Regd. No. C-3911

VOL. 32 INDIAN JOURNAL OF PHYSICS No. 1

(*Published in collaboration with the Indian Physical Society*)

AND

VOL. 41 PROCEEDINGS No. 1

OF THE

INDIAN ASSOCIATION FOR THE CULTIVATION OF SCIENCE

JANUARY, 1958

PUBLISHED BY THE

INDIAN ASSOCIATION FOR THE CULTIVATION OF SCIENCE

JADAVPUR, CALCUTTA 32

BOARD OF EDITORS

R. K. ASUNDI — P. S. GILL

K. BANERJEE — S. K. MITRA

D. M. BOSE — P. RAY

S. N. BOSE — K. R. RAO

K. R. DIXIT — S. C. SIRKAR (*Secretary*)

B. N. SRIVASTAVA

EDITORIAL COLLABORATORS

PROF. D. BASU, PH.D.

DR. A. BOSE, D.SC.

DR. N. N. DASGUPTA, M.SC., PH.D.

PROF. A. K. DUTTA, D.SC., F.N.I.

DR. S. GHOSH, D.SC.

DR. S. R. KHASTGIR, D.SC., F.N.I., F.R.S.E.

PROF. P. K. KICHLU, D.SC., F.N.I.

PROF. D. S. KOTHARI, D.SC., F.N.I.

DR. K. S. KRISHNAN, D.SC., F.R.S.

PROF. B. D. NAG CHOWDHURY, PH.D.

PROF. S. R. PALIT, D.SC., F.R.I.C., F.N.I.

DR. S. PARTHASARATHY, D.SC., F.N.I.

DR. H. RAKSHIT, D.SC., F.N.I.

DR. R. GOPALAMURTY RAO.

DR. VIKRAM A. SARABHAI, M.A., PH.D.

PROF. N. R. TAWDE, D.SC., F.N.I.

DR. P. VENKATESWARLU.

ASSISTANT EDITOR

MR. A. N. BANERJEE, M.SC.

Annual Subscription—

Inland Rs. 20

Foreign £ 2

NOTICE TO INTENDING AUTHORS

Manuscripts for publication should be sent to the Assistant Secretary, Indian Journal of Physics, Jadavpur, Calcutta 32.

The manuscripts submitted must be type-written with double space on thick foolscap paper with sufficient margin on the left and at the top. The original copy, and not the carbon copy, should be submitted. Each paper must contain an abstract at the beginning.

All references should be given in the text by quoting the surname of the author, followed by year of publication, *e.g.*, (Ghosh, 1954). The full reference should be given in a list at the end, arranged alphabatically, as follows; Ghosh, D. K., 1954, *Ind. J. Phys.*, **28**, 485.

Line diagrams should be drawn on white Bristol board or tracing paper with black India ink, and letters and numbers inside the diagrams should be written neatly in capital type with India ink. The size of the diagrams submitted and the lettering inside should be large enough so that it is legible after reduction to one-third the original size. A simple style of lettering such as gothic, with its uniform line width and no serifs should be used, *e.g.*,

A·B·E·F·G·M·P·T·W·

Photographs submitted for publication should be printed on glossy paper with somewhat more contrast than that desired in the reproduction, and should, if possible, be mounted on thick white paper.

Captions to all figures should be typed in a separate sheet and attached at the end of the paper.

The mathematical expressions should be written carefully by hand. Care should be taken to distinguish between capital and small letters and superscripts and subscripts. Repetition of a complex expression should be avoided by representing it by a symbol. Greek letters and unusual symbols should be identified in the margin. Fractional exponents should be used instead of root signs.

INDIAN JOURNAL OF PHYSICS

VOL. 32

AND

PROCEEDINGS

OF THE

Indian Association for the Cultivation of Science, Vol. 41

(Published in Collaboration with the Indian Physical Society)

(With Seventeen Plates)

Printed by Kalipada Mukherjee, Eka Press, 204/1. B. T. Road, Calcutta
and published by the Registrar, Indian Association for the Cultivation
of Science, Jadavpur, Calcutta 32

1958

BOARD OF EDITORS

R. K. ASUNDI — P. S. GILL
K. BANERJEE — S. K. MITRA
D. M. BOSE — P. RAY
S. N. BOSE — K. R. RAO
K. R. DIXIT — S. C. SIRKAR (*Secretary*)
B. N. SRIVASTAVA

EDITORIAL COLLABORATORS

PROF. D BASU, PH.D.

DR. A BOSE, D.SC.

DR. N. N DASGUPTA, M.SC., PH.D.

PROF. A. K. DUTTA, D.SC., F.N.I.

DR. S. GHOSH, D.SC.

DR. S R. KHASTGIR, D SC, F.N.I., F.R.S.E.

PROF. P. K. KICHLU, D SC, F.N I.

PROF. D. S. KOTHARI, D.SC., F.N.I.

DR. K. S. KRISHNAN, D.SC, F.R.S.

PROF. B. D. NAG CHOWDHURY, PH.D.

PROF. S. R. PALIT, D.SC., F.R.I.C., F.N.I.

DR. S. PARTHASARATHY, D.SC., F N I.

DR. H. RAKSHIT, D.SC., F.N.I

DR. R. GOPALAMURTY RAO.

DR. VIKRAM A. SARABHAI, M.A., PH.D.

PROF. N. R. TAWDE, D.SC., F.N.I.

DR. P. VENKATESWARLU.

ASSISTANT EDITOR
SRI A. N. BANERJEE, M SC.

Annual Subscription—
Inland Rs. 20
Foreign £ 2 or $ 6

NOTICE TO INTENDING AUTHORS

Manuscripts for publication should be sent to the Assistant Secretary, Indian Journal of Physics, Jadavpur, Calcutta 32.

The manuscripts submitted must be type-written with double space on thick foolscap paper with sufficient margin on the left and at the top. The original copy, and not the carbon copy, should be submitted. Each paper must contain an abstract at the beginning.

All references should be given in the text by quoting the surname of the author, followed by year of publication, *e.g.*, (Ghosh, 1954). The full reference should be given in a list at the end, arranged alphabatically, as follows; Ghosh, D. K., 1954, *Ind. J. Phys.*, **28**, 485.

Line diagrams should be drawn on white Bristol board or tracing paper with black India ink, and letters and numbers inside the diagrams should be written neatly in capital type with India ink The size of the diagrams submitted and the lettering inside should be large enough so that it is legible after reduction to one-third the original size. A simple style of lettering such as gothic, with its uniform line width and no serifs should be used, *e.g.*,

A·B·E·F·G·M·P·T·W·

Photographs submitted for publication should be printed on glossy paper with somewhat more contrast than that desired in the reproduction, and should, if possible, be mounted on thick white paper.

Captions to all figures should be typed in a separate sheet and attached at the end of the paper.

The mathematical expressions should be written carefully by hand. Care should be taken to distinguish between capital and small letters and superscripts and subscripts. Repetition of a complex expression should be avoided by representing it by a symbol Greek letters and unusual symbols should be identified in the margin. Fractional exponents should be used instead of root signs

INDIAN JOURNAL OF PHYSICS. 32, 1958

CONTENTS

No 1. January

PAGE

1. Spectroscopic Constants of Molecules. VI. Dependence of Force Constant on Electronegativity—Yatendra Pal Varshni ... 1
2. An X-Ray Study of Some Leathers—D. M. Chakraburtty and B. Chakravarti 10
3. X-Ray Analysis of Frozen Pyridine and its Solution at-180°C --S. G. Biswas 13
4. A Study on the Cosmic Ray Nuclear Interactios in Lead at 9000 ft. —R. N. Mathur and P. S. Gill 19
5. Improved Transmission of Ions with Inhomogeneous Magnetic Fields —S. B. Karmohapatro 26
6. The Effect of a Uniform Magnetic Field on Electrodeless Discharge in a Tube and Measurement of Electronic Mobility. I. Air.—S. N. Goswami 35
7. X-Ray Study of Alpha-Beta Transformation in Keratin—V. D Gupta 42

LETTERS TO THE EDITOR

1. Possibility of Polarization of Free Electrons—S Yamaguchi ... 45
2. Thermoluminescence Spectra of LiF—A. K. Ghosh and B C Dutta 47

No. 2. February

8. The Dielectric Properties of Ester Gum—A. K. Sen and G. N. Bhattacharya 49
9. Velocity of Ultrasonic Waves in Solutions of Electrolytes—Satya Prakash and Satish Chandra Srivastava 62
10. A Comparative Study of Betatron and Direct Injection in the Electron Synchrotron Proposed for the Institute of Nuclear Physics, Calcutta—M. N. Viswesvariah and S. K. Sen 66
11. A Warble Tone Generator.—R. R. Duttagupta 75
12. High Energy Neutron-Proton Scattering With Spin-Orbit Interaction. —H. N. Yadav and L. S. Singh 80
13. An Electronic Differential Analyser.—A. K. Choudhury and B. R. Nag 91

No. 3. March

14. On Linear Delayed Control Systems. Part I—Considerations of Stability.—N. B. Chakraborti 109

PAGE

15. The Influence of Constant Electric and Magnetic Fields on the Spin of the Particle— S. Sarkar 124
16. On the Calculational Procedures in the Derivation of the Vibrational Transition Probabilities of the First Negative ($b^4\Sigma^- g \rightarrow a^4\Pi_u$) Bands of O_2^+— N. R. Tawde and N. Sreedhara Murthy 128
17. X-Ray Crystallographic Data on Rubidium Fumarate, Monohydrate ($Rb_2C_4H_2O_4,H_2O$)— M. P. Gupta and G. P. Dube 133
18. X-ray Analysis of Frozen Stryene At − 180°C.— N. K. Roy ... 137
19. Analogue Multiplier and Function Generator with Cathode Ray Tube—A. K. Choudhury and B. R. Nag 141
20. Quadrupole Vibrations and the Electric Quadrupole Moment of Some Closed Shell Plus (or Minus) a Single Nucleon Nuclei —P. N. Mukherjee and I Dutt 149

No 4 April

21. Spectral Study of Thermoluminescence Emission from KBr and NaBr - - B. C. Dutta and A. K. Ghosh 155
22. On the Axial Stability of a Deformed Nucleus I— P. N. Mukherjee and I. Dutt 165
23. Extension of the Table for the Calculation of Surface Tension from Measurements of Sessile Drops—K. G Parvatikar 174
24 Spin of an Electron from Five-Dimensional Wave Equation— C. C Banerjee 179
25. The Study of Noise Pulses and a Liquid Scintillator- Brat Pal Singh, H. S. Hans and P. S. Gill 183
26. On the Raman Spectra of Solutions of Ortho-Chlorophenol - Deb Kumar Mukherjee 192
27 X-Ray Study of Agave Vera Cruz Fibre - - N. N. Saha and Thanda Pe 198

No 5 May

28. Use of Laguerre Filters for Realisation of Time Functions and Delay — A K. Choudhury and N. B Chakraborti 205
29. On the Application of an Electronic Differential Analyser for Finding the Roots of a Polynomial— B. R. Nag 212
30. Ultraviolet Absorption Spectrum of Acetophenone— R. N. Bapat 218
31. New Visible Band Systems of the PO Molecule— K. Kanaka Durga and P. Tiruvenganna Rao 223
32 Stability of Magnetic Stars in a Decay Field—S. P. Talwar ... 230
33. The Effect of a Uniform Magnetic Field on Electrodeless Discharge in a Tube and Measurement of Electronic Mobility. II. Oxygen, Nitrogen, Carbon-Dioxide and Hydrogen—S. N Goswami ... 241

PAGE

34. Electron Scattering and Image Contrast in Electron Microscopy —P. Sadhukhan 249

No. 6. June

35. New Evidence for a Particle of Mass $525m_e$— Milima Basu and M. S. Sinha 259
36. Automatic Recorder of the Waveforms of Atmospherics— B. A. P. Tantry 267
37. On the Thermal Neutron Capture Cross-Sections— H. S. Hans and M. L. Sehgal 276
38. On the Making of Electret Measurement of the Changes of Dielectric Constant of a Polarised Electret Forming Material with Time —T. C. Bhadra 281

LETTERS TO THE EDITOR

3. Diurnal Variation of Deviative Absorption in the F_2 Region of the Ionosphere— S. K. Sharma 297
4. Indexed Powder Diffraction Data on Dihydroxyfumaric Acid, Anhydrous, $C_4H_4O_6$— M. P. Gupta and G. P. Dube ... 299
5. Afterglow in *p*-Chlorotoluene at −180°C—D. C. Biswas ... 301

No. 7. July

39. Studies on a Rhombic Antenna with Cylindrical Helices as the Arms — Ashoke Kumar Sen 303
40. Radial Pulsations of an Infinite Cylinder in the Presence of Magnetic Field— J. N. Tandon and S. P. Talwar 317
41. Ultraviolet Absorption Spectra of Solutions of Pyridine in Different Solvents and at Different Temperatures— S. B. Roy ... 323
42. On Core-to-Particle Interaction from Classical Point of View— S. Mukherjee and A. Gupta 330
43. Scattering of Electron from Five Dimensional Wave Equation — A. K. Mitra 336

LETTERS TO THE EDITOR

6. Relationship between Adiabatic Compressibility and Concentration of Solutions of Electrolytes— Satish Chandra Srivastava ... 340
7. Five Dimensional Wave-Equation for Hydrogen Atom— V. B. Kelkar and K. M. Ghata 342

No. 8 August

44. On the Infra-Red Spectra of Solutions of *o*-Chlorophenol and Phenol— S. C. Sirkar, A. R. Deb and S. B. Banerjee ... 345
45. Polarisation of a Dirac Particle and Proton-Neutron Scattering— S. P. Misra 355

PAGE

46. Dipole Moments of some Substituted Benzenes and Pyridines. Part II Meta Disubstituted Benzenes— C. R K. Murty ... 365
47. An Electron Diffraction Camera of Simplified Design—S. N. Chatterjee 369
48. Range-Energy Relation for Protons in Various Substances—Yatendra Pal Varshni 373
49. Dielectric Relaxation-Effect of Temperature—K. V. Gopala Krishna 387

LETTERS TO THE EDITOR

8. Soft X-Ray Emission Spectroscopy of Graphite and the Suggestion of a Suitable Brillouin Zone for it —Ajit Kumar Dutt ... 397

BOOK REVIEW 400

No 9 September

50. The Emission Spectrum of Chlorine (Cl_2^{+})—P. B. V. Haranath and P. Tiruvengamma Rao 401
51. Determination of the Beta Ray Energy Spectrum from the Absorption Curves of Beta Rays—N. K. Saha and K. L. Kaila ... 418
52. On the Absorption Coefficients and Energy Spectra of Gamma-Rays from Ra(B + C) under thick Layers of Pb Absorber—P. K. Sen Chaudhury 430
53. The Variation of Compressibility of Water and Electrolytic Solutions with Temperature—Prafulla Kumar Mahapatra and Baman Charan Ray 439
54. Calorimeter for the Measurement of Specific Heat of Lac—Surendra Nath Srivastava 443

LETTERS TO THE EDITOR

9. On the Magnetic Susceptibility and Anisotropy of V^{3+} under a Crystalline Electric Field having Predominantly Cubic Symmetry with a Small Trigonal Component—A. S. Chakraborty ... 447

BOOK REVIEW 450

No. 10. October

55. Infra-Red Absorption Spectra of Solutions of Ethylene Dichloride in Certain Solvents—Monomohan Mazumder 451
56 Crystal Structure of Frozen Cyclohexane at —180°C—G. S. R. Krishnamurti 460
57. A Compact Instrument for the Measurement of Surface Tension of Liquids—P. D. Pathak and R. M. Patel 464
58. 150 KV Cockcroft-Walton Type Particle Accelerator—C. S. Khurana and H. S. Hans 468

PAGE

59. Evidence for Formation of Molecular Groups in Liquids at Low Temperatures— G. S. Kastha 473
60. On the Electron Production Rate in the F_2 Region of the Ionosphere — S. Dutta 483
61. Dipole Moments of some Substituted Benzenes and Pyridines. Part III. Chloro-and Bromo Ethyl Benzenes — C. R. K. Murty 492

No. 11. November

62. Structure of the Spectrum of Singly Ionised Bromine— Y. Bhupala Rao 497
63. Dipole Moments of some Substituted Benzenes and Pyridines— C. R. K. Murty 516
64. Correction for Stokes' Law — N. R. Gokhale and K. M. Gatha ... 521
65. Electronic Spectra of *o*-Chlorophenol in Different Environments and at Different Temperatures— S. B. Roy 525

LETTERS TO THE EDITOR

10. Charge-Transfer Transition in Cl_2^{+}— V. Venkateswara Rao and P. Tiruvenganna Rao 534

No. 12 December

66. A New Wideband Discriminator— N. B. Chakraborti ... 537
67. Calculations of the Dipole Moments of Tri-Substituted Benzenes 1, 2, 3-, 1, 2, 4-and 1, 3, 5-Substitutions— D. V. G. L. Narasimha Rao 547
68. The Dielectric Properties of Rosin— A. K. Sen and G. N. Bhattacharya 556
69. Colour Centres in Pentahydrate Crystal of Sodiumthiosulphate — Kapil Deo Prasad 566
70. Absorption of Microwaves in Solutions of Ortho-Chlorophenol — Tarak Jiban Bhattacharyya 573

LETTERS TO THE EDITOR

11. Thermoluminescence and Phosphorescence Spectra of some Pure and Impurity Activated Alkali Halides— B. C. Dutta and A. K. Ghosh 578
12. On the Calculation of Relaxation Times— C. R. K. Murty ... 580
13. Configurational Interaction in Molecular Orbital Theory as Applied to Indene— S. Ramamurty 582
14. Predicted Electronic Shifts in Flourinated Napthalenes— S. Ramamurty 584

AUTHOR INDEX

Author	Subject	Page
Banerjee, C. C.	Spin of an electron from five-dimensional wave equation	179
Banerjee, S. B.	See Sirkar, S. C.	345
Bapat, R. N.	Ultraviolet absorption spectrum of acetophenone	218
Basu, Nilima and M. S. Sinha	New evidence for a particle of mass 525 m_e	259
Bhadra, T. C.	On the making of electret and measurement of the changes of dielectric constant of a polarised electret forming material with time	281
Bhattacharyya, G. N.	See Sen, A. K.	49
,, ,,	,, ,,	556
,, Tarak Jiban	Absorption of microwaves in solutions of ortho-chlorophenol	573
Biswas, D. C. (L)	After glow in *p*-chlorotoluene at −180°C	301
Biswas S. G.	X-ray analysis of frozen pyridene and its solutions at −180°C	13
Chakraborty, A. S. (L)	On the magnetic susceptibility and anisotropy of V^{3+} under a crystalline electric field having predominantly cubic symmetry with a small trigonal component	447
Chakraborti, N. B.	On linear delayed control system. Part 1. Consideration of stability	109
	See Choudhury, A. K.	205
	A new wide band discriminator	537
Chakraburtty, D. M. and	An X-ray study of some leathers	10
,, B. Chakravarti	See Chakraburtty, D. M.	10
Chatterjee, S. N.	An electron diffraction camera of simplified design	369
Choudhury, A. K. ahd B. R. Nag	An electronic differential analyser	91
,, ,, and B. R. Nag	Analogue multiplier and function generator with cathoderay tube	141
and N. B. Chakraborti	Use of Laguerre filters for realisation of time function and delay	205
Deb, A. R.	See Sirkar, S. C.	345
Dube, G. P.	See Gupta, M. P.	133
	,, ,, ,,	299

Author	Subject	Page
Durga, K. Kanaka and P. T. Rao	New visible band system of PO molecule	223
Dutta, Ajit Kumar	Soft X-ray Emission spectroscopy of graphite and the suggestion of a suitable Brillouine zone for it. (L)	397
Dutta, B. C. and A. K. Ghosh	Spectral study of thermoluminescence emission of KBr and NaBr	155
,, ,,	See A. K. Ghosh	47
,, ,, and A. K. Ghosh	Thermoluminescence and phosphorescence spectra of some pure and impurity activated alkali halides (L)	578
Dutt, I.	See Mukherjee, P. N.	149
,, ,,		165
Dutta, S.	On the electron production rate in the F_2 region of the ionosphere	483
Duttagupta, R. B.	A Warble tone generator	75
Gatha, K. M.	See Kelkar, V. B.	342
Gatha, K. M.	See Gokhale, N. R.	521
Ghosh, A. K. and B. C. Dutta	Thermoluminescence spectra of LiF (L)	47
,, ,,	See Dutta B. C.	155
,, ,,	,, ,, ,,	578
Gill, P. S.	See Mathur, R. N.	19
,, ,,	See Singh, B. P.	183
Gokhale, N. R. and K. M. Gotha	Correction for Stokes' law	521
Gopalakrishna, K. V.	Dielectricrelaxation-Effect of temperature	387
Goswami, S. N.	The effect of a uniform magnetic field on electrodeless discharge in a tube and measurement of electronic mobility. I. Air	35
	,, ,, ,, ,, ,, II Oxygen, nitrogen, carbon dioxide and hydrogen	241
Gupta, A.	See Mukherjee, S.	330
Gupta, M. P. and G. R. Dube	Indexed powder diffraction data on dihydroxy fumaric acid, anhydrons $C_4H_4O_6$ (L)	299
Gupta, M. P. and G. P. Dube	X-ray crystallographic data on rubidium fumarate monohydrate ($Rb_2C_4H_2O_4,H_2O$)	133

Author	Subject	Page
Gupta, V. D.	X-ray study of alpha-beta transformation in keratin	42
Hans, H. S.	See Singh, B. P.	183
,, ,, and M. L. Sehgal	On the thermal neutron capture cross-section	276
	See Khurana, C. S.	468
Haranath, P. B. V. and P. T. Rao	The emission spectrum of chlorine (Cl_2^+)	401
Kaila, K. L	See Saha, N. K.	418
Karmohapatro, S. B.	Improved transmission of ions with inhomogeneous magnetic fields	26
Kastha, G. S.	Evidence for formation of molecular groups in liquids at low temperatures	473
Kelkar, V. B. and K. M. Gatha	Five dimensional wave-equation for hydrogen atom. (L)	342
Khurana, C. S and H. S. Hans	150 KV Cockcroft-Walton type particle accelerator	468
Krishnamurti, G. S. R.	Crystal structure of frozen cyclohexane at −180°C	460
Mahapatra, P. K. and B C. Ray	The variation of compressibility of water and electrolytic solutions with temperature.	439
Mathur, R. N. and P. S. Gill	A Study on the cosmic ray nuclear interactions in lead at 9000ft.	19
Mazumder, M. M.	Infra-red absorption spectra of solutions of ethylene dichloride in certain solvents	451
Misra, S. P.	Polarisation of a Dirac Particle and proton-neutron scattering	355
Mitra, A. K.	Scattering of electron from five-dimensional wave equation	336
Mukherjee, D. K.	On the raman spectra of solutions of Ortho-chlorophenol	192
Mukherjee, P. N. and I. Dutt	Quadrupole vibrations and the electric quadrupole moment of some closed shell plus (or minus) a single nucleon nuclei.	149
	On the axial stability of a deformed nucleus I	165

Author	Subject	Page
Mukherjee, S. and A. Gupta	On core-to-particle interaction from classical point of view	330
Murty, C. R. K.	Dipole moments of some substituted benzenes and pyridines II (Meta disubstituted bengenes)	
,, ,,	,, ,, ,, ,, III (chloro-bromobthyl ,,)	492
,, ,,	,, ,, ,, ,, IV	516
,, ,,	On the calculation of relaxation times. (L)	580
Nag, B. R.	See Choudhury A. K.	91
	,, ,, ,,	141
,, ,,	On the application of an electronic differential analyser for finding the roots of a polynomial	212
,, ,,		
Patel, R. M.	See Pathak, P. D.	464
Pathak, P. D. and R M. Patel	A compact instrument for the measurement of surface tension of liquids	464
Parvatikar, K. G.	Extension of the table for the calculation of surface tension from measurements of sessile drops	174
Pe, Thanda	See Saha, N. N.	198
Prakas, Satya and Satish Chandra Srivastava	Velocity of ultrasonic waves in Solutions of electrolytes	62
Prasad, K. D.	Colour centres in pentahydrate crystal of sodiumthiosulphate	566
Ramamurty, S.	Configurational interaction in molecular orbital theory as applied to indene. (L)	582
	Predicted electronic shifts in flourinated (napthalenes (L)	584
Rao, P. Tiruvenganna	See Durga K Kanaka	223
	See Rao, V. V.	534
	See Haranath, P. B. V.	401
Rao, Narasimha, D. V. G. L.	Calculations of the dipole moments of tri-substituted benzenes 1, 2, 3-, 1, 2, 4-and, 3, 5-Substitutions	547
Rao, V. Venkateswara and P. T Rao	Charge-transfer transition in Cl_2^+ (L)	534

Author	Subject	Page
,, Y. Bhupala	Structure of the spectrum of singly ionised bromine	497
Ray, B. C.	See Mahapatra, P. K.	439
Roy, N. K.	X-ray analysis of frozen styrene at −180°C	137
,, S. B.	Ultraviolet absorption spectra of solutions of pyridine in different solvents and at different temperatures	323
	Electronic spectra of *o*-chlorophenol in different environments and at different temperatures	525
Sadhukhan, P.	Electron scattering and image Contrast in electron microscopy	249
Saha, N. K. and K. L. Kaila	Determination of the beta-ray energy spectrum from the absorption curves of beta-rays	418
Saha, N N. and Thanda Pe	X-ray study of agave vera cruz fibre	198
Sarkar, S.	The influence of constant electric and magnetic fields on the spin of the particle	124
Sehgal, M. L.	See Hans , H. S.	276
Sen, A. K.	Studies on a rhombic antenna with cylindrical helices as the arms	303
Sen, A. K. and G. N. Bhattacharya	The dielectric properties of ester gum	49
	The dielectric properties of rosin	556
Sen, S. K.	See Viswesvariah, M. N.	66
Sen, Choudhury, P. K.	On the absorption coefficients and Energy spectra of gamma-rays from Ra (B+C) under thick layers of Pb absorber	430
Sharma, S. K.	Diurnal variation of deviative absorption in the F_2 region of the ionosphere (L)	297
Sinha, M. S.	See Basu Nilima	259
Sinha, B. P., H. S. Hans and P. S. Gill	The study of noise pulses and a liquid scintillator	183
Sinha, L. S.	See Yadav, H. N.	80

Author	Subject	Page
Sirkar, S. C., A. B. Deb and S. B. Banerjee	On the infra-red spectra of solutions of *o*-chlorophenol and phenol	345
Sreedharamurthy, N.	See Tawde, N. R.	128
Srivastava, S. C.	See Prakash Satya	62
	Relationship between adiabatic compressibility and concentration of solutions of electrolytes (L)	340
Srivastava, S. N.	Calorimeter for the measurement of specific heat of lac	443
Talwar, S. P.	Stability of magnetic stars in a decay field	230
" "	See Tandon, J. N.	317
Tandon, J. N. and S. P. Talwar	Radial pulsations of an infinite cylinder in the presence of magnetic field	317
Tantry, B. A. P.	Automatic recorder of the waveforms of atmospherics	267
Tawde, N. R. and Sreedharamurthy, N.	On the calculational procedures in the derivation of the vibrational transition probabilities of the first negative ($b^4\ \Sigma^- g \rightarrow a^4 \Pi_u$) bands of O_2	128
Varshni, Y. P.	Spectroscopic constants of molecules. VI. dependence of force constanton electronegativity	1
	Range-Energy relation for protons in various substances	373
Viswesvariah, M. N. and S. K. Sen	A comparative study of betatron and direct injection in the electron synchrotron proposed for the Institute of Nuclear Physics, Calcutta	66
Yadav, H. N. and L. S. Singh	High energy neutron-proton scattering with spin-orbit interaction	80
Yamaguchi, S.	Possibility of polarization of free electrons. (L)	45

SUBJECT INDEX

Subject	Author	Page
Absorption of microwaves in solutions of orthochloro phenol	Tarak Jiban Bhattacharya	573
Adiabatic compressibility of concentration of solutions of electrolytes. Relationship between (L)	Satish Chandra Srivastava	340
Afterglow in *p*-chlorotoluene at −180°C (L)	D. C. Biswas	301
Analogue multiplier and function generator with cathode ray tube	A. K. Choudhury and B. R. Nag	141
Automatic recorder of waveforms of Atmospherics	B. A. P. Tantry	267
Axial stability of a deformed nucleus. On the	P. N. Mukherjee and I. Dutt	165
Beta-ray energy spectrum from the absorption curves of beta-rays. Determination of the	N. K. Saha and K. L. Kaila	418
Betatron and direct injection in the electron synchrotron proposed for Institute of Nuclear Physics, Calcutta. A comparative study of	M. N. Viswesvariah and S. K. Sen	66
Charge transfer transition in Cl_2^+ (L)	V. V. Rao and P. T. Rao	534
Cockcroft-Walton type accelerator. 150 KV	C. S. Khurana and H. S. Hans	468
Colour centres of penta hydrate crystals of sodium thiosulphate	Kapil Deo Prasad	566
Compressibility of water and electrolytic solutions with temperature. The variation of	P. K. Mahapatra and B. C. Roy	439
Configurational interaction in molecular orbital theory as applied to indene. (L)	S. Ramamurty	582
Core-to-particle interaction from classical point of view. On	S. Mukherjee and A. Gupta	330
Cosmic ray nuclear interactions in lead at 9000 ft. A study on the	R. N. Mathur and P. S. Gill	19
Crystal structure of frozen Cyclohexane at −180°C	G. S. R. Krishnamurti	460
Dielectric properties of ester gum. The	A. K. Sen and G. N. Bhattacharyya	49
Dielectric properties of rosin. The	G. N. Bhattacharyya	556

Subject	Author	Page
Dielectric relaxation-effect of temperature.	K. V. G. Gopalakrishna	387
Dipole moments of some substituted benzenes and pyridenes. Part II	C. K. R. Murty	365
,, ,, ,, Part III	,,	492
		516
Dipole moments of tri-substituted benzenes 1, 2, 3-, 1, 2, 4, and 1, 3, 5, substitutions. Calculation of the	D. V. G. L. Narasimha Rao	547
Dirac particle and proton-neutron scattering. Polarisation of a	S. P. Misra	355
Duirnal variation of deviative Absorption in F_2—region of the ionosphere (L)	S. K. Sharma	297
Electric and measurement of the changes of dielectric constant of a polarised electret forming material with time. On the making of	T. C. Bhadra	281
Electrodeless discharge in a tube and measurement of electronic mobility . I. Air. The effect of uniform magnetic field on	S. N. Goswami	35
Electrodeless discharge in a tube and measurement of electronic mobility. II. Oxygen, nitrogen, carbondioxide and hydrogen. The effect of a uniform magnetic field on	S. N. Goswami	241
Electronic differential analyser. An	A. K. Choudhury and B. R. Nag	91
Electronic shifts in fluorinated naphthalenes. Predicted (L)	S. Ramamurty	584
Electronic differential analyser for finding the roots of a polynomial. On the application of an	B. R. Nag	212
Electron diffraction camera of simplified design. An	S. N. Chatterjee	369
Electron production rate in F_2-region of the Ionosphere. On the	S. Dutta	483
Electron scattering and image contrast in electron miscroscopy.	P. Sadhukhan	249
Five dimensional wave equation for hydrogen atom	V. B. Kelkar and K. M. Gatha	342

Subject	Author	Page
Gama-rays from Ra (B+C) under thick layers of Pb absorber. On the absorption coefficients and energy spectra of	P. K. SenChoudhury	430
Indexed powder diffraction data on dihydroxyfumaric acid analydrous $C_4H_4O_6$. (L)	M. P. Gupta and G. P. Dube	299
Laguerre filters for realisation of time functions and delay. Use of	A. K. Choudhury and N. B. Chakraborti	205
Linear delayed control systems. Part I. consideration of stability. On	N. B. Chakraborti	109
Magnetic stars in a delay field. Stability of	S. P. Talwar	230
Magnetic susceptibility and anisotropy of V^{3+} under a crystalline electric field having predominantly cubic symmetry with a small trigonal component. On the (L)	A. S. Chakraborty	447
Molecular Groups in liquids at low temperatures. Evidence of formation of	G. S. Kastha	473
Neutron-proton scattering with spin-orbit interaction. High energy	H. N. Yadav and L. S. Singh	80
Noise pulses and a liquid scintillator. The study of	H. S. Hans and P. S. Gill	183
Particle of mass 525 m_e. New evidence for a	Nilima Basu and M. S. Sinha	259
Polarisation of free electrons. Possibility of (L)	S. Yamaguchi	45
Quadrupole variations and electric quadrupole moments of some closed shell plus (or minus) a single nucleon nuclei	P. N. Mukherjee and I. Dutt	149
Radial pulsation of an infinite cylinder in the presence of magnetic field.	J. N. Tandon and S. P. Talwar	317
Range-energy relations for protons in various substances	Y. P. Varshni	373
Relaxation times. On the calculation of (L)	C. R. K. Murty	580
Rhombic antenna with cylindrical helices as the arms. Studies on a	A. K. Sen	303

Subject	Author	Page
Scattering of electrons from five dimensional wave equations	A. K. Mitra	336
Specific heat of Lac. Conorimeter for measurement of	S. N. Srivastava	443
SPECTRA		
Electronic spectra of *o*-chlorophenol indifferent environments and at different temperatures	S B. Roy	525
Emission spectrum of chlorine (Cl_2^+). The	P. B. V. Haranath and P. T. Rao	401
Infra-red absorption spectra of solutions of ethylene dichloride in certain solvents	M. M. Mazumder	451
Infra-red spectra of solutions of *o*-chlorophenol and phenol On the	S. C. Sirkar, A. R. Deb and S. B. Banerjee	345
Raman spectra of solutions of *o*-chlorophenol. On the	D. K. Mukherjee	192
Spectrum of ingly ionised bromine. Structure of the	Y. Bhupala Rao	497
Ultraviolet absorption spectrum of Acetophenone	R. N. Bapat	218
Ultraviolet absorption spectra of solutions of pyridene in different solvents and at different temperatures.	S. B. Roy	323
Spectroscopic constants of molecules, VI. Dependance of force constants on electronegativity	Y. P. Varshni	1
Spin of an electron from five-dimensional wave equations	C. C. Banerjee	179
Spin of the particles. On the influence of constant electric and magnetic fields on the	S. Sarkar	124
Stokes' law. Correction for	N. R. Gokhale and K. M. Gatha	521
Surface tension from measurement of sessile drops. Extension of the table for the calculation of	K. G. Parvatikar	174
Surface tension of liquids. A compact instrument for the measurement of	P. D. Pathak and R. M. Patil	464

Subject	Author	Page
Thermal neutron capture cross-sections. On the	H. S. Hans and M. L. Sahgal	276
Thermoluminescence spectra of LiF (L)	A. K. Ghosh and B C. Dutta	47
Thermoluminescence emission from KBr and NaBr. Spectral study of	B. C. Dutta and A. K. Ghosh	155
Thermoluminescence and phosphorescence spectra of some pure and impurity activated alkalihalides (L)	B. C Dutta and A K. Ghosh	578
Transmission of ions with inhomogeneous magnetic fields. Improved	S. B. Karmohapatro.	26
Ultrasonic waves in solutions of electrolytes—Velocity of	S. Prakash and S. C. Srivastava	62
Vibrational transition of probabilities of the first negative ($b^4\Sigma_g^- \rightarrow a^4\pi_u$) bands of O_2^+. On the calculations of the procedures in the derivation of the	N. R Tawde and N Sreedharamurty	128
Visible band systems of PO molecules New	K Kanak Durga and P T. Rao	223
Warble tone generator. A	R. R. Duttagupta	75
Wideband discriminator. A new	N B. Chakraborti	537
X-ray analysis of frozen pyridene and its solutions at $-180°C$	S G. Biswas	13
X-ray analysis of frozen styrene at $-180°C$	N K. Roy	137
X-ray crystallographic data on rubidium fumarate, monohydrate ($Rb_2 C_4H_2O_4, H_2O$)	M. P. Gupta and G. P. Dube	133
X-ray emission spectroscopy of Graphite and the suggestions of a suitable Brillouin zone for it. Soft(L)	Ajit Kumar Dutt	397
X-ray study of Agave Vera Cruz fibre	N. N Saha and Thanda Pe	198
X-ray study of alpha-beta transformation in keratin	V. D. Gupta	42
X-ray study of some leathers. An	D. M Chakraburtty and B. Chakravarti	10

SPECTROSCOPIC CONSTANTS OF MOLECULES. VI. DEPENDENCE OF FORCE CONSTANT ON ELECTRONEGATIVITY

YATENDRA PAL VARSHNI

DEPARTMENT OF PHYSICS, ALLAHABAD UNIVERSITY, ALLAHABAD

(*Received, January* 5, 1957)

ABSTRACT. For diatoms formed out of elements belonging to the same sub-group of the periodic table, it has been shown that

$$\log k_e = g \log x_A x_B + h$$

where g and h are constants and x_A and x_B are the electronegativities.

A relation between the force constants of diatoms AA and AH has also been suggested:

$$k_e(AH) = p\, k_e(AA) + q$$

where p and q are constants for each group.

INTRODUCTION

The concept of "electronegativity" introduced by Pauling (1932, 1944) has proved to be very useful in the understanding of the chemical bond. Electronegativity (x) is a measure of the power of an atom to attract electrons to itself. It has achieved an astonishing success "in correlating a vast field of chemical knowledge and experience"

Pauling's original values of electronegativities have been revised and extended by him and others, and various comparisons have been made between electronegativities computed on basis of Pauling's assumptions and those computed in other ways. Recently the subject has been exhaustively reviewed by Pritchard and Skinner (1955). Gordy and Thomas (1956) have compared electronegativity values derived by different methods and have suggested the "best" values.

A number of attempts have been made to investigate the dependence of molecular properties *e.g.* dipole moment, force constant, ionic character etc. on electronegativity.

Gordy (1946a, b) has found that for bonds of similar nature

$$k_e = aN \left[\frac{x_A x_B}{r_e^2} \right]^{3/1} + b \qquad \ldots (1)$$

where k_e — force constant

r_e — internuclear distance

N — bond order

a, b — constants

An interesting feature of eq. (1) is the fact that x_A and x_B are involved as product $x_A x_B$ rather than as a difference Exceptions to Gordy's relation have been found by several workers (Cottrell and Sutton, 1947)

Recently, Williams (1956) has proposed that for elements of groups IV to VII :

$$x_A = .761(z_A/r_A)^{.7} \qquad (2)$$

where z is the number of valence electrons in the atom and r_A is its covalent radius Combining eq (2) with Gordy s eq (1) he derives

$$k_e = \alpha(z_A z_B)^{.525}/r_e^{2.525} + \beta \qquad (3)$$

From this, Williams puts forward the view that force constant is primarily a function of number of valence electrons, rather than that of electronegativities

NEW RELATIONS

In diatomic molecules formed out of elements A and B, both belonging to the same sub-group of the periodic table, the valence forces are very similar In view of this it was conjectured that the k_e of such molecules may show simple relationship with the electronegativities of the constituent atoms

It has been found that for such molecules log k_e is linear with log $x_A x_B$. The relationship can be represented as

$$\log k_e = g \log x_A x_B \qquad (4)$$

where g and h are constants for each molecular group

Pritchard and Skinner (1955) and Gordy and Thomas (1956) have suggested the "best" values of electronegativities While for most of the elements the two scales agree, for IVb group elements there are serious differences A compromised set of values selected with the guiding principle that electronegativity should decrease regularly as one passes downwards in any subgroup of the periodic table (Fajans, 1928 , Walsh, 1951) is given in Table I and has been used in the present paper

TABLE I

Ia		4b		6b		7b	
Li	95	C	2 5	O	3 5	F	3 9
Na	9	Si	1 9	S	2 6	Cl	3 0
K	.80	Ge	1 8	Se	2 4	Br	2 8
Rb	78	Sn	1 7	Te	2 1	I	2 5
Cs	75	Pb	1 6				

The applicability of equation (4) has been illustrated for 1a–1a, 6b–6b and 7b–7b groups in figures 1, 2 and 3 respectively The values of the constants

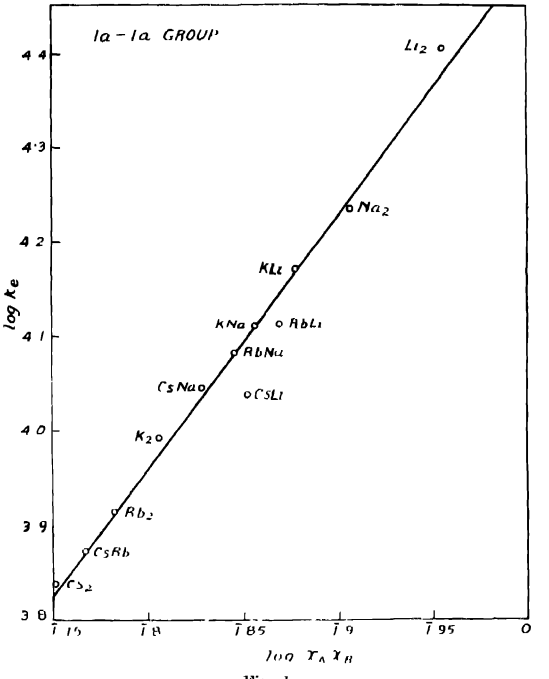

Fig. 1.

y and h are recorded in Table II. Numerical results have been tabulated in Table III. All force constants are in Des. (10^5 dynes/cm.). Uncertain values are in parentheses.

The applicability of relation (4) for such molecules in which the two atoms belong to two different groups was examined but the results are not very encouraging Figure 4 shows log k_e against log $x_A x_B$ for 4b–6b group. Force constant data were taken from Varshni and Majumdar (1955).

TABLE II

Group	y	h
1a—1a	2 684	4 498
6b—6b	1 59	4 357
7b—7b	1 55	4 004

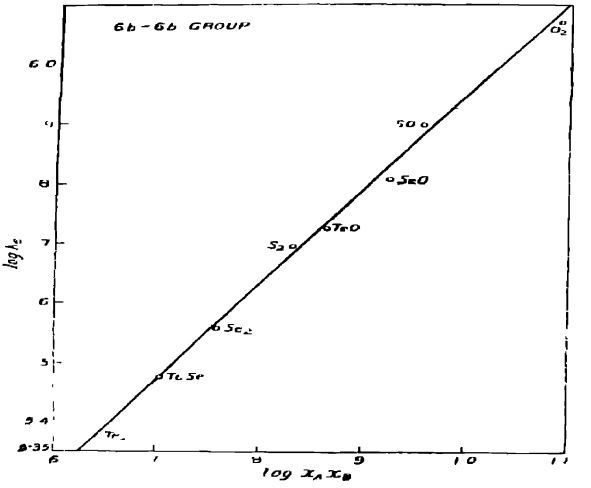
6b-6b GROUP
log k_e
log $x_A x_B$
O_2
SO
SeO
TeO
S_2
Se_2
TeSe
Te

Fig. 2

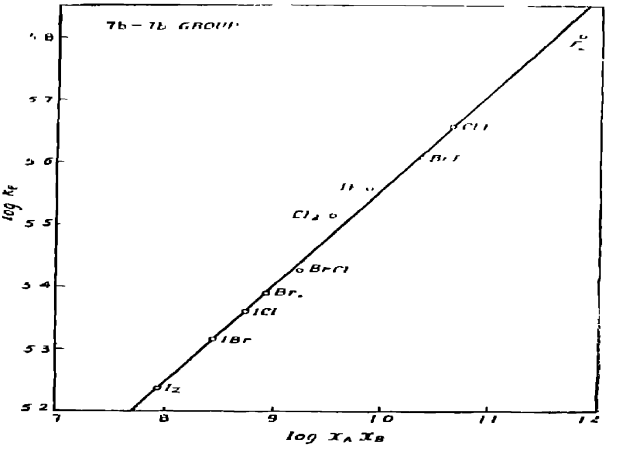
7b-7b GROUP
log k_e
log $x_A x_B$
Cl_2
BrCl
Br_2
ICl
IBr
I_2

Fig. 3

TABLE III

Group	Diatom	k_e obs.	k_e calc.	% error
1a—1a	LiLi	2552	2389	− 6 39
	NaNa	1717	1803	+ 5 00
	KK	0985	0950	3.55
	RbRb	.08205	0829	+ 1.03
	CsCs	06902	0672	− 2 64
	KLi	(.1487)	1507	+ 1 34
	RbLi	(1294)	1408	+ 8 81
	CsLi	(.1094)	1267	+ 15.81
	KNa	1296	1303	+ 54
	RbNa	.1213	.1218	+ 41
	CsNa	(.1109)	1096	+ 1 17
	CsRb	.0748	.0747	− 13
6b—6b	OO	11.76	12 22	+ 3 91
	SS	4.959	4 75	− 4 21
	SeSe	3 613	3 682	+ 1 91
	TeTe	2 368	2.401	+ 1 41
	SO	7 93	7 62	− 3.91
	SeO	6 446	6 707	+ 4 05
	TeO	5.304	5 425	+ 2.28
	TeSe	3 002 S_1	2 977	83
7b—7b	FF	6.336 eV_1	6 869	(+ 8 41)
	ClCl	3 279	3 044	− 7 17
	BrBr	2 457	2 459	+ 08
	II	1.721	1 73	+ 52
	ClF	4.562	4 573	+ 24
	BrF	4 071	4.11	+ 95
	IF	3 621 D_1	3.446	− 4 83
	BrCl	(2 675)	2 736	+ 2 28
	ICl	2 296	2 295	04
	IBr	2 064	2 063	05
	See notes below Table V		Average	+ 2 95

Walsh (1951) noticing that the variation of force constants of diatomic hydrides is very similar to Pauling's electronegativities, has suggested that the force constant of a diatomic hydride AH may be considered to be a measure of the electronegativity of the corresponding atom A. This suggests the possibility of a connection between $k_e(AA)$ and $k_e(AH)$. It was found that in this case $k_e(AA)$ is linear with $k_e(AH)$. Thus

$$k_e(AH) = p\ k_e(AA) + q \tag{5}$$

Figures 5 and 6 depict the relation graphically The numerical values of p and q for different groups are given in Table IV. Observed and calculated values of $k_e(AH)$ have been compared in Table V.

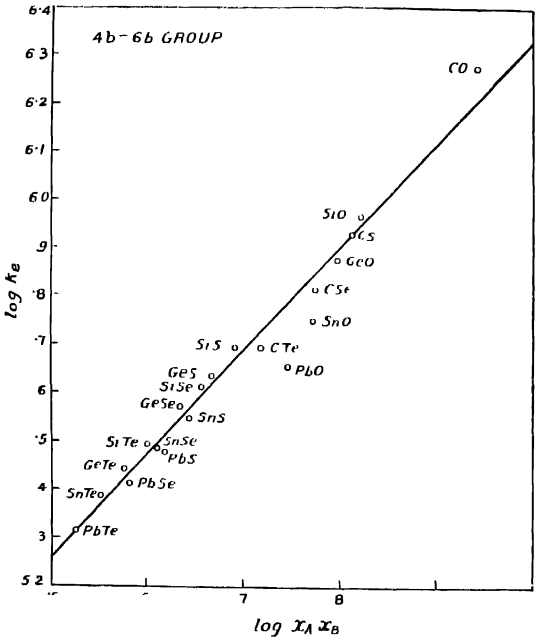

Fig. 4.

TABLE IV

Group	p	
1a–H	2.952	.273
6b–H	.5602	1.206
7b–H	1.405	.665

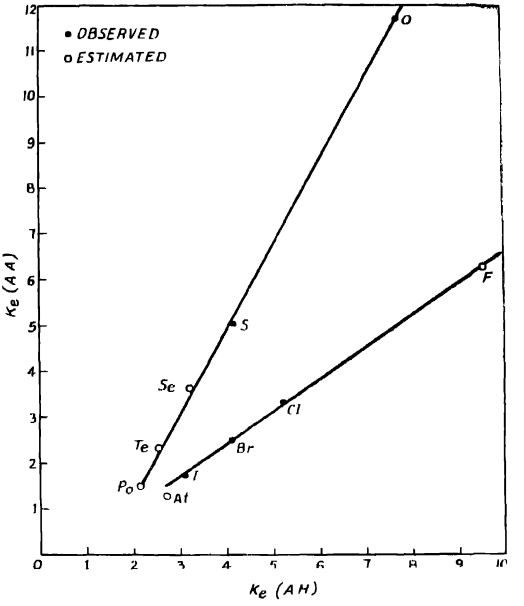

Fig. 5

TABLE V

Group	Diatom AA	$k_e(AA)$ obs	Diatom AH	$k_e(AH)$ obs.	$k_e(AH)$ calc.
Ia	LiLi	2552	LiH	1.026	1 026
	NaNa	1717	NaH	781	.780
	KK	.0985	KH	5614	564
	RbRb	0820	RbH	5148	5150
	CsCs	.0690	CsH	467	477
	FrFr	0595 eC$_1$	FrH		.449
6b	OO	11 76	OH	7 792	7.794
	SS	4 959	SH	4 193 L$_2$	3 984
	SeSe	3 613	SeH	3 18 eS$_3$	3 23
	TeTe	2.368	TeH	2 53 eS$_3$	2 533
	PoPo	1.51 eC$_1$	PoH	2 1 eS$_3$	2.052
7b	FF	6 336 eV$_1$	FH	9 655	9.567
	ClCl	3.279	ClH	5 157	5.272
	BrBr	2 457	BrH	4.117	4 117
	II	1 721	IH	3 142	3 083
	AtAt	1.213 eC$_1$	AtH	2.7 eS$_3$	2.37

Notes on Tables III and V. Except for the follow ng, other data have been taken from Herzberg (1951)

e—estimated value, C$_1$—Clark (1937), D$_1$—Durie (1951), L$_2$—Leach (1954), S$_3$—Sheline (1950). Force Constant of AtH has been freshly estimated, S$_4$—Sharma, private communication, V$_3$—Majumdar and Varshni (1954).

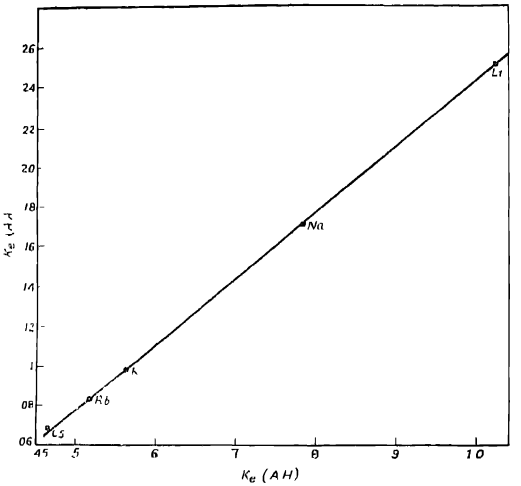

Fig. 6.

DISCUSSION

First relation .

Equation (4) (Figures 1 to 3 , Table III) . Making due allowance for the uncertainties in the electronegativity values, the relationship is well followed However, in case of CsLi the calculated value is much higher than the observed value. It may be pointed out that the observed value is uncertain and that other methods also predict a higher value of ω_e for this diatom (Varshni, 1955). It is not unlikely that further investigations on this molecule may lead to a higher observed value In figure 3, for FF, the estimated value of k_e (Majumdar and Varshni 1954) which is higher than the reported value has been plotted The position of FF in the figure supports the estimated value

Second relation

Equation (5) (Figures 5 and 6 , Table V) The linearity is well obeyed.

Line for 7b group further supports the estimated value of k_e (FF) (Majumdar and Varshni 1954)

ACKNOWLEDGMENT

The author is thankful to the U P Scientific Research Committee for a research grant.

REFERENCES

Clark, C. H D., 1937, *Trans Faraday Soc.*, **33**, 1398.
Cottrell, T. L. and Sutton, L E., 1947, *Quart. Revs.*, **2**, 260.
Durie, R. A., 1951, *Proc. Roy Soc.*, *A* **207**, 388
Fajans, K , 1928, *Z. Elektrochem.*, **34**, 507.
Gordy, W., 1946a, *Phys. Rev.*, **69**. 130
Gordy, W , 1946b, *Jour. Chem. Phys.*, **14**, 305
Gordy, W. and Thomas, W J. O., 1956, *Jour. Chem Phys.*, **24**, 439.
Herzberg, G., 1951, Spectra of Diatomic Molecules (D Van Nostrand Inc , New York)
Leach, S., 1954, *Jour. Chem Phys.*, **22**, 1261
Majumdar, K and Varshni, Y P., 1954, *Ind. J. Phys.*, **28**, 209.
Pauling, L., 1932, *J Amer. Chem. Soc.*, **54**, 3570
Pauling, L., 1944, The Nature of the Chemical Bond (Cornell University Press, Ithaca, N.Y.)
Pritchard, H. O. and Skinner, H. A., 1955, *Chem. Revs.* **55**, 745.
Shelne, R. K., 1950, *Jour. Chem. Phys.*, **18**, 927.
Varshni, Y. P., 1955, *Z. Phys. Chem.*, **204**, 188.
Varshni, Y. P. and Majumdar, K., 1955, *Ind. J. Phys.*, **29**, 38.
Walsh, A. D., 1951, *Proc. Roy. Soc.*, *A* **207**, 13.
Williams, R L., 1956, *Jour Phys Chem.*, **60**, 1016.

2

AN X-RAY STUDY OF SOME LEATHERS

D M. CHACKRABURTTY AND B CHAKRAVARTI

DEPARTMENT OF GENERAL PHYSICS AND X-RAYS
INDIAN ASSOCIATION FOR THE CULTIVATION OF SCIENCE, JAVADPUR,
CALCUTTA

(*Received, May* 15, 1957)

Plate I

ABSTRACT The spacings of the diffuse intense band of some leather samples were measured. It was observed that the spacings were varying from sample to sample. The variations are explained on the basis of Pauling's model of collagen-gelatin structure.

INTRODUCTION

The outstanding works on leathers and skins which are classified under collagen-gelatin protein group were mainly confined to the measurement of meridional and equatorial reflections and the interpretation of such reflections It was pointed out by Bear (1944) that the principal meridional arc was varying from 2 82 Å to 2 90Å, and the principal equatorial reflection between 10.4 Å to 15.5 Å The variation of the equatorial reflection was accounted for but the variation of spacings of meridional reflection has never been seriously looked into. Pauling (1951), however, proposed a model of the polypeptide chains in collagen-gellatin protein with special reference to dried tendon for which he accepted the value of the principal equatorial reflection as 10.4Å and the meridional reflection as 2 86Å and set up a satisfactory structure by assuming alternation of two cis groups and a trans group in polypeptide chain and three such polypeptide chains coiled into helix, the binding between the chains being achieved by intramolecular hydrogen bonds. The coiling of the chains were achieved at the α-carbon atom. The important features of such structure are (1) the dihedral angle at these carbon atoms is 97°, (2) the helix formed by a single chain of collagen molecule has nearly a 9-fold screw axis of symmetry and (3) the value for C–N–C in polypeptide chain is 123° A set of co-ordinates were derived for different atoms on the above considerations and the derivation of the form factor F led to the calculated intensity and spacings of certain bands The important diffuse intense band of some considerable intensity was calculated to be 4 72Å.

EXPERIMENTAL OBSERVATION

The verification of the structure requires an accurate measurement of the band spacing particularly that of the calculated intense band at 4.72Å. For dried tendon only the observed spacing of such band was reported as 4.4 Å by

Indian Journal of Physics, Vol XXXII, No. 1.

Fig

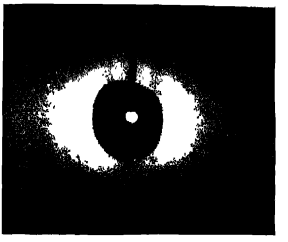

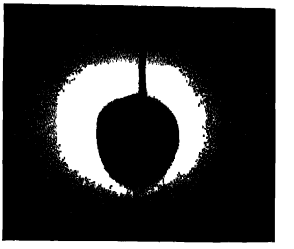

Fig 2

Fig 3

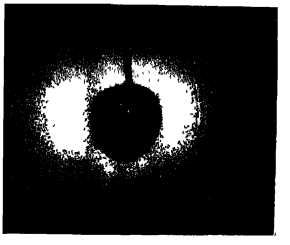

Fig 4

Fig 5

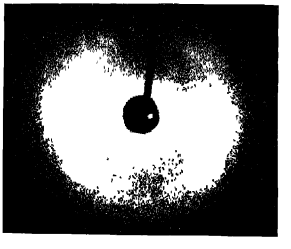

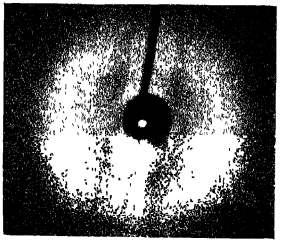

Fig. 6

Fig. 7

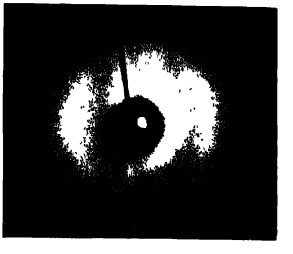

X-ray photographs of leather samples

Astbury (1940) and 4.37Å by Pauling and Corey (1951). In the present investigation we have concentrated our attention on the measurement of the diffuse band in different samples of leather with the idea of correlating the observed and calculated spacings. Each leather or skin specimen was cut into thin strip and mounted on a frame. This frame was in turn mounted on a goniometer head of X-ray camera and pictures were taken in CuKα and Co$K\alpha$ radiations which showed bands and in several cases faint lines of chemicals like NaCl used during tanning. Using the observed 200 reflection of NaCl as the internal standard in some cases, the spacing of the diffuse band was calculated and some of the results were verified by taking photometric records. For accurate measurement some of the pictures were taken in cobalt radiation instead of copper radiation. The results are tabulated in Table I and the pictures are shown separately in Plate I.

TABLE I

Samples	Camera radius	Radiation used	Spacing of the diffuse intense band
Sample I	3 cms.	Copper	4.32 Å
Sample II	3 cms.	Copper	4.47 Å
Sample III	3 cms.	Copper	4.33 Å
Sample IV	4.13 cms	Copper	4.49 Å
Sample V	4.55 cms	Copper	4.32 Å
Sample VI	4.55 cms	Cobalt	4.44 Å
Sample VII	4.13 cms	Cobalt	4.74 Å

DISCUSSION OF THE RESULT

It is difficult to find out a systematic correlation between the observed values and calculated value 4.72Å. In samples II, IV, VI and VII the observed results are nearer to the calculated value, but in others the observed values are too low. To account for the low values we have assumed certain distortions and deviations in the structure already proposed. Although we are unable to establish our views from the pictures obtained by us, we predict that it is possible to obtain the calculated band spacing lower than 4.72 Å for a particular value of meridianal reflection ranging between 2.82 Å—2.90 Å, but other than the value of 2.86 Å, bearing, of course, in mind the variations of meridianal reflection reported by Bear (1944). Proportionally the C–N–C angle must be changed slightly to account for (1) the helix formed by a single individual chain of collagen molecule to retain a 9-fold screw axis and (2) the intramolecular bonds binding the three

polypeptide chains The other structural features will remain similar to that proposed in Pauling's structure.

ACKNOWLEDGMENTS

The authors express their gratitude to Prof. B. N. Srivastava for help, encouragement and guidance throughout the progress of the work.

REFERENCES

Astbury, W T., 1940. *Jour Inst Soc. Leather Traders Chem*, **24**, 69.
Bear R. S, 1944, *Jour. Am. Chem. Soc.*, **66**, 1297
Pauling L. and Corey R. B., 1951, *Proc. Acad of Sci, Washington*. **37**, 272.

3

X-RAY ANALYSIS OF FROZEN PYRIDINE AND ITS SOLUTION AT −180°C

S. G. BISWAS

OPTICS DEPARTMENT, INDIAN ASSOCIATION FOR THE CULTIVATION OF SCIENCE, JADAVPUR, CALCUTTA.

(*Received for publication, September 2, 1957*)

Plate II

ABSTRACT. Debye-Scherrer patterns of pure pyridine and its solution in the frozen state at −180°C have been studied and two different patterns due to crystals of pyridine have been observed. Analysis of the patterns show that the first modification belongs to the space group Q^1_h with $a=12.16$ A.U., $b=9.14$ A.U., $c=8.18$ A.U. and the second modification belongs to the space group Q^2_h with cell dimensions $a=11.00$ A.U., $b=9.27$ A.U., $c=9.02$ A.U. The density of the crystals has also been measured and the number of molecules in the unit cell is found to be 8 in both the cases.

It is pointed out that pyridine molecule is asymmetric in both the modifications and that the formation of weak bonds among the molecules in the solid state may be the cause of such asymmetry. The frozen mixture is found to be amorphous. These results are compared with those of the investigations on the Raman spectra of crystals of pyridine and of frozen mixtures of pyridine by previous workers and it is concluded that complex groups of molecules produced new Raman band in the frozen mixtures.

INTRODUCTION

The Debye-Scherrer patterns of toluene and its mixtures with alcohol in the solid state at −180°C were studied recently by Biswas and Sirkar (1957) and it was observed that frozen toluene belongs to the space group C_{2v}^7, and that certain frozen mixtures of toluene and alcohol which appear to form glass are amorphous. These results, combined with those of the investigations on the Raman spectra of these substances (Kastha, 1956a), throw some light of the nature of intermolecular forces present in these solid masses at −180°C.

It was further observed by Kastha (1956) that solid pyridine at −180°C produces new Raman lines in the low frequency region and that frozen mixtures of pyridine with alcohol produce a new Raman band instead of a few new lines given by pure pyridine in the solid state. It was not known, however, whether the mixtures of pyridine with alcohol in the solid state are crystalline and the crystal structure of pyridine was also not known. The present investigation was undertaken to study the Debye-Scherrer patterns of frozen pyridine and of its solutions in alcohol at −180°C in order to correlate the results with those observed in the investigations on the Raman spectra of these substances. It was also

intended to find the space group of the crystals of pure pyridine and to determine the symmetry of the molecule in the crystal.

EXPERIMENTAL

Pyridine used in the investigation was of chemically pure quality. Debye-Scherrer patterns of pyridine and of 50% solution of pyridine in dehydrated ethyl alcohol in the frozen state at - 180°C were photographed using a low-temperature camera of special design The liquid was sealed in thin-walled glass tube which was fixed vertically along the axis of a cylindrical camera and was rotated slowly during the exposure by an electric motor and a gear system A narrow stream of liquid oxygen was falling continuously through a funnel on the tube containing the liquid from a Dewar vessel of special design fitted on the lid of the cylindrical camera which was evacuated continuously with a pump With this arrangement well-defined Debye-Scherrer rings were produced by frozen pyridine, but a halo due to liquid oxygen was superposed on the pattern. The radius of the camera was measured by photographing the Debye-Scherrer pattern due to rock salt

A Seifert X-ray tube running at 32 KV and 26 mA was used to photograph the Debye-Scherrer patterns The X-ray tube was provided with a copper target and a nickel filter was used to cut off the Kβ radiation An exposure of $2\frac{1}{2}$ hours was sufficient to record each pattern with moderate intensity. Several photographs were taken in each case to confirm the genuineness of the results It was observed, however, that in some of these photographs the pattern was similar to that due to a fibre, while in the other photographs uniform rings were obtained So both these patterns were recorded carefully to find out whether they indicated different structures

RESULTS AND DISCUSSION

The two types of pattern due to frozen pyridine at 180°C are reproduced in figures 1 and 2, Plate II. The values of $\sin^2\theta$, calculated from these Debye-Scherrer photographs of frozen pyridine at $-180°$C, are given in Tables I and II respectively These values indicate that the structure is not the same in the two cases. By applying Lipson's method (Lipson, 1949) to the values of $\sin^2\theta$ the crystal system was found to be ortho-rhombic in both the cases The values of $\lambda^2/4a^2$, $\lambda^2/4b^2$, and $\lambda^2/4c^2$ deduced from the values of $\sin^2\theta$ by Lipsons' method are given below :

(a) *Modification I* (figure 1) $\lambda^2/4a^2 = .00401$, $\lambda^2/4b^2 = .00710$

$$\lambda^2/4c^2 = .00825.$$

From these we get

$$a = 12.16 \text{ A.U}, \; b = 9.14 \text{ A.U} \quad c = 8.48 \text{ A.U}.$$

To calculate the number of molecules per unit cell, the density of pyridine at −180°C was required, but it was not found in the existing literature. So the density of frozen pyridine at −180°C was measured in the same way as in the case of toluene (Biswas and Sirkar, 1957) and it was found to be 1.134. The number of molecules per unit cell calculated with this value of the density is approximately 8.

The values of $\sin^2\theta$, calculated with those of $\lambda^2/4a^2$, $\lambda^2/4b^2$ and $\lambda^2/4c^2$ mentioned above, the spacings and indices of the corresponding planes are, also included

TABLE I

$\sin^2\theta$ (observed)	$\sin^2\theta$ (calculated)	Difference	Spacings in A.U.	Indices and Intensities
.01650	.01604	.00046	5.99	200 (m)
.02826	.02840	.00014	4.58	020 (m)
.03287	.03300	.00013	4.25	002 (vs)
.03735	.03701	.00034	3.98	102 (w)
.04264	.04319	.00055	3.73	310 (vw)
.04857	.04904	.00047	3.49	202 (s)
.05319	.05269	.00050	3.34	221 (s)
.07089	.07126	.00037	2.89	410 (s)
.07939	.07951	.00012	2.73	411 (s)
.09670	.09716 .09690	.00046 .00020	2.47	402 (vw)* 032
.11330	.11360	.00030	2.29	040 (w)
.13220	.13200	.00020	2.12	004 (w)
.14940	.14969	.00029	1.99	340 (m)
.16230	.16264	.00034	1.91	242 (vw)
.17680	.17644	.00036	1.83	224 (w)
.19630	.19616	.00014	1.74	404 (vw)

*br

TABLE II

$\sin^2\theta$ (observed)	$\sin^2\theta$ (calculated)	Difference	Spacings in A.U	Indices and Intensities
.02785	02760	00025	4 61	020 (s)
02966	02920	00046	4 47	002 (vs)
03384	03380	00004	4 19	211 (s)
.04100	.04120	00020	3.80	112 (vw)
04857	04880	00023	3 49	202 (s)
.05423	05450	00027	3 31	221 (m)
06947	06940	00007	2 92	031 (s)
07877	07840	00037	2 74	400 (s)
09656	09620	.00036	2 48	132 (m)
11070	11040	.00030	2 32	040 (m)
.13000	.13000	00000	2.13	240 (w)
13610	13640	00030	2 09	204 (vw)
14420	14440	.00020	2 03	024 (m)
14940	14930	.00010	1 99	124 (m)
15110	15100	.00010	1 98	413 (w)
15930	.15920	.00010	1 93	342 (w)
16810	16780	.00030	1 88	314 (vw)
17640	17640	.00000	1 83	600 (m)
19400	19430	.00030	1 75	115 (m)

in Table I. The intensities are indicated roughly by the letters "s, m, w" etc in parentheses It can be seen from Table I that there is no restriction for the occurrence of reflection from the planes. The ring due to (400) is masked by the liquid oxygen halo The want of restriction leads to the conclusion that the space group C_h^1 and as the number of molecules in the unit cell is eight, the molecule has no symmetry in the frozen state at - 180°C. So, there is neither a plane of symmetry nor a two-fold axis of symmetry in the molecule in this modification of the crystal This indicates that probably there is unusual bond-formation among the molecules in the solid state. This also supports the view put forward by Kastha (1956) that groups of pyridine molecules formed in the solid state produce new Raman lines in the low-frequency region.

Fig. 1

Fig 2

Fig 3

Fig. 4

Fig

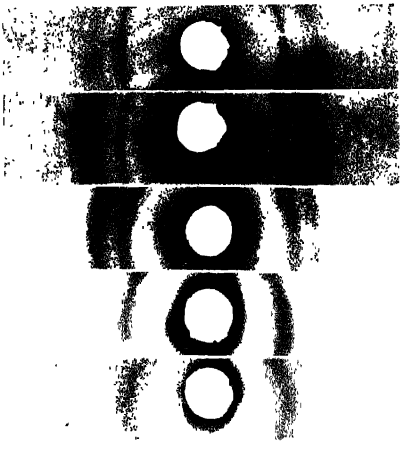

X-ray photographs

Fig. 1 Pyridine (modification I) at −180°C
Fig 2 ,, (modification II) ,, ,,
Fig. 3 50% mixture at −180°C
Fig 4 50% ,, at 30°C
Fig 5 Pure pyridine at 30°C

(b) *Modification II.*

In this case the values of $\lambda^2/4a^2$, $\lambda^2/4b^2$ and $\lambda^2/4c^2$, which explain the observed values of $\sin^2\theta$ given in Table II satisfactorily, are .0049, .00690 and .00735 respectively. These give the following cell dimensions·

$$a = 11.00 \text{ A.U.}, \quad b = 9.27 \text{ A.U}, \quad c = 9.02 \text{ A.U.}$$

If the density is taken as 1.134 in this case also the number of molecules per unit cell comes out as 7.94. This shows that the number of molecules per unit cell is 8 in both the modifications and the differences between this value and those calculated in the two cases may be due to some uncertainty in the value of the density.

Table II shows that planes (221), (124) and (115) produce Debye-Scherrer rings in this case. These rings could not be assigned alternative indices. So there seems to be no restriction in this case also except that (okl) is halved if $(k+l)$ is odd, (hol) is halved if $(h+l)$ is odd and (hko) is halved if $(h+k)$ is odd. These restrictions and the number of molecules per unit cell indicate that the space group is Q_h^2 and the molecules are all asymmetric in this case also. It appears that rotation through a small angle of the molecules about the b-axis is responsbile for producing the second modification.

II. *Structure of frozen solutions of pyridine.*

The patterns due to a 50% solution of pyridine in ethyl alcohol both in the solid state at −180°C and at the room temperature and that due to pure pyridine in the liquid state are reproduced in figures 3, 4 and 5 (Plate II) respectively. Pure pyridine in the liquid state produces a broad halo giving a mean spacing of 4.65 A.U. The mixture in the liquid state produces a similar halo corresponding to a spacing of 4.43 A.U The frozen solution shows a single halo inside another halo due to liquid oxygen and the spacing is 4.17 A.U.

It was reported earlier (Biswas and Sirkar, 1957) that frozen ethyl alcohol produces ring corresponding to a spacing of 3 78 A.U. Hence the spacing observed in the case of mixture of pyridine in ethyl alcohol is just the mean of the spacings due to two pure liquids. This shows that the mixture is a homogeneous one. Further, the spacings observed in the frozen mixture of pyridine in ehtyl alcohol is much larger than that in the frozen in cybotactic groups in solid ethyl alcohol This shows that in this mixture there are certain frozen-in cybotactic groups formed by interpenetrating pyridine and ethyl alcohol molecules. Evidently the new Raman band at 95 cm^{-1} observed by Kastha (1956) in the Raman spectrum of such a frozen mixture is produced by frozen-in groups of molecules in which both pyridine and alcohol molecules are present. Since the whole structure is amorphous, the intermolecular vibration, which gives rise to this band, must be confined to very small groups of molecules, each group containing both types of mole-

cules. The value of the frequency-shift indicates that the weak bond which holds the two types of molecules together in these smaller groups must be many times stronger than the Van der Waals forces expected to be present in the lattice. Hence, all these results indicate that formation of some weak bonds between pyridine and ethyl alcohol molecules takes place in the frozen mixture and very small groups oriented in the same way in small portion throughout the volume form frozen-in cybotactic groups in the amorphous mass

ACKNOWLEDGEMENT

The work has been carried out under a scheme financed by the Council of Scientific and Industrial Research and the author is indebted to the Council for the financial help The author is also indebted to Professor S C. Sirkar, D.Sc., F.N.I., for his kind interest and guidance during the progress of the work

REFERENCESS

Biswas, S G. and Sirkar, S C., 1957, *Ind. J Phys.*, **31**.
Kastha, G S., 1956a, *Ind. J Phys.*, **30**, 313.
" " 1956b, *Ind J. Phys.*, **30**, 519
Lipson, H., 1949, *Acta Cryst.*, **2**, 43.

4

A STUDY ON THE COSMIC RAY NUCLEAR INTERACTIONS IN LEAD AT 9000 ft.

R. N. MATHUR AND P. S. GILL

GULMARG RESEARCH OBSERVATORY, GULMARG (KASHMIR)

(*Received July* 15, 1957)

ABSTRACT Nuclear disintegration rates in lead plates of different thicknesses have been studied under no absorber and under 280 gms./cm^2 of lead absorbers The transition phenomena is exhibited by both the unfiltered and filtered N-radiation. A comparative study, however, reveals a change in the characteristics of the N-radiation when filtered through the absorber. Unfiltered N-radiation shows a broad maximum around 25 gms./cm^2 of Pb. For filtered N-radiation, however, there appears to be an upward shift in the position of the maximum The interaction mean free path of the unfiltered N-radiation is obtained equal to 200 gms./cm^2 of lead. Filtered N-radiation, however, seems to have an interaction mean free path greater than 250 gms./cm^2 of lead. The absorption mean free path of the N-radiation is obtained as 340 gms./cm^2 of lead.

INTRODUCTION

A weak transition effect in lead of the star-producing radiation has been described by various workers Using neutron counter pile detecting systems Simpson (1953) and Treiman and Fonger (1952) have reported a similar effect. Though the transition maxima for the star-producing and the neutron-producing radiations have been obtained for almost the same thicknesses of lead plates, the magnitude of the effect for the stars has been observed to be considerably smaller than that for the neutrons The interpretation of the phenomena becomes difficult due to the fact that the reported thicknesses of lead plates, which intervene in the said effect, are in the range 10-20 gms./cm^2 and are, therefore, smaller by an order of magnitude from the characteristic interaction length of the N-radiation. The present investigation was undertaken to find out whether the N-radiation undergoes any change in its characteristics when filtered through large absorber. The present experiment was carried out to measure the neutron production rates by the N-radiation unfiltered and filtered through 280 gms./cm^2 of lead as a function of thickness of the producer plates.

EXPERIMENTAL ARRANGEMENT

The experimental set up for the study of N-radiation with and without filter has been sketched in figure 1 (a) &(b) The neutron detecting pile consisted of a pair of BF_3 proportional counters embedded in a block of paraffin of dimen-

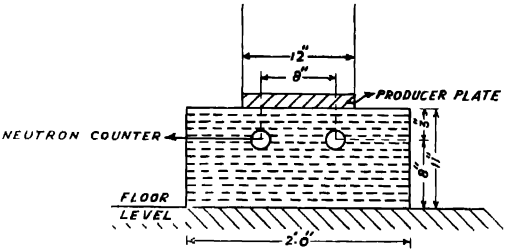

Fig. 1(a)

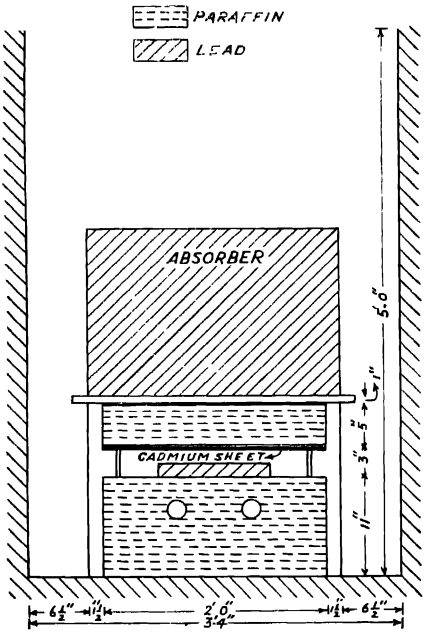

Fig. 1(b).

sions 24″×22″×11″. For the filtered N-radiation the pile was transferrod inside a pit so as to reduce the background.

Boron trifluoride counters used in these investigations had the following specifications (Mathurh, 1956)

overall length	24″
outer diameter	1.75″
anode wire diameter	0.003″
gas filling	BF_3(natural boron) at 45 cms. of Hg+argon at 5 cms of Hg. pressure.

The two counters were connected in parallel and then coupled to a cathode-follower which, in turn, was coupled to a Jordan-Bell type of a wide-band amplifier (Model 204 C of the Atomics Instruments Co Ltd.).The discriminator output of the amplifier was fed to a fast scaling unit (Model 162 of Nuclear Instruments and Chemicals Corporation Ltd.) the output from which was used to drive a mechanical register. Check on the consistent operation of the pile was carried out by frequently drawing the plateau and bias curves as also measuring the rates with and without cadmium thimble over the counters.

OBSERVATIONS

Counting rates were obtained for different thicknesses of the producer plates over the detecting pile, first in the increasing order followed by a decreasing one. The observations were repeated several times such that the periodic variations of cosmic rays were smoothed out The difference in counting rates with the producer plate in position and without it had been taken to be proportional to the nuclear disintegrations in the producer plates.

The correction terms due to (1) the change in geometry of the detecting unit with respect to the producer plates– displacement factor (2) scattering of the neutrons produced in the upper layers of the producer plates by its lower layers-scattering factor, were obtained from Simpson's (1953) displacement curve and Geiger's (1956) results respectively.

ANALYSIS OF THE DATA

The corrected production rates have been plotted as a function of thickness of the producer plates for both unifiltered and filtered N-radiation on a semi-logarithmic graph in figure 2. The data are shown in curves I and II of figure 2. The initial parts of these curves may be represented by an equation of the form

$$N_x = A + B\{1 - \exp(-x/L)\}$$

where N_x is the production rate for the plate of thickness x, $A = N$ for $x = 0$; B would then be a constant to be given by the product of the intensity of N-radiation and the efficiency of the detecting system, including the geometry of the plates

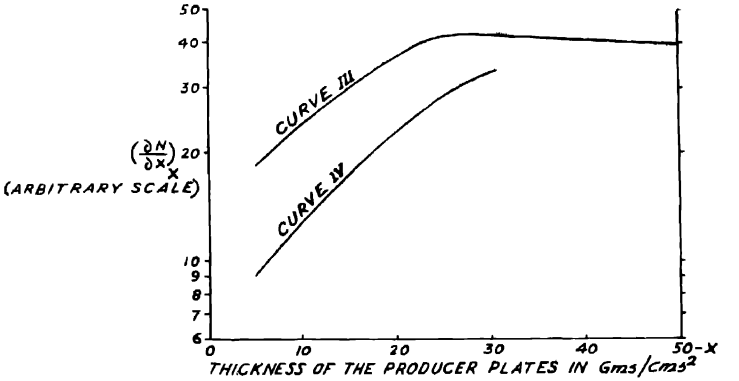
50
40
30
$\left(\frac{\partial N}{\partial x}\right)_x$ 20
(ARBITRARY SCALE)
10
9
8
7
6
CURVE III
CURVE IV
0
10
20
30
40
50-X
THICKNESS OF THE PRODUCER PLATES IN Gms/Cms²

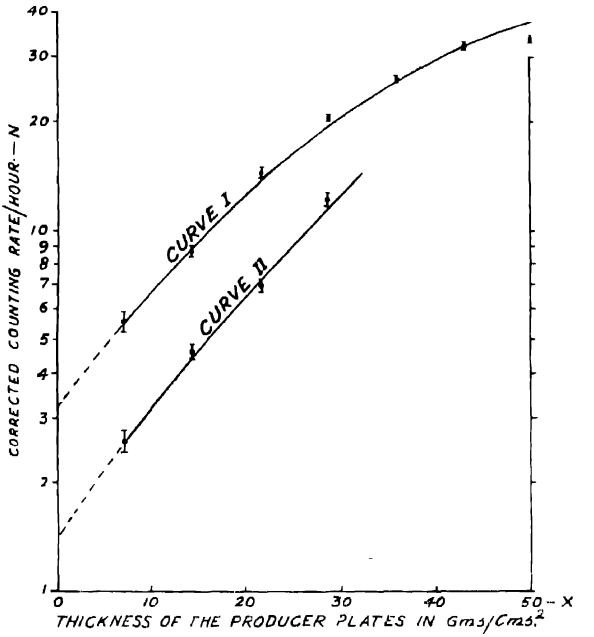
40
30
20
10
9
8
7
6
5
4
3
2
1
CORRECTED COUNTING RATE/HOUR — N
CURVE I
CURVE II
0
10
20
30
40
50 - X
THICKNESS OF THE PRODUCER PLATES IN Gms/Cms.²

Fig. 2.

with respect to the detecting unit, L is the interaction mean free path of N-radiation in lead. Using chi-square test, the best values of B and L were obtained for a good fit of the calculated values with curve I in its initial part. L is thus obtained equal to 200 gms./cm² of lead. For comparison, the values of the interaction mean free path of N-radiation obtained by other workers has been given in Table I. A similar method applied to curve II leads to a value of L greater than 250 gms./cm² of lead.

TABLE I

Cosmic ray phenomena	Int m f p of the N-radiation	
Penetrating showers	160 ± 15 gms./cm² of Pb	Cocconi, G. (1949 a, b)
	196 ± 13 gms./cm² of Pb	Sitte, K. (1950)
π-mesons	82 ± 35 gms./cm² emulsion	Cammi *et al.* (1950)
Stars	102 ± 27 gms./cm² emulsion	
N radiation		
(*i*) unfiltered	200 gms./cm² of Pb	Present work
(*ii*) filtered through 280 gms./cm² of	greater than 250 gms./cm²	Present work

From curves I and II, their differential curves III and IV were obtained. Evidently, neutron production per unit thickness of the producer plates is very much dependent upon the amount of lead the N-radiation has immediately passed through. Curve III shows a transition effect with a broad maximum around 25 gms./cm² of lead. The curve IV, however continues to show a rising trend up to 30 gms./cm². This curve has a slope greater than that of the previous one.

Transition curve III above 25 gms./cm² can be used for an estimation of the absorption mean free path of N-radiation. This estimation leads to a value of the absorption mean free path equal to 330 ± 30 gms./cm² of lead. The absorption mean free path of N-radiation can also be obtained by comparing neutron production rates by the filtered and the unfiltered N-radiation. Using the equation

$$\frac{I_1}{I_2} = \exp(x_2 - x_1) = \frac{N_1}{N_2}$$

the initial parts of the curves III and IV yield a value of absorption mean free path equal to 340 gms./cm². of lead.

DISCUSSION

A few interesting points follow immediately from the above analysis. Curves III and IV establish the existence of the transition effect for the unfiltered as also for the filtered N-radiation. The transition curve III has a broad maximum

at $\sim$ 25 gms./cm^2 as compared to 15 gms./cm^2 obtained by Simpson (loc. cit) and also by Treiman and Fonger (loc. cit).

In the present work the difference of the counting rates with and without producer plates in position has been taken to be proportional to nuclear disintegrations in the plates. This implicitly assumes that the background counting rate, represented by the rate obtained without the plate in position, is not disturbed when the plate of any thickness is placed over the detecting unit. The background counting rate consists of two parts only : (i) Cosmic ray fast neutrons; (ii) disintegration neutrons from the moderating medium. The effect of the plates on the former is a small reduction for the range of thicknesses of plates that intervene in the transition effect. The latter might change because of (a) absorption of N-radiation in producer plates, (b) back scattering of the disintegration neutrons produced in the moderator, so as to get detected by the counters; (c) a possible increase in the low-energy star production in paraffin because of the release of energetic secondaries from the nuclear disintegrations in the plates; (d) the interactions in the producer plates of the energetic back-directed secondaries of the nuclear disintegrations in paraffin. Contributions from processes (a) and (b) are known to be quite small for thicknesses of lead plates involved and being opposite in sign, they are likely to minimise the total effect due to them However, processes (c) and (d) might make a significant change in the background counting rate. Barton *et. al* (1951) have shown that it is the isotropic class of the secondaries which is important in accounting for any increase in the star frequencies under absorbers. These processes might also be able to account for an apparent production rate for no producer plates.

Transition curve IV for the filtered N-radiation shows comparatively a steeper rise than that obtained for the unfiltered one. This curve also exhibits a rising trend up to 30 gms./cm^2 of lead. Evidently the N-radiation under the absorber has slightly different characteristics than that with no absorber. This change in the behaviour of N-radiation, after passing through a large absorber, can come about because of either (i) a change in the average energy of the N-radiation, (ii) a change in the composition of the N-radiation, or (iii) both. The present data, however, make it difficult to discriminate between these possibilities.

A comparison of the production rates in producer plates of same thicknesses by the filtered and unfiltered N-radiation brings out another interesting point. This ratio varies from $\sim$ 1 6 to $\sim$ 2.2 for plate thicknesses from 30 gms./cm^2 to 5 gms./cm^2, whereas the ratios for thinner plates lead to values of abs. *m.f.p.* comparable to the ones obtained by other workers and approximately equal to the geometrical value, the ratios for thicker plates lead to progressively higher values. It is quite possible that the mode of production of most of the neutrons in thicker plates by the filtered N-radiation is somewhat different from that by

the unfiltered N-radiation. The probability for more than one interaction in the plates increases with thickness and as such for this reason alone the values of the ratio for thinner plates only need be taken into consideration for the calculation of abs. *m.f.p.*

ACKNOWLEDGEMENTS

One of the authors (R.N M.) acknowledges with thanks the receipt of financial aid from the Govt of India. Thanks are also due to Mr. Ajit Singh, glass-blower, for his expert handling of the counter construction.

REFERENCES

Barton, J. C., George, E. P and Jason, A C., 1951, *Proc. Phys. Soc. A.*, **64**, 175.
Camirim *et al.*, 1950, *Phil. Mag.* **41**, 413.
Cocconi, G., 1949a, *Phy. Rev.*, **75**, 1079.
,, ,, 1949b, *Phy. Rev.*, **76**, 984.
Geiger, K. W., 1956, *Canad. Jour. of Phy.*, **34**, 288.
Mathur, R. N., Ph.D, Thesis, Muslim University, Aligarh, 1956.
Sampson, J. A. 1953, *Phy. Rev.*, **90**, 44.
Sitte, K , 1950, *Phy. Rev.*, **78**, 714.
Treiman, S. B. and Fonger, W., 1952, *Phy. Rev.*, **85**, 364.

5

IMPROVED TRANSMISSION OF IONS WITH INHOMOGENEOUS MAGNETIC FIELDS

S B. KARMOHAPATRO

INSTITUTE OF NUCLEAR PHYSICS, CALCUTTA.

(*Received July* 10, 1957)

ABSTRACT. Design parameters for symmetrical and asymmetrical first order focussing conical shaped inhomogeneous magnetic analysers with field varying as r^{-n} where $0.5 < n < 1$ are considered for utilising their high resolving power with improvements in transmission of ions Some representative cases for such a 180°-magnetic analyser are shown with a discussion for using such magnets with different sector angles in mass spectroscopy, which will be more advantageous than the conventional flat type homogeneous magnetic analysers, when solid angle and resolving power of the instruments are simultaneously considered

Application of the inhomogeneous magnetic analysers, having field shape

$$H = H_0 \left(\frac{r_0}{r} \right)^n \qquad \ldots \quad (1)$$

derived by Kerst and Serber (1941), have been frequently used for betatron and synchrotrons and have now extended to the field of β-ray and mass spectrometry. Siegbahn and Svartholm (1946) have utilised this type of inhomogeneous magnets for two directional focussing of the β-particles at an angle $\sqrt{2}\pi$ with $n = 0.5$. Higher order focussing for improved resolution has been considered by Shull and Dennison (1947), Verster (1950), Stoker *et al.* (1954), Lee-Whiting and Taylor (1957), Judd and Bludman (1957) and others with two directional focussing magnetic analysers. Such first and second order focussing magnetic analysers are now used in β-ray spectrometry Svartholm (1951) proposed conical magnets for an average two directional focussing of the charged particles and a β-ray spectrometer by Arbman and Svartholm (1955) has been constructed on this suggestion

Two directional focussing of the charged particles with an inhomogeneous magnet having an angle $\sqrt{2}\pi$ has been considered by Judd (1950), Rosenblum (1950) and others. The possibility of using such an analyser with a shaped pole boundary was discussed by the author (Karmohapatro, 1955) in connection with the design of a mass spectrometer. Sternheimer (1952) has discussed the focussing of charged particles with such inhomogeneous magnets with proper consideration to the focussing effect caused by the fringing field of a sector magnet. In case of a magnetic analyser, in which the source and the detector are within the magnetic field, the focussing or defocussing effect due to fringing field does not arise. But for a sector magnet, even with a homogeneous flat field, axial focuss-

ing is possible in the inhomogeneous fringing field region as shown by Camac (1951) and Cross (1951).

Sternheimer (1952) derived a generalised expression determining the parameters of a first order focussing inhomogeneous magnetic analysers with proper consideration to the fringe-field focussing. Though the aim of this derivation was mainly for reducing the distance of source and detector from the pole boundary of a two directional fringe-field focussing magnetic analyser by introducing a slight inhomogeneity in the magnet with a field index $n = 0.5$, the scope of the work, being a generalised treatment, is extensive and is applicable to such inhomogeneous magnetic analysers with any field index $n \leqslant 1$.

If we consider the case of a symmetrical sector shaped inhomogeneous magnetic analyser having field index n, sector angle ϕ, and ϵ being the angle made by the central beam with the normal at the entrance and exit of the pole boundary, the radial focussing of the charged particles is possible at a distance

$$l = \frac{(1-n)^{\frac{1}{2}} \cot (1-n)^{\frac{1}{2}}\phi + \tan\epsilon + (1-n)^{\frac{1}{2}} \operatorname{cosec} (1-n)^{\frac{1}{2}}\phi}{(1-n) - \tan^2\epsilon - 2(1-n)^{\frac{1}{2}} \cot (1-n)^{\frac{1}{2}}\phi \tan\epsilon} \qquad (2)$$

where l is also the distance of the source in unit of the equilibrium orbit r_0, which is hereafter used in all cases indicating any length. This formula is directly derived from Sternheimer's expression (1952) This formula reduces to

$$l = \frac{\cot\phi + \tan\epsilon + \operatorname{cosec}\phi}{1 - \tan^2\epsilon - 2\cot\phi\tan\epsilon} \qquad \ldots \quad (3)$$

when $\qquad n = 0$

and $\qquad l = \cot\phi + \operatorname{cosec}\phi \qquad \ldots \quad (4)$

when $\qquad n = 0, \qquad \epsilon = 0.$

The above formulae are due to Herzog (1949) and applicable to homogeneous flat type magnetic analysers extensively used in mass spectroscopy.

For $\quad \epsilon = 0, \qquad n \neq 0$ exp. (3) reduces to

$$l = \frac{1}{(1-n)^{\frac{1}{2}}} \left[\cot (1-n)^{\frac{1}{2}}\phi + \operatorname{cosec} (1-n)^{\frac{1}{2}}\phi\right] \qquad \ldots \quad (5)$$

This is the case derived for an asymmetric inhomogeneous magnet with field index n as treated by Judd (1950) and Rosenblum (1950) in connection with the two directional focussing of charged particles with $n = 0.5$

The axial focussing of the charged particles also occurs at a distance

$$l' = \frac{n^{\frac{1}{2}} \cot n^{\frac{1}{2}}\phi - \tan\epsilon + n^{\frac{1}{2}} \operatorname{cosec} n^{\frac{1}{2}}\phi}{n - \tan^2\epsilon + 2n^{\frac{1}{2}} \cot n^{\frac{1}{2}}\phi \tan\epsilon} \qquad \ldots \quad (6)$$

for a symmetrical magnetic analyser. This expression reduces to

$$l' = \frac{2 - \phi \tan \epsilon}{2 \tan \epsilon - \phi \tan^2 \epsilon} \qquad \ldots \quad (7)$$

for $n = 0$ and it is equivalent to the expressions derived by Camac (1951) and Cross (1951) for focussing of charged particles with the fringing field of a homogeneous sector magnet.

It should be mentioned here that a positive real value of l' cannot be found out for the axial focussing alone with an inhomogeneous symmetrical magnetic analyser.

It is interesting to note that the dispersion of the charged particles with inhomogeneous magnetic analysers of field index n is $\frac{1}{1-n}$ times greater than the homogeneous ones This advantageous property has been utilised for achieving double dispersion along with higher transmission with a two directional focussing magnetic analyser having $n = 0.5$ as described by Siegbahn and Svartholm (1946).

It is evident that for $n = 0.8$ or $n = 0.9$, the dispersion will respectively be 5 or 10 times greater than the homogeneous magnetic fields The Russian authors Alseevesky and Prudkovsky (1955) have constructed mass spectrometers with field index $n = 0.8$ and 0.9. Dubroniv and Balabina (1955) have constructed one which has a resolving power of $\sim 10^5$ and can measure atomic masses to an accuracy of $\sim 10^{-6}$. Since velocity focussing electrostatic analysers are absent and electrometer detection can be used instead of photographic plates, the instrument becomes simpler

It should be mentioned that since $n > 0.5$, axial focussing is not attained. The resolving power R of a mass spectrometer is expressed as

$$R = \left(\frac{M}{\Delta M} \right)_{max} = \frac{D}{A}$$

where M is the average mass of the two masses and ΔM is their difference, D is the dispersion of the magnetic analyser and A is the width of the beam consisting of aberation due to the analysers, velocity dispersion of ions, etc

The solid angle of such an inhomogeneous magnetic analyser is

$$\frac{\Omega}{A} = \frac{1}{\left[l^4 + \frac{1 + l^2}{n(1-n)} \right]} \ \tfrac{1}{2} \text{ steradian} \qquad \ldots \quad (9)$$

where Ar_0^2 is maximum available cross-section area for the ion path.

We now consider expression (5) for radial focussing of ions with a magnetic analyser having $n > 0.5$ The graphs (figure 1) determining the values of l with

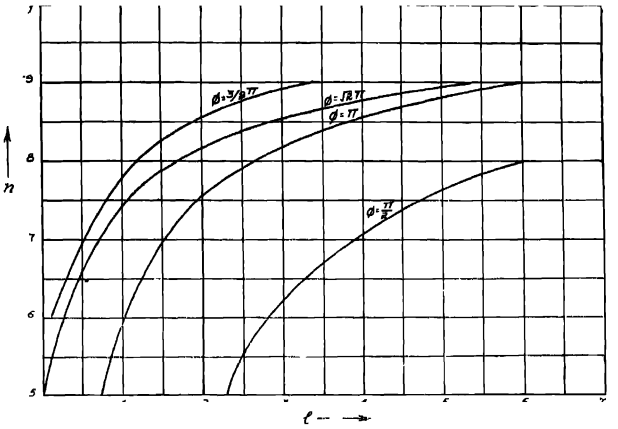

Fig. 1 Relations between the object distance and field index n for an inhomogeneous symmetrical magnetic analyser with different sector angles

different sector angle ϕ and $n = 0.8$ or 0.9 show that l increases with higher values of n For the same n-value l decreases for higher values of ϕ

The resolving power of such a magnetic analyser can on principle be increased without reducing intensity by reducing the aberration A, which consists of the terms as follows :

$$A = a + b + r_0\alpha^2 + \text{ velocity dispersion etc.} \tag{10}$$

where a and b are entrance and exit slit widths and $r_0\alpha^2$ is the second order aberration due to the magnetic analyser, α being the half divergence angle The term $r_0\alpha^2$ can be reduced to the third order by shaping the pole boundaries of sector homogeneous magnet as suggested by Kerwin (1949) and Hintenberger (1949). For a given resolving power, reduced aberration gives an advantage of increasing a and b for attaining a better transmission. For inhomogeneous symmetrical magnetic analysers having $n = 0.8$ or 0.9 such second order focussing with a straight pole boundary is also possible The condition for such a focussing with the ions, not incident normally to sector boundary, is expressed as

$$l = -\frac{1}{3\tan\epsilon} = \frac{2\cot(1-n)^{\frac{1}{2}}\phi/2}{3(1-n)^{\frac{1}{2}}} \tag{11}$$

$$\tan\epsilon = -\tfrac{1}{2}(1-n)^{\frac{1}{2}}\tan(1-n)^{\frac{1}{2}}\phi/2 \tag{12}$$

With this expression different parameters of an analyser for $n = 0.8$ and 0.9 have been calculated and given in Table I.

The table shows also a reduction in the value of l compared to figure 1 in which perpendicular incidence of ions is considered. Thus expressions (9) and (10) show that this type of magnet will give us a two-fold advantage for attaining higher transmission

This is to a certain extent off set by the low dispersion attained with these type of magnets in comparison to those with perpendicular incidence of ions.

Moreover, this method will not be very helpful in practice, since the axial defocussing effect due to the fringing field, may destroy the improved focussing effect. This difficulty is also encountered in case of the homogenous magnets However, Kerwin (1950) has constructed such a homogeneous sector magnet and attained proper second order focussing of ions. In case of the inhomogeneous magnets, there is also the possibility of utilizing the parameters of Table I to construct a suitable magnet for second order focussing of ions with high dispersion.

TABLE I

n	ϕ	ε	l
0 9	$3\pi/2$	8°17′	2 275
0 9	$\sqrt{2}\pi$	−7°38′	3 623
0 9	π	−4°53′	3 92
0 9	$\pi/2$	2°17′	8.426
0 8	$3\pi/2$	−21°25′	82
0 8	$\sqrt{2}\pi$	10°43′	1 753
0 8	π	-8°54′	1 163
0 8	$\pi/2$	-4°18′	4 026

Another way to improve transmission of ions with these high dispersion magnets lies in reducing the value of l without axial defocussing by utilising the focussing effect due to fringing field of the inhomogeneous sector magnet. Unfortunately combining expressions (2) and (6), suitable parameters for a symmetrical magnetic analyser with radial and axial focussing cannot easily be found out. It is worthwhile to consider the cases of asymmetric sector magnetic analysers having conical shape and the same first order focussing effect as described by Sternheimer

(1952). The schematic diagram of such an analyser is shown in figure 2 and it satisfies the following conditions for a first order radial focussing.

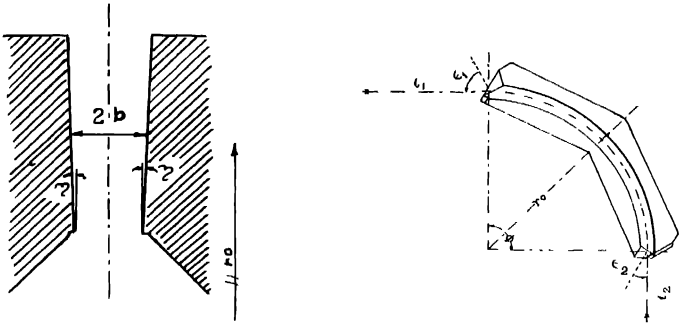

Fig. 2 (*a*) End view of the pole face of the conical magnet showing the parameters which determine the field index n. (*b*) Side view of the magnetic analyser showing the parameters for focussing of ions

$$2 \tan \epsilon_2 = \frac{(1-n)^{\frac{1}{2}}}{\cot\{(1-n)^{\frac{1}{2}}\phi + x\}} \quad \frac{n^{\frac{1}{2}}}{\cot\{n^{\frac{1}{2}}\phi + y\}} \tag{13}$$

where

$$\cot x = \frac{(1-n)^{\frac{1}{2}} l_1}{l_1 \tan \epsilon_1}$$

$$\cot y = \frac{n^{\frac{1}{2}} l_1}{1 - l_1 \tan \epsilon_1}$$

and

$$l_2 = \frac{\cot\{n^{\frac{1}{2}}\phi + x\}}{n^{\frac{1}{2}} + \tan \epsilon_2 \cot\{n^{\frac{1}{2}}\phi + x\}} \tag{14}$$

Here l_1 and l_2 are distance of the source and detector from the entrance and exit pole boundaries respectively, ϵ_1 and ϵ_2 are the angles made by the central beam of ions with the normals to the entrance and exit pole boundaries respectively, and ϕ, n are same as before.

A few parameters for such high dispersion asymmetric magnetic analysers for values of $n = 0.8$ and 0.9 are calculated and some representative cases are shown in figures 3 and 4,.

Under the same conditions implied in the Sternheimer's findings, any sector angle can be considered with $0.5 < n < 1$ for high dispersion as well as better transmission by suitable choice of the parameters

If we compare figure 1 with figures 3 and 4, it is seen that due to reduced l_1 with shaped pole boundaries, transmission increases to a great extent. As,

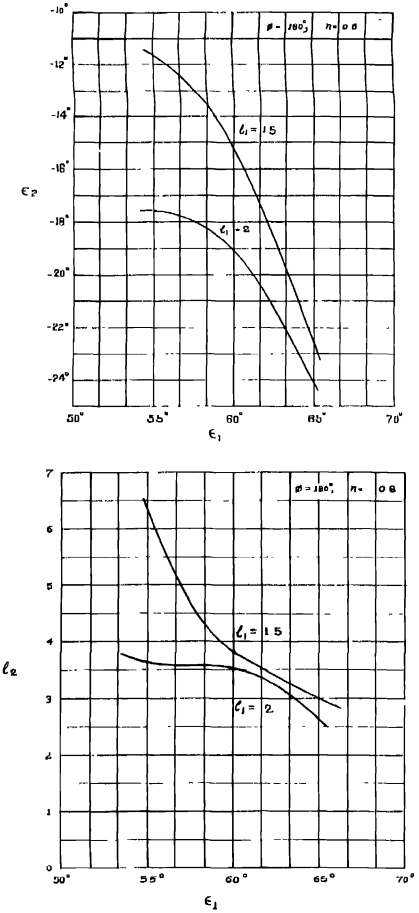

Fig 3. Relations among entrance and exit angles (ϵ_1, ϵ_2) and image distance l_2, object distance l_1, for focussing of ions with a magnet having $\phi = 180°$, $n = 0.8$.

for example, with $\epsilon_1 = 60°$, a 180° annular magnetic analyser with $n = 0.9$, one will have a solid angle $= 0.1183$ sterad instead of 0.0249 for $\epsilon_1 = 0$, for the same

available cross-section area for the ion trajectory and for 10 times better dispersion than a homogeneous magnet for both the cases.

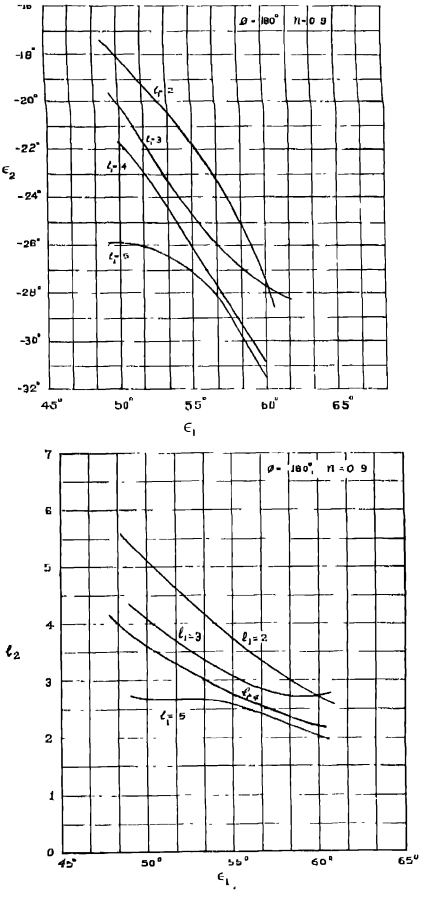

Fig. 4. Relations among entrance and exit angles (ε_1, ε_2) and image distance l_2, object distance l_1 for focussing of ions with a magnet having $\phi = 180°$, $n = 0.9$.

It is also possible to utilise the conditions of second order focussing principle due to Kerwin (1949) and Hintenberger (1949) with these types of magnet with which the resolution or the solid angle can be increased further by choice of suitable

parameters and the reduced distance of the source or the detector adds some advantage to it.

For mass spectroscopes, in which high intensity ion sources are not usually used except for isotope separation, improvement in transmission of ions as suggested above will be of some importance. With suitable parameters, a moderately high resolution mass spectrometer with less complicated ion source and detection system can be designed on this principle, which will be superior to a conventional flat type instrument, when the resolving power and the solid angle are simultaneously considered

ACKNOWLEDGEMENT

The above ideas were developed in connection with the design-studies for constructing a mass spectrometer for this laboratory and the author is grateful to Prof B. D Nag for his guidance and constant encouragement in this work.

REFERENCES

Alseevesky, N. E., Prudokvsky, G P., Kusomov, G. I. and Filimnov, S. I., 1955, *Proc Acad. Sci.*, (*U S S R.*) **100**, 229
Arbman, E. and Svartholm, N. 1955, *Arkiv. For Fysik*, **10**, 1
Camac, M, 1951, *Rev. Sci Inst.*, **22**, 197.
Cross, W. G., 1951, *Rev. Sci Inst.*, **22**, 717.
Dubroniv, A. V. and Balabina, G V., 1955, *Proc Acad. Sci*, (*U S.S.R.*), **102**, 719.
Herzog, R., 1934, *Phys Z*, **89**, 447, and 786
Hintenberger, H., 1949, *Rev. Sci Inst*, **20**, 748
Judd, D. L., 1950, *Rev. Sci Inst.*, **21**, 213.
Judd, D L. and Sidney A Bludman, 1957, *Nuclear Instruments*, **1**, 46
Karmohapatra, S. B 1955, *Ind. Jour. Phys.*, **29**, 393
Kerst, D. W. and Serber, R. 1941, *Phys. Rev.*, **53**, 60
Kerwin, L 1949, *Rev. Sci. Inst.*, **20**, 36.
Kerwin, L., 1950, *Rev. Sci. Inst.*, **21**, 96.
Lee-Whiting, G. E. and Taylor, E. A., 1957, *Canad J. Phys*, **35**, 1
Rosenblum, E. S., 1950, *Rev. Sci. Inst.*, **21**, 586.
Shull, F B. and Denision, D. N., 1947, *Phys Rev.*, **71**, 681.
Sternheimer, R. M., 1952, *Rev. Sci Inst.*, **23**, 629.
Stoker, P. H, ongping Hog, de Haan, E. F. and Sizoo, G. J, 1954, *Physica*, **20**, 337.
Svartholm, N., 1951, *Arkiv. For Fysik*, **2**, 115
Svartholm, N. and Siegbahn, K, 1946, *Arkiv For Mate. Astr. Fysik.*, **33A**, *nr*21, 24.
Verster, N. F., 1950, *Physica*, **19**, 195

6

THE EFFECT OF A UNIFORM MAGNETIC FIELD ON ELECTRODELESS DISCHARGE IN A TUBE AND MEASUREMENT OF ELECTRONIC MOBILITY I. AIR

S. N. GOSWAMI

DEPARTMENT OF PHYSICS, HOOGHLY MOHSIN COLLEGE, CHINSURA.

(*Received July* 18, 1957.)

ABSTRACT. Results of measurements of the percentage increase in the breakdown potential in a discharge tube filled with dry air and excited with a 50-cycles alternating voltage, under a uniform magnetic field and of the electronic mobility have been reported. Measurements are made for different pressures and under magnetic fields inclined at different angles with the electric field Results are discussed from the standpoint of the theory proposed by Deb and Goswami (1956).

INTRODUCTION

The change in the values of the discharge current in both an ozoniser and an electrodeless discharge tube under the influence of a uniform magnetic field has been observed previously by several workers, viz., Bhiday *et al.* (1951) and Goswami (1954). In the course of further study with electrodeless discharge in a tube of simple geometry, it was recently reported by Deb and Goswami (1956) that in the range of pressures investigated, the value of the breakdown potential was always increased in the presence of a unifrom magnetic field. Experimental values of the breakdown potential, both with and without a superimposed magnetic field, were given, and a theory, based on electron ballistics, was presented to explain the increase in the value of the breakdown potential An expression for the electronic mobility was derived therefrom when the angle between the electric and magnetic fields was $\frac{\pi}{2}$. The value of the electronic mobility at a pressure of 1 mm Hg. thus calculated, agreed in order of magnitude with that given earlier by Brose. In this paper, measurements of the breakdown potential at different pressures, with and without a superimposed magnetic field, at different inclinations with the electric field, have been made, and values of electronic mobility obtained. The measurements have been repeated for several values of the magnetic field. The values of electronic mobility and its nature of variation with pressure agree fairly with those of Brose (1925) and Nielsen and Bradbury (1936, 1937).

EXPERIMENTAL

The discharge system used was one of the simplest possible geometry *e.g.*, a cylindrical tube (figure 1). An arrangement for revolving the discharge tube

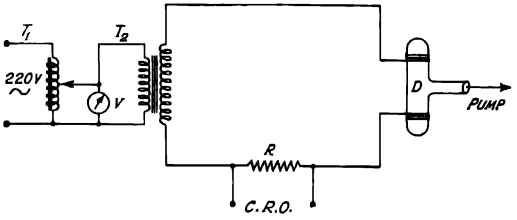

Fig. 1

about an axis perpendicular to its own and passing through its centre was provided in order to vary the inclination of the magnetic field with respect to the electric field. The tube was filled with dry air and was subjected to electrodeless discharge —the discharge being excited with 50 cycles alternating voltage obtained from the secondary winding of a step-up transformer T_2 The transformer primary was fed by the output of a variac T_1 which enabled one to smoothly vary the applied potential The pressure was reduced by means of a Cenco-hyvac pump and was recorded with a vacuoscope The magnetic field was obtained from an electromagnet with adjustable pole-pieces The wave-form of the discharge current was observed by applying the potential drop across a resistance R connected in series with the discharge circuit to the deflecting plates of a cathode-ray oscilloscope. Observations were made over the range of pressure 0.3 3.0 mm Hg, a range of exciting potential 0.45—4.06 KV(R.M.S.), and for magnetic fields 1575, 2000, 2475, 2950, 3175 and 3400 gauss.

The distance between the pole-pieces of the electromagnet was kept fixed at 4 3 cm. In making a set of observations, the discharge tube was first adjusted at a certain angle with the magnetic field, which was set at the desired value by varying the current in the electromagnet The pressure was next adjusted to a suitable value and with the magnetic field switched off the applied potential was gradually increased till pulses of discharge current just appeared on the screen of the oscilloscope The corresponding applied potential was noted. The magnetic field was then switched on and the new value of the applied potential at which the current pulses appeared again was noted The measurements were repeated for different values of pressure The discharge tube was next adjusted at a different angle with the magnetic field and in this new position similar measurements were carried out.

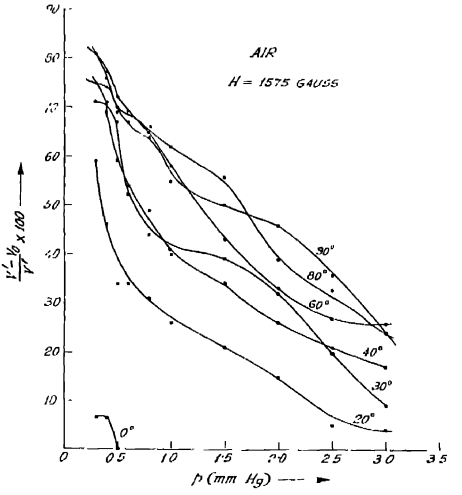
AIR
H = 1575 GAUSS
90°
80°
60°
40°
30°
20°
0°
p (mm Hg)

Fig. 2

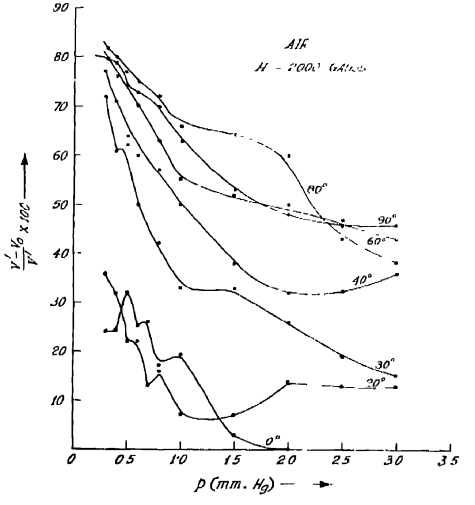
AIR
80°
90°
60°
40°
30°
20°
0°
p (mm. Hg)

Fig. 3.

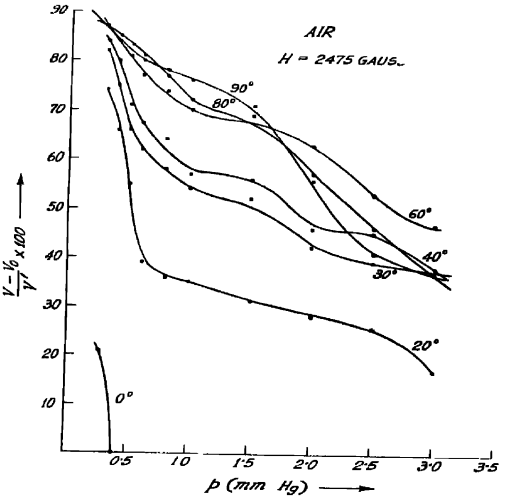
AIR
H = 2475 GAUSS
90°
80°
60°
40°
30°
20°
0°
$\frac{V-V_0}{V} \times 100$
p (mm Hg)

Fig. 4.

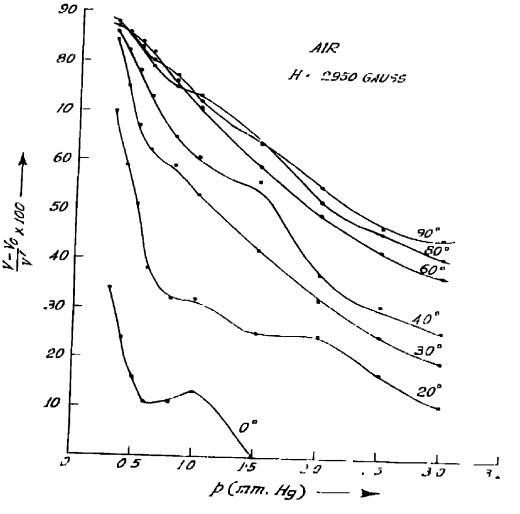
AIR
H = 2950 GAUSS
90°
80°
60°
40°
30°
20°
0°
$\frac{V-V_0}{V} \times 100$
p (mm. Hg)

Fig. 5.

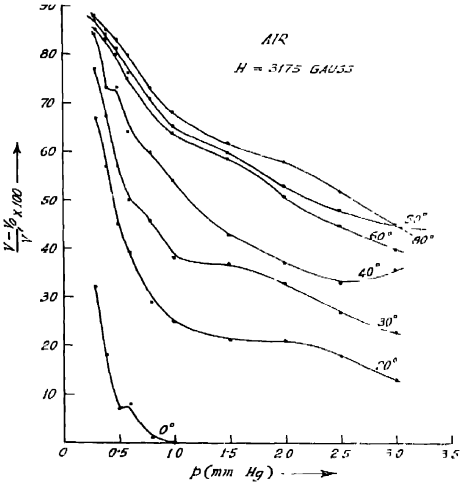
AIR
H = 3175 GAUSS
90°
80°
60°
40°
30°
20°
0°
$\frac{V-V_0}{V_0} \times 100$
p (mm Hg)

Fig. 6

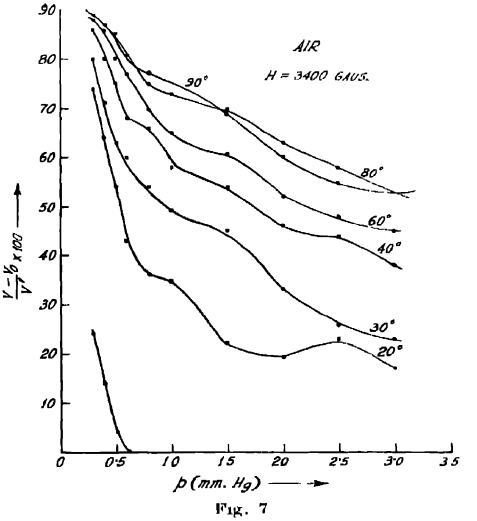
AIR
H = 3400 GAUS.
90°
80°
60°
40°
30°
20°
$\frac{V-V_0}{V_0} \times 100$
p (mm. Hg)

Fig. 7

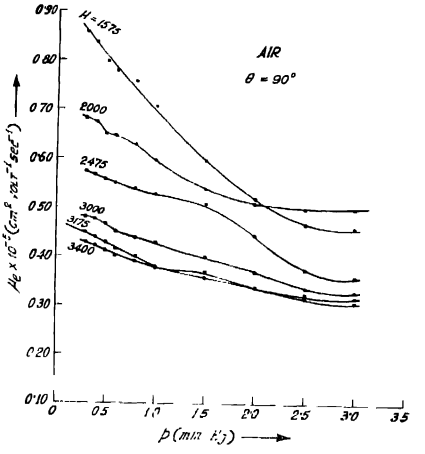

Fig 8

DISCUSSION OF RESULTS

The results obtained are shown in figures 2–8. On an examination of the curves the following facts may be summarised :

(i) The percentage effect $\frac{V'-V_0}{V'} \times 100$ diminishes with increase in pressure.

(ii) The percentage effect is, in general, higher for higher values of θ, the angle between electric and magnetic fields.

(iii) Electronic mobility decreases with increase of pressure

(iv) Electronic mobility at a given pressure is less, the higher the magnetic field.

These observed facts receive simple explanation in the light of the theory given already in a previous communication (Deb and Goswami, 1956) where ϕ and μ_e are shown to be

$$\phi = \frac{He\lambda}{m\bar{v}c} \qquad \ldots \quad (1)$$

$$\mu_e = \frac{\cos^{-1}\left[1 - \frac{V'-V_0}{V'}\right]}{H} \times 10^8 \text{ cm}^2/\text{volt. sec.} \qquad \ldots \quad (2)$$

and

$$\frac{V'-V_0}{V'} = 1 - \cos\phi \qquad \ldots \quad (3)$$

When the angle between the electric and magnetic fields is θ, Eqns (1) and (2) take the form

$$\phi = \frac{H \sin\theta \, . \, e\lambda}{m\bar{v}\, c} \qquad \ldots \quad (4)$$

and

$$\mu_e = \frac{\cos^{-1}\left[1 - \frac{V' - V_0}{V'}\right]}{H \sin\theta} \; 10^8 \text{ cm}^2/\text{volt sec} \qquad \ldots \quad (5)$$

As the pressure is increased, λ diminishes and it follows from Eqn. (4), that, for given values of H and θ, ϕ will decrease. This is in agreement with (i) above. Again from (4) it follows that other things remaining the same ϕ must increase with θ which explains (ii). The observed decrease in μ_e with increasing pressure [as in (iii) above] is also in agreement with the theoretical relation given by Nielsen & Bradbury (1936). Further, the higher is the magnetic field the greater is the proportion of total energy appearing as the lateral component and this brings about an apparent dependence of μ_e on H as noted under (iv) above. It is to be noted that the true value of μ_e is obtained only for very small values of H.

ACKNOWLEDGMENTS

The work described above was carried out in the Institute of Radiophysics and Electronics, Calcutta University. The author wishes to acknowledge his indebtedness to Prof. J. N. Bhar for his kind permission to work in the laboratory and to Dr. S. Deb for guidance in the course of the investigation. He is also thankful to Prof. S. K. Mitra for encouragement.

REFERENCES

Bhiday, M. R., Bhide, V. G., Asolkar, G. V., 1951, *Nature*, **168**, 1006.
Bose, H. L., 1925, *Phil. Mag.*, **1**, 536.
Deb, S. and Goswami, S. N., 1956, *Sci. and Cult.*, **22**, 283.
Goswami, S. N., 1954, *Sci. and Cult.*, **20**, 97.
Nielsen and Bradbury, 1936, *Phys. Rev.*, **49**, 338.
Nielsen and Bradbury, 1937, *Phys. Rev.*, **51**, 69.

7

X-RAY STUDY OF ALPHA-BETA TRANSFORMATION IN KERATIN*

V. D. GUPTA

PHYSICS DEPARTMENT, UNIVERSITY OF ALLAHABAD, ALLAHABAD

(*Received November* 12, 1957)

ABSTRACT. A measure for the degree of order introduced in alpha-beta transformation in keratin fibres is defined and its determination is carried out in three varieties of human hair It is concluded that the behaviour of golden hair is much nearer to the black than to the white.

INTRODUCTION

The X-ray study of alpha-beta transformation in keratin was made first by Herzog and Jancke (1921) and Astbury and Street (1932) Since then it has always occupied a pivotal position in all attempts to arrive at the molecular structure determination of proteins Configurations for the polypeptide chains have been proposed by Astbury and Bell (1941), Huggins (1943) and by Bragg, Kendrew and Perutz (1950) The most satisfactory model has been the one proposed by Pauling, Corey and Branson (1951). In their model the protein chain is considered as coiled into a 3 7 residue helix of pitch 5.4 A U. and a repeat distance of 1.5 A.U parallel to the axis. The successive turns of the spiral are held together by a hydrogen bond between a CO group and a nitrogen atom and it crumples up very much like certain type of fabrics which contain elastic threads Recently, Bendit (1957) has reported in case of Lincoln wool the variation of peak intensities of the 4.6 A.U , 5.1 A U. and 9 8 A.U reflections against percentage extension He concluded that Astbury's hypothesis of a molecular transformation based on a 1 · 1 correspondence of the intensity variation of the first two reflections is not tenable Pauling's model has also been supported by the researches of Cochran and Crick (1952). However, so far no quantitative X-ray study of the degree of order introduced with extension has been reported.

The outstanding reflections in the alpha photograph of human hair are the meridional strong arc of spacing 5.1 A.U. made up of (020) flanked on either side by (120) and the composite equatorial reflections (001), (101), (300) and (201). This is spread over three A.U. and has a mean spacing of 9.8 A.U. The (100) reflection because of its closeness to the centre does not lend itself to an easy evaluation and is, therefore, omitted During the course of transformation from alpha to beta which sets in *at* about 30% extension, the meridional arc begins to close up.

*Communicated By Prof. K. Banerjee, D.Sc., F.N.I.

However, it never completely disappears In addition to this there appears on the equator a new spot of 4.6 A.U. and the over-all definition of the photograph also improves. If we denote the intensity of the meridional and equatorial reflections by I_m and I_e respectively, the degree of order Ω may be defined by the relation :

$$\Omega = \frac{I_e - I_m}{I_e + I_m} \times 100$$

This expression has the advantage of being independent of all exposure factors.

EXPERIMENTAL

In order to carry out an experimental determination of this degree for the three different varieties of human hair, X-ray photographs of suitable intensity were taken of bundles of fibres well combed to ensure parallelism CuK_α radiation from a Seifert's sealed tube working at 40 K V and 20 m A and monochromatised

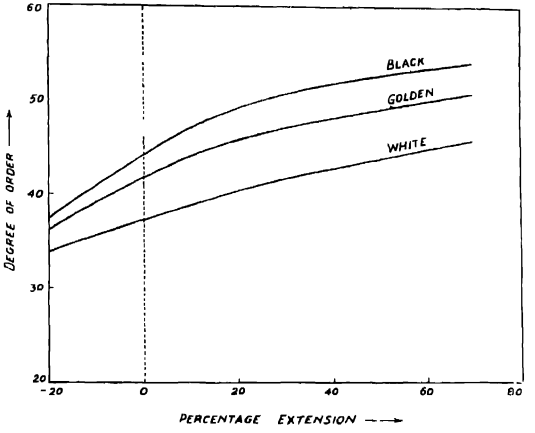

Fig 1

by reflection from a calcite crystal was used with specimen to film distance of 5 cm. The fibres were held taut between two pin-vices, one of which was movable and carried a screw gauge to measure extension. The fibres were always stretched in water at room temperature and super-contracted by stretching first in steam and later on allowing them to recover in steam itself. Intensity measurements were made by Moll's recording type microphotometer In a few cases the intensity measurements were also checked by rotating the film. Under these conditions a spot was uniformly spread out over an annular area and two scannings were given at right angles to each other. The average value of these intensities was

7

X-RAY STUDY OF ALPHA-BETA TRANSFORMATION IN KERATIN*

V. D. GUPTA

PHYSICS DEPARTMENT, UNIVERSITY OF ALLAHABAD, ALLAHABAD

(*Received November* 12, 1957)

ABSTRACT. A measure for the degree of order introduced in alpha-beta transformation in keratin fibres is defined and its determination is carried out in three varieties of human hair. It is concluded that the behaviour of golden hair is much nearer to the black than to the white.

INTRODUCTION

The X-ray study of alpha-beta transformation in keratin was made first by Herzog and Jancke (1921) and Astbury and Street (1932) Since then it has always occupied a pivotal position in all attempts to arrive at the molecular structure determination of proteins. Configurations for the polypeptide chains have been proposed by Astbury and Bell (1941), Huggins (1943) and by Bragg, Kendrew and Perutz (1950) The most satisfactory model has been the one proposed by Pauling, Corey and Branson (1951). In their model the protein chain is considered as coiled into a 3 7 residue helix of pitch 5.4 A.U. and a repeat distance of 1.5 A.U. parallel to the axis. The successive turns of the spiral are held together by a hydrogen bond between a CO group and a nitrogen atom and it crumples up very much like certain type of fabrics which contain elastic threads Recently, Bendit (1957) has reported in case of Lincoln wool the variation of peak intensities of the 4 6 A.U , 5 1 A U. and 9 8 A U reflections against percentage extension. He concluded that Astbury's hypothesis of a molecular transformation based on a 1 : 1 correspondence of the intensity variation of the first two reflections is not tenable Pauling's model has also been supported by the researches of Cochran and Crick (1952). However, so far no quantitative X-ray study of the degree of order introduced with extension has been reported

The outstanding reflections in the alpha photograph of human hair are the meridional strong arc of spacing 5.1 A.U made up of (020) flanked on either side by (120) and the composite equatorial reflections (001), (101), (300) and (201) This is spread over three A.U. and has a mean spacing of 9.8 A.U. The (100) reflection because of its closeness to the centre does not lend itself to an easy evaluation and is, therefore, omitted During the course of transformation from alpha to beta which sets in *at* about 30% extension, the meridional arc begins to close up.

*Communicated By Prof. K. Banerjee. D.Sc., F.N.I.

However, it never completely disappears. In addition to this there appears on the equator a new spot of 4.6 A.U. and the over-all definition of the photograph also improves. If we denote the intensity of the meridional and equatorial reflections by I_m and I_e respectively, the degree of order Ω may be defined by the relation :

$$\Omega = \frac{I_e - I_m}{I_e + I_m} \times 100$$

This expression has the advantage of being independent of all exposure factors.

EXPERIMENTAL

In order to carry out an experimental determination of this degree for the three different varieties of human hair, X-ray photographs of suitable intensity were taken of bundles of fibres well combed to ensure parallelism (CuK_α radiation from a Seifert's sealed tube working at 40 K.V. and 20 m.A and monochromatised

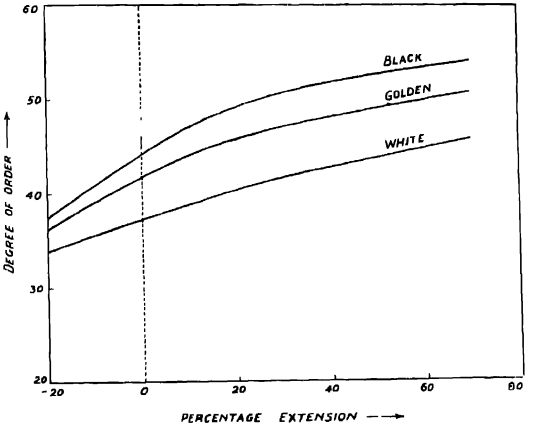

Fig. 1

by reflection from a calcite crystal was used with specimen to film distance of 5 cm. The fibres were held taut between two pin-vices, one of which was movable and carried a screw gauge to measure extension. The fibres were always stretched in water at room temperature and super-contracted by stretching first in steam and later on allowing them to recover in steam itself. Intensity measurements were made by Moll's recording type microphotometer. In a few cases the intensity measurements were also checked by rotating the film. Under these conditions a spot was uniformly spread out over an annular area and two scannings were given at right angles to each other. The average value of these intensities was

multiplied by the factor obtained on dividing the annular area by the area traversed by the exploring beam in one scanning. It was found that the intensity measurements in the two cases were within experimental error and agreed fairly well. All measurements were reduced to the same scale. The results obtained are tabulated below

Variety	Supercontracted	Unstretched	Stretched 40%	60%	70%	Treated with cupra-ammonium hydroxide
Black	38.13	43.97	51.9	53.19	54.09	0
Golden	37.58	41 80	48.01	50.12	51.12	0
White	34.21	37 03	43.82	45.83	46.60	0

DISCUSSIONS

The above results which have also been graphically represented show that the change is exponential. Initially there is a relatively rapid rise in the degree of order but later on the change not very large when the extension varies from 60% to 70%. Further, the behaviour of golden hair is nearer to that of the black than that of the white The difference may be ascribed to the change in pigment, presence of air bubbles in white hair and other changes produced during the course of metabolism. On treatment with cupra-ammonium hydroxide it was found that the fibre photograph completely disappeared because of the contraction having arisen from an extra folding of the chains induced by co-ordination of the absorbed copper with appropriate groups in the keratin chains A study of this "reversible supercontraction" produced on washing with dilute H_2SO_4 is also being made and a detailed account of the work would be shortly published elsewhere.

ACKNOWLEDGMENTS

The author is grateful to Professor K Banerjee, D Sc., F.N I , for his valuable guidance and encouragement throughout the progress of the work

REFERENCES

Astbury, W T. and Street, A. 1932. *Phil Trans. Roy. Soc , A*, 230, 75.
Astbury, W T. and Bell, F. O. 1941, *Nature (London)*, 147, 696
Huggins, M. L 1943, *Chem. Rev.*, 32, 195
Bragg, L., Kendrew, J. C. and Perutz, M. F. 1950, *Proc Roy. Soc.*, 203*A*, 321
Pauling, Linus; Corey, Robert B and Branson, H. R. 1951. *Proc. Nat. Acad Sciences (Washington)*, 37, 205.
Bendit, E. G. 1957, *Nature (London)*, 179, 535
Cochran, W and Crick, 1952, *Nature (London)*, 169, 234.

Letters to the Editor

The Board of Editors will not hold itself responsible for opinions expressed in the letters, published in this section. The notes containing reports of new work communicated for this section should not contain many figures and should not exceed 500 words in length. The contributions must reach the Assistant Editor not later than the 15th of the second month preceding that of the issue in which the Letter is to appear. No proof will be sent to the authors.

1. POSSIBILITY OF POLARIZATION OF FREE ELECTRONS

S YAMAGUCHI

SCIENTIFIC RESEARCH INSTITUTE, 31 KAMIFUJI (HONGO), TOKYO, JAPAN

(*Received November* 4, 1957)

Powder of permanent magnet (coercive force, about 700 Oe) was oriented on a magnet substrate An electron beam (wavelength, about 0.03 A) was tunnelled through the magnet particles, as is shown in figure 1. A diffraction pattern here

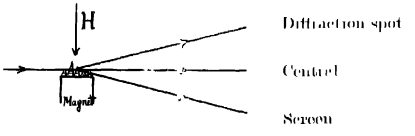

Fig 1. Arrangement of experiment

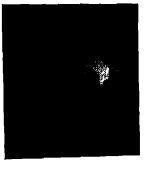

Fig 2, Diffraction pattern obtained from the magnet. Wavelength: 0 0286A. Camara length: 495 mm

Fig. 3. The central spot found in Fig. 2, 40 times enlarged optically. Splitting of electron beam is noticeable.

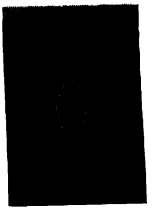

Fig. 4. The electron beam without touching the magnet There is no splitting here.

obtained is shown in figure 2. The central spot found in figure 2 was optically enlarged 40 times, as is seen in figure 3. It would be noticed in figure 3 that the

electron beam is splitup after it has passed through the magnet body. The form of the electron beam, which did not touch the magnet, is shown in figure 4. In figure 4 there is no splitting of the beam. The author has tried to elucidate this splitting phenomenon as polarization of electrons.

There is a steep gradient of the magnetic field in the magnet This gradient appears at the border between Weiss' magnetic domain and Bloch's magnetic wall. There is an interaction between the electron spins in the incidence and the magnetic field with the gradient. The geometric relation between the incident

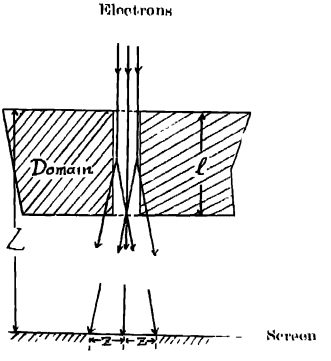

Fig. 5. Relation between the incident electrons and the inner magnetic field.

electrons and the inner field is illustrated in figure 5 In the arrangement of the experiment, the deflection of the electron beam is expressed by

$$\Delta Z = \frac{1}{2} B \left| \frac{\partial H}{\partial Z} \right| m \left(\frac{\lambda l}{h} \right)^2 \qquad \dots \quad (1)$$

where B is the magnetic moment of Bohr's magneton (0.93×10^{-20} erg/gauss), $\frac{\partial H}{\partial Z}$ is the gradient of the field, m is electron mass ($9.1 \times 10^{-28} g$), l is the path of the beam, λ is the wavelength of the beam (0.0286 Å), and h is Planck's constant (6.6×10^{-27} erg.sec).

In figure 5 we have a relation

$$\frac{\Delta Z}{Z} = \frac{l}{L} \qquad \dots \quad (2)$$

where Z means the distance between the splitup spots in figure 3. In figure 3 we can estimate $Z = 0.02$ cm. And if we assume $l = 10^{-3}$ cm, that is, the known linear dimension of Weiss' domain, then we obtain from Eq. (1) and Eq. (2)

$$\left| \frac{\partial H}{\partial Z} \right| = 4 \times 10^{13} \text{ gauss/cm} \qquad \dots \quad (3)$$

It is expected that this steep gradient of magnetic field is realised at the border between Weiss' domain and Bloch's wall It is known that the thickness of Bloch's wall $\Delta\zeta$ is about 100 Å. If we assume

$$\frac{\partial H}{\partial Z} = \frac{\Delta H}{\Delta\zeta/2}$$

we have from Eq. (3)

$$\Delta H = 10^7 \text{ Gauss},$$

where ΔH means the strength of Weiss' field. This observed value coincides with the known strength of Weiss inner field

Discussion here performed is not quantal, but it is classical Quantum mechanics may treat this problem as result of exchange force between electron spins in the incidence and those in the magnet The author has regarded here Weiss' molecular field as real This thought is quite similar to the Bragg's thought that regards the interplanar spacings in crystal as real

2 THERMOLUMINESCENCE SPECTRA OF LIF

A. K GHOSH AND B C DUTTA*

KHAIRA LABORATORY OF PHYSICS, UNIVERSITY COLLEGE OF SCIENCE, CALCUTTA

(*Received for publication, November 11, 1957*)

Lithium fluoride bombarded with 10 KV cathode rays at room temperature fluoresces weakly and the thermoluminescence glow is too weak for spectral analysis, however when exposed to cathode rays at 90°K it fluoresces blue and on prolonged irradiation the sample becomes red luminescent On rapid heating, the coloured sample gives two glow peaks at approximately 140°K and 650°K. The first glow is intense but of short duration while the second is weak and persists for an appreciable time The spectral distributions of these glows have been recorded by means of an automatic rapid scanning spectrophotometer by Dutta and Ghosh (1956) The spectra of the glows are found to be different. The band maximum at the first glow peak temperature is 435 mμ (frame No. 4) while that for the second is 597 mμ (frame No. 5). During the first thermoluminescence glow, in the temperature range 122°K to 140°K, there is an indication of a weak diffuse band on the shorter wave length side of the main band. The position of this band is indicated by an arrow in the spectral record At about 128°K to 134°K another weak band appears on the longer wave length side, its position being marked by a double arrow in the record

*Present address : Physics Dept., Birkbeck College, London

The first glow peak temperature agrees fairly well with those obtained by Pringsheim and Yuster (1950), Ghormley (1952) and also Sharma (1952). In fact, the emission of a blue glow peak at -135°C, as reported by them, is found to be the first glow peak having band maximum at 435 mμ. Ghormley and Levy (1952) reported that the phosphorescence (thermostimulated) spectrum of gamma irradiated LiF is characterized by two broad bands at about 270 mμ and 440 mμ. The photomultiplier used in the present acse is insensitive below 330 mμ and hence if the 270 mμ band be present in the thermoluminescence emission it cannot be detected. The second glow peak temperature is in accordance with that obtained by Sharma (1952).

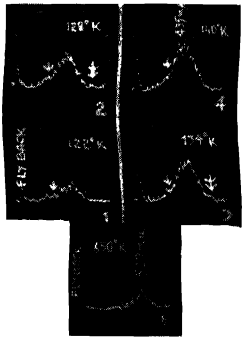

Fig. 1. Thermoluminescence spectra of LiF at different temperatures during the glow (Frames No. 1-4)

The experimental results obtained clearly show that the spectral nature of the glows is not identical. This is attributable to a process of the release of electrons from different traps at different temperatures, undergoing preferential transitions during the emission process.

A series of spectra were recorded one in each second for the thermoluminescence emission and a few of these are given in the spectral record.

ACKNOWLEDGMENT

The authors wish to thank Prof. S. N. Bose for his constant interest in the work and to Dr. K. Dasgupta for helpful discussions.

REFERENCES

Dutta, B. C. and Ghosh, A. K., 1956, *Ind. J. Phys.*, **30**, 570.
Pringsheim, P. and Yuster, P., 1950, *Phys. Rev.*, **78**, 293.
Ghormley, J. A. and Cevy, A. A., 1952, *J. Chem. Phys.*, **56**, 548.
Sharma, J., 1952, *Phys. Rev.*, **67**, 535.

Fig. 2. Thermoluminescence Spectra of LiF at the glow peak temperature 650°K. (Frame No. 5).

THE DIELECTRIC PROPERTIES OF ESTER GUM

A. K. SEN AND G N. BHATTACHARYA

DEPARTMENT OF APPLIED PHYSICS, UNIVERSITY OF CALCUTTA, CALCUTTA.

(*Received (of publication April* 6, 1957 , *after revision November* 16, 1957)

ABSTRACT. The dielectric properties of ester gum have been measured over a wide range of temperature and frequency viz., from 22°C to 140°C and from 400 cycles per second to 300 kc/s. The resin shows characteristic polar properties and the region of anomalous dispersion extends over a wide range. The maximum value of dielectric loss at any frequency is less than that demanded by Debye's theory and the $\varepsilon''/\varepsilon''_m$ plot against f/f_m gives a much blunter curve than the theoretical one indicating thereby a distributed relaxation time of the orientating dipoles. The radius of the rotating unit, calculated from data reported here and the melt-viscosity data published earlier, gives an average value of 1.5 Å only, which

ERRATA

Vol. 31, No. 12

Page 644, 1st and 2nd line read 'ether' instead of 'ethyl alcohol' and 4th line, read 'axes' for 'axis'.

heating and solidify on cooling, the process being reversible and (b) the thermo-setting resins, which sometimes soften on heating but solidify on continued heating, the process being irreversible These two types of behaviour are believed to be due to the difference in their molecular structure The thermoplastic resins usually have a long chain molecular structure, whereas the thermo-setting ones have a cross-linked structure. Hence the molecules of a thermoplastic resin are in a position to respond more freely to impressed external forces such as heat or electric field than those of a thermo-hardening type

According to Debye's dipole theory, all polar substances are expected to show anomalous dispersion and the accompanying dielectric loss somewhere in the frequency range determined by the size and shape of dipoles and the inner friction coefficient, which again depends upon temperature. Important information regarding their physical structure may thus be obtained from a study of their behaviour in an alternating electric field under varying conditions of temperature and frequency. Debye's simple dipole theory can very well account for such dispersion in case of substances having smaller molecules with single relaxation

The first glow peak temperature agrees fairly well with those obtained by Pringsheim and Yuster (1950), Ghormley (1952) and also Sharma (1952) In fact, the emission of a blue glow peak at 135°C, as reported by them, is found to be the first glow peak having band maximum at 435 mμ. Ghormley and Levy (1952) reported that the phosphorescence (thermostimulated) spectrum of gamma irradiated LiF is characterized by two broad bands at about 270 mμ and 440 mμ. The photomultiplier used in the present acse is insensitive below 330 mμ and hence if the 270 mμ band be present in the thermoluminescence emission it cannot be detected. The second glow peak temperature is in accordance with that obtained by Sharma (1952)

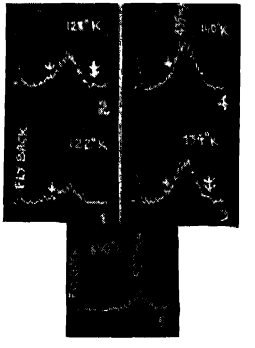

Fig. 1 Thermoluminescence spectra of LiF at different temperatures during the glow. (Frames No. 1-4)

The experimental results obtained clearly show that the spectral nature of the glows is not identical This is attributable to a process of the release of electrons from different traps at different temperatures, undergoing preferential transitions during the emission process

A series of spectra were recorded one in each second for the thermoluminescence emission and a few of these are given in the spectral record

ACKNOWLEDGMENT

The authors wish to thank Prof. S N. Bose for his constant interest in the work and to Dr. K Dasgupta for helpful discussions

REFERENCES

Dutta, B. C. and Ghosh, A K , 1956, *Ind. J. Phys* , **30**, 570.
Pringsheim, P. and Yuster, P., 1950, *Phys. Rev.*, **78**, 293.
Ghormley, J. A. and Levy, A A., 1952, *J. Chem. Phys.*, **56**, 548
Sharma, J., 1952, *Phys. Rev.*, **67**, 535.

Fig. 2. Thermoluminescence Spectra of LiF at the glow peak temperature 650°K. (Frame No. 5).

8

THE DIELECTRIC PROPERTIES OF ESTER GUM

A. K. SEN AND G. N. BHATTACHARYA

DEPARTMENT OF APPLIED PHYSICS, UNIVERSITY OF CALCUTTA, CALCUTTA.

(*Received for publication April 6, 1957 ; after revision November 16, 1957*)

ABSTRACT. The dielectric properties of ester gum have been measured over a wide range of temperature and frequency viz , from 22°C to 140°C and from 400 cycles per second to 300 kc/s. The resin shows characteristic polar properties and the region of anomalous dispersion extends over a wide range The maximum value of dielectric loss at any frequency is less than that demanded by Debye's theory and the ϵ''/ϵ''_m plot against f/f_m gives a much blunter curve than the theoretical one indicating thereby a distributed relaxation time of the orientating dipoles. The radius of the rotating unit, calculated from data reported here and the melt-viscosity data published earlier, gives an average value of 1.5 Å only, which is the same as that of a hydroxyl group. From the consideration of composition of ester gum it has been postulated that the dielectric loss of this resin is mainly due to the presence of glyceryl mono- and di-abietates in this resin.

INTRODUCTION

Resins in general are quite different from both crystalline solids and ordinary liquids; in their bulk mechanical properties they resemble solids, while as far as details of molecular mechanics are concerned they have many of the properties of liquids. According to their behaviour towards heat treatment, resins may have two other classifications, viz, (a) the thermoplastics, which soften on heating and solidify on cooling, the process being reversible and (b) the thermosetting resins, which sometimes soften on heating but solidify on continued heating, the process being irreversible These two types of behaviour are believed to be due to the difference in their molecular structure The thermoplastic resins usually have a long chain molecular structure, whereas the thermo-setting ones have a cross-linked structure Hence the molecules of a thermoplastic resin are in a position to respond more freely to impressed external forces such as heat or electric field than those of a thermo-hardening type.

According to Debye's dipole theory, all polar substances are expected to show anomalous dispersion and the accompanying dielectric loss somewhere in the frequency range determined by the size and shape of dipoles and the inner friction coefficient, which again depends upon temperature. Important information regarding their physical structure may thus be obtained from a study of their behaviour in an alternating electric field under varying conditions of temperature and frequency. Debye's simple dipole theory can very well account for such dispersion in case of substances having smaller molecules with single relaxation

time and yields important data regarding their physical structure. But sometimes such direct and quantitative application of Debye's equations becomes difficult in the case of a substance having large molecules with distributed relaxation time, as in the case of a complex polar resin whose polar groups may not be free but anchored to a common chain It has been observed that in many such cases these groups only orient with the alternating field instead of the whole molecule.

Chemically speaking ester gum is the glycerol ester of rosin acids about 98% of which is abietic acid. It is a thermoplastic resin having a softening range of temperature near about 79°C. Ester gum is largely used in various industries although wood rosin is considered as an inferior resin owing to its high acid value Its molecular weight is about 900, hence although the molecule is small compared to most polymeric resins, it may be sufficiently large for the quantitative application of Debye's equations. It is, therefore, of considerable interest to study the dielectric properties of this thermoplastic resin with a view to getting an idea of the size of the rotating unit.

THEORETICAL

The dielectric properties of a substance which exhibits the phenomenon of absorption or dielectric loss may be expressed in terms of a real and an imaginary part of the complex dielectric constant, viz ,

$$\epsilon = \epsilon' - j\epsilon''$$

where ϵ = the complex dielectric constant,

ϵ' = the real or ordinary dielectric constant or permittivity,

and ϵ'' = the imaginary part or the dielectric loss factor

The relation between the dielectric loss factor ϵ'' and the dielectric constant ϵ' is generally expressed as

$$\epsilon'' = \epsilon' \cos \phi$$

ϕ being the phase angle by which the current vector leads the voltage vector across a condenser filled with the given dielectric material. In the case of a perfect dielectric this angle would be 90°. The angle δ which measures the lag of the phase angle from 90°, is called the loss angle and is usually very small in case of dielectric materials.

Since δ is very small and $\phi + \delta = 90°$, we have

$$\epsilon'' = \epsilon' \cos \phi = \epsilon' \sin \delta = \epsilon' \tan \delta$$

where $\tan \delta$ is called the power factor of the condenser. The dielectric constant ϵ' and the power factor $\tan \delta$ of a condenser may be determined in the usual manner and the dielectric loss ϵ'' may be computed.

EXPERIMENTAL

Apparatus : For the measurements of permittivity and power factor of ester gum a General Radio type 716-C capacitance bridge was used. The generator was a G.R. type 1330-A bridge oscillator and the detector-amplifier was a G.R. type 1212-A unit null-detector having a suitable gain of amplification over the range of frequency investigated.

Throughout this investigation a vertical type parallel plate condenser was used. The metal plates were fixed on a fused quartz plate. The condenser could be placed inside a small beaker containing the material to be investigated upon in the liquid state. This vertical type condenser was preferred to the horizontal type as the adherent air bubbles could easily escape from the former. The details of construction of this type of condenser has been described previously (Bhattacharya, 1944).

Method of Procedure · Preliminary tests were made on the condenser as regards the constancy of its value and was found to be quite satisfactory. The condenser was placed inside a completely shielded enclosure and leads were taken out through coaxially shielded quartz tube The outer shield and one set of the condenser plates were connected to the ground terminal of the bridge which was earthed. Keeping the condenser in this position its air-capacity was determined by using chemically pure benzene up to a certain mark on the beaker. Hence, by measuring the capacity of the test cell filled up to the said mark with the material its dielectric constant could be determined.

Ester gum was melted in a crucible and poured in the beaker and kept inside a hot air oven alongside the condenser to allow the dissolved air bubbles to rise gradually up to the surface. The hot condenser was then slowly put in the molten ester gum taking care to avoid adherent air bubbles. The temperature of the oven was then slowly brought down to the room temperature. A thin cork pad in the form of a ring was placed between the rim of the beaker and the quartz plate in order to avoid undue strain during the setting of the resin on cooling. The temperature of the oil bath was controlled by a thermostat within $\pm$ 0.2°C. Measurement of d.c. resistivity was carried out using the same condenser. The details of this measurement have already appeared (Sen and Bhattacharya, 1957).

DISCUSSION

In figures 1, 2 and 3, the power factor tan δ, the dielectric constant ϵ' and the dielectric loss ϵ'' have been plotted as respective functions of temperature. All these curves can be explained in terms of orientation of polar molecules in the light of Debye's theory. According to Debye the dielectric loss is caused by the orientation of polar molecules, when placed in an alternating electric field, against an

RESULTS

TABLE I

Dielectric constant—temperature data.

Temperature in °C	Dielectric constant ε′ at						
	400 c/s.	1 kc/s.	5 kc/s.	10 kc/s.	50 kc/s.	100 kc/s	300 kc/s.
22°	2 717	2 714	2 708	2 704	2.702	2 698	2 692
30°	2 719	2.719	2 712	2 712	2 707	2 702	2 700
40°	2 748	2 745	2 733	2 738	2 733	2.732	2 727
50°	2.790	2 781	2 775	2 771	2 763	2.763	2 753
60°	2 831	2 816	2 798	2 790	2 779	2.775	2 771
70°	2.969	2 900	2 836	2.827	2 805	2 796	2.790
80°	3 360	3 154	2 954	2 917	2 851	2 829	2 805
90°	3 748	3 569	3 310	3 119	2 962	2.910	2 854
100°	3 858	3.783	3.616	3 455	3 175	3.073	2 949
110°	3 848	3.810	3 681	3 584	3 362	3.300	3 054
120°	3.835	3.787	3.768	3 740	3 619	3.489	3.323
130°	3 810	3 796	3 784	3 773	3 709	3 637	3.512
140°	3.777	3 773	3.766	3 755	3 733	3.702	3 618

TABLE II

Power factor—temperature data

Temperature in °C	Power factor tan δ (corrected for d.c. conductivity) at						
	400 c/s.	1 kc/s	5 kc/s.	10 kc/s.	50 kc/s	100 kc/s.	300 kc/s.
22°	0 0018	0 0018	0 0014	0 0014	0.0018	0 0020	0.0027
30°	0 0017	0 0017	0 0013	0.0013	0 0017	0 0019	0.0027
40°	0 0012	0 0014	0.0012	0 0012	0 0016	0.0018	0 0027
50°	0.0036	0 0030	0.0022	0 0020	0 0020	0.0022	0 0033
60°	0 0105	0 0077	0 0052	0.0043	0 0031	0.0031	0 0039
70°	0.0388	0 0240	0.0132	0 0105	0 0067	0.0060	0.0057
80°	0.0800	0.0600	0 0370	0.0295	0.0170	0 0140	0.0111
90°	0.0644	0.0685	0 0755	0.0577	0 0380	0.0320	0 0222
100°	0.0254	0 0370	0 0581	0 0720	0 0625	0 0585	0.0427
110°	0.0099	0.0173	0 0350	0 0405	0.0680	0 0750	0.0615
120°	0.0033	0 0057	0.0169	0.0229	0 0515	0.0662	0.0741
130°	0.0011	0 0025	0.0079	0 0123	0 0314	0 0465	0.0660
140°	0.0018	0.0010	0 0040	0 0058	0 0171	0.0267	0.0480

TABLE III

Dielectric loss-temperature data

Temperature in °C	Dielectric loss ε″ (corrected for d.c. conductivity) at						
	400 c/s	1 kc/s	5 kc/s.	10 kc/s.	50 kc/s.	100 kc/s	300 kc/s.
22°	0.0049	0 0050	0 0038	0.0038	0.0480	0.0054	0.0073
30°	0 0046	0.0046	0 0034	0.0035	0.0047	0.0051	0.0073
40°	0 0033	0.0038	0.0033	0 0033	0.0046	0.0049	0.0074
50°	0.0101	0.0085	0.0062	0.0055	0 0055	0 0061	0 0091
60°	0.0297	0 0216	0 0147	0.0120	0 0086	0 0087	0.0108
70°	0 1152	0 0696	0 0376	0 0297	0.0189	0 0168	0 0159
80°	0 2669	0 1892	0 1093	0 0861	0.0485	0 0396	0.0311
90°	0.2414	0 2440	0.2499	0.1800	0.1126	0.0931	0.0634
100°	0.0980	0.1400	0 2100	0 2488	0.1985	0.1798	0.1261
110°	0 0377	0.0659	0.1288	0.1451	0.2310	0 2429	0.1878
120°	0.0127	0.0216	0.0636	0.0858	0.1864	0 2310	0 2462
130°	0.0042	0.0097	0.0300	0.0466	0.1166	0.1690	0 2317
140°	0.0067	0.0038	0.0152	0 2174	0.0640	0.0988	0.1737

internal frictional force or viscosity. At lower temperature, when the substance is more or less in a solid state, the inner frictional force or viscosity is so great that the dipoles are unable to orient themselves in response to the impressed alternating

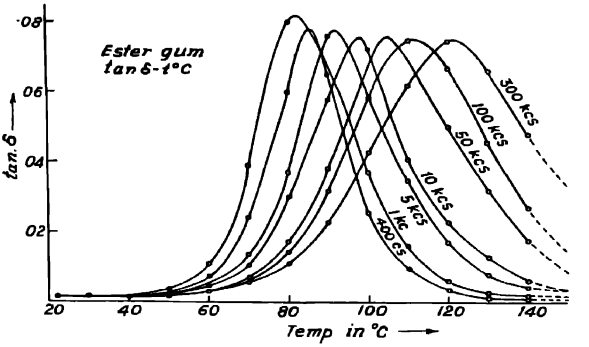
Ester gum
tan δ-t°C
tan δ
·08
06
04
02
300 kcs
100 kcs
50 kcs
10 kcs
5 kcs
1 kcs
400 cs
20
40
60
80
100
120
140
Temp in °C

Fig. 1

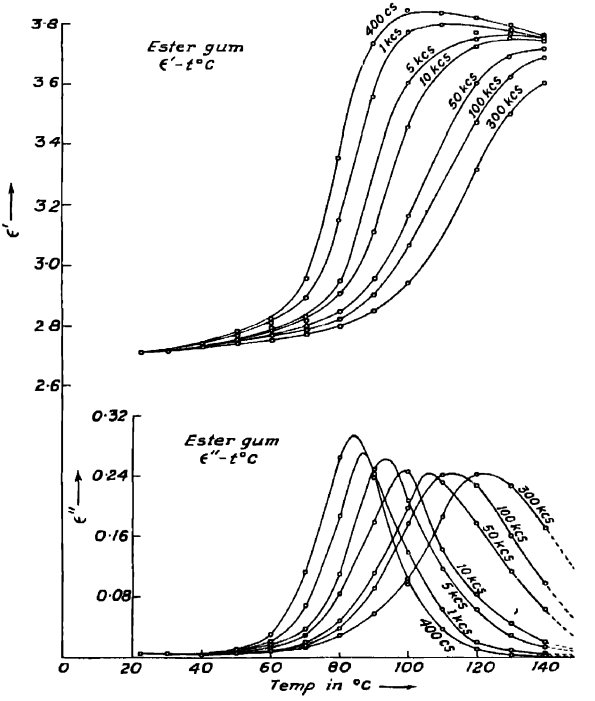
Ester gum
ε'-t°C
ε'
3·8
3·6
3·4
3·2
3·0
2·8
2·6
400 cs
1 kcs
5 kcs
10 kcs
50 kcs
100 kcs
300 kcs
Ester gum
ε''-t°C
ε''
0·32
0·24
0·16
0·08
300 kcs
100 kcs
50 kcs
10 kcs
5 kcs
1 kcs
400 cs
0
20
40
60
80
100
120
140
Temp in °C

Fig. 2 & 3.

field as if they are "frozen in". Consequently, the dielectric loss and the power factor are low The value of the dielectric constant is also low and is mainly due to the electronic polarisation as any contribution from dipole polarisation is almost nil. At very high temperatures thermal agitation tends to produce a random distribution of dipoles thereby making a very few dipoles available to orient themselves in response to the field And even those few dipoles that orient absorb little energy from the field as the resistance to such orientation is very small owing to the logarithmic decrease of viscosity with temperature. Thus at high temperatures, too, the loss and the power factor are low. Between these two extremes there will be states at which the dipoles can respond more or less freely to the alternations of the impressed field against the opposing forces of both the internal viscous forces of the material as well as those due to thermal agitation With the increase of temperature the forces due to thermal agitation increase, whereas those due to viscosity decrease. At any temperature, therefore, the loss is determined by the frequency of the alternating field as well as the viscosity of the substance and the size and shape of the dipoles giving the characteristic relaxation time τ

As the softening point of the substance is approached with the increase of temperature, the internal viscosity decreases rapidly and more and more polarisation takes owing to increased participation of the "frozen in" dipoles in the orientation, resulting in a steep rise in the value of the dielectric constant. Then the dielectric constant tends towards a maximum indicating a liquid state with the maximum number of oriented dipoles and the high value of the dielectric constant approaches ϵ_0', the "static value" of the substance at the particular temperature. With a further rise in temperature the opposing forces due to thermal agitation predominate and so the number of oriented dipoles diminish, resulting in a lower value of the dielectric constant It may be seen from figure 2 that this stooping portion of the dielectric constant-temperature curve was obtained for the frequencies, 400 c/s and 1000 c/s only while those for other frequencies seem to lie at temperatures higher than the range of investigation.

Now, for a given substance the amount of dipole polarisation depends upon the relative values of relaxation time τ and the period of the alternating field $2\pi/\omega$. When this period is very small *i.e.* for very high frequencies compared with $1/\tau$, the dipole polarisation is negligible, hence both the dielectric constant and the dielectric loss are low. This may be seen from figures 2 and 3. When the period of the field is large compared with τ, complete polarisation takes place in each half of the cycle and the dielectric constant approaches the maximum value. Because of the low value of τ compared with the period of the field, orientation also does not lag behind the field alternations, thus resulting in a low loss. The change of the dielectric constant from a low value to a large one occurs in the region in which the half period of the applied field is of the same order as

the relaxation time. Again, in this region polarisation can not keep pace with the field alternations and it lags appreciably behind the field, with the result that both dielectric loss and power factor approaches maximum values. It may be noted from figures 2 and 3 that the peak of any loss curve corresponds to a temperature at which the maximum variation of dielectric constant takes place in the corresponding ϵ'—temperature curve.

As with the increase of temperature relaxation time decreases, it follows that the dielectric loss peaks corresponding to different frequencies would occur at higher and higher temperatures as the frequency is increased. This may be seen from figure 3. At the frequency of 400 c/s the maximum dielectric loss takes place at 84°C while for the frequencies of 1, 5, 10 and 50 kc/s the peaks occur at 87°C, 94°C, 99°C and 106°C respectively For 100 kc/s and 300 kc/s, the peaks, which are blunter than the previous ones, occur at still higher temperatures viz., at 112°C and 122°C respectively. Thus within the above frequency band the peaks spread through a range of about 38°C. From the curves it may again be noted that the value of the maximum loss ϵ''_m of each curve increases as we proceed towards lower temperatures Thus ϵ''_m for the curve corresponding to 400 c/s is 0.296 the maximum occurring at 84°C, whereas ϵ''_m for 300 kc/s is only 0.246 at 122°C.

It is quite appparent that all the curves given above are in qualitative agreement with the expected behaviour of polar molecules according to Debye's theory. But the electrical properties of polar systems containing large molecules differ markedly from those in which the molecules are small. The properties of the latter are well accounted for by Debye's theory in which the fundamental assumption is the single relaxation time and the small size and simple shape of the rotator.

But in the case of a polar substance having large molecules, such as polar polymers, polar groups sometimes are attached to a common chain or to other polar groups attached to the chain. The different possible configurations of the chain and their random distribution under thermal agitation give rise to a band of distributed relaxation times for the entire molecule instead of a single one as in the case of a simple polar molecule (Fuoss and Kirkwood, 1941). Now from theoretical considerations (Wagner, 1913 and Yager, 1936) it has been shown that the characteristic difference between a polymeric system and a system describable in terms of a single relaxation time is revealed by a diminution in the value of the maximum loss ϵ''_m from that demanded by Debye's equation as well as by the widening of the dispersion band.

The maximum value of the dielectric loss of a polar liquid at any temperature, according to Debye's theory, can be represented as

$$\epsilon''_m = \frac{\epsilon_0' - \epsilon_\infty'}{2}$$

where $\epsilon_m'' =$ the maximum value of the loss,

$\epsilon_0' =$ the static dielectric constant at the particular temperature,

and $\epsilon_\infty' =$ the value of the dielectric constant at very high frequencies.

For ester gum, the value of ϵ_0' at 100°C can be estimated from figure 4 to be 3.89 and that of ϵ_∞' 2.79. Hence on the basis of Debye's relation the value of the maximum loss at 100°C should have been 0.55. But the experimental value, as

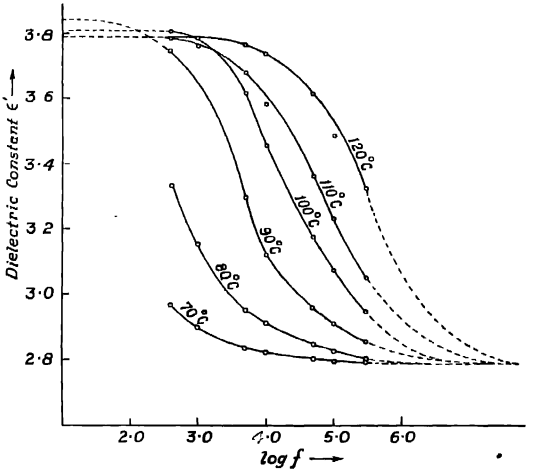

Fig 4.

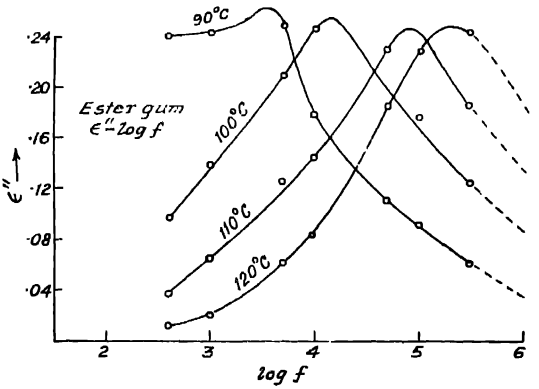

Fig 5

can be seen from figure 5, is 0 256 which is only half of the theoretical value. Thus the quantitative application of Debye's relation is found to be invalid in this case.

It may be seen from ϵ'-frequency and ϵ''-frequency curves of figures 4 and 5 that both the regions of dispersion as well as of absorption extend over a wide range of frequency not less than 6 or 7 decades. The values of ϵ''/ϵ_m'' for ester gum, obtained from the 100°C data of figure 5, are plotted against $\log f/f_m$ and the resulting curve is shown in figure 6. The Debye curve is also shown in the same

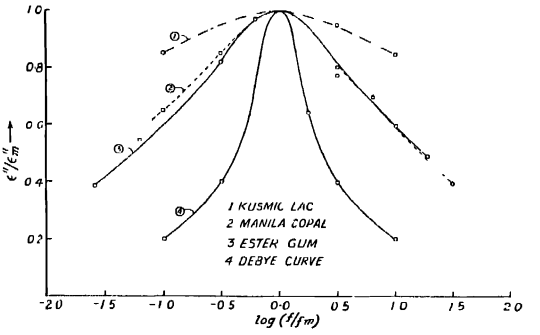

Fig. 6.

figure for the sake of comparison and it may be seen that the curve for ester gum is much blunter than the theoretical curve Similar curves for several other resins are also represented in figure 6 for the sake of comparison. It may be seen that the curve for ester gum almost coincides with that for Manila copal obtained previously by one of us (Bhattacharya, 1946). Thus the effects of distributed relaxation times are quite evident in the case of ester gum by the blunter shape of the absorption curve as well as by the wide departure of the observed value of the maximum loss from the calculated one.

As stated previously, the phenomenon of dielectric loss of polar materials caused by the orientation of dipoles in an alternating electric field, is, according to Debye, a relaxation mechanism controlled by an internal frictional force. The relation between the relaxation time and the internal frictional torque encountered by a dipole in an alternating field, is

$$\tau = \frac{\xi}{2kT}$$

where τ = relaxation time, ξ = frictional torque, k = Boltzmann constant, and T = absolute temperature.

In the case of a liquid where a spherical shape of the rotator can be assumed, ξ can be written as equal to $8\pi\eta a^3$, according to Stoke's law, so that

$$\tau = \frac{4\pi\eta a^3}{kT} \qquad \ldots \quad (1)$$

where η = coefficient of viscosity and a = radius of the rotator.

Now τ can be calculated from another relation due to Debye, viz.,

$$\omega\tau = \frac{\epsilon_\alpha' + 2}{\epsilon_0' + 2} \qquad (2)$$

at a temperature where the dielectric loss is maximum for any frequency and ϵ_0' and ϵ_∞' are the static dielectric constant and the dielectric constant at very high frequencies respectively at that temperature.

From the last two relations it is quite apparent that if the values of η and τ for the temperature at which the maximum dielectric loss takes place for a particular frequency are known, the radius of the dipole unit a can be determined The coefficient of viscosity of this resin has already been determined over the range of temperature investigated (Sen and Bhattacharya, 1957) The relaxation time τ for a particular temperature can be determined from the ϵ'—log f curve using relation (2). The results of this computation are shown in Table IV below.

TABLE IV.

Frequency (in kc/s.)	T_m (Temp. in °C at which ϵ_m'' occurs)	ϵ_0' (at T_m)	ϵ'_∞	τ (Relaxation time in sec)	log η (at T_m)	a (in Å)
1	87°	3.850	2 790	1.304×10^{-4}	5 26	1 41
5	94°	3.860	2.790	$2\ 605\times10^{-5}$	4.54	1.44
10	99°	3.890	2 790	$1\ 294\times10^{-5}$	4 13	1.58
50	106°	3 870	2.790	2.597×10^{-6}	3.49	1.52
100	112°	3.860	2.790	1.301×10^{-6}	3.07	1.67

From Table IV it may be clearly seen that the radii of the rotator units, although computed from various data corresponding to different frequencies, are in close agreement and they all lie within a narrow region around the most probable value of 1.5 Å.

The smallness of these values is one of their most striking features. From the molecular structure of abietic acid, as given by Ruzicka and his co-workers (1932, 1933), it is quite evident that ester gum, which is mainly a glycerol ester of abietic

acid, can not in any possibility have such a small dimension if we assume the whole molecule to rotate in response to the alternating field. On the other hand, the value of the radius of OH group has been fairly established from X-ray and other methods as having 1.5 Å. The exact coincidence of these two values suggests that perhaps it is the hydroxyl group in the ester gum molecule which mainly participates in the orientation when placed in an alternating field instead of the whole molecule.

Hartshorn and co-workers (1940) arrived at a similar conclusion in case of some synthetic phenolic resins. One of us (Bhattacharya, 1944) also demonstrated that in case of several lac resins the rotator unit was the hydroxyl group.

Ester gum is obtained commercially by the esterification with glycerol of wood rosin about 98% of which is abietic acid. Abietic acid molecule contains only one —COOH group, according to the structure suggested by Ruzicka and co-workers (1932, 1933). Glycerol, being a trihydric alcohol, would require three molecules of abietic acid for complete esterification to form glyceryl tri-abietate and no free hydroxyl group is expected in this ester. Doubts naturally arise as to the propriety of identifying the rotating unit in the ester gum molecule with hydroxyl group. But Ellis (1935) has pointed out that complete esterification is very difficult in the formation of ester gum from glycerol and abietic acid and in usual practice ester gum obtained consists of glyceryl tri-abietate together with some amounts of mono- and di-abietates. In the glyceryl mono- or di-abietates one or two of the three hydroxyl groups of glycerol remain unesterified. Perhaps it is these unesterified hydroxyl groups which contribute towards the dipole orientation and their dimensions have been obtained in the calculation of the rotator size.

ACKNOWLEDGMENTS

The authors are grateful to the Government of India, the Ministry of Education, for a grant-in-aid under fundamental research for the purchase of some equipment used in this investigation. They also wish to express their thanks to Messrs, Napier Paint Works Ltd. for the supply of a sample of ester gum.

REFERENCES

Bhattacharya, G. N., 1944, *Ind. J. Phys.*, **18**, 1.
Bhattacharya, G. N., 1946, *J. Sc. and Ind. Res*, **4B**, 713.
Ellis, C., 1935, The Chemistry of Synthetic Resins, (Reinhold Publishing Corporation., New York), **1**, 791.
Fuoss, R. M., and Kirkwood, J. G., 1941, *J. Amer. Chem. Soc.*, **63**, 385.
Hartshorn, L., Megson, N. J. L. and Rushton, E., 1940, *Proc. Phys. Soc.*, **52**, 796.
Ruzicka, L., Ankersmit, P. J. and Frank, B., 1932, *Helv. Chim. Acta.*, **15**, 1289.
Ruzicka, L., Waldman, H., Meier, P. J. and Hosli, H., 1933, *Helv. Chim. Acta*, **16**, 169.
Sen, A. K. and Bhattacharya, G. N., 1957, *J. Assoc. App. Physicistis*, **4**, 72.
Wagner, K. W., 1913, *Electrotech. Zeit.*, **34**, 1279.
Yager, W. A., 1936, *Physics*, **7**, 434.

VELOCITY OF ULTRASONIC WAVES IN SOLUTIONS OF ELECTROLYTES

SATYA PRAKASH AND SATISH CHANDRA SRIVASTAVA*

(DEPARTMENT OF CHEMISTRY, ALLAHABAD UNIVERSITY)

(*Received for publication August* 21, 1957)

ABSTRACT. An equation for the velocity of ultrasonic waves in solutions of electrolytes has been developed on the basis that electrostatic forces between the ions increase the pressure whereby the volume elasticity is increased, increasing the velocity.

Mohanty and Deo (1955) published their results on ultrasonic velocities in zinc and magnesium sulphate solutions at different concentrations and over different ranges of temperatures. Similar experimental results published by Krishnamurthi (1950, 51) are available for solutions of electrolytes like potassium iodide, potassium bromide, potassium fluoride, sodium fluoride, sodium nitrate, potassium nitrate, strontium nitrate and barium nitrate.

Whereas it is easier to explain the variation of ultrasonic velocities in case of solutions of non-electrolytes, the treatment becomes extremely difficult for solutions of electrolytes.

Salts are ionised in solution and consequently the electrostatic forces exerted by the ions cause an extra local pressure and since the pressure of the liquid is increased, the liquid becomes harder to compress, *i.e.*, the compressibility β or $-\frac{dv}{vdp}$ decreases. In other words, we may also say that back and forth motions of the particles or the ions are guided by two forces; firstly, the normal pressure P experienced by the particles as if the salt was non-ionised and secondly, the pressure P' due to the electrostatic forces in case of electrolytes. These two pressures combined together, contribute towards the compressibility of, or the velocity in, the solutions of the electrolytes. From the equations,

$$I = 2\pi\nu V d A^2 \qquad \ldots \quad (1)$$

$$\dot{x} = 2\pi\nu A \qquad \ldots \quad (2)$$

$$p = -\frac{K}{V} \cdot \dot{x} \qquad \ldots \quad (3)$$

we may write,

$$V = \frac{p^2}{2Id} \qquad \ldots \quad (4)$$

* Present address—Department of Physical Chemistry, I.A.C.S., Calcutta-32.

where I is the intensity of ultrasonic waves in ergs/sec/sq. cms. ν is the frequency; V is the velocity of the waves in the medium, d is the density of the solution; A is the maximum particle displacement ; $\dot{x}$ is particle velocity; K is the volume elasticity.

As already stated this pressure p is the sum of the two pressures P and P' and equation (4) may be written as,

$$V = \frac{(P+P')^2}{2Id} \qquad \ldots \quad (5)$$

Now P' may be calculated as given below The potential of an ion in solution may be written from Debye-Huckel theory of electrolytes as

$$\psi_i = \mp \frac{Z_i \epsilon \kappa}{D} \qquad \ldots \quad (6)$$

where Zi is the valency of an ion, ϵ is electronic charge, D is dielectric constant of the medium and

$$\kappa = \left(\frac{4\pi\epsilon^2 \Sigma\, n_i Z_i^2}{DkT} \right)^{1/2} \qquad \ldots \quad (7)$$

(where k is Boltzmann constant given by $\frac{R}{N}$; N being the Avogadro number and R the gas constant, T is temperature, n_i is the number of ions per c.c. of ith kind.

From the well known laws of electrostatics the force per unit area between two charged particles at a potential difference of ψ is given by

$$\text{force per unit area} = \frac{D\psi^2}{8\pi}$$

where D is the dielectric constant of the medium. Hence force per unit area, *i.e.* pressure is given by

$$P' = \frac{D\left(\mp \frac{Z_i \epsilon \kappa}{D}\right)^2}{8\pi}$$

$$= \frac{Z_i^2 \epsilon^2 \kappa^2}{8\pi D} \qquad \ldots \quad (8)$$

Thus from equations (5) and (8)

$$V = \frac{\left[P + \frac{Z_i^2 \epsilon^2 \kappa^2}{8\pi D}\right]^2}{2Id} \qquad \ldots \quad (9)$$

Equation (9) may be simplified with the help of the following equations,

$$\frac{NC_i}{1000} = n_i \qquad \ldots \quad (10)$$

$$\Sigma\, C_i\, Z_i^2 = 2\mu \qquad \ldots \quad (11)$$

where C_i is the number of gm. ions per litre ; μ is ionic strength.

The final form of the equation may be written as,

$$V^{\frac{1}{2}} = \frac{P}{(2Id)^{\frac{1}{2}}} + \frac{BZ_i^2\,(2\mu)}{D^2T(Id)^{\frac{1}{2}}} \qquad \ldots \quad (12)$$

where $$B = \frac{N^2 \,.\, c^4}{1000 \,.\, 2\sqrt{2R}}$$

Assuming the pressure P in equation (12) to be constant (this includes one constant term and the other term for osmotic pressure which can be expanded for accuracy) to an extent of approximation, equation (12) represents a straight line. In figure 1 we have plotted $(V \,.\, d)^{\frac{1}{2}}$ against μ (ionic strength) from the

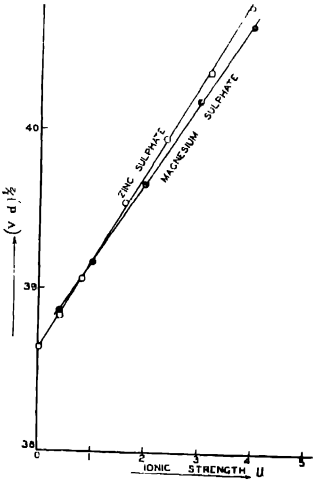

Fig. 1.

data published by Mohanty and Deo (loc. cit), for zinc and magnesium sulphate. The graphs are straight lines. It is interesting to note, as is expected from our

equation, that the slopes of the straight lines for the two electrolytes are almost the same.

ACKNOWLEDGMENTS

We owe our best thanks to Dr. Bal Krishna for his kind suggestions.

REFERENCES

Krishnamurthi, Bh., 1950, *J. Sci. Ind. Res.*, **9B**, 251,
" " 1951 *ibid.*, **10B**, 149, 1951.
Mohanty, B. S. and Deo, B. B., *Ind. J. Phys.*, 1955, **29**, 578.

1. GRAPH 1. Plot of $(V.d)^{\frac{1}{2}}$ against μ,

10

A COMPARATIVE STUDY OF BETATRON AND DIRECT INJECTION IN THE ELECTRON SYNCHROTRON PROPOSED FOR THE INSTITUTE OF NUCLEAR PHYSICS, CALCUTTA.

M. N. VISWESVARIAH AND S. K. SEN

INSTITUTE OF NUCLEAR PHYSICS, CALCUTTA

(*Received for publication July* 16, 1957)

ABSTRACT. The operation of an electron synchrotron in relation to the types of injection is described briefly and the capture efficiency at the time of start of the synchrotron phase of motion has been calculated. In the two cases the approach of calculation has been different depending on the fact that the motion of electrons towards the end of the betatron phase and the motion at the time of injection from the external injector are different

The merits of the two types of injection have been discussed.

INTRODUCTION

The synchrotron, which has proved a successful successor to the betatron for acceleration of electrons to very high energies (up to theoretical limit of 2 GEV), is derived from the classical principles of Veksler (1945) and McMillan (1945). It has an a.c. magnet as in the betatron, but the acceleration is provided by an r.f. system as in the cyclotron.

Goward and Barnes (1946) first demonstrated the practical possibility of the electron synchrotron by converting a 4 Mev betatron into an 8 Mev synchrotron simply by increasing the magnet excitation and placing an r.f. resonator outside the donut.

Figures (1) and (2) are block dragrams of the components of a typical machine.

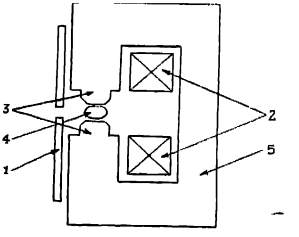

Fig. 1. A "C" Section of synchrotron magnet
1. Betatron flux bar
2. Magnet excitation windings
3. Magnet poles
4. Acceleration chamber or donut
5. Magnet flux return path

Injection into a betatron started synchrotron takes place at 50 to 100 KV from an electron gun and electrons are accelerated by betatron action up to relativistic energies. In 'direct' injection electrons of 2 to 3 Mev are injected into

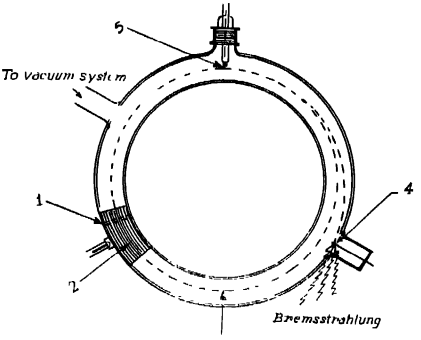

Fig. 2. Details of acceleration chamber or donut
1. Acceleration gap
2. Quarter wave resonator
3. Equilibrium or bit
4. Target
5. Electron gun (injector)

the synchrotron from a linac, Van de Graaff, pulse transformer etc. (Salvini 1955). In the betatron phase of motion, the electrons move in instantaneous orbits which start from the injector position. The instantaneous orbits contract towards the equilibrium orbit r_0 as the energy of the electrons increases along with the increase of the magnetic field. Electrons which are not exactly on their instantaneous circles execute radial and vertical oscillations about the instantaneous circles. The frequency of these radial and vertical oscillations are proportional to $(1-n)^{\frac{1}{2}}$ and $n^{\frac{1}{2}}$ respectively (Kerst 1941) where n is known as the magnetic field index and is given by $-\frac{r}{H}\frac{dH}{dr}$. The amplitudes of these oscillations decrease as the energy increases. Towards the end of the betatron phase of motion, the electron oscillation amplitudes are so small that their effect when the synchrotron phase of motion begins can be neglected.

In the case of 'direct' injection or injection at relativistic energy from an external injector, there is no increase of energy during the time of injection and the instantaneous circles contract due to the increase of magnetic field.

The amplitude of oscillation of electrons which are not on their proper orbits do not decrease but remain as free oscillations. So when the synchrotron action begins there are electrons with free oscillation amplitudes ranging from zero to the clearance between the injector and the stable orbit.

Calculation of efficiency of capture into synchronous motion will depend on the type of motion the electrons are undergoing before the synchrotron phase begins.

GENERAL THEORY

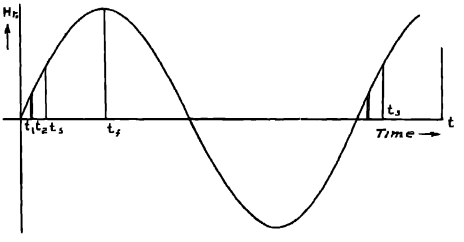

Fig. 3(a). Variation of magnetic field with time and timing of events in betatron injection

Event	Total energy	Time from zero field	Magnetic field at r_0
t_1 (Injection start)	0.56 Mev	9.5 μ Sec	30 gauss
t_2 (Injection stop)	,,	10.22 μ Sec	32 gauss
t_s (R.F.on)	2 Mev	84.9 μ Sec	267 gauss
t_f (R.F.off)	75 Mev	50000 μ Sec	10 K Gau s

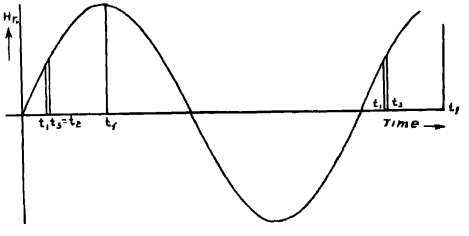

Fig. 3(b). Magnetic field *vs* time and time of event in direct injection

Event	Total energy	Time from zero field	Magnetic field at r_0
t_1 (Injection starts)	2 Mev	82 μ sec	258 gauss
t_2 (Injection Stops R.F. on) $=t_s$	,,	84.7 μ sec	266 gauss
t_f (R.F. off)	75 Mev	5000 μ sec	10, K gauss

Figure 3 (*a*) & (*b*) shows the variation of magnetic field with time at any radius r. The magnetic field varies with radius and time according to the formula

$$H = H_{max}\left(\frac{r}{r_0}\right)^n \sin 2\pi f_m t \tag{1}$$

where H_{max} = maximum magnetic field at the equilibrium orbit radius r_0,
f_m = frequency of magnetic field.

The frequency of the r.f. cycle and the relation of magnetic field with electron energy are given by (Livingston 1954).

$$f_S = \frac{C}{2\pi r_0} \tag{2}$$

$$H = \frac{[E^2 - E^2_0]^{1/2}}{Cer_0} \tag{3}$$

where E_0 = rest energy of the electron.
e = electronic charge in e.s.u.
C = velocity of light

The case of betatron injection.

The spread of radii at the end of the betatron phase and the spread of radii at its beginning are related by

$$\rho_0 = \rho_I\left(\frac{E_I\beta_I}{E_S\beta_S}\right) \tag{4}$$

where ρ_0 = radial spread at the end of betatron phase.
ρ_I = initial spread of radii
E_I = injection energy
E_S = final energy (betatron phase)
β = velocity of electron/velocity of light

The equation of motion of an electron captured into synchronous motion is shown to be an oscillation in phase about a mean positive phase with respect to the r.f. wave (McMillan, 1945, Bohm and Foldy, 1946, Frank 1946). This phase oscillation corresponds to a radial oscillation given by (Goward, 1949).

$$\rho = \frac{\rho_S}{\sqrt{2}}\,[\cos\theta + \cos\theta_S - (\pi - \theta_S - \theta)\sin\theta_S]^{1/2} \tag{5}$$

ρ_S corresponds to amplitude of oscillation when $\theta_S = 0$, where θ_S is the equilibrium phase angle.

$$\text{Capture efficiency} = \frac{\text{area common to the proper } \theta_S \text{ curve and rectangle}}{\text{area of rectangle.}}$$

(See figure 4)

The case of Direct Injection.

In this case, as these are electrons with all possible amplitudes of free oscillation between 0 and ρ_I, where ρ_I is the clearance between injector and stable orbit, the condition for capture is that the sum free and synchrotron oscillation amplitudes should be less than ρ_I. From this it can be shown that (Persico, 1955)

$$X_M \leqslant \rho_I - \frac{\sigma}{T} t \tag{6}$$

where X_M = synchrotron oscillation amplitude
σ = orbit contraction per rotation
T = period of one rotation
t = instant of injection during injection interval.

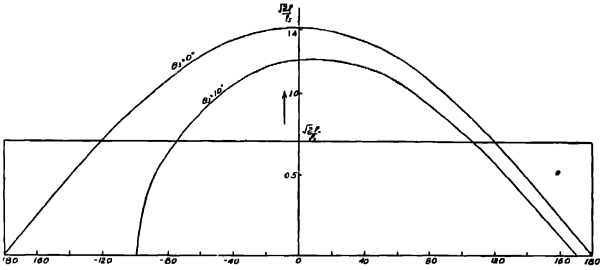

Fig. 4.

X^2_M can be shown to be proportional to a function $\eta(\theta)$ given by

$$\eta(\theta) = [F(\theta) - F(\theta_{max})]$$

where

$$F(\theta) = \frac{\cos\theta}{\sin\theta_s} + \theta$$

Figure (5) is plot of $\eta(\theta)$ against θ. With $\eta(\theta)$ calculated from X_M, as ordinate, a horizontal line is drawn in figure (5). The length of this straight line intercepted by the curve of figure (5) divided by an abscissa length corresponding to 2π gives the captured fraction of electrons injected at time t.

Several such fractions are calculated and plotted in figure (6), where a rectangle is also drawn with ordinate equal to unity (the area of this rectangle corresponds to the number of electrons injected).

$$\text{Capture efficiency} = \frac{\text{area below the curve of figure (6)}}{\text{area of rectangle}}$$

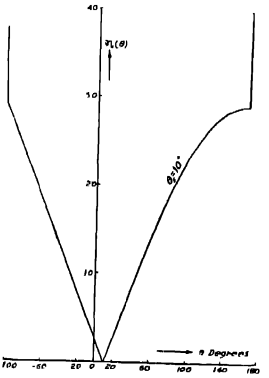

Fig. 5.

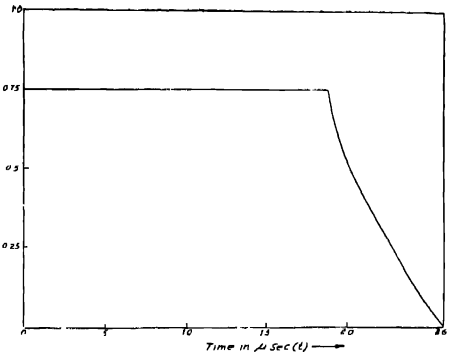

Fig. 6.

Based on these ideas our calculations give the results shown in Tables I, II and III.

TABLE I

Table of common parameters for the electron synchrotron with betatron or direct injection

Parameter	Symbol	Value
Final energy of beam energy	E_f	75 Mev
Peak magnetic field at stable orbit	H_{max}	10^4 gauss
Stable orbit radius	r_0	25 cms.
Peak accelerating voltage	V	725 volts
Radio frequency	f_S	191 Mc/s.
Magnetic field frequency	f_m	50 c/s.
Magnetic field index	n	0.7
Equilibrium phase angle	θ_S	10°
Maximum increase in voltage per rotation	v_0	125 volts
Distance of injector from equilibrium orbit	ρ_I	3 cms.

TABLE II

Additional specifications for betatron injected synchrotron

Parameter	Symbol	Value
Injection energy	E_I	50 K.V. (kinetic)
Starting of time of injection after the magnetic field rises from zero value	t_1	9.5 microseconds
End of injection	t_2	10.22 ,,
Time when betatron stops and R.F. is made on	t_S	84.7 ,,
Electron energy at transition	E_S	2 Mev.
Spread of radii at the end of betatron phase	ρ_0	0.3476 cm.
Size of donut (with elliptical section)	—	4.7 inches half width
	—	3.1 inches half height
The operating pressure	—	1×10^{-5} mm. of Hg.
The max. vertical amplitude due to gas scattering which is attained at four times the injection energy (using Blachman and Courant theory)	—	1 cm.
Fraction of electrons at the end of betatron phase accepted into stable synchronous orbit	—	64.28%

TABLE III

Direct injection parameters

Parameter	Symbol	Value
Injection energy	E_I	2 Mev.
Time of injection start	t_1	82.1 micro-sec.
Time of end of injection and R F. on	$t_2 = t_S$	84 7 micro-sec.
Donut dimensions—semi major axis	—	4 5″
semi minor axis	—	2.2″
The operating pressure about	—	1×10^{-5} mm. Hg.
At $3\ 6 \times 10^{-6}$ mm. of H_g the max. vertical amplitude due to gas scattering	—	0.003676 cm.
Fraction of electrons absorbed into stable orbits after missing the injector	—	64 88%

DISCUSSION

For injection at 50 KV, the magnetic field at the start of injection should be 30 gauss and for injection at 2 Mev the field should be 266 gauss. A higher magnetic field at the time of injection means less difficulty of controlling and shaping the magnetic field.

The theory of gas scattering as worked out by Blackman and Courant (1948) has been shown by Riddiford (1951) to explain approximately the minimum vertical cross section of the donut observed in synchrotrons below which the output of the machine falls rapidly to zero (Elder, Langmuir, Pollock 1948). Using Riddiford's approach we find that the contribution to the oscillation amplitude is negligible in the case of high energy injection Thus the donut can be operated at higher pressures or the dimensions of the donut can be reduced, as also the cost of the magnet.

The angular spread of an electron beam from a high energy injector is much smaller than that of the conventional betatron injector.

The possibility of electrons missing the injector in the high energy injection case is more than in the betatron injection case as the rate of instantaneous orbit contraction is greater in the former case than in the latter.

The case of betatron injection is simpler, as the additional flux needed is derived by flux bars attached to the poles of the main magnet. In the case of direct injection much additional equipment is needed to bend the high energy beam along the direction of the circular orbits.

High energy injection becomes more and more economical as the maximum energy for which the synchrotron is designed increases as the cost of the injector is nearly the same for all machines.

ACKNOWLEDGMENTS

Our acknowledgments are due to Prof. B. D. Nag, Director of the Institute of Nuclear Physics, who entrusted this work to us and for his constant guidance and several helpful discussions during the course of this study. Our grateful acknowledgments are also due to the Atomic Energy Commission under whose auspices the synchrotron project has been undertaken.

REFERENCES

Bohm, D and Foldy, L , 1946, *Phy. Rev* . **70**, 764.
Blackman, M. and Courant, E. D , 1948, *Phy. Rev.*, **74**, 140
Elder, Langmuir, Pollock, 1948, *R. S. I.*, **19**, 121.
Frank, N. H , 1946, *Phy. Rev* , **70**, 177
Goward, F. K. and Barnes, D E , 1946, *Nature*, **158**, 413
Goward, F. K., 1949, *Proc of Phy. Soc. A.*, **62**, 617.
Kerst, D. W. and Serber, R., 1941, *Phy. Rev.*, **60**, 53
Kaiser, T R , 1950, *Proc. Phy Soc A.*, **63**, 52
Livingston, M. S., 1954, High Energy Accelerators, p 39.
MacMillan, E. M., 1945, *Phys. Rev.*, **68**, 143
Persico, E., 1955, *Nuo Cemento*, Series X Vol. II Suppl. I., p. 459.
Riddiford, L., 1951, *Proc. Phy. Soc.* (*Lond*), **64A**, 10
Salvini, G., 1955, *Nuo Cemento*. Suppl. I to Vol II, Series X, p. 442
Veksler, V., 1945, *J Phys. U S S R* , **9**, 153.

A WARBLE TONE GENERATOR

R. R. DUTTA GUPTA

DEPARTMENT OF COMMUNICATION ENGINEERING, INDIAN INSTITUTE OF TECHNOLOGY KHARAGPUR, INDIA

(*Received for publication, July* 25, 1957)

ABSTRACT. A warble tone generator using a simple phase shift oscillator has been described. Actually two similar oscillators are used, one having a very low fixed frequency corresponding to the frequency of wobbulation This low frequency oscillator voltage is applied to the grid of a triode which is used as a variable resistance element in the main oscillator of varying frequency. The relative importance of the different R C sections of a phase-shift oscillator from the point of view of frequency stability has also been discussed. It has been shown, for example, that the variation of the first resistance of the three sections gives maximum percentage variation of frequency

1. INTRODUCTION

The need of a warble tone generator in acoustic measurements is well known. Thus in measurement of reverberation time of an auditorium if a pure tone is sounded it is likely that a number of normal modes will be excited. As a result, when the sound source is turned off, the sound pressure at any point in the auditorium decays in an irregular manner. Such irregularities can be reduced by using a warble tone

Hunt (1936) and Burger (1943) have described methods of producing warble tones. The former uses a rotating condenser which is connected in parallel with the main capacitance of an $L-C$ circuit and this in turn varies the frequency of the oscillator circuit. The latter, however, uses a multivibrator for generating a sawtooth wave which is then amplified by a valve whose average plate current also serves to magnetize the core of a variable reactor which is connected to its plate. This variable reactor, in parallel with condensers connected across it, forms a frequency modulated oscillator circuit. In Hunt's method one has to use a mechanically rotating part which, from the point of view of operation, is not quite convenient. Burger's method of producing warble tone is, on the other hand, very round about. In the following is described a new type of warble tone generator which is very simple in design and at the same time avoids all mechanically rotating parts.

2. PRINCIPLE OF THE NEW GENERATOR

The circuit of the new warble tone generator is shown in figure 1. It represents a conventional phase shift oscillator [Ginzton and Hollingsworth 1941,]

with three sections of resistance capacitance networks at the output of the 6AC7 oscillator tube. The plate load R_L is chosen to be low so that the 6AC7 plate voltage is exactly 180° out of phase with regard to its grid voltage. The additional

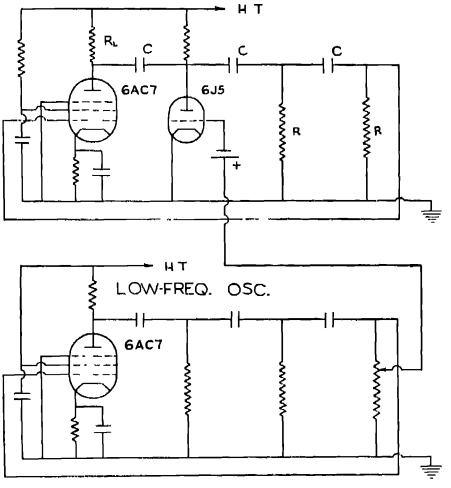

Fig. 1. Circuit diagram of the warble tone generator.

180° phase shift for oscillations to occur is provided by the *R-C* sections as usual. The 6J5 triode acts as a variable resistance tube which is effectively connected in shunt with the resistance on its plate. The variation of this resistance gives 180° phase shift in the network at different frequencies and thus the oscillator frequency changes. The degree and speed of frequency modulation depends respectively upon the voltage and frequency applied at the grid of the modulation tube 6J5. This voltage is supplied from a similar low frequency phase shift oscillator.

In the circuit of figure 1 the first resistance of the three R-C sections was varied because this gives maximum frequency modulation. Considering the simplified circuit as given in figure 2., we can write

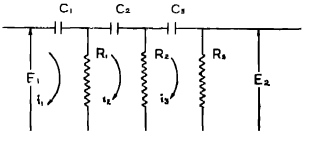

Fig. 2. Phase shifting network

$$\begin{bmatrix} E_1 \\ 0 \\ 0 \end{bmatrix} = [Z] \begin{bmatrix} i_1 \\ i_2 \\ i_3 \end{bmatrix}$$

where $[Z]$ = matrix of the transformation.

$$= \begin{bmatrix} \left(R_1+\frac{1}{j\omega C_1}\right) & -R_1 & 0 \\ -R_1 & \left(R_1+R_2+\frac{1}{j\omega C_2}\right) & -R_2 \\ 0 & -R_2 & \left(R_2+R_3+\frac{1}{j\omega C_3}\right) \end{bmatrix}$$

or,
$$\begin{bmatrix} i_1 \\ i_2 \\ i_3 \end{bmatrix} = [Z]^{-1} \begin{bmatrix} E_1 \\ 0 \\ 0 \end{bmatrix}$$

where, $[Z]^{-1}$ = inverse matrix of $|Z|$

If $|Z|$ = network determinant,

$$i_3 = \frac{E_1 R_1 R_2}{|Z|}$$

or, transfer function $T = \frac{E_2}{E_1} = \frac{R_3 i_3}{E_1} = \frac{R_1 R_2 R_3}{|Z|}$ ... (1)

For oscillation to take place, phase shift in the network must equal π. This condition is satisfied if the imaginary part of $|Z|$ vanishes.

Or, $\frac{1}{\omega C_3}\left(R_1^2 - \frac{1}{\omega^2 C_1 C_2}\right) + \frac{R_1(R_2+R_3)}{\omega}\left(\frac{1}{C_1}+\frac{1}{C_2}\right) + \frac{R_2 R_3}{\omega C_1} + \frac{R_1 R_2}{\omega C_3} = 0$

This gives,

$$f = \frac{\omega}{2\pi} = \frac{1}{2\pi\sqrt{\left(\frac{R_1R_2+R_2R_3+R_3R_1}{C_1}+\frac{R_1R_2+R_1R_3}{C_2}+\frac{R_1R_2}{C_3}\right)C_1C_2C_3}} \quad \text{... (2)}$$

Now, if $C_1 = C_2 = C_3 = C$,

$$f = \frac{1}{2\pi C\sqrt{3R_1R_2+2R_1R_3+R_2R_3}} \quad \text{... (3)}$$

From this expression we see that when the three resistances are of the same nominal value and one of them is varied, the change in frequency of oscillation is maximum due to variation of R_1. If, therefore, good frequency stability is required, greatest attention should be given to R_1. On the other hand, if large variation in frequency is wanted by varying one of the three resistances it is R_1 which should be made to vary by the modulating signal.

If, furthermore $R_2 = R_3 = R$, the expression for f becomes,

$$f = \frac{1}{2\pi RC\sqrt{1 + \frac{5R_1}{R}}} \qquad \ldots (4)$$

This is the frequency which holds in our set up.

3 RESULTS

The results of static modulation characteristics of the main oscillator are given in Table I and are plotted in figure 3.

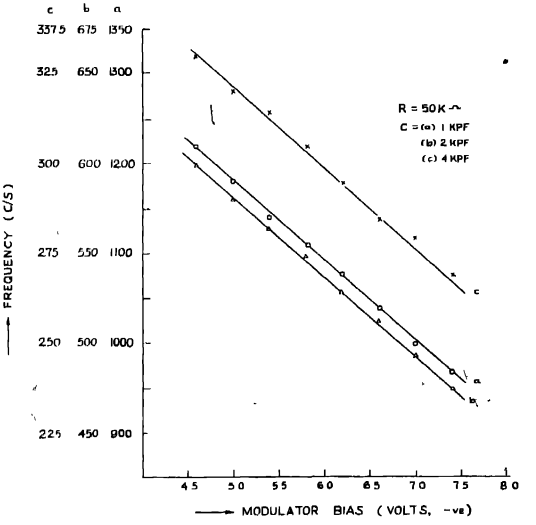

Fig. 3. Static characteristics of the warble tone generator.

TABLE I

Modulator bias (Volts, $-VE$)	Frequency of oscillator (c/s)		
	$R = 50K\ \Omega$ $C = 1\ KPF$	$R = 50K\ \Omega$ $C = 2\ KPF$	$R = 50K\ \Omega$ $C = 4\ KPF$
4.6	1220	600	330
5.0	1180	580	320
5 4	1140	565	315
5.8	1110	550	305
6.2	1080	530	295
6 6	1040	515	285
7.0	1000	495	280
7 4	970	475	270

It is to be noted that the shunt resistances of the R-C sections have been kept fixed and the series capacitances only have been changed for obtaining different centre frequencies, because otherwise both the degree and linearity of modulation would be affected as seen from eqn (4).

It is seen from the above table that linear frequency variation is obtained up to about $\pm$ 12% of the centre frequency. With further increase in deviation, however, the amplitude changes—the smaller the bias the smaller is the resistance 6J5, and lower is the amplitude of oscillation. The amplitude modulation has been found to be quite small over a range of about $\pm$12% of the centre frequency

For effective measurement of reverberation time of an auditorium the warble tone is generally frequency-modulated to about 10% of the centre frequency. Further, as pointed out by Hunt (1933), the ratio of twice the maximum frequency deviation from the mean frequency to the modulating frequency should exceed 3. This meant that the modulating frequency should be less than one-fifteenth of the oscillator mean frequency If the lowest mean frequency be 100 c/s, fm should not exceed 7 and, therefore, if the l f oscillator is designed for a frequency of 7 c/s. all the requirements are fulfilled.

ACKNOWLEDGMENTS

The author records his grateful thanks to Prof. H. Rakshit, D.Sc., F.Inst.P., F.N.I , Head of the Dept. of Electronics and Elec. Communication Engineering, Indian Institute of Technology, for constant encouragement and helpful discussions.

REFERENCES

Burger, B., 1943, *Hochfrequenztechnik und Electroakustik*, **61**, 75.
Ginzton, E. L., and Hollingsworth, L. M., 1941, *Proc. I.R E.*, **29**, 43.
Hunt, F. V., 1933, *Jour. Acous. Soc. Amer.*, **5**, 127.
Hunt, F. V., 1936, *Jour. Acous. Soc. Amer.*, **8**, 34.

HIGH ENERGY NEUTRON-PROTON SCATTERING WITH SPIN-ORBIT INTERACTION.

H. N. YADAV AND L. S. SINGH*

UNIVERSITY DEPARTMENT OF PHYSICS, PATNA UNIVERSITY, PATNA

(*Received for publication, June* 21, 1957)

ABSTRACT The angular distribution and total cross sections have been calculated for high energy n–p scattering in the energy-range 83–415 Mev (laboratory system). The interaction considered is of a symmetrical type with spin-orbit and tensor force in the triplet states. Yukawa potential has been used with ranges 1.18×10^{-13} cm. and 1.60×10^{-13} cm. in the singlet and triplet states respectively. The parameters of the potential are fitted to explain the low energy scattering cross section and the properties of the deuteron. The calculated high-energy cross sections are, as usual, large The symmetrical meson theory with tensor force and spin-orbit interaction does not seem to be capable of explaining the high-energy scattering data.

1. INTRODUCTION

The theoretical investigations of high energy n – p scattering with non-central interaction have been carried out by a number of workers [Ashkin and Wu, (1948), Massey, Burhop and Hu (1948) Hsu and Hu (1948), Eisenstein and Rohrlich (1948), Burhop and Yadav (1948, 1949), Yadav (1952), Castillejo and Richardson (1949), Jastrow (1950, 1951)]. The calculated cross section is too large compared with the experimental results. More recently, Gammel and Thaler (1956), Wertheim, Hull and Saperstein (1956) and Christian, Gammel and Thaler (1957) have performed calculations with phenomenological nucleon-nucleon potential, but the results are, as usual, far from satisfactory.

In view of the present circumstances, it is interesting to see the effect of a velocity dependent force (such as a spin orbit force) in the nucleon-nucleon interaction. Case and Pais (1950) were the first to consider the spin-orbit term of the type L.S., where L is the orbital angular momentum vector and S the spin vector for the two-nucleon system. They used Born approximation to fit the 32 Mev and 350 Mev scattering data using a highly singular radial dependence of potential with L. S. term. But it has been shown by Swanson (1953) that Born approximation gives unreliable results with singular potentials even at very high energy However, the qualitative conclusion of Case and Pais is that L.S. term gives preference to 90° scattering (in the centre-of-mass system), which is exactly what is wanted to explain the scattering data. Also Goldfarb and Feldman (1952)

* Now at the Physics Department, University College, London.

have shown that only L. S. interaction in triplet odd states is incapable of explaining the experimental p—p scattering data.

As no exact calculations with L.S. term in the nucleon-interaction are available since the Born approximation estimate of Case and Pais (1950), the investigation of L. S. potential in high energy nucleon-nucleon scattering deserves further study. Consequently, it was considered worthwhile to undertake the exact calculations with tensor force and spin-orbit term in the triplet interaction with exchange properties given by symmetrical meson theory. Since the present work began, Chnuma and Feldman (1956) made a phase-shift analysis of the experimental cross sections at 150 Mev and their conclusion is that almost every set of acceptable phase-shifts favours the inclusion of spin-orbit potential. The existence of spin-orbit potential in nucleon-nucleon interaction is also supported by the work of Wolfenstein (1956) and also from the success of the shell model for complex nuclei.

The results obtained in the present attempt are large as usual, and possibly the spin-orbit term (along with tensor force), used with conventional potentials (spherical, Gaussian, exponential, Yukawa) is not enough to explain the scattering data. Also the symmetrical theory gives too much backward scattering ($\theta = 180°$) which is not in agreement with experiment except at very high energy $\simeq 300$ Mev. Calculations were performed in the energy range 83 to 415 Mev (lab. system).

2. THE INTERACTION POTENTIAL

(i) *Triplet states* : The interaction potential with exchange properties as given by symmetrical meson theory was chosen as it has been found to fit the experimental data better [Hsu and Hu (1949), Christian (1952)]. The potential taken is of the form

$$^3V = \frac{1}{3}\vec{\tau}_1 \cdot \vec{\tau}_2 \frac{\hbar^2}{Mr_0^2} \left\{ \frac{a}{4} (\vec{\sigma}_1 \cdot \vec{\sigma}_2 + 3) + a\gamma S_{12} + g(\vec{\sigma}_1 \cdot \vec{\sigma}_2 - 1) + a\alpha\, \mathbf{L.S} \right\} v(r/r_0) \quad \ldots \quad (1)$$

where $\vec{\sigma}_1$ and $\vec{\sigma}_2$ are the spin-vector operators, τ_1, τ_2 the corresponding isotopic spin operators and $\mathbf{r}$ the relative position vector for the two particles. S_{12} is the tensor force operator and is equal to $\frac{3}{r^2}\{(\vec{\sigma}_1 \cdot \mathbf{r})(\vec{\sigma}_2 \cdot \mathbf{r})\} - \vec{\sigma}_1 \cdot \vec{\sigma}_2$, a, γ, g, α are dimensionless constants and $v(r/r_0)$ is a function that defines the radial dependence of potential of range r_0; $\mathbf{L.S}$ is the spin-orbit force introduced in the interaction, $\mathbf{L}$ is the orbital angular momentum and S the spin vector for the two-nucleon system. Assuming the radial dependence of potential to be of Yukawa type, the potentials for triplet even and odd states are respectively

$$^3V_{even} = -\frac{\hbar^2}{Mr_0^2} \{a + a\gamma S_{12} + a\alpha \mathbf{L} \cdot \mathbf{S}\} \frac{e^{-r/r_0}}{r/r_0} \quad (2)$$

$$^3V_{odd} = -\frac{1}{3}\,^3V_{even} \qquad \ldots \quad (3)$$

where the triplet range $r_0 = 1.60 \times 10^{-13}$cm.

All the constants were calculated to fit the low energy scattering and the properties of the deuteron in the usual manner (Yadav, 1952 ; Hu and Massey, 1949). The values obtained are

$$a = 1.816\ ; \qquad \gamma = 0.756\ , \qquad \alpha = -0.603.$$

D-state admixture for the ground state of the deuteron = 3.16%

(ii) *Single states* —The singlet potential is

$$^1V = -\frac{\hbar^2}{Mr^2_s}\,\vec{\tau}_1 \cdot \vec{\tau}_2\, g\,\frac{e^{-r/r_s}}{r/r_s} \qquad (4)$$

which for even and odd states become respectively

$$^1V_{even} = -\frac{\hbar^2}{Mr^2_s}\, g\,\frac{e^{-r/r_s}}{r/r_s} \qquad (5)$$

$$^1V_{odd} = +3\,^1V_{even} \qquad (6)$$

This is taken from the calculations of Hsu and Hu (1949) and Breit *et al.* (1952). The constants are, $r_s = 1.18 \times 10^{-13}$ cm., and $g = 1.575$ and fit the results of low energy n–p and p–p scattering correctly.

3. THEORY OF CALCULATION

(i) *Triplet states* — The phase-shifts for the coupled states $^3S_1$ and $^3D_1$ and for uncoupled states $^3P_0$, $^3P_1$ and $^3D_1$ were calculated from the exact solutions of the radial wave equations obtained by numerical integration by Gauss and Jackson method [Jeffreys and Jeffreys, 1946] The phases for higher angular momentum states, being very small, were taken into account by Born approximation. The procedure followed in brief is given below.

Introducing the potential (2) in Schroedinger's equation for the two-body system in the centre-of-mass co-ordinates, we have

$$\Delta^2\psi + \left[\frac{ME}{\hbar^2} - \frac{a}{r^2_0}(1+\gamma S_{12}+\alpha \mathbf{L.S})\ \frac{e^{-r_0/r_0}}{r/r_0}\right]\psi = 0 \qquad \ldots \quad (7)$$

where the eigen value of the $L.\ S.$ operator $= \frac{1}{2}\{J(J+1) - L(L+1) - S(S+1)\}$ J being the total angular momentum vector, $\mathbf{J} = \mathbf{L} + \mathbf{S}$.. Putting the value of

the triplet state wave function (Hu and Massey (1949) in (7), we get after some usual manipulations

$$\left\{\frac{d^2}{dr^2}+\frac{k^2}{r_0^2}-\frac{L(L+1)}{r^2}\right\} f_{JJ_zL} = \left(\frac{M}{\hbar^2}\int \sum_{L'} F^*_{JJ_zL} V F_{JJL'} f_{JJ_zL'}\, d\,\Omega\right)$$

where $k^2 = \frac{ME}{\hbar^2} r_0^2$, and other notations are the same as in the paper referred to above. Introducing the value of ${}^3V_{even}$, the equation for the triplet even state is

$$\left\{\frac{d^2}{dr^2}+k^2-\frac{L(L+1)}{r^2}\right\} f_{JJ_zL} = -\frac{1}{r_0^2}\sum_{L'}\left[a\delta_{LL'}+a\gamma\langle L|S_{12}|L'\rangle\right.$$

$$\left.+a\alpha\,\mathbf{L.S}\;\delta_{LL'}\right] f_{JJ_zL'}\,\frac{e^{-r/r_0}}{r/r_0} \qquad \ldots (9)$$

where the matrix elements $\langle L\,|\,S_{12}\,|\,L'\rangle = \langle \overset{*}{F}_{JJ_zL}\,|\,S_{12}\,|\,F_{JJ_zL}\rangle$

$=2$, for $J = L$, and all other matrix elements vanish. The differential equation for triplet even states for $J = L$, is

$$\left[\frac{d^2}{dx^2}+k^2-\frac{L(L+1)}{x^2}+a(1+2\gamma-\alpha)\frac{e^{-x}}{x}\right] f_{JJ_zL} = 0 \qquad \ldots (10)$$

where $x = \frac{r}{r_0}$

And, for triplet odd states for $J = L$, the equation is the same as (10) with a replaced by $-\frac{a}{3}$.

Considering the case for $L = J-1$, $\langle L|S_{12}|L'\rangle$ has the following values

$$\langle J-1\,|\,S_{12}\,|\,J-1\rangle = -\frac{2(J-1)}{2J+1}.$$

$$\langle J-1\,|\,S_{12}\,|\,J+1\rangle = -\frac{6[J(J+1)]^{\frac{1}{2}}}{2J+1}$$

$$\langle J-1\,|\,S_{12}\,|\,J\rangle = 0.$$

and the eigen value of $L.S = J-1$, for $L = J-1$. The right-hand side of (9) becomes

$$= -\frac{a}{r_0^2}\left[1+\alpha(J-1)-2\gamma-\frac{(J-1)}{2J+1}\right]\frac{e^{-x}}{x} f_{JJ_z,\,J+1} - \frac{6a}{r_0^2}\gamma\,[J(J+1)]^{\frac{1}{2}}$$

$$\times\frac{e^{-x}}{x} f_{JJ_z,\,J+1}$$

and the equation for triplet even states for $L = J-1$, becomes

$$\left[\frac{d^2}{dx^2}+k^2-\frac{L(L+1)}{x^2}+a\left\{1+\alpha(J-1)-2\gamma\frac{(J-1)}{2J+1}\right\}\frac{e^{-x}}{x}\right]f_{JJ_z,\,J-1}$$

$$+6a\gamma\frac{\{J(J+1)\}^{\frac{1}{2}}}{2J+1}\frac{e^{-x}}{x}f_{JJ_z,\,J+1}=0 \qquad \ldots \quad (11)$$

Replacing a by $-a/3$ in the above equation, we get the corresponding equation for triplet odd states.

Finally, for $L=J+1$, $L.\,S=-(J+2)$, and

$<L|S_{12}|L'>$ has the following values

$$<J+1|S_{12}|J+1>=-\frac{2(J+2)}{2J+1}.$$

$$<J+1|S_{12}|J>=0.$$

$$<J+1|S_{12}|J-1>=\frac{6[J(J+1)]^{\frac{1}{2}}}{2J+1}.$$

The right-hand side of (9) is

$$=-\frac{a}{r_0^2}\left[1-\alpha(J+2)-2\gamma\frac{(J+2)}{2J+1}\right]\frac{e^{-x}}{x}\cdot f_{JJ_z,\,J+1}$$

$$-6\frac{a}{r_0^2}\gamma\frac{[J(J+1)]^{\frac{1}{2}}}{2J+1}\frac{e^{-x}}{x}\cdot f_{JJ_z,\,J-1}$$

and, we have the differential equation for even states with $L=J+1$.

$$\left[\frac{d^2}{dx^2}+k^2-\frac{L(L+1)}{x^2}+a\left\{1-\alpha(J+2)-\frac{2\gamma(J+2)}{2J+1}\right\}\frac{e^{-x}}{x}\right]f_{JJ_z,\,J+1}$$

$$+6a\gamma\frac{[J(J+1)]^{\frac{1}{2}}}{2J+1}\frac{e^{-x}}{x}f_{JJ_z,\,J-1}=0 \qquad \ldots \quad (12)$$

and similar equation for odd states with a replaced by $-a/3$.

(ii) *Singlet states* :—

In this case the equations are

$$\frac{d^2u}{dx^2}+\left[k_s^2-\frac{L(L+1)}{x^2}+g\frac{e^{-x}}{x}\right]u=0 \qquad \ldots \quad (13)$$

for even states.

and

$$\frac{d^2u}{dx^2}+\left[k_s^2-\frac{L(L+1)}{x^2}-3g\frac{e^{-x}}{x}\right]u=0 \qquad \ldots \quad (14)$$

for odd states.

where $k_s^2 = \frac{ME}{\hbar^2} r_s^2$, $x = r/r_s$, and u = wave function for the state in question; r_s = the range in singlet states = 1.18×10^{-13} cm.

The equations for $^3S_1 + {}^3D_1$, $^3P_0$, $^3P_1$, and $^3D_2$ states were solved exactly, the method of obtaining the initial solution and the procedure followed are outlined by Mott and Massey (1949). Similarly for the singlet $^1S_0$, $^1P_1$ and $^1D_2$ states exact solutions were performed. The phase shifts for the above-mentioned states were calculated. In order to take the higher states into account by Born approximation, phases were also calculated for the above states by Born approximation following Ashkin and Wu (1948). The procedure for taking into account the higher angular momentum states has been given by one of us [Yadav, 1952]. The scattering cross sections were also calculated entirely by Born approximation for comparison. The method of calculating the matrix elements for scattering amplitudes in Born approximation is well known [Burhop and Yadav, 1949; Askhin and Wu, 1948] and will not be given here.

4. RESULTS

The phases are given in radians in Table I, and the angular distribution in 10^{-26} cm.^{2}/sterad. in Table II. The real and imaginary parts of the triplet coupled phases satisfied the relations given by Rarita and Schwinger (1949).

In the table, A stands for $(e^{2i\eta} - 1)$, and B for $2i\delta$; where η = exact phases, and δ = phases calculated by Born approximation, m = magnetic quantum number = 0, $\pm$ 1.

TABLE I

(a) Triplet coupled phases for states $^3S_1$ and $^3D_1$.

Energy in Mev.		$^3S_1$		$^3D_1$	
		$m = \pm 1$	$m = 0$	$m = \pm 1$	$m = 0$
83	A.	$-1.604+0.860i$	$-1.418+0.784i$	$-0.151+0.264i$	$+0.034+0.188i$
	B.	$+1.164i$	$+1.799i$	$-0.131i$	$+0.496i$
166	A.	$-1.253+1.026i$	$-1.012+0.876i$	$-0.208+0.374i$	$+0.032+0.225i$
	B.	$+1.083i$	$+1.586i$	$+0.078i$	$+0.520i$
249	A.	$-1.051+1.053i$	$-0.791+0.856i$	$-0.234+0.435i$	$+0.028+0.237i$
	B.	$+1.032i$	$+1.335i$	$+0.205i$	$+0.508i$
332	A.	$-0.916+1.047i$	$-0.649+0.818i$	$-0.245+0.470i$	$+0.022+0.240i$
	B.	$+0.993i$	$+1.194i$	$+0.290i$	$+0.491i$
415	A.	$-0.818+1.032i$	$-0.549+0.778i$	$-0.251+0.496i$	$+0.020+0.242i$
	B.	$+0.963i$	$+1.086i$	$+0.349i$	$+0.472i$

TABLE I (*contd.*)

(b). Triplet uncoupled phases

Energy in Mev.	Phases	$^3P_0$	$^3P_1$	$^3D_2$
83	η (exact)	+0 130	−0.180	+0 602
	δ (Born)	+0.069	−0 263	+0.344
166	η	+0.119	−0.224	+0.644
	δ	+0.075	−0 285	+0 448
249	η	+0.111	−0.236	+0.655
	δ	+0 075	−0.286	+0.489
332	η	+0.106	−0.241	+0.650
	δ	+0.074	−0 283	+0.509
415	η	+0.101	−0.240	+0.643
	δ	+0 073	−0 278	+0.518

(c). Singlet phases

Energy in Mev.	Phases	$^1S_0$	$^1P_1$	$^1D_2$
83	η (exact)	+0 771	−0.345	+0.314
	δ (Born)	+0 628	−0.559	+0 066
166	η	+0 665	−0 486	+0 272
	δ	+0.589	−0.669	+0 100
249	η	+0.604	−0.543	+0.263
	δ	+0.554	−0.704	+0.117
332	η	+0 563	−0.574	+0.254
	δ	+0.525	−0.716	+0 128
415	η	+0.531	−0.591	+0.248
	δ	+0 502	−0.718	+0.134

TABLE II

(a) Exact differential cross section $\sigma(\theta)$ in 10^{-26} cm.^{2} sterad. (θ = angle of scattering in the centre-of-mass system).

θ \ Energy in Mev.	83	166	249	332	415
0	3.484	3.171	3.199	3.268	3.341
15	2.794	1.738	1.419	1.362	1.267
30	2.066	1 041	0.695	0.507	0 392
60	0.861	0.349	0.201	0.134	0.098
90	0.630	0.234	0 130	0.084	0.060
120	1.067	0.471	0.276	0 184	0.128
150	4.179	2.572	1.828	1.375	1.079
165	6.684	5.656	5.421	5.205	4.960
180	7 472	6.215	5.972	5.890	5.875

(b) Born differential cross sections

θ \ Energy	83	166	249	332	415
0	3.558	3.791	3 892	3 950	3.987
15	1.295	1 274	1.275	1.250	1.204
30	0 783	0.522	0.383	0.295	0.234
60	0.303	0.120	0.067	0.043	0 031
90	0.380	0.146	0.079	0 050	0.035
120	0.973	0.450	0.265	0 177	0.113
150	3.305	2.335	1.727	1.328	1.054
165	5 344	5.376	5 354	5.218	5 001
180	6.043	6.132	6.171	6.192	6.206

(c) Total collision cross sections (in 10^{-26} cm.^{2}/sterad).

Energy in Mev.	Exact	Born	Experimental	References
83	19.34	12.99	8 3	Cook et al. (1947, 1949); Hadley et al. (1948, 1949); Dejuren (1950); Wallace (1951); Selove et al. (1953); Chin (1954); Stahl & Ramsay (1954); Chin and Powell (1957).
166	10.81	8.59	5.1	Dejuren et al. (1950, 1951); Randle et al. (1952); Taylor et al. (1951, 1953).
249	8.10	7.34	3 9	Pangher (1955); Dejuren (1950) a 269 Mev.
332	6.39	5.63	3.6	Pangher (1954, 1955) at 302 Mev. t
415	5.64	5 06	3 3	Nedzel (1953, 1954) at 410 Mev. Hartzler et al (1954) at 400 Mev.

5. DISCUSSION AND CONCLUSION

The calculated differential cross sections are much larger than the observed ones. The total cross sections obtained by Born approximation is in better agreement with experiments than the exact ones, but the former are unreliable and sometimes misleading It has been found that though the differential cross sections do not differ markedly, the partial singlet and triplet cross sections are not so. The singlet Born cross section $\sigma_s(\theta)$ is higher than the exact one, but opposite is the case for triplet cross sections $\sigma_{tr}(\theta)$ and as such when $\sigma_s(\theta)$ and $\sigma_{tr}(\theta)$ are combined to give the differential cross section $\sigma(\theta)$, an agreement is obtained. Moreover, the minimum in the cross section occurs near 60° in Born approximation, while the exact calculation gives a minimum near 90° in agreement with experiments. Also the theoretical cross section is asymmetric about 90°, $\sigma(\pi)/\sigma(0) =$ 2.1—1.8 in the energy range 83—415 Mev. This asymmetry has been observed experimentally at high energy $\sim$ 300 Mev by Pangher (1954, 1955) who found $\sigma(\pi)/\sigma(0) = 2$ nearly This is in sharp contradiction to the predictions of the Serber potential which was invoked to offer an explanation for the deep minimum and the almost symmetry about 90° near 90 Mev.

As the Yukawa potential gives the lowest cross sections (Burhop and Yadav, 1949), the L.S term used with other conventional potentials (spherical, exponential, and Gaussian) will give still larger values of cross section in disagreement with observed facts.

It seems that possibly the analysis of the high energy data in terms of static potential is doomed to a failure. We know that in the energy-range considered here, mesons are produced in nucleon-nucleon collisions and as such mesonic

structure of the nucleons may play a significant role in scattering. It is probable that the meson cloud, which surrounds the nucleons and which is responsible for interaction between the nucleons, is polarized in high energy collisions. This polarization of the meson cloud round the nucleon would be expected to lead a marked change in the apparent interaction (Sachs, 1955) which may affect the scattering results considerably.

ACKNOWLEDGMENTS

The authors wish to express their indebtedness to Dr. E. H. S. Burhop (Physics Department, University College, London) for his keen interest and advice in the calculation. Thanks are also due to Dr R. A. P. Singh for his kind help in determining the constants of interaction in triplet states and to Professor B. N. Singh for providing us facilities for work.

REFERENCES

Ashkin, J., and Wu, T. Y., 1948, *Phys. Rev.*, **73**, 973.
Burhop, E. H. S., and Yadav, H. N , 1948, *Nature*, **162**, 738.
,, ,, ,, ,, , 1949, *Proc. Roy. Soc A* , **197**, 505.
Case, K. M., and Pais, A., 1950, *Phys. Rev* , **79**, 185.
,, ,, , *ibid.*, **80**, 203.
Castillejo, L., and Richardson, H. T., 1949, *Phys. Rev.*, **76**, 1732.
Chih, C. Y., and Powell, W. M., 1957, *Phys Rev.*, **106**, 539
Christian, R. S., 1952, *Report on Prog. in Phys.*, **15**, 68.
Cook, L. J., McMillan, E. M., Peterson, J. M , and Sewell, D. C., 1947, *Phys. Rev.*, **72**, 1264.
,, ,, ,, ,, 1949, *Phys. Rev.*, **75**, 7.
De juren, J., 1950, *Phys. Rev.*, **80**, 27.
De juren, J., and Moyer, B. J., 1951, *Phys Rev.*, **81**, 919.
Eisenstein, J. and Rohrlich, F., 1948, *Phys. Rev.*, **73**, 641 & 1411.
Goldfarb, L. J. B., and Feldman, D , 1952, *Phys. Rev.*, **88**, 1099.
Gammel, J. L., and Thaler, R M , 1956, *Phys. Rev.*, **103**, 1874.
Gammel, J. L., Christian, R. S. and Thaler, R M., 1957, *Phys. Rev* , **105**, 311.
Hadley, J., Kelly, E., Leith, C., Segre, E., Wigand, C., and York, H , 1948, *Phys Rev.*, **73**, 1114.
,, ,, ,, ,, 1949, *Phys. Rev.*, **75**, 351.
Hartzler, A. J., Siegel, R T , and Opitz, W., 1954, *Phys. Rev.*, **95**, 591.
Hsu, K. N., and Hu, T. M., 1949, *Phys. Rev.*, **75**, 987.
Jastrow, R., 1950, *Phys. Rev* , **79**, 389.
,, 1951, *Phys. Rev.*, **81**, 165.
Jeffrey, H., and Jeffrey, B. S., 1946, Methods of Mathematical Physics, 276.
Massey, H. S. W., Burhop, E H. S , and Hu, T. M., 1948, *Phys. Rev.*, **73**, 1403.
Mott, N. F., and Massey, H. S. W., 1949, The theory of Atomic Collisions, 130.
Nedzel, V. A., 1954, *Phys. Rev.*, **94**, 174.
Ohnuma, S., and Feldman, D., 1956, *Phys Rev* , **102**, 1641.
Pangher, J. De, 1953, *Phys. Rev.*, **92**, 1084.
,, 1954, *Phys. Rev.*, **95**, 578.
,, 1955, *Phys. Rev.*, **99**, 1447.

Randle, J. C., Taylor, A. E., and Wood, E., 1952, *Proc. Roy. Soc. A. .), Lond* **213**, **392**.
Rarita, W. and Schwinger, J., 1941, *Phys. Rev.*, **56**, 436 & 556.
Sachs, R G , 1955, Nuclear Theory, *P.* 155.
Selove, W., Strauch, K. and Titus, F., 1953, *Phys. Rev.*, **92**, 724.
Stahl, R H and Ramsay, N. F., 1954, *Phys. Rev.*, **96**, 1310.
Swanson, Don, R., 1953, *Phys. Rev.*, **89**, 740.
Raylor, A. E., Pickavence, T. G , Cassels, J. M , and Randle, T. C., 1951, *Phil. Mag.*, **42**, 20.
Taylor, A. E., 1953, *Phys. Rev.*, **92**, 1071
Wallace, R., 1951, *Phys. Rev.*, **81**, 493.
Wortheim, M. S., Hull, M. H., and Saperstein, A. M., 1956, *Phys. Rev.*, **104**, 764.
Wolfenstein, L., 1956, *Bull Am. Phys. Soc., Series II*, **1**.
Yadav, H N., 1952, *Ind J Phys.*, **26**, 337.
Yovits, M. C , Smith, R. L., Hull, M H., Bengston, J., and Breit, G., 1952, *Phys. Rev.*, **85**, 540

13

AN ELECTRONIC DIFFERENTIAL ANALYSER

A. K. CHOUDHURY AND B. R NAG

INSTITUTE OF RADIO PHYSICS AND ELECTRONICS, CALCUTTA UNIVERSITY

(*Received for publication, July* 15, 1957)

ABSTRACT. An electronic differential analyser having sixteen operational amplifiers is described. The analyser is specially designed for solving equations arising in connection with research works on circuit theory, servo-mechanism and electron trajectories. The analyser works both repetitively and non-repetitively. Different sources of error of the computer elements are also discussed Accuracy of the solutions obtainable by the machine is illustrated by some examples

INTRODUCTION

In the course of last ten years, electronic differential analysers have come to be recognised as useful tools for solving differential equations with moderate accuracy. (Ragazinni *et al.*, 1947; Williams and Ritson, 1947, Mc Nee, 1949; Meneley and Morill, 1953 ; Paul and Thomas, 1957, Biswas *et al.*, 1955). In the present paper is described an electronic differential analyser, built with a view to solving equations arising in connection with research work in circuit theory, servo mechanisms and electron trajectories. Very often interest is mainly centered on the qualitative rather than on the quantitative aspect of the solution. Hence in designing the computer emphasis was laid on low cost, moderate accuracy, ease of construction and flexibility.

The analyser can be used to solve both linear and non-linear equations. In the present paper only the linear computing elements are described. In the first part of the paper, the different sources of error in the computing elements and the factors governing the choice of the time scale of the computer are discussed. The actual hardware of the machine is described in part two. The accuracy obtainable by the machine is illustrated by examples. The non-linear components will be described in a paper to be published later

PART I

BASIC COMPUTING ELEMENTS FOR SOLVING LINEAR DIFFERENTIAL EQUATIONS WITH CONSTANT CO-EFFICIENTS

The basic computing elements required for solving linear differential equations with constant co-efficients are (1) adders, (2) integrators and (3) co-efficient setting potentiometers. Adders and integrators are constructed with operational

amplifiers by the application of feedback. The general arrangement of feed back in the operational amplifier is shown in figure 1. $Z_1, Z_2, \ldots Z_n$ are the input impedance elements and Z_f is the feedback impedance element. Output voltage

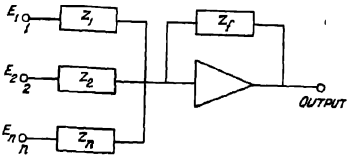

Fig. 1—Operational amplifier with feedback.

E_{out} of the amplifier due to the input voltages $E_1, E_2, \ldots, E_n$ applied respectively at the n input terminals is

$$_{out} = -\left[\frac{Z_f}{Z_1} E_1 + \frac{Z_f}{Z_2} E_2 + \ldots + \frac{Z_f}{Z_n} E_n\right] \qquad \ldots (1)$$

Operational amplifier is assumed to have ideal characteristics *i.e.* its gain, bandwidth and input impedance are infinitely large, output impedance infinitesimally small, and it has no drift.

When $Z_1 = Z_2 = \ldots Z_n = Z_f$, E_{out} is the inverted sum of the voltages applied at the different inputs. The operational amplifier with this feedback arrangement is said to act as an adder. If, input is applied to only one terminal, it acts as an inverter.

When $Z_1 = Z_2 = \ldots, Z_n = R$ (a resistance) and $Z_f = \frac{1}{pC}$ (*i.e.* the feedback impedance is due to a capacitance), E_{out} is the inverted sum of integrals of the inputs, scaled by CR. An operational amplifier with this feedback arrangement is referred to as an integrator.

A linear differential equation is solved by combining the adders and integrators to form a system whose response equation is the same as the equation to be solved. The coefficients of the equation are set by potentiometers.

Adder and Integrator errors.

E_{out} of an adder or integrator deviate from the ideal value given by Eq(1). due to,

(1) non-ideal behaviour of the operational amplifier.

(2) inaccuracy of the feedback and input network elements.

A practical amplifier has always a finite value of gain, bandwidth, input impedance or output impedance and also a finite drift. The exact equivalent

circuit for the operational amplifier together with the network elements is shown in figure 2 (Mc. Donald, 1950)

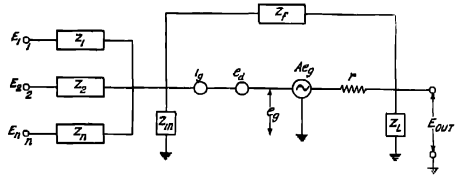

Fig. 2—Equivalent circuit of the operational amplifier with feedback.

Now,

$$E_{out} = -\frac{E_1 \frac{Z_f}{Z_1} + E_2 \frac{Z_f}{Z_2} + \dots + E_n \frac{Z_f}{Z_n} + e_d \left[1 + \frac{Z_f}{Z_1} + \dots + \frac{Z_f}{Z_{in}} \right] + Z_f i_g}{1 - \frac{1}{A'} \left[1 + \frac{Z_f}{Z_1} \dots + \frac{Z_f}{Z_n} + \frac{Z_f}{Z_{in}} \right]}$$

where $$A' = A \cdot \frac{Z'}{r + Z'}, \; Z' = \frac{Z_L \times Z''}{Z_L + Z''}, \; Z'' = Z_f + \frac{1}{\sum_{i=1} \frac{1}{Z_i}}$$

A = the gain of the amplifier,
Z_{in} = the amplifier input impedance.
r = the amplifier output impedance.
Z_L = load impedance terminating the amplifier
i_g is a constant current generator to represent the drift due to grid current.
e_d is a constant voltage generator, with an output voltage e_d to represent the drift due to supply voltage variations, filament supply variations, contact p.d., amplifier parameter variations etc

If $$Z_1 = Z_2 \dots = Z_n = Z_0$$

$$E_{out} = -\frac{E_1 + E_2 \dots + E_n + Z_0 i_g + e_d \left[n + \frac{Z_0}{Z_f} + \frac{Z_0}{Z_{in}} \right]}{\frac{Z_0}{Z_f} - \frac{1}{A_1}} \tag{2}$$

where,

$$A_1 = \frac{A'}{n + \frac{Z_0}{Z_f} + \frac{Z_0}{Z_{in}}} \tag{3}$$

and

$$A' = A\,\frac{Z'}{r+Z'}\ ,\ Z' = \frac{Z \times Z''}{Z_L+Z''}\ ,\ Z'' = Z_f + \frac{Z_0}{n}.$$

Thus, the effect of the non-ideal behaviour of the operational amplifier is to introduce the term $\frac{1}{A_1}$ in the denominator, and $Z_0\, i_g + e_d\left(n + \frac{Z_0}{Z_{in}} + \frac{Z_0}{Z_f}\right)$ in the numerator. Error due to the former may be called the response error while that due to latter is called the drift error.

Response error.

1. Frequency response error :

Let $-|A_1(\omega)|\, e^{-(\omega)}$ represent the value of A_1 at any frequency ω. Substituting this in Eqn. 2

$$E_{out} = -\frac{E_1 + E_2 + \ldots + E_n + e}{\left[\left|\frac{Z_0}{Z_f}\right| \cos\psi + \left|\frac{1}{A_1(\omega)}\right| \cos\phi(\omega)\right] + j\left[\left|\frac{Z_0}{Z_f}\right| \sin\psi + \left|\frac{1}{A_1(\omega)}\right| \sin\phi(\omega)\right]} \quad \ldots(4)$$

where

$$\left|\frac{Z_0}{Z_f}\right| e^{j\psi} = \frac{Z_0}{Z_f}$$

and

$$e = Z_0\, i_g + e_d\left[n + \frac{Z_0}{Z_f} + \frac{Z_0}{Z_{in}}\right]$$

Thus, E_{out} differs from the ideal in both amplitude and phase. The deviation in the amplitude normalised by the ideal value is called the amplitude error and the deviation in phase is the phase error.

For an adder $\left|\frac{Z_0}{Z_f}\right| = 1$ and $\psi = 0$, Hence, the output voltage of the adder is

$$E_{a\,(out)} = -\frac{E_1 + E_2 + \ldots + E_n + e}{\left|\frac{1}{A_1(\omega)}\right| \cos\phi(\omega) + 1 + j\left|\frac{1}{A_1(\omega)}\right| \sin\phi(\omega)}$$

The adder amplitude error, at any frequency ω is

$$\epsilon_a(\omega) = 1 - \frac{1}{\sqrt{1 + \frac{1}{|A_1(\omega)|^2} + \frac{2}{|A_1(\omega)|}\cos\phi(\omega)}} \approx -\frac{\cos\phi(\omega)}{|A_1(\omega)|} \quad \ldots \quad (5a)$$

Adder phase error $\delta\phi_a(\omega)$ is

$$\delta\phi\ (w) = \tan^{-1}\frac{\sin\phi(\omega)}{|A_1(\omega)| + \cos\phi(\omega)} \approx \tan^{-1}\frac{\sin\phi(\omega)}{|A_1(\omega)|}$$

$$\approx -\frac{\sin\phi(\omega)}{A_1(\omega)} \qquad \ldots \quad (5b)$$

For an integrator

$$\left|\frac{Z_0}{Z_f}\right| = \omega cR = \frac{\omega}{\alpha_0},\ \alpha_0 = \frac{1}{CR} \text{ and } \psi = \pi/2$$

Hence output of the integrator is

$$E_{out} = -[E_1+E_2+\ldots+E_n+e]\frac{1}{\dfrac{\cos\phi(\omega)}{|A_1(\omega)|} + j\left(\dfrac{\omega}{\alpha_0} + \dfrac{\sin\phi(\omega)}{|A_1(\omega)|}\right)}$$

Thus the integrator amplitude error at any frequency ω is

$$\epsilon_i(\omega) = 1 - \frac{1}{\sqrt{1 + \dfrac{1}{|A_1(\omega)|}\dfrac{\alpha_0^2}{\omega^2} + \dfrac{2\sin\phi(\omega)}{|A_1(\omega)|}\dfrac{\alpha_0}{\omega}}}$$

$$\approx \frac{1}{|A_1(\omega)|}\frac{\alpha_0}{\omega}\left[\sin\phi(\omega) + \frac{\alpha_0}{2\omega}\frac{1}{|A_1(\omega)|}\right] \qquad \ldots \quad (6a)$$

and integrator phase error is

$$\delta\phi_i(\omega) = \frac{\pi}{2} - \tan^{-1}\frac{\dfrac{\omega}{\alpha_0} + \dfrac{\sin\phi(\omega)}{|A_1(\omega)|}}{\dfrac{\cos\phi(\omega)}{|A_1(\omega)|}} \approx \frac{\cos\phi(\omega)}{\sin\phi(\omega) + |A_1(\omega)|\dfrac{\omega}{\alpha_0}} \qquad \ldots \quad (6b)$$

At frequencies for which $\dfrac{\omega}{\alpha_0} << 1$

$$\epsilon_i(\omega) \approx \frac{1}{2}\frac{\alpha_0^2}{\omega^2}\frac{1}{|A_1(\omega)|},\ \delta\phi_i(\omega) = \frac{\alpha_0}{\omega|A_1(\omega)|}$$

while at frequencies for which

$$\frac{\omega}{\alpha_0} >> 1$$

$$\epsilon_i(\omega) \approx \frac{\sin\phi(\omega)}{A_1(\omega)|}\frac{\alpha_0}{\omega},\ \delta\phi_i(\omega) \approx \frac{\cos\phi(\omega)}{|A_1(\omega)|\,\omega/\alpha_0}$$

Now Z_L, the impedance terminating the amplifier is either due to a potentiometer or the input resistance element of an adder or integrator. When Z_L is due to a potentiometer $Z' = Z_L = R_p$, R_p is the resistance of a potentiometer and is assumed to be small compared to Z_f and $\frac{Z_0}{n}$. Hence $A' = A \frac{R_p}{r+R_p}$. On the other hand, when Z_L is due to input resistance of an adder or integrator $Z_L = R$, R is the resistance connected between the input terminal and grid of operational amplifier. So $A' = A \frac{R}{r+R}$. In both the cases A is multiplied by a constant factor which is very near unity.

Z_{in} is the input impedance of the operational amplifier and can be written as $\frac{1}{Z_{in}} = \frac{1}{R_{in}} + pC_{in}$. R_{in} and C_{in} being the input resistance and capacitance of the operational amplifier.

Hence A_1 is related to A by the relations

$$A_1 = \frac{A}{n+1+\frac{R}{R_{in}}+pRC_{in}} \quad \text{(for adder)} \qquad \ldots \text{(7a)}$$

$$= \frac{A}{n+\frac{R}{R_{in}}+pR(C+C_{in})} \quad \text{(for integrator)} \qquad \ldots \text{(7b)}$$

If the operational amplifier is a low pass one, $|A(\omega)|$ decreases with increase of frequency. Hence the largest error in the adder occurs at the highest operating frequency. A measure of the frequency response error of the adder can be obtained by knowing the highest frequency ω at which the amplitude error is ϵ_a % and denoted by $\omega_a(\epsilon)$. The integrator error, however, increases both at high and low frequencies. If $|A(\omega)|$ does not decrease very rapidly, the largest error in the integrator occurs at the lowest operating frequency. A measure of the integrator frequency error can be obtained by knowing the lowest frequency at which the integrator amplitude error is ϵ_i % and denoted by $\omega_i(\epsilon)$.

2. *Time Response Error* :

Adder error. A unit step applied to one of the inputs of the adder should ideally give at its output a unit step. But due to imperfection of the operational amplifier the output is different from a unit step. Determination of the actual output requires an exact knowledge of the frequency response characteristics of the operational amplifier. For a multistage, high gain d.c. amplifier exact frequency response characteristic is difficult to determine. However, in order that the adder

be stable it is necessary that $|A_1(\omega)|$ be less than 1 when $\phi(\omega)$ approaches 180°. This is ensured by so designing the operational amplifier that A_1 can be taken to have effectively two poles. One of the poles being due to the input networks, operational amplifier contributes a single pole (say at α_1).

Thus A_1 can be written as

$$A_1 = -\frac{A_{10}\alpha_a\alpha_1}{(p+\alpha_a)(p+\alpha_1)} \text{ where } A_{10} = \frac{A_0}{(n+1+R/R_{in})} \tag{8a}$$

A_0 is the d.c. gain of the operational amplifier.

$$\alpha_a = \frac{1}{RC_{in}\,\overline{n+1+R/R_{in}}} \tag{8b}$$

Then, output of the adder E_{out} due to a unit step is as given below :

Case I: When $(A_{10}+1)\alpha_a\,\alpha_1 < \left(\frac{\alpha_a+\alpha_1}{2}\right)^2$

$$E_{out} = -\frac{A_{10}}{(\alpha_1'-\alpha_2')(A_{10}+1)}\left[(\alpha_1-\alpha_2')+\alpha_2'\epsilon^{-\alpha_1't}-\alpha_1'e^{-\alpha_2't}\right]$$

α_1', α_2' are the roots of the equation.

$$p^2+(\alpha_a+\alpha_1)p+(A_{10}+1)\alpha_a\alpha_1 = 0$$

Case II : When $(A_{10}+1)\,\alpha_a\alpha_1 = \left(\frac{\alpha_a+\alpha_1}{2}\right)^2$

$$E_{out} = -\frac{A_{10}}{(A_{10}+1)}\left[1-e^{-(\alpha_1+\alpha_a)t}\left\{1+(\alpha_1+\alpha_a)t\right\}\right]$$

Case III : When $(A_{10}+1)\alpha_a\alpha_1 > \left(\frac{\alpha_a+\alpha_1}{2}\right)^2$

$$E_{out} = -\frac{A_{10}}{A_{10}+1}\left[1-\frac{\sqrt{(A_{10}+1)\alpha_a\alpha_1}}{\sqrt{(A_{10}+1)\alpha_a\sigma_1-\left(\frac{\alpha_a+\alpha_1}{2}\right)^2}}\,e^{-\frac{\alpha_a+\alpha_1}{2}t}.\right.$$

$$\sin\left\{\left(\sqrt{(A_{10}+1)\alpha_a\alpha_1-\frac{\alpha_a+\alpha_1}{2}}\right)t+\right.$$

$$\left.\left.\tan^{-1}\frac{\sqrt{(A_{10}+1)\alpha_a\alpha_1-\left(\frac{\alpha_a+\alpha_1}{2}\right)^2}}{\frac{\alpha_a+\alpha_1}{2}}\right\}\right]$$

In all the three cases for large values of t, $E_{out} = -\frac{A_{10}}{A_{10}+1}$. Hence adder time response error for large values of t is

$$\epsilon_a(\text{large}) = \frac{1}{A_{10}} = \frac{n+1+R/R_{in}}{A_0} \qquad \ldots \quad (9a)$$

For small values of t, however, the error is much larger and the machine solution for small values of time has to be neglected. A measure of this small time error can be obtained by determining the error time, defined as the time measuring from zero after which the error is less than twice the large time error. Adder error time for the three cases can be obtained from

Case I : $$t_a \simeq \frac{1}{\alpha_2'} \ln \frac{1}{\epsilon_a(\text{large})} \quad \text{If } \alpha_1' \gg \alpha_2' \qquad \ldots \quad (9b)$$

Case II : $$t_a \simeq \ln \frac{1+(\alpha_a+\alpha_1)t_a}{\epsilon_a(\text{large})} \qquad \ldots \quad (9c)$$

Case III : $$t_a \simeq \frac{1}{\alpha_a+\alpha_1} \ln \frac{1}{\epsilon_a(\text{large})} \qquad \ldots \quad (9d)$$

Integrator Error.

The integrator should give a voltage $E_{out} = t/CR = \alpha_0 t$ at its output when a unit step is applied to one of its inputs (other inputs being grounded).

Now, for an integrator $$A_1 = -\frac{A_{10}\alpha_i\alpha_1}{(p+\alpha_i)(p+\alpha_1)}$$

where $$A_{10} = \frac{A_0}{n+R/R_{in}} \qquad \ldots \quad (10a)$$

$$\alpha_i = \frac{n+R/R_{in}}{R(C+C_{in})} \qquad \ldots \quad (10b)$$

Hence on neglecting small order terms, since it can be assumed that

$$\left(A_{10}\frac{\alpha_i}{\alpha_0}+1\right)\alpha_i+\alpha_1 \gg 4\alpha_i\alpha_1$$

$$E_{out} = A_{10}\left[1-e^{-\frac{\alpha_0}{A_{10}}t} - \frac{\alpha_0}{A}\,\frac{e^{-\left(\frac{A_{10}}{\alpha_0}\alpha_i+1\right)\alpha_1 t}}{\left(\frac{A_{10}\alpha_i}{\alpha_0}+1\right)\alpha_1}\right]$$

Also, when $$\frac{\alpha_0}{A_{10}}\, t \ll 1$$

$$E_{out} \simeq A_{10}\left[\frac{\alpha_0}{A_{10}}\, t - \left(\frac{\alpha_0}{A_{10}}\right)^2 t^2 - \frac{\alpha_0}{A_{10}}\,\frac{e^{-\left(\frac{A_{10}\alpha_1}{\alpha_0}+1\right)\alpha_1 t}}{\left(\frac{A_{10}\alpha_1}{\alpha_0}+1\right)\alpha_1}\right]$$

Thus the integrator time response error is

$$\epsilon_i(t) = \frac{\alpha_0 t - E_{out}}{\alpha_0 t}$$

$$= \frac{\alpha_0}{A_{10}}\, t + \frac{e^{-\left(\frac{A_{10}}{\alpha_0}\alpha_1+1\right)\alpha_1 t}}{t\left[\frac{A_{10}\alpha_1}{\alpha_0}+1\right]\alpha_1}$$

$$= \frac{\alpha_0}{A_{10}}\, t + \frac{e^{-(A_0+1)\alpha_1 t}}{(A_0+1)\alpha_1 t}$$

The integrator error is, therefore, large both for small values and for large values of time For large values of t, ϵ_i (large) $= \dfrac{\alpha_0 t}{A_{10}}$ (13)

If T is the operation-time of the machine *i.e.* the time for which the solution is observed then ϵ_i (large) $= \dfrac{\alpha_0 T}{A_{10}}$ ... (14)

Error time t_i of the integrator is obtained from

$$\frac{\alpha_0}{A_{10}}\, t_i + \frac{e^{-(A_0+1)\alpha_1 t_i}}{(A_0+1)\alpha_1 t_i} = \epsilon_i \text{ (large)} \qquad \ldots (15)$$

Drift Error.

It is seen from equation (2), that the effect of drift of the amplifier is to add a voltage $e = Z_0 i_g + e_d\left[n + \dfrac{Z_0}{Z_f} + \dfrac{Z_0}{Z_{in}}\right]$ to one input of the adder or integrator. In an adder the total drift error when referred to the inputs is thus $R_{ig}+(n+1+R/R_{in})e_d$, e_d is assumed to vary slowly with time. Drift error for the integrator referred to the input is $R_{ig}+(n+R/R_{in})e_d$. The actual error in the output depends on the nature of variation of i_g and e_d with time.

Component Error.

In deducing Eq.(2) it was assumed that $Z_1 = Z_2 = \ldots = Z_n = Z_0$. When these impedances are due to elements whose value is accurate to within α%,

in adding an input voltage an error of $2\alpha\%$ may be committed in the adder. Also the integrator equation was deduced assuming Z_f to be due to a loss-less condenser. However, condensers which are used have a finite loss which can be represented by assuming a resistance R_e to be present in parallel with the capacitance C.

The integrator output is then

$$E_{out} = -[E_1 + E_2 + \ldots + E_n + e] \frac{1}{pCR - \frac{1}{A_1} + \frac{R}{R_e}}$$

Hence the frequency response equations modify to

$$\epsilon_i(w) = \frac{1}{2}\frac{\alpha_0^2}{w^2}\frac{1}{|A_1(w)|} + \frac{\alpha_0}{w}\frac{\sin\phi(w)}{|A_1(w)|} + \frac{1}{2}\frac{\alpha_0^2}{w^2}\left(\frac{R}{R_e}\right)^2 + \frac{\cos\phi(w)}{|A_1(w)|}\frac{R}{R_e}\frac{\alpha_0^2}{w^2}$$

and

$$\delta\phi_i(w) = \frac{\cos\phi(w) + |A_1(w)|\, R/R_e}{|A_1(w)|\,\frac{w}{\alpha_0} + \sin\phi(w)}$$

The time response error equations are

$$\epsilon_i(\text{large}) = \frac{\alpha_0(1 + A_{10}R/R_e)}{A_{10}}\, T.$$

and

$$\frac{\alpha_0(1 + A_{10}R/R_e)}{A_{10}}\, t_i + \frac{e^{-(A_0+1)\alpha_1 t_i}}{(A_0+1)\alpha_1 t_i} = \epsilon\,(\text{large})$$

Effect of the condenser leakage is to increase the error in the integrator low frequency response and also increasing the value of ϵ_i (large), for the same operation time.

Characteristics of the operational amplifier

The measured frequency response characteristics of the operational amplifier are given in figure 3 The operational amplifier has a d.c. gain of 12000, and the

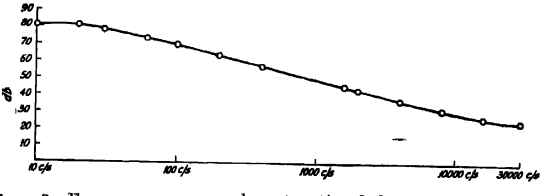

Fig. 3—Frequency response characteristic of the operational amplifier.

first pole is at 30 c/s. Input capacitance is less than 10pf. Output impedance is 600 ohm. In or that the output impedance should not contribute a fraction

of the adding resistance by more than 0.1%, the adder resistors should be made greater than 600K Ω. A value of $1M$ was hence chosen. In the following Table I is given the values of the adder and integrator errors calculated from the above data :

TABLE I

Adder Errors	No. of inputs			Used as scaler with scaling factor		
	$n = 1$			2	5	10
The highest frequency at which amplitude error is						
1) less than 0.1% $\omega_a(.1)$				100 c/s	40 c/s	25 c/s
2) less than 1% $\omega_a(1)$	1.6 kc/s	1 kc/s	0 8 kc/s	1 kc/s	0 6 kc/s	300 c/s
Large time error	015%	025%	03%	025%	.05%	.1%
Adder error time	less than 10 μ sec.					

Integrator error	No. of inputs		
	$n = 1$	$n = 2$	$n = 3$
The lowest frequency at which the amplitude error is			
1) less than 0.1% $\omega_i(.1)$	.08 $\alpha_0$rad/sec	.15 $\alpha_0$rad/sec	.25 $\alpha_0$rad/sec
2) less than 1% $\omega_i(1)$	008 $\alpha_0$rad/sec	.016 $\alpha_0$rad/sec	.025 $\alpha_0$rad/sec
Large time error in % (Operation time T)	$.008\alpha_0 T$	$.016\alpha_0 T$	$0\ 25\alpha_0 T$

Choice of the Computer Time scale

The above table has been prepared with a view to choosing the proper value α_0. It is seen that if the adders are required to scale by a factor of 10, the highest oscillation frequency of the system should be kept lower than 25 c/s. On the other hand, the lowest oscillation frequency ω should be such that $\frac{\omega}{\alpha_0}$ is greater than .25. Thus, to handle equations having characteristic frequencies, such that the ratio of the highest to lowest characteristic frequency is less than 100, α_0 has to be chosen to be equal to 6 rad/sec in order to ensure that the amplitude errors at the highest and lowest oscillation frequencies are less than .1%. The required value of the integrator capacitor works out to $1/6\mu F$. It should be noted that, when preparing a problem, it should be so arranged, that the lowest oscillation frequency is greater than $.25\alpha_0$ and the highest less than 25 c/s.

PART II

THE ANALYSER

General Description.

There are 16 operational amplifiers, four in one chasis, arranged as shown in the figure 4. Eight operational amplifiers are arranged to work as adders and eight as integrators.

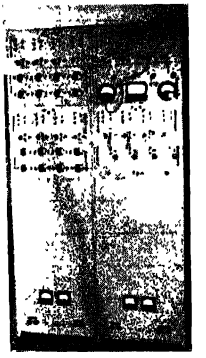

Fig 4. A photograph of the electronic differential analyser.

There are provisions for three inputs and two outputs of the adders through jack. The input resistors and feedback resistors, matched to within 0.1% are wired in the chassis. But the feedback resistors can be disconnected from the input of the operational amplifier by disconnecting an external link between terminals numbered 2 and 3 in figure 5. Access to the input and the output of

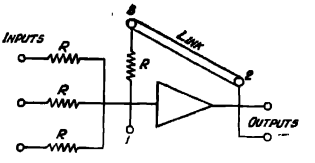

Fig. 5. Adder circuit.

the operational amplifier is provided by terminals 1 and 2 respectively. The arrangement enables one to replace the feedback resistor by another fixed resistor or potentiometer, or to connect input to the adder through any other resistor.

The integrator input resistors are also wired in the chassis. Each integrator has provisions for three inputs. Integrator capacitors are arranged in a different pannel. The integrator capacitors and resistors are matched to make the time constant of all the integrator equal to within .1%. Initial conditions are set in the machine by charging the integrator capacitors. Integrator circuit arrangement is shown in the figure 6. In the reset position the input of the operational amplifier is connected to terminal 2 and the integrator condenser is charged to the

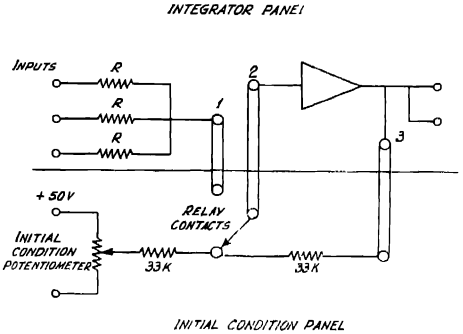

Fig. 6. Integrator circuit.

potential set by initial condition potentiometer In the compute position the input of the operational amplifier is connected to the common terminal of the input resistors. The terminals of the integrator are connected by external links to the initial condition panel terminals.

Switching of input between the terminals 1 and 2 is done by a relay, the arrangement of which is shown in figure 7. Relay 1 and relay 2 provide the eight one pole two-way contacts required for the 8 integrators. In the reset condition

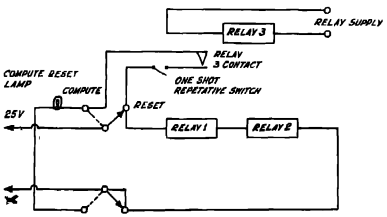

Fig. 7. Compute-reset relay circuit.

the relays are energised and while in the compute condition they are de-energised. Relay 3 makes the compute condition repetitive. The driving circuit for relay

3 is shown in figure 8. The repetition rate is determined by a multivibrator and can be set to 1 c/s, 0.5 c/s, 0.1 c/s. The computer is made repetitive or single shot by the one-shot-repetitive switch.

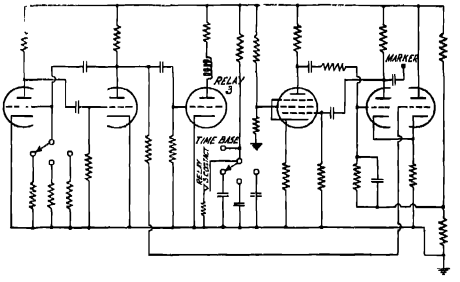

Fig. 8. Time base, marker and relay 3 driving circuit.

Coefficients are set by helipot potentiometers of 0.1% accuracy with loading error correction. The machine solution can be viewed in meters or in an oscilloscope having long persistance tube. For one-shot operation, the oscilloscope time base is worked on single shot while for repetitive operation the time base is supplied by the relay 3 driving circuit. The time is marked by time markers generated by a pulsed audio oscillator. Permanent record of the solution at present is made by photographing the oscilloscope output.

The values of the solution at different times are measured by an arrangement shown in figure 9. During the reset cycle inputs to the adder are disconnected by relays and the oscilloscope line indicates the zero level of its output. The value of the solution at any time is measured by adding to the solution a voltage which

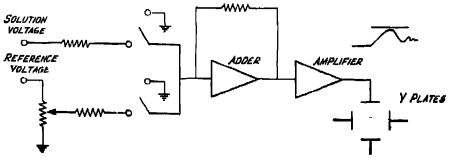

Fig. 9. A circuit for measuring the values of the solution at different times.

makes the oscilloscope spot coincide with the zero line at that time. With an amplifier gain of 100, the zero can be distinguished to within 10 mv. Also the voltage added being set by a helipot potentiometer can be measured to within 0.1%

Illustrative solutions.

In the following tables are given the solutions of three problems as obtained by the analyser.

In Table II is given percentage overshoot for different values of b in the equation,

$$\frac{d^2y}{dt^2} + b\frac{dy}{dt} + y = H(t)$$

ep function.

TABLE II

b	% Overshoot	
	Calculated value	Experimentally obtained value
1	16 33	16 3
845	23.10	22 8
.684	31.86	31.7
.518	43.10	43 0
.347	57.50	57.4
.174	75.96	75 7
0	100.00	99.7

Table III gives the measured overshoot and rise time for Butterworth functions up to the sixth order. Figure 10 gives the response of the Butterworth functions due to a unit step.

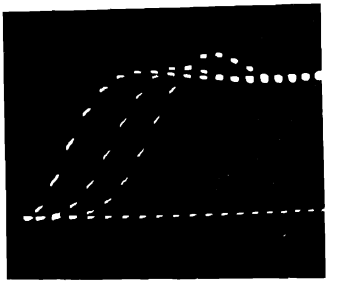

Fig. 10. Step response of Butterworth function of different orders,

TABLE III

Order of the function	% Overshoot	
	Calculated value	Experimentally obtained value
2	4 3	4.1
4	10.9	10.5
6	14 3	14.0

In Table IV is given the different combinations of the values of the coefficients in the equation

$$\frac{d^3y}{dt^3} + a\frac{d^2y}{dt^2} + b\frac{dy}{dt} + cy = 0$$

which make the solution a continuous oscillatory function.

TABLE IV

a	b	c	
		Calculated value for maintained oscillation	Experimental value for maintained oscillation
3.00	2.00	6 00	6.06
3.00	3 00	9 00	8 99
3 00	4.00	12.00	12.02
3.00	5.00	15.00	14.99

It may be noted that the above equations were taken as representative of the types of equations that will be met with in practice. The results obtained indicate that whatever be the errors in the individual computing elements, the overall solution is accurate enough for practical purposes.

In order to illustrate the use of the differential analyser in solving electron trajectory problems, the motion of an electron when injected into a region containing a uniform electric field in the y-direction and a uniform magentic field in the Z-direction, is considered. The equations of motion of the electron can be written as

$$\ddot{y} = a - \omega\dot{x}$$

$$\ddot{x} = \omega\dot{y}$$

where

$$\omega = \frac{eH}{m} \quad \text{and} \quad a = \frac{eX}{m} \quad e, m, X \text{ and } H \text{ have their usual meaning.}$$

The set up of the computer for solving the above equations is shown in figure 11. Evidently, ω is equal to $1/CR$ and a is set by the magnitude of the input

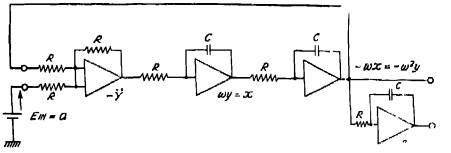

Fig. 11. Set up of the computer for obtaining the electron trajectory in crossed uniform electric and magnetic field.

voltage. Photographs of the trajectories for different initial velocities of the electron as obtained by the computer are given in figure 12.

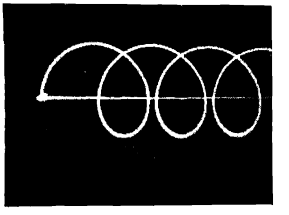

(*a*) (*b*)

Fig. 12. Photographs of the electron trajectory as obtained by the computer.

$$\left.\begin{array}{l} \text{a) } \dot{x} = \dot{y} = 0 \\ \text{b) } \dot{x} = 0 \quad \dot{y} = \dot{y}_0 \end{array}\right\} \text{at } t = \sigma$$

CONCLUDING REMARKS

In solving a practical problem in circuit theory, servo-mechanism etc. with the differential analyser, the percentage overshoot, rise time and stability conditions are the important results that one is usually interested in. All differential analysers are such that the solutions obtained with them are accurate only over a certain range of values of time or frequency. But, by properly chosing the time scale of the computer, one can determine the overshoot, rise time or stability with sufficient accuracy.

ACKNOWLEDGMENTS

The authors are deeply indebted to Prof. S. K. Mitra for his kind interest in the work and to Prof J. N Bhar , Head of the Department of Radio Physics and Electronics, for his constant help and guidance. Thanks are also due to Sri N. B. Chakrabarty for helpful discussions.

REFERENCES

Biswas, N. N., Chiplonkar, V. N. and Rideout, V L., 1955, *J. Ind. Insti. of Sci.* **37**, 186.

McNee, A. B., 1949, *Proc. I. R. E.*, **37**, 1315.

McDonald, D., 1950, *Rev. Sc. Instr.*, **21**, 154.

Menoley, C. A. and Morill, C. D., 1953, *Proc. I. R. E.*, **41**, 1487.

Paul, J. A. and Lloyd Thomas, E., 1957, *J. Brit. I. R. E.*, **17**, 49.

Ragazinni, J. R , Randall, R. and Russell, F. A., 1947, *Proc. I. R. E* 35 [illegible]

Williams, F. C. and Ritson, F. A., 1947, *J. I. E. E.* (Part IIA), 80, 112

ON LINEAR DELAYED CONTROL SYSTEMS. PART I—CONSIDERATIONS OF STABILITY

N. B. CHAKRABORTI

INSTITUTE OF RADIO PHYSICS AND ELECTRONICS, CALCUTTA UNIVERSITY

(*Received for publication August* 5, 1957)

ABSTRACT. In this paper the problem of stability of delayed control systems has been studied. The location of the roots of some characteristic equations which can be considered as the sum of a rational function and a transcendental function has been discussed. Results are derived regarding stability of systems having the characteristic equation

$$(p^3+ap^2+bp+c)e^p+rp^n = 0$$

It is shown that by the application of simple graphical methods, viz., the dual loci technique and the dual Nyquist diagram, the location of the roots can be rapidly determined and information regarding stability readily obtained.

INTRODUCTION

In a feedback control system it is required that the controlled condition should settle to the desired value after any disturbance to which the system may be subjected. It is the aim of a good control design to keep the deviation of the controlled condition to a minimum and bring it to the desired value as quickly as possible.

One of the most important factors governing the control performance is the fact that the full effect of any corrective action is not immediately felt. The delay in response assumes disturbing proportions in systems employing pneumatic, thermal and hydraulic elements. This lag is due to the finite velocity of the physical entities-pressure, or heat or mass, travelling around the loop and bears close analogy to delays in distributed parameter electrical circuits. The presence of the lag gives rise to special problems in respect of stability and time response ; the characteristic equation becomes a transcendental one and instantaneous response to a command is an impossibility.

The present author has examined in some details the problem of stability and time response of delayed control systems. In this Part I of the paper, the results of the study of stability only of certain simple systems of frequent occurrence have been discussed. The location of the roots of some characteristic equations are first considered, the principal aim being to find out the regions in the complex frequency plane where the roots with positive real parts will first appear, as the delay or the magnitude of the delayed term is varied. Analytical and graphical methods are then formulated to derive results regarding stability of certain systems.

1. *Properties of the roots of the characteristics equation*

We shall first endeavour to indicate the properties on which the boundedness of the solution of the delayed control systems depends and the regions on the complex frequency plane, where the roots of the characteristic equation with positive real parts may occur. We shall also compare the dead-time lag and distributive lag systems in respect of the location of the roots of the characteristic equation.

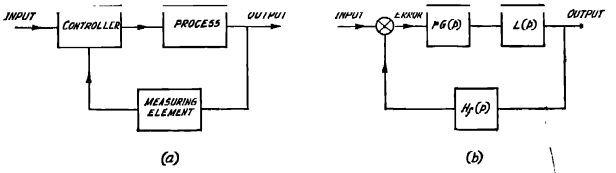

Fig 1. Block diagram of a process control system

The input-output relationship of the system of figure 1(b) is given by

$$\frac{C}{R} = \frac{G(p)L(p)r}{1+G(p)\,L(p)\,.\,rH_f(p)} = \frac{rG(p)L(p)}{1+rG(p)\,L(p)},$$

if $H_f(p) = 1$.

The characteristic roots of the system are then obtained from the zeros of

$\frac{1}{G(p)}+L(p)r$. Putting $\frac{1}{G(p)} = H_0(p)$, we have

$$H(p) = H_0(p)+re^{-p}(\text{or } re^{-\sqrt{p}}) \qquad \ldots \quad (1a)$$

$$= H_0(p)+ rL(p) \qquad \ldots \quad (1b)$$

where $H_0(p)$ is a ratio of two polynomials, *i.e*

$$H_0(p) = \frac{\Sigma a_r p^r}{\Sigma b_r p^r} = \frac{N(p)}{D(p)} \qquad \ldots \quad (2)$$

Let n be the difference between the highest exponents of $N(p)$ and $D(p)$ Putting $p = \sigma+i\omega$ we have for a root of $H(p)$

$$A_0(\sigma, \omega)e^{i(\sigma,\omega)} = -re^{-(\sigma+i\omega)}\left[or-r^{-\left[\left(\frac{\sqrt{\omega^2+\sigma^2}+\sigma}{2}\right)^{\frac{1}{2}}+i\left(\frac{\sqrt{\omega^2+\sigma^2}-\sigma}{2}\right)^{\frac{1}{2}}\right]}\right] \ldots \quad (1c)$$

where $A_0(\sigma, \omega)$ and $\phi(\sigma, \omega)$ are the amplitudes and phase of $H_0(p)$. Let the roots of $N(p)$ and $D(p)$ be bounded by the line $\sigma = \sigma_0$ to the right. Then if $n > 0$,

for $\sigma > \sigma_0$, $A_0(\sigma, \omega)$ continuously increases with σ, while $L(\sigma, \omega)$ decreases. Thus the real parts of the roots of $H(p)$ are bounded above. On the other hand, if $n < 0$, $A_0(\sigma, \omega)$ decreases with σ, and there is no upper bound of the roots of $H(p)$. We observe also that for values of σ smaller than the minimum of the real parts of the roots of $N(p)$ and $D(p)$ and $n > 0$ (which will indeed be the commonest case) both $A_0(\sigma, \omega)$ and $L(\sigma, \omega)$ increase. For large negative values of σ the amplitude equation for a dead lag system can be written as $\pi(\omega^2-\alpha_m) = r^2e^{-2\sigma}$, which reduces to $\omega^{2n} = r^2e^{-2\sigma}$. Hence at a root $p_k+i\omega_k$, $\omega_k >> \sigma_k$.

In a distributive lag system, for a given σ, sufficiently removed from the poles and zeros of $H_0(p)$, $A_0(\sigma, \omega)$ increases with ω, while $L(\sigma, \omega)$ decreases. And hence the possible roots are clustered round the real axis.

It is useful to note that a little removed from the rectangle containing the poles and zeros of $H_0(p)$, $\phi(\sigma\ \omega)$ is a slowly varying uniform function, so that the separation of the roots along ω of a pure lag system and along σ of a distributive lag system is approximately 2π.

Let us now consider the equation $H(p) = 0$, inside the rectangle containing all the roots of $N(p)$ and $D(p)$. We shall assume for convenience and $N(p)$ and $D(p)$ are Hurwitz. (If they are not, we have only to shift the imaginary axis to the right and our arguments and results remain valid). It is easily seen that the roots with the largest σ occur near the minima of $A_0(\sigma, \omega)$ closest to the imaginary axis. For a system with low pass properties, it is sufficient then to investigate the region near the origin in the p-plane. It is easy to observe that if $A(\sigma, \omega) > r$ for all ω, there can be no roots of $H(p)$ with non-negative real part. A root (or a pair, if complex) will occur in the neighbourhood of every zero, $\sigma+i\omega$, of $H_0(p)$ -- to the right or to the left of it, depending on the phase condition.

An estimate of system performance can be obtained if the location of the first few roots in order of magnitude of the real part and the residues there at be known. It should be noted that the position of occurrence of the delay elements affects the values of the residues but not the position of the roots. It is not difficult to find the region where the real roots, if any, will occur. The complex roots are, however, less easily located. A detailed treatment of this and other related topics will be found in what follows.

2. *Roots of some transcendental equations*

We shall now consider some simple systems in respect of the location of the roots and stability.

Consider first the equation $p = c'\,e^{-p} = -c_e^{-j\,\theta}e^{-p}$ where c is real. Putting $-p = Z = u+iv$, one has easily

$$v^2 = c^2e^{2u}-u^2 \qquad \ldots \quad (3a)$$

$$v \cot (v+\theta) = u \qquad \ldots \quad (3b)$$

It is easily verified that (i) the closed branch of 3(a) exists only for $c \leqslant e^{-1}$ and (ii) the whole of the open branch of 3(a) lies to the right of its intersection with the real axis. (See figure 2 where curves A_1 and A_2 correspond to 3(a) with $c = 1$

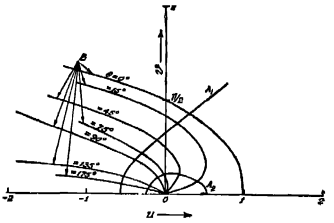

Fig. 2. Plot of (A) $v^2 = c^2 e^{2u} - u^2$
(B) $v \cot (v+\theta) = u$.

and 0.1 respectively and curves B to 3(b) for different values of θ). We note that the slope of the curve 3(a)

$$\frac{dv}{du} = \pm \frac{c^2 e^{2u} - u}{\sqrt{c^2 e^{2u} - u^2}}$$

is finite except at $u = ce^u$. Further, Eqns. 3(a) and 3(b) can be combined into $\log \frac{v \operatorname{cosec}(v+\theta)}{} = v \cot (v+\theta)$. For $v > 0$, $v \cot (v+\theta)$ has a local maximum at $2v = \sin (v+\theta)$, whereafter it uniformly decreases up to $v = \pi - \theta$; while for $v < 0$, it uniformly increases, going to ∞ at $v = -\theta$. It is apparent that if $c < e^{-1}$ there will be no roots except those in the interval $-\pi+\theta < v < \pi+\theta$. Hence the condition that the roots of $p = -c_e{}^{-p} e^{-j\theta}$ lie to the left of $Re(p) = K$ is

$$c < e^k (v^2+k^2)^{\frac{1}{2}} \tag{4}$$

where v is a root of $v \cot (v+\theta) = -k$ and $-(\pi+\theta) < v < \pi - \theta$.

The result (4) is directly applicable to cases where the characteristic polynomial is factorisable into terms of the form $p - c_r e^{-p}$.

We now consider the equation $p_1{}^n = c_1 e^{-p_1 \delta}$. This is reducible to $p^n = c^n e^{np}$. The curves, the intersections of which give the location of the roots are

$$v^2 = c^2 e^{2u} - u^2 \tag{5a}$$

$$v \cot \left(\frac{v+2m\pi}{n}\right) = u \tag{5b}$$

where m is any integer (for $c < 0$, replaces $2m$ by $2m+1$).

Equations (5) are identical with the equations (3) if we put $\theta = \frac{2m\pi}{n}$ and the results deduced regarding the latter hold in this case also. We observe that

there will be n branches of 5(b) and, in general, n roots will occur in the interval $r\pi < v < (r+1)\pi$, r being any integer, and the curve 5(b) is symmetrical about the $= 0$ axis. The root with the largest negative real part corresponds to the intersection of 5(a) with the curve 5(b) having θ or $\pi-\theta$ smallest, that is, the intersection occurring in the region $-\pi < v < \pi$. As regards boundedness, it is seen that all roots of $p^n = c^n e^{-np}$ lie to the left of $Re(p) = k$ if

$$c^2 < (v^2+k^2)\, e^{2k} \qquad \ldots \quad (5c)$$

where v is the root of $v \cot\left(v+\frac{2m\pi}{n}\right)$ in the interval $-\pi < v < \pi$. This result 5(c) is very useful when the characteristic polynomial, a part from the delay term, has a multiple root.

Next we consider the equation $p^2+2ap+b_0+r_1p^ne^{-p} = 0$. We take first the case $n = 0$, arising in connection with a position controlled servo. On putting $p+a = z$, the equation reduces to $z^2+c+re^{-z} = 0$ where $c = b_0-a^2$ and r, $e^a = r$. Now putting $Z = u+iv$, we have

$$u^2+2uv \cot v-v^2+c = 0 \qquad (6a)$$

$$v^4+2v^2(u^2-c)+(u^2+c)^2-r^2e^{-2u} = 0 \qquad (6b)$$

In 6(b), in order that the real solutions of v exists, it is clearly necessary that (i) when $c > 0$, $r^2 e^{-2u} > 4cu^2$ and $u^2 < c+\sqrt{r^2e^{-2u}-4cu^2}$ and (ii) when $c < 0$, $u^2 < c+\sqrt{r^2e^{-2u}-4cu^2}$. We may recall that $c > 0$ corresponds to an under-damped two-pole structure and $c < 0$ to the overdamped case. For $c > 0$, 6(b) has cuspidal tangents at $(u^2+c)^2 = r^2e^{-2u}$, which may occur at $u > 0$ if r is large enough ($|r| < c$). If $c > |r| > 0$, 6(b) starts at the cusp, bifurcates into the upper and lower half planes. Considering the upper branch, it rises from the cusp with a positive slope, turns at $u^2+v^2 = c$ and finally goes to $u = -\infty$, $v = \infty$. The lower branch is clearly an image of the upper. The part with the largest positive u lies in the region where v lies between $\sqrt{b_0}$ and 0. If, however, $c < 0$ the curve is single valued and the part with the largest real part lies near $v = 0$. Now the curve 6(a) has two branches in each half plane. Considering the upper, if $c < 0$ or $c \leqslant 1$, the two branches start at $-1+\sqrt{1-c} = u$ and $-1-\sqrt{1-c} = u$. For $c > 1$, they start at v_0, where $\frac{\sin v_0}{v_0} = \frac{1}{\sqrt{c}}$ (clearly $0 < v_0 < \pi$) where they bifurcate and rise. We notice that at $v = (2k+1)\frac{\pi}{2}$ the two branches are at equal distances $\left(\pm\sqrt{\left((2k+1)\frac{\pi}{2}\right)^2-c}\right)$ from the $u = 0$ axis and that at $v = m\pi$ one branch is on the $u = 0$ axis and the other is at infinity, with one notable property that the slope, excepting for the part near v given by $\frac{\sin v}{v} = \frac{1}{\sqrt{c}}$, is everywhere

positive. In figure 3 the values of c and r are : $c = 4$, $r = 1$; $c = 4, r = 10$; $c = -4$, $r = 10$ for the curves A_1, A_2, and A_3 respectively and the values of c for B_1 and B_2 are respectively 4 and -4.

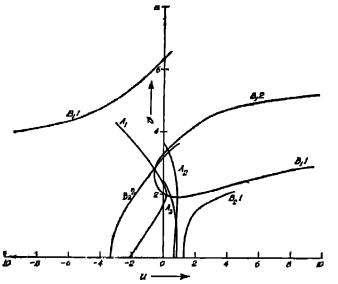

Fig. 3. Plot of (A) $\nu^4+2\nu^2(u^2-c)+(u^2+c)^2-r^2 e^{-2u}$

(B) $\nu \cot \nu = \dfrac{v^2-u^2-c}{2u}$

From the foregoing we have the results : (i) there will, in general, be two roots of the equation $p^2+2ap+b_0+re^{-p} = 0$ in the interval $m\pi < v < (m+1)\pi$, m being any integer, (ii) the root with the largest positive real part occurs at the intersection of 6(a) and 6(b) in the region where $\pi+b_0-a^2 > |v| > 0$, if $\sqrt{b_0-a^2}$ is real; otherwise in the region $0 < v < \pi$.

Similar graphical constructions are possible for the equation $p^2+2ap+b_0+rpe^{-p} = 0$ $(n = 1)$. For this case we consider instead the mapping of the p-plane into the planes $S_1 = x_1+iy_1$ and $S_2 = x_2+iy_2$. We draw contours corresponding to $u =$ constant and $v =$ constant in the p-plane Since S is an analytic function of p, the transformation will be conformal and the squares in the p-plane will transform into approximate squares in the S-plane. The line $u = 0$ is the locus of S_1 at real frequencies.

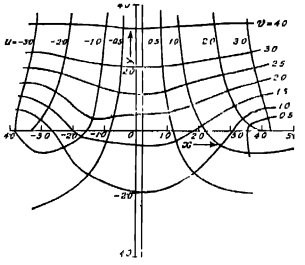

Fig 4. U-constant and v-constant contours of $\dfrac{p^2+0.2p+3}{p}$

The location of a root is found from the confluent intersections of the u-constant and v-constant curves of S_1 and S_2. It is easy to ascertain from the chart the value of r for which the largest value of the real part of the roots does not exceed, say, k. (See figure 4 which is plotted for $2a = 0.2$ and $b_0 = 3$. The plot of S_2 being very simple is not shown).

The equation $p^2+2ap+b_0+rp^2e^{-p} = 0$ $(n = 2)$ can be treated on similar lines.

The study of the equation with $n > 2$ is very instructive. Considering, for example, the equation with $n = 3$, we note that the magnitude and phase condition for a root is given by

$$(b_0+2au+u^2-v^2)^2+v^2(2u+2a)^2 = (u^2+v^2)^3e^{-2u} \qquad \ldots \quad (7a)$$

$$\tan^{-1}\frac{v(2u+2a)}{b_0+2au+u^2-v^2} = 3\tan^{-1}\frac{v}{u} - v + k\pi \qquad \ldots \quad (7b)$$

Considering the first equality, we note that it can be satisfied for any positive u, however large, and also for small negative values ; but it cannot be satisfied for a large negative u. Noting that the curve representing the second equality extends, in general, from $u = -\infty$ to $u = \infty$ for every π interval of v, we conclude that the roots of the equation are not bounded above. This result is, in fact, true for all $n > 2$. We now consider the equation $p^n = c^{2n}e^{-2n\sqrt{p}}$. The substitution

$$\sqrt{p} = \sqrt{\sigma+i\omega} = u+iv \text{ yields}$$

$$u^2 + v^2 = c^2e^{-2u} \qquad \ldots \quad (8a)$$

$$v \cot\left(\frac{v + 2k\pi}{n}\right) = -u \qquad \ldots \quad (8b)$$

Clearly for a large positive u, 8(a) requires $u^2+v^2 \simeq 0$, and for large negative u, $v^2 >> u^2$, hence the boundedness. The roots with positive $\sigma = R_e(p)$ correspond to the roots in the region between the lines $u = v$, $u = -v$ and the real axis.

For the case where $n = 1$, the curves we have to construct are $u^2+v^2 = c^2e^{-2u}$ and $v \cot v = -u$. These have already been drawn in another connection (see figure 2). We have here the easily verifiable result : The real part of the roots of $p = c^2e^{-2\sqrt{p}}$ will be non-positive if at the intersection of $v \cot v = -u$ and the line $u = v$,

$$c^2e^{2u} > 2u^2. \qquad \ldots \quad (9)$$

3. *Stability*

We shall now consider the stability of the solution of

$$p^3 + ap^2 + bp + c + rp^ne^{-p} = 0 \qquad \ldots \quad (10)$$

Coefficients a, b and c here are all real, and positive while r is real but may be either positive or negative. Such equations occur in process control systems as well as in the kinetics of circulating fuel reactors.

We refer here to Pontrajagin theorems · (I). If the polynomial $P(Z, e^Z) = P(Z, W)$ has a leading term, the real parts of the zeros of $P(Z, W)$ will be uniformly bounded above.

(II). Let $H(Z) = P(Z, e^z)$, where $P(Z, W)$ is a polynomial with a leading term. We write $H(iy) = F(y)+iG(y)$; if all the zeros of the function lie to the left of the imaginary axis then the zeros of the functions $F(y)$ and $G(y)$ are real, interlaced and

$$F(y)G'(y) - F'(y)G(y) > 0 \qquad \ldots \quad (11)$$

for all values of y. Conversely, in order that the roots of the function should lie to the left of the imaginary axis, it is sufficient that at least one of the conditions given below should be satisfied :

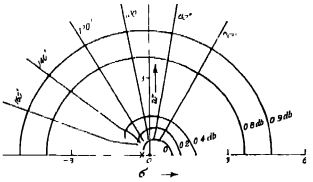

Fig. 5. (a) Equiamplitude and equiphase contours of $p^2/p+0.3$

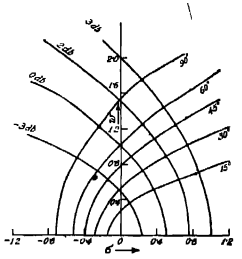

(b) Equiamplitude and equiphase contours of $c-\sqrt{p}$

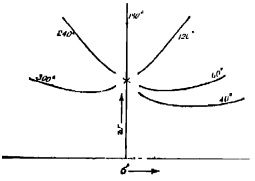

Fig. 6. (a) Equiphase contours of a pair of complex poles.

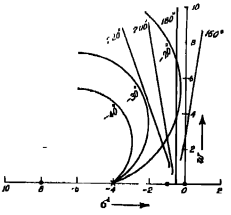

(b) Superposed equiphase contours of $p(p+1)$ and $\frac{p+8}{p+4}$

(i) All the roots of the functions $F(y)$ and $G(y)$ are real and interlaced and the inequality (11) holds for at least one value of y.

(ii) All the roots of $F(y)$ are real and the inequality which now reduces to $F'(y)\ G(y) < 0$ holds for each of them.

(iii) All the roots of $G(y)$ are real the inequality (11) holds for each of them *i.e.* $G'(y)\ F(y) > 0$.

The meaning of the theorems in terms of polar plot is that the total phase $\tan^{-1}\dfrac{G}{F}$ should be uniformly increasing with y and that the $\mathbf{F}+\mathbf{G}$ vector will unwind itself on the y-axis as many times as it has wound itself on the infinite semi-circle to the right of the y-axis. One observes that on the semi-circle of radius $R(R\to\infty)$ the zeros of F and G occur at $(2k+1)\dfrac{\pi}{2} = n\theta+y$, and at $m\pi = n\theta+y$, respectively and thus each has exactly $4l\pi$ roots in an interval $2l\pi$ of y Thus for

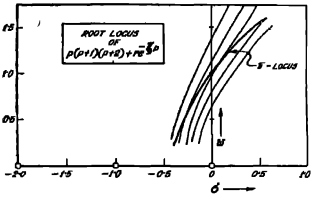

Fig. 7. (a) Root locus of $p(p+1)(p+2)+re^{-p}$

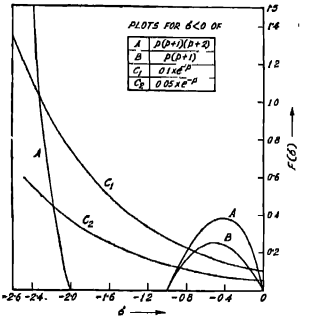

(b) Illustrates shift of real roots of $p(p+1)(p+2)+re^{-p}$ with r.

H to have no root to the right of the y-axis it is necessary that this situation be repeated on the y-axis. We now return to Eqn. (10) which can be re-written as

$$H(p) = (p^3+ap^2+bp+c)e^p+rp^n = 0 \qquad \ldots \quad (12)$$

For the presence of a leading term we require $n \leqslant 3$. Let us consider the case of $n = 0$ in some detail. Writing $p = iw$ we have

$$H(iw) = F(w)+iG(w)$$
$$= (c-aw^2)\cos w+(w^3-bw)\sin w+r+i\{(c-aw^2)\sin w+(b-w^2)\,w\cos w\}$$

This can be written as

$$H(iw) = A(w)\cos(w+\phi)+r+i\ A(w)\sin(w+\phi)$$

where $A(w) = [(c-aw^2)^2+w^2(b-w^2)^2]^{\frac{1}{2}}$ and $\phi w) = \tan^{-1}\dfrac{w(b-w^2)}{c-aw^2}$.

Then

$$G'(w)\,F(w) = \{A(w)\cos(w+\phi)+r\}\{A'(w)\sin(w+\phi)+(1+\phi'(w)\,A(w)\cos(w+\phi)\}.$$

We may note that the positiveness of the slope of $\phi(w)$ is ensured by the fact that the roots of $p^3+ap^2+bp+c=0$ lie in the left half of the p-plane. Since $\phi'(w)$ is always positive, the condition $F(w)\,G''(w)>0$ at the roots of G *i.e.* at $w\cot w = \dfrac{c-aw^2}{w^2-b}$, requires that

$$\cos(w+\phi)\,.\left[\cos(w+\phi)+\frac{r}{A(w)}\right]>0.$$

The inequality is best tested near the minimum of $A(w)$. Now there are two cases to consider . (a) when the roots are all real (b) when a pair is complex. If the roots are all real, it suffices to test the inequality in the region $0 \leqslant w \leqslant 3\pi$ If a pair be complex, a minimum exists if the quadratic $3x^2+2(a^2+b)x+b^2-2ac$ has a real positive root. Also k defined by $w+\phi = k\pi$, should be taken as odd if $r>0$, or else even.

Now let the maximum value of $u = \dfrac{r}{A(w)}$ occur at w_0 (found from the condition that at w_0 the discriminant of the cubic $x^3+(a^2-2b)x^2+(b^2-2ac)x+c^2+\dfrac{r^2}{u^2}$ is zero). Then the condition that $H(p)$ has no root with positive real part is : At the root of $w\cot w = \dfrac{c-aw^2}{w^2-b}$ closest to the maximum of $\dfrac{r}{A(w)}$,

$$1-\frac{r}{A(\omega)}>0 \qquad \ldots \quad (13)$$

We next consider Eqn. (12) for $n=1$. Thus $H(h) = (p^3+ap^2+bp+c)e^{-rp}$. From the condition $G(w)F'(w)<0$ at the roots of $F(w)$ *i.e.* at $w\tan w = \dfrac{c-aw^2}{b-w^2}$ it follows that

$$\{A'(w)\cos(w+\phi)-A(w)\,.\,(1+\phi'(w))\sin(w+\phi)\}\{A(w)\sin(w+\phi)+rw\}<0.$$

Remembering that at a root of $F(w)$, $w+\phi=(2k+1)\dfrac{\pi}{2}$, the condition reduces to $1>\dfrac{rw}{A(w)}$ at a root of $F(w)$. Now the maximum value of $u=\dfrac{rw}{A(w)}$ renders the discriminant of the cubic $x^3+(a^2-2b)x^2+\left(b^2-2ac-\dfrac{r^2}{u^2}\right)^2+c^2$ to zero.

It can thus be readily seen that $H(p)$ will have no root with positive real part if

$$1-\frac{rw_m}{bw_m-w_m^3}\cos w_m>0 \qquad \ldots \quad (14)$$

where w_m is the sole positive root of $w\tan w = \dfrac{c-aw^2}{b-w^2}$ in the interval $m\pi < w$

$<(m+1)\pi$ closest to the maximum of $\frac{rw}{A(w)}$, and provided that k in $(w+\phi) = (2k+1)\,\pi/2$ is geven when $r < 0$ or else odd.

We now give the corresponding results for the equations with $n = 2$ and 3.

The Eqn. $(p^3+ap^2+bp+c)e^p+rp^2$ will have no root with positive real part if

$$1-\frac{rw_m^2}{c-aw_m^2}\cos w_m > 0\,. \qquad \ldots \quad (15)$$

where w_m is the root of $w \cot w = \frac{c-aw^2}{w^2-b}$ closest to the maximum of $u = \frac{rw^2}{A(w)}$, and k defined by $w+\phi = k\pi$ is odd if $r < 0$ or else even.

The eqn. $(p^3+ap^2+bp+c)e^p+rp^3$ will have no root with positive real part if

$$1-\frac{r\,w_m^3}{A(w_m)} > 0\,, \qquad \ldots \quad (16)$$

where $A(w_m)$ is the magnitude of p^3+ap^2+bp+c at $p = iw_m$ and w_m is the root of $w \tan w = \frac{c-aw^2}{b-w^2}$ closest to the maximum of $\frac{rw^3}{A(w)}$.

It should be emphasised that the technique employed here is readily adapted to higher order cases. For an example, let us take the equation

$$(p^4+ap^3+bp^2+cp+d)e^p+r = 0.$$

Here we shall have two distinct cases according as the minimum value of $(w^4-bw^2+d)^2+w^2(w^2-c)^2$ occurs at $w = 0$ or not. Let it occur at w_m. We have now to find the condition for $F(w)G'(w) > 0$ at the root of $G(w)$ *i.e.* at $w \cot w = \frac{w^4-bw^2+d}{w^2-c}$ closest to w_m.

4. *Graphical methods*

We shall now study the location of the roots and the stability of delayed systems by graphical methods, viz., the dual loci technique and the dual Nyquist diagram.

Dual loci technique

It is known that the amplitude and phase due to poles and zeros of a network function are analogous to the potential and stream functions respectively of a set of filamentary charges of proper sign. The equipotentials and stream function contours of a single filamentary charge consist of a system of circles and radial lines. Labelling the equipotentials in logarithmic units, it is easy to draw

by simple addition the resultant equi-amplitude (V) and equi-phase (ϕ) contours due to a number of poles and zeros.

We observe that the V = constant, ϕ = constant contours of re^{-p} are a set of lines parallel to the axes while those of $re^{-\sqrt{p}}$ are given by the parabolas,

$$\sqrt{\sigma^2+w^2}+\sigma = K_1 \quad \text{and} \quad \sqrt{\sigma^2+w^2}-\sigma = K_2 \quad \text{(figure 5b)}$$

By superposing the equi-amplitude and equi-phase curves on the same graph, one can easily obtain the roots of the characteristic equation and evaluate the residues at the roots. Obviously this method facilitates prediction of system performance with adjustment and compensation.

The inverse of the overall transfer function $G_0(p)$ is given by $\frac{1}{G_0(p)} = \frac{1}{rG(p)L}$ $+H_f(p)$. The singularities of $\frac{1}{G(p)}$ and $H_f(p)$ are first plotted on the p-plane. The equi-phase and equi-amplitude contours for $\frac{1}{G\,H_f(p)}$ and $L(p)[re^{-p}$ or $re^{-\sqrt{p}}]$ are then drawn. The next step is to plot the phase locus, *i.e.*, the locus on which the total phase equals π radians, and to insert the gain values at selected points on it.

It is useful to note some properties of the loci. Let $H_0(p)$, to restate, be $\frac{N(p)}{D(p)}$ and let n, the difference of the orders of N and D, be positive. The asymptotic amplitude and phase characteristics are the same as those of a zero of order n at the centre of charge of the system. (The root distributions of such simple systems have already been described in Sec. 2). At any particular σ one may profitably use the Bode asymptotes with proper regard, however, to the position of the singularities with respect to the σ = constant line. The phase due to a zero at a point σ, w to its right is $\tan^{-1}\frac{w-w_k}{\sigma-\sigma_k}$ and at a point to its left is $\pi-\tan^{-1}\frac{w-w_k}{\sigma-\sigma_k}$. The phase angle of $H_0(p)$ on the real axis is π radians over the segments to the right of which the number of singularities is odd. Hence if $r > 0$, the real roots of $H_0(p)+re^{-p}$ will occur only on such segments, while the roots of $H_0(p)+re^{-\sqrt{p}}$ can occur only at the points $\sigma = -m^2\pi^2$, m is any integer.

The phase loci for complex roots of delayed systems will clearly be more bent towards the right than those of non-delayed systems. Now on any π-locus the magnitude of $H_0(p)$ may increase or decrease as the real part of p increases. Confining our attention to the locus determining the location of the predominant

pair of complex roots, we note that if the locus has a positive gradient and if $H_0(p)$ decreases with $Re(p)$, instability in delayed control systems sets in at a smaller value of open loop gain and the frequency of oscillation is lower.

An increase in gain, it is evident, will cause the roots to shift to regions of higher $\frac{H_0(p)}{L(p)}$ and the amount of shift will depend on the nature of the system, non-delayed, pure delay or distributive. In delayed systems $L(p)$ decreases uniformly with increase of $Re(p)$. Hence if gain is reduced, a root will shift to the right if $H_0(p)$ decreases with $Re(p)$ and to the left if $H_0(p)$ increases with $Re(p)$; the former movement will be less and the latter more than that occurs in non-delayed systems in similar situations. (See figure 8 depicting the location of the real roots of $p(p+1)+re^{-p}$ and $p(p+1)(p+z)+re^{-p}$ for $r = 0.1$ and $r = 0.05$).

Dual Nyquist diagram for stability

For the purposes of a dual Nyquist diagram the characteristic equation is considered as a sum of two functions $F_1(p)$ and $F_2(p)$, and the diagram consists of two polar plots of $-F_1(j\omega)$ and $F_2(j\omega)$. Instability will be revealed by the value of the total phase change over the contour formed by the imaginary axis and the infinite semi-circle in the right-half plane. This technique permits a rapid study of stability property as one, say F_2 is varied, as well as of the amplitude response.

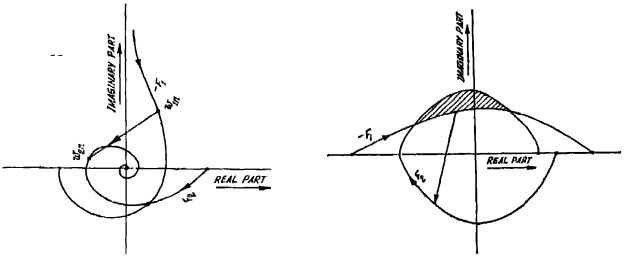

Fig. 8. A dual Nyquist diagram to illustrate
(a) Space and intersection (b) Shell.

The procedure for determining the stability of the system is stated below. On first plots the functions $-F_1(j\omega)$ and $F_2(j\omega)$. We call the points corresponding to ω_n in $-F_1$ and F_2 the terminal points ω_{1n} and ω_{2n} respectively. The region enclosed by F will be termed F-space and the region enclosed together by the arcs of F_1 and F_2 a shell. The following rules with regard to stability are easily derived:

(i) The system is stable if ω_{1n} originates inside the F_2-space and leaves it before ω_{2n} reaches the point of exit.

(ii) The system is unstable if one locus completely encloses the other.

(iii) The system is unstable if ω_{1n} enters the F_2-space and does not leave it.

(iv) The system is unstable if ω_{1n} and ω_{2n} find each other inside any shell.

We shall now consider the application of the dual Nyquist diagram in connection with the expression :

$$\frac{p^2+ap+b_0}{p^n}+rL(p) = \frac{1}{G(p)}+F(p)$$

where $L(p)$ is either e^{-p} or $e^{-\sqrt{p}}$ for certain specific cases.

1. First consider the case where $n = 0$. We note that if $\left|\frac{1}{G(j\omega)}\right| > r$ for all ω there can be no intersections of the plots of $-\frac{1}{G}$ and F. Let us assume that $\left|\frac{1}{G(j\omega)}\right| < r$ for a range of values of ω. Now two distinct cases arise according as there is only one intersection or two (It is to be noted that $\left|\frac{1}{G(j\omega)}\right|$ exhibits a minimum only if $2b_0 > a^2$) In the former case the system is stable if $-1/G$ leaves R_A (figure 9) before F reaches it, and in the latter the system is stable if the terminal points do not meet inside the shell $M_1\ N_1$ (figure 11).

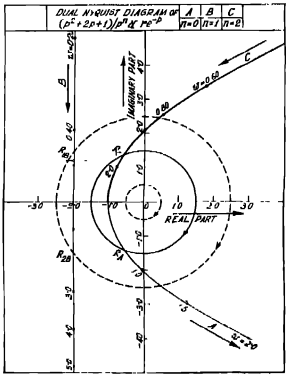

Fig. 9. Dual Nyquist diagram of $\frac{p^2+2p+1}{p^n}$ and re^{-p}

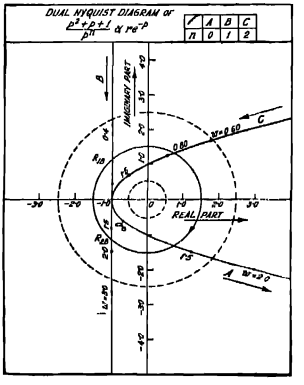

Fig 10. Dual Nyquist diagram of $\frac{p^2+p+1}{p^n}$ and re^{-p}

2. The case $n = 1$. The system is stable if the terminal points do not meet inside the shell $R_{1B}-R_{2B}$ (see figures 9 and 10).

3. The case $n = 3$. The number of intersections may be one or two. In the former case it is required for stability that the terminal points be not lodged

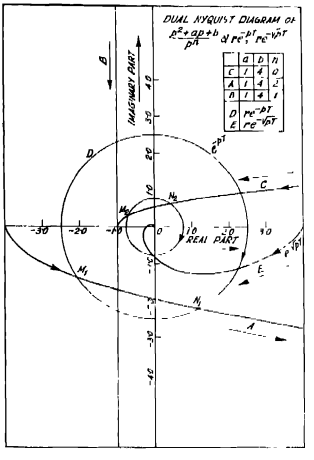

Fig. 11. Dual Nyquist diagram of $\frac{p^2+p+4}{p^n}$ and re^{-p}

inside $F(j\omega)$ (figure 9) and in the latter, the terminal points do not meet inside the shell M_2N_2 (figure 11).

ACKNOWLEDGMENT

The author is deeply indebted to Professor J. N Bhar for guidance and helpful suggestions and to Mr. A. K. Chowdhury and Mr. B R. Nag for valuable assistance during the progress of the work.

He is also grateful to Professor S. K. Mitra, for his encouragement and kind interest in the work.

The grant of a Senior Research Scholarship made by the Ministry of Education, Government of India, is thankfully acknowledged.

REFERENCESS

Ansoff, H. I., 1949. *Jour. of Appl. Mech.* **16**, 158.

Callender, A., Hartree, D. R. and Porter, A., 1936. *Phil. Trans. Royal Soc. London*, Ser. A., **235**, p. 415-444.

Farrington, Automatic Control Systems.

Hayes, N. D., 1950. *Jour. Lond. Math. Soc.*, **25**, 226.

N. Minorsky, 1948. *Jour. of Appl. Phys.*, **19**, 332.

15

THE INFLUENCE OF CONSTANT ELECTRIC AND MAGNETIC FIELDS ON THE SPIN OF THE PARTICLE

S SARKAR

DEPARTMENT OF THEORETICAL PHYSICS, INDIAN ASSOCIATION FOR THE CULTIVATION OF SCIENCE, JADAVPUR, CALCUTTA-32

(*Received for publication, September* 28, 1957)

ABSTRACT. If we assume that the particle obeys the second order equation obtained in the usual way of operating twice the Dirac's linear Hamiltonian, we find that the change of momentum and spin direction of a particle subjected to magnetic and electric fields is the same as for a particle obeying Dirac's first order equation

INTRODUCTION

Tolhoek (1951) has discussed the change of momentum and spin orientation of an electron beam when subjected to constant transverse and longitudinal electric and magnetic fields. He has treated the problem for the electron according to three methods, viz , Klein-Gordon's equation, Pauli spin theory and Dirac's linear equation. The result for the change of momentum direction obtained from the Klein-Gordon equation is the same as one gets from the Dirac's equation, whereas the result from the Pauli spin theory is the non-relativistic approximation of the above For the change of spin orientation what the Pauli spin theory gives is again the non-relativistic limit of what is obtained from Dirac's theory.

If we operate twice the Dirac linear Hamiltonian, we obtain the following equation :

$$\left[(E-e\phi)^2-(c\boldsymbol{p}-c\boldsymbol{A})^2-m^2c^4+e\hbar c\sigma \,.\, \boldsymbol{H}+ie\hbar c\alpha.\ \vec{c} \right] \psi_u = 0 \qquad \ldots \quad (1)$$

Let us consider the influence of transverse electric field along y-axis on the orientation of spin direction of the electron moving along x-axis and obeying the above equation.

We have

$$\epsilon = \epsilon \boldsymbol{j}, \quad \phi = \epsilon y, \quad \boldsymbol{A} = 0 \qquad \ldots \quad (2)$$

As before we put

$$\psi = e^{ief(x,y)}\, \psi_0 \qquad \ldots \quad (3)$$

where ψ_0 is the usual solution of the Dirac's equation for a free electron

$$\psi_0 = \begin{pmatrix} -\dfrac{cp_zA}{E+mc^2} - \dfrac{c(p_x-ip_y)B}{E+mc^2} \\ -\dfrac{c(p_x+ip_y)A}{E+mc^2} + \dfrac{cp_zB}{E+mc^2} \\ A \\ B \end{pmatrix} e^{\frac{i}{\hbar}(\boldsymbol{px}-et)} = \begin{pmatrix} -\dfrac{cpB}{E+mc^2} \\ -\dfrac{cpA}{E+mc^2} \\ A \\ B \end{pmatrix} e^{\frac{i}{\hbar}(px-Et)} \quad \ldots (4)$$

Since $p_y = p_z = 0$ and $p_x = p$. Under the conditions of (2), equation (1) becomes

$$[E^2 - m^2c^4 - c^2p_x^2 - c^2p_y^2 - c^2p_z^2 + 2eE\epsilon y + i\hbar c\alpha_y\epsilon]\,\psi = 0 \quad \ldots (5)$$

Substituting (2) into (5), we have

$$\partial f/\partial x - \frac{i\hbar}{2p}(\partial^2 f/\partial x^2 + \partial^2 f/\partial y^2 + \partial^2 f/\partial z^2) - \frac{Ecy}{c^2hp} - \frac{ic\alpha_y}{2p} = 0 \quad \ldots (6)$$

Equation (6) can be satisfied by the following relation

$$f = (\epsilon E/\hbar pc^2)xy + i(c/2pc)\alpha_y \quad \ldots (7)$$

$$\psi = \begin{pmatrix} \psi_1 \\ \psi_2 \\ \psi_3 \\ \psi_4 \end{pmatrix} = e^{i\epsilon}[(\epsilon E/\hbar pc^2)xy]\left[1 + \frac{ie\epsilon}{2pc}x\begin{pmatrix} 0 & 0 & 0 & 1 \\ 0 & 0 & -1 & 0 \\ 0 & 1 & 0 & 0 \\ -1 & 0 & 0 & 0 \end{pmatrix}\right]\begin{pmatrix} -\dfrac{cpB}{E+mc^2} \\ -\dfrac{cpA}{E+mc^2} \\ A \\ B \end{pmatrix} e^{\frac{i}{\hbar}(px-Et)} \quad \ldots (8)$$

We can write

$$\begin{pmatrix} \psi_3 \\ \psi_4 \end{pmatrix} = \begin{pmatrix} A \\ B \end{pmatrix} K(x, y, t) + \frac{ie\epsilon}{2pc}x\,\frac{cp}{E+mc^2}\begin{pmatrix} -A \\ B \end{pmatrix} K(x, y, t) \quad \ldots (9)$$

$$= \left(1 - \frac{i}{2}\sigma_z\frac{e\epsilon}{E+mc^2}x\right)\begin{pmatrix} A \\ B \end{pmatrix} K(x, y, t) \quad \ldots (11)$$

where $K(x, y, t) = e^{(i/\hbar)(px-Et)+ie(\epsilon E/hpc^2)xy}$

According to Darwin (1928)

$$-B/A = \cot\frac{\chi}{2}e^{i\omega} \qquad \ldots \quad (12)$$

where χ and ω are colatitude and longitude of electron spin respectively From (10)

$$-\frac{\psi_4}{\psi_3} = -\frac{B}{A}\cdot\frac{1+\dfrac{iecx}{2(E+mc^2)}}{1-\dfrac{iecx}{2(E+mc^2)}} \approx \cot\tfrac{1}{2}\chi\, e^{i\omega}\,.\, e^{i\frac{e\epsilon}{E+mc^2}x} \qquad \ldots \quad (13)$$

Therefore we obtain for the rotation of spin axis about z-axis

$$\Delta\alpha_{\epsilon 1} = [e\,\epsilon/(E+mc^2)]x \qquad \ldots \quad (14)$$

Also

$$\Delta p_x = 0, \quad \Delta p_z = 0, \quad \Delta p_y = (e\,\epsilon E/pc^2)x, \quad \Delta\gamma_\epsilon = \frac{\Delta p_y}{p_z} = \frac{eE\epsilon}{p^2c^2}\,x \qquad \ldots \quad (15)$$

$$\Delta\alpha_{\epsilon 1}/\Delta\gamma_\epsilon = p^2c^2/E(E+mc^2) = E_{min}/E \qquad \ldots \quad (16)$$

By $\Delta\alpha_{\epsilon 1}/\Delta\gamma_\epsilon$ we compare the rotation of spin orientation with the deflection of the beam.

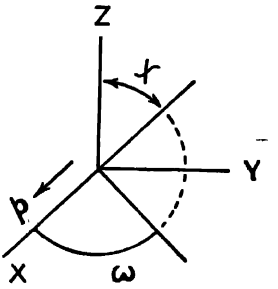

Fig. 1

From (16) we see that the spin orientation remains nearly constant in space for small kinetic energies. The corresponding value for transverse magnetic field is given by

$$\Delta\alpha_{\beta\perp}/\Delta\gamma_\beta = 1$$

where $\Delta\alpha_{\beta\perp} = -(e_\beta/pc)x. \qquad \Delta\gamma_\beta = -(e_\gamma/pc)x.$

The reason for this discrepancy is that the electric moment is v/c times less effective so far as rotation of spin direction in electric field is concerned than that of the magnetic moment and the deflection in magnetic field is v/c times less strong than that in electric field for the same magnitude of both electric and magnetic fields. In a similar manner we can treat the case of longitudinal electric field and also of the magnetic fields.

ACKNOWLEDGMENT

The author is grateful to Dr. D. Basu for suggesting the problem and for his valuable discussion during the progress of the work.

REFERENCES

Darwin, C. G., 1928, *Proc. Royal Soc.*, **120**, 621.
Tolhoek, H. A., 1951, *Physica*, **17**, 17.

ON THE CALCULATIONAL PROCEDURES IN THE DERIVATION OF THE VIBRATIONAL TRANSITION PROBABILITIES OF THE FIRST NEGATIVE ($b^4\Sigma^-_g \rightarrow a^4\Pi_u$) BANDS OF O_2^+

N. R. TAWDE AND N. SREEDHARA MURTHY

DEPARTMENT OF PHYSICS, KARNATAK UNIVERSITY, DHARWAR

(*Received for publication, November* 18, 1957)

ABSTRACT. Recently, Rao and Ranade have published some calculations of vibrational transition probabilities of the bands of O_2^+ (first negative) system A study of that paper has revealed two very serious errors in the calculations and in the usage of the methods applied by the authors The first error is due to the wrong usage of mathematical technique of Manneback for the calculation of vibrational transitional probabilities, and the other error is in the interpretation and derivation of transition probabilities by the application of the method of Manneback and Rahman.

Rao and Ranade (R & R) (1957) gave calculations of what, according to them, are transition moments and vibrational transition probabilities of the bands of the first negative system of $O_2^+(b^4\Sigma_g^- \rightarrow a^4\pi_u)$. They have applied the methods of (i) Manneback (1951) and (ii) Manneback and Rahman (1954) to compute these values. These data have been studied by them in terms of the available values of transition probabilities of Jarmain, Fraser and Nicholls (1955) on this system As a result of this comparative study, they have emphasised the earlier conclusions of Shuler (1950, 1952) on OH ($A \rightarrow X$) system, that howsoever one may take the mechanical anharmonicity of the wave function into account in any theory of vibrational transition probability, the contribution at the same time, of the variation of electronic transition moment with internuclear separation R, could not be neglected, as it is an important factor for consideration.

The application of the theory of Manneback and Rahman to such problems requires the knowledge of the exact relation of electronic transition moment with R for the particular band system. For without it, the contribution of this variation to the vibrational transition probability in relation to that of mechanical anharmonicity cannot be judged. To our knowledge, neither this relation, nor the experimental vibrational intensities for any of the bands of this system, from which this relation could be obtained, are on record. This aspect aroused our interest in the calculations of (R & R). A careful scrutiny of their paper brought out certain very fundamental points and issues which nullify their results and the conclusions based on them. It was therefore thought imperative to put these findings on record, in order to see the work of (R & R) in its proper perspective.

I

It has been shown already by Tawde, Patil, Sreedhara Murthy and Katti (1957) in the case of OH($A \rightarrow X$) system that Hutchisson's and Manneback's analytical treatments, although differing in complexity, lead to exactly identical results. This test has been applied here to the first negative band system of O_2^+ under consideration, employing the same constants as those used by Rao and Ranade (1957). The transition probabilities are calculated by Hutchisson's and Manneback's methods and these results are presented in Table 1 in columns 2 and 3 For comparison, the values of (R & R) by Manneback's method are reproduced side by side in column 4.

TABLE I

Calculated transition probabilities.
O_2^+(First negative) $b^4\Sigma_g \rightarrow a^4\pi_u$

Band v', v''	Hutchisson (present authors)	Manneback (present authors)	Manneback (R & R)
0,0	0 255	0.255	0 255
0,1	0 373	0.373	0 323
0,2	0.246	0.246	0.181
0,3	0 096	0.096	0.059
1,0	0.323	0 323	0.373
1,1	0 033	0.033	0 033
1,2	0 092	0 092	0 082
1,3	0.258	0 258	0.195
2,0	0 228	0.228	0.300
2,1	0 050	0 050	0.061
2,2	0.159	0 159	0 164
2,3	0 000_3	0 000_3	0 000_2
3,0	0.118	0.118	0.175
3,1	0.168	0 168	0.226
3,2	0 009	0.009	0 010
3,3	0.127	0 127	0.135

It is evident from the table that even in the case of this system as in OH ($A \rightarrow X$) system, there is complete agreement between the results emerging from both the methods, viz., Hutchisson's and Manneback's, and this is as it should be, as made out in the work of Tawde, Patil, Sreedhara Murthy and Katti (1957), and will be further shown by mathematical equivalence between the two in a forthcoming paper. The fact that the calculated values of (R & R) by the same mathematical treatment do not agree with ours indicates that they have badly erred in following the method of Manneback (1951), and applying it to the problem in hand. In arriving at this conclusion, we have applied whatever internal checks were necessary at each step of the calculations, leading to the results of columns 2 and 3 (Table I), and we have reproduced the values at every stage.

Although, the method of Hutchisson is cumbersome and requires laborious calculations over protracted period, we have, as an external check, employed it here only to be sure of the correctness of our procedures in working out the data from Manneback's method.

While attempting to locate the source of the values arrived at by Rao and Ranade it was found that they resulted from the misunderstanding on the part of the authors, of the use of the two general formulae I and II given by Manneback for the calculation of $C(n' n'')$ matrix These formulae contain the quantities. Δ, k, a and b, and are valid for any of these values including negatives as stated by Manneback. Correct values of transition probabilities would follow by the direct use of these quantities with their proper signs in the two formulae. The values happen to be negative in the particular case of O_2^+ (first negative) system, and are to be directly used with their signs in the general formulae for the evaluation of $C(n' n'')$ matrix The square of $C(n' n'')$ then gives the transition probabilities. This way have resulted our data of column 3 in Table I An alternative but simpler way suggested by Manneback when negative values of the above are encountered, is to interchange the meaning of upper and lower states, *i.e.* of n' and n'', while retaining their positive values. This simpler way has been adopted by (R & R) but in using it, they have not correctly interpreted the meaning of it, which is obviously more than mere interchange of n' and n''. (R & R) have taken the above remark of Manneback to mean merely the interchange of quantum numbers, n' and n'', without considering the real meaning of it, viz., interchange also of the quantities involved in the upper and lower states along with the interchange of n' and n''. The consequence is that wrong values have emerged for $C(n' n'')$ and hence the transition probabilities, and they are represented as such in their paper. We have also tried this alternative but simpler way with its correct meaning given above, and arrived at the values identical with those of column 3 (Table I). In following the correct use of Manneback's mathematical technique, the method of Manneback has to be understood in the context of Hutchisson's analytical treatment.

II

In their attempt to include the contribution of variation of electronic transition moment with R, to the transition probability against the background of the above results, the authors have also erred in their fundamental approach to this question This problem is sought to be investigated through the application of Manneback and Rahman's treatment. But, in doing so, they have made untenable assumptions. This can be understood from the following analysis

Following Shuler (1950), Manneback and Rahman start from the integral involving the wave functions of the upper and lower states :

$$| M_{n'n''} | = \int \psi_{n'}(R) M_{e'e''}(R) \psi \quad (R) dR \qquad \ldots \quad (1)$$

where $M_{e'e''}(R)$, the electronic transition moment can be taken to be constant, or a variable of R. The main object of Manneback and Rahman's treatment has been to take the latter into account in the theory, viz., the variability of electronic transition moment with R, and they considered the variation according to the linear relation of Shuler viz., $M_{e\,e''}(R) = c(1+\rho R)$, ρ being the expansion coefficient. With the introduction of this relation in equation (1), the integral $|M_{n'n''}|$ becomes

$$|M_{n'n''}| = c\,[\int \psi_{n'}(R)\ \psi_{n''}(R)dR + \rho \int \psi_{n}(R)\psi_{n''}(R)RdR| \qquad \ldots \quad (2)$$

This expression (2) is written in the from

$$|M_{n'n''}| = c[C(n'\,n'') + \rho D(n'n''| \qquad \ldots \quad (3)$$

where $$C(n'\,n'') = \int \psi_{n'}(R)\ \psi_{n''}(R)dR \qquad \ldots \quad (3a)$$

and $$D(n'\,n'') = \int \psi_{n'}(R)\psi_{n''}(R)RdR \qquad \ldots \quad (3b)$$

The square of the quantity $|M_{n'n''}|$ gives the transition probability, p. The expression for $|M_{n'n''}|$ consists therefore of two terms. The first term $C(n'\,n'')$ in the bracket is the same integral as referred to in Manneback's theoretical application discussed in Section 1 above The second term is the additional one brought about as a result of the electronic transition moment being considered to vary with R It consists of two factors. (a) ρ, the expansion coefficient and (b) $D(n'\,n'')$, another integral stated above As a close parallel to the treatment for $C(n'\,n'')$ matrix, Manneback and Rahman have given the following formula for computing the $D(n'\,n'')$ matrix

$$D(n'\,n'') = XC(n'\,n'') + Yn'C(n'-1,\,n'') + Zn''C(n',\,n''-1) \qquad \ldots \quad (4)$$

where the quantities X, Y and Z have the meaning defined by them. $D(n'\,n'')$ matrix can therefore be computed if $C(n'\,n'')$ martrix is known

The quantity $|M_{n'n''}|$ in equation (3) is therefore calculable from $C(n'\,n'')$ and $D(n'\,n'')$, provided the value of ρ is known. The value of constant, c, could be eliminated by considering the relative values of transition probabilities for a pair of bands. But ρ for this particular system of O_2^+(first negative) is not known, nor have (R & R) derived any value for it. Hence $|M_{n'n''}|$ and therefore p cannot be estimated. It is therefore not understood how (R & R) could get the values of $|M_{n'n''}|$ and hence p. It has, however, been noticed that (R & R) have assumed $D(n'\,n'')$ to be itself the "overlap integral" and have taken the square of it to be the value of p for the condition under which the electronic transition moment is supposed to vary with R. This is obviously wrong, since it involves the assumptions that $C(n'\,n'') = 0$, $c = 1$ and $\rho = 1$, which are untenable. As has been shown,

$D(n' n'')$ taken along with the factor ρ is only an additional term to $C(n' n'')$, to take account of the variation of electronic transition moment with R in the calculation of transition probabilities. Further, the numerical values given by (R & R) for $D(n' n'')$ are also wrong since the values of $C(n' n'')$ on which they depend have been shown to be erroneous.

Apart from the two fundamental defects from which the calculations of (R & R) suffer, there are some minor corrections required which are not so significant as to need a particular note. As a consequence of these defects the main results of their calculations are erroneous. Hence, the conclusions drawn by them from the comparative study of those results in terms of the values of Jarmain, Fraser and Nicholls (1955) cannot sustain.

ACKNOWLEDGMENT

One of the authors (N.S M.) acknowledges his gratitude to the Ministry of Education, Government of India, for the award of a Senior Research Training Scholarship which enabled him to participate in this particular piece of work in the general programme in hand.

REFERENCES

Jarmain, W. R., Fraser, P. A., and Nicholls R W., 1955, *Astrophys. J.*, **122**, 55.
Manneback, C., 1951, *Physica*, **17**, 1001.
Manneback, C. and Rahman, A., 1954, *Physica*, **20**, 497.
Rao, P. S. and Ranade, J. D., 1957, *Ind. J. Phy.*, **31**, 491.
Shuler, K. E., 1950, *J. Chem. Phys.*, **18**, 1221.
,, 1952, *Proc. Phys. Soc. (London)*, **A65**, 70.
Tawde, N. R., Patil, B S., Sreedhara Murthy, N. and Katti, M. R., 1957, *Physica*, **23**, 154.

X-RAY CRYSTALLOGRAPHIC DATA ON RUBIDIUM FUMARATE, MONOHYDRATE ($Rb_2C_4H_2O_4, H_2O$)

M. P. GUPTA AND G. P. DUBE

DEPARTMENT OF PHYSICS, RANCHI COLLEGE, RANCHI

(*Received for publication, January* 18, 1958)

Plate III

ABSTRACT. Single crystal photographs show rubidium fumarate, monohydrate ($Rb_2C_4H_2O_4, H_2O$) to be triclinic with,

$$a = 9.23\text{Å}, \quad b = 7.51\text{ Å}, \quad c = 6.66\text{ Å}$$

$$\alpha = 81°5', \quad \beta = 96°42', \quad \gamma = 91°48'$$

There are two formula units in the cell. The space group is suggested to be $P\bar{1}$. Attention is drawn towards the pseudo-monoclinic symmetry. Indexed power diffraction data for the compound is given at the end in tabular form.

Several potassium and rubidium salts of fumaric acid have been reported in Beilstein's Organische Chemie (Band II, Syst. No. 179, p. 637) and their X-ray crystallographic examination was completed by Gupta (1953) and Gupta and Barnes (1958). While the work on the determination of the crystal structure of potassium fumarate, dihydrate ($K_2C_4H_2O_4, 2H_2O$) was in progress, the desirability of preparing an isomorphous rubidium salt, rubidium fumarate, dihydrate ($Rb_2C_4H_2O_4, 2H_2O$) was felt. This compound is not reported anywhere in the chemical literature but it was anticipated that by mixing stoichiometric proportions of fumaric acid and rubidium carbonate, such a compound could be prepared. In the event that the compound so prepared did not turn out to be isomorphous with the corresponding potassium fumarate, this result is being published.

Preparation : One gram of rubidium carbonate (Fischer, reagent) was mixed with the stoichiometric amounts of fumaric acid in water solution and the resulting solution was warmed, filtered off and left for crystallization (by the method of slow evaporation) in crystallizing dishes. After a fortnight, several platy crystals were obtained with the (100) as the platy face. These were considered suitable for X-ray work after the usual examination in the polarizing microscope.

Unit cell : The unit cell which was found to be triclinic was determined by mounting a single crystal (1 mm × 1 mm × 0.25 mm) on the Buerger precession camera. The reciprocal cell angles γ^* and β^* were measured directly on the zero level precession photographs showing the reciprocal nets a^*-b^* and a^*-c^* respectively while the interaxial direct cell angle $\alpha(b\frown c)$ was measured directly

from the precession camera dial readings. These lead, using the formula for a triclinic cell, to the following values of the interaxial angles

$$\alpha = 81°5', \quad \beta = 96°42', \quad \gamma = 91°48'$$

The values of a^*, b^*, c^* measured from zero level precession photographs showing the a^*-b^* net and a^*-c^* net and the above values of α, β and γ lead to the following values of the unit cell lengths :

$$a = 9.23 \text{ Å}, \quad b = 7.51 \text{ Å}, \quad c = 6.66 \text{ Å}$$

$$d_{100} = 9.17 \text{ A}, \quad d_{010} = 7.42 \text{ A}, \quad d_{001} = 6.54 \text{ A}.$$

Radiation used throughout was Mo K_α, $\lambda = 0.7107$ Å. The reciprocal net a^*-b^* shows a marked amount of monoclinic pseudo-symmetry (Plate III).

The density, measured by floatation method using a mixture of methyl iodide (density 2 279 gm/cc) and toluene (density 0.867 gm/cc) was found to be 2.23 gm/cc. Using the above values of the cell constants, the volume of the unit cell = 452.99 A^3 and the weight of the unit cell contents = 608.54 (atomic units). Theoretical molecular weight for $Rb_2\ C_4\ H_2\ O_4$ is 284 88 (atomic units) If there are two such formula units per unit cell, the balance of 38.78 (atomic unit) can be ascribed only to the presence of two water molecules in the unit cell ($2 \times 18 = 36$ atomic units). Thus the chemical formula of the compound was uniquely fixed as $Rb_2C_4\ H_2O_4$, H_2O, no other possibility being consistent with the above data

Space group : The diffraction symmetry observed is, of course, $P\bar{1}$ With the presence of two molecules per unit cell and in view of the pseudo-monoclinic symmetry that the crystal shows (figure. 1) the space group is suggested to be $P\bar{1}$.

The corresponding potassium salt of fumaric acid ($K_2\ C_4\ H_2\ O_4$) crystallizes with two molecules of water of crystallization and is monoclinic, space group $P2_{1/c}$. Since the rubidium salt ($Rb_2\ C_4\ H_2\ O_4$) crystallizes with only one molecule of water, this would explain that the potassium and rubidium salts are not isomorphous, the rubidium salt crystallizing with lower triclinic symmetry, although pseudo-monoclinic symmetry persists. It may be noted in passing that a similar lack of isomorphism exists in other corresponding rubidium and potassium salts of fumaric acid (Gupta, 1956).

In order to check whether a higher hydrated form of $Rb_2\ C_4\ H_2\ O_4$ exists or not a powder photograph of $Rb_2\ C_4H_2O_4$, H_2O, sealed in a Lindemann glass capillary tube was taken. One end of the capillary tube was then broken and this was made to touch a trace of water. By capillary action, the whole tube was then saturated with water. The resulting powder pattern of this water saturated sample did not show any changes from the corresponding powder photograph of $Rb_2C_4H_2O_4$, $H_2\ O$. Thus the possibility of a higher hydrated form of $Rb_2C_4\ H_2\ O_4$ had to be ruled out.

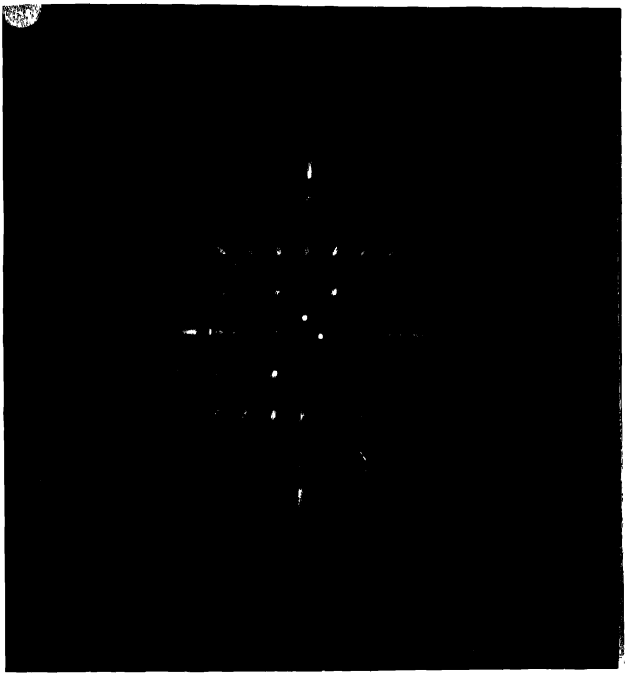

Fig. 1. Zero level precession photograph of rubidium fumarate, monohydrate. Triclinic. a*—b* net with a* along the horizontal axis. $\mu = 30^{\circ}$, F = 6.00 cms Mo Kα radiation, λ = 0.7107 A. The pseudo-orthogonality of the net may be noticed The four spots in the centre making a square array are due to accidental leakage of light in the camera.

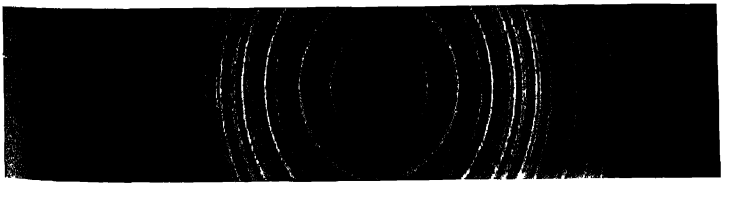

Fig. 2 X-ray diffraction powder photograph of rubidium fumarate, monohydrate. Camera diameter = 114.6 mm ; radiation, Cu Kα.

The powder photograph of $Rb_2C_4H_2O_4$, H_2O is reproduced in figure 2, while the indexed powder data are given in Table I. The powder data (film method) were also checked by obtaining a diffraction curve from the Norelco Geiger counter

TABLE I

X-ray diffraction powder data (Indexed upto $d \simeq 2A$)

I/I	$d(A)$ Observed	$d(A)$ Calculated	hkl
20	9.22	9.17	100
9	6.52	6 54	001
29	5.66	5.63	101
10	5 30	5 33	011
10	5 04	5.05	101
9	4 62	4 58	200
30	4 39	4.39	111
50	3 98	3 97	$20\bar{1}$
25	3 69	3 71	020
25	3 58	3 56	201
30	3 45	3 45	120
		3 45	021
		3 42	120
75	3 32	3.31	211
		3 31	121
15	3.24	3.27	002
50	3.16	3.18	012
		3.18	102
		3.16	121
100	3.09	3 13	$2\bar{1}1$
50	3 02	3 03	$02\bar{1}$
35	2.89	2.90	$2\bar{2}0$
		2.90	112
		2 90	$30\bar{1}$
		2.86	$\bar{2}21$
35	2.81	2.83	$01\bar{2}$
		2 84	$\bar{1}21$
		2.81	310
		2.81	$20\bar{2}$
		2.84	$3\bar{1}0$
25	2.76	2.77	$\bar{3}11$
		2.76	212
35	2 65	2 65	301
		2 64	$1\bar{1}2$
		2.66	022
		2.67	221
20	2 56	2 57	$22\bar{1}$
12	2 53	2 54	311
		2 53	202
		2.52	$21\bar{2}$
8	2 49	2.47	030
		2 48	221
		2 49	122
		2 48	212
25	2 40	2.40	130
		2.41	$\bar{2}22$
13	2 34	2 34	$3\bar{2}0$
		2.34	$\bar{3}12$
35	2.31	2.32	131
		2.31	212
5	2 27	2.25	$12\bar{2}$
12	2.20	2 18	$2\bar{3}0$
		2.21	410
		2 20	013
		2 19	$03\bar{1}$
		2 21	113
8	2.16	2 16	230
		2 17	$10\bar{3}$
16	2.12	2.11	302
		2.13	032
		2.12	$1\bar{3}1$
		2 12	$\bar{1}32$
		2 11	$41\bar{1}$
		2.13	$\bar{3}22$

TABLE I (*contd.*)

I/I_1	$d(A)$ Observed	$d(A)$ Calculated	hkl
10	2 08	2.08	312
9	2.05	2.06	$20\bar{3}$
20	1.99	1.99	411
		1.99	$3\bar{1}2$
		1 98	$\bar{4}21$
		1 99	222
4	1 95		
4	1 90		
10	1 87		
10	1 85		
5	1.81		
3	1.78		
4	1.74		
4	1.71		

I/I	$d(A)$ Observed	$d(A)$ Calculated	hkl
5	1 69		
7	1.68		
9	1.65		
4	1 63		
3	1.60		
3	1 58		
3	1.55		
3	1.52		
3	1 50		
4	1.46		
4	1 43		

diffractometer capable of greater resolution. There were good agreements regarding the diffraction angles but not regarding the intensities for which the agreement with film method was only qualitative. This may be due to preferred orientation of grains in the sample prepared for the Norelco diffractometer and absorption

ACKNOWLEDGMENT

The experimental work was done during part of Exchange Visit Programme P-72 at the Polytechnic Institute of Brooklyn, N.Y , and one of us (Gupta) is greatly indebted to Prof. I. Fankuchen for providing all the laboratory facilities

REFERENCES

Gupta, M. P. 1953, Ph. D. Thesis, University of London.
Gupta, M. P., and Barnes, W H , 1958, *Canadian Journal of Chemistry* (in press)
Gupta, M. P., 1956, *Acta Cryst*, **9**, 263.

X-RAY ANALYSIS OF FROZEN STYRENE AT −180°C

N. K. ROY

OPTICS DEPARTMENT, INDIAN ASSOCIATION FOR THE CULTIVATION OF SCIENCE, CALCUTTA-32

(*Received for publication, January* 15, 1958)

Plate IV

ABSTRACT Debye-Scherrer pattern of pure monomeric styrene frozen and cooled to −180°C has been studied. Analysis of the pattern shows that the crystals might belong to C_{2v}^{1} space group assuming the molecule to possess a plane of symmetry or to C_{2h}^{1} space group, in case there is no symmetry in the molecule. The dimensions of the unit cell are found to be $a = 9.90$ Å, $b = 8.89$ Å and $c = 7.84$ Å. The number of molecules in the unit cell as determined from the measured density of the crystals is found to be four.

Similar pattern of polystyrene at 30°C shows four diffuse halos corresponding to the spacings of 7.51 Å, 3.49 Å, 2.39 Å and 1.95 Å, of which the first is the most intense one.

INTRODUCTION

From the results of the investigation on the Raman spectra of styrene and its polymer at −180°C it was concluded (Roy, 1954) that the low-frequency Raman lines observed in the case of monomer at −180°C might be due to the translational oscillation of the benzene nuclei connected to each other through virtual bonds giving some regular arrangements in the surrounding molecules. In the case of the polymer a continuous wing accompanying the Rayleigh line upto 90 cm^{-1} was observed, and this was attributed to the irregular arrangement of the molecules. As shown by Whitby (1927), the polymer is amorphous. The frozen monomeric styrene appeared to be crystalline, but its structure was not known. The object of the present investigation was to determine the crystal structure of frozen monomeric styrene at −180°C, because such information might be helpful in understanding the origin of the low-frequency Raman lines. For this purpose the Debye-Scherrer patterns of monomeric styrene at −180°C have been photographed and the results of the analysis of the patterns have been discussed in the present paper. For comparison, the Debye-Scherrer pattern of poly-styrene at 30°C has also been studied in order to find out the predominant spacings shown by the halos.

EXPERIMENTAL

A sample of styrene (monomer) was carefully purified as described earlier (Roy, 1954) and was used to photograph the Debye-Scherrer patterns. The polymer prepared in the laboratory from pure monomeric styrene (Roy, 1954) was also

used for studying the Debye-Scherrer pattern. A Seifert X-ray tube running at 32KV and 26 mA was used to photograph these patterns. The X-ray tube was provided with a copper target and a nickel filter was used to cut off the $K\beta$ radiation. An exposure of about 2 hours was required for recording each pattern.

The patterns at $-180°C$ were photographed by the method described by Krishnamurti and Sen (1956), but the sample was rotated about a vertical axis intermittently. The radius of the camera was measured accurately by taking a Debye-Scherrer pattern of rock salt.

RESULTS AND DISCUSSION

The pattern due to monomeric styrene at $-180°C$ is reproduced in figure 1, Plate IV, and that due to polymeric styrene at 30°C in figure 2, Plate IV.

The pattern due to monomeric styrene at $-180°C$ shows a large number of rings, and therefore, the substance is crystalline at this temperature The values of $\sin^2\theta$ for the rings were calculated and these are given in the first column of Table I. The first three spacings were assumed to be those due to (100), (010) and (001) planes respectively, and following Lipson's (1949) method, the differences between $\sin^2\theta$ were plotted on a graph paper. It was observed that the differences 0.024, 0.030 and 0.010 are repeated several times. So the assignments were assumed to be correct and the following values of the constants were assumed to calculate the spacings of the planes on the assumption that the crystal belongs to the orthorhombic system :

$$\frac{\lambda^2}{4a^2} = 00604, \qquad \frac{\lambda^2}{4b^2} = .00750, \qquad \frac{\lambda^2}{4c^2} = .00964.$$

From these values of the constants we get, $a = 9.90$Å, $b = 8.89$Å, and $c = 7.84$ Å.

The density of the frozen monomer at $-180°C$ was measured by a method previously described by Biswas and Sirkar (1957) and was found to be 1.012, taking the density of liquid styrene at 31°C to be 0.8966. This gives the number of molecules in the unit cell as 4.07 which may be taken as 4.

From a consideration of the results in Table I and the above value of the number of molecules per unit cell two possible space groups may be ascribed to the crystals of frozen monomeric styrene at $-180°C$. On the assumption of existence of a plane of symmetry in the monomeric styrene molecule, which is not unlikely from its molecular formula, and the number of asymmetric molecules required per unit cell to be 8, *i.e.*, double of the calculated value, the space group of the crystals may be C_{2v}^1. In case there is no symmetry in the molecules Q_h^1 space

Indian Journal of Physics, Vol XXXII, No. 3

Fig

Fig 2

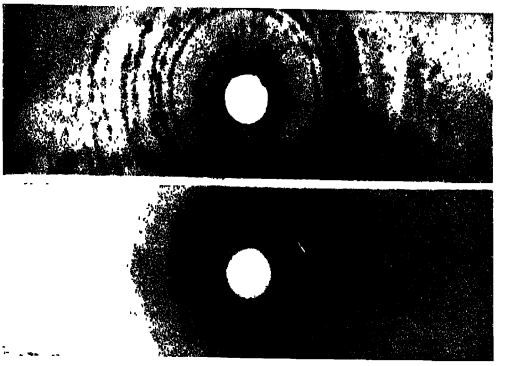

Debye-Scherrer patterns
Radius of the camera, 4·5 cms

Fig 1. Frozen monomeric styrene at −180°C
Fig 2 Polystyrene at 30°C

TABLE I

Radius of the Camera 4.50 cm.

Data for the Debye-Scherrer pattern of styrene at −180°C

$\sin^2\theta$ (observed)	$\sin^2\theta$ (calculated)	Difference	Spacings in Å	Proposed indices & intensities
.00604	.00604	.00000	9.90	100 (s)
.00750	.00750	.00000	8.89	010 (s)
.00964	.00964	.00000	7.84	001 (m)
.02402	.02416	.00014	4.97	200 (s)
.03054	.03000	.00054	4.40	020 (m)
.03187	.03166	.00021	4 31	210 (v.s)
.03651	.03604	.00047	4.03	120 (m)
.03860	.03856	.00004	3 92	002 (s)
.05253	05210	.00043	3.36	112 (w)
.05478	.05416 .05436	.00062 .00042	3.29	220 300 (m)
.06439	.06400	.00039	3.03	301 (m)
.06714	.06750	.00036	2.97	030 (m)
.08271	.08318	.00047	2.68	131 (w)
.08662	.08676	.00014	2.62	003 (m)
.10030	.10030	.00000	2.43	113 (m)
.1198	.1200	.0002	2.22	040 (m)
.1304	.1302	.0002	2.13	232 (m)
.1407	.1409	.0002	2.05	223 (m)
.1590	.1586	.0004	1.93	042 (m)
.1645	.1641	.0004	1 90	430 (s)
.2113	.2117	.0004	1 67	250 (w)
.2326	.2321	.0005	1.60	152 (s)

group can be ascribed to the crystals. It is not possible to decide from these data whether the molecule has a plane of symmetry in the crystal or not.

The Debye-Scherrer pattern of the polymer at 30°C shows one very intense halo and three comparatively weaker halos. The corresponding spacings are 7.51Å, 3.49 Å, 2.39 Å and 1.95 Å respectively. It is interesting to note that

although these spacings are near to some spacings observed in the case of the frozen monomer the relative intensities are entirely different in the latter case. In the of case the polymer the spacing 7.51 Å is the most predominant one and this may correspond to the width of the molecule.

ACKNOWLEDGMENT

The author is indebted to Professor S. C Sirkar, D.Sc., F.N.I for his kind interest and constant guidance during the work.

REFERENCES

Krishna Murti, G. S. R. and Sen, S. N., 1956, *Ind. J. Phys*, **30**, 242
Lipson, H, 1949, *Acta Cryst.*, **2**, 43.
Roy, N. K., 1954, *Ind J Phys.*, **28**, 365
Whitby, G S., 1927, *India Rubber J.*, **73**, 638.

ANALOGUE MULTIPLIER AND FUNCTION GENERATOR WITH CATHODE RAY TUBE

A. K. CHOUDHURY AND B. R. NAG

INSTITUTE OF RADIOPHYSICS & ELECTRONICS, UNIVERSITY OF CALCUTTA

(*Received for publication, September* 18, 1957)

ABSTRACT. A multiplier and a function generator using a cathode ray tube with a capacitative pick up device are described. The device simplifies the construction of the multiplier and function generator without impairing the speed of response or the accuracy of the instrument.

INTRODUCTION

Function generators and multipliers using cathode ray tubes have been described by many authors (MacNee, 1949, Mackay, 1947; Deely and Mackay, 1949; Sunstein, 1949). Use of the electron beam of the C. R. tube as the dynamic element in these function generators and multipliers results in high speed and makes them specially suited for applications in high speed analogue computers. However, in all such function generators and multipliers, the voltage giving the function or the product is obtained with the help of photocells placed in front of the C. R. tube. Instead of the photocells as the pick up device, MacNee suggested the use of metallic pick up plates mounted inside the C. R. tube. Evidently, this is only suited for the multiplier. If it is to be used for the function generator a separate C. R. tube is required for each new function. In this paper a multiplier and function generator with a new pick up device is described. The device is simple and can be easily replaced so that the same C. R. tube can be used for the multiplier or for generating different types of functions.

PRINCIPLE OF THE MULTIPLIER

The electron beam in a cathode ray tube, when subjected to an electric field $\mathbf{E}_x$ in the X-direction and a magnetic field $\mathbf{H}_z$ in the Z-direction, is deflected in the Y-direction and the deflection is given by y, where

$$y = K_1 \mathbf{E}_x \times \mathbf{H}_z$$

Since, velocity of the spot in the Y-direction is proportional to $\mathbf{E}_x \times \mathbf{H}_z$.

The deflection in the Y-direction is proportional to the product of the electric and magnetic field intensities. One of the voltage to be multiplied (V_1) is applied to the X-plates (figure 1). Thus $\mathbf{E}_x$ is made proportional to V_1. The other voltage V_2 is applied to an amplifier which sends a current proportional to V_2 through a

coil mounted coaxially on the neck of the tube between X and Y plates. The resulting Y-deflection is proportional to the product of V_1 and V_2.

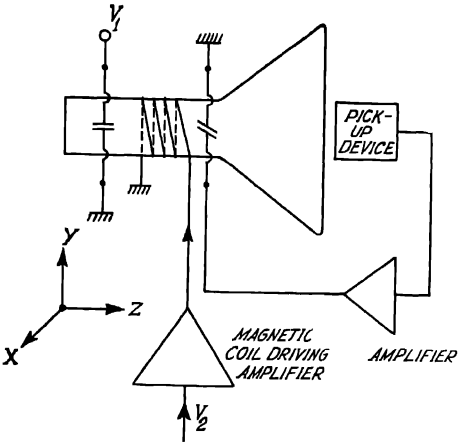

Fig. 1 · Block diagram of the multiplier.

On the face of the cathode ray tube is mounted a pick up device. It gives an output voltage which varies as the spot is deflected from the zero-Y line. If the output voltage of the pick up device is proportional to the spot deflection, it is also proportional to the product of V_1 and V_2 Usually this is not so, and to obtain a voltage proportional to the product, the output of the pick up device is amplified and applied to the Y-plates, in such a phase that it tries to bring the spot back to its initial position, whenever it is deflected due to the applications of V_1 and V_2. Let the pick up device give an output voltage v per unit Y deflection and δ_y be the Y-plate deflection sensitivity of the tube. Then, evidently the voltage appearing at the output of the amplifier, when voltages V_1 and V_2 are applied, is V_{out}, where

$$V_{out} = \frac{K_2 V_1 V_2}{\delta_y - \frac{1}{vA}} = \frac{K_2/\delta_y}{1 - \frac{1}{\delta_y vA}} V_1 V_2. \qquad \ldots (1)$$

A is the gain of the amplifier and K_2 is a constant related to K_1, the X-plate sensitivity and the constant relating V_2 with V_1. If the gain of the amplifier is made so large, that $\frac{1}{\delta_y vA}$ is very small compared to 1. V_{out} is proportional to the product of V_1 and V_2.

PICK UP DEVICE

The pick up device consists of metallic plates mounted on the face of the cathode ray tube as shown in the figure 2. One of the plates is directly grounded and the other is connected to ground through a high impedance element. The electron beam of the C. R. tube is intensity modulated. As a result the charge appearing before the plates varies with time and thereby induces charges on the

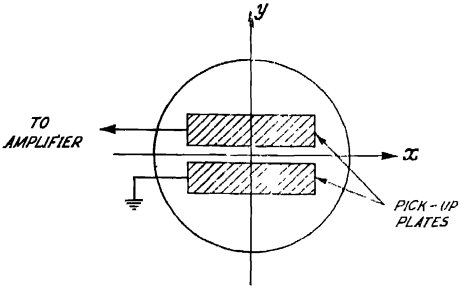

Fig. 2. Shape of the pickup plates for the multiplier.

plates which also vary with time. The varying charge on the metallic plate connected to ground through high impedance causes a voltage to be developed across the impedance. Evidently the magnitude of this voltage depends on the position of the cathode ray spot relative to this pick up plate and decreases as the spot recedes from its edge. The presence of the grounded plate enhances this rate of variation.

CIRCUITRY OF THE MULTIPLIER

The amplifier circuit following the pick up device is shown in figure 3. The high impedance element connected to the pick up plate consists of a heavily damped parallel tuned circuit. It is tuned to the frequency at which the electron beam is intensity modulated, which is 400 kc/s. The oscillator supplying the intensity modulation voltage is crystal controlled. The voltage developed across the pick up device is amplified by R-C coupled amplifiers in two stages, and then rectified by a thermionic diode. The rectified voltage is applied to the input of a d.c. amplifier. The output of the d.c. amplifier is adjusted to be zero when the spot is on the zero-Y line by the zero adjuster. Also the phase of the output voltage is so adjusted that as the spot tries to leave the zero-Y line, the amplifier output voltage, when applied to the Y-plate, brings it back. The gain of the amplifier is such that $v\delta_y A$ is equal to 1000. Thus error introduced from this source is less than 1 in 1000.

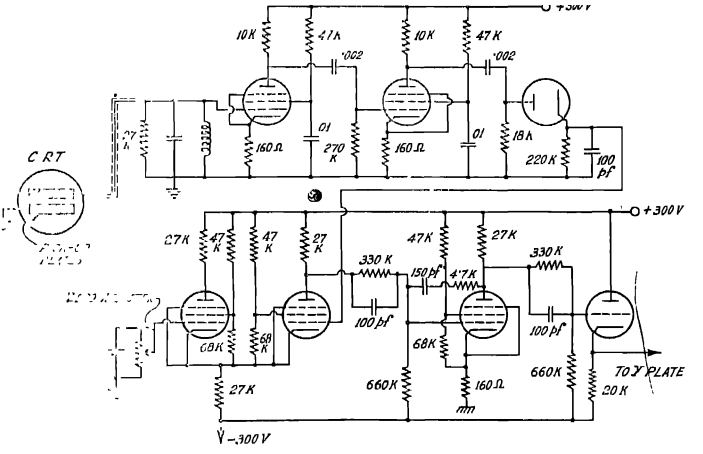

Fig. : Circuit arrangement of the amplifier.

The circuit arrangement of the amplifier supplying the current to the magnetic deflection coil is shown in figure 4. The frequency response of this amplifier is flat up to 3 Kc/s. The magnetic deflection coil consists of 5000 turns of 46 gauge copper wire and has a resistance of 1 K Ω. The C-R tube used for the multiplier is of the type 5BP1.

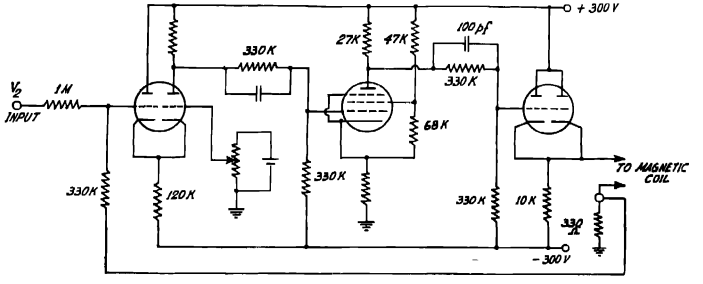

Fig. 4. : Magnetic-deflection amplifier circuit.

MULTIPLIER CHARACTERISTICS

The measured d.c. characteristics of the multiplier is shown in figure 5. It shows an accuracy of 2% of full output. The frequency response of the multiplier is flat up to 5 Kc/s for voltages applied to the X-plates and up to 3Kc/s for voltages applied to the magnetic-deflection coil.

The accuracy of the multiplier is limited by limitations of mechanical alignments. The edges of the pick up plates are not perfectly parallel to the zero-Y deflection line and also the axis of the magnetic deflection coil cannot be accurately aligned with the tube axis. With better mechanical arrangements the accuracy figure can be further improved. In this connection, it may be noted that as the

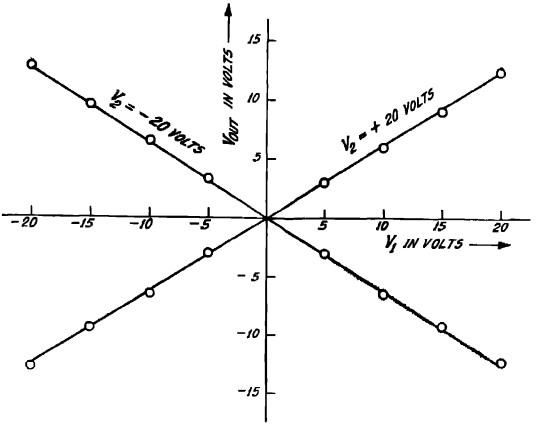

Fig 5 : Multiplier D. C. characteristics.

spot is deflected from its centre position it gets defocussed. This defocussing is further increased when the magnetic field is applied. However, defocussing only reduces the output of the pick-up plate and thereby affects the overall gain. The reduction in the gain does not affect the accuracy much since even the reduced gain is well over 700 and this may contribute an error of only 1 in 700.

The frequency response of the multiplier for voltages applied at the Y-plate may be further improved by using a higher frequency for beam intensity modulation and increasing the bandwidth of the parallel-tuned circuit. The frequency response for voltage applied at the magnetic deflection coil also may be improved by increasing the bandwidth of the magnetic deflection amplifier. This requires the use of a magnetic-deflection coil with smaller number of turns and therefore involves greater power consumption. Since, however, the differential analyser of which the multiplier forms a part has a fixed value of CR equal to 1/4, further improvement of the frequency response was thought unnecessary.

Solution of an equation with the multiplier

The performance of the multiplier in its actual use in the computer is illustrated by solutions of Mathieu equation obtained by the differential analyser using the multiplier.

Mathieu equation in its general form is written as

$$\frac{d^2y}{dz^2} + (a - 2q \cos 2z)y = 0 \qquad \ldots \quad (2)$$

The set-up of the computer for solving the equation is shown in figure 6. Cos $\omega_1 t$ is generated in a different part of the analyser. The computer set-up solves the equation

$$\frac{d^2y}{dt^2} + \omega_0^2(\alpha_1 - \alpha_2 \cos \omega_1 t)y = 0 \qquad \ldots \quad (3)$$

where $\omega_0^2 = 1/(CR)^2$.

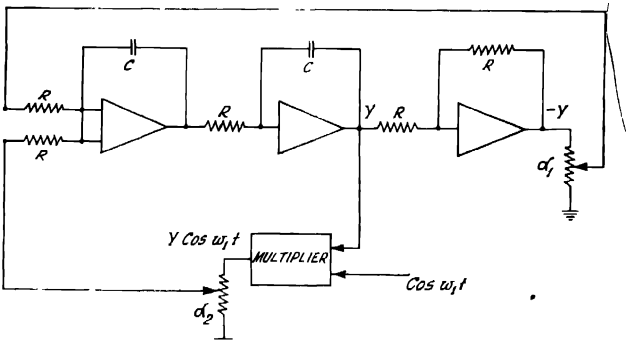

Fig. 6 · Computer set up for solving the equation,

$$\frac{d^2y}{dz^2} + (a - 2q \cos 2z)y = 0.$$

On substituting $2z$ for $\omega_1 t$ Eqn. (3) reduces to

$$\frac{d^2y}{dz^2} + \left[\frac{4\omega_0^2}{\omega_1^2} \alpha_1 - 2 \cdot \frac{2\omega_0^2}{\omega_1^2} \alpha_2 \cos 2z \right] y = 0.$$

Hence $$a = \frac{4\omega_0^2}{\omega_1^2} \alpha_1, \text{ and } q = \frac{2\omega_0^2}{\omega_1^2} \alpha_2.$$

In figure 7 is given the solution of the equation as obtained by the analyser for $a = 3$, $q = 2$ and $\dot{y} = 0$.

FUNCTION GENERATOR

Let the function to be generated be given by $f(V_1)$. The pick up plate mounted on the face of the C.R. tube is replaced by two other plates with their edges shaped to the form given by $f(V_1)$. The form of the pick up plates for $f(V_1) = V_1^2$ is shown

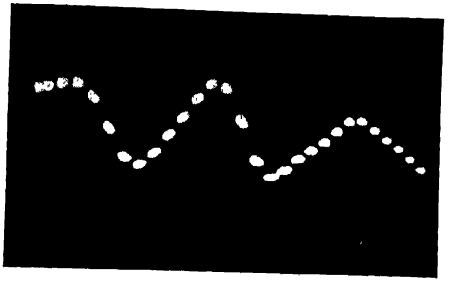

Fig. 7 : Computer solution of Mathieu equation for $a = 3, \quad q = 2, \quad \dot{y}_0 = 0.$

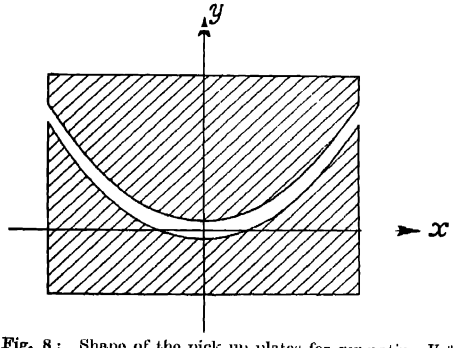

Fig. 8 : Shape of the pick up plates for generating V_1^2.

Fig. 9 : Plot of V_1^2 generated by the function generator against V_1.

in figure 8. Now for generating V_1^2, V_2 is made zero and V_1 applied to the X—plates. As V_1 is applied, the spot moves along the X-axis, but the feed back device keeps it in between the edges of the two plates. As in the case of the multiplier if the gain of the amplifier is large, the spot moves along the centre line between the edges, and since the plate edges are shaped to V_1^2, the voltage appearing at the output of the amplifier is proportional to V_1^2.

V_1^2 plotted against V_1 as generated by the function generator is shown in figure 9. The frequency response of the function generator is flat up to 5 Kc/s, which, however, can be improved further as indicated before by increasing the beam intensity modulation frequency.

CONCLUSION

The new pick up device described in this paper can be used successfully for constructing a multiplier or a function generator employing a C. R. tube. The use of this device does not affect the speed of response. The accuracy is mainly limited by mechanical mis-alignments.

ACKNOWLEDGMENTS

The authors are deeply indebted to Prof. S. K. Mitra for his constant help and guidance in the work. Thanks are also due to Prof. J. N. Bhar, Head of the Department of Radio Physics and Electronics, Calcutta University, for his kind interest in the work.

REFERENCES

Deely, E. M. and Mackey, D. M., 1949, *Nature*, **163**, 650.
MacNee, A. B., 1949, *Proc. I.R.E.*, **37**, 1315.
Mackey, D. M., 1947, *Nature*, **159**, 406.
Sunstun. D. E., 1949, *Electronics*, **22**, 100.

QUADRUPOLE VIBRATIONS AND THE ELECTRIC QUADRUPOLE MOMENT OF SOME CLOSED SHELL PLUS (OR MINUS) A SINGLE NUCLEON NUCLEI

P. N. MUKHERJEE AND I. DUTT

INSTITUTE OF NUCLEAR PHYSICS, CALCUTTA

(*Received for publication, October* 30 1957)

ABSTRACT. A critical survey has been made in this paper on the present position of the quadrupole moment of closed shell plus (or minus) a single nucleon nuclei. It is found that collective model formalism of the quadrupole moment is essentially correct if one calculates the rigidity of the core from the data on the vibrational spectra of even-even nuclei. Using the available data on vibrational levels the strength of surface coupling has been calculated and it is found that in the region of closed shell, an intermediate coupling picture holds true. The values of the quadrupole moment are also improved in this scheme.

1. INTRODUCTION

It is well known that although spin and energy levels of nuclei can sometimes be satisfactorily explained by the shell model, it is very difficult to account for the magnitude of their magnetic moments and electric quadrupole moments. Specially the latter is very sensitive to the choice of the ground state wave function. In the extreme single particle model the ground state quadrupole moment for a closed shell plus a single proton nucleus is given by

$$Q_j = < r^2(3\cos^2\theta - 1) >_{j=m}$$

$$= -\frac{2j-1}{2(j+1)} < r^2 > \qquad \ldots \quad (1)$$

where $\mathbf{j}$ is the total angular momentum of the satellite proton, m its Z-component and $\mathbf{r}$ its position vector.

On the average $< r^2 >$ can be taken as $3/5\, R_0^2$ (Mayer and Jensen, 1955), where R_0 is the nuclear charge radius. It is well known that

$$R_0 = KA^{1/3} \qquad \ldots \quad (2)$$

where $K = 1.19 \times 10^{-13}$cm (as given by electron scattering experiments). If there is a hole instead of a proton then the sign of (1) is to be interchanged. This explains the fact that just before a magic number the quadrupole moment is positive and after a magic number it is negative. But apart from this qualitative agree-

ment, the single particle model is not adequate to account for the magnitude of the quadrupole moments. In fact, the ratio Q_{obs}/Q_j is sometimes as large as forty.

In 1950, Rainwater showed that if instead of a central field $V(r)$, a spheroidal field of the form $V(r, \theta)$ is taken then the value of Q_j is somewhat increased. This was further developed in the collective model of nuclei by A. Bohr in 1952. In this model the closed shell part of the nucleus is treated as a liquid drop, capable of collective oscillations and around this core one or more particles are moving in their shell orbits. As a result of the surface coupling the core will be distorted and its equilibrium shape will be a spheroid.

As a consequence of this there will be a good amount of contribution to the quadrupole moment from the core.

It can be easily proved (Bohr and Mottelson, 1953) that for core plus a single proton

$$Q = Q_c + Q_j$$

$$= -\left[1 - 3 \cdot \frac{2I+1}{(I+1)(2I+3)} \cdot \frac{x^2}{\sqrt{x^4+4/9}}\right] \frac{3}{4\pi} \cdot \frac{2I-1}{2(I+1)} \cdot \frac{k}{C} Z R_0^2$$

$$- \frac{3}{5} \cdot \frac{2I-1}{2(I+1)} \cdot R_0^2 \quad \ldots \quad (3)$$

In (3) k is a term appearing in the interaction hamiltonian of the particle and surface. Its sign is reversed if the particle is replaced by a hole. On the average $k \simeq 40$ Mev. The factor C which appears in (3) is known as the nuclear rigidity. For a uniformly charged nucleus of constant surface tension S

$$C = 4R_0^2 S - \frac{3}{10\pi} \cdot \frac{Z^2 e^2}{R_0} \text{ [A. Bohr, 1952]} \quad \ldots \quad (4)$$

The dimensionless parameter

$$x = \sqrt{\frac{5}{16\pi}} \cdot \frac{k}{\sqrt{\hbar \omega j C}} \quad \ldots \quad (5)$$

It is a measure of the strength of coupling between the particle and the surface. In (5) ω is the frequency of collective oscillations of the core. It can be shown (A. Bohr, 1952) that

$$\omega = \sqrt{\frac{C}{B}} \quad \ldots \quad (6)$$

where B is the nuclear inertial parameter.

For a uniform liquid in irrotational flow,

$$B = \frac{3}{8\pi} \cdot AMR^2_0 \qquad \ldots \quad (7)$$

Using (4) and (7), Bohr and Mottelson (1953) have calculated Q for various nuclei and found that in general Q is many times larger than its actual value (see Table 1. column 15). This is hardly surprising since both (4) and (7) are very approximate equations. It is obvious that both B and C should depend strongly on the shell structure of the core.

Marumori *et al.* (1956) showed that C, the surface rigidity depends strongly on the shell structure configuration of the core. Using a simple form of interaction they have calculated the values of C and found that these values of C give excellent values of the quadrupole moment. But here again the agreement has little meaning since these authors have used the same irrotational value of B as given by equation (7).

The purpose of the present paper is to show that the collective model formalism of the quadrupole moment, as given in equation (3), is essentially correct.

2. CALCULATION OF QUADRUPOLE MOMENT FROM THE DATA OF THE VIBRATIONAL LEVEL OF EVEN-EVEN NUCLEI

The core of the nuclei under our consideration are even-even nuclei and hence they are capable of oscillation about a spherical equilibrium shape when the extra particle is absent (Alder *et al.* 1956). The lowest mode will be obviously of quadrupole type if the nucleus is to remain symmetric. The energy of the first excited level is given by the well known oscillator equation.

$$E_2 = \hbar\omega$$

$$= \hbar\sqrt{\frac{C}{B}} \qquad \ldots \quad (8)$$

It is well established that the spin of the first excited level of even-even nuclei is almost always 2 and the dominant mode of decay is by E_2 radiation. That the observed excitation is of collective origin is exhibited by the fact that the reduced transition probability $B(E_2)$ is many times larger than the single particle estimate.

If one assumes that these vibrations correspond to one photon excitation then it is easy to show that

$$B(E_2, 0 \rightarrow 2) = \Sigma \mid < 0 \mid m(E_2\mu) \mid 1 > \mid^2$$

TABLE I

The values of quadrupole moment

Isotope	Configuration Proton	Configuration Neutron	Core	Spin	E_2 Mev	$B(E_2)$ $\times 10^{-48}$ cm4.e²	$B(E_2)$ / $R(E_2)$ sp	C_2 Mev	λ	$P_q(x)$	In Barn Q_o	Q_s	Q_j	$Q = Q_s + Q_j$	Q BM	Q obs
$_5B^{11}$	$(1p_{3/2})^{-1}$	—	$_6C^{12}$	3/2	4 40	0 009	11 42	14	1.31	0 258	0 121	0.031	0.016	.047	0 093	0.036
$_{27}Co^{59}$	$(1f_{7/2})^{-1}$	—	$_{28}Ni^{60}$	7/2	1.33	0.12	17 80	59	0 76	0 650	0 656	0 426	0.085	0.511	0.90	0.5
$_{31}Ga^{69}$	$(2p_{3/2})^{-1}$	—	$_{32}Ge^{70}$	3/2	1 08	0 077	9.62	120	0 93	0 363	0.245	0.089	.058	.147	0.52	0.23
$_{31}Ga^{71}$	$(2p_{3/2})^{-1}$	—	$_{32}Ge^{72}$	3/2	0.83	0 23	26.77	32	1.999	0.211	0.937	0.197	0.058	.255	0.52	0.14
$_{79}Au^{197}$	$(2d_{3/2})^{-1}$	—	$_{80}Hg^{198}$	3/2	0.41	1.0	30.3	88	1 714	0 22	1.688	0.371	0 115	0.486	0.967	0.48
$_{32}Ge^{73}$	—	$1g_{9/2}$	$_{32}Ge^{72}$	9/2	0 83	0 23	26 77	32	1.154	0 593	−1 703	−1.01	0	−1.01	−1.1	−0.2

$$= \left(\frac{3}{4\pi} ZeR_0^2 \right)^2 \sum_{\mu} | < 0 | \alpha_{2\mu}^* | | 1 > |^2$$

where $\alpha_{2\mu}$ is the familiar deformation parameter.

$$= 5. \left(\frac{3ZeR_0^2}{4\pi} \right)^2 \cdot \frac{\hbar}{2(BC)^{1/2}} \qquad \ldots \quad (9)$$

From (8) and (9)

$$C = \frac{45}{32\pi^2} \cdot \frac{Z^2e^2R_0^4E_2}{B(E_2, 0 \rightarrow 2)} \qquad \ldots \quad (10)$$

Thus here is a nice way to determine the value of C as well as x from the data of the first excited state of even-even nuclei. From (5) it is obvious that

$$x = \sqrt{\frac{100}{2\pi j E}} \qquad (11)$$

where we have taken $k = 40$Mev and E_2 and C are expressed in Mev.

To be sure that the levels we have used to calculate C and, x are of collective origin, we have compared the experimental $B(E_2)$ values with that of single particle estimate. (Blatt and Weisskoff, 1952).

$$B_{sp}(E_2, 0 \rightarrow 2) = \frac{9}{20\pi} e^2R_0^4 \qquad \ldots \quad (12)$$

This is presented in Table I column 8, where one can see that the ratio $\frac{B_{exp}(E_2)}{B_{sp}(E_2)}$ is always much greater than one.

The coupling strength x as calculated from (11) is presented in column 10 of the same table. It is seen that x is almost always of the order of one, indicating an intermediate coupling. It is of interest to note that x depends sensitively on the orbital angular momentum of the satellite particle. Thus for $_{32}Ge^{72}$ core $x \sim 2$ when the outside particle is in $2p$ orbit, while $x \sim 1.1$ when the particle is in $1g$.

The last three columns of Table I give our calculated values of Q, the previous hydrodynamical values Q_{BM}, and observed values Q_{obs}. It will be seen that our values agree better with the observed values. One exception is that of $_{32}Ge^{73}$. This can be accounted for by the fact that the core $_{32}Ge^{72}$ has or more rigid neutron core ($N = 40$) than proton core, and the values of C as determined from the vibrational spectra gives essentially the rigidity of the proton core.

ACKNOWLEDGMENTS

The authors want to express their deep gratitude to Prof. A. K. Saha for his kind interest in the problem.

They are also grateful to the Department of Atomic Energy, Government of India, for the award of Research Fellowships which enabled them to work in this Institute.

REFERENCES

Alder, Bohr, Huus, Mottelson and Winther, 1956, *R.M.P.*, **28**, No. 4. 432.

Blatt, J. M. and V. F. Weisskopf., Theoretical Nuclear Physics (John Wiley & Sons, Inc, New York (1952)

Bohr, A., 1952, *Dan. Mat. Fys. Medd.* **26**. No. 14.

Bohr, A., and Mottelson, B., 1953, *Dan. Mat. Fys. Medd.* **27**, No. 16.

Marumori, T., Suekane & Yamamoto, 1966, *Prog. Theo. Phys, Japan.* **16**, No. 4, 120.

Mayer & Jenson, Elementary Theory of Nuclear Shell Structure. John Wiley & Sons, Inc, New York.

Rainwater. *J. Phys. Rev.* 1950, **79**, 432

SPECTRAL STUDY OF THERMOLUMINESCENCE EMISSION FROM KBr AND NaBr.

B. C. DUTTA* AND A. K GHOSH

KHAIRA LABORATORY OF PHYSICS, UNIVERSITY COLLEGE OF SCIENCE, CALCUTTA

(*Received for publication, October* 21, 1957)

ABSTRACT. The results obtained from the spectral study of thermoluminescence emission from KBr and NaBr coloured at 90°K by 10 KV electron bombardment are reported. An automatic rapid scanning quartz spectrophotometer capable of recording spectrum in one second is used to record the spectral distribution in the emission The thermoluminescence of KBr consists of four strong glow peaks at approximately 163°K, 226°K, 330°K, and 498°K. Each of the first, second and the fourth glow peaks consists of a single band with maximum at 522mμ, 520mμ, 498mμ, respectively There are two bands in the third glow peak with maxima at 443mμ and 516mμ The thermoluminescence glow of NaBr is characterized by two strong glow peaks at about 145°K and 286°K and emission band maximum at 457mμ and 500mμ respectively.

INTRODUCTION

Colour centres are formed in alkali halides irradiated by ionizing radiations. There is bleaching and changes in some of these centres at specific temperatures, usually accompanied by thermoluminescence emission (Dutton *et al.*, 1953; Sharma, 1952, 1956, Halperin *et al* 1957) The results reported by different workers on luminescence emission at various temperatures together with the principal changes in colour centres, if there be any, are summarized in Tables I and II

It is to be seen from the tables that the findings of the different workers are not in accord with each other This may in all probability be due to the differences in the nature and amount of irradiation, rate of heating, thermal history, physical nature and impurity contents of the phosphor

The present work deals with the behaviour and distribution of the spectral emission during thermoluminescence glow The spectra recorded are shown in figures 1-4. The curve in each of the frame indicates the spectral and intensity distribution of the thermoluminescence glow with rise of temperature at an interval of one second. The area under each curve when plotted against its corresponding temperature gives the "glow curve"

EXPERIMENTAL TECHNIQUE

The spectral distribution of thermoluminescence is recorded by an automatic rapid scanning spectrophotometer, the construction of which was reported

* Now at Birkbeck College, London.

earlier (Dutta *et al* 1956). The finely ground phosphor (E. Merck, guaranteed reagent quality) is rubbed to the flat surface of the sample holder. A high rate of heating, 6°–7°C per second, is preferred so as to increase the intensity of emission. Care is taken to retain the purity of the sample

3. EXPERIMENTAL RESULTS AND DISCUSSIONS

Potassium Bromide:

Potassium bromide fluoresces weakly on cathode ray bombardment at liquid oxygen temperature and the sample becomes blue on prolonged irradiation—

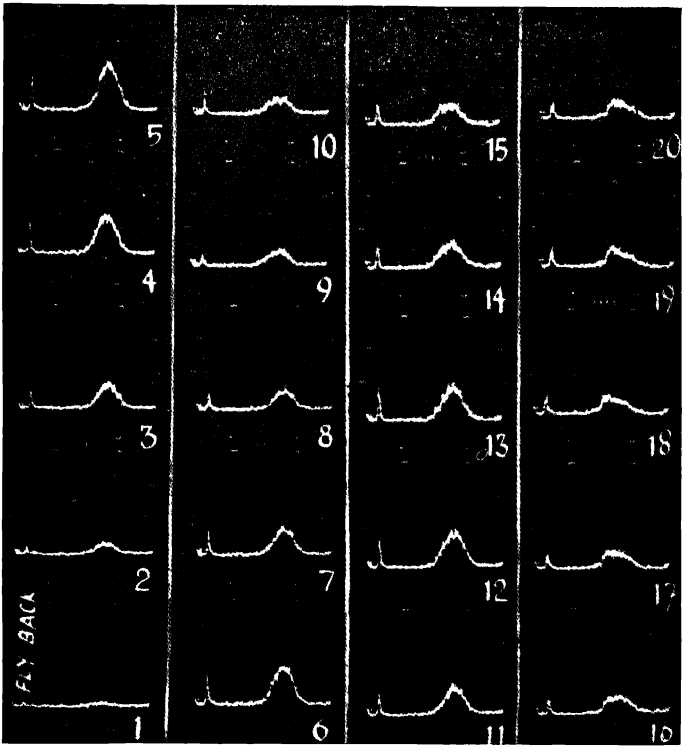

Fig. 1.—Thermoluminescence spectra of KBr irradiated by cathode rays at 90°K.

possibly due to *F* band (630 mμ). At low temperature the after-glow intensity is rather poor; but at high temperature it perceptibly increases. From the study

of the shape and size of the glow curves (Sharma, 1956) and the corresponding spectra, it is found that the glow curves (except for the lowest temperature) are broad and extended, overlapping one another greatly; this means that the trap depths in this crystal are not as sharp as in the other crystals studied and he distributed over wider limits.

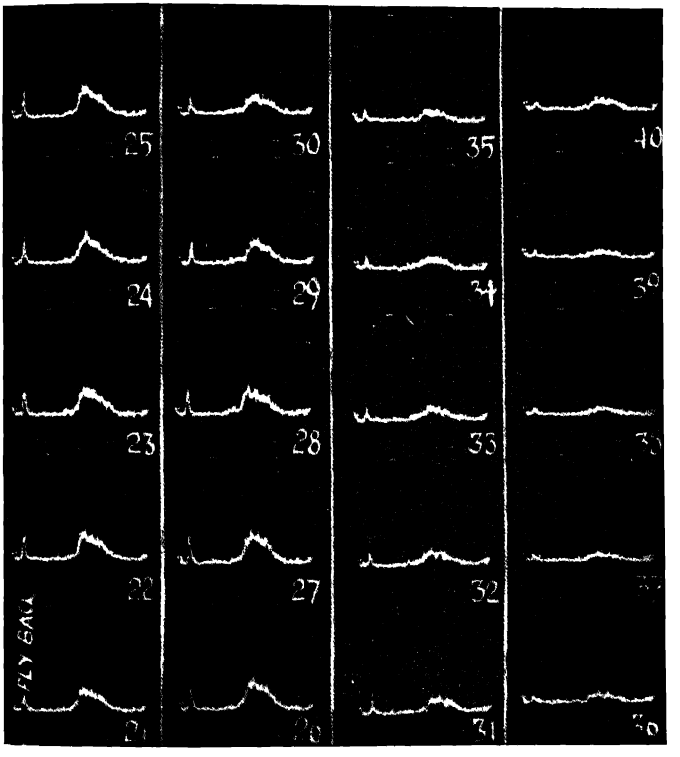

Fig. 2—Thermoluminescence spectra of KBr irradiated by cathode rays at 90°K. (*contd.*)

The thermoluminescence of KBr is characterised by four strong glow peaks at temperatures 163°K, 226°K, 330°K and 498°K. The spectra of the first two glow peaks seem to be identical. Immediately after the second glow peak, the effect of the third is reflected in the successive thermoluminescence spectra. The third glow peak is characterised by a strong short wave-length emission (443 mμ)

together with an indication of a long wave-length component (516 mμ) which persists over a wide temperature range. Either due to overlapping of the bands

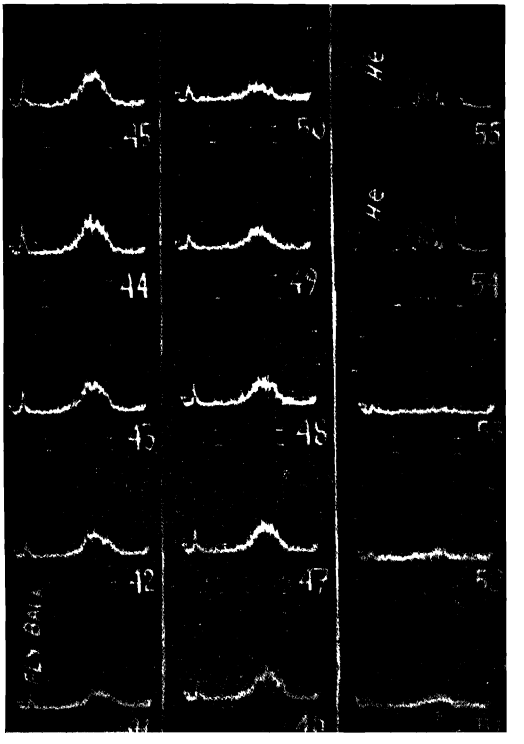

Fig. 3—Thermoluminescence spectra of KBr irradiated by cathode rays at 90°K. (*contd.*)

or due to temperature shift or due to both, the short wave-length band maximum of 443 mμ at 330°K appears to be shifted to 483 mμ at 402°K; the other band maximum ceases to be perceptible beyond ~370°K. The fourth glow spectrum is a single band. The position of the band maximum seems to remain completely unaffected by the temperature. The nature of the spectral emission of thermoluminescence of KBr will be evident from figures 1—4 and Table III.

It is observed that the blue colour of the sample disappears with the 163°K peak. Since thermal ionization of the F centre is improbable at this temperature, it may be that due to thermal ionization of V_1 centres holes are released and migrate to the F centres where recombination of the free holes and trapped elec-

trons occur resulting in the destruction of the F centre, the cause of the blue colour of the sample. Dutton *et al.* (1953), reported such a phenomenon though at a somewhat lower temperature The spectrum of the second glow is a broad band and its emission occurs over a wide temperature range. The band maximum is compatible with that reported by Dutton *et al.* for the emission associated with the disappearance of the V_4-band. The process occurring during the third glow seems to be complex; the V_2 and V_3 bands are likely to be bleached in this temperature range. The thermoluminescence spectrum of the last glow is distinctly different from the others Possibly the thermal ionization of the F centre occurs at this temperature. By colouring the sample at room temperature the blue colour disappears in this temperature range.

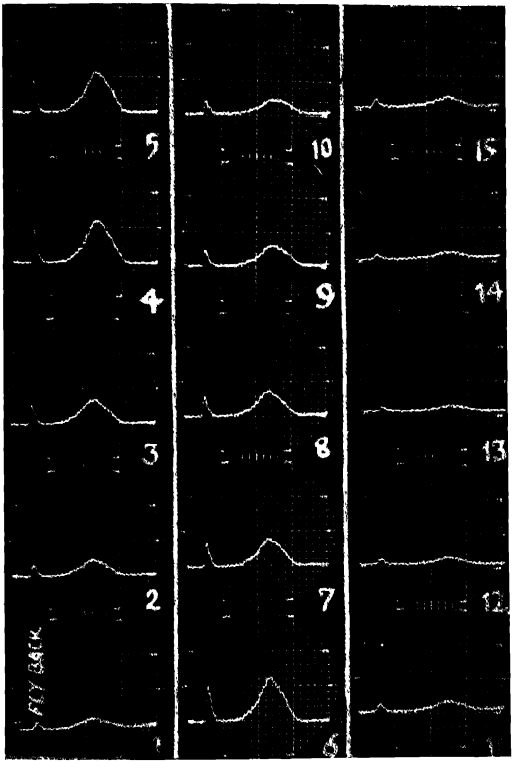

Fig. 4—Thermoluminescence spectra of NaBr irradiated by cathode rays at 90°K.

TABLE I

Luminescence peaks of KBr at various temperatures together with the principal changes in colour centres as reported by different workers.

Peak temperature in °K	Principal changes in absorption band	Luminescence peaks in $m\mu$	Method	Authors
115 143 185 225 246	V_4 F^1 " " V_4	$\lambda > 500$ $\lambda < 380$ $\lambda > 500$ — $\lambda > 500$	Luminescence glow and current peak measurement after X-ray irradiation at 90°K	Dutton and Maurer (1953)
123 203 263	– – –	320 and 500 500 290 and 450	Phosphorescence glow measurement after γ-ray irradiation at nitrogen temp.	Ghormley and Levy (1952)
176 235 281 330 415 525	– – – – – –	– – – – – –	Thermoluminescence and diffuse reflectance measurements after electron bombardment at 90°K.	Sharma (1956)
163 226 330 498	– – – –	522 520 433 and 516 498	Spectral study of Thermoluminescence by spectrophotometric method after electron bombardment at 90°K	Present authors.

TABLE II

Luminescence peaks of NaBr at various temperatures together with the principal changes in colour centres reported by different workers.

Peak temperature in °K	Principal change in absorption band	Luminescence peaks in $m\mu$	Method	Authors
133 194 225 300 480	– – – – F	– – – – –	Thermoluminescence and diffuse reflectance measurements after electron bombardment at 90°K.	Sharma (1956)
145 286	– –	457 500 and 570	Spectral study of thermoluminescence by spectrophotometric method after electron bombardment at 90°K.	Present authors

TABLE III

KBr

(Excited at liquid oxygen temperature)

Frame No.	Peaks $m\mu$	Half-width $m\mu$	Temperature °K
1	—	—	137
2	532	—	143
3	532	—	149
4	530	—	156
5 (Max)	522	476 — 589	163
6	527	—	170
7	527	—	178
8	527	—	186
9	535	—	194
10	535	—	202
11	535	—	210
12	525	—	218
13 (Max)	520	470 — 593	226
14	516	—	234
15	510	—	242
16	510	—	250
17	510	—	258
18	460	—	266
19	448	—	274
	537		
20	450	—	282
	537	—	
21	450		290
	526		
22	443	—	298
	526		
23	443	—	306
	516		
24	443	—	314
	516		
25	443	—	322
	516		
26 (Max)	443	—	330
	516		
27	457		338
28	466	—	346
29	466	—	354
	516		
30	466	—	362
	516		
31	473		370
32	473		378
33	483	—	386
34	483	—	394
35	483	—	402
36 — 40	—	—	411 — 448
41	498	—	458
42	498	—	468
43	498		478
44	498	—	488
45 (Max)	498	448 — 582	498
46	498	—	508
47	498	—	518
48	498	—	528
49	498	—	538
50	498	—	548

TABLE IV

NaBr

(Excited at liquid oxygen temperature)

Frame No.	Peak $m\mu$	Half-width $m\mu$	Temperature °K
1	443	—	114
2	443	—	120
3	443	—	126
4	448	398 — 510	132
5	452	400 — 512	138
6 (Max)	457	418 525	145
7	461	418 525	152
8	461	418 525	159
9	463	426 — 530	166
10	465	426 — 530	174
11	476	445 — 546	182
12	482	449 — 558	190
13	482	- -	198
14	—	.	206
15	498	- -	230
16	507	460 — 580	238
17	507	460 — 580	246
18	507	460 — 583	254
19	510	460 - 583	262
20	498 551	450 590	270
21	500 551	445 — 600	278
22 (Max)	500 570	446 — 600	286
23	502 575	440 — 600	294
24	498	440 — 600	302
25	498	—	310
26	496	—	318
27	496	—	326
28	493	—	334
29	493	—	342

Sodium Bromide :

Sodium bromide has a bluish-green fluorescence–emission on cathode ray bombardment at liquid oxygen temperature NaBr even under prolonged irradiation cannot be visibly coloured It is to be noted that the phosphor is coloured yellow when heated to 250°K after irradiation at liquid oxygen temperature. This colour also appears on irradiating the sample at room temperature. Fluorescence emission of NaBr is characterised by an intense ultra-violet band extended from 350 $m\mu$ to 250mμ or beyond; other bands are also present in the visible region (Bose *et al.*, 1950).

The thermoluminescence of NaBr consists of two strong glow peaks at 145°K and 286°K. The spectral nature of the emission at different temperatures will be evident from figures 4 and 5 and Table IV. From a study of the nature of the emission, it is clear that the emission extends into the ultra-violet region; the ultra-violet part of the emission is missed because of the insensitivity of the phototube.

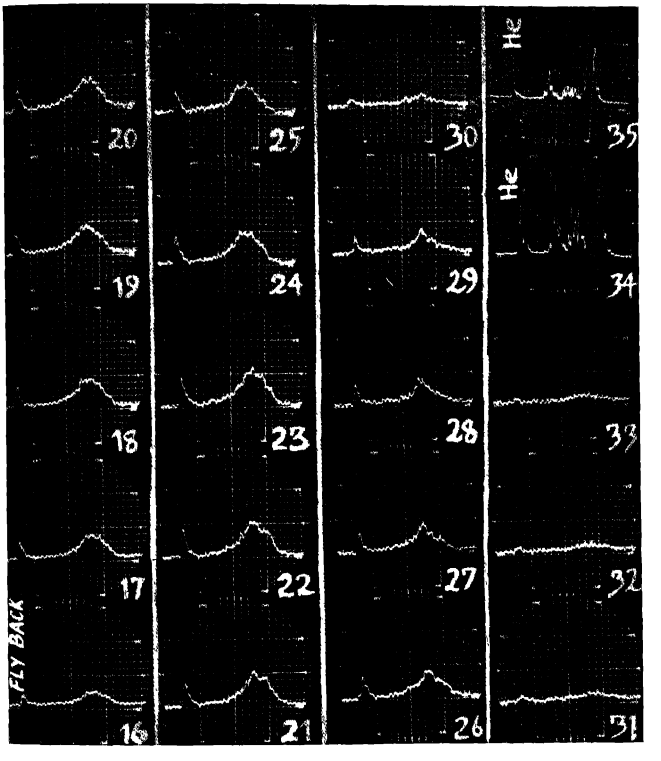

Fig. 5—Thermoluminescence of NaBr irradiated by cathode rays at 90°K. (*contd.*)

The lowest temperature glow peak occurs in the shorter wave-length region with band maximum at 457 mμ while the other one lies in the longer wave-length region with band maxima at 500 mμ and 570 mμ.

From the study of the emission it appears that there is a gradual change

taking place throughout the process of thermoluminescence. Thus, for the first glow, emission at the initial and final stages has a band maximum at 443 mμ when the temperature is 114°K and at 482 mμ when the temperature is 198°K. During the second glow, initially, emission band maximum appears at 498 mμ corresponding temperature being 230°K; at about 270°K emissions show another long wave-length component with band maximum at 551 mμ. At the glow peak temperature 286°K there are two maxima in the emission band at 500 mμ and 570 mμ respectively.

If one takes into account the effect of mutual overlapping of two diffuse bands it can be easily seen that the development of a new diffuse band on the long wave-length side in the emission may cause the peak position of the original band to be shifted towards the longer wave-length. Thus it is reasonable to conclude that the emission band with maximum at 457 mμ(at 145°K) which is gradually shifted towards longer wave-length with increasing temperature, is present in all the glows observed.

Sodium bromide is a pronounced ultra-violet emitter; as such the measurements cannot be considered as complete for obvious reasons. From Table II we observe that Sharma associates the glow peak at 480°K, with the thermal bleaching of the F centre and it is assumed to be so Due to its low intensity the spectrum of this glow could not be recorded. Comparing results with KBr and other phosphors it is guessed that the glow peaks at 145°K and 280°K are associated with the bleaching of the V_1 and V_4 centres. The additional long wave-length emission may be provided by the possible bleaching of the F' centres in the corresponding temperature range

Additional work is needed before one tries to picture the kinetics of the emission process, and moreover the measurements, being confined to the visible region, are incomplete. Since absorption measurements have not been made, the identification of the glow peaks with thermal bleaching of the colour centres as reported are to be taken as suggestions rather than experimental findings.

ACKNOWLEDGMENTS

We are grateful to Prof. S. N. Bose for his helpful discussions and constant interest in the work Thanks are also due to the Ministry of Education, Govt. of India, for granting scholarships to both the authors.

REFERENCES

Dutton, D and Maurer, R. J., 1953, *Phys Rev.*, **90**, 126.
Ghormley, J. A. and Levy, H. A., 1952, *J. Phys. Chem.*, **56**, 548.
Sharma, J., 1952, *Phys. Rev.*, **85**, 692 and **87**, 335; D. Phil. Dissertation, Calcutta University.
,, 1956, *Phys. Rev.*, **101**, 1295.
Halporn, A, *et al.*, 1957 *Phys. Rev.*, **108**, 928. *Phys Rev*, **108**, 932.
Dutta, B. C. *et al.*, 1956, *Ind. J. Phys.*, **30**, 570.
Bose, H. N. *et al.*, 1950, *Proc. Nat. Inst. Sc., India*, **26**, 47.

ON THE AXIAL STABILITY OF A DEFORMED NUCLEUS I

P. N. MUKHERJEE AND I. DUTT

INSTITUTE OF NUCLEAR PHYSICS, CALCUTTA

(*Received for publication, February* 13, 1958)

ABSTRACT. The energy eigen values of a single particle moving in an anisotropic harmonic oscillator potential have been calculated assuming that the equipotential surface coincides with the nuclear surface It has been found that in the rare-earth region the shell model energy levels of a single particle depend sensitively on the deviation of the nuclear shape from cylindrical symmetry. Calculations have been done upto Ca^{40} core and it is found that the energetically stable form of the nucleus corresponds to either $\gamma = 0$ or $2\pi/3$. It is also found that the total energy of an oblate nucleus is about 2 Mev greater than that of a prolate one, which is consistent with the observed positive excess of quadrupole moment in the rare-earth region.

1. INTRODUCTION

In the region of the rare-earth nuclei (A — 150 to 190) very large positive quadrupole moments have been observed, which indicates that these nuclei are strongly deformed. Moreover, it has been found (A. Bohr, 1954) that the first excited level of the majority of these nuclei are of collective rotational origin. The fact that the energies of these levels are proportional to I (I + 1) (where I is the spin of the level), indicates that these nuclei have cylindrical symmetry. From these two observations one can infer that the nucleon configuration in the rare-earth region prefers energitically a prolate deformation The object of the present paper is to see whether this is so, if the nucleons are assumed to be moving in an average deformed potential.

From the self-consistency condition it is obvious that the strength of the nuclear potential is proportional to the particle density inside the nucleus. Hence one can conclude that at the nuclear surface the equipotential surface more or less coincides with the nuclear surface. Starting from this the energy eigen values of a single particle have been calculated by various workers, (Moszkowski, 1955 ; Nilsson, 1955 ; Gottfried, 1956) using rectangular well of infinite depth, harmonic oscillator potential and rectangular well of finite depth respectively. But they have tentatively assumed a cylindrical symmetry of the nucleus. Gottfried (1956), however, showed that for a rectangular well of finite depth the nucleus prefers a cylindrical symmetry. But in his calculations the positive and negative quadrupole moments are found to be equally probable.

We have taken here an anisotropic harmonic oscillator potential and applying the usual perturbation treatment have calculated the energy eigen values for different ellipsoidal shapes. This paper contains the results up to $N = 20$, while the exact machine calculation for higher levels are in progress and will be reported in due course.

2. MATHEMATICAL FORMULATION

Let the hamiltonian of a single particle of mass M, moving in an average field, $V(\mathbf{r})$ be

$$H = -\frac{\hbar^2}{2M}\Delta' + V(\mathbf{r}') + C\,\mathbf{l}.\mathbf{S} + D\mathbf{l}^2 \qquad \ldots (1)$$

where the last two terms are added to get the zero-order shell structure levels. (Nilsson 1955).

For anisotropic harmonic oscillator field one can write,

$$V(\mathbf{r}') = \tfrac{1}{2} M(\omega^2_{x'} x'^2 + \omega^2_{y'} y'^2 + \omega^2_{z'} z'^2). \qquad \ldots (2)$$

where $\mathbf{r}'$ gives the position of the particle with respect to a body-fixed system of axes (X', Y', Z') It is customary to choose (X', Y', Z') as the principal axes of the nucleus. (A. Bohr 1953) whose surface is

$$r_S = \lambda^{-1}R_0[1 + a_0 Y_{20}(\theta'\phi') + a_2\{Y_{22}(\theta'\phi') + Y_{2-2}(\theta'\phi')\}] \qquad \ldots (3)$$

The parameter λ in (3) preserves the nuclear volume. By straightforward integration one can show from (3) that

$$\lambda^3 = 1 + \frac{3}{4\pi}(a_0^2 + 2a_2^2) + \frac{16}{35}\left(\frac{5}{16\pi}\right)^{3/2}(a_0^4 - 6a_0a_2^2) \qquad \ldots (4)$$

(without any approximation)

Equating the length of the major axes from (2) and (3), and noting that the volume of the nucleus remains constant under deformation, it is easy to see that (2) can be written as

$$V(\mathbf{r}') = \tfrac{1}{2} MKR_0^{-2}\lambda^{-1}[\{1 + f_1(a_0a_2)\}r'^2 + f_2(a_0a_2)r'^2 Y_{20}(\theta'\phi') + f_3(a_0a_2)r'^2 \{Y_{22}(\theta'\phi') + Y_{2-2}(\phi'\theta')\}] \qquad \ldots (5)$$

where $(KR_0^{-2})^{\frac{1}{2}} = \omega_0^0$ is the zero-order harmonic oscillator frequency, and

$$f_1(a_0a_2) = -\frac{5}{4\pi}\sqrt{\frac{5}{16\pi}}\,a_0^3 + \frac{15}{4\pi}\sqrt{\frac{5}{4\pi}}\,a_0a_2^2 + \frac{75}{256\pi^2}a_0^4 + \frac{75}{64\pi^2}a_0^2\alpha_2^2 + \frac{75}{64\pi^2}\cdot a_2^4 \qquad \ldots (6a)$$

$$f_2(a_0a_2) = -2a_0 + 3\sqrt{\frac{5}{16\pi}}\, a^2_0 - \frac{3}{2}\sqrt{\frac{5}{\pi}}\, a^2_2 - \frac{25}{256\pi^2}\sqrt{\frac{16\pi}{5}}\, a_0^4$$

$$- \frac{75}{64\pi^2}\sqrt{\frac{16\pi}{5}}\, a^2_0\, a^2_2 + \frac{75}{64\pi^2}\cdot\sqrt{\frac{16\pi}{5}}\, a_2^4\,. \qquad \ldots \quad (6b)$$

$$f_3(a_0a_2) = -2a_2 - \frac{15}{8\pi}\sqrt{\frac{16\pi}{5}}\, a_0a_2 - \frac{25}{32\pi^2}\cdot\sqrt{\frac{16\pi}{5}}\, a^3_0a_2 \qquad \ldots \quad (6c)$$

neglecting higher order terms.

So (1) becomes

$$H = -\frac{\hbar^2}{2M}\Delta' + \tfrac{1}{2}M\omega_0^2(a_0a_2)r'^2[1 + p_2(a_0a_2)Y_{20}(\theta'\phi') + p_3(a_0a_2)$$

$$\{Y_{22}(\theta'\phi') + Y_{2-2}(\theta'\phi')\}\, C\mathbf{l}\,.\,\mathbf{s} + D\mathbf{l}^2] \qquad \ldots \quad (7)$$

where $$\omega_0(a_0a_2) = \omega_0^0\,\lambda^{-2}\{1 + f_1(a_0a_2)\}^{1/2} \qquad \ldots \quad (8a)$$

and $$p_2(a_0a_2) = \frac{f_2(a_0a_2)}{1 + f_1(a_0a_2)} \qquad \ldots \quad (8b)$$

$$p_3(a_0a_2) = \frac{f_3(a_0a_2)}{1 + f_1(a_0a_2)} \qquad \ldots \quad (8c)$$

Introducing the usual dimensionless co-ordinate

$$x = \sqrt{\frac{M\omega_0(a_0a_2)}{\hbar}}\; x' \text{ etc and two new parameters}$$

$$\chi = -\tfrac{1}{2}\frac{C}{\hbar\omega^0_0} \qquad \ldots \quad (9a)$$

$$\mu = \frac{2D}{C} \qquad \ldots \quad (9b)$$

equation (7) becomes

$$H = -\frac{\hbar\omega_0(a_0a_2)}{2}(\nabla - r^2) + \hbar\chi\omega_0^0 R \qquad \ldots \quad (10)$$

where

$$R = \tfrac{1}{2}\xi r^2\left[Y_{20}(\theta\phi) + \frac{f_3(a_0a_2)}{f_2(a_0a_2)}\{Y_{22}(\theta\phi) + Y_{2-2}(\theta\phi)\}\right] - 2\mathbf{l}\mathbf{s} - \mu\mathbf{l}^2. \qquad \ldots (11)$$

In (11) we have introduced a new parameter

$$\xi = \frac{p_2(a_0a_2)}{\chi} \cdot \frac{\omega_0(a_0a_2)}{\omega_0^0}$$

$$= \frac{f_2(a_0a_2)}{\chi} \cdot \lambda^{-4}. \qquad \ldots \quad (12)$$

3. DETERMINATION OF THE ENERGY-LEVELS

It can be shown that the r-dependent part of the hamiltonian H as given by equation (10) commutes with the operators l, l_z & S_z, where $\mathbf{l}$ is the orbital angular momentum, l_z its projection on z-axis and S the z-component of the spin $\mathbf{S}$ of the particle. Hence the base vector $| Nl\, l_z S_z >$ can be obtained from the zero-th order equation of motion

$$-\frac{\hbar\omega_0^0}{2} (\nabla - r^2) \mid Nl\, l_z S_z > = E_0 \mid N\, l\, l_z S_z > \qquad \ldots \quad (13)$$

The radial part of the eigen ket appearing in (13) looks like

$$| Nl > \simeq \sqrt{\frac{2\Gamma(n+1)}{[\Gamma(n+l+3/2]^3}}\; r^l e^{-\frac{1}{2}r^2} L_n^{l+\frac{1}{2}} (r^2) \qquad \ldots \quad (14)$$

while the orbital part is $Y_{ll_z}(\theta\phi)$, with usual notation.

In (14) $N = 2n+l$ (where n can assume positive integral values, defines the radial quantum number.

Unfortunately none of the above operators commute with the total hamiltonian H as given in equation (10). But it can be readily shown that to a first approximation, j_z commutes with H, where j_z is the z-component of the total angular momentum $\mathbf{j}$ $(= \mathbf{l} + \mathbf{s})$ of the particle. Thus one can take the actual eigen function of a single particle in an ellipsoidal field as

$$| Nj_z > = \sum_l [A_{lj_z-\frac{1}{2}} \mid Nlj_z - \tfrac{1}{2}\, \tfrac{1}{2} > + A_{lj_z+\frac{1}{2}} \mid Nlj_z + \tfrac{1}{2}, -\tfrac{1}{2} >] \qquad \ldots \quad (15)$$

Using this wave function the energy eigen values can be easily calculated from equation (10) from a set of secular equations. The expression for total energy of a single particle moving in an ellipsoidal field is

$$E(Nj_z a_0 a_2) = (N+3/2)\hbar\omega_0(a_0a_2) + \hbar\chi\omega_0^0 < R > \qquad \ldots \quad (16)$$

The evaluation of $< R >$ is shown in the appendix.

The parameters χ and ω_0^0 in (16) are so chosen that the energy levels correspond to the Klinkenberg's (1952) level scheme in the limit of zero deformation, $(a_0 = a_2 = 0)$. For $A > 100$, $\hbar\omega_0^0 \sim 8.8 M$ev and χ is 0.05. The parmeter μ

defined in equation (9b) is of importance only when $N > 2$. In general, its value is ~ 0.4.

In calculating the energy eigen values we have introduced two new deformation parameters β and γ defined by

$$a_0 = \beta \cos \gamma \qquad \ldots \quad (17a)$$

$$a_2 = \frac{1}{\sqrt{2}} \beta \sin \gamma \qquad \ldots \quad (17b)$$

A look at equation (3) will show that if $\gamma = 0$ the surface of the nucleus becomes a prolate spheroid about Z'-axis and if $\gamma = \pi$ it is an oblate spheroid. In between these two values of γ the surface is a general ellipsoid.

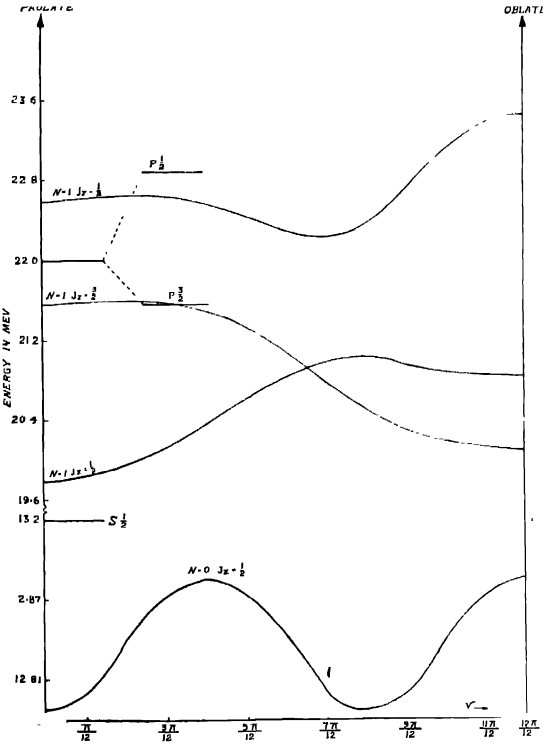

Fig. 1. The variation of the energy eigen values of a single particle moving in an anisotropic harmonic oscillator potential with γ for $N = 0$ and 1.

We have taken β as 0.3 which approximately corresponds to the deformation of Lu^{175} (as calculated from the intrinsic quadrupole moment). The variations of the energy eigen value of a single particle with γ are presented in figures 1 and

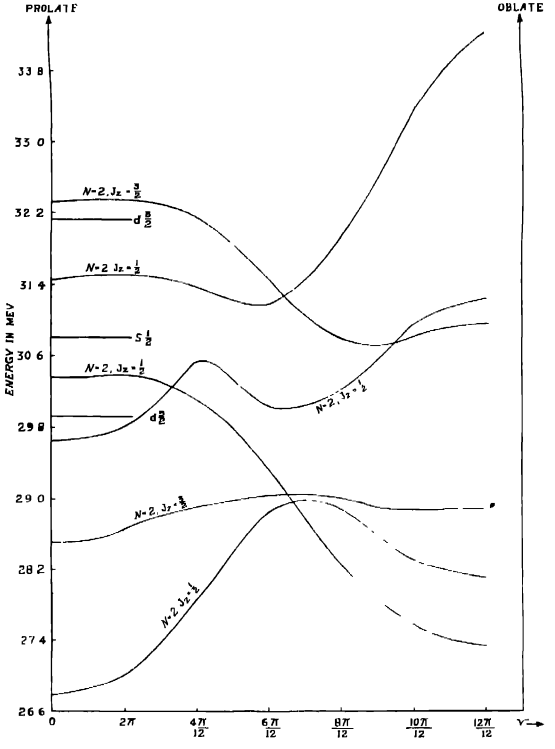

Fig. 2. The variation of the energy eigen values of a single particle with γ for $N = 2$.

2 for $N = 0$, 1 and 2 respectively. From these figures it is obvious that the positions of the energy levels depend sensitively on the choice of γ. The energy levels of a single particle in a central field approximation ($a_0 = a_2 = 0$) have also been shown in figures 1 and 2. Figure 3 illustrates the variation of the parameter ξ with γ.

Since the interactions between the nucleons are neglected in assuming an average field, the total energy of the nucleus is simply given by the sum of the energies of the individual particles. In this way total energy of the Ca^{40}-core part of Lu^{175} is plotted against γ in figure 4, from which one can see that there are

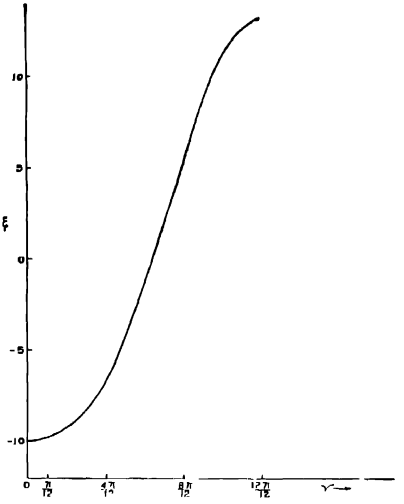

Fig. 3. The deformation parameter ξ against γ.

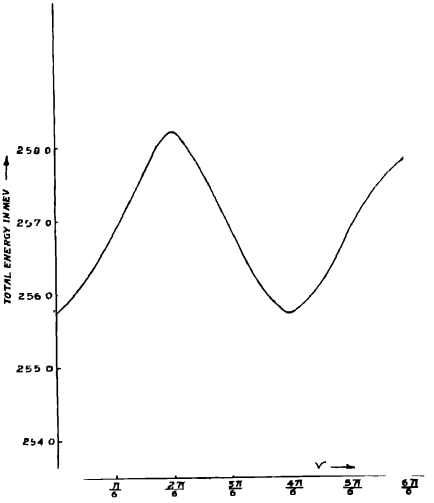

Fig. 4. The calculated total energy for the Ca^{40} core plotted against γ.

two minima, one at $\gamma=0$ and the other at $\gamma = 2\pi/3$ of which the first corresponds to a prolate shape. It is rather surprising that such a minimum should occur at $\gamma = 2\pi/3$, which does not preserve axial symmetry of the nucleus. Up till now we have not been able to explain this, but this may be smoothed out if one goes above the magic number 20. It is found that the difference in energy is approximately 2 Mev between a prolate and an oblate nucleus which is rather encouraging since the nuclei under our consideration prefer a prolate form.

Similar calculations for $N>2$ are in progress and will be reported in due course.

ACKNOWLEDGMENTS

The authors wish to express their deep gratitude to Professor A. K. Saha for his kind interest in the problem. Thanks are also due to Dr. M. K. Banerjee for many valuable discussions

Finally, the authors are grateful to the Department of Atomic Energy, Government of India, for the award of Research Fellowships which enabled them to work in this Institute.

APPENDIX

The evaluation of the matrix R

For $N \leqslant 2$, it is easy to see

$$< R > = < N'l'l'_z S'_z | \tfrac{1}{2}\xi r^2 Y_{20} - 2l \,.\, \bar{S} | Nl\, l_z s_z > \qquad \ldots \quad (1a)$$

$$= \tfrac{1}{2}\xi \left[\frac{\Gamma(n+1)\Gamma(n'+1)}{\Gamma(n+t-\nu+1)\,\Gamma(n'+t-\nu'+1)} \right]^{1/2} \nu\,!\,\nu'\,!\,.$$

$$\sum_{\sigma} \frac{\Gamma(t+\sigma+1)}{\sigma!(n-\sigma)!(n'-\sigma)!\,(\sigma+\nu-n)!(\sigma+\nu'-n)!}$$

$$\cdot\sqrt{\frac{5}{4\pi}}\sqrt{\frac{2l+1}{2l'+1}} < l2l_z0 | l2l'l'_z > . < l200 | l2l'0 >.$$

$$-2 < l'l'_z S'_z | l \,.\, \bar{S} | l\, l_z S_z > \qquad \ldots \quad (1b)$$

where $\nu = \tfrac{1}{2}(l'-l+2)$

$\nu' = \tfrac{1}{2}(l-l'+2)$

and $t = \tfrac{1}{2}(l+l'+3)$

The condition on the summation variables σ is

$$\begin{matrix} n \\ n' \end{matrix} \geqslant \sigma \geqslant \begin{matrix} n-\nu \\ n'-\nu' \end{matrix}$$

The Clebsch-Gordon coefficients appearing in equation (1b) are those defined by Condon and Shortley (1936).

The non-vanishing elements of $< l' l_z' S_z' | \bar{l} \, . \, \bar{S} | l \, l_z S_z >$

are
$$< l \, l_z \pm 1, \mp \tfrac{1}{2} | \bar{l} \, . \, \bar{S} | l \, l_z, \pm \tfrac{1}{2} > = \tfrac{1}{2} \sqrt{(l \mp l_z)(l \pm l_z + 1)} \quad \ldots \quad (2a)$$

and
$$< l \, l_z, \pm \tfrac{1}{2} | l \, . \, \bar{S} | l \, l_z \pm \tfrac{1}{2} > = \pm \tfrac{1}{2} l_z \qquad (2b)$$

In (1a) the $Y_{22}(\theta\phi) + Y_{2-2}(\theta\phi)$ term has been neglected since in the first order approximation, its contribution is negligible. The non-diagonal terms ($N \neq N'$) in equation (1b) are also of second order importance.

REFERENCES

Bohr, A., 1954, Rotational states in atomic nuclei (Ejnar Munksgaard, Copenhagen).

Bohr, A., 1953, *Dan. Mat. Fys. Medd.*, **26**, No. 14.

Condon, E. U. and Shortley, G. H., 1926, Theory of Atomic Spectra (Oxford).

Gottfried, K., 1956, *Phys. Rev.*, **103**, 1017.

Klinkenberg, P. F. A., 1952, *Rev. Mod. Phys*, **24**, 63.

Moszkowski, S. A., 1955, *Phys. Rev.*, **99**, 803.

Nilsson, S. G., 1955, *Dan. Mat. Fys. Medd.*, **29**, No. 16.

EXTENSION OF THE TABLE FOR THE CALCULATION OF SURFACE TENSION FROM MEASUREMENTS OF SESSILE DROPS

K. G. PARVATIKAR

DEPARTMENT OF PHYSICS, KARNATAK COLLEGE, DHARWAR

(*Received for publication, February* 13, 1958)

ABSTRACT. The calculations presented are an extension of the work of Tawde and Parvatikar on sessile drops. A table is prepared of the values of a^2/r^2 against h/r in the range from 0 570 to 0 978 at interval of 0.001.

The use of sessile drops for the measurement of surface tension has been suggested by several workers such as Worthington (1885), Fergusson (1913), Rayleigh (1915) and Porter (1933), but it is only recently that the method was placed on better foundations for exact work by Taylor and Alexander (1944). These authors have fitted up an empirical equation from which the values of a^2/r^2 are obtained for the corresponding values of h/r where a^2 is the capillary constant which connects the surface tension γ of a liquid by the relation $\frac{2\gamma}{g\rho}$, ρ being the effective density of the liquid, r, the radius of the sessile drop and h, the height of it from the equatorial plane. Thus the final derivation of surface tension from the knowledge of the measurable quantity h/r involves the use of the tabular functions connecting h/r with a^2/r^2.

Recently, Tawde and the author (1951) have shown that this function of h/r and a^2/r^2 could also be obtained by modifying the standard tables of Bashforth and Adams (1883). The table thus drawn up from fundamental considerations has been put to a rigorous test for its usefulness by using the experimental measurements on sessile drops. By a critical study, it has been shown that this table is equally dependable for applicability to experimental measurements. This table gave values of h/r and a^2/r^2 for the values of β ($\beta = 2b^2/a^2$, where b is the radius of curvature at the apex of the drop) ranging from 25 to 50 at interval of unity and from 50 to 100 at interval of two. Later, Tawde and Parvatikar (1954) have prepared a more detailed and conprehensive table of h/r *vs.* a^2/r^2, but, however, only in the range from 0.5100 to 0.5708.

Now it is interesting to consider whether it is necessary to extend this table beyond the range for which it was worked out. It can easily be seen that for a given area of a flat circular tip, the drops of a liquid formed on the tip will not have diameters beyond a certain limit. Thus the range of the shape factor h/r of a

TABLE I

h/r vs a^2/r^2 for sessile drops.

h/r	0	1	2	3	4	5	6	7	8	9
0.57	0.36393	0.36589	0.36784	0.36984	0.37182	0.37382	0.37581	0.37785	0.37988	0.38196
0.58	0.38403	0.38609	0.38813	0.39028	0.39238	0.39454	0.39665	0.39876	0.40091	0.40312
0.59	0.40530	0.40748	0.40968	0.41192	0.41412	0.41637	0.41865	0.42090	0.42318	0.42550
0.60	0.42779	0.43012	0.43249	0.43484	0.43721	0.43960	0.44198	0.44443	0.44687	0.44928
0.61	0.45173	0.45424	0.45675	0.45926	0.46178	0.46434	0.46689	0.46945	0.47202	0.47460
0.62	0.47721	0.47986	0.48252	0.48517	0.48786	0.49056	0.49328	0.49601	0.49876	0.50155
0.63	0.50434	0.50715	0.50994	0.51279	0.51565	0.51854	0.52145	0.52434	0.52723	0.53017
0.64	0.53313	0.53613	0.53915	0.54219	0.54524	0.54830	0.55134	0.55444	0.55759	0.56074
0.65	0.56388	0.56706	0.57027	0.57353	0.57680	0.58003	0.58335	0.58670	0.59005	0.59342
0.66	0.59683	0.60024	0.60366	0.60711	0.61056	0.61405	0.61758	0.62112	0.62466	0.62828
0.67	0.63193	0.63561	0.63929	0.64302	0.64675	0.65051	0.65428	0.65805	0.66188	0.66575
0.68	0.66965	0.67355	0.67749	0.68149	0.68551	0.68957	0.69366	0.69774	0.70184	0.70597
0.69	0.71014	0.71434	0.71858	0.72284	0.72717	0.73150	0.73583	0.74024	0.74467	0.74915

TABLE I (*contd.*)

h/r vs. a^2/r^2 for sessile drops.

h/r	0	1	2	3	4	5	6	7	8	9
0 70	0.75365	0 75815	0 76272	0.76737	0 77202	0 77666	0 78134	0 78603	0 79081	0.79560
0.71	0.80047	0.80535	0.81026	0 81518	0 82020	0.82525	0 83036	0.83550	0 84066	0.84584
0.72	0.85106	0 85637	0 86169	0 86711	0 87252	0 87798	0 88344	0.88898	0 89457	0.90018
0 73	0 90587	0 91158	0 91735	0 92315	0.92897	0 93492	0.94087	0 94689	0 95297	0.95904
0.74	0.96522	0 97140	0 97763	0 98398	0 99033	0.99679	1 0033	1.0098	1.0164	1.0231
0 75	1.0298	1.0366	1.0434	1.0502	1.0572	1 0642	1.0713	1 0784	1 0857	1.0929
0.76	1.1003	1 1077	1 1152	1.1227	1.1304	1.1381	1 1458	1 1536	1.1615	1.1695
0.77	1 1774	1.1856	1.1938	1.2020	1.2104	1.2188	1 2273	1 2358	1 2445	1.2534
0.78	1.2622	1.2711	1 2801	1 2893	1.2985	1.3077	1 3171	1.3267	1 3363	1.3458
0.79	1 3556	1 3655	1 3754	1.3853	1 3953	1.4058	1 4163	1 4268	1.4372	1 4480
0.80	1.4589	1.4699	1 4808	1.4918	1 5032	1 5148	1 5264	1.5380	1.5495	1 5617
0.81	1.5739	1 5861	1 5983	1 6105	1.6232	1.6362	1.6492	1 6622	1 6751	1.6883
0.82	1 7021	1.7159	1 7297	1.7435	1.7573	1 7717	1 7865	1 8014	1 8162	1.8311
0.83	1.8459	1 8614	1 8774	1.8934	1.9094	1.9254	1.9414	1.9577	1.9751	1 9925
0 84	2.0099	2 0273	2 0447	2 0621	2 0804	2 0995	2 1185	2.1376	2.1567	2.1757

TABLE I (*contd.*)

h/r vs. a^2/r^2 for sessile drops.

h/r	0	1	2	3	4	5	6	7	8	9
0 85	2 1948	2 2148	2 2359	2 2570	2 2780	2.2991	2 3202	2 3412	2 3623	2 3858
0 86	2.4093	2 4329	2 4564	2 4800	2 5035	2 5271	2 5506	2.5773	2.6030	2 6318
0.87	2.6576	2.6843	2 7111	2 7379	2 7647	2.7930	2 8241	2 8552	2 8863	2.9174
0 88	2 9485	2.9796	3 0107	3.0417	3.0737	3 1105	3 1472	3 1839	3.2206	3.2573
0 89	3.2940	3 3308	3 3675	3 4042	3 4425	3 4874	3 5323	3 5772	3 6220	3 6669
0 90	3.7118	3 7567	3.8016	3 8465	3 8914	3 9409	3 9981	4 0553	4 1126	4.1698
0 91	4.2270	4 2843	4 3415	4 3987	4 4560	4 5132	4 5704	4 6387	4.7164	4 7941
0 92	4 8717	4 9494	5 0271	5 1048	5 1825	4 2601	5.3378	5 4155	5 4932	5 5709
0.93	5 6686	5 7849	5 9012	6 0174	6 1337	6 2500	6 3662	6 4825	6 5988	6 7150
0 94	6.8313	6 9476	7 0638	7 1801	7 3036	7 5096	7 7157	7 9217	8 1277	8.3338
0 95	8 5398	8 7359	8.9519	9 1580	9 3640	9.5700	9 7761	9 9822	10 188	10 403
0 96	10.600	11.087	11 692	12.170	12 711	13 253	13 794	14 335	14 876	15 418
0.97	15.959	16 505	17.041	17 583	18 124	18 665	19 207	19 748	20.289	—

liquid is governed by the tip used. This range can be easily altered by employing a different tip Therefore, if the table of h/r *vs.* a^2/r^2 is limited in its range a suitable tip will have to be chosen so as to form drops of a liquid having h/r within this range.

It can be seen from the observations of Taylor and Alexander (1944) that this shape factor h/r is within the range 0 46505 and 0.48462, whereas this range is between 0.5203 and 0 5539 for the observations of Tawde and the author (1951) This shift of range of h/r is to be attributed to the different tip employed for the formation of drops. But it is a point to be noted here that r or h/r does not vary much from each other in the two sets of observations This is to be expected due to the circular tips employed in the two independent investigations having nearly the same diameter. Unfortunately, since the diameter of the flat circular tip used has not been given by Taylor and Alexander (1944) in their paper, it is not possible to verify the above conclusion But the experience of the author on similar expermental investigations shows that the conclusions drawn may not be far from truth. Therefore, if tips selected vary widely, it is possible to produce drops of liquids having values of h/r in different regions The standard tables of Bashforth and Adams (1883) in the case of sessile drops are at intervals 0.1 in β in the range 0.0 to 46.7 As pointed out earlier the table of h/r *vs.* a^2/r^2 has been worked out only in the range of $h/r = 0.5100$ to 0.5708 (or $\beta = 22.0$ to 46.7), and therefore, it is thought desirable to extend this table for the remaining values of β available in the work of Bashforth and Adams This has been done and a table is drawn in the range of $\beta = 0\ 0$ to 22.0 The method of calculation to obtain the values of h/r and a^2/r^2 was the same as shown in the earlier work

Direct interpolation was used to arrive at a^2/r^2 corresponding to the desired value of h/r The table thus prepared is given below with h/r values at interval of 0.001. This table allows for direct interpolation of intermediate values of h/r

REFERENCES

Bashforth and Adams, 1883, An Attempt to Test the Theories of Capillary Action Cambridge University Press.

Fergusson, 1913, *Phil. Mag.*, **25**, 509.

Porter, 1933, *Phil. Mag.*, **15**, 163.

Rayleigh, 1915, *Proc. Roy. Soc.*, **92***A*, 184.

Taylor and Alexander, 1944, *Proc. Ind. Acad. Sc.*, **19***A*, 149.

Tawde and Parvatikar, 1951, *Ind. J. Phy.*, **25**, 473.

Tawde and Parvatikar, 1954, *Ind. J. Phy.*, **28**, 345.

Worthington, 1885, *Phil. Mag.*, **20**, 51.

SPIN OF AN ELECTRON FROM FIVE-DIMENSIONAL WAVE EQUATION

C. C. BANERJEE

DEPARTMENT OF THEORETICAL PHYSICS,

INDIAN ASSOCIATION FOR THE CULTIVATION OF SCIENCE, JADAVPUR, CALCUTTA-32

(*Received for publication, February* 13, 1958)

ABSTRACT. The author attempts a general solution of five dimensional analogue of Klein-Gordon equation and finds that an intrinsic angular momentum of the electron similar to the spin appears as a consequence of the solution.

1. INTRODUCTION

In a previous paper the author (Banerjee, 1957) has obtained Sommerfeld's fine structure formula in exact form from five dimensional analogue of the Klein-Gordon wave equation. There it has been found that the introduction of the fifth co-ordinate influences the energy levels of the electron in the same way as the existence of its spin does it may be remarked here that the connection between the fifth co-ordinate of a particle and its spin is not, however, apparent. The idea to represent the motion of a particle in five-dimensional space-time continuum has engaged the attentions of Kaluza (1921), Klein (1926, 1946), Einstein (1931, 1932), Pauli (1933), Wilson (1928), Fisher (1929), Flint (1946), Corben (1952) and others , they have, however, confined themselves to purely theoretical lines It has been felt that it may be worthwhile to see how the idea fares with regard to its practical application and this feeling has enabled the author to obtain Sommerfeld's fine structure formula which result gives us the hope that this representation may throw more light on the mysteries of quantum phenomena It is further hoped that further investigation may give us better insight as to whether or how the fifth co-ordinate is connected to spin.

The author in the previous paper has obtained for the five dimensional equation a special solution when the two of the four quantum numbers coincided In the present paper that restriction has been removed and a general solution leading to the appearance of four quantum numbers has been obtained. It has been found that the square of the angular momentum has eigen values $j(j+1)\hbar^2$ where $j = l + \frac{1}{2}$; the appearance of half integers indicates that spin of the electron has entered into picture in a subtle way. The extra quantum number p, which appears here as a consequence of the additional co-ordinate, does not affect the energy levels of the electron subjected only to a coulomb field. It is necessary to pursue the line to find out what part the extra quantum number plays in atomic and nuclear processes.

2. GENERAL SOLUTION OF THE WAVE EQUATION

The relativistic wave equation in polar co-ordinates in five dimensions is given by

$$\frac{\partial^2\psi}{\partial r^2}+\frac{3}{r}\frac{\partial\psi}{\partial r}+\frac{1}{r^2\sin^2\chi\sin\theta}\frac{\partial}{\partial\theta}\left(\sin\theta\frac{\partial\psi}{\partial\theta}\right)+\frac{1}{r^2\sin^2\chi\sin^2\theta}\frac{\partial^2\psi}{\partial\phi^2}$$

$$+\frac{1}{r^2\sin^2\chi}\frac{\partial}{\partial\chi}\left(\sin^2\chi\frac{\partial\psi}{\partial\chi}\right)+\left(A+\frac{2B}{r}+\frac{Z^2\alpha^2}{r^2}\right)\psi=0 \qquad \ldots (1)$$

where $A=\frac{W^2-m_0{}^2c^4}{\hbar^2c^2}$, $B=WZ\alpha^2$ and $\alpha=\frac{e^2}{\hbar c}$

(This equation is the same as the equation (4a) of the previous paper). We may separate the above equation into two equations given below

$$\frac{r^2}{\psi_r}\left[\frac{\partial^2\psi_r}{\partial r^2}+\frac{3}{r}\frac{\partial\psi_r}{\partial r}+\left(A+\frac{2B}{r}+\frac{Z^2\alpha^2}{r^2}\right)\psi_r\right]=l(l+2) \qquad \ldots (2)$$

and

$$\frac{1}{\psi_\theta}\frac{1}{\sin^2\chi\sin\theta}\frac{\partial}{\partial\theta}\left(\sin\theta\frac{\partial\psi_\theta}{\partial\theta}\right)+\frac{1}{\psi_\varphi}\frac{1}{\sin^2\chi\sin^2\theta}\frac{\partial^2\psi_\varphi}{\partial\phi^2}+\frac{1}{\psi_\chi}\frac{1}{\sin^2\chi}\frac{\partial}{\partial\chi}$$

$$\left(\sin^2\chi\frac{\partial\psi_\chi}{\partial\chi}\right)=-l(l+2) \qquad \ldots (3)$$

where l is a positive integer. The equation (2) leads to the fine structure formula in exact form which has been done in the previous paper and the equation (3) may be split up into two following equations.

$$\frac{1}{\psi_\theta}\frac{1}{\sin\theta}\frac{\partial}{\partial\theta}\left(\sin\theta\frac{\partial\psi_\theta}{\partial\theta}\right)+\frac{1}{\psi_\varphi}\frac{1}{\sin^2\theta}\frac{\partial^2\psi_\varphi}{\partial\phi^2}=-p(p+1) \qquad \ldots (4)$$

and

$$\frac{1}{\psi_\chi}\frac{\partial}{\partial\chi}\left(\sin^2\chi\frac{\partial\psi_\chi}{\partial\chi}\right)+l(l+2)\sin^2\chi=p(p+1) \qquad \ldots (5)$$

where p is a positive integer.

The equation (5) becomes on substitution $\psi_\chi=(\sin\chi)^{-\frac{1}{2}}\omega$ where ω is a function of χ,

$$\sin\chi)^{-\frac{1}{2}}\left[\frac{1}{\sin\chi}\frac{\partial}{\partial\chi}\left(\sin\chi\frac{\partial\omega}{\partial\chi}\right)+(l+\tfrac{1}{2})(l+\tfrac{3}{2})\omega-\frac{(p+\frac{1}{2})^2}{\sin^2\chi}\omega\right]=0 \qquad \ldots (6)$$

Putting $j = l+\frac{1}{2}$ and $q = p+\frac{1}{2}$ and since $(\sin\chi)^{-1/2} \neq 0$ we have

$$\frac{1}{\sin\chi}\frac{\partial}{\partial\chi}\left(\sin\chi\,\frac{\partial\omega}{\partial\chi}\right)+j(j+1)\omega-\frac{q^2}{\sin^2\chi}\,\omega=0 \qquad \ldots \quad (7)$$

The solution of the equation (7) is $P_j^q(\cos\chi)$ and this is expressible in the form of a rational integral function of $\cos\chi$ and $\sin\chi$ when $j-q$ is a positive integer (Thomson and Tait, 1879) Hence the time-independent ψ-function in five-dimensional continuum may be written as

$$\psi = \psi_r\, P_p^m(\cos\theta)\, e^{im\phi}\,(\sin\chi)^{-1}\, P_{l+1/2}^{p+1/2}(\cos\chi) \qquad .. \quad (8)$$

where ψ_r denotes the solution of the radial equation (2). The above solution reduces to our solution in the previous paper when $l=p$ It is seen from the general solution given above that it contains an extra quantum number (p) which, however does not affect the eigen energies of the bound electron Further the appearance of half integers makes one feel that the spin of the electron has been embedded in the formalism in a curious way.

3 INTRINSIC ANGULAR MOMENTUM OR SPIN

In three dimensional space (*i e.* four dimensional continuum) the square of the angular momentum operator is given by

$$L^2 = -\hbar^2\left[\frac{1}{\sin\theta}\frac{\partial}{\partial\theta}\left(\sin\theta\,\frac{\partial}{\partial\theta}\right)+\frac{1}{\sin\theta}\frac{\partial^2}{\partial\phi^2}\right] \qquad .. \quad (9a)$$

Replacing $\frac{\partial^2}{\partial\phi^2}$ by $-m^2$, we have

$$L^2 = -\hbar^2\left[\frac{1}{\sin\theta}\frac{\partial}{\partial\theta}\left(\sin\theta\,\frac{\partial}{\partial\theta}\right)-\frac{m^2}{\sin\theta}\right] \qquad .. \quad (9b)$$

We maintain that in our four dimensional space (*i e.* five dimensional continuum) the square of the angular momentum operator, which we shall denote by J^2 maintains the same form as in three dimensional space.

Now from equations (6) and (7) we have an operator

$$-\hbar^2\left[\frac{1}{\sin\chi}\frac{\partial}{\partial\chi}\left(\sin\chi\,\frac{\partial}{\partial\chi}\right)-\frac{q^2}{\sin^2\chi}\right]$$

which has the desired form and we associate this operator in our four dimensional space as the square of the angular momentum operator. The eigen values of this operator is evidently given by $j(j+1)\hbar^2$ and hence $J = \sqrt{j(j+1)}\hbar$. When $l = 0$, we have $J^2 = 3/4\,\hbar^2$, $J = \sqrt{\frac{1}{2}(\frac{1}{2}+1)}\hbar$ and $j\hbar = \hbar/2$. Since $l = 0$ corresponds to

the state of the particle independent of θ, ϕ and χ we may assign these values to be due to the intrinsic angular momentum or what is called the spin of the particle

ACKNOWLEDGMENT

The author desires to express his sincere thanks to Prof. D Basu, Ph.D , for valuable discussions and helpful comments during the progress of the work.

REFERENCES

Banerjee, C. C , 1957, *Ind Jour of Phys.*, **31**, 242
Corben, H. C., 1952, *Phys. Rev*, **88** 677
Einstein, A., 1931, *Berl. Ber.*, 541 .
1932, *Berl Ber* , 130
Fisher, J. W , 1929, *Proc. Roy. Soc* . *A* **123**, 490
Flint, H. T., 1946, *Proc Roy. Soc* , *A*. **185**, 14.
Kaluza Th., 1921, Sitzungsber. Pruss Akad. d Wiss., 966
Klein, O., 1926, *Zeit f Physik*, **37**, 895.
,, 1946, *Arkiv. Mat Astron. Fysik*, **34***A* No. 1.
Pauli, W , 1933, *Ann d Physik*, **18**, 305 and 337.
Thomson, W and Tait P G., 1879, Natural Philosophy, Vol 1, App B.
Wilson, W , 1928, *Proc. Roy Soc.*, *A* **123**, 490.

THE STUDY OF NOISE PULSES AND A LIQUID SCINTILLATOR

BRAT PAL SINGH*, H. S. HANS† AND P. S. GILL

DEPARTMENT OF PHYSICS, MUSLIM UNIVERSITY, ALIGARH

(*Received for publication, January* 20, 1958)

ABSTRACT. Analysis of noise pulses of RCA photomultiplier 5819 has been made with about 350 volts between photocathode and first dynode. The differential distribution of noise pulses has been studied at different voltages and temperatures. Two distinct distributions are apparent in these curves. One has been interpreted as due to thermal noise and the other due to after-pulses caused by ion feedback. Response of stilbene in xylene liquid scintillator has been studied for Co^{60} gamma-rays with high collection efficiency and at low temperature. From the differential distribution of these pulses, the Compton edge due to Co^{60} gamma-rays is clearly indicated.

1. INTRODUCTION

It is well known that the collection efficiency between the cathode and the first dynode increases at high voltages between the two (Engstrom *et al.*, 1952). But at these high voltages the noise in the photomultiplier also goes up considerably. The pulse height distribution of these noise pulses is of considerable importance especially when the genuine pulses are of small size, as for example, in liquid scintillators.

The origin of these noise pulses has been the subject of analysis by many workers (Engstrom, 1947; Rodda, 1949; Morton and Mitchell, 1949; Curran, 1953 and others). From these investigations it appears that the main causes of the noise may be summarised as (i) amplified thermionic emission from the photocathode, (ii) positive ion feedback, (iii) the generation of photons inside the photomultiplier and (iv) ohmic leakage. In the early work of Engstrom, Rodda and others only the integrated effect of the noise pulses *i.e.* the noise current was studied. Morton and Mitchell made some studies of differential distribution of the noise pulses. Later Mueller (1952), Harrison (1952) Davison (1952), Lanter and Corwin (1952) and Breitenberger (1955) studied the after-pulses which are mainly produced by the feedback of ions created by the electrons of the main pulse.

A systematic study of pulse height distribution of the noise pulses was therefore essential to analyse the pulses from the liquid scintillator. This also helps one to understand the origin of the noise pulses

* Research Scholar, Ministry of Education, Government of India.

† Senior Research Fellow of the National Institute of Sciences of India.

2. EXPERIMENTAL

For the study of noise pulses, RCA photomultiplier 5819 was mounted in a light-tight chamber. The assembly which contained the 5819 tube with Mu-magnetic shield, associated voltage dividing resistance network, and cathode follower (scintillation head), was enclosed in a thermostatically controlled cabinet. The temperature in the cabinet could be varied from 30°F to 75°F.

The voltage between the cathode and the first dynode was about seven times the voltage between the other dynodes in order to get very high collection efficiency. The pulses from the cathode follower were fed to the Atomic's linear amplifier model 204C and the pulse height analysis was made by Atomic's pulse height analyser model 510, after which the pulses were scaled and recorded.

Stilbene in xylene (3 gms/litre) introduced by Kallmann and Frust (1950) is our liquid scintillator, whose response was studied for Co^{60} gamma-rays. A thin-walled glass cell (diameter 4.8 cm and length 11 cm) was filled with the scintillator liquid solution and was covered from sides with aluminum to serve as reflector. The cell was fixed to the photomultiplier with silicone grease, with a perspex piece in between to provide a flat surface and to act as a light pipe.

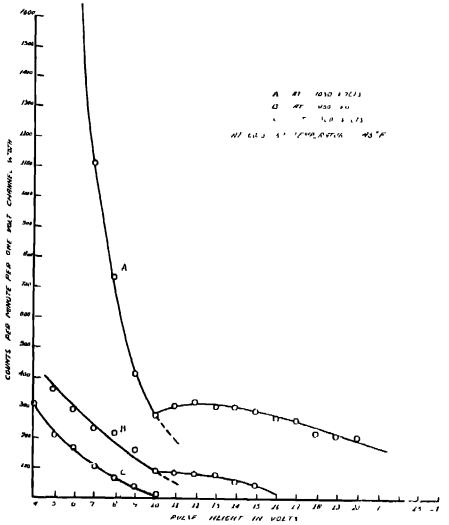

Fig. 1 Differential pulse height spectrum of noise pulses at various total voltages applied to the photomultiplier when the temperature of the photomultiplier was kept constant at 45° F.

For attaining a particular temperature the system was left in the cabinet for about $1\frac{1}{2}$ hours to attain the equilibrium, which was checked by observing the counting rate at a particular pulse height which remained constant with time.

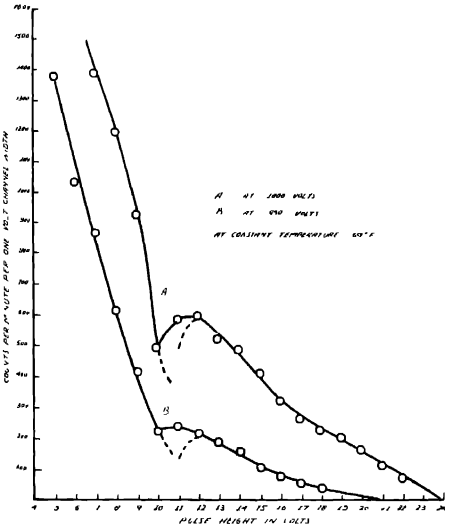

Fig. 2. Differential pulse height spectrum of noise pulses at various total voltages applied to the photomultiplier when the temperature of the photomultiplier was kept constant at 69°F.

3. OBSERVATION AND RESULTS

Figures 1 and 2 show the curves of differential distribution of noise pulses at different voltages, keeping the temperature constant, while figures 3 and 4 show the curves at different temperatures keeping the voltage constant Voltages were varied from 900 to 1050 volts while the temperatures were kept at three different settings, 37°F, 56°F and 69°F.

An interesting feature of these curves is that each curve appears to consist of two parts, the first part coming down smoothly and the second part having a maximum Also it is clear from the curves that the total noise is decreased at lower temperatures and lower voltages.

Figure 6 gives the distribution of the pulses from the liquid scintillator for Co^{60} gamma-rays, after substracting the background. Peak due to Compton edge is clearly visible. It was noted that only xylene without stilbene did not give any pulse above 4 volts.

4. DISCUSSION

Though the first part of the curves for the noise pulses more or less resembles the trend of the curves reported by a number of workers, (Morton and Mitchell,

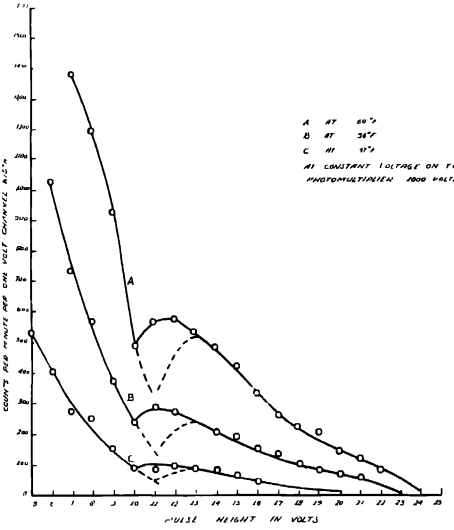

Fig. 3. Differential pulse height spectrum of noises at various temperatures of the photomultiplier when the total voltage on the photomultiplier was kept constant at 1000 volts.

1949 and others), the second part with a hump seems to be a peculiarity of these curves. Comparatively very high voltage applied between the cathode and the first dynode appears to be the main difference between this experiment and that of other workers.

In our conditions, the gain of the photomultiplier could be taken roughly as 4×10^4, the total stray capacity at the anode as 10 pf and the gain of the linear amplifier as 8000. One electron from the photocathode, therefore, gives pulse of about 4 to 5 volts.

The pulses due to ohmic leakage are known to be small in size as discussed by Morton and Mitchell (*loc, cit*), Engstrom (1947), Rodda (1949) and others. They are expected to be around or below 5 volts Therefore in the analysis of these curves, we need consider only thermionic noise and ion feedback, as the main contributing factors. According to the above authors also, these two effects contribute most to the noise in the region of our interest.

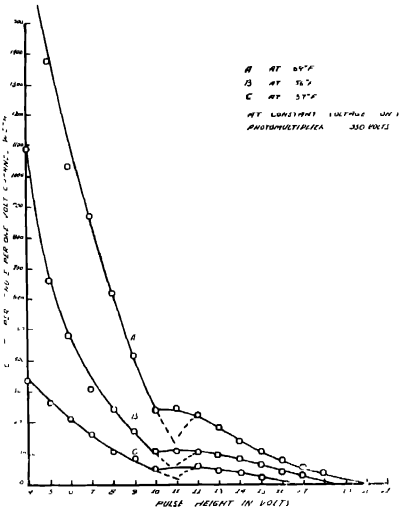

Fig 4 Differential pulse height spectrum of noise pulses at various temperatures of the photomultiplier when the total voltage on the photomultiplier was kept constant at 950 volts.

As mentioned above, the hump portion in our curves appears to be related with the high voltage between the cathode and the first dynode. This is borne out by figure 1, where at an overall voltage of 900, when the voltage between the cathode and the first dynode is 335 volts this portion disappears, while at overall voltage of 1050, when the voltage between the cathode and the first dynode is 390 volts, this portion is very dominant The fact that the pulse height, in this portion are comparatively high, rules out the possibility of its arising from any other dynode, except from the cathode. It also appears that this is due to some secondary effects, connected with the initial electrons starting from the photocathode. It is well known that the thermal electrons, which are the only primary

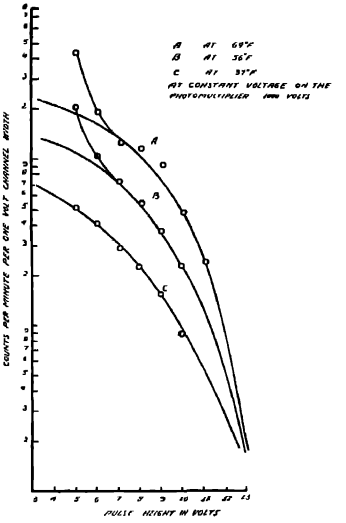

Fig 5. Differential pulse height spectrum of noise pulses at various temperature of the photomultiplier when the total voltage on the photomultiplier was kept constant at 1000 volts (Semilog graph).

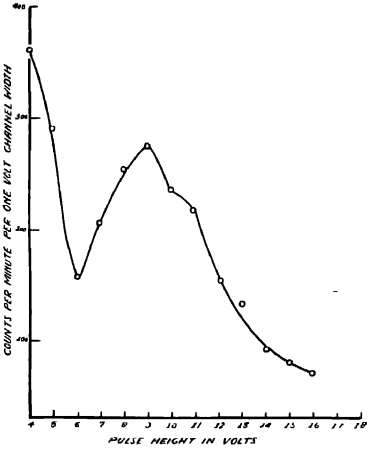

Fig. 6 Differential pulse height spectrum of pulses from stilbene in xylene liquid scintillator due to Co^{60} gamma rays.

electrons from the cathode in our case, give noise pulses whose pulse height distribution curve comes down smoothly following some sort of distribution law. Most of the curves of noise pulses found in the literature bear this out They are normally taken at comparatively low voltages between the cathode and the first dynode where the positive ion feedback effect will not be dominant and therefore the curves may be assumed to be wholly due to thermal noise. Normally change of voltage is expected to change the number and the pulse height but the general trend of the curves due to thermal electrons should remain the same.

The most predominant secondary cause of noise pulses is the positive ion feedback The primary electrons starting from the cathode may ionize the atoms of the residual gas, which on reaching the cathode may release further electrons, to give one more pulse. These pulses are expected to be delayed with respect to the primary ones Though this effect should be present even at comparatively low voltages, its probability of occurrence shoots up at higher voltages. This is borne out by Huxford (1939) who ploted γ, the average number of electrons released by each positive ion falling on Cs-Ag-O photo-surface, versus the field through which positive ion moves It appears from his curve that while γ remains constant at a value of about 0.5 for fields loss than 150 volts per cm, at higher fields the value of γ goes up quite steeply so that at 250 volts/cm, γ is about 4 and if the trend of the curve is assumed to remain the same even for little higher fields, γ for 350 volts/cm or so may be still higher. The trend of this curve for γ suggests that it is feasible that after a certain field between the cathode and the first dynode, the pulses, due to positive ion feedback may attain heights, to deviate appreciably from the curves due to the primary electrons. The above arguments therefore, suggest that the humped portion may be attributed to the positive ion feedback.

Photons produced inside the photomultiplier due to de-excitation of the residual gas may be ruled out as the cause of this part of the curve, because the efficiency for electron emission for photons is extremely small It requires about 25 photons in the photo-sensitive region to emit one electron

Pulses due to positive ion feedback which are delayed with respect to the primary pulses, have been studied by Harrison, (1952) Davison, (1952) Mueller *et al.*, (1952) Lanter and Corwin (1952), and Breitenberger. (1951) According to Harrison the amplitude and the distribution of these is consistent with their being caused by single positive ions, produced by the electrons of the main pulse. Mueller *et al* observed that after-pulses which are produced by the initial pulses due to the single electrons, are of the same height or slightly taller than the main pulses. Lanter and Corwin, however, observed that at higher gain the maximum height of the after-pulse corresponds to more than one photoelectron and depends on the height of the main pulse. It appears from the oscillograph traces given in this paper that the after-pulses

follow some sort of distribution law in heights. But according to Davison, the number, but not the amplitude of the after-pulses seems to be related to the amplitude of the main pulse. Further, he observed that the visual comparison of the after-pulses produced by a single electron seems to indicate that the pulse height distributions of the two are identical

At the low voltage between the cathode and the first dynode the value of γ as given in the curve of Huxford is of the order of 0 5, which may be interpreted that the after-pulses will be mostly due to one electron This seems to be borne out by the experiments of the workers mentioned above. However, at comparatively high voltages at which the present experiments were carried out, probability of emission of more than one electron is appreciably high. It is even possible that the most probable number of electrons emitted by a single positive ion at high voltages may be five or six etc in which case one should expect a sort of pulse height distribution with a maxima corresponding to the average value of γ This explains the hump in our curves.

In figure 5 the first part of the curve of figure 3 is replotted on a semilogarithmic graph Two interesting facts emerge from these curves, firstly, these curves follow more or less a parabolic shape and secondly, at higher temperatures and higher voltages a deviation from the parabolic shape is observed. It seems that these deviations are due to preponderance of small pulses caused by ohmic leakage or certain effects arising from dynodes. The parabolic shape confirms our conclusion that the first portion of these curves is mostly due to thermionic emission from the photocathode.

It is further clear from the curves in figures 1 to 4, that (1) the number of noise pulses decreases at low temperatures. (2) the number of pulses at higher pulse heights decreases more slowly with temperature than the number at the smaller pulse heights, (3) the number of small pulses seems to go up very rapidly with higher voltages and (4) in general, the structure of the curves remains the same.

5. RESPONSE OF STILBENE IN XYLENE LIQUID SCINTILLATOR

Luminescence efficiency of liquid scintillator is much less as compared to NaI(TL) crystal. It should, therefore, be quite interesting to study their response under our conditions of extraordinary high collection efficiency.

The scintillators containing atoms of low atomic number, like the one in this experiment, respond to gamma-rays of about 1 Mev, mainly through Compton effect. Co^{60} emits two gamma-rays of energies of 1.17 Mev and 1 33 Mev. Under very good conditions the two Compton edges due to Co^{60} gamma-rays have been clearly indicated by McIntyre and Hofstadter (1950) using NaI(TL) crystal as detector.

Figure 6 gives the differential distribution of pulses from stilbene in xylene liquid scintillator with Co^{60} gamma-rays This spectrum was taken with 390 volts between the cathode and the first dynode and at a temperature of 37°F. These conditions increase the collection efficiency and decrease the noise pulses. This curve was drawn after substracting the noise pulses of the type mentioned earlier.

The peak at 9 volts may be interpreted as due to Compton edge At 11volts also there is an indication of an edge If the peak at 9 volts is taken to be due to Compton edge of 1.17 Mev. gamma-rays and if the scintillator is assumed to be linear, the Compton edge due to 1.33 Mev gamma rays should come out to be at 10 6 volts However, one should be cautious in attributing the Compton edge at 11 volts due to 1 33 Mev. gamma-raya, because the primary pulses from the scintillator are also expected to give after-pulses which will have their maximum at about 12 volts These after-pulses cannot be subtracted. Though their number is expected to be small still it can not be ruled out that the edge at 11 volts may be mostly due to them Also because of low luminescence efficiency the scintillator is not expected to be good enough to resolve the two Compton edges. Peak at 9 volts is, of course, definitely due to Compton edge of Co^{60} gamma-rays

A comparison was made of pulse heights produced in NaI(TL) and stilbene in xylene by the same energy gamma-rays under the same conditions This gave the ratio of photoelectron yield of our liquid scintillator and NaI(TL) as 0.0045 for gamma-rays of Co^{60}

REFERENCES

Birks, J. B., 1954, "Scintillation Counters", Pergamon Press.

Breitenberger, E., 1955, *Prog. Nuclear Physics*, **4**, 56.

Curran, S C., 1953, "Luminescence and the Scintillation Counters".

Davison, P. W., 1952, *Nucleonics*, **10**, 3, 33.

Engstrom, R. W., 1947, *Journal of Opt Soc. Of America*, **37**, 6, 420.

Engstrom *et al.*, 1952, *Nucleonics*, **10**, **4**, 58.

Harrison, F. B. 1952, *Nucleonics*, **10**, 3, 33.

Huxford, W. J , 1939, *Phy. Rev.*, **55**, 754.

Kallmann, H., Frust, M., 1950, *Phy. Rev* , **79**, 857.

Lanter, R. L and Corwin, R W., 1952, *Rev. Sci. Instruments*, **23**, 507.

McIntyre, J A. and Hofstadter, R., 1950, *Phy. Rev.*, **78**, 617.

Morton, G A and Mitchell, J. A., 1949, *Nucleonics*, **4**, 1, 16.

Mueller, D. W., 1952, *Nucleonics*, **10**, 3, 33.

Mueller, D. W. *et al* , 1952, *Nucleonics*, **10**, 6, 53.

Rodda, R. S., (1949, *Jour. Sci. Inst.*, **26**, 65.

ON THE RAMAN SPECTRA OF SOLUTIONS OF ORTHO-CHLOROPHENOL

DEB KUMAR MUKHERJEE

OPTICS DEPARTMENT, INDIAN ASSOCIATION FOR THE CULTIVATION OF SCIENCE, CALCUTTA-32

(*Received for publication February 4, 1958.*)

Plate V

ABSTRACT. The Raman spectra of 15% and 30% solutions of *o*-chlorophenol in carbon tetrachloride, chloroform and cyclohexane have been investigated and the relative intensity of the line 3533 cm^{-1} due to O–H valence oscillation has been measured with respect to that of the line 1416 cm^{-1}. It has been observed that the intensity of the line increases when the liquid is dissolved in the solvents and it increases further when the concentration is diminished from 30% to 15%. It has been concluded from these results that at a very low concentration the intensity of the line 3533 cm^{-1} is expected to increase still further. It has been pointed out that as this line is assigned to the O–H valence oscillation in the molecule with the O–H group in the trans position, such molecules become predominant in the solution at very low concentrations, and therefore, the strong infrared absorption peak at 6910 cm^{-1} observed in 0·1 molal solution in carbon tetrachloride cannot be ascribed to O–H vibration in the group in the cis position. It is suggested that the peak may be due to vibration in the O–H group in the trans position under the influence of surrounding carbon tetrachloride molecules. It has been suggested that infrared absorption band at 6610 cm^{-1} of the pure liquid might be due to a combination tone in the molecule of cis form.

INTRODUCTION

It was observed by previous workers that in the Raman spectra of both phenol and *o*-chlorophenol there is a weak line of Raman frequency about 3520 cm^{-1} (Kohlrausch and Pongratz, 1933, 1934). Wulf and Liddell (1935) on the other hand, while studying the infrared absorption spectra of solutions of organic compounds containing OH group in carbon tetrachloride observed that the solution of phenol shows a single absorption peak at 7050 cm^{-1} while *o*-chlorophenol gives two peaks at 6910 cm^{-1} and 7050 cm^{-1} respectively, the former being much stronger than the latter. These peaks correspond to the first harmonic of the fundamental O–H frequency 3520 cm^{-1}, and this difference between the behaviour of *o*-chlorophenol and that of phenol was first explained by Pauling (1936) who pointed out that in the solution of *o*-chlorophenol there might be two types of molecules, one having the OH group in the cis position and the other in the trans position with respect to the chlorine atom. Errera and Mollet (1935) also studied the infrared abosrption spectrum of pure *o*-chlorophenol in the region 1.3μ–1.8μ and observed a peak at 6620 cm^{-1} in place of the two peaks due to the solution in carbon tetrachloride mentioned above. The Raman spectrum of solution of *o*-chlorophenol in carbon tetrachloride was later

studied by Batuev (1945) who observed the OH line to be at 3533 cm^{-1} in the Raman spectrum of the pure liquid and the solution also yielded only a single line at 3540 cm^{-1}. Recently, Biswas (1954) studied the Raman spectra of o-chlorophenol in the liquid and solid states and observed that the line 3533 cm^{-1} due to O–H valence oscillation persists even when the crystals of the compound are cooled to −180°C. The results reported by Batuev (1945) do not indicate that the frequency of the O–H valence oscillation diminishes when the liquid is dissolved in carbon tetrachloride and are therefore contradictory to those on the infrared absorption in the region of 7000 cm^{-1} reported by previous workers It was, therefore, thought worthwhile to study the Raman spectra of solutions of o-chlorophenol in different solvents more carefully and to compare the intensity of the line 3533 cm^{-1} due to the pure liquid with that of the corresponding line due to the solution in order to find out whether any change either in the frequency or in the intensity of the line occurs when the liquid is dissolved in simple organic liquids. The present paper deals with these results

EXPERIMENTAL

The solvents used for the study of the Raman spectra of the solutions were carbon tetrachloride, chloroform and cyclohexane, the last one being chosen to avoid halogen atoms in the solvent molecules Ortho-chlorophenol of laboratory reagent quality was purchased from City Chemical Corporation of New York All the liquids were distilled under reduced pressure, as usual, and the Raman spectra of 15% and 30% solutions were photographed using a Fuess spectrograph having a dispersion of about 11 5 Å/mm in the 4046 Å region As the line 3533 cm^{-1} is very weak the spectra were photographed with long exposures to bring out this line clearly The spectrum was also photographed with the 4046 Å group of Hg lines cut off with rhodamine 6 GBM filter in order to assign the lines correctly. As preliminary investigations indicated that the intensity of the line 3533 cm^{-1} changes when the liquid is dissolved in the solvents mentioned above attempt was made to estimate the relative intensities of certain lines using blackening-log-intensity curves which were drawn with the help of microphotometric records of the continuous spectra of light from a tungsten filament lamp recorded with different known widths of the slit of the spectrograph As the line 3533 cm^{-1} is weak the background intensity had to be subtracted from the total intensity in order to derive the actual intensity of the line Microphotometric records of the spectra were obtained with the help of a Kipp and Zonen type recording microphotometer

RESULTS AND DISCUSSION

Some of the spectrograms are reproduced in figure 1, Plate V and some of the microphotometric records are reproduced in figure 2. It can be seen from

the latter figure that the line 3533 cm^{-1} excited by the 4046 Å line is weak and broad in comparison with a weak line at 1416 cm^{-1} excited by 4358 Å line in the spectrum due to the pure liquid, but in the spectra due to the solutions the line 3533 cm^{-1} is much stronger than the 1416 cm^{-1} line. The ratio of the intensity of the line 3533 cm^{-1} to that of the line 1416 cm^{-1} observed in the spectra due to the pure liquid and the solutions in carbon tetrachloride and chloroform are given in Table I. This ratio could not be determined in the case of the solution in cyclohexane, but in this case the Raman frequency of the line seems to increase to about 3550 cm^{-1}.

TABLE I

Ratio of intensities of the lines 3533 cm^{-1} and 1416 cm^{-1}

Substance	I_{3533}/I_{1416}
o-Chlorophenol pure	0.8470
30% solution in CCl_4	1.55
15% solution in CCl_4	1.88
30% solution in $CHCl_3$	1.47
15% solution in $CHCl_3$	1.62

Figure 1(a) shows that there is no line of Raman frequency slightly lower than 3533 cm^{-1} in the spectrum due to the pure liquid. The infrared spectra of the pure liquid in the region between 6000 cm^{-1} and 7200 cm^{-1} studied by Errera and Mollet (1935) and of the solution in carbon tetrachloride studied by Wulf *et al* (1935) show that in the case of the pure liquid there is a strong and broad absorption peak at about 6620 cm^{-1} with the indication of weak absorption at about 7050 cm^{-1}, and in the case of the solution there are two absorption peaks at 6910 cm^{-1} and 7050 cm^{-1} respectively, the former being nine times as large as the latter. These peaks are assumed to be due to harmonics of the O–H valence oscillations and the peak at 6910 cm^{-1} due to the solution was assigned by Pauling (1935) to the harmonic of the oscillations in O–H group in the cis position of the molecule with respect to the chlorine atom and the line 7050 cm^{-1} to the harmonic of such oscillations in the O–H group in the trans position. Similarly, the peak 6620 cm^{-1} given by the pure liquid was attributed to the harmonic of the oscillation in O–H group in the cis position with the oxygen atom of the O–H group forming a hydrogen bond with the hydrogen atom of the O–H group of a neighbouring molecule. It is, however, surprising that the Raman spectrum of the pure liquid does not show, besides the line at 3533 cm^{-1}, another line at 3310 cm^{-1} which would be the fundamental frequency corresponding to the harmonic at 6620 cm^{-1}. Similarly, the Raman spectrum due to the solution in carbon tetrachloride does not show a strong line at 3455 cm^{-1}

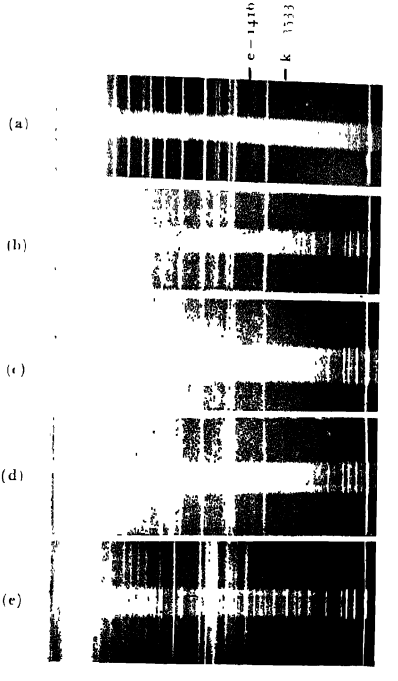

Raman spectra of ortho-chlorophenol

(a) Pure liquid
(b) ,, ,, excited with 4046 A. U. cut off
(c) 15% solution in CCl_4
(d) 30% solution in $CHCl_3$
(e) 15% solution in cyclohexane

as the fundamental of the harmonic at 6910 cm^{-1} observed in the infrared spectra. These facts seem to be anomalous.

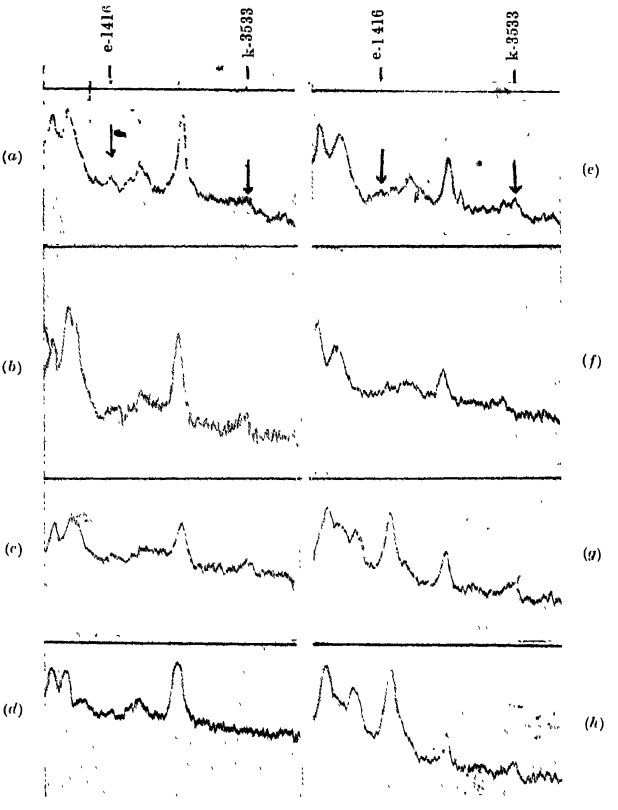

Fig. 1. Microphotometric records of Raman spectra.

(*a*) Pure *o*-chlorophenol in liquid state
(*b*) 30% solution in CCl_4
(*c*) 15% " " "
(*d*) Pure *o*-chlorophenol excited with 4046 A.U. group cut off.
(*e*) 30% solution in $CHCl_3$
(*f*) 15% " $CHCl_3$
(*g*) 30% " in cyclohexane
(*h*) 15% " " "

It is evident from the above facts that probably it is necessary to find out an alternative interpretation of these infrared absorption bands. As the Raman spectrum of the pure *o*-chlorophenol shows a faint line at 3533 cm^{-1} this line is to be assigned to the valence oscillation in the OH group which is not attached to the chlorine atom, as in the phenol molecule. This line is produced evidently by only a very small percentage of molecules in the pure liquid The corresponding oscillation in the cis position of the O–H group may have almost the same frequency, but probably the O–H vibration in this case cannot be excited without exciting simultaneously the C–H valence oscillation of the molecule Hence we expect to observe a combination line of Raman shift about 6600 cm^{-1} and the corresponding band was actually observed by Errera and Mollet (1935) in the infrared region The band at 1 51μ observed by them is probably not due to the harmonic of O- H valence oscillation, but it may be due to the combinational mode mentioned above. There is, however, a little absorption in the region 7050 cm^{-1} in the curve reproduced by Errera and Mollet, and this absorption may be due to the harmonic of the line 3533 cm^{-1} excited in a very small percentage of the molecules, as observed in the Raman spectrum of the pure liquid.

This alternative interpretation of the infrared bands of the pure liquid is offered, because the structure of the dimer which is assumed to be present in the pure liquid by Pauling (1935) indicates the presence of two types of O H groups, but in the Raman spectrum only one line due to O–H valence oscillation is observed Also, the formation of the hydrogen bond between the two molecules is expected to produce a shift in the electronic energy level with the change from the vapour to the liquid phase of the substance The ultraviolet absorption spectra of the vapour and the liquid were compared by Swamy (1953) but no appreciable shift was observed to take place with liquefaction of the vapour although large shifts were observed to take place with this change of state in the case of parachlorophenol This shows that such a change in the electronic energy level is produced by the chlorine atom the influence of which is diminished by the attachment of the hydrogen atom of the O–H group to it

As indicated in Table I the Raman spectra of the solutions show that the intensity of the line 3533 cm^{-1} increases when the liquid is dissolved in the solvents and it increases further when the concentration is diminished from 30% to 15%. As this line is to be assigned to O–H vibration in the molecule with the O–H group in the trans position the number of such molecules increases with lowering of concentration of the solutions. It is, therefore, quite unlikely that at a concentration of 01 molal 90% of the molecules in the solution in carbon tetrachloride may have the OH group in the cis position. The strong peak at 6910 cm^{-1} observed by Wulf *et al* (1935) is due to a 01 molal solution in carbon tetrachloride and the interpretation that 90% of the molecules in the solution have

the O-H group in the cis position and that these molecules produce this peak at 6910 cm^{-1} has probably to be revised in view of the results given in Table I. It has to be assumed now that at 01 molal concentration of the solution in carbon tetrachloride studied by Wulf *et al* (1935) almost all the *o*-chlorophenol molecules have the O–H group in the trans position It is, however, quite probable that this conversion from the cis to the trans form is caused by the chlorine atoms of the carbon tetrachloride molecule to which the hydrogen atom of the O–H group in most of the *o*-chlorophenol molecules may be loosely attached. Such an attachment is expected to diminish the frequency of the O-H valence oscillation, and this explains the diminution of the frequency of the harmonic from 7050 cm^{-1} to 6910 cm^{-1}. The weak peak at 7050 cm^{-1} is probably produced by the small percentage of molecules in which the hydrogen atom of the O-H group is not attached to the neighbouring carbon tetrachloride molecules. The lowest concentration of the solutions of which the Raman spectra have been studied in the present investigation is 15%. Even at this concentration the Raman line due to the O–H oscillation is very weak and therefore the majority of the molecules have the O–H group in the cis position. At this concentration probably the O–H group in the trans position in the remaining few molecules are not attached to the neighbouring carbon tetrachloride molecules owing to the influence of the *o*-chlorophenol molecules with the O–H group in the cis position which are still predominant in the solution at such a concentration.

In the case of the solution in cyclohexane such a diminution in the O-H frequency owing to the influence of the molecules of the solvent is not expected and it would be interesting to study the infrared spectrum of the solution in the region from 1 5μ to 1 7μ. The fact that the O–H frequency increases slightly in this solution shows that even in the pure liquid the intermolecular field slightly lowers the frequency of this vibration

ACKNOWLEDGMENT

The author is indebted to Professor S C Sirkar, D Sc , F.N.I. for kindly suggesting the problem and also for his guidance during the progress of the work.

REFERENCES

Batuev, M. I. (1945), *Doklady Akad Nauk, S.S.S.R.*, **47**, 100.
Biswas, D. C., 1954, *Ind. J. Phys.*, **28**, 85.
Errera, J. and Mollet, P., 1935, *Jour. de Physique*, **6**, 281
Kohlrausch, K. W. F. and Pongratz, A , 1933 *Sitz Akad. Wiss. Wien.*, **142**, 633.
Kohlrausch, K. W. F. and Pongratz, A., 1934, *Wiener Anz. Nr.*, **22**, 281.
Pauling, L., 1936, *J. A. C S.*, **58**, 94.
Swamy, H. N., 1953, *Ind. J. Phys* , **27**, 119
Wulf, O. R, and Liddel, U., 1935, *J. A. C. S.*, **57**, 1464.

X-RAY STUDY OF AGAVE VERA CRUZ FIBRE

N. N. SAHA AND THANDA PE

DEPARTMENT OF PHYSICS, UNIVERSITY OF RANGOON

(*Received for publication, ,February* 20, 1958)

Plate VI A & B

ABSTRACT. The structure and properties of Agave vera cruz have been studied with the help of X-ray diffraction analysis. This particular type of leaf fibre, which is used by local weavers in Burma for making longyi, has not so far received due attention as far as its structural study by X-ray method is concerned. The length of the (002) arcs has been found to be greater than that in any bast fibre. It has also been found that, unlike cotton, the strength of the fibre decreases with the decrease in spiral angle and also that the strength of the fibre decreases with the increasing concentration of mercerising solution. An explanation of this phenomenon has been incorporated in the paper

1. INTRODUCTION

It is well known that cotton occupies a unique position in the family of natural textile fibres. Next comes jute which belongs to the 'bast fibre' group. Another group classed as 'leaf fibres' is a comparatively newcomer in the domain of textile industry. Till now, leaf fibres are mainly used in cor industry. The bare fact they have not made their mark as quality textile fibres in the past does not necessarily rule out the possibility of their economic utilisation in the future. In fact, a particular type of leaf fibre—Agave vera cruz, which finds its use in longyi industry in Burma, forms the subject matter of our present investigation

An exhaustive study of natural fibres has already been made by many investigators (Meyer and Mark 1928; Sirkar and Saha 1944; Sisson, 1943). The results of the investigations are so well known that a resume here may appear redundant Nevertheless, some salient features deserve mention. The chains of which a fibre is built may lie either closely parallel to or a long a spiral path around the fibre axis. It was later suggested that all natural fibres have their crystallites arranged in spiral manner. It should be pointed out that a very steep spiral amounts almost to parallel configuration. In ramie, crystallites are arranged in a very steep spiral form, *i e.* in parallel configuration. This so called parallel orientation, howsoever perfect from crystallographic point of view, is not an ideal configuration so far as textile properties of a fibre are concerned It is true that this perfect alignment of the crystallites in ramie provides to the fibre very good strength and rigidity, but there is an associated brittleness in the transverse direction. In cotton, the crystallites are arranged in spirals making an angle of about 30° with

the fibre axis. Though cotton has less intrinsic strength than ramie, it is more resilient and weaves into a softer fabric.

The degree of steepness of a spiral finds its manifestation in the length of the (002) arcs. A cellulose fibre having crystallites arranged in steep spirals will give an X-ray diagram having well defined spots. But as the spiral arrangement is more and more flat, *i e.* spiral makes larger angles to the fibre axis, the reflections are drawn out into larger and larger arcs.

The width of the (002) reflection, however, depends on the size of crystallites, the fluctuation in arrangement of crystallites along the spiral and on the presence of constituents other than cellulose in a marked degree. A correct idea of the orientation and the size of the crystallites can, therefore, be obtained from the length and width of the (002) reflections It may be mentioned that the measurement of intensity along different directions of the (002) reflection provides a good method of classification of fibres (Sirkar and Saha, 1946).

It needs hardly any mention that a precise knowledge of the molecular structure of a fibre is essential to have a deeper understanding and clear insight of the properties of a fibre; and the X-ray diffraction analysis is the best available method for the purpose. In view of the fact that the leaf fibres have not yet received any systematic and extensive study by X-ray method, the present investigation on the X-ray study of the structure and properties of Agave vera cruz has been undertaken by us.

2. EXPERIMENTAL

Raw leaves of Agave vera cruz were retted as usual in our laboratory and the fibres thus obtained from the retted leaves were thoroughly washed, dried and combed before taking X-ray photographs The specimens were prepared in the form of a bundle containing about twenty strands, each cut into 2.5 cm in length. The individual fibres in the specimen were made parallel to each other by applying a little tension and the bundle thus made was fixed on a specially made specimen holder with the fibre axis vertical. The specimen was then placed against the X-ray beam collimated through a slit of 0.05 cm in diamter and 6 cm in length. Filtered Cu Kα radiation from a demountable 'Raymax 60' X-ray tube was used all throughout the investigation.

Samples mercerised with 15%, 20%, 25% and 30% NaOH solution at room temperature were also photographed. Two samples with different conditions of pre-treatment were bleached by passing chlorine gas in the fibres kept in water. The physical properties such as fineness and intrinsic strength of the fibres, both raw and treated with mercerising solutions of different strength, were determined.

All X-ray photographs reproduced in this paper were taken with Unicam single crystal goniometer; the film to specimen distance in each photograph being 3 cm.

Calibration was made by taking X-ray pattern on the same film of a copper wire whose spacings are known accurately.

3. RESULTS AND DISCUSSIONS

X-ray patterns of raw and treated Agave vera cruz are reproduced in Plate VI A & B. The pattern due to raw fibre (Fig. 1) corresponds to that of native cellulose, though some differences in finer details are observed. The equatorial reflections $A_1(101)$ and $A_2(10\bar{1})$ are nearly fused together. The $A_1(002)$ arcs, which are most intense, end rather abruptly and continue with weaker intensity along the diffraction ring. The spacings calculated from figure 1 (Plate VI A) are given in Table below.

TABLE 1

Spacings in Å	tensity	Planes (*hkl*)
14 45	w.	?
9 57	m.w.	?
5 92	s	101
5 42	s	$10\bar{1}$
3.93	v s.	002
6.35	m.w.	110
5 15	w.	020
4.3	m.s.	120
4.2	m.	?
2 56	m.s.	040

The unit cell dimension calculated from these spacings was found to be quite in agreement with that of native cellulose. It can be seen from the table above that three spacings whose planes are not identified do not belong to cellulose spacings. Figure 1 shows the presence of a few irregular spots scattered all over the diagram. These are due to diffraction by calcium oxalate crystals present in the fibre. Our preliminary chemical analysis indicated the presence of these crystals. Our findings do not support the suggestion made by Kubo (1940) that the cellulose present in Agave fibres is in the modified form, known as Cellulose T

Our chemical analysis shows that the cellulose content of this fibre is about 75% and the next major constituent lignin is about 15%. Two reflections near the central spots of spacings 14 35A and 9.57A (Table I) appear to be due to lignin. It is well known that stronger the caustic soda solution used for mercerisation, the larger is the quantity of lignin removed from the fibres It can be seen from X-ray patterns (figures 5, 6, 7, 8 of Plate VI B) of mercerised fibre that these two reflections get gradually weaker as the strength of mercerising solution is increased. This suggests that these two spacings are due to lignin present in the fibre. Another reflection of spacing 4.2A(Table I), intense on the meridian, seems to be due to

Indian Journal of Physics, Vol. XXXII, No. 4.

PLATE VI A

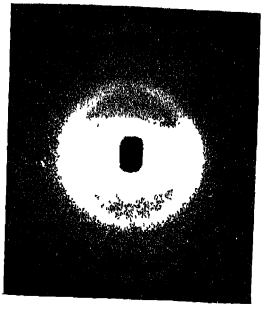

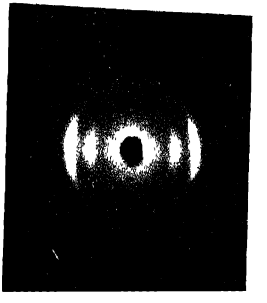

Fig. 2

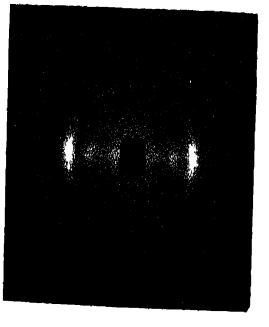

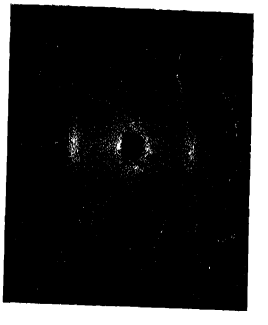

Fig. 4

X-ray diffraction patterns

Fig. 1. Raw Agave vera cruz

Fig. 2. Bleached fibre (lignin partially removed)

Fig. 3. Bleached fibre (lignin removed in higher degree)

Fig. 4. Fibre kept in boiling water for one hour

Fig 5

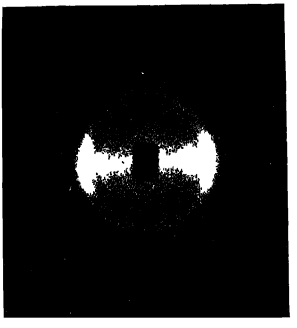

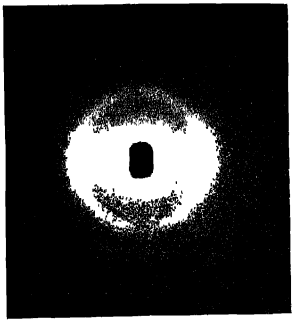

Fig 6

Fig 7

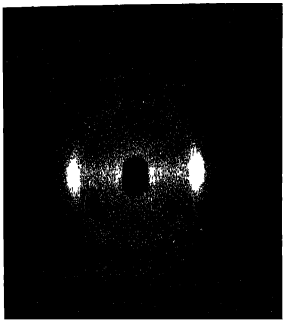

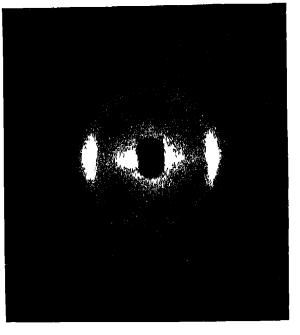

Fig 8

X-ray diffraction patterns

Fig 5 Mercerised with 15% NaOH solution.
Fig. 6 ,, ,, 20% ,, ,,
Fig 7 ,, ,, 25% ,, ,,
Fig 8. ,, ,, 30% ,, ,,

wax in the fibre. That this spacing is due to wax has been confirmed by taking the X-ray photograph of the dewaxed sample where this particular reflection is absent.

All our X-ray photographs show that the (002) reflections are drawn out into arcs which are longer than those due to bast fibres. The length of the arc in the case of raw Agave fibre has been found to be about 60° (figure 1). The extented arcs indicate that the pattern corresponds to cellulose crystallites oriented in spiral form, the spiral making an angle of 30° with the fibre axis Four fainter arcs distributed diagonally on the meridian can also be seen in figure 1. They correspond to (021) reflections and are not as sharp as they are in ramie or flax. The lack of sharpness as well as the extension of the arcs in the present case may be due to the flat spiral configuration A comparison of the (002) arcs in figure 1 with those in the X-ray pattern of cotton showed that the arcs in the former are much wider. This pronounced width suggests that the size of the crystallites in this case is smaller. It also indicates a lower degree of lateral order and a marked fluctuation of the orientation of crystallites around the spiral.

X-ray photographs of two Agave vera cruz samples from which lignin was removed in different degree and bleached thereafter by passing chlorine gas revealed some interesting informations A careful examination of figure 2, which is due to the sample from which the lignin and other intercrystalline materials were removed only partially, shows that the (002) reflection is sharper and the pattern as a whole is cleaner than those due to raw fibre (figure 1) Figure 3, which is due to the sample from which the lignin and amorphous constituents were removed in a higher degree, shows that the pattern (figure 3) is undoubtedly cleaner than figure 2 and the (002) reflection is almost as sharp as it is in cotton which is regarded as almost pure cellulose. It should be noted that the strength of the latter was markedly less than the former (figure 3). This marked loss of strength in the latter sample, therefore, seems to be due to the higher degree of removal of lignin and other intercrystalline constituents A comparative study of figures 2 and 3 also reveals that the reflections due to lignin of spacings 14.35Å and 9.57Å are very poor or nearly absent in figure 3. This finding suggests that lignin helps in retaining the strength of the fibre

It may be observed from the X-ray photograph (figure 4) of fibres kept in boiling water for about an hour that the reflections are sharper and the pattern as a whole is cleaner than those due to raw fibre. It is also to be pointed out that the (020) reflection on the meridian is more clearly visible and the length of the (002) arcs is less than that in raw fibre, i.e. 50°. This reduced length of the (002) arcs and their sharpness indicate better orientation and crystallinity. No change in spacings was, however, observed.

X-ray photographs of samples mercerised with 15%, 20%, 25% and 30% caustic soda solutions are reproduced respectively in figures 5, 6, 7 and 8

(Plate VI B). A careful examination reveals that in all these photographs, in addition to the usual spacings of mercerised cellulose, two reflections of spacings 5.92Å and 5.4Å due to 101 and $10\bar{1}$ planes of the native cellulose are present. This shows that both native and mercerised cellulose (Saha, 1948; Sisson and Saner, 1941) are present in the samples. The mercerisation is not complete even in the sample treated with 30%NaOH solution. The size of the unit cell calculated from the spacings in the mercerised patterns, given in Table II below, was found to be the same as that in hydrated cellulose (Sirkar and Saha, 1946, Andress, 1929).

TABLE II

Spacings in A	Intensity	Planes (*hkl*)
7.36		101
4.4		101
4.03		002
5.2		020
4.35		120, 021
2.56		040
5.92		101 } Native
5.4		101 } Native

In cotton, mercerisation was found to be complete when it was treated with 18% NaOH solution, but in the present case even a 30% solution could not effect complete mercerisation. This appears to be due to the predominance of intercrystalline materials present in this fibre which affects mercerisation adversely. It may be mentioned that the degree of mercerisation is more pronounced in a sample kept in boiling water before being mercerised. The degree of mercerisation in the sample kept in boiling water for about an hour and then mercerised with a 30% NaOH solution has been found to be more complete, as revealed by X-ray examination, than that in the sample which was mercerised as usual with the same concentration of mercerising solution (figure 8). This enhanced degree of mercerisation appears to be due to the swelling—a factor favouring mercerisation—effected by boiling; and also perhaps due to the removal of some intercrystalline constituents which affect mercerisation.

It may be noted that the nature of the diffraction pattern, particularly the (002) arcs, gives an idea of the strength of the fibre. The longer the arcs, the greater is the departure of the orientation of spiral with respect to the fibre axis, which, as is well known, accounts for the loss of strength. Table III below shows the relationship between the intrinsic strength of the fibres, both raw and and

mercerised, and the length of the (002) arcs or the spiral angle. It also shows the relationship between the intrinsic strength and the concentration of the mercerising solutions.

TABLE III

Per cent NaOH	Intrinsic strength $10^6 \frac{gm}{gm/cm}$ $\left(\frac{strength}{fineness}\right)$	Spiral angle (in degrees)
Raw fibre	2.35	
15 %	1.41	
20 %	1.18	22 5
25 %	×	20
30 %	0.97	

It can be seen that the raw fibre with spiral angle 30° has intrinsic strength 2 35, which means that 23 5 kilometres length of fibre will break by its own weight. It is evident from Table III that as the concentration of the mercerising solutions increases, the intrinsic strength decreases. Table III also shows that the intrinsic strength decreases with the decrease in spiral angle. These observations are in contrary to that observed in cotton, where the intrinsic strength increases with the decrease in spiral angle.

It may be noted that this fibre, unlike cotton, contains about 15% lignin, which, as mentioned before, acts as a cementing material. Though lignin is absent in some strong fibres like ramie and cotton, it adds to the strength of the fibres if and where it is present. It is well known that lignin is removed on mercerisation and this is evident from our X-ray photographs (figures 5, 6, 7, 8) where we find the gradual fading, though not complete disappearance, of the two reflections which are ascribed to lignin. As lignin is supposed to be the cementing force, removal of it will naturally result into the loss of strength of the fibre.

That the crystallites are better oriented as a result of mercerisation is evident from the graudal decrease in the length of the (002) arcs, as can be seen in our mercerised patterns It is expected that this preferred orientation, i.e. steeper spirals would increase the strength of the fibre. But our findings show that the strength decreases. It seems that the increase in strength due to better orientation as a result of mercerisation has been outweighed by the loss of strength due to the removal of lignin in course of mercerisation. It, therefore, explains the seemingly contradictory findings as to why in spite of gradual decrease in intrinsic strength, the length of the arcs becomes gradually shorter.

It is also well known that the length of the micelle is one of the most important factors which go to build up the strength of fibres. Our investigation on the

determination of the length and width of the micelle (Laue, 1926) in raw and mercerised fibres is in progress. These results will be published shortly.

It may be pointed out that the single fibres which are used by local weavers here are coarse and this is rather a handicap to them so far as the use of this fibre in finer garments is concerned. Our optical study has revealed that these socalled single fibres get splitup into a number of finer fibrils under the action of very dilute acids. Investigation in this line is also in progress. In conclusion, it may be mentioned that if this particular type of leaf fibre, which is so abundant in Burma and also in India, along with some other members of the 'leaf fibre' group could be studied with the intensity and care it deserves, it is expected that there will be some more welcome additions in the family of ideal textile fibres.

REFERENCES

Andress, K. R., 1929, *Z. Phys. Chem. B*, **4**, 190
Kubo, T., 1940, *Z. Physik. Chem. A*, **187**, 297.
Laue, M. von, 1926, *Z. Krist*, **64**, 115.
Meyer, K. H. and Mark, H., 1928, *Ber.*, **61***B*, 593.
Saha, N. N., 1948, *Ind. Jour. Phys.*, **22**, 141.
Sirkar, S. C, Saha, N. N., *et al.*, 1944, *Proc. Nat Inst. Sc*, **10**, 325.
Sirkar, S. C. and Saha, N. N., 1946, *Nature*, **157**, 839.
Sirkar, S. C. and Saha, N. N., 1946, *Proc. Nat. Inst. Sc*, **12**, 151.
Sisson, W. A., 1943, 'X-ray Examination', High Polymer Vol 5, Interscience Publishers
Sisson and Saner, 1941, *J. Phys. Chem*, **45**, 717.

Statement about ownership and other particulars about "INDIAN JOURNAL OF PHYSICS"

FORM IV

1 Place of Publication ± ... 2 & 3 Lady Willingdon Road, Calcutta 32.

2 Periodicity of its publication ... Monthly

3 Printer's Name ... ... Kalipada Mukherjee,
Nationality ... ... Indian,
Address ... ... 204/1, B. T. Road, Alambazar, Calcutta-35

4 Publisher's Name ... ... Samarendra Nath Sen
Nationality ... ... Indian,
Address ... ... 2 & 3 Lady Willingdon Road, Calcutta-32

5 Editor's Names
Nationality
Address

1. Prof R. K. Asundi
Indian
16, Juhu Road,
Bombay-23.

2. Prof K. Banerjee
Indian
Hd. of the Dept. of Phys,
Allahabad University,
Allahabad.

3. Prof. D M. Bose,
Indian,
Bose Institute,
93/1 Upper Circular Rd.
Calcutta-9

4. Prof. K. R. Dixit,
Indian,
Prof. of Physics,
Gujarat College,
Ahmedabad-6.

5. Prof. P. S. Gill,
Indian,
Prof. of Physics,
Muslim University,
Aligarh

6 Prof S. N. Bose
Indian
Vice-Chancellor
Biswa-Bharati
Bolpur, Dt. Birbhum.

7. Prof S. K. Mitra,
Indian,
Institute of Radio Physics Electronics,
92, Upper Circular Road
Calcutta-9.

8. Prof P. Ray,
Indian,
Indian Association for the Cultivation of Science
Calcutta-32.

9. Prof K. R. Rao,
Indian,
Principal & Hd. of the Dept, of Physics,
Andhra University.
Waltair.

10. Prof S. C Sirkar
Indian,
Indian Association for the Cultivation of Science
Jadavpur, Calcutta-32

11. Prof. B. N. Srivastava,
Indian,
Indian Association for the Cultivation of Science,
Jadabpur, Calcutta-32

6 Name and address of the proprietor ... Indian Association for the Cultivation of Science, Jadavpur, Calcutta-32.

I, Samarendra Nath Sen, hereby declare that the particulars given above are true to the best of my knowledge and belief.

(Sd) Samarendra Nath Sen,
Signature of Publisher

Date 16-3-58

NEWS RELEASE

Publication of Index to Scientific Journals

Indian Journal of Physics is among the 510 periodicals that are being indexed by subject and author in a new publication announced recently.

The primary subjects included in these indexes are solid state physics, nucleonics, radiation, optics, mechanics, astrophysics, radio, electronics, sound, astronomy, rockets, guided missiles, artificial satellites and space travel. These indexes, comprising several hundred thousand entries, have been compiled by the Library of the U. S. Naval Research Laboratory.

The original index cards are to be reproduced in book form by offset printing, 21 cards per page, 10″ × 14″. Author, and subject, sections, and the monthly, quarterly and annual supplements to each, can be purchased separately.

The publication will be available only to those who subscribe in advance of printing, which will start in the 3rd quarter of this year.

The publication is offered by Micro-Photography Co., 97 Oliver Street, Boston 10, Massachusetts.

USE OF LAGUERRE FILTERS FOR REALISATION OF TIME FUNCTIONS AND DELAY

A. K. CHOUDHURY AND N. B. CHAKRABARTI

INSTITUTE OF RADIO PHYSICS AND ELECTRONICS, UNIVERSITY OF CALCUTTA

(*Received for publication, September 26, 1957*)

ABSTRACT. In this paper is presented a method of realising time functions, delays and delayed integrations by making use of Laguerre filters. Circuit arrangements for realising two classes of Laguerre functions are described. The method has the merit that the adjustments required for obtaining different operations present no difficulty.

1. INTRODUCTION

In a simulator, the components of the original system are replaced by analogous devices having similar performance characteristics. One of the basis of such simulation is the time response. Further, in simulation of process control systems, one is required to realise operations of delay and delayed integration.

It is known that for the indicial response of a system a sectionalised delay line may be used. (Corrington *et al.* 1954). But, for low frequency applications, the construction of such delay line is difficult. For the realisation of time delays, a method employing operational amplifiers has been described (Morill, 1954); this method labours under the disadvantage that it requires a large number of elements and is not adaptable to the realisation of time functions.

2. LAGUERRE FUNCTIONS

The simplest means of generating a function would be to sum a number of easily realisable functions. For this purpose it would be a great advantage if the coefficients could be easily determined. The Laguerre functions, besides being orthogonal, also possess rational Fourier transforms, and are thus eminently suited for the realisation of arbitrary time and frequency functions.

A set of Laguerre functions due to Tricomi is defined as

$$T_n(t) = \sum_{0}^{r=n} \binom{n}{r} \frac{(-t)^r}{r!} = \mathcal{L}^{-1} \frac{(p-1)^n}{p^{n+1}} = \mathcal{L}^{-1} T_n(p) \qquad \ldots \quad (1)$$

Now

$$\mathcal{L}^{-1} e^{-\alpha t} T_n(t) = \frac{1}{p+\alpha} \left(\frac{p+\alpha-1}{p+\alpha} \right)^n \qquad \ldots \quad (2)$$

Hence writing $g(p) = \frac{1}{p+\alpha} \Sigma a_n \left(\frac{p+\alpha-1}{p+\alpha}\right)^n$, one has

$$L^{-1}g(p) = F(t) = e^{-\alpha t} \Sigma a_n T_n(t) \qquad \ldots \quad (3)$$

The coefficients a_n are given by the series

$$(p+\alpha)\, g(p) = \Sigma a_n Z^n = F(Z) \qquad \ldots \quad (4)$$

where the transformation $Z = \frac{p+\alpha-1}{p+\alpha}$ has been adopted. This relation transforms any circle $|Z| = a$ in the z-plane into a circle on the p-plane which may be made to enclose all the singularities of $(p+\alpha)\, g(p)$ by choosing suitable values of a and α.

We now consider the different functions obtained by giving values to α.

α	Z	Transformation	Radius of convergence of $F(z)$	Time functions
0	$\frac{p-1}{p}$	Half plane $R(p) < 0$ into the half plane $R() > 1$	$R(Z) < 1$	$\sum \binom{n}{r} \frac{(-t)^r}{r!} = T_n(t)$
$\frac{1}{2}$	$\frac{p-1/2}{p+1/2}$	Half plane $R(p) < 0$ into an area outside the unit circle	Inside the unit circle	$e^{-t/2} \sum \binom{n}{r} \frac{(-t)^r}{r!} = L_n(t)\,(-1)^n$
1	$\frac{p}{p+1}$	Left half-plane of p into the right half plane of Z	$\lvert Z \rvert = \frac{1}{2}$ at $Z = \frac{1}{2}$	$e^{-t} \sum \binom{n}{r} \frac{(-t)^r}{r!} = \beta_n(t)$

It is to be noted that only the symmetric function corresponding to $\alpha = 1/2$ permits expansion of $F(Z)$ in powers of Z around $Z = 0$. Therefore even in realising a function in terms of $\beta_n(t)$ the preliminary mathematical steps should employ only the set $L_n(t)$. The conversion is safely effected by noting that

$$\frac{p}{p+1} = 1/2 \left(1 + \frac{p-1}{p+1}\right)$$

3. GENERATION OF ARBITRARY TIME FUNCTIONS

Let $f(t)$ be the impulse response of the system to be simulated and $g(p)$ be the Laplace transform of $f(t)$. The steady value of $f(t)$ is assumed to be zero. If it is not, we consider the function $f(t) - [f(t)]_\infty = F(t)$. We may now write

$$F(t) = \sum^{n} a_k L_k(t) = e^{-t} \Sigma \beta_k t^k$$

which means that it is desired to approximate $F(t)e^t$ by a polynomial in t. The relation between the coefficients a_k and β_k is simple. For the purpose we note that

$$\frac{t^k e^{-t}}{k!} = \mathcal{L}^{-1} \frac{1}{(p+1)^{k+1}} = \mathcal{L}^{-1} \frac{1}{2^k(1+p)} = \left(1+\frac{1-p}{1+p}\right)^k$$

$$= 1/2^k \mathcal{L}^{-1} [L_0(p)+kL_1(p)+\ldots\ldots] \qquad \ldots \quad (5)$$

In case $g(p)$ is known analytically or approximately by the expansion in terms of the moments of $f(t)$ we effect the transformation

$$g\left(\frac{Z-1}{Z+1}\right) \cdot (1+Z) = \Sigma a_n Z^n \qquad \ldots \quad (6)$$

It is clear that the procedure seeks to find the numerator coefficients on the assumption of a given denominator polynomial $(1+p)^{n+1}$. Besides in a few cases expansions of the arbitrary functions are readily recognisable. For example, one finds easily that

$$J_0(2\sqrt{x\,t}) = e^{-t/k} \sum_0^{n=\infty} \frac{1}{n!} \left(\frac{t}{k}\right)^n L_n(kx)(-1)^n \qquad \ldots \quad (7)$$

$$\frac{erf(\sqrt{t})}{\sqrt{\pi}} = e^{-t} \sum_0^{n=\infty} \frac{(n+\frac{1}{2})}{n!} (-1)^{n-1} L_{n-1}(t) \qquad \ldots \quad (8)$$

For realisation of a square pulse of duration T, one has only to evaluate

$$a_n = \int_0^T L_n(t)\, dt.$$

We give below expansions of some simple functions in terms of Laguerre function.

1. Delay Operator :

$$e^{-pT} = \frac{1}{p+1} \sum_0^{\infty} (-1)^n L_n(T) \frac{(1-p)^n}{(1+p)^n}$$

2. Square wave of duration T :

$$\frac{1-e^{-pT}}{p} = \frac{1}{p+1} \sum_0^{\infty} \left(\frac{1-p}{1+p}\right)^n \int_0^T L_n(t)dt$$

3. Integrator :

$$\frac{1}{p} = \frac{1}{p+1} \sum_0 \left(\frac{1-p}{1+p}\right)$$

4. Delayed Integration :

$$\frac{1}{p} - \frac{1-e^{-pT}}{p} = \frac{1}{p+1} \sum_{n}^{n=\alpha} \left(\frac{1-p}{1+p}\right)^n \left[1 - \int_0^T L_n(t)dt \right]$$

To realise an arbitrary function it is only necessary to add different order Laguerre function multiplied by appropriate coefficients in proper phase. The values of the co-efficients for generating a square pulse is presented in Table I It will be noted that the operation of delayed integration can be realised more easily by subtracting the output of a system realising a square pulse of duration T from the output of the conventional integrator when both are excited by the same input. It is only necessary to adjust the time constant of the integrator to equal the duration T.

It is to be noted that different order Laguerre functions have been realised by CR networks. The time scale is therefore normalised with respect to the CR time constant of the networks.

4. CIRCUIT FOR GENERATION OF LAGUERRE FUNCTIONS

The Laplace transform of the Laguerre functions of the two sets corresponding to $\alpha = 1$ and $\alpha = \frac{1}{2}$ can be written as

$$e^{-bt}T_n(bt) = L^{-1} \frac{1}{p+b} \left(\frac{p}{p+b}\right)^n$$

$$(-1)^n e^{-bt}T_n(2bt) = L^{-1} \frac{1}{p+b} \left(\frac{b-p}{b+p}\right)^n$$

TABLE I

For square pulses of duration T.

Duration	Coefficients of different Laguerre functions										
T	L_0	L_1	L_2	L_3	L_4	L_5	L_6	L_7	L_8	L_9	L_{10}
0 25	0 442	.336	.248	.174	.114	065	026	.006	−.023	−.048	− 051
0.50	0 787	426	181	.021	− 072	− 120	−.134	−.129	− 107	−.083	− 051
1 00	1 264	.207	−.207	− 283	−.207	− 087	.024	.091	.133	.198	.137
1.50	1.557	−.215	− 454	− 215	.048	186	199	.129	053	−.074	− 097
2.00	1.729	−.647	−.436	.079	278	.227	.041	− 102	−.170	−.147	− 079
2.50	1.836	−1.015	−.216	.353	.207	.011	−.188	− 209	−.105	.031	.122
3.00	1.900	−1 303	.108	.490	.108	−.228	−.250	− 074	.018	.183	.172
3.50	1.940	−1 517	.460	450	−.157	−.333	−.111	.144	.218	.119	−.038
4.00	1.963	−1 670	.791	.283	−.381	− 232	.051	.324	.069	−.011	−.245

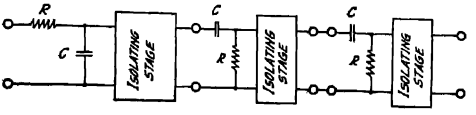

Fig. 1(a). Schematic circuit for realising Laguerre functions corresponding to $\alpha = 1$

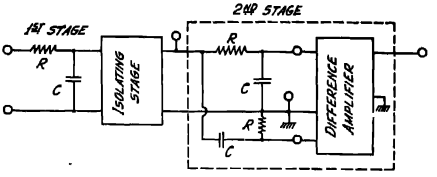

Fig. 1 (b). Corresponding to $\alpha = \frac{1}{2}$

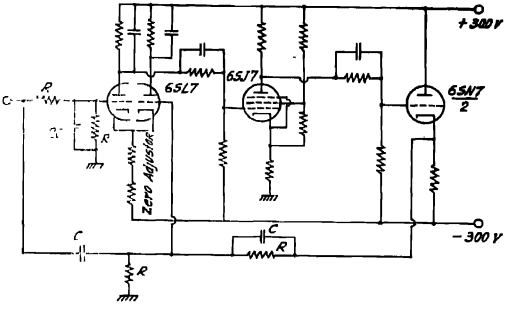

Fig. 1(c). Circuit arrangement for realising Laguerre function corresponding to $\alpha = \frac{1}{2}$

Schematic circuits for realising the Laguerre functions corresponding to $\alpha = 1$ and $\alpha = 1/2$ are shown in figure 1(a) and 1(b) respectively. In figure 1(b) the output from the first stage having the transfer function $1/pCR+1$ is fed through an isolating cathode follower into networks having transfer functions $1/pCR+1$ and $pCR/pCR+1$. The output of the networks are fed into the two inputs of a unity gain difference amplifier The transfer function of the stage is therefore $\dfrac{1-pCR}{1+pCR}$. The practical circuit arrangement is shown in figure 1(c).

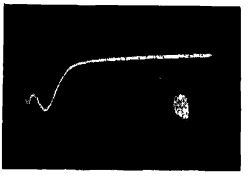

Fig. 2 (*a*). Photographs of step response of the different order Laguerre functions corresponding to $\alpha = \frac{1}{2}$ 3rd order;

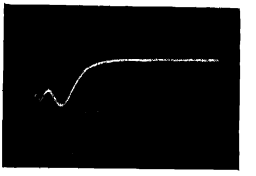

Fig. 2 (*b*). 4th order;

Fig. 2 (*c*). 6th order;

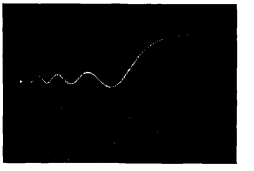

Fig. 2 (*d*). 8th order;

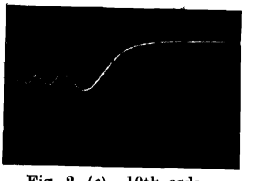

Fig. 2. (*e*) 10th order

Photographs of the step response of the different order Laguerre functions is shown in figure 2.

5. EXAMPLES TO ILLUSTRATE FUNCTION GENERATION

In the system built there are ten Laguerre filters (with $\alpha = \frac{1}{2}$) connected in cascade. The output from each filter is fed into a potentiometer for coefficient multiplication. The addition of the Laguerre functions in proper phase is done

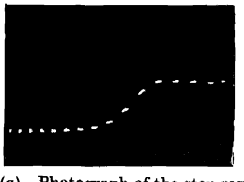

Fig. 3(*a*). Photograph of the step response of a delay function synthesised with Laguerre filters with a delay of 0.6 sec.

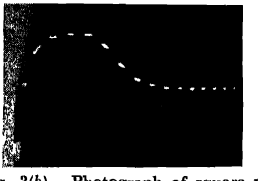

Fig. 3(*b*). Photograph of square pulse

by feeding the outputs from the different potentiometers into the proper terminals of a unity gain difference amplifier.

Photographs of step response of a delay function with a delay of 0.6 sec. and a square wave function of duration 0.6 sec. are shown respectively in figures 3(a) and 3(b).

6. CONCLUSION

In the study of process control systems with the help of a differential analyser the Laguerre filters can be used to realise time delays with advantage. The filters can also be used for simulation of the components of the original system.

ACKNOWLEDGMENTS

The authors are indebted to Prof. J. N. Bhar for his constant help and guidance. Thanks are due to Prof. S. K. Mitra for his kind interest in the work. One of the authors (N. B. C.) is grateful to the Union Government for the award of Senior Research Scholarship.

REFERENCES

Corrington, T., Multar, S., Murakmi and Richard W. Somenfeldt, 1954, Convention of I.R.E., National Convention Part 2, Circuity Theory, page 30.

C. D. Morrill, 1954, *I. R. E.*, Transactions-Electronic Computer Issue, page 45.

ON THE APPLICATION OF AN ELECTRONIC DIFFERENTIAL ANALYSER FOR FINDING THE ROOTS OF A POLYNOMIAL

B. R. NAG

INSTITUTE OF RADIO PHYSICS AND ELECTRONICS, CALCUTTA UNIVERSITY

(*Received for publication, August* 20, 1957)

ABSTRACT. A method of finding the roots of a polynomial with real coefficients by an electronic differential analyser is described. The principle underlying the method is to set up in the analyser a system having a transfer function, of which the numerator is the polynomial whose roots are to be obtained. The denominator of the transfer function is a suitably chosen polynomial. Roots of the polynomial are then obtained by determining the frequencies at which the system gives zero output.

INTRODUCTION

Different methods of utilising a differential analyser for finding the roots of a polynomial have been investigated. Atkinsen has described a method of obtaining the real roots of a polynomial by electromechanical analysers. The same method can also be applied for obtaining complex roots by breaking the polynomial into real and imaginary parts. However, simpler methods using an electronic analyser have been described, which give both real and complex roots directly.

In the harmonic synthesis method the variable is represented as $re^{j\omega t} = r \cos \omega t + jr \sin \omega t$. The polynomial is constructed by generating the terms $r \cos \omega t$, $r \sin \omega t$, $r^2 \cos 2\omega t$, $r^2 \sin 2\omega t$.....etc., multiplying them by the proper coefficients of the polynomial and adding them. The quantities $\cos \omega t$, $\sin \omega t$, $\cos 2\omega t$, $\sin 2\omega t$, ... etc. are first generated by setting oscillators on the analyser having the frequencies $\omega, 2\omega, \ldots$ etc. Multiplication of these quantities by r, $r^2 \ldots$ etc. is done by a set of ganged potentiometers. Evidently, a root of the polynomial can be obtained by determining the value of r and ωt which make both the real and the imaginary parts of the polynomial vanish simultaneously. The method is simple but has the disadvantage of requiring a large number of operational amplifiers. An n degree polynomial may require as many as $(5n+2)$ operational amplifiers.

In another method suggested by Cahn (1956) the roots of a polynomial are obtained by determining the frequencies of maintained oscillations of a system having a transfer function, the denominator polynomial of which is identical to the given polynomial. This method requires a smaller number of computing

elements, an n degree polynomial requiring $(2n+1)$ operational amplifiers. This reduction in the number of operational amplifiers is a great advantage when the polynomial is of high degree. However, in this method, after obtaining one root, the polynomial has to be reduced in order to obtain the remaining roots. This reduction may impair the accuracy of the roots and also involves a new arrangement of the computer for finding each root Determination of the frequency of a maintined oscillation also requires a large time in slow computers

In this paper a method is suggested, which requires a small number of operational amplifiers and no reduction of the polynomial. The method is similar to that employed in potential analogues. The roots are obatined by determining the frequencies of zero output of a system having a transfer function the numerator of which is the given polynomial. The denominator polynomial is, however, chosen suitably. In contrast to the potential analogue method, the residues of the transfer function at the poles are not required to be calculated and the poles can be easily varied without altering the set up of the analyser This facilitates accurate determination of the frequencies of zero output of the system.

PRINCIPLE OF THE METHOD

Let the polynomial be given by

$$f(z) = a_n z^n + a_{n-1} z^{n-1} + \dots + a_0$$

where $a_n, a_{n-1} \dots a_0$ are all real.

The variable z may be represented by the complex frequency p Now, theoretically, a system having the transfer function $f(p)$ can be set on an analyser This system requires differentiators, which, when put in cascade, give at their outputs the voltages pE_{in}, p^2E_{in},... etc when E_{in} is applied to the input of the cascaded system These when multiplied by the respective coefficients and added, gives $f(p)\ E_{in}$. However, in practice, it is difficult to set such a system. Since the system gain increases with frequency, it has a tendency to become unstable due to stray coupling between the output and input In addition, extraneous noise is very much amplified in this system.

On the other hand, a system having the transfer function $\frac{f(p)}{D(p)}$ can be easily constructed where $D(p)$ is a polynomial of the same order as $f(p)$ and has roots with real parts negative and greater than 1.

We first note that $\frac{f(p)}{D(p)}$ can be written as $\frac{1}{1+\frac{D_1(p)}{f(p)}}$, where $D_1(p) = D(p) - f(p)$. Thus if a system having the transfer function $\frac{D_1(p)}{f(p)}$ is available one can

realise a system of transfer function $\frac{f(p)}{D(p)}$ in the manner indicated in figure 1

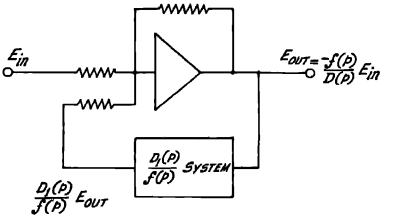

Fig. 1. Arrangement of the analyser for realising a system having the transfer function $\frac{f(p)}{D(p)}$ when a system having the transfer function $\frac{D_1(p)}{f(p)}$ is available.

For obtaining the system with the transfer function $\frac{D_1(p)}{f(p)}$, the analyser is arranged to solve the equation $f(p)E_{out} = E_{in1}$. Then from the outputs of the integrators are obtained the voltages $\frac{p^n}{f(p)} E_{in1}$, $\frac{p^{n-1}}{f(p)} E_{in1}$ . . etc., which, when multiplied by the coefficients of $D_1(p)$ and added, give $\frac{D_1(p)}{f(p)} E_{in1}$.

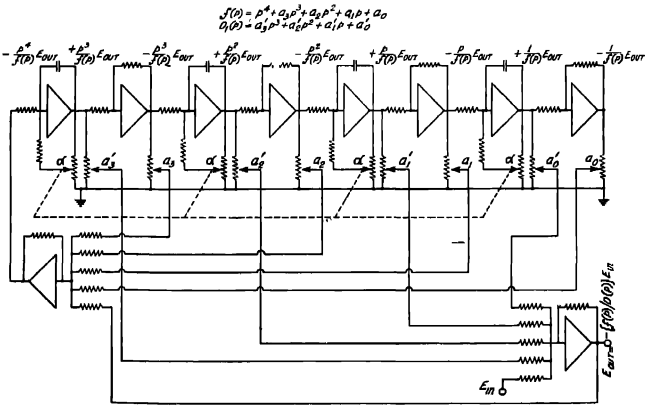

Fig. 2. Arrangement of the analyser for finding the roots of a fourth degree polynomial

The above principle is illustrated in figure 2 which shows the set up of the analyser for finding the roots of a polynomial of fourth degree. $a_3', a_2' \ldots a_0'$ are the coefficients of $D_1(p)$.

Evidently, the values of p for which this system gives zero output are the roots of the polynomial.

METHOD OF SEARCHING THE ROOTS

Roots of the polynomial may be real, imaginary or complex.

For searching real and complex roots, there should be provison for transforming the system with transfer function $\frac{f(p)}{D(p)}$ into one having the transfer function $\frac{f(p+\alpha)}{D(p+\alpha)}$, where α is a real quantity and can be varied between $+1$ to -1. This transformation is done by applying feedback from the output of the integrators to the inputs through potentiometers set to α. For making α negative, the feedback is applied from the output of the inverter following the integrator. On ganging all the α-potentiometers, as shown in figure 2, α can be easily varied between the required limits

For searching real roots a d.c. voltage is applied to the input and the α-potentiometers adjusted for zero output. The setting of α which gives a zero E_{out} is a real root of the polynomial.

For searching complex roots a sinusoidal voltage is applied to the input. The frequency of this voltage and α are varied alternately till a zero output is obtained. It may be noted that on transforming the system $\frac{f(p)}{D(p)}$ to the system $\frac{f(p+\alpha)}{D(p+\alpha)}$, effectively the imaginary axis in the p plane is shifted to the right by α. Hence if α is so adjusted that the complex root lies on the shifted imaginary axis the output becomes zero when the input has a frequency equal to the imaginary part of the root. Thus the frequency of the input and the setting of α for zero output give respectively the imaginary and real part of the complex root. To make the searching of the complex root systematic, the input voltage may be supplied by a sweep frequency oscillator and then one has only to vary α to find the root. Once a root is approximately located it may, however, be located accurately later by close searching

For searching an imaginary root it is obvious that one needs only set α zero and find the frequency of the input voltage for zero output.

The method enables location of roots having real parts respectively within the range $+1$ to -1 and imaginary within the range $\omega_h CR$ to $\omega_l CR$, where ω_h and ω_l are the highest and lowest frequencies of the oscillator and CR is the time

constant of the integrators. Roots lying outside these limits can be found by properly transforming the polynomial.

Choice of $D(p)$

The roots of $D(p)$ are the poles of the transfer function of the system and since, while searching the roots of the polynomial, α may be set to -1, the real part of the roots of $D(p)$ should be negative and greater than 1. The roots of $D(p)$ may be made real and placed far away from the region where the roots of $f(p)$ are searched. In that case the output of the system will vary exactly in accordance with the nature of the polynomial. However, placing of the roots of $D(p)$ far away results in reduction of the gain of the system on one hand, and on the other, increases the values of the coefficients of $D(p)$. These effects obviously necessitate the use of a high gain null detector and large gain operational amplifiers. To avoid these difficulties the roots of $D(p)$ are placed only slightly away to the left of -1, and to ensure that the d.c. loop gain is not inconveniently increased when α is set -1, the roots are chosen to be complex.

Once the roots of $f(p)$ are approximately known, $D(p)$ may be modified by altering the coefficients of $D_1(p)$ so that its roots lie very near to the left of the root of $f(p)$ being searched. This would facilitate location of the roots of $f(p)$, specially when they are close together

ACCURACY OF ROOT LOCATION

The straightforward method of determining the accuracy of the roots obtained by an experimental method is to check them against the actual roots of the polynomial. However, a good measure of the accuracy of a root is also provided by the value of the polynomial obtained by substituting this root in it. Obviously if this value is zero, it indicates that the root is cent per cent accurate. In polynomials, in which the value depends very critically on the values of the coefficients this method of estimating the accuracy may indicate large error. In such cases one may alternatively judge the accuracy by forming a polynomial with the roots obtained and checking how far the coefficients of the polynomial so found agree with those of the original polynomial. If the variation is found to lie within the tolerance limits expected from instrumental limitations, the roots are accepted

The limits of tolerance expected of the analyser as a whole may be estimated by ascertaining the errors introduced due to imperfections of the computing elements and to inaccuracies in the values of the computing networks. The amplifiers used in the adders and integrators have finite gain and band-width, hence they perform the operations required of them over a limited range of frequency with a certain prescribed accuracy. However, when the time scale of the computer is properly selected, the adders introduce errors which may be included in

the values of the network elements. The integrators, however, always operate by $\frac{1}{p+\alpha_0}$ instead of by $\frac{1}{p}$, α_0 being determined by the d.c gain of the amplifier and loss resistance of the integrating capacitor. This results in an error in the value of α However, α_0 can be determined and corrected for in the value of the root obtained. The inaccuracy of the computing networks introduces inaccuracy in the coefficients of the polynomial and can be estimated on knowing the tolerance of the network elements for any particular polynomial.

The method discussed here has been applied to determine the roots of a few polynomials employing the electronic differential analyser, installed at the Institute of Radio Physics and Electronics, Calcutta The roots were found to be accurate up to the second decimal place.

ACKNOWLEDGMENTS

The author is deeply indebted to Professor J. N. Bhar for his constant help and guidance. He wishes to express his gratitude to Sri A K. Choudhury and Sri N. B Chakraborty for valuable discussions

The author is also grateful to Professor S. K Mitra for his kind interest in the work.

REFERENCES

Cahn C R., 1956, *Rev. Sc Instr.*, **27**, 856.

Cherry, E. C., 1952, Proceedings of the Symposium on Modern Network Synthesis (New York, N.Y.), 140.

Johnson, C. L., 1956, Analog Computer Technique (Mc-Graw Hill Book Co. Inc., New York).

Soroka, W W, 1954, Analog Methods in Computation and Simulation (Mc-Graw Hill Book Co. Inc., New York).

ULTRAVIOLET ABSORPTION SPECTRUM OF ACETOPHENONE

R. N. BAPAT

PHYSICS DEPARTMENT, COLLEGE OF SCIENCE, NAGPUR

(*Received for publication, July* 10, 1957)

Plate VII

ABSTRACT The absorption spectrum of acetophenone was studied at different temperatures and with different lengths of the absorbing column. There are four regions of absorption, two in the region of 2400Å, third at about 2800Å and the fourth at about 3200Å New bands in absorption have been observed in these studies and an interpretation for the same is discussed.

INTRODUCTION

Acetophenone forms an important starting point for a class of compounds in which C = O is conjugated to phenyl ring. Benzaldehyde, which is the first member of such a class, has been extensively investigated by various workers The absorption spectrum of acetophenone was studied by Kato and Someno (1938) in liquid solution and absorption bands were reported by them at wave numbers 34900, 35900 and 37000 It was further studied by Deb (1951) and he has reported three broad bands with centres at 35744, 38748 and 40277 cm $^{-1}$ respectively. The ultraviolet absorption and fluorescence was studied by Vanselow and Duncan (1953). They have observed at room temperature (about 1 mm pressure) three bands at 2832, 2770 and 2695Å in a 20 cm path of the absorbing column. They also report that a new band appears at about 60 mm pressure with centre at about 3250 Å. Apart from earlier work, absorption of acetophenone in the vapour state has been recently investigated by Imanishi, Semba, Ito and Anno (1952). These workers, as also the work on solution spectrum, have clearly established that the complete ultra-violet spectrum consists of three regions of absorption. The longest wave length region near 3200 Å is assigned to an $n-\pi$ transition of the C = O group. The region between about 2900-2400Å corresponds to the 2600Å absorption of benzene suitably modified by substitution. Absorption on the lower ultraviolet below 2400Å has been assumed to correspond to the 1900 Å benzene band and is tentatively assigned due to $N-V$ transition of carbonyl group. Imanishi *et al.* have studied the absorption system between 2900—2400Å. Duncan *et al.* were mainly concerned with the 3200Å absorption system and the corresponding fluorescence of this molecule. The 2800Å band

system has been studied in the present investigations at various temperatures and at different path-lengths.

EXPERIMENTAL

Experiements have been carried out at room temperature (30°C) using saturated vapour of acetophenone in columns of lengths varying from 2 cm to 4 m. Experiments were carried out also with a tube in which the vapour pressure was that saturated at 60°C and the tube was heated to various temperatures. A hydrogen lamp was used to give the continuum. A Hilger medium quartz spectrograph and B 20 plates were used. The wide diffuse bands were photographed on a Hilger small quartz spectrograph. At least three plates were measured on a comparator reading to 0.001 mm. As the bands are diffuse readings were taken at the centre of the bands The liquid used was distilled at the temperature corresponding to the boiling point and the first and the last portions of the distillate were discarded collecting the liquid only after the first portions were removed. The liquid was put in the bulb and quartz windows were attached at both ends by sealing wax and the open end of the bulb was connected to a vacuum pump and then sealed off. A comparison spectrum of copper was superposed in the centre.

EXPERIMENTAL RESULTS

With 2 cm cell and temperature of the liquid at 24°C at an exposure time of 20 minutes, an absorption band was observed with its centre at 2389 Å (Plate VII, Fig. 1). With 5 cm length of the absorbing column at room temperature only two bands at 2826 Å and 2752 Å were observed. When the length of the column was 50 cm, all bands mentioned in the 2800 Å region appeared at room temperature. When the temperature of the bulb was maintained at 5°C bands at 2826 and 2752 Å were still there and accompanied by another diffuse band with centre at 2389 Å and a very broad diffuse band from 2330Å to 2249 Å (Plate VII, Fig. 2) By increasing the length of the absorbing column to 100 cm or more, the bands as mentioned in the table below appeared. (Plate VII, Fig. 4 & 5. When the length of the absorbing column was 4 metres the diffuse band with centre at 3250 Å was clearly seen (Plate VII, Fig. 3). On heating the cell so that the temperature of the bulb and the cell was the same no additional bands were observed on the longer wave length side of the (0—0) band though the temperature was raised from 36°C to 110°C (Plate VII, Fig. 6). The data on the bands are given in Table I.

DISCUSSION

The spectrum can be divided into two types of bands.—A prominent set of diffuse bands which are very similar in nature and of which the first member is the 0- 0 band; and three sets of a group of three comparatively sharp bands in between

TABLE I

Wave length (Å) in air	Nature of band	Wave number in vacuo	Assignment
2826	b.d.	35375	0,0
2797	s.d.	35742	0,+367
2790	s.d	35831	0,+456
2781	s.d	35947	0, +572
2752	b.d.	36326	0,+951
2725	s d	36686	0, + 951 +360
2718	s.d.	36780	0,+951+454
2709	s.d.	36903	0,+951+577
2681	b.d.	37288	0, +951 +962
2656	s.d.	37639	0,+2(956)+351
2649	s.d.	37738	0,+2(956)+450
2641	s.d.	27853	0, +2(956)+565
2614	b d.	38244	0, + 2(956) +956

* b.d. = broad diffuse. s.d. = sharp diffuse.

the diffuse bands. The disposition and nature of these bands seem to indicate that they do not belong to the series of diffuse bands and although belonging to the same electronic transition they form a different series.

Acetophenone belongs to the C_s symmetry group and as such has only two symmetry types, namely, A' and A'', symmetric and anti-symmetric to the plane of symmetry. The transitions between these are allowed. The successive reduction of symmetry from D_{6h} of benzene to acetophenone C_s through C_{2v} shows that the $A_{1g}-B_{2u}$ transition of benzene becomes $A'-A'$ under the reduced symmetry and is hence allowed by selection rules. The assignment of (0—0) band is in agreement with Imanishi *et al.* whose selection of the band was, however, quite arbitrary. Absorption was recorded at various temperatures and no extension of the 2800 system was found beyond the band at 2826Å The intensity distribution in the system of bands at higher temperatures when compared to that obtained at lower temperatures showed that the first strong band at 35375 cm^{-1} is the 0—0 band of the system.

Indian Journal of Physics, Vol. XXXII, No. 5.

Fig. 1

Fig. 2

Fig. 3

Absorption spectra of acetophenone

Fig. 1. 2389 A U. band (41845 cm^{-1})

,, 2. Broad diffuse band

,, 3. Diffuse band at 3250 A. U. (30760 cm^{-1})

Fig. 4

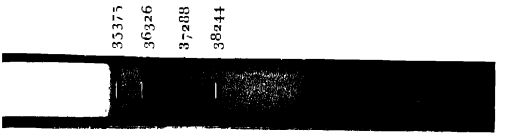

Fig. 5.

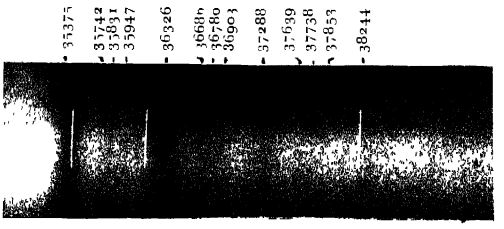

Fig. 6

Fig. 7

Fig. 8

Absorption spectrum of acetophenone

Fig. 4 Contact print 2800 system of bands.

„ 5. Enlarged print showing sharp diffuse bands

„ 6. Absorption at 36°C

„ 7. Absorption at 80°C

„ 8 Absorption at 110°C

It is significant to note that even at a temperature of 110°C no further bands are observed on the longer wave length side of the 2826 Å band. This is in contrast to benzaldehyde where quite a large number of small frequencies in the ground state are excited with increase of temperature or path length.

The principal progression with frequency of 956 is observed as in most cases of substituted benzene. This progression has been explained as due to the excited state frequency corresponding to the totally symmetric frequency of about 1000 cm^{-1} in the ground state which corresponds to the totally symmetric vibration frequency 992 cm^{-1} in benzene. Long progressions of bands corresponding to excitation of this type of vibration have been observed in most of the simple substituted benzenes.

The ground state frequencies corresponding to the excited ones of the order of 360, 450 and 570 giving rise to the three comparatively sharp bands are not excited at the temperatures employed in the present experiments. This is rather peculiar to the molecule because similar ground state vibrations have been observed in the spectrum of benzaldehyde (Garg, 1953).

Of these three vibrations two must correspond to the two vibrations arising out of the 606 cm^{-1} e_{2g} degenerate benzene vibration. Imanishi *et al.* have assigned 360 and 570 to the excited state frequencies corresponding to 371 and 617 in the ground state, these being the two vibrations corresponding to 606 of benzene. Under the C_s symmetry both belong to a' symmetry and thus give rise to bands of about the same intensity That the assignment is essentially correct can be seen by comparison with the spectrum of benzaldehyde and other benzene derivatives The smaller of the two frequencies shows a decrease with the increasing weight of substituent and the value calculated according to formula given by Garg comes to be of the order assumed here. The higher frequency component of the split frequency is rather invariable with the substituent Both show appreciable depolarization in Raman effect and hence belong to a' summetry.

The third frequency (450) may be excited frequency of 588 in the ground state, in analogy with the spectrum of acetaldehyde where Rao and Rao (1954) have assigned 527 cm^{-1} and the corresponding ground state frequency 562 cm^{-1} to C—C = O bending vibration of a' type. This is a very prominent frequency in the acetaldehyde spectrum.

The excited frequency ~570 in acetophenone corresponds to the excited frequency ~544 in benzaldehyde in which it occurs only in combination with the (0– 0) band. In acetophenone, however, the vibration (~570) is present associated with successive quanta of the totally symmetric vibration. This frequency therefore corresponds to the e_{2g} of benzene where under the D_{6h} symmetry it is excited

only to one quantum for the $A_{1g}-B_{2u}$ transition. It appears that whereas benzaldehyde still retains some part of residual benzene character, acetophenone seems to have lost all of it.

ACKNOWLEDGMENTS

The author is indebted to Professor R. K. Asund and Dr. M R. Padhy for their interest in the work

REFERENCESS

Deb, A. R., 1951, *Ind. J. Phys* **34**, 433
Garg, S. N., 1953-54, *J Sci. Res.* B.H.U
Imanishi, Semba, Ito and Amo., 1952, *Jan Bull. Ch. Soc. Japan*, **190**.
Kato, S. and Someno, F 1938, *Sci. Pap. Inst. Phys. Chem. Res. Tokyo*, **34**, 912
Rao, V. Ramkrishna and Rao, I. Achyuta, 1954, *Ind. J. Phys* **28**.
Vanselow R. D , and Duncan, A. B. F., 1953, *J. A. Chem Soc* **75**.

31

NEW VISIBLE BAND SYSTEMS OF THE PO MOLECULE

K. KANAKA DURGA AND P. TIRUVENGANNA RAO

DEPARTMENT OF PHYSICS, ANDHRA UNIVERSITY

(*Received for publication, November* 20, 1957)

Plate VIII

ABSTRACT. Two new band systems attributed to the PO molecule, have been observed in the visible region in a high frequency discharge, when moist red phosphorous is excited under low pressure conditions. Of the four new groups of bands observed, two are assigned to one system designated as $D-B$ while the other two groups are assigned to another system designated as $D'-B$. The common lower state B is identified as the upper state of $B-X$ ultraviolet system of PO The D level is identified as theupper state of the $D-X$ system of PO having a doublet separation of 27 K. The structure of the two systems seem to indicate $^2\Delta_a - {}^2\Pi_b$ and $^2\Delta_a$ $^2\Pi_b$ transitions for the systems D' B and D - B systems respectively, the upper states being different. The D' level has a doublet separation of 97 K.

The electronic states of PO and related molecules are discussed in terms of electron configurations.

INTRODUCTION

The band spectrum of the PO molecule long since has been known to give rise to two characteristic band systems one near λ2600 Å and the other near λ3300 Å Of these two systems the former which is analogous to the well known 'γ' system of NO has been investigated in detail by Ghosh and Ball (1931) and Sen Gupta (1935) It is well known from this year's work that this system is due to an electronic transition $^2\Sigma \longrightarrow {}^2\Pi$ with a $^2\Pi$ ground state having a doublet separation of 223.8 cm^{-1}. The band system near λ3300Å was investigated by many workers (Curry, Herzberg and Herzberg 1933), Ramanatham, Rao and Ramasastry (1946) and more recently by K Dressler (1955).) The recent work of this latter author (Dressler) has shown that these bands occurring in the region λ3190Å $-\lambda$3560Å belong to a single system having for its lower state the $^2\Pi$ ground state, identified as the ground state of PO and for its upper state a Hund's case (b) state. In addition to the above two systems Dressler reported three new systems of doublet bands occurring in the regions λ1975Å--λ2140Å, λ2050Å—λ2170Å, and λ1825Å—λ1930Å in a Geissler discharge tube used as a light source. The vibrational analysis of these band systems indicate that the lower state is common and identified as the $^2\Pi$ ground state of PO, the upper states corresponding to different excited electronic states of the PO molecule. The various excited electronic levels

identified from the analysis of the above mentioned systems were designated by Dressler as B, A, C, D, E written in the order of increasing energy. Of these 'D' level is known to be a doublet state having a separation of about 30 cm^{-1}, while the B and E levels are known to belong to Hund's case (b). The Λ value of these two states and the nature of the 'C' level are however not yet known.

Besides the discrete band systems reported for PO, a number of diffuse and unresolved bands have been observed by Karl Rumpf in the visible region extending from $\lambda 6500-\lambda 4750$. These bands were observed in the flame of burning phosphorous in the presence of CO_2 and photographed under low dispersion of about 80Å per mm. at $\lambda 5000$ Å. A tentative analysis of these bands on the basis of two systems given by the above author is, however, not convincing.

As compared to NO, our knowledge of the nature of the excited electronic levels of PO is less complete, the authors considered it worthwhile to reinvestigate the emission spectrum of the PO molecule. The present paper describes the new results obtained in this reinvestigation.

EXPERIMENTAL

Method of excitation ·

The two band systems $A-X$, $B-X$ were reported by early workers as occurring in a carbon arc source fed with P_2O_5. The $B-X$ system was observed by Dressler as occurring in a Geissler discharge tube in which a free flow of oxygen is maintained over heated phosphorous. The remaining systems were also reported as occurring in the same source. The diffuse bands occurring in the region $\lambda 6500$ Å$-\lambda 4750$ Å were reported by Karl Rumpf in the flame of burning phosphorous in the presence of CO_2.

In our present experiments the spectrum was excited in a high frequency discharge from a high power (100 watt) oscillator. Red phosphorous in the wet condition was taken in an ordinary H.F. discharge tube and the tube was evacuated by a Cenco high vacuum pump through a series of absorption towers. No external heating of the substance was found necessary as the R. F. heating of the electrodes was sufficient to maintain a free flow of P_2 vapour due possibly to the dissociation of P_4 into P_2 molecules.

DESCRIPTION OF THE BANDS AND THEIR ORIGIN

During the first five minutes after the oscillator was switched on, an intense line spectrum was observed in the whole visible region. After this interval of time the line spectrum disappeared and a characteristic pale yellow discharge was observed and the spectrum photographed under these conditions. The photographs of the spectra in the visible region taken on the Fuess instrument (dispersion about 35 Å/mm at $\lambda 5600$.) and three prism glass Littrow instrument

Indian Journal of Physics, Vol. XXXII, No. 5.

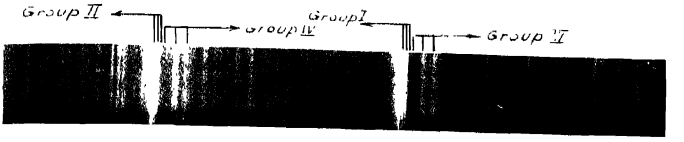

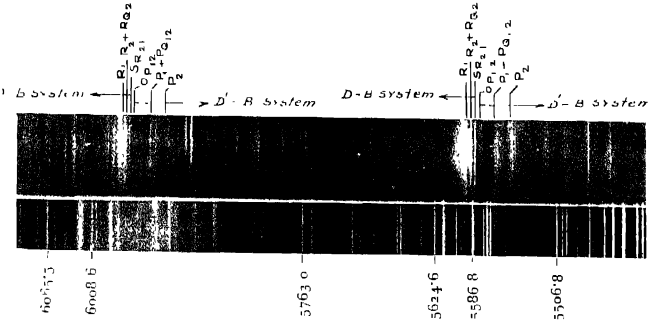

Spectra of the two new systems of PO molecules

(dispersion about 24Å/mm. at λ5600 Å) are reproduced in Plates VIII(a) and (b) respectively. In the ultraviolet region the extensive P_2 band system and the well known 'γ' system of PO are observed and the spectrum was photographed under the same conditions on a Hilger medium quartz instrument.

Plates VIII(a) and 1(b) are seen to consist of characteristic groups of bands extending from λ5400 to λ6000. A close examination of Plate VIII(a) reveals a characteristic group of three red degraded bands designated as group I at wavelengths λ5584.3, λ5588.2 and λ5592.2. Strikingly similar in appearance to this group of bands, there is another characteristic group of three red degraded bands designated as group (II) at wavelengths λ5962.3 Å, λ5966.7 Å and λ5973.1 Å. On the short wavelength side of group I bands another group of three violet degraded bands designated as group (III) occurs at wavelengths λ5549.5Å, λ5564.3 Å and λ5580.0 Å. A similar group of violet degraded bands designated as group (IV) is also observed on the short wavelength side of group (II). The spectrum as reproduced in plate 1(b) reveals also a partial resolution of the rotational structure of the groups (I) and (III) bands.

In attempts to identify the emitter of the groups of bands reproduced in plates 1(a) and 1(b) a comparison is made with the spectra of the commonly occurring impurities like CO, CO^+, C_2, N_2, N_2^+, CN etc., in the visible region. The measurements of the wavelengths of the band heads of these groups of bands do not agree with any of those given in the list of table of persistent band heads due to impurities as given by Pearse and Gaydon's book "On the identification of molecular spectra". Thus there remain the three following possibilities for the emitter of the bands namely P_2, PO and PH. The last two possibilities PO and PH have to be considered in view of the fact that these new bands are observed when phosphorous is excited in the presence of water vapour. A detailed vibrational analysis as described in the following pages has definitely established that the emitter of the bands is PO.

ANALYSIS OF BANDS

Intensity considerations point to the group of bands designated as group (I) as constituting unambiguously the $\Delta v = 0$ sequence and group (II) as forming the $\Delta v = -1$ sequence. The wavenumber intervals between the first, second and third members of groups I and II are obtained as 1136.0, 1134.8 and 1136.9 respectively. The average $\Delta G_{1/2}''$ difference as shown in Table I is obtained as 1133.9 cm^{-1}. This first $\Delta G_{1/2}''$ interval agrees very well with the first $\Delta G_{1/2}''$ interval of the B upper state of the two subsystems $B-{}^2\Pi_{1/2}$ and $B-{}^2\Pi_{3/2}$ as shown in Tables (II and III). This agreement shows conclusively that the lower state of this new system shown in Table (I) is upper state D of the PO molecule. This also confirms the view that the emitter of this new band system is PO. Further this $\Delta G_{v1/2}'$ interval does not agree with the $\Delta G_{v1/2}$ interval of the upper or lower

states of any of the band systems of either P_2 or PH molecule, this interval being too big for P_2 and too small for PH. As the $\Delta v = -2$ sequence is expected to occur at λ6400Å and is not recorded on our plates. The $x_e\omega_e$ value of 14.1 derived by Dressler for the B state has been adopted by us The vibrational frequency of the lower state of the new system is thus obtained as 1164 cm^{-1}. The bands in groups III and IV which are degraded to shorter wavelengths and are comparatively weaker in intensity, obviously seem to belong to another system From intensity considerations the groups III and IV are regarded as $\Delta v = 0$ and $\Delta v = -1$ sequences respectively. The vibrational scheme shown in Table (IV) indicates that the first average $\Delta G''_{v+1/2}$ interval is again 1132 cm^{-1} This suggests that the two systems have a common lower state which is to be identified as the B state of PO The two systems shown in Tables (I and IV) may be designated as $D-B$ and $D'-B$ systems respec- tively.

TABLE I

$D-B$ system $^2\Delta_{3/2,\,5/2} \rightarrow {}^2\Pi_b$

v' \ v''	0		1
$S_{R_{21}}$	17903 7	1136 0	16767 7
$R_2+R_{Q_{21}}$ 0	17891 5	1134 8	16756 7
R_1	17876 8	1136 9	16739.9

Average value of $\Delta G''_{1/2} = 1135\ 9$

$\omega'' = 1135.9 + 2x_e''\omega_e''$

$\omega'' = 1135\ 9 + 2 \times 14.1$

$\omega'' = 1164$

$\omega' \leqslant 1164$

Position of $^2\Delta_{3/2}$ above the ground state $= 48718$

Position of $^2\Delta_{5/2}$ above the ground state $= 48745$

$^2\Delta_{5/2} - {}^2\Delta_{1/2} = 27 = A$

Coupling constant (approximately).

TABLE II

$^2\Pi_1 \rightarrow {}^2\Pi_b$

v' \ v''	0	1	2	3	4
0	30796 4	1217.3 29579.1	1204.7 28374.4		
$\Delta G'_{1/2}$		1131.2	1134.0		
1		30710 3	1201.9 29508.4	1191 1 28317 3	
$\Delta G'_{3/2}$			1077.0	1105.1	
2			30585.4	1163.0 29422 4	1177 1 28245.3
					1073 0
3					29318.9

TABLE III

$^2\Pi_{3/2} \longrightarrow {}^2\Pi_b$

v' \ v''	0	1	2	3
0	30567.6	1213.4 29354 2	1203.5 28150.7	
			1131.2	
1			29281.9	1189 7 28092.2
				1100.0
2				29192.2

TABLE IV

D' B system $^2\Delta_{3/2,\ 5/2} \longrightarrow {}^2\Pi$

v' \ v''	0	1	2
$^0P_{1/2}$	17916 2	1136 7 16779 5	
$P_1+PQ_{1/2}$ 0	17965.8	1130 3 16835.5	
P_2	18013 4	1128 7 16884 7	
$P_1+PQ_{1/2}$ 1			16976 1
P_2			17027.6

Average value of $\Delta G''_{1/2}$ = 1131.9

ω'' = 1131 9 + $2\nu\omega_e'$

ω'' = 1131.9 + 2 × 14 1

ω'' = 1160

ω'' $\simeq$ 1301

Position of $^2\Delta_{3/2}$ above the ground state = 48757 5

Position of $^2\Delta_{5/2}$ above the ground state. = 48854.7

$^2\Delta_{5/2} - {}^2\Delta_{3/2}$ = 97 2 cm^{-1} = A = coupling constant (approximately).

From his analysis of the B—$^2\Pi$ system of PO Dressler concluded that the B state belongs to Hund's case (b). However he did not definitely suggest the Λ value of this state. It may be either $a^2\Sigma$ or $a^2\Pi_b$ or $^2\Delta_b$ state. Of these three alternatives $^2\Pi_b$ term is considered more likely for the B state, as this would account for the observed double headed nature of the B—$X^2\Pi$ system and also the coarse vibrational structure of the two new systems reported here.

The vibrational structure of the D—B system shown in Table (I) can be interpreted on the basis of $a^2\Delta_a \rightarrow {}^2\Pi_b$ transition. Such a transition is expected to give rise to four head forming branches. $^SR_{2\ 1}$, $R_2+{}^RQ_{2\ 1}$, R_1 and $Q_1+{}^OR_{1\ 2}$ and the last $Q_1+{}^OR_{1\ 2}$ is generally obscured in the shading of the R_1 head. Thus both the (0, 0) and (0, 1) bands appear to be triple headed as observed. The appearance of this system is strikingly similar to the well known red CN system arising from a

transition between two doublet states. Since ${}^{S}R_{2\,1}$ and R_1 heads occupy similar positions in the two subsystems of $a^2\Delta_a - {}^2\Pi_b$ transition, they will be separated by a wave number interval which is approximately of the order of the coupling constant A for the upper ${}^2\Delta$ state. This interval is obtained as 27 cm^{-1} approximately and represents the interval between ${}^2\Delta_{5/2}$ and ${}^2\Delta_{3/2}$ components of the ${}^2\Delta_a$ state. Adopting the $\nu_{H(0\cdot 0)}$ values (${}^{S}R_{2\,1}$ and R_1 heads) the heights of the ${}^2\Delta_{3/2}$ and ${}^2\Delta_{5/2}$ above the ground state are obtained as 30841.3+17876.8 = 48718.1 and 30841.3+17903.7 = 48745.0 respectively. These compare favourably with the approximate value 48690 and 48720 given by Dressler for the two components of the D state of PO from his analysis of $D-X$ system. Thus both the doublet intervals and the positions of these levels suggest that the upper state of the above new system is to be identified as the D state. Further, as in the $D-X$ system of PO, predissociation is observed in the $v' = 1$ level of this new system as well.

The vibrational scheme shown in Table (IV) relates to the $D'-B$ system of PO. It is seen that the (0, 0) band consists of three sub bands. The vibrational structure of these bands is interpreted on the basis of ${}^2\Delta_a \rightarrow {}^2\Pi_b$ transition, the lower state ${}^2\Pi_b$ being the common lower state of both the systems. The upper state ${}^2\Delta$ belongs to a separate higher excited state of the PO molecule. The two doublet components ${}^2\Delta_{3/2}$ and ${}^2\Delta_{5/2}$ will give rise to four head forming branches ${}^{O}P_{1\,2}, P_1 + {}^{P}Q_{1\,2}$ and $P_2, Q_2 + {}^{Q}P_{2\,1}$. Of these the $Q_2 + {}^{Q}P_{2\,1}$ head is generally being obscured in the shading of the P_2 head and the (0, 0) band appears triple headed. The two corresponding heads ${}^{0}P_{1\,2}$ and P_2 which occupy similar positions in the two sub systems are separated by a wave number interval which is approximately equal to coupling constant A of the ${}^2\Delta$ state. This is obtained approximately as 97 cm^{-1}. The heights of the two components above the ground state are derived as 48757.5 (= 30841.3+17916.2) and 48854.7 (= 30841.3+18013.4) for the ${}^2\Delta_{3/2}$ and ${}^2\Delta_{5/2}$ respectively.

Predissociation :

It is noteworthy that no bands are observed belonging to the $\Delta v = +1$ sequence. This may be due to the occurrence of predissociation at the $v' = 1$ level in the two upper states D and D'. This predissociation may then also account for the absence of the (1,0) band in the $D-X$ system analysed by Dressler.

PREDICTED ELECTRONIC STATES FROM ELECTRONIC CONFIGURATIONS IN PO AND RELATED MOLECULES

The electronic configuration giving rise to a ${}^2\Pi_r$ state in each of the related molecules NO, NS, PO, PS and SiF is well known to be

$$K.K.....(z\sigma)^2(y\sigma)^2(x\sigma)^2(w\pi)^4(v\pi)...{}^2\Pi_r \qquad \ldots (1)$$

In this configuration the last $(v\pi)$ electron is an antibonding electron. According to Mulliken the symbols z, y, x, w, v denote the order of decrease in firmness

of binding energy of molecular orbitals of the electrons, from a detailed discussion of the electronic states of NO and O^+_2. Assuming that in PO as well the same order of orbitals the first excited electronic configuration of PO may be written as

$$K.K...(z\sigma)^2(y\sigma)^2(x\sigma)^2(w\pi)^3(v\pi)^2...{}^2\Pi_i,\ {}^2\Pi_r,\ {}^2\Pi,\ {}^4\Pi_i \text{ states} \quad ... \quad (2)$$

Of these the $^2\Pi$ term may represent the B-state in PO and belongs to Hund's case (b). However the transition of an electron from a $w\pi$ to a $v\pi$ orbital is accompanied by only a slight reduction in frequency from 1232 to 1166 cm^{-1} in contrast to a large diminution in NO. This probably indicates that the $w\pi$ electrons in PO are weakly bonding. The second excited electronic configuration corresponds to the transition of an electron from $x\sigma$ to $v\pi$ orbital giving rise to the states

$$K.K....(z\sigma)^2(y\sigma)^2(x\sigma)(w\pi)^4(v\pi)^2...{}^2\Sigma^+,\ {}^2\Sigma^-,\ {}^2\Delta, {}^4\Sigma^- \text{ states} \quad ... \quad (3)$$

The $^2\Delta$ term belonging to configuration (3) may represent the D state of PO. In the $D-B$ transition an $x\sigma$ electron changes into a $w\pi$ electron. This change is accompanied by probably a slight reduction in vibrational frequency as indicated by the evidence of slight degradation of the bands in the $D-B$ system towards the red. This indicates that the $x\sigma$ orbital in PO is slightly more bonding than $w\pi$.

The third excited electronic configuration corresponding to the transition of $y\sigma$ to $v\pi$ as in configuration (4) gives rise

$$K.K...(z\sigma)^2(y\sigma)(x\sigma)^2(w\pi)^4(v\pi)^2...{}^2\Sigma^+,\ {}^2\Sigma^-,\ {}^2\Delta,\ {}^4\Sigma^- \text{ states} \quad ... \quad (4)$$

to $a^2\Delta$ term in addition to $^2\Sigma^+$, $^2\Sigma^-$ and $^4\Sigma^-$. This $^2\Delta$ term may very well represent the D' level in PO. The transition of an antibonding $y\sigma$ electron to a $w\pi$ orbital is expected to be accompanied by an increase in vibrational frequency It is probable that the $x\sigma$ orbital has only slightly greater firmness of binding. In consequence the two $^2\Delta$ states resulting from (3) and (4) lie close to each other. Since the two states satisfy Kronig's selection rules for predissociation the observed predissociation at the $v' = 1$ level can thus be accounted for.

ACKNOWLEDGMENT

The authors wish to express their respectful thanks to Prof. K. R. Rao for his interest in this work.

REFERENCES

Curry, Herzberg and Herzberg, 1933, *Z. Physik*, **86**, 348.
Dressler, K. 1955, *Helv. Phys. Acta.*, **28**, 563-590.
Ghosh and Ball, 1931, *Z. Physik.*, **71**, 362.
Kark Rumpf, 1938, *Zeit. Physi. Chemi.*, **B38**, 469.
Mulliken, R. S., 1932, *Rev. Mod. Phys.* **4**, 1.
Pearse and Gaydon "On the Identification of Molecular Spectra".
Ramanathan, Rao and Rama Sastry, 1946, *Ind. J. Phys.* **20**, 161.
Sen Gupta, 1935, *Proc. Phys. Soc.* (*London*), (*A*), **47**, 247.

STABILITY OF MAGNETIC STARS IN A DECAY FIELD

S. P. TALWAR

DEPARTMENT OF PHYSICS, UNIVERSITY OF DELHI, DELHI

(*Received for publication, December* 11, 1956)

ABSTRACT. The question of stability of a magnetic star in a slowly decaying axially symmetric magnetic field is investigated. Poloidal and toroidal fields are considered and the initial magnetic energies evaluated. From the condition of dynamical stability the expression for the critical primitive magnetic fields which can exist in the star is worked out. The magnetic energies and the critical fields for instability are tabulated.

Further the effect of a magnetic field, toroidal as well as poloidal (less than the critical) on the equilibrium of a sphere of constant conductivity is investigated. It is found that the sphere is not an equilibrium form and tends to deform into a spheroidal shape. The effect of a toroidal field is to turn it into a prolate spheroidal shape, whereas in a poloidal field the sphere has a tendency to become an oblate spheroid of small ellipticity. The expressions for the ellipticity of the spheroidal form are worked out in each case.

1. INTRODUCTION

The mechanical equilibrium of a magnetic star has been the subject of investigation during recent years, (Chandrasekhar and Fermi, 1953;) Ferraro, 1954; Gjellestad, 1954; Roberts, 1955; Auluck and Kothari, 1956; Prendergast, 1956; Talwar, 1957). The fluid sphere, in these cases, is assumed to be incompressible, *infinitely conducting*, and situated in vacuum. In this paper, we investigate the problem of the dynamical stability and the equilibrium of an incompressible, gravitating, fluid sphere, in which prevails a slowly decaying magnetic field, which arises due to the Joule heating of a correspondingly decaying current system in the medium of constant electric conductivity σ. The magnetic star is further assumed to be lying at rest in empty space so that the current density j vanishes outside the sphere.

The equations governing a slowly decaying magnetic field in a homogenous sphere of permeability unity, are (using e.m.u.)

$$\text{curl } \boldsymbol{H} = 4\pi \boldsymbol{j}, \qquad \text{curl } \boldsymbol{E} = -\frac{\partial \boldsymbol{H}}{\partial t} \qquad \ldots (1)$$

$$\boldsymbol{j} = \sigma \boldsymbol{E}$$

hence

$$\nabla^2 \boldsymbol{H} = 4\pi\sigma \frac{\partial \boldsymbol{H}}{\partial t} \qquad \ldots (2)$$

This equation (2) holds for the interior of the sphere. For regions outside the sphere, the current density j is zero, so that

$$\nabla^2 \boldsymbol{H} = 0 \qquad (3)$$

Elsasser (1946) showed that it is possible to construct three independent solutions of the decaying field equation (2), and the solutions can be written as,

$$\boldsymbol{U} = R\,\Delta\psi,\ \boldsymbol{T} = \text{curl}\,(\boldsymbol{r}\,\psi),\ \boldsymbol{S} = R\ \text{curl curl}\,(\boldsymbol{r}\,\psi) \qquad \ldots \quad (4)$$

where $\boldsymbol{r}$ is the radius vector from the centre,, R is the radius of the sphere and ψ is a scalar generating function satisfying,

$$\nabla^2\psi + k^2\psi = 0 \quad \text{(inside)} \qquad \ldots \quad (5)$$

and

$$\nabla^2\psi = 0 \quad \text{(outside)} \qquad \ldots \quad (6)$$

Here $\qquad k^2 = 4\pi\sigma/\tau, \quad \tau$ being the decay time.

Elsasser calls these functions $\boldsymbol{T}, \boldsymbol{S}, \boldsymbol{U}$ as 'toroidal', 'poloidal' and 'scleoidal' respectively. We shall be concerned in our present work with the toroidal and poloidal functions, and shall be studying the stability of an incompressible sphere, in two cases, one where the field is continuous across the surface of the sphere and the other where the field vanishes on the boundary of the sphere and in the entire space outside it. We shall call these cases as 'Case I' and 'Case II' respectively.

CASE I

2 *Initial magnetic energy, and dynamical instability.*

When equations (5) and (6) are solved with the boundary condition that ψ and $\partial\psi/\partial r$ are continuous at $r = R$, the solutions inside and outside the sphere are given as (Jenson, 1955; Elsasser, 1946)

$$\psi_{ns}{}^m = Z_n N_n{}^m (R/r)^{\frac{1}{2}} J_{n+\frac{1}{2}}(k_{ns}r) P_n{}^m(\mu) e^{im\phi} \qquad (r \leqslant R) \qquad \ldots \quad (7)$$

and

$$\psi_{ns}{}^m = Z_n N_n{}^m (R/r)^{n+1}\, J_{n+\frac{1}{2}}\,(k_{ns}R) P_n{}^m\,(\mu) e^{im\phi} \quad (r \geqslant R) \quad \ldots \quad (8)$$

where Z_n, $N_n{}^m$ are constants and the characteristic values of k are the zeros of the Bessel function $J_{n-\frac{1}{2}}(k_{ns}R)$.

The equation (4) gives the following components of the functions $\boldsymbol{T}$ and $\boldsymbol{S}$,

$$\boldsymbol{T}_{ns}{}^m = \left[\ 0, \frac{1}{\sin\theta}\frac{\partial\psi_{ns}{}^m}{\partial\phi}, -\frac{\partial\psi_{ns}{}^m}{\partial\theta}\right]$$

$$\boldsymbol{S}_{ns}{}^m = \frac{R}{r}\left[\ n(n+1)\psi_{ns}{}^m,\ \frac{\partial}{\partial r}\left(r\frac{\partial\psi_{ns}{}^m}{\partial\theta}\right), \frac{1}{\sin\theta}\frac{\partial}{\partial r}\left(r\frac{\partial}{\partial\phi}\psi_{ns}{}^m\right)\right] \qquad \ldots \quad (9)$$

We are interested in an axially symmetric field so that the functions T, S do not depend upon the variable ϕ. The components of the internal magnetic field are therefore written as

$$\boldsymbol{H}^{(i)} = \Big[\ C(R/r)^{3/2}n(n+1)J_{n+\frac{1}{2}}(k_{ns}r)P_n(\mu),\ -C\,\frac{R^{3/2}}{r}\,\frac{d}{dr}\Big\{\,r^{\frac{1}{2}}J_{n+\frac{1}{2}}\,(k_{ns}r)\Big\}\,P_n^{\,1}(\mu),$$

$$C(R/r)^{\frac{1}{2}}J_{n+\frac{1}{2}}\,(k_{ns}r)P_n^{\,1}(\mu)\ \Big] \quad \ldots \quad (10)$$

The corresponding components of the field outside the sphere are

$$\boldsymbol{H}^{(e)} = [Cn(n+1)(R/r)^{n+2}J_{n+\frac{1}{2}}(k_{ns}R)P_n(\mu),\ Cn(R/r)^{n+2}J_{n+\frac{1}{2}}(k_{ns}R)P_n^{\,1}(\mu),$$

$$C(R/r)^{n+1}J_{n+\frac{1}{2}}(k_{ns}r)P_n^{\,1}(\mu)] \quad \ldots \quad (11)$$

where C is a constant defined in terms of the polar values of the field H_p, as

$$C = \frac{H_p}{n(n+1)J_{n+\frac{1}{2}}(k_{ns}R)} = \frac{(H_p)_0 e^{-t/\tau}}{n(n+1)J_{n+\frac{1}{2}}(k_{ns}R)} \quad \ldots \quad (12)$$

where $(H_p)_0$ denotes the primitive polar field (at time $t = 0$).

The total magnetic energy, m, is composed of two parts; $m^{(i)}$, the internal magnetic energy and $m^{(e)}$, the external magnetic energy. The internal or external magnetic energy further consists of (i) the contribution $m_p^{(i)(e)}$ due to the poloidal field (r, and θ-components) and (ii) the contribution $m_\tau^{(i)(e)}$ due to the toroidal field (the azimuthal component H_ϕ).

The magnetic energy, m_p, of the configuration due to the poloidal field defined by the components in the r- and θ- directions in equations (10) and (11), is written as

$$m_p = m_p^{(i)} + m_p^{(e)} = \frac{n(n+1)}{4(2n+1)}\,C^2R^3(k_{ns}R)^2.\ J^2_{n+\frac{1}{2}}(k_{ns}R) \quad \ldots \quad (13)$$

Using equations (10) and (11) the contribution to the magnetic energy due to the toroidal field H_ϕ, is written as

$$m_\tau^{(i)} = \frac{n(n+1)}{4(2n+1)}\,C^2R^3J^2_{n+\frac{1}{2}}(k_{ns}R) \quad \ldots \quad (14)$$

$$m_\tau^{(e)} = \frac{n(n+1)}{4(2n+1)(2n-1)}\,C^2R^3J^2_{n+\frac{1}{2}}(k_{ns}R) \quad \ldots \quad (15)$$

so that,

$$m_T = m_T^{(i)} + m_T^{(e)}$$

$$= \frac{n(n+1)}{4(2n-1)} C^2 R^3 J^2_{n+\frac{1}{2}}(k_{ns}R) \qquad \ldots \quad (16)$$

Thus the total magnetic energy of the configuration is given by

$$m = m_T + m_p$$

$$= \frac{n(n+1)}{4} \; C^2 R^3 J^2_{n+\frac{1}{2}}(k_{ns}R) \left[\frac{k^2_{ns}R^2}{2n+1} + \frac{1}{2n-1} \right] \qquad \ldots \quad (17)$$

or, in terms of the primitive polar field

$$m = \frac{(H_p)_0^2 R^3}{4n(n+1)} \cdot \left[\frac{k_{ns}^2 R^2}{(2n+1)} + \frac{1}{(2n-1)} \right] e^{-2t/\tau}$$

In Table 1, we have tabulated the primitive magnetic energies in units of $H_p^2 R^3$.

The gravitational potential energy of a homogenous sphere is given by

$$\Omega = -\frac{3}{5}\frac{GM^2}{R} \qquad \ldots \quad (18)$$

For dynamical stability the magnetic energy (eq 17) should be less than the gravitational energy (eq. 18); thus the critical magnetic field parameter C^* is given by

$$C^* = \left[\frac{12}{5} \frac{(2n-1)(2n+1)}{\{n(n+1)\}\{(2n-1)k_{ns}^2R^2+(2n+1)\}} \right]^{1/2} \frac{G^{1/2}M}{R^2 J_{n+1/2}(k_{ns}R)} \qquad \ldots \quad (19)$$

The condition for dynamical stability can be alternatively written in terms of the primitive polar field $(H_p)_0$, as

$$(H_p)_0 < \left[\frac{12}{5} \frac{n(n+1)(2n-1)(2n+1)}{(2n-1)k_{ns}^2R^2+(2n+1)} \right]^{1/2} \frac{G^{1/2}M}{R^2} \qquad \ldots \quad (20)$$

Here $k_{ns}R$ denote the zeros of the Bessel function $J_{n-\frac{1}{2}}(k_{ns}R)$. Table. II is derived from the equation (20) for a star having solar dimension and mass.

The equation (19) defines the critical maximum magnetic field which can exist with a sphere with constant electrical conductivity. In the following section (3) we investigate the effect of a decaying magnetic field less than the critical field (the field for dynamical instability to set in) on the mechanical equilibrium of star.

TABLE I

The magnetic energies in some modes for a sphere of uniform conductivity

n	s	Magnetic energy in units of $H_p^2R^3$	n	s	Magnetic energy in units of $H_p^2R^3$
1	1	0.536	3	1	0.110
1	2	1 770	3	2	0.251
1	3	3.827	3	3	0.458
1	4	6.707	3	4	0.738
1	5	10.410	3	5	1.056
2	1	0.182			
2	2	0 620			
2	3	1.093			
2	4	1.726			
2	5	2.519			

TABLE II

Critical primitive polar fields for instability for a magnetic star of solar dimensions

n	s	$H_p \times 10^{-7}$gauss	n	s	$H_p \times 10^{-7}$gauss
1	1	5.37	2	3	3.94
1	2	2.94	2	4	3.06
1	3	1.98	2	5	2.49
1	4	1 50	3	1	11.70
1	5	1 2	3	2	7.56
2	1	9 06	3	3	5.72
2	2	5.50	3	4	4.38
			3	5	3.77

3. *Equilibrium of a sphere under poloidal and toroidal fields (eq. 10, 11).*

For the purpose of investigating whether a sphere is an equilibrium form under the magnetic field defined by equations (10) and (11), we give the sphere a virtual displacement which changes the boundary $r = R$ of the sphere into one defined

$$r(\mu) = R + \epsilon P_l(\mu) \qquad \ldots \quad (21)$$

and calculate the change in the total energy of the configuration (magnetic plus gravitational). If the change in the total energy of the configuration vanishes, to the first order in ϵ for all values of l in equation (21), (for all modes of P_l – deformation), we can then conclude that a sphere is a form of equilibrium. If,

on the other hand, it vanishes for only some particular values of l, the maximum we can conclude is that the sphere is a form of equilibrium only for these particular modes of P_l-deformation and not *in general* so that the sphere is not a form of *true* equilibrium.

In order to evaluate the change in the total energy of the configuration, we need expressions for the change in gravitational potential energy, $\Delta\Omega$, and for the change in the magnetic energy, Δm, due to the P_e-deformation (21). The former is calculated by Chandrasekhar and Fermi (1953) and is given by,

$$\Delta\,\Omega_l = \frac{3(l-1)}{(2l+1)^2}\,\epsilon^2\,\frac{GM^2}{R^5} \tag{22}$$

which is of second order in ϵ and is always positive. If Δm also turns out to be of second order in ϵ and positive, then the sphere is a stable form of equilibrium. We shall find that the expression for the change in magnetic energy is non-vanishing, up to first order in ϵ, for a P_2-deformation, and is zero for all other deformations ($l\neq 2$). Thus we can conclude that the magnetic star (sphere) is unstable for a P_2-deformation, and would tend to become spheroidal although for any other deformation, we cannot decide about the stability question unless we go upto second order in ϵ. This, however, is beyond the scope of the present work.

The change in the magnetic energy, Δm, as a consequence of the P_l-deformation, can be written as,

$$\Delta m = -\int \boldsymbol{\xi}_e\cdot(\boldsymbol{J}\times\boldsymbol{H})d\tau \tag{23}$$

The result shall be true up to first order in ϵ when the volume integral is taken over the undisturbed body and $\boldsymbol{J}$ and $\boldsymbol{H}$ denote the undisturbed current density and field.

In equation (23), $\boldsymbol{\xi}_e$ denotes the displacement corresponding to deformation (21), and is written as (Chandrasekhar and Fermi, 1953),

$$\xi_r = \epsilon(r/R)^{l-1}P_e(\mu),\ \ \xi_\theta = -\epsilon/l(r/R)^{l-1}P_l^1(\mu) \qquad \ldots \tag{24}$$

The current density $\boldsymbol{J}$ in zero outside the sphere, whereas in the interior of the sphere it is given by,

$$4\pi\boldsymbol{J} = \text{curl}\ \boldsymbol{H} \qquad \ldots \tag{25}$$

so that we can write, using equation (10),

$$4\pi j_r = \frac{CR^{\frac{1}{2}}}{r^{3/2}}\ J_{n+\frac{1}{2}}(k_{ns}r)n(n+1)\,P_n(\mu)$$

$$4\pi j_\theta = -\frac{CR^{1/2}}{r^{3/2}}\ [\,-nJ_{n+\frac{1}{2}}(k_{ns}r)+k_{ns}rJ_{n-\frac{1}{2}}(k_{ns}r)]\,P_n^1(\mu) \tag{26}$$

and

$$4\pi j_\phi = \frac{Ck_{ns}^2}{r^{1/2}} R^{3/2} J_{n+\frac{1}{2}}(k_{ns}r)(1-\mu^2)^{\frac{1}{2}} P_n'(\mu)$$

The Lorenty force is written as,

$$F = [j \times H] = [j_\theta H_\phi - j_\phi H_\theta, j_\phi H_r - j_r H_\phi, j_r H_\theta - j_\theta H_r] \quad \ldots \quad (27)$$

Thus the expression (23) can be rewritten as,

$$\Delta m = -\int_\tau (\xi_r F_r + \xi_\theta F_\theta) d\tau = -\int_\tau [\xi_r (j_\theta H_\phi - j_\phi H_\theta) + \xi_\theta (j_\phi H_r - j_r H_\phi)] d\tau$$

$$= \Delta m_p + \Delta m_T \quad \ldots \quad (28)$$

where

$$\Delta m_p = -\int [\xi_r(-j_\phi H_\theta) + \xi_\theta (j_\phi H_r)] d\tau \quad \ldots \quad (29)$$

and

$$\Delta m_T = -\int [\xi_r (j_\theta H_\phi) + \xi_\theta (-j_r H_\phi)] \, d\tau \quad \ldots \quad (30)$$

The expression (29) gives the change in the magnetic energy of a sphere due to a P_l deformation , when the magnetic field assumed is purely poloidal (r, θ components), whereas equation (30) gives the change in magnetic energy for the same deformation when the magnetic field is purely toroidal in character.

The equation (29) can be written as, making use of the equations (10), (24), and (26),

$$\Delta m_p = -\frac{\epsilon C^2 R^3 k_{ns}^2}{2R^{l-1}} \int_{-1}^{+1} \int_0^R \Big[[P_n^1(\mu)]^2 P_l(\mu) r^{l-1} J_{n+\frac{1}{2}}(k_{ns}r) \times \{-nJ_{n+\frac{1}{2}}(k_{ns}r) +$$

$$k_{ns} r J_{n-\frac{1}{2}}(k_{ns}r)\} - \frac{n(n+1)}{l} r^{l-1} [J_{n+\frac{1}{2}}(k_{ns}r)]^2 P_l^1(\mu) P_n^1(\mu) P_n(\mu)] dr d\mu \quad \ldots \quad (31)$$

Since the integration over μ in equation (31) vanishes for $(2n+l)$ = odd i.e. l = odd, we conclude that

$$\Delta m_p = 0 \quad \text{for all } n, \quad \text{but } l = \text{odd} \quad \ldots \quad (32)$$

Further, it can be easily shown that for $n = 1$ the change in the poloidal magnetic energy, Δm_p, vanishes for all l, except $l = 2$, which corresponds to a

P_2-deformation. For a P_2-deformation, the change, Δm_p, in poloidalm agnetic energy is of first order in ϵ, and is given by

$$\Delta m_p = -\frac{\epsilon C^2 R^2 k_{ns}^2}{2}\left[\frac{2n(n+1)\{n(n+1)-3\}}{(2n-1)(2n+1)(2n+3)} \times \int_0^R rJ_{n+\frac{1}{2}}\{-nJ_{n+\frac{1}{2}}+k_{ns}rJ_{n-\frac{1}{2}}\}dr\right.$$

$$\left. -\frac{n(n+1)}{2}\int_0^R\int_{-1}^{+1} P_2^1(\mu)P_n^1(\mu)P_n(\mu)r[J_{n+\frac{1}{2}}(k_{ns}r)]^2 dr\, d\mu\right] \quad \ldots \quad (33)$$

For the simplest decay field, corresponding to $n = 1$, we have

$$\Delta m_{1s} = 0 \text{ for } l \neq 2$$

and

$$\Delta m_{\substack{1s\\(l=2)}} = \frac{2}{15} C^2\epsilon R^2 \left[(k_{1s}R)^2 J_{3/2}(k_{1s}R) + \frac{1}{\pi}\left\{k_{1s}R - \frac{3}{4}\sin 2k_{1s}R + \frac{k_{1s}R}{2}\cos 2k_{1s}R\right\}\right] \quad \ldots \quad (34)$$

Since $k_{1s}R$ are zeros of the function $J_{\frac{1}{2}}(k_{1s}R)$, the above expression for the change in the poloidal magnetic energy, for a P_2—deformation, can be put down as

$$[\Delta m_{1s}]_p = \frac{7}{15}\epsilon s C'^2 R^2 = \frac{7}{120}\pi^2 s^2 \epsilon (H_p)_0^2 R^2 e^{-2t/\tau} \quad \ldots \quad (35)$$

Thus we see that in contrast to $\Delta\Omega$, (equation 22), which is of second order in ϵ and always positive, the change, Δm_p, in the poloidal magnetic energy has a contribution even up to first order in ϵ for a P_2-deformation. Hence we conclude that a magnetic sphere of constant conductivity with poloidal field given by equation (10), is not an equilibrium form and would tend to an oblate spheroidal form for a P_2-deformation. The extent of the collapse towards the oblate shape in the simplest decay field, can be found immediately by minimising the total change $(\Delta\Omega + \Delta m_{1p})$ for a P_2-deformation . This leads us to the expression

$$(\epsilon/R)_{1s} = -\frac{35}{144} s^2\pi^2 \frac{(H_p)_0^2 R^4}{GM^2} e^{-2t/\tau} \quad \ldots \quad (36)$$

The other part, Δm_τ, in equation (28), which represents the change in the toroidal magnetic energy, can be evaluated, with the help of equation (10), (24) and (26). The results are expressed as,

$$\Delta m_\tau = 0 \quad \text{for all } n, \quad \text{but } l = \text{odd}$$

$$= 0 \quad \text{for } n = 1, \quad \text{but } l \neq 2 \quad \ldots \quad (37)$$

For a P_2-deformation, $(l = 2)$, the change in the magnetic energy due to the toroidal component, Δm_T, is non-vanishing and is given by, for the simplest decay field,

$$[\Delta m_{1s}]_T = -\frac{4}{15}\frac{C^2\epsilon R^2}{\pi^2 s} \quad \ldots \quad (38)$$

Thus the change in the total magnetic energy, Δm, due to a P_l-deformation of a sphere, with both toroidal and poloidal decaying fields, is

$$\begin{aligned} \Delta m &= \Delta m_T + \Delta m_p \\ &= 0 \quad \text{for all } n, \quad \text{but } l = \text{odd} \\ &= 0 \quad \text{for } n = 1, \quad \text{but } l \neq 2 \end{aligned} \quad \ldots \quad (39)$$

and

$$[\Delta_1 m_s]_{r=2} = \frac{7}{15}\epsilon s C^2 R^2 \left(1 - \frac{4}{7\pi^2 s^2}\right) \quad \ldots \quad (40)$$

Since s is a positive integer, Δm, does not vanish for any value of s. Thus we see that the change, Δm, in the magnetic energy is of first order in ϵ, whereas the change $\Delta\Omega$ is of second order in ϵ and is always positive. We conclude, therefore, that with both toroidal and poloidal field (eq.10,11) the sphere is not in real equilibrium and would deform into a spheroidal shape of ellipticity ϵ/R, given by

$$(\epsilon/R)_{1s} = -\frac{35}{144}\frac{s^2\pi^2 R^4}{GM^2}(H_p)_0^2 e^{-2t}\left(1 - \frac{4}{7\pi^2 s^2}\right) \quad \ldots \quad (41)$$

$$= -3.5(H_p/H_p^{\times})_0^2 e^{-2/\tau}\left[1 - \frac{4}{7\pi^2 s^2}\right]$$

in terms of the critical primitive polar field.

If only toroidal field were present, its effect is to deform the sphere into a prolate spheroid of ellipticity,

$$(\epsilon/R)_{1s} = \frac{10}{9s\pi^2}\frac{C^2 R^4}{GM^2} \quad \ldots \quad (42)$$

CASE II

4: Stability of a sphere with poloidal and and toroidal field, vanishing at surface.

When the internal field vanishes on the surface, $r = R$, of the sphere and in the space outside it, the calculations differ from Case I in that the characteristic values l_{ns} are zeros of the Bessel function $J_{n+\frac{1}{2}}(l_{ns}R)$.

The field components can then be written as,

$$H = \Big[\, C'n(n+1)(R/r)^{3/2} J_{n+\frac{1}{2}}(l_{ns}r) P_n(\mu),\ -\frac{C'R^{3/2}}{r}\frac{d}{dr}$$

$$\{r^{\frac{1}{2}} J_{n+\frac{1}{2}}(l_{ns}r)\} P_n^1(\mu), C'(R/r)^{\frac{1}{2}} J_{n+\frac{1}{2}}(l_{ns}r) P_n^1(\mu)\,\Big] \quad \ldots \quad (43)$$

The corresponding magnetic energy is

$$m = \frac{n(n+1)}{4(2n+1)} C'^2 R^3 [1 + l^2_{ns} R^2], \quad \ldots \quad (44)$$

so that the sphere shall be dynamically stable for values of the field parameter C', less than the critical defined by,

$$C'^{\times} = \left\{ \frac{12(2n+1)^{\frac{1}{2}}}{5n(n+1)} \right\} \frac{G^{\frac{1}{2}}M}{R^2} \frac{1}{(1 + l^2_{n\cdot} R^2)^{\frac{1}{2}} J_{n-\frac{1}{2}}(l_{ns}R)} \quad \ldots \quad (45)$$

Again for fields less than this critical, the change $\Delta\eta$ in the magnetic energy, due to a P_l -deformation of the sphere, is written as,

$$\Delta m = 0 \qquad \text{for all } n, \quad \text{but} \quad l = \text{odd} \quad \ldots \quad (46)$$

and

$$\Delta m = 0 \qquad \text{for } n = 1, \quad \text{but } l \neq 2$$

For a P_2-deformation, the change Δm_s in magnetic energy is non-vanishing and is given by, (for $n = 1$),

$$\Delta m_{1s} = (\Delta m_{1s})_T + (\Delta m_{1s})_p \quad \ldots \quad (47)$$

The change, $[\Delta m_{1s}]_p$ in the poloidal magnetic energy can be easily worked out and is given by,

$$[\Delta m_{1s}]_p = \frac{2}{15} C'^2 \epsilon R^2 \left[J^2_{\frac{1}{2}}(l_{1s}R) + \frac{l_{1s} R}{2\pi\{1 + l^2_{1s} R^2\}} \right] l^2_{1s} R^2 \quad \ldots \quad (48)$$

and the corresponding expression for the change $[\Delta m_{1s}]_T$ in the toroidal energy is,

$$[\Delta m_{1s}]_T = -\frac{2}{15} C'^2 \epsilon R^2 \left[\frac{J^2_{\frac{1}{2}}(l_{1s}R)}{4} + \frac{l_{1s}R}{2\pi\{1 + l^2_{1s} R^2\}} \right] \quad \ldots \quad (49)$$

so that the total change in magnetic energy due to a P_2-deformation of a sphere with simplest decay field (poloidal+toroidal) becomes

$$\Delta m_{1s} = \frac{2}{15} C'^2 \epsilon R^2 \left[J^2_{\frac{1}{2}}(l_{1s}R)\{l^2_{1s} R^2 - \tfrac{1}{4}\} + \frac{l_{1s}R\{l^2_{1s} R^2 - 1\}}{2\pi\{l^2_{1s} R^2 + 1\}} \right] \quad \ldots \quad (50)$$

Thus we see that the sphere is not in true equilibrium with the decay field (poloidal+toroidal) vanishing at the surface and in the space outside, since the change in magnetic energy is non-vanishing for P_2-deformation. The sphere shall deform to a spheroidal shape, and the extent of deformation is easily written as (for $n = 1$)

$$(\epsilon/R)_{1s} = -\frac{5}{9}\frac{C'^2R^4}{GM^2}\left(J^2_{\frac{1}{2}}(l_{1s}R)\left\{ l_{1s}^2R^2 - \frac{1}{4}\right\} + \frac{l_{1s}R\{l^2_{1s}R^2-1\}}{2\pi\{l_{1s}^2R^2+1\}}\right) \quad \ldots \quad (51)$$

If the field prevalent in the sphere is purely toroidal, the sphere will tend to a prolate spheroidal shape of ellipticity,

$$(\epsilon/R)_{1s} = \frac{5}{9}\frac{C'^2R^4}{GM^2}\left[\frac{J^2_{\frac{1}{2}}(l_{1s}R)}{4} + \frac{l_{1s}R}{2\pi\{1+l^2_{1s}R^2\}}\right] \quad \ldots \quad (52)$$

ACKNOWLEDGMENTS

The author is indebted to Professor D. S. Kothari and Professor F. C. Auluck for their interest in this work.

REFERENCES

Auluck, F. C. and Kothari, D. S., 1956, *Proc. Nat. Inst. Sci* (In press).
Chandrasekhar, S. and Fermi, E., 1953, *Ap. J.* **118**, 116.
Elsasser, W M., 1946, *Phy Rev.*, **69**, 106
Ferraro, V C. A., 1954, *Ap. J.* **119**, 407.
Gjellestad, G., 1954, *Ap J* **120**, 172.
Jonson, E., 1955, *Ap. J.* (Supplement No. 16), 141.
Lust, R. and Schluter, A., 1954, *ZAp.* **34**, 263
Prendergast, K H., 1956, *Ap. J.* **123**.
Roberts, P. H, 1956, *Ap. J.* **122**, 508.
Stratton, J. A., 1941, Electromagnetic Theory (McGraw Hill Book Co., Inc., New York) Chap 7.
Talwar, S. P, 1957, *Zeits. f. Ap.* **42**, 42.

THE EFFECT OF A UNIFORM MAGNETIC FIELD ON ELECTRODELESS DISCHARGE IN A TUBE AND MEASUREMENT OF ELECTRONIC MOBILITY II. OXYGEN, NITROGEN, CARBONDIOXIDE AND HYDROGEN.

S. N. GOSWAMI

DEPARTMENT OF PHYSICS, CENTRAL CALCUTTA COLLEGE, CALCUTTA.

(*Received for publication, September* 10, 1957)

ABSTRACT. Results of measurements of the percentage increase in the breakdown potential and of electronic mobility in a discharge tube filled with O_2, N_2, CO_2 and H_2, and excited with a 50-cycles alternating voltage, under a uniform magnetic field have been reported. Measurements are made at different pressures and under magnetic fields inclined at different angles with the electric field.

INTRODUCTION

In a previous communication the author (Goswami, 1958) reported that the value of the breakdown potential in dry air in an electrodeless discharge tube, excited with a 50-cycles alternating voltage, is increased in a magnetic field. The percentage increase in the breakdown potential is dependent upon the pressure, the strength of the magnetic field and its inclination with the electric field. The main features of the observed phenomena were satisfactorily explained in the light of the theory presented by Deb and Goswami (1956). In the present investigation, results of similar measurements in oxygen, nitrogen, carbondioxide and hydrogen are reported and compared with those in dry air.

EXPERIMENTAL

The experimental arrangement was practically identical with the one described in our previous communication, except that particular attention was given to make the discharge system free from moisture, grease-vapour etc.

RESULTS AND DISCUSSION

The results of measurement are given in Tables I-IV from which the variations of the percentage effect and the electronic mobility with pressure for different values of the magnetic field at different inclinations can be obtained. The variations, with pressure, of the percentage effect are also graphically represented for only two values of the magnetic field for each of the gases in figures 1—8 and of the electronic mobility in figures 9—12.

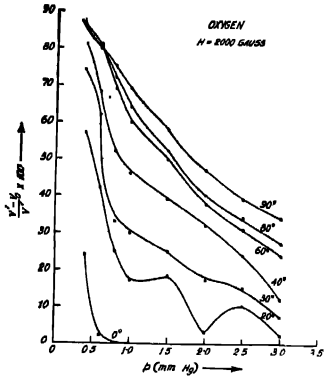

Fig. 1.

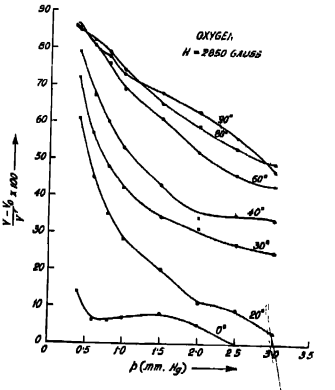

Fig. 2.

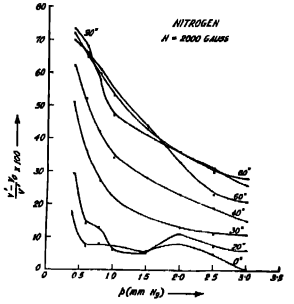

Fig. 3.

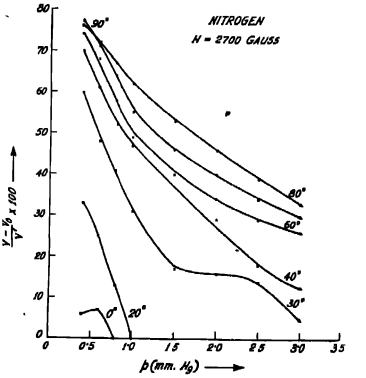

Fig. 4.

A comparison of the results with those for dry air reported previously (Goswami, 1958) shows that the variations in both cases are similar. Table I-IV.

It may be seen that the curves representing the variation of $\frac{V'-V_0}{V'}$ with pressure as also of the electronic mobility with pressure have trends more or less similar to rectangular hyperbolas. It is interesting to note that this result is in agreement with the theory.

TABLE I

Values of $\frac{V'-V_0}{V'}$ and μ_e for oxygen

	$\frac{V'-V_0}{V'}$												$\mu_e \times 10^{-5}$ ($\theta = 90°$) cm²/volt. sec.		
	$\theta = 0°$			30°			60°			90°					
p-mm Hg \ H in gauss	1525	1750	3325	1525	1750	3325	1525	1750	3325	1525	1750	3325	1525	1750	3325
0.4	.00	.17	.15	.61	.61	.76	76	78	80	.75	81	85	.86	.79	.43
0.6	.00	.12	.06	.48	.41	64	.70	.67	.74	70	.73	.80	.83	.74	.41
0.8	.00	.14	.00	.36	.35	52	63	.54	.65	.56	.65	77	.73	.69	.40
1.0	.00	.12	.00	.24	.36	.46	.52	.46	.57	.44	.58	.72	.64	.65	.39
1.5	.00	.15	.00	.13	.31	31	.40	.40	.50	.34	.50	.66	.56	.60	.37
2.0	.00	.12	.00	.14	.27	.26	.28	34	.46	.32	.42	.59	.54	.54	35
2.5	.00	.16	.00	.13	.23	.23	.21	.29	.44	.24	.31	50	46	.46	.32
3.0	.00	.10	.00	.08	.14	18	.18	.25	.33	.24	.26	.41	.46	.42	.28

TABLE II.

Values of $\frac{V'-V_0}{V'}$ and μ_e for nitrogen

	$\frac{V'-V_0}{V'}$												$\mu_e \times 10^{-5}$ ($\theta = 90°$) (cm²/volt. sec.)		
	$\theta = 0°$			30°			60°			90°					
p-mm.Hg \ H in gauss	1750	2225	2500	1750	2225	2500	1750	2225	2500	1750	2225	2500	1750	2225	2500
0.4	.11	16	.15	.51	49	.47	.71	.76	.74	.75	.69	.79	.75	.56	.54
0.6	06	.06	.11	.44	.46	40	.66	.70	.64	.70	.66	.76	.72	.55	.53
0.8	.07	.07	.08	.38	.36	31	.63	.64	.54	.62	.56	.72	.68	.50	.52
1.0	.00	.05	.04	.33	.31	.11	.57	.60	.47	.54	.47	.62	.62	.46	.47
1.5	.00	.00	.07	.28	.29	.13	.50	.54	40	.47	.42	.52	.58	.43	.43
2.0	.00	.00	.00	.25	.27	.14	.42	.47	.34	.43	.34	.44	.55	.38	.39
2.5	.00	.00	.00	.19	.24	.08	39	.43	.26	.37	.27	.37	.51	.34	.36
3.0	.00	00	.00	.15	.18	.06	.34	.36	.23	.30	.28	.30	.45	.34	.32

TABLE III.

Values of $\frac{V'-V_0}{V'}$ and μ_e for carbon-dioxide

	$\frac{V'-V_0}{V'}$												$\mu_e \times 10^{-3}$ ($\theta = 90°$) cm²/volt. sec.		
	$\theta = 0°$			30°			60°			90°					
p-mm. Hg. \ H in gauss	2500	2950	3225	2500	2950	3225	2500	2950	3225	2500	2950	3225	2500	2950	3225
0.4	.08	.24	.28	72	.69	70	77	.80	79	79	80	82	54	.48	.43
0.6	00	16	.23	.64	60	.63	74	74	74	77	78	75	54	46	41
0.8	00	12	11	53	46	50	.71	72	.69	75	.72	73	53	.44	40
1.0	00	14	09	36	38	42	61	.62	62	62	70	66	.47	.43	.38
1.5	.00	.15	00	.22	23	32	.50	.53	55	57	.62	.58	45	40	.35
2.0	.00	.08	00	12	.16	23	.39	46	48	.37	55	50	.36	38	.33
2.5	.00	.05	00	04	09	.17	.31	.43	.41	.31	.47	44	.32	.34	.30
3.0	.00	.00	.00	.00	06	.05	20	.35	.32	.24	.40	.37	28	.31	.28

TABLE IV.

Values of $\frac{V'-V_0}{V'}$ and μ_e for hydrogen

	$\frac{V'-V_0}{V'}$												$\mu_e \times 10^{-5}$ ($\theta = 90°$) cm²/volt. sec.		
	$\theta = 0°$			30°			60°			90°					
p-mm. Hg. \ H in gauss	2325	2550	3175	2325	2550	3175	2325	2550	3175	2325	2550	3175	2325	2550	3175
0.4	.25	.22	.20	.59	.62	66	.76	77	.79	.79	.78	.82	.59	.53	.44
0.6	.18	12	16	47	.46	.55	71	.71	73	.75	.74	.77	.57	.51	.42
0.8	.08	.07	17	.28	.36	46	.64	67	.68	67	.68	.74	53	.49	.41
1.0	.15	.03	.14	.17	.27	38	55	58	.63	.58	.60	.70	49	.45	.40
1.5	05	.00	.06	.09	.21	31	.47	52	55	51	.55	.67	.46	.43	.39
2.0	.09	00	05	.04	.16	21	39	43	.49	.48	.43	.55	.41	.40	.35
2.5	.00	.00	.00	.05	15	.20	.32	.35	.44	.41	.43	.51	40	.38	.33
3.0	.00	.00	.00	00	11	12	29	25	35	.36	.34	44	.38	.33	.31

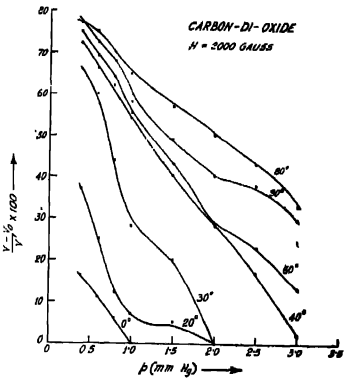

Fig. 5.

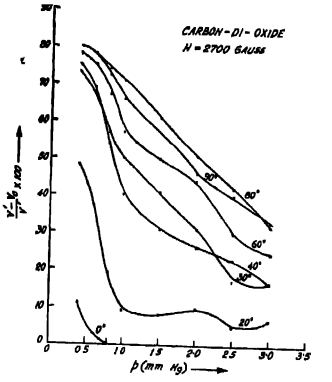

Fig. 6.

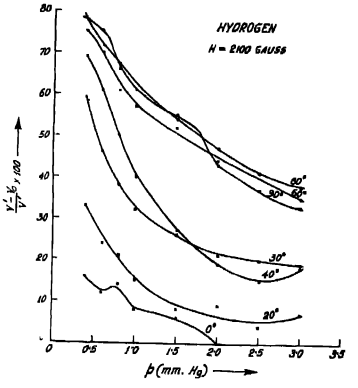

Fig. 7.

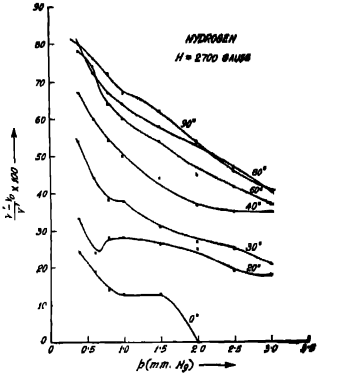

Fig. 8.

We have seen that $$\phi = \frac{He\lambda}{m\bar{v}c} \qquad \ldots \quad (1)$$

$$\mu_e = \frac{\cos^{-1}\left[1-\frac{V'-V_0}{V'}\right]}{H} \times 10^8 \text{ cm}^2/\text{volt. sec} \qquad \ldots \quad (2)$$

and $$\frac{V'-V_0}{V'} = 1-\cos\varsigma \qquad \ldots \quad (3)$$

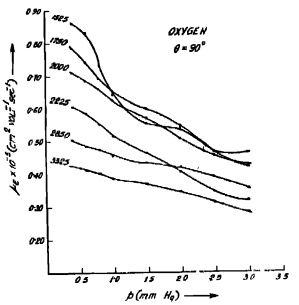

Fig. 9

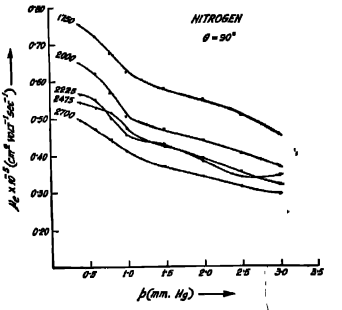

Fig. 10

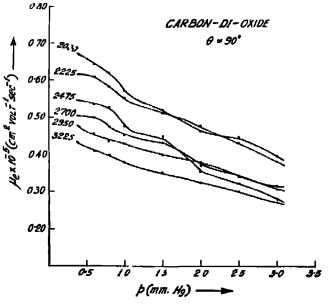

Fig. 11

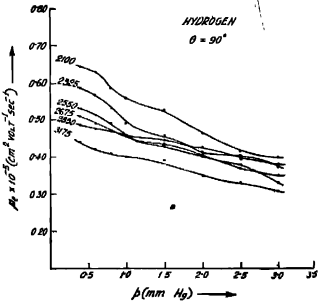

Fig. 12.

At constant temperature. $\lambda \propto \frac{1}{p}$, it follows from (1), (2) and (3) that under the present experimental conditions for a given H, both $p\phi$ and $p\mu_e$ are constant.

ACKNOWLEDGMENTS

The work was carried out in the Institute of Rādio Physics and Electronics and the author wishes to acknowledge his indebtedness to Prof. J. N. Bhar for his kind permission to work in the laboratory, and to Dr. S. Deb for guidance. He is also grateful to Prof. S. K. Mitra for his encouragement and help.

REFERENCES

Deb, S. and Goswami, S. N., 1956, *Sci. and. Cult.*, **22**, 283.
Goswami, S. N., 1958, *Ind. Jour. Phys.*, **32**, 35

ELECTRON SCATTERING AND IMAGE CONTRAST IN ELECTRON MICROSCOPY.

P. SADHUKHAN

BIOPHYSICS DIVISION, INSTITUTE OF NUCLEAR PHYSICS, CALCUTTA-9

(*Received for publication, February 18, 1958*)

ABSTRACT. In the present paper, the elastic scattering cross-sections for a 60 k.v. electron beam have been calculated for several different elements from the equations of Moliere and Lenz. The variation of the scattering cross-section with the aperture angle and with the beam voltage has been considered. The inelastic scattering cross-sections for the same elements have also been estimated from Lenz equations. The values of different cross-sections have been compared and their relative importance in the production of contrast in an electron microscopic image has been estimated.

1. INTRODUCTION

The degree of scattering of electrons in a specimen determines the contrast in the image formed by an electron microscope. Thin metallic films are often used for enhancing the contrast of biological specimens, because the electron scattering power of the specimen is then artificially increased due to deposit of heavy atoms on its surface. It is, therefore, important to estimate the contrast to be expected for the deposit of a known thickness of metal vapour.

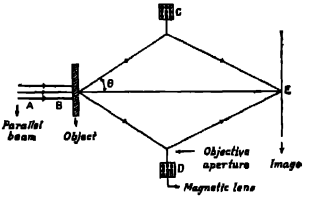

Fig. 1. Elastic cross-section due to Moliere and Lenzfor 60 k.v. electrons as a function of θ for different elements.

In figure 1, a parallel beam of electrons is incident on the specimen The electrons are scattered in all directions and emerge out of the specimen as a divergent beam. The electrons scattered at angles less than θ with the optic axis are allowed by the objective aperture and focussed by the lens on the image plane, while the electrons which are scattered beyond θ are lost to the image.

The scattering by free electrons and multiple scattering are usually neglected in electron microscopic specimens which are normally very thin. The incident

electrons on encountering the specimen are mainly scattered in two different ways :

a) elastic scattering with no energy loss, but change of direction,

b) inelastic scattering resulting in excitation or ionisation of the atom.

The total scattering cross-section is, therefore, given by,

$$\sigma = \sigma_e + \sigma_i \qquad \ldots \quad (1)$$

where, σ_e = elastic scattering cross-section, and σ_i = inelastic scattering cross-section. σ_e and σ_i have been calculated in the following sections for uranium, gold, palladium and chromium —the elements frequently used in shadow casting cross-sections for carbon have also been estimated as all biological materials consist mostly of carbon.

II. ELASTIC SCATTERING CROSS-SECTION

Various elastic scattering formulae have been proposed to estimate the scattering cross-sections. Starting with the theory of differential corss-section of scattering by Williams (1939), Chaudhuri (1952) of this laboratory derived a formula of elastic cross-section. In his review, Von Borries (1949) favoured the formula of Mohere (1947) which is based on Thomas-Fermi atom model. But the formula derived by Lenz (1954) has been found to be in better agreement with experimental results by various investigators [Biberman (1949), Leonhard (1954), Haine and Agar (1956), Kempf and Lenz, 1956]. In this paper scattering cross-sections based on both Mohere and Lenz-equations have been calculated and compared.

a) *Elastic Scattering According to Moliere.*

According to Moliere, for a beam of electrons of energy $e\phi_R$ the differential cross-section of scattering per unit solid angle between an angle θ and $\theta + d\theta$ for fast electrons is given by,

$$\frac{d\sigma_e}{d\Omega} = \frac{d(N/N_0)}{d\Omega}$$

$$= 6.77 \times 10^{-17} \times Z^{2/3} \cdot \left[\sum_{i=1}^{i=3} \frac{a_i}{b_i^2 + \left(\frac{\theta}{\theta_0}\right)^2} \right] \qquad \ldots \quad (2)$$

where,

$$d\Omega = 2\pi\theta \,.\, d\theta.$$

$$a_i = 0.1, \quad 0.55, 0.35$$

$$b_i^2 = 36, \quad 1.44, \quad 0.09$$

$$\theta_0 = \frac{4.17 \times Z^{1/3}}{\phi_R^{1/2}},$$

and θ is defined in figure 1. With the usual aperture diameters of 2.75, 5.5, 27.5, 55 and 275μ and object to aperture distance of 2.75 mm, we get five values of θ viz, 5×10^{-4}, 10^{-3}, 5×10^{-3}, 10^{-2} and 5×10^{-2}

Substituting, $X = \left(\frac{\theta}{\theta_0}\right)^2$,

we get,

$$\sigma_e = \int_\theta^\infty d\sigma_e$$

$$= 4\,255\times10^{-16}\times Z^{2/3}\times\frac{\theta_0^2}{2}\left[\int_0^\infty\left(\sum\frac{u_i}{b_i^2+x}\right)^2 . dx\right]$$

$$= \frac{3.699\times10^{-15}\times Z^{4/3}}{\phi_R}\times\left[\int_\theta^\infty f(\theta, Z, \phi)\right] \qquad \ldots (3)$$

With the help of equation (3), the elastic scattering cross-sections have been calculated for U(92), AU(79), Pd(46), Cr(24) and C(6). For $\phi = 60$ k v. and 5 values of $\theta = 5\times10^{-4}$, 10^{-3}, 5×10^{-3}, 10^{-2}, 5×10^{-2} radians which are frequently used in electron microscopic work. The calculated cross-sections are contained in Table I.

TABLE I

Calculated values of elastic scattering cross-sections (σ_e) from Moliere's equation for different elements and for different aperture angles, ϕ is assumed to be 60 k.v.

ϕ in k v.	θ in radians	Elastic scattering cross section σ_e in 10^{-18} cm^2				
		C	Cr	Pd	Au	U
	5×10^{-4}	1.51	9 60	22.84	47.01	57.63
	10^{-3}	1.50	9.57	22.81	46.95	57.55
60	5×10^{-3}	1 26	8 87	21.69	45.31	55.73
	10^{-2}	0.89	7.36	18.99	41 05	50.94
	5×10^{-2}	0.15	1 83	5.67	14.27	18.46

b) *Elastic Scattering According to Lenz.*

According to Lenz, the differential elastic scattering cross-section per unit solid angle is given by,

$$\frac{d\sigma_e}{d\Omega} = \frac{4Z^2}{a_H^2}\cdot\frac{1}{(q^2+1/R^2)^2} \qquad \ldots (4)$$

where,

$$d\Omega = 2\pi\theta \,.\, d\theta$$

$$a_H = 0.528 \times 10^{-8} \text{ cm.}$$

$$R = a_H \,.\, Z^{-1/3}.$$

$$q = \frac{2\pi\theta}{\lambda}$$

and,

$$\lambda = \frac{12.3 \times 10^{-8}}{\phi_R^{1/2}} \text{ cm.}$$

$$\therefore \qquad d\sigma_e = \frac{8\pi Z^2}{a_H^2} \cdot \frac{\theta d\theta}{(q^2+1/R^2)^2} \,. \qquad \ldots (5)$$

Substituting,

$$q^2 = x, \quad \text{i.e.,} \quad \frac{4\pi^2\theta^2}{\lambda^2} = x; \quad \frac{4\pi^2}{\lambda^2} \,.\, 2\theta d\theta = dx.$$

$$\therefore \quad \theta \,.\, d\theta = \frac{\lambda^2}{8\pi^2} \,.\, dx.$$

$$\therefore \qquad d\sigma_e = \frac{8\pi Z^2}{a_H^2} \cdot \frac{\lambda^2}{8\pi^2} \cdot \frac{dx}{(x+1/R^2)^2} \,. \qquad \ldots (6)$$

$$\therefore \qquad \sigma_e = \int_\theta^\infty d\sigma_e = \frac{Z^2\lambda^2}{\pi a_H^2} \cdot \int \frac{dx}{(x+1/R^2)^2} \,.$$

$$= \frac{Z^2\lambda^2}{\pi a_H^2} \cdot \left[-\frac{1}{(x+1/R^2)} \right]_\theta^\infty = \frac{Z^2\lambda^2}{\pi a_H^2} \left\{ \frac{1}{q^2+1/R^2} \right\} \qquad \ldots (7)$$

TABLE II.

Elastic scattering cross-sections (σ_e) calculated from Lenz's equation for different elements and for different aperture angles, ϕ is assumed to be 60 k.v.

ϕ in k.v.	θ in radians	Elastic scattering cross-section σ_e in 10^{-18} cm^2				
		C	Cr	Pd	Au	U
	5×10^{-4}	0.83	5.25	12.49	25.71	31.50
	10^{-3}	0.83	5.25	12.49	25.70	31.49
60	5×10^{-3}	0.80	5.18	12.39	25.55	31.32
	10^{-2}	0.73	4.97	12.06	25.08	30.80
	5×10^{-2}	0.18	2.20	6.58	15.80	20.11

With the help of equation (7), the elastic scattering cross-sections have also been calculated for the above elements for $\phi = 60$ k.v. and different scattering angles. The calculated cross-sections are contained in Table II.

The results for σ_e by Moliere (Table I) and Lenz (Table II) are shown in figure 2. It has been found that the values of σ_e calculated from Moliere's equation

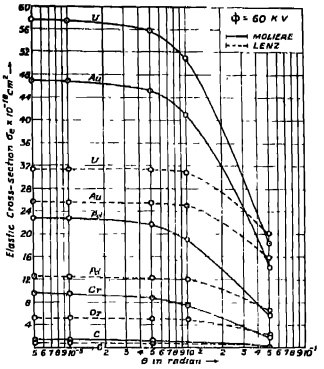

Fig. 2. Inelastic cross-section due to Lenz for 60 k.v. electrons as a function of for θ different elements

are almost double than those of Lenz at small angles. The two values become nearly equal at an angle of 5×10^{-2} radians. The curves also indicate that for angles less than about 5×10^{-3} radians, the elastic cross-sections do not change appreciably with aperture angles.

III. INELASTIC SCATTERING CROSS-SECTION

The atomic electrons will give rise to independent scattering as a result of which they are either raised to a higher level or ejected out of their orbits. The cross-section of this inelastic scattering has been shown by Lenz as.

$$\sigma_i = \int_{\theta}^{\infty} d\sigma_i$$

$$= \frac{2\lambda^2 R^2 Z}{\pi a_H^2} \cdot \left[\frac{1}{2(q^2R^2+1)} + \log_e \cdot \frac{1}{\left(1+\frac{1}{q^2R^2}\right)} \right]_q^{\infty}$$

$$= \frac{2\lambda^2 R^2 Z}{\pi a_H^2} \cdot \left[-\frac{1}{2(q^2R^2+1)} - \log_e \frac{1}{\left(1+\frac{1}{q^2R^2}\right)} \right]$$

$$= \frac{2\lambda^2 R^2 Z}{\pi a_H^2} \cdot \left[\log_e \left(1 + \frac{1}{q^2 R^2}\right) - \frac{1}{2(q^2 R^2 + 1)} \right] \tag{8}$$

with the notations defined in equation (4).

With the help of equation (8), the cross-sections for inelastic scattering have been calculated for U, Au, Pd, Cr and C for 5 values of θ and $\phi = 60$ k.v. The calculated cross-sections are contained in Table III.

TABLE III

Calculated values of inelastic scattering cross-sections (σ_i) for different elements for different aperture angles, ϕ is assumed to be 60 k.v.

ϕ in k v.	θ in radians	Inelastic scattering cross section σ_i in 10^{-18} cm^2				
		C	Cr	Pd	Au	U
	5×10^{-4}	2.05	3.66	4.79	5.96	6.34
	10^{-3}	1.67	3.06	4.03	5.06	5.40
60	5×10^{-3}	0.80	1.66	2.29	2.98	3.20
	10^{-2}	0.46	1.08	1.56	2.09	2 27
	5×10^{-2}	0.04	0 15	0.26	0.42	0.48

Comparing figs.(2) and (3) it will be noticed that the inelastic cross-sections

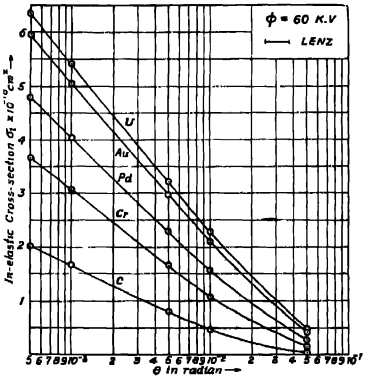

Fig. 3. Elastic and Inelastic cross-sections of Gold due to Moliere and Lenz for aperture angle 10^{-2} radians as a function of beam potential ϕ

for the heavy metals Pd, Au and U are very small compared to the elastic cross-sections. Only in the case of C and Cr, the inelastic cross-sections are comparable to the elastic cross-sections.

IV. VARIATION OF SCATTERING CROSS-SECTION WITH BEAM POTENTIAL

With the help of equations (3), (7) and (8), the cross-sections for elastic and inelastic scattering have been calculated for Au, the metal most frequently employed for shadowing in electron microscopy for $\theta = 10^{-2}$ radians and 4 values of ϕ = 40, 60, 80 and 100 k.v. The results are contained in Table IV, and are also plotted in figure 4 as a function of the beam potential ϕ.

TABLE IV.

Calculated values of elastic (σ_e) and inelastic (σ_i) scattering cross-sections for Gold, for different beam potentials ϕ, θ is assumed to be 10^{-2} radians.

θ in radians	ϕ in k.v.	Scattering cross-section in 10^{-18} cm^2		
		σ_e (Moliere)	σ_e (Lenz)	σ_i (Lenz)
	40	65.58	38 68	3.62
10^{-2}	60	41.05	25 08	2 09
	80	28 98	18 31	1 40
	100	21.89	14 26	1 01

It will be seen from figure 4 that for all voltages the inelastic scattering cross-section is negligible compared to elastic cross-section for gold.

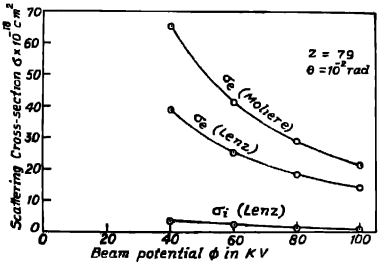

Fig. 4. Contrast diagram due to any thickness of C, Cr, Pd, Au and U—films for 60 k.v. electrons and aperture angle 10^{-2} radians, assuming Moliere's equation of elastic cross-section and Lenz's equation of inelastic cross-section.

V. CONTRAST IN ELECTRON MICROGRAPHS

A specimen of thickness t may be supposed to be divided into infinitesimal

layers of thickness dt, it can then be shown that if I_0 be the incident beam intensity and I_t the transmitted intensity, we have the relation,

$$I_t = I_0 \cdot e^{-nt\sigma(\theta)} \qquad \ldots \quad (9)$$

where $\sigma(\theta)$ is the total cross-section per atom for scattering above a limiting angle θ, and n the number of atoms per unit volume of the specimen. θ is defined by the objective aperture as shown in figure 1.

The contrast g in the image is determined by the difference between the incident and the transmitted beam expressed as the fraction of the incident beam and can be expressed as

$$\begin{aligned} g &= (I_0 - I_t)/I_0 \\ &= 1 - e^{-nt\sigma(\theta)} \\ &= 1 - e^{-\frac{N}{A} \cdot \rho t \sigma(\theta)} \end{aligned} \qquad \ldots \quad (10)$$

TABLE V

Element and atomic number 'Z'	Film thickness 't' in A.U.	Contrast 'g' in percentage (σ_e by Moliere)	Contrast 'g' in percentage (σ_e by Lenz)
	5	11 89	7.57
	10	22 37	14 56
U(92)	15	31.60	21 02
	20	39.73	27.00
	25	46.90	32.52
	30	53.22	37.63
	5	12.01	7.74
	10	22.57	14 89
Au(79)	15	31 87	21.48
	20	40 05	27.56
	25	47.24	33.17
	30	53.58	38.34
	5	6.85	4.59
	10	13.24	8.98
Pd(46)	15	19.18	13.16
	20	24.72	17.16
	25	29.88	20.96
	30	34.68	24.59
	5	3 20	2.03
	10	6.28	4.54
Cr(24)	15	9 28	6.74
	20	12.17	8.89
	25	14.98	10.99
	30	17.69	13.03
	5	0.77	0 68
	10	1 52	1.34
C(6)	15	2.27	2.01
	20	3.02	2.66
	25	3.76	3 32
	30	4.50	3.97

where N = Avogadro number,
A = Atomic weight
ρ = Density of scattering substance in gm. cm^{-3}
t = Thickness in cm.

and, $\sigma(\theta) = \sigma_e(\theta) + \sigma_i(\theta)$, total integral scattering cross-section between $\theta - \infty$.

With the help of equation (10) and the previously calculated values of $\sigma_e(\theta)$ and $\sigma_i(\theta)$, the contrasts corresponding to different film thicknesses are estimated taking both the elastic and inelastic scattering cross-sections into consideration. The results are contained in the Table V. Column 3 of this table shows the calculated values of contrasts based on the cross-section due to Moliere, while column 4 contains the values of contrast to be expected if Lenz equations are valid. Figures 5 and 6 show the contrast values for the elements most frequently used in shadow-casting. These diagrams are the plots of the results contained in Table V with g in per cent taken as abscissa and the corresponding film thickness in Angstroms taken as ordinate.

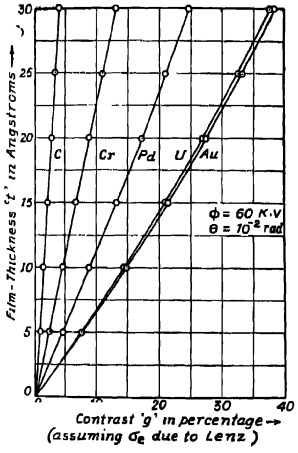

Fig. 5. Contrast diagram due to any thickness of C, Cr, Pd, Au and U—films for 60 k.v. electrons and aperture angle 10^{-2} radians, assuming Lenz's equations of elastic and inelastic cross-sections.

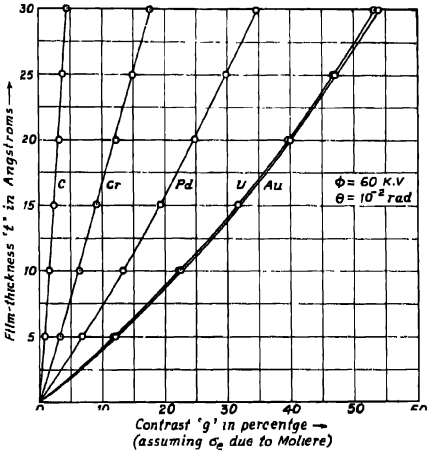

Fig. 6.

VI. DISCUSSIONS

Contrast in the image of an electron micrograph is influenced, in addition to the scattering, by such factors as (a) the spherical aberration of the objective lens

which depends on the angular aperture of the objective, (b) voltage sensitivity of the photographic plate used in recording the image. For the lowest values of the aperture angles, the effect of aberration ($\sim c_s \theta^3$) is negligible and if one decides to work at a fixed accelerating beam potential then obviously the effect of the beam potential on the photographic response need not be considered, So these two factors have been neglected in the present communication; only the effect of scattering of electrons by the specimen has been considered which is the main source of the production of contrast in electron micrograph.

In the light of the results presented in the paper, it is found that if 10% contrast is considered adequate for good representation, then the thicknesses of metals required are given in Table VI.

TABLE VI

Metal and atomic number 'Z'	Film thickness 't' in A.U. from fig. (5)	from fig. (6)
Uranium—92	4 1	6 7
Gold—79	3 8	6.2
Palladium—46	9 8	11 0
Chromium—24	16 2	22.0

Hence from the accurate measurement of contrast with thin films of heavy elements at the lowest value of the aperture angle and at a fixed accelerating beam potential it should be possible to find the relative merits of the two formulations.

ACKNOWLEDGMENTS

The author gratefully acknowledges his indebtedness to Prof. N. N. Das Gupta and Sri M. L. De for suggesting the problem and for their helpful suggestions and to the Ministry of Education, Government of India for the award of a Research Training Scholarship.

REFERENCES

Borries, B. V., 1949, *Z. Naturforsch*, **4a**, 51.
Biberman, L. M., *et al* 1949, *C. R. Akad. Sci. U.S.S.R.*, **69**, 519.
Chaudhuri, A. K., 1952, *Proc. Nat. Inst. Scie. Ind.*, **18**, 585.
Haine, M. E. and Agar, A. W., 1956, Electron Microscopy, Proc. Stockholm Confc., 1956 (Almqvist & Wiksell, Boktryckeri Aktiebolag, Uppsala, 1957), pp. 64.
Kempf, G. and Lenz, F., 1956, Electron Microscopy, Proc. Stockholm Confc., 1956 (Almqvist & Wiksell, Boktryckeri Aktiebolag, Uppsala, 1957) pp. 67.
Lenz, F., 1954, *Z. Naturforsch*, **9a**, 185.
Leonhard, F., 1954, *Z. Naturforsch*, **9a**, 1019.
Moliere, G., 1947, *Z. Naturforsch*, **2a**, 133.
Williams, E. J., 1939, *Proc. Roy. Soc., A*, **169**, 531.

NEW EVIDENCE FOR A PARTICLE OF MASS ~ 525 m_e

NILIMA BASU AND M. S. SINHA

BOSE INSTITUTE, CALCUTTA

(*Received for publication, March* 28, 1958)

ABSTRACT. While photographing stopped muons in a multiplate cloud chamber at Calcutta (sea level 12°N) nine pictures were obtained in which the rate of change of ionisation of the particles and their residual ranges were not compatible with that shown either by mu-mesons or by protons. Their mass values were obtained by measuring their change in ionisation in the successive gaps and their decrease in residual ranges. Ionisation was measured by drop counting. It was found that five of these particles gave an average mass value 528 ± 34 m_e and the remaining four an average of 280 ± 21 m_e. The close proximity of the latter value with the pion mass is a strong indication for the correctness of the method employed. A probable decay event of the particle of mass ~ 528 m_e has also been given.

1. INTRODUCTION

The experiments of Alikhanyan *et al.* (1948) and his collaborators at an altitude of 3250 mertes with several sets of G.M. counters and lead absorbers placed in a magnetic field indicated for the first time the possible existence of mesons of various masses as deduced from their magnetic deflections and residual ranges. The same group of workers also confirmed this evidence from observations in photographic plates In 1952 a few events were obtained by Shapire (1952) and Perkins (1952) in photographic emulsions in which a primary particle of mass $\sim 525\, m_e$ was observed to undergo a small deflection after which the average scattering of the particle increased two fold pointing to a decrease in mass by a factor of two. These authors interpreted the data as the decay of a particle which was called $\zeta^{\pm}$ according to the mode

$$\zeta^{\pm} \rightarrow \pi^{\pm} + \pi^{0} + Q(\text{a few Mev}) \tag{1}$$

Later, Daniel and Perkins (1954) stated that all such events, except only one, could be explained as a normal spread of mass values centred on the pion mass. There were, furthermore, three cases obtained by Leighton and Wanlass (1952) in a cloud chamber operated in a magnetic field where a visual estimate of ionisation and measured momentum gave the mass value 450 ± 150, 550 ± 150, 750 ± 150 of which the first two are highly incompatible with either the pion or the K-meson mass. Three doubtful cases of the existence of such particles have been reported by Inoki *et al.* (1957) from the study of slow meson masses.

Recently an investigation was carried out by the authors (1957) to determine the slow meson intensity at Calcutta (12°N) by stopping these particles in a multi-

plate cloud chamber fitted with five half inch Cu-plates and triggered by a three-fold coincidence cum anti-coincidence method. In course of analysis of the pictures nine cases were observed, where the change in ionisation of the track of the particle from gap to gap was much slower than that of a normal mu-meson but more rapid than that of a proton or a K-meson. The ionisation produced by these particles was estimated by drop counting in the different gaps and the mass of each particle was determined by two methods, which although slightly interdependent, help to reduce the statistical error. It is found that five of these particles exhibit a mean value of mass 528 ± 34 m_e and the remaining four a mean value 280 ± 21 m_e. The close proximity of the mass value of the second group with the pion mass appears to be a strong evidence for the correctness of the method. A preliminary report has been given by the authors (1958) in *Science and Culture*, March, 1958.

2. THE METHOD

The change in ionisation of a singly charged particle on passing through a certain thickness of matter can be easily converted into the corresponding change in $p/\mu (= \beta/\sqrt{1-\beta^2})$ of the particle from one side of the plate to the other from the $I/I_m - p/\mu$ curves (figure 1). We then use the following equation of Rossi and Greisen (1941) valid for a small momentum interval.

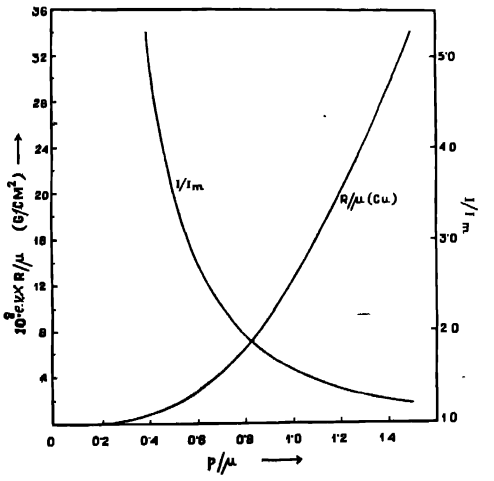

Fig. 1.

$$\Delta R = R\left(\frac{p_2}{\mu}\right) - R\left(\frac{p_1}{\mu}\right) = \frac{M}{2CB}\left[\frac{(p_2/\mu)^2+2}{\{(p_2/\mu)^2+1\}^{\frac{1}{2}}} - \frac{(p_1/\mu)^2+2}{\{(p/\mu)^2+1\}^{\frac{1}{2}}}\right] \quad \ldots \quad (2)$$

where ΔR is the thickness in g/cm² of the plate, on passing through which the ionisation of the particle changes by such an amount as to reduce the value of its p/μ from p_2/μ to p_1/μ. M is its mass in electron mass units, C is a constant for the material used and B is a slowly varying function of p/μ. For copper, the material used in this cloud chamber,

$$C = 6.84 \times 10^{-2} \text{ and } B = 15.71 + 9.21 \log_{10}(p/\mu) - \frac{2}{1+(p/\mu)^{-2}}$$

It should be noted that ΔR is known accurately and the accuracy of the value of the mass determined from equation (2) essentially depends on the accuracy with which the ionisation of the particle can be measured in the different gaps and the number of gaps available for such measurement. It should also be emphasised that this method of mass determination is quite unsuitable for very heavy particles, such as protons where the change in ionisation from plate to plate is quite small and also for very light particles such as mu-mesons where the number of gaps available for measurement (after $I/I_m > 1.5$) is one or atmost two. But, for a particle of mass $\sim 500\ m_e$, the change in I/I_m as well as the number of gaps in which such changes can be estimated are optimum for the determination of the mass from equation (2).

First of all drop counting was made on thirty selected mu-meson tracks of uniform minimum ionisation which showed less than 0.5° of scattering in all the five half inch copper plates inside the chamber. They were obtained by triggering the chamber with 3-fold coincidence only. The track in each gap was divided into about thirty cells of length equal to the width of the track and the number of drops in each cell was counted after magnifying the track to eight times its actual dimension at the time of formation. Back-ground counts of silver grains were made on both sides of the track at the same time and subtracted from the total counts per cell on the track. The statistical fluctuation of the background counts was small and uniform and the overall statistical error in the final counts per cell of the thirty minimum ionisation tracks was less than 6%. Whenever a portion of minimum ionisation track was available in the picture containing the heavy track, drop counts were made on it and found to agree with the value obtained from the measurement on the thirty mu-meson tracks. The cloud chamber pressure, the delay of light flash, and the developing procedure of the film were kept uniformly constant throughout the experiment. Out of about five hundred particles stopped inside the cloud chamber the rate of change of ionisation in the successive gaps was apparently smaller than that of mu-mesons in nine cases. Seven of the particles stopped in the fourth plate and two in the third plate and in

each of them drop counts were made on both the stereo views in all the gaps Back ground counts made on the same negative on the two sides of the track were

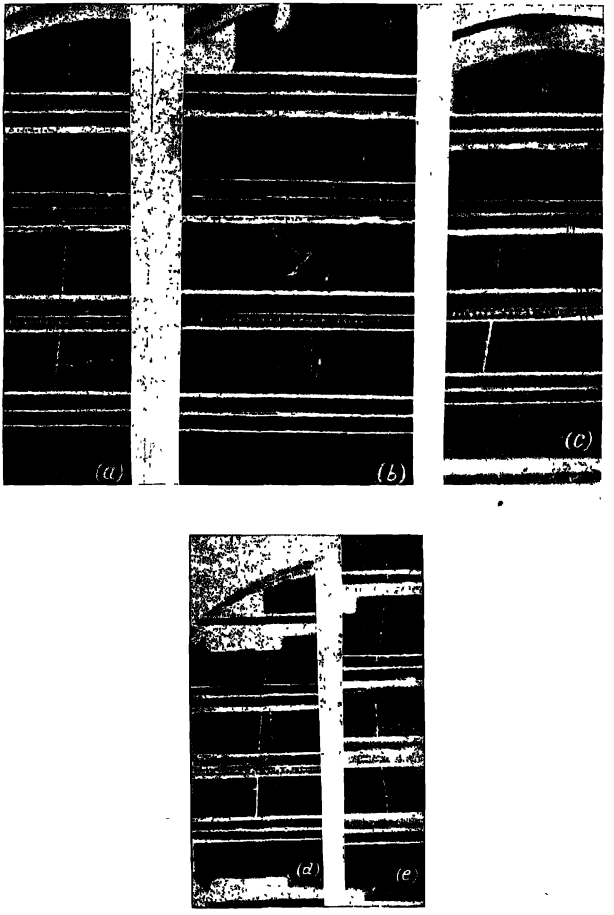

Fig. 2.

then subtracted and the resulting number of drops per unit cell found out. The ratio of the average count in any gap to the average count for the thirty mu-meson tracks was taken to be the ionisation of the particle in that gap. The

chamber gas was argon and the number of ion-pairs produced per cell was so high that the error due to overlap of drop images was more than fifteen per cent when the track showed more than three times minimum ionisation and no attempt at estimation of ionisation was made above this value. The values of ionisation of the nine particles in the different gaps obtained in this way are given in Table I.

All the five tracks of the heavy particles are shown in figure 2(a), (b), (c) (d) and (e) and two of the lighter tracks which gave mass values close to the pion mass are shown in figure 3(a), (b) of which the latter shows a visible decay electron. It will be seen from Table I, that although seven of the nine particles stopped in the fourth plate, ionisation measurements in the fourth gap were too high to be measured in two cases. Measurements on the first gap of those tracks which were near minimum in those portions were not carried out extensively. Measurement in gap 2 of picture no. 11505 could not be made owing to the distorted nature of the track in this gap.

Fig. 3.

All these ionisation estimates were then converted into p/μ values from the $I/I_m - p/\mu$ curve (figure 1) valid for an argon filled chamber. From Table I we find that at least three such p/μ values were available for each particle which provided us with three independent estimates (12, 23, 13) of the mass value from equation 2. Obviously p/μ values have asymmetric statistical errors and so

TABLE I

Ionisation estimates of nine particles

Picture number	Value of I/I_m above plate number			
	1	2	3	4
11505	1.46 ± 0.15		2.02 ± 0.18	2.92 ± 0.22
12050		1.61 ± 0.13	1.01 ± 0.18	2.54 ± 0.20
8610	1.52 ± 0.14	1.70 ± 0.17	2.65 ± 0 23	
2700	1.59 ± 0.16	1.94 ± 0.18	2.60 ± 0.20	
3705		1.47 ± 0.17	1.79 ± 0.19	2.31 ± 0.20
1605	1.33 ± 0.11	1 57 ± 0.12	2.74 ± 0.21	
12616	1.40 ± 0.12	1.66 ± 0.14	2.70 ± 0.20	
1715		1.32 ± 0.11	1.65 ± 0.14	3.18 ± 0.32
3700		1.34 ± 0.18	1.76 ± 0.20	3.11 ± 0 34

also these three individual mass values, which together with their six extreme values were combined to obtain an average mass for the particle and its standard deviation. These average values are shown in column two of Table II.

It is well known that apart from the error in counting and the error due to overlap of the drops in highly ionising tracks, the ionisation process itself is a statistically fluctuating phenomenon, and the correction due to this was incorporated in the following way. The p/μ values obtained for the various gaps were converted to R/μ values for Cu (shown in figure 1) and then for each gap the total expected residual range of the particle was found out from the mean value of the mass obtained for that particle in the above manner and its R/μ value for that gap. In this way the expected residual ranges of a particular particle after each of three gaps were known from the ionisation in these gaps and since the thickness of each plate is known accurately, the data gave us the mean expected range of the particle in the plate in which it stopped. It should be noted that in obtaining the range of the particle in the *last plate* we have taken into account the ionisation of the particle in at least three gaps and the mean of this range is given in column 3 of Table II. The experimental residual range at any gap is now fixed, being the total matter subsequently passed through by the particle plus its mean range in the last plate as obtained above.

If we now combine the R/μ values as obtained from figure 1 from the ionisation estimates of the particle in each gap with its experimental residual range corresponding to that gap we shall get a value of the mass of the particle. We have given in column 4, Table II, the mass values obtained by the second method.

The two mass values thus obtained for each particle are then combined and the mean with its standard deviation given in the fifth column. It will be seen that the mean values obtained for the first five particles (first group) are highly incompatible with the mass of a pion or a K-meson, whereas the mean values obtained for the last four particles (second group) are quite consistent with the pion-mass. We have lastly assumed that the particles in the first group have actually the same mass and so also those in the second group and a grand mean for the two groups is given in the last column with its *probable error* as computed from the whole data for that group.

TABLE II

Mass values of the nine particles

Picture number	ΔR—$\Delta(p/\mu)$ method m_e	Range in last plate (g/cm² of Cu)	R–R/μ method m_e	Mean mass m_e	Grand mean m_e
11505	538 ± 171	8.5	607 ± 141	572 ± 91	
12505	568 ± 120	11.0	610 ± 120	589 ± 65	
8610	484 ± 210	0.7	573 ± 210	528 ± 123	528 ± 34
2700	483 ± 187	0	584 ± 156	533 ± 103	
3705	416 ± 156	8.6	426 ± 102	421 ± 76	
1605	250 ± 70	4.1	259 ± 45	254 ± 21	
12615	317 ± 69	4.8	328 ± 65	322 ± 26	
1715	256 ± 65	2.8	273 ± 61	264 ± 26	280 ± 21
3700	271 ± 79	3.0	291 ± 85	281 ± 32	

Annis, Bridge and Olbert (1953) have indicated a method of rough estimation of mass of particles stopping inside a multiplate cloud chamber by measuring the projected angle of multiple scattering in a certain plate and the residual range of the particle at that plate. The values of the product $\eta^2 = \phi^2 R^{2\alpha}$ for each plate was computed, where ϕ is the projected angle of scattering in a certain plate, R the residual range at the scattering plate and $\alpha = 0.55$ for all elements. The average value of η^2 for a large number of scatterings is found out and then equated to a theoretical expression which is a function of the mass of the particle, the thickness of the scattering material and a factor which is constant for a particular scatterer. Although this method is not very accurate even when at least seven or more scattering angles are available, we made an attempt to find in this way the mass of the particle in group one above by measuring the three projected angles of scattering and the residual ranges. The final mean value of the mass so determined is 537 m_e with an as symmetric statis-

tical error of nearly 20 per cent, if we assume that all the particles in group one are of the same mass, and exclude the scattering of the particle 2(b), 12505 in the third plate which is too high to be due to multiple scattering. The general agreement of this value with the grand mean of group one particles in Table II is a strong support for the contention that the particles do exhibit a mass value $\sim 525 m_e$.

Lastly, we want to mention that if the particle actually has a decay mode given by equation (1) it will be hard to observe the charged decay product in a multiplate cloud chamber since the resulting $\pi\pm$ will have a small range. The π^0 can however under suitable conditions be recognised by its subsequent decay into two photons and their resultant electron cascade. It is very interesting to note that the stopping of the particle (12505) in figure 2(b) in the fourth plate results in a heavy particle coming up towards the right which is stopped in the first plate it enters into and there is a pair of soft electrons towards the left. The heavy particle may be interpreted as the low energy pion and the pair of electrons the effect of π^0. Alikhanyan *et al.* (1956) have also observed a pair of electrons coming out in two cases from the point of stopping of such a particle. These authors further report that particles of mass $\sim 550 m_e$ always appeared singly in their chamber and this agrees well with our observations that all the five particles have entered the chamber unaccompanied by any secondary.

ACKNOWLEDGMENTS

This work was performed with financial support from the A.E.C., Government of India. The authors are indebted to Dr. D. M. Bose, Director, Bose Institute for his constant advice and encouragement.

REFERENCES

Alikhanyan, A I., *et al.*, 1948, *J. Exp. Theor. Phys.*, **18**, 673.
Alikhanyan, A. I. *et al.*, 1956, *ibid*, **31**, 955.
Annis, M., Bridge, H. S. and Olbert, 1953, *Phys. Rev.*, **89**, 1216.
Basu, N. and Sinha, M. S., 1956-57, *Trans. Bose Res. Institute*, 21.
Basu, N. and Sinha, M. S., 1958, *Science and Culture*, **23**, 496.
Daniel, R. R. and Perkins, D. H., 1954, *Proc. Roy. Soc. A.*, **221**, 365.
Inoki, M., Yasaki, T., Machida, M. and Matsukairu, Y. 1957, *Phys. Rev.*, **105**, 1872.
Leighton, R. B. and Wanlass, S. D., 1952, *Phys. Rev.*, **86**, 426.
Perkins, D. H., 1952, Third Annual Rochester Confer, Report 72.
Rossi, B. and Greisen, K. 1941, *Rev. Mod. Phys.*, **13**, 248.
Shapiro, M., 1952, Third Annual Rochester Conference Report, p. 71.

AUTOMATIC RECORDER OF THE WAVEFORMS OF ATMOSPHERICS

B. A. P. TANTRY

BANARAS HINDU UNIVERSITY

(*Received for publication, November* 1, 1957)

ABSTRACT. An automatic atomospherics recorder was constructed for recording the electric field-changes during the various lightning discharges. It consisted of several suitable units which were designed for obtaining complete, accurate and non-overlapping oscillograms with minimum waste of the recording film. The details of the component units and of the various associated circuits are described in the paper.

INTRODUCTION

For studying the waveforms of atmospherics, an automatic recorder was designed and constructed in the laboratory. The main object was to obtain a full and faithful record of the electric field-changes during the various lightning discharges. It was therefore necessary to set up several suitable units for delineating and photographing the electric field-changes on the fluorescent screen of a cathoderay oscillograph after suifficient amplification without distortion and adequate time-resolution. Suitable trigger circuits were constructed and employed for the intensity-modulation of the oscillograph. Necessary circuits were set up for recording the initial part of the electric field variation which was of small magnitude. Arrangements were also made for avoiding overlapping of the oscillograms and for the automatic recording of the electric field-changes during the lightning discharges.

COMPONENT UNITS IN THE ATMOSPHERICS RECORDER

The various component units were not constructed in their final form at the same time. Some of the circuits were developed by stages after testing the performance of the entire equipment. No attention is, therefore, paid to the chronological sequence in describing the various associated circuits of the different units.

In what follows, we shall describe the different units of automatic atmospherics waveform recorder.

1. AERIAL UNIT

In the earlier experimental studies of the waveforms of atmospherics, an open-air horizontal aerial of effective height, 12 metres, and self-capacity, 265 $\mu\mu F$, was used as the receiving antenna, but in the later investigations, a smaller

aerial of similar type with an effective height of 4 metres and self-capacity of 100 $\mu\mu F$. was employed. The vertical leads from the aerial were led into the observation room through proper insulators and they were well shielded to reduce the 50-cycles hum from the power mains.

A resistance R of $1k\ \Omega$ and a condenser C_1 of capacity, $0.001\mu F$, (figure 1 were placed in series with the aerial, so that the latter was rendered aperiodic

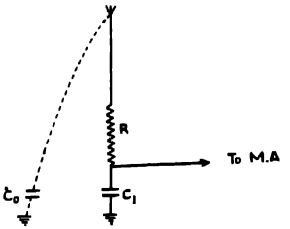

Fig. 1. Aerial unit.

with a time-constant which was small in comparison with the duration of the atmospherics.

2. MAIN AMPLIFIER

A wide-band, R-C coupled, Class A, three-stage voltage-amplifier, having a flat frequency-response from 100 c/s to 100 kc/s was constructed and used as the main amplifier. Two 6AC7 (V_1 and V_2) valves, each having a high figure of merit were used in the first and the second stage of the amplifier, whereas a power pentode, 6AG7 (V_3), was found very suitable as an output valve. As these high-transconductance pentodes are quite microphonic, the whole amplifier was fitted with rubber cushions in order to protect it from mechanical vibrations. Due care was taken about the lay-out and the wiring of the amplifier to reduce the pick-up of the 50-cycles hum by the amplifier.

For the manual control of the total gain (80 db) of the amplifier, two calibrated carbon potentiometers were used as grid-leak resistances in the first and the third stage of the amplifier. The phase-shift distortion measured oscillographically and the amplitude distortion determined by the 'fundamental supression method' were found to be negligible in the useful frequency range of the amplifier.

The detailed circuit diagram of the amplifier is shown in figure 2.

3. SQUARE-WAVE TRIGGER UNIT

For recording the oscillograms without over-lapping, the intensity- modulation of the cathode-ray oscillograph required for making it operative only on the

arrival of the atmospherics, was effected with the help of a positive square-wave trigger circuit in the following manner :

A part of the output voltage from the main amplifier adjustable by means of a potentiometer was fed into a single stage $R-C$ coupled triode (V_4—6SC7) amplifier, the output of which was connected to a cathode-follower phase-inverter

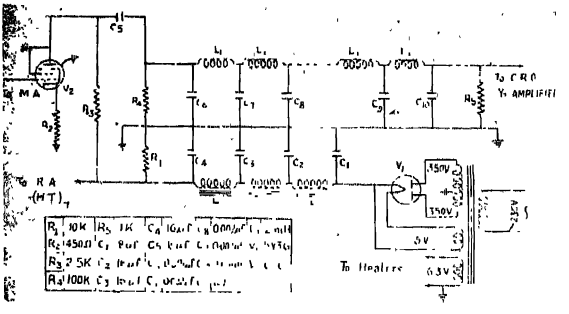

Fig. 2. Main amplifier.

(V_5—6L6). The input of the latter could thus be adjusted to any desired level without disturbing the gain of the main amplifier. The balanced output voltages (with respect to the ground) from the phase-inverter were so fed into a double-diode (V_8—6H6) *via* two peak-clippers (V_6, V_7—6L6), that whatever might be the polarity (positive or negative) and the amplitude of the initial portion of the atmospherics pulse, a positive voltage of almost fixed value (nearly 40 volts) was developed between the cathode of the diode and the ground. The output voltage from this double diode was then applied to a univibrator (V_9—6SN7) which remained quiescent until its action was initiated by a positive voltage of about 40V at its input. The univibrator was so arranged as to have a *quasi*-stable state of controllable time from 0.5 to 2.0 seconds. The rectangular voltage output from the univibrator was differentiated and then applied to a clamping circuit with a diode, (V_{10}—6H6), from which only the sharp positive pulse was derived which was utilised to trigger another univibrator (V_{11}—6SN7) the output of which gave a rectangular pulse of about 40V with a *quasi*-stable state of about 6 milli-seconds. This was applied to the modulating grid (usually kept at a high negative potential with respect to the ground) of the cathode-ray oscillograph thus allowing in cathode-ray beam to reach its full brilliance during the *quasi*-stable state of the pulse.

During the *quasi*-stable state of the first univibrator, lasting for a time of 0.5 to 2.0 seconds, no further intensity-modulating pulse could be derived from the subsequent atmospherics. The entire triggering circuit would thus have a

quiescent time of the same duration after each triggering pulse, preventing thereby overlapping of oscillograms.

The detailed circuit diagram of the whole square-wave triggering unit is shown in figure 3.

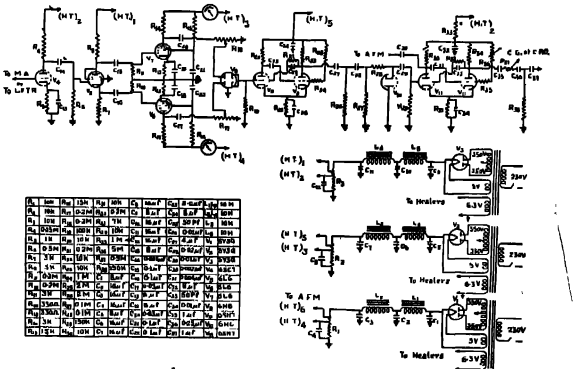

Fig. 3. Square-wave trigger unit.

4. DELAY LINE UNIT

As a square-wave trigger unit would require a positive voltage of predetermined value, there must be a definite time-lapse between the arrival of the atmospherics pulse and the restoration of the brilliancy of the cathode-ray beam, the magnitude of the time delay depending upon the initial rise-time of the wave-form of an atmospherics pulse. Hence in order to restore the initial portion of the wave form lost in the oscillographic record, before triggering, it was necessary to delay the signal by about 60μs, whereas the undelayed signal was used for triggering the square-wave trigger unit.

The delay-line was of a negligible rise-time and was of the form of a low-pass, ladder-type filter having 30 sections. The theoretical cut-off frequency of the delay line was kept as high as 150 kc/s, so that negligible phase distortion would be introduced in the useful frequency spectrum of the transmitted pulse. Because of the low normal characteristic impedance of the delay-line, an impedance-matching amplifier was introduced between the delay-line and the main amplifier. The impedance-matching amplifier was essentially a cathode-degenerated *R-C* coupled voltage-amplifier with a very small coupling resistance. A high transconductance valve (6L6), used as a triode, was found suitable as an amplifier tube, since it could accommodate a large signal voltage with negligible distortion in the output voltage.

The circuit diagram of the delay-line unit is shown in figure 4.

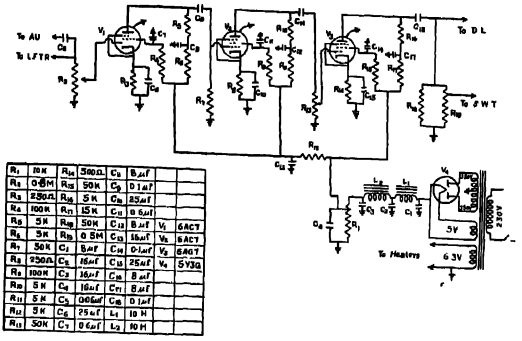

R_1	10K	R_{14}	500Ω	C_9	8 μμf		
R_2	0·5M	R_{15}	50K	C_{10}	0·1 μf		
R_3	250Ω	R_{16}	5K	C_{11}	25 μμf		
R_4	100K	R_{17}	15K	C_{12}	0·6 μf		
R_5	5K	R_{18}	50K	C_{13}	8 μf	V_1	6AC7
R_6	5K	R_{19}	0·5M	C_{14}	16 μμf	V_2	6AC7
R_7	50K	C_1	8 μf	C_{15}	0·1 μf	V_3	6AG7
R_8	250Ω	C_2	16 μf	C_{16}	25 μμf	V_4	5Y3G
R_9	100K	C_3	16 μf	C_{17}	8 μf		
R_{10}	5K	C_4	16 μf	C_{18}	8 μμf		
R_{11}	5K	C_5	0·05 μf	C_{19}	0·1 μf		
R_{12}	5K	C_6	25 μf	L_1	10 H		
R_{13}	50K	C_7	0·6 μf	L_2	10 H		

Fig. 4. Delay line unit.

5. OSCILLOGRAPH UNIT

A Cossor double-beam oscillograph (Model No. 1035) with a cathode-ray tube of flat blue fluorescent screen was employed very successfully for recording the waveforms of atmospherics. Usually the atmospherics signal from the delay-line was given to the Y_2-amplifier of the oscillograph.

Puckle's hard-valve linear time-base of the oscillograph was found suitable as X-sweep, because of its perfect linearity in the useful range of the sweeps. The time-range switch of the oscillograph would allow the variation of the transverse speed, the duration ranging from 15 microseconds to 150 milliseconds. The required transverse speeds were previously calibrated with the help of a standard audio-oscillator, employing the frequency comparator principle. The fly-back suppression was made inoperative in order to trace the course of the horizontal lines in the raster arrangement.

6. RASTER ARRANGEMENT

In the raster arrangement there was a linear time-base using a thyratron (V_2—884 R.C.A.) followed by a two-stage *R-C* coupled amplifier. The first stage of the latter worked as a voltage-amplifier (V_3—6AC7) and the second stage was an impedance-matching amplifier (V_4—6L6, used as a triode) similar to the one which was used in the delay-line unit. The linear time-base of the cathode-ray oscillograph would by itself deflect the cathode-ray spot horizontally. When the raster linear time-base with a period which was an integral multiple of that of the horizontal sweep was applied simultaneously to the vertical deflector plates of the cathode-ray oscillograph, several horizontal lines, one above another, were swept out and exhibited on the fluorescent screen of the oscillograph. Since the output from the main amplifier was applied to the same vertical

deflector plates of the oscillograph through the delay-line unit, any electrical field-change due to an atmospheric pulse would produce a corresponding vertical deflection on the raster lines.

The purpose of the raster arrangement was to provide for the longer duration of the oscillographic records without overlapping, at the same time permitting a greater time-resolution in the waveform observations.

The detailed circuit diagram of the above arrangement is shown in figure 5.

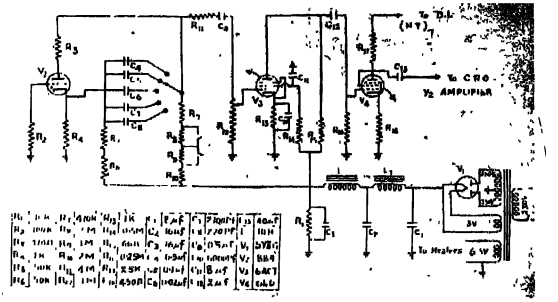

Fig. 5. Raster arrangement

7. AUTOMATIC FILM-MOVING UNIT

The function of the automatic film-moving unit was to move the photographic film forward through a distance of about 2 cms after each exposure and its working may be briefly explained as follows :

The intensity-modulating pulse derived from the square-wave trigger unit was differentiated and applied to a diode-clamping circuit, the output of which gave a positive pulse which was used to trigger a univibrator. A solenoidal relay placed in the plate circuit of the cut-off valve of the univibrator was energised during its *quasi*-stable state, thus completing the power supply of a capacitor-

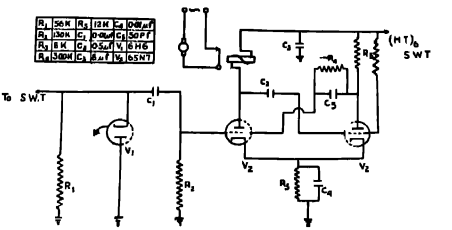

Fig. 6. Automatic film-moving unit.

type motor which was free from electrical interference and fitted with a reducing gear system. The motor-drive was transmitted to the spindle of the camera unit through a friction-clutch, so that the exposed film could be automatically moved forward about 2-cms distance during the *quasi*-stable state of the univibrator.

The circuit diagram of the automatic film-moving unit is shown in figure 6.

8. CAMERA UNIT

The camera unit consisted of a F/1.9 lens of 10.4 cm focal length with which the oscillograms could be photographed continuously, either manually or automatically, on a perforated 35 mm film with the image reduction ratio of 3.6. The exposed film moved forward by the conventional sprocket-drive method. Actually the body of the camera unit contained a main casting locating the driving sprockets, the guide rollers and a film driving spindle which could be coupled to the motor-drive unit.

While taking observations, the camera shutter was kept open and the fluorescent screen of the oscillograph kept blank with the help of the 'intensity-control' knob, so that the oscillograph would be intensity-modulated only on the arrival of the atmospherics, with the result that the oscillograms would be exposed to the film without any delay. After each exposure, however, the exposed film would move forward automatically by the automatic film-moving unit, so that the unit would be ready for recording the subsequent oscillogram.

9. LOW-FREQUENCY TUNED AMPLIFIER

This unit was essentially a narrow-band low-frequency tuned receiver having a maximum gain of 65 db. The receiver was a transformer-coupled amplifier (V_2—6AC7) with a tuned secondary, tunable to any frequency between 14 kc/s to 18 kc/s. The output of this stage was coupled to a conventional *R-C* coupled amplifier (V_3—6SJ7). A cathode-follower (V_1—6SJ7) with a step-attenuator as an input stage to the amplifier provided a high input impedance to the receiver, so that the receiver when coupled to the aerial unit in parallel with the main amplifier would offer negligible shunting effect to the main amplifier.

The purpose of the unit was to develop any rapid electrical variations, in the initial portion of an atmospheric pulse, to an extent sufficient to trigger the square-wave trigger circuit for intensity-modulating purposes. This kind of triggering was found at times advantageous (especially when the electrical noise in the locality of the equipment was higher than usual) over the usual method of triggering which has already been described. Being a tuned receiver, it was capable of discriminating the low-frequency electrical noise from the atmospherics pulses, so that the high electrical noise was unable to trigger the square-wave trigger unit. As a consequence the wastage of the film was avoided.

The circuit diagram of the low-frequency tuned amplifier is shown in figure 7.

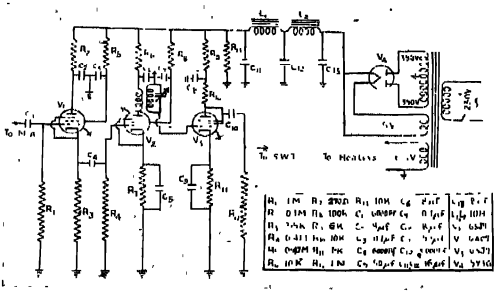

Fig. 7. Low frequency tuned amplifier.

10. TRANSIENT GENERATOR UNIT

In this unit, a condenser was charged and then discharged through a suitable inductance in series with a suitable resistance by means of make-and-break key. The L-C-R of the circuit was so adjusted that the discharge was oscillatory giving a *quasi*-period of about a millisecond. This unit was found very useful for periodical testing of the performance of the automatic atmospherics recorder.

A block diagram of the automatic atmospherics waveform recorder, indicating its various units is shown in figure 8. A few oscillograms representing electric field-changes during lightning discharges are shown in figure 9.

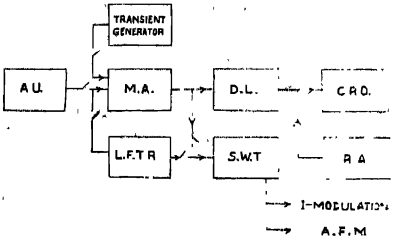

Fig. 8. Block diagram of the automatic waveform recorder.

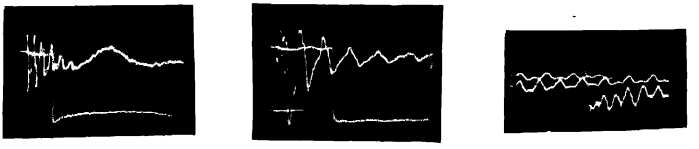

Fig. 9. Oscillograms representing electric field-changes during lightning discharges.

CONCLUSION

The automatic atmospherics waveform recorder described above was employed successfully in the investigations on the wave-forms of atmospherics since 1952. A preliminary report of the recorder in the early stage of its development was already published by the author (Tantry, 1952). The construction of the recording equipment was initiated as early as July 1950, so that some of the circuits which are in some respects similar to those employed by Clarke and Mortimer (1951) and Caton and Pierce (1952) were designed almost about the same time.

ACKNOWLEDGMENTS

The work was carried out under a Research Project sponsored by the Council of Scientific and Industrial Research. My thanks are due to the C.S.I.R. for the Research Assistantship held by me for two years. I am also grateful to Prof. S. R. Khastgir, D.Sc., F.N.I. for his guidance and help. I also sincerely thank Mr. R. S. Srivastava, M.Sc. for his collaboration in a part of the constructional work.

REFERENCES

Caton, P. G. F. and Pierce, E. T., 1952, *Phil. Mag.*, **43**, 393.
Clarke, C. and Mortimer, D. E., 1951, *Wireless Engineer*, 406.
Tantry, B. A. P., 1952, *Jour. Sc. & Indust. Res.*, **11B**, 218.

ON THE THERMAL NEUTRON CAPTURE CROSS-SECTIONS

H. S. HANS AND M. L. SEHGAL

DEPARTMENT OF PHYSICS, MUSLIM UNIVERSITY, ALIGARH

(*Received for publication, March 17, 1958.*)

ABSTRACT. Experimental and theoretical values of thermal neutron capture cross-sections have been compared for a number of cases. An attempt is made to explain the discrepancy in many cases. It is proposed that in the case of Ag^{107}, Ni^{62}, In^{113}, Hg^{199}, Mo^{97}, and Hf^{179}, there exist negative energy levels close to zero energy. Radiation width in the case of Co^{59} is considered to be 0.6 ev, instead of 0.2ev as given by Segrè.

1. INTRODUCTION

Thermal neutron absorption as well as activation cross-sections have been more or less exhaustively measured. They have been tabulated in the AECU-2040 (1955) report. It is possible to evaluate exactly the thermal neutron capture cross-sections theoretically, if the various parameters of the resonances near the zero energy are exactly known. Breit-Wigner single level dispersion formula should be valid in most of these cases, where resonances are separated enough to neglect any interference effects It will be interesting to compare the experimental and theoretical values of these cross-sections. Any discrepancy between these values should reveal that either the information about the parameters of the nearest known resonances is inadequate or there are still other resonances on the positive or negative side of the zero energy.

2. DISCUSSION

In Tables I and II are presented the theoretical and experimental values of thermal neutron capture cross-sections at 0.025ev. The experimental values are invariably taken from AECU–2040 (1955) report . The theoretical values are calculated from Breit-Wigner single level formula (Blatt and Weisskopf, 1952).

$$\sigma_0(n, \gamma) = \frac{g\lambda_0^2}{4\pi} \frac{\Gamma_n \Gamma_\gamma}{(E_0 - E_r)^2 + (\frac{1}{2}\Gamma)^2} \left(\frac{E_0}{E_\gamma}\right)^{1/2}$$

where $\sigma_0(n, r)$ is the cross-section at 0.025ev; g is the statistical weight factor; λ_0 is the neutron wave length at 0.025 ev Γ_n and Γ_γ are the neutron and the radition widths of the reasonance under consideration; $E_0 = 0.025$ev; E_r is the resonance energy in electron volts and Γ is the total width given by

$\Gamma = \Gamma_n + \Gamma_\gamma + \ldots$. Interference effects due to the nearness of two levels of the same J and parity are, of course, neglected. The sources from which the values of various parameters are taken are given in the tables.

Table I represents those cases where the ratio R is 1 within the uncertainties involved either in the resonance parameters used in the Breit-Wigner formula or in the experimental values of σ_0. In cases where I the total angular momentum of the target nucleus is very much greater than one, the value of J is taken to be $I+\frac{1}{2}$ which anyhow does not differ very much from the value $I-\frac{1}{2}$. The values of J of the compound nucleus of other cases given in Table I are normally taken from the existing literature.

In Table II are listed those cases for which the ratio R is generally quite different from 1. In the first three cases i.e. Hf^{177} I^{127}, and Tb^{159}, it is found that the contribution to σ_0 from resonances other than the nearest one is comparable to the first one. The case of I^{127} is of particular interest where the contribution from the first level is hardly ten per cent of the total value. While in the case of Hf^{177} the experimental σ_0 is fully explained by taking into account the other resonances, the discrepancies in Tb^{159} and I^{127} are still unexplained. It appears possible that negative energy levels may be contributing appreciably in these cases. Other cases in this table cannot be explained by the known positive energy resonances even taking into account the experimental uncertainties involved. Careful consideration of the resonances of Ag^{107}, Ni^{62}, In^{113}, Hg^{199} and

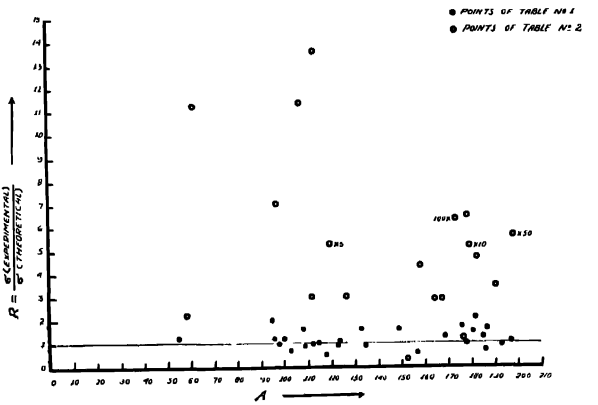

Fig. 1

Mo^{97} where the value of R is very high, suggests very strongly the existence of negative energy resonances. In the case of Ag^{107} and Hg^{199} the negative energy resonances are also pointed out by Wood (1956) and Segre (1953). In calcula-

TABLE I

S.N.	Isotope	J value of compound nucleus	σ_0 in barn		Ratio R	Reference
			Calculated	Experimental		
1	Mn^{55}	2	11.1	13.2	1.2	Bollinger *et al.* (1955)
2	Mo^{95}	3	6.5	13.4	2.0	AECU–2040 (1955)
3	Mo^{96}	½	1.0	1.2	1.2	–do–
4	Mo^{98}	½	0.16	0.4	1.0	–do–
5	Mo^{100}	½	0.41	0.5	1.2	–do–
6	Rh^{103}	0	71.8	150	2.0	–do–
		1	215.5	150	0.7	
7	Pd^{108}	½	7.4	12	1.6	Segre (1953)
8	Ag^{109}	1	92.5	84	0.9	Wood (1956)
9	Cd^{113}	1	19974	20800	1.0	Sailor (1956)
10	In^{115}	4	181	197	1.0	AECU–2040 (1955)
11	Sn^{118}	½	0.02	0.01	0.5	–do–
12	Te^{123}	1	413	390	0.9	–do–
13	Sn^{124}	½	0.17	0.20	1.1	–do–
14	Cs^{133}	4	17.5	29.0	1.6	–do–
15	Xe^{135}	2	2.94	2.7	0.9	AECU–2040 (1955) Deutsch (1956)
16	Sm^{149}	4	31420	50000	1.6	AECU–2040 (1955)
17	Gd^{157}	3	256964	160000	0.6	–do
18	Tm^{169}	1	86	118	1.3	–do–
19	Lu^{176}	15/2	2361	4000	1.7	–do–
20	Hf^{178}	½	71.1	75	1.0	–do–
21	Ta^{181}	4	13.7	21.3	1.5	Wood (1956)
22	W^{182}	½	9.1	19	2.1	AECU–2040 (1955)
23	Re^{185}	3	74.5	100	1.3	–do–
24	W^{186}	½	45.4	34	0.7	–do–
25	Re^{187}	3	39.4	63	1.6	Segre (1953) AECU–2040 (1955)
26	Ir^{193}	$gn=0.4\times10^{-3}$ev	140.9	130	0.9	Segre (1953)
27	Au^{197}	2	89.5	98	1.1	AECU–2040 (1955)

TABLE II

S.N.	Isotope	J value of compound nucleus	σ_0 in barns calculated	σ_0 in barns experimental	Ratio R	References
1	I^{127}	3	0.19+0.89 +1.10=2.18	6 7	3 0	AECU–2040 (1955)
2	Tb^{159}	2	4.9+5.1+ 0.2=10.2	44	4.3	–do–
3	Hf^{177}		214+83+5 =302	380	1.2	Igo *et al*, (1956) Segre (1953) AECU–2040 (1955)
4	Co^{59}	4	16.4	37	2.2	AECU–2040 (1955) Segre (1953)
5	Ni^{62}	$\frac{1}{2}$	1.33	15	11.2	AECU–2040 (1955)
6	Mo^{97}	3	0.3	2.1	7.0	–do–
7	Ag^{107}	1	2.6	30	11.4	Wood (1956) AECU–2040 (1955)
8	Sn^{112}	$\frac{1}{2}$	0.42	1.3	3 0	AECU–2040 (1955)
9	In^{113}	5	4.3	58	13.6	–do
10	Sn^{120}	$\frac{1}{2}$	0.005	0.14	26.4	–do–
11	Eu^{153}	3	1233	420	0.34	Segre (1953) AECU–2040 (1955)
12	Ho^{165}	4	21.8	64	2.9	AECU–2040 (1955)
13	Yb^{168}	$\frac{1}{2}$	3768	11000	2.9	–do–
14	Hf^{174}	$\frac{1}{2}$	2.35	1500	638	–do–
15	Hf^{179}	1	10	65	6.5	–do–
16	Hf^{180}	$\frac{1}{2}$	0.25	13	52	–do–
17	W^{183}	1	2.3	11	4.7	–do–
18	Ir^{191}	$g\Gamma_n=0.2 \times 10^{-3}$ ev	267	960	3.5	Segre (1953)
19	Hg^{199}	1	8.8	2500	284	AECU–2040 (1955)

ting σ_0 (theoretical) for Co^{59}, Γ_γ is taken to be 0.3ev as given by Segre (1953). This value of Γ_γ could be in error. In the case of Mn^{55} also Γ_γ is 0.2ev according to Segre (1953), but from the recent measurements made by Bollinger and Dahlberg (1955), $\Gamma_\gamma = 0.6$ev. As CO^{59} and Mn^{55} are very near to each other in atomic weights, and Γ_γ changes only slowly with atomic weight as pointed out by Levin and Hughes (1955), Γ_γ for Co^{59} may be taken to be $\simeq 0.6$ev. This gives the ratio R nearly equal to 1. As all the resonances in Ho^{165} and Hf^{179} are claimed

to be known by Harvey *et al.* (1955), the discrepancies between the experimental and theoretical value of σ_0 cannot be accounted for by the known positive energy resonances. These again may be the cases where the negative energy resonances play some part. The rest of the cases involve so many uncertainties in the various measurements that it is very difficult to assign any particular reason for the discrepancies. In the case of isotopes of Sn and Hf, the possibility of some of the unresolved resonances is quite strong. In the case of rare earths small impurities can make great contributions in the cross-sections which could be the cause of error in some cases. Figure 1. gives the value of the ratio R for various atomic weights. The cases of discrepancy are self-evident.

ACKNOWLEDGMENTS

The authors wish to express their sincere thanks to Prof. P. S. Gill for his kind interest in this work. One of the authors (M.L.S.) is thankful to the Union Education Ministry for the grant of a Senior Research Scholarship.

REFERENCES

AEC Neutron Cross-section Advisory Group, U.S. Atomic Energy Commission Document AECU-2040 (1955)

Blatt, J. M., and Weisskopf, V. F., 1952, Theoretical Nuclear Physics, pp. 470.

Bollinger, L. M. *et al.* 1955, *Phys. Rev.*, **100**, 126.

Deutsch, R. W., 1956, *Phys. Rev.*, **104**, 555.

Harvey, J. A., *et al.* 1955, *Phys. Rev.*, **99**, 10.

Igo, G., and London, H. H., 1956, *Phys. Rev.*, **101**, 726.

Levin, J. S. and Hughes, D. J., 1955, *Phys. Rev.*, **98**, 1161.

Sailor, V. L.,1956, *Phys. Rev.*, **104**, 736.

Segre, E. (Editor), 1953, Experimental Nuclear Physics, Vol. II, pp. 324.

Wood, R. E., 1956, *Phys. Rev.* **104**, 1425.

ON THE MAKING OF ELECTRET AND MEASUREMENT OF THE CHANGES OF DIELECTRIC CONSTANT OF A POLARISED ELECTRET FORMING MATERIAL WITH TIME*

T. C. BHADRA

BOSE INSTITUTE : CALCUTTA

(*Received for publication, April* 22, 1958)

ABSTRACT. Electrets were made with commerically available carnauba wax.

Influences of voltage and temperature on the formation of electrets were studied.

Attempts were made to measure the surface charges with an electrometer.

Variation of dielectric constant ε and tan δ were measured with time by means of a universal capacity bridge.

On application of the field in the molten condition of the material, only a fraction of the dipoles orient in the direction of the field, larger portion orient randomly in all other possible directions. Alignments of the dipoles in the parallel direction increases the dielectric constant. Depending on time more of the dipoles orient in the parallel direction due to the field induced by the dipoles, thereby increasing the value of dielectric constant In the present investigation, abnormally high increase in the value of dielectric constant along the direction of the field was obtained. But when the dielectric constant was measured at right angles to the direction of the field, the values of the treated material were found to be lower than those for the control sample.

A. C. conductivity of the material was calculatded from the measured values of ε and tan δ.

1. INTRODUCTION

Adams (1927) found that electret materials were piezo-electric. But Gemant (1935) and Nakata (1927) could not find any piezo-electric effects, and Thiessen (1936) and co-workers obtained only small deflections of the electrometer upon the application of pressure, which they ascribed to capacity changes rather than to piezo-electricity. In view of this apparent contradiction, it was thought worthwhile to undertake further investigations to elucidate the question.

The experimental investigation here reported was undertaken with the hope of finding out some materials which on being electrically conditioned, might attain piezo-electric property. An artificially made piezo-electric material may be

---

* Part of the results has been published in *Phys. Rev.* 1955, 98, 1728.

This paper contains the essential materials of the subsidiary part of a thesis approved by the Calcutta University for the degree of Doctor of Philosophy (1957).

fruitfully utilized to the best advantage as a substitute for piezo-electric quartz crystal and also magnetostriction type transducer to generate ultrasonic energy in a certain frequency range—specially in the lower frequency region 20-100 kc/s. Intensive private commercial investigations have been made. But their findings are of no use to the scientific investigators as they are naturally unwilling to disclose their findings.

Materials having permanent dipole moment may attain the property of piezo-electricity, when they are electrically treated. Under this condition, they may be said to have attained the property known as electro-strition. Likewise, in the field of magnetism, there is magneto-striction. By electro-striction it is understood that the volume of the dielectric material changes, resulting from electric polarisation. Of considerably greater interest is the production of permanent polarity in a dielectric whereby a polarised baror plate of dielectric behaves like a permanently polarised steel bar or plate; such an object was called by Heaviside (Engineering, 1885, quoted from Physical Chemistry by Partington, J R.) an 'electret'. Usually the properties of the polarised material measured do not include that of eletro-striction but includes the measures of ϵ and tan δ.

When an electric field is applied to a polarised material along the direction of the permanent polarisation, the material lengthens. If the applied field is reversed, a shortening occurs. Thus an alternating field applied along the same line as the polarisation causes the material to alternately lengthen and shorten its dimension along this line. This effect is used directly in driving thickness vibrations in the direction of the applied field. It is used indirectly through Poisson-effect in driving radial vibrations of a disc, and length vibrations of a bar when field is perpendicular to length. By applying the driving field perpendicular to the direction of permanent polarisation a shear strain is produced.

Electrets were investigated experimentally by a number of workers (see references). A mixture of wax, specially carnauba wax, a little beeswax and rosin are used and the fused mixture is allowed to solidify in a strong electric field. It has been found that the charge so produced on the surface is not removed by a flame, treatment with X-rays, washing with various liquids or shaving off the surface with a knife. When the charge on the surface is removed it re-appears after a time. The surface charge is measured by an electrometer. The initial surface charge is a hetero-charge, opposite in sign to the charge on the metal plate during the preparation, but there is a rapid change to a homocharge, of the same as that on the plate. The anode layer assumes a short-lived positive charge, rapidly subsiding to a steady somewhat lower positive charge which is constant for several days. The general conclusion is reached that the charge on an electret is not due to polarisation of the dielectric throughout the mass, but is in the nature of a surge charge communicated from the electrodes.

In the present investigation, initially, an attempt was made to measure the surface charge against time by means of a Wulf's type electrometer. But no satisfactory results were obtained. The electret was found to behave like an electrophorous and so measurements with this electrometer was discontinued. Subsequently measurements were made of the change of dielectric constant of the electret forming material with time, after it had been treated with unidirectional electric field. The property of the polarised material includes the measure of ε and tan δ.

In course of the measurements of the dielectric constant ε and tan δ some remarkable findings were obtained. It was found that the dieletric constant increased to an abnormally high value after some days. This high value after hovering for some days dropped down to a lower value. In the present report, the changes of dielectric constant with time under different conditions of the formation of electrets, are presented. The piezo-electric effects of electret will be reported later on. The results obtained are shown in the diagrams (figures 2–6).

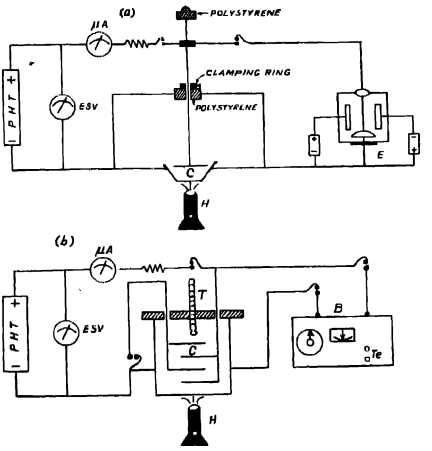

Fig. 1.—The schematic experimental arrangements for making an electret and devices to measure charge, dielectric constant ε and tan δ.

P.H.T.—Polarising High Tension ESV–Electrostatic voltmeter; μA–Microammeter; C–Capacitor unit which contains the dielectric under investigation; E–Electrometer; B–Universal capacity bridge; T–Thermometer; Te–Headphone; H–Bunsen burner.

2. THEORETICAL CONSIDERATIONS

Molecules are composed of positively and negatively charged particles in such numbers that they are neutral as a whole. In polar molecules there is finite distance of separation between what may be termed the centres of gravity of posi-

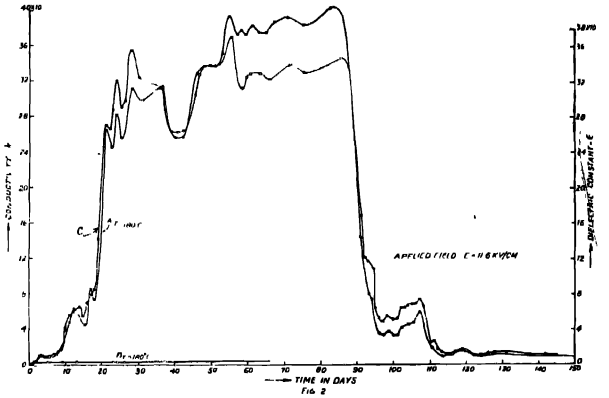

Fig. 2. Graph A shows the plot for the change of dielectric constant of the specimen under test against time in days. A_T180°C–Temperature, when the field was applied. Graph B shows the plot for the change of dielectric constant of the control specimen against time B_T180°Crefers to temperature up to which it was raised. Polarising field E = 11.6 Kv/cm. Graph 2C–shows the change of a.c. conductivity R of the polarised material against time.

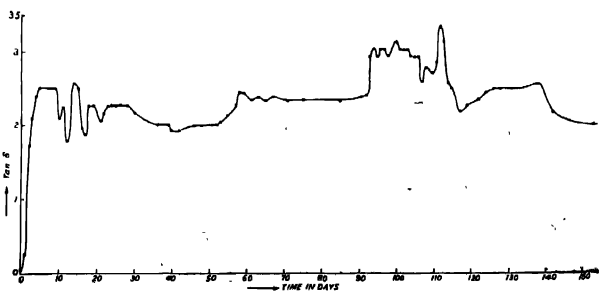

Fig. 3. The change of tanδ against time

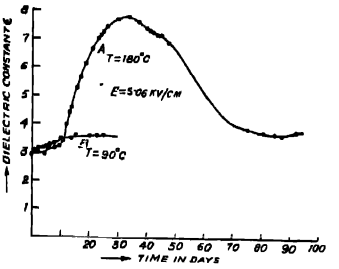

Fig. 4. Graphs A$_T$180°C and B$_T$90°C show the effect of temperature of the material at which the field was applied on the change of dielectric constant with time.

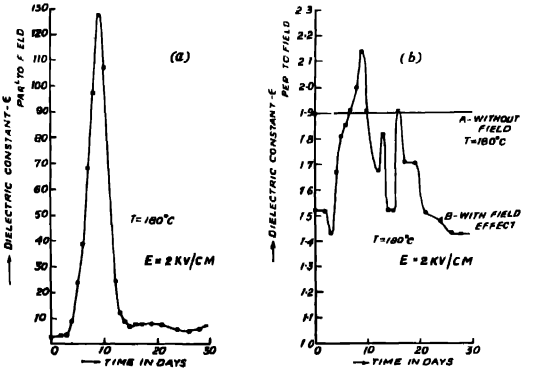

Fig. 5. The change of dielectric constant against time. Fig (5a)—Along the direction of field; Fig. (5b), Curve B–change at right angles to the direction of field and curve A–shows the change for the control specimen in the capacitor placed perpendicular to the field.

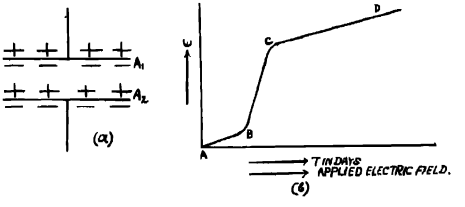

Fig- 6.

tive and negative electricity, and the polarity of a molecule becomes less as these centres of gravity in a molecule approach each other. When placed in an electrical field a polar molecule will tend to orient itself in such a way that the positive part of the molecule points towards the negative electrodes and the negative part points to the positive electrodes. The force required to orient the molecules will depend on the magnitude of the charges and on the distance between them. The dipole moment is defined as the product of one of the charges and the distance between the two average centres of positive and negative electricity.

On application of external electric field, the dipoles of the domain structure orient in the direction of the applied field. It is assumed that orientations of molecules in all directions are equally probable. The alignments may be in parallel, antiparallel and other directions. Under the aligned condition, the medium is said to be polarised. Saturation electric polarisation, apparently, cannot be reached without dielectric breakdown. For this breakdown of the dielectric medium an electric field of the order 10^8V/cm is required. From the practical point of view, it is too difficult a situation to be materialised easily. But in the neighbourhood of an ion, or the dipole, the field may be as high as 10^8V/cm. There is also a dependence of dielectric constant on the applied field and electrostriction.

On account of the regular distribution, the dipoles are mutually coupled in a special way by the very powerful internal field in the structure. If a weak field is applied, the internal field enhances it by resulting orientation of the dipoles. The spontaneous parallel arrangement of all dipoles gives rise to a high dielectric constant, but also occasions a very large dielectric loss due to hysteresis. The oriented dipoles exert supplementary forces and the resulting change of dimensions leads to new positions of stability.

Solid substances, such as Rochelle salt, ammonium dihydrogen phosphates and barium titanate have got unusually high permeabilities (or dielectric constants). These are the analogues in electrical properties of the so-called ferromagnetic bodies with abnormally high magnetic permeabilities and also showing the properties of hysteresis and permanent magnetism. The correspoding dielectrics, in view of their essential property, the unusually high dielectric constant, are termed as hyperelectrics. Many of the fundamental ideas have been carried over to the electrical analogues, in particular that of domain structure. While considering the domain structure, the elementary dipoles are identified with domains containing a large number of atoms, the permanent dipole moment of which are aligned in one direction inside each domain. This alignment is assumed to be due to a permanent intra-molecular field extending over the whole volume of the domain, the existence of the field is supposed to characterise a hyperelectric material. Many investigations have been carried on Rochelle salt, AD phosphates and barium titanate. But no investigation has yet been

carried along these lines on carnauba wax. In the present investigation, an attempt was made to investigate the case of carnauba wax.

(a) *Calculation of polarisability*

Let the material under investigation contain N_1 molecules per cubic centimetre, all of the same kind and in the same state a. The polarisation of the medium will be

(1) $P = N_1 R$, where R stands for dipole moment.

For an isotropic medium, the Lorentz field,

(2) $E^1 = E + 4\pi P/3$ may be denoted as the effective field. Expressing E^1 by this relation, the expression for the polarisation of the medium may be written as

(3) $P = N_1 \; E/\left(\frac{1-4\alpha \, N_1 \pi}{3}\right)$ where α stands for the polarisability of the molecule in the state a.

From electromagnetic theory, the electric displacement vector D may be expressed in the following way,

(4) $D = \epsilon E = E + 4\pi P$, where ϵ is the dielectric constant of the medium.

In terms of polarisability, the dielectric constant may be written as

$$(5) \qquad \epsilon = 1 + \frac{4\pi N_1 \alpha}{1 - 4\pi N_1 \alpha/3} \quad \text{or} \quad \frac{\epsilon - 1}{\epsilon + 1} = \frac{4\pi N_1 \alpha}{3}$$

With the help of the equation (5), the amount of polarisation produced in the electrically polarised dielectric material can be estimated. This partial polarisation is supposed to be responsible for the piezo-electric effect.

(b) *Calculation of a.c. conductivity of the dielectric material*

An alternating field,

(6) $E = E_0 \sin (2\pi t/T)$, where T is the period, when it acts on a dielectric, the current through the dielectric is represented by

(7) $I(t) = I_0 \cos (2\pi t/T - \delta) = I_0 \cos \delta \cos (2\pi t/T) + I_0 \sin \delta. \; \sin 2\pi t/T.$

The cosine term represents the displacement current and the sine term, the conduction current. If C is the capacity

(8) $I_o \cos \delta = (2\pi/T) \, C. \; E_0$; $I_0 \sin \delta = (4\pi R/\epsilon) \; CE_0$, where R is the conductivity and ϵ is the dielectric constant. The loss angle δ is determined from equation (8) by

(9) $\tan \delta = 2TR/E$

Or $\quad R = \epsilon \tan \delta/2T$

3. EXPERIMENTAL ARRANGEMENTS

The entire experimental arrangements are shown in the schematic diagrams figures 1(a) and 1(b).

Figures 1(a) and 1(b) show the arrangements of melting, polarising by applying external fields, and the respective apparatus for measuring charges, dielectric constant ϵ and tan δ. Temperature was recorded by means of the thermometer T. In figure 1(a), the electrodes dipped into the molten dielectric were of tin and those in the figure 1(b) were the commercially available condenser plates. The external field applied to polarise the material was measured by means of an electrostatic voltmeter and the current through the material during the time of polarising was observed by means of a microammeter, connected as shown in the figures 1(a) and 1(b). These meters remained connected till the material was cooled down in air.

Carnauba wax, the material under investigation in the present experiment, was melted and the temperature was raised to some higher level above the melting point. At a particular temperature (kept approximately constant by manual manipulation of the flame) the external field was applied, and the material was kept under tension of this applied field at that temperature for about 15 minutes. Then the flame was removed and allowed to cool in air. It required about 8 to 10 hours to solidify. (This was verified by actual experiment). After solidification the external field was removed and the charge was measured by a Wulf's type electrometer, and the dielectric constant ϵ and tan δ were measured by means of a universal capacity bridge. From the magnitudes of the measures of charges or change of dielectric constant the amount of polarisation produced in the material were estimated and thereby confirming whether the specimens of material under investigation were turned into an electret or not. Electrets were made under the following conditions :

S. No.	Temperature in 0°C	Applied field KV/cm
(1)	90	5.1
2(a)	180	2.0
(b)	180	5.1
(3)	180	11.6

(4) Two condenser units arranged in such a way so that the plates of one unit is orthogonal to the other unit.

This is to measure dielectric constant both par^l to the direction of the applied field and perp. to the direction of the applied field.

(5) Material was melted and temperature was raised to 180°C and then allowed to cool in air. In this case no external field was applied. This specimen served as a control.

4. MEASURING INSTRUMENTS

1. Wulf's single string electrometer

A schematic diagram of the electrometer is shown in figure 1. The fibre is placed in a uniform electric field between two knife edges. The lower end of the fibre rests on a quartz bow and the upper end being connected to an electrode which passes through a high grade insulator. The arrangement of connecting the specimen under investigation and the electrometer is shown in figure 1. The fibre deflection is observed on a micro-scale fitted in the eye-piece of a telescope. The capacity of the system being previously determined, the charge stored by the electrometer can be ascertained.

2. *Marconi universal capacity bridge Type No. TF* 868/1. This instrument incorporates an oscillator to generate a.c. voltage of 1000 c.p.s. There is an a.c. bridge circuit arrangement in which the oscillator output voltage of definite magnitude is applied. Any change in the capacity of a condenser is observed from the deflection of the meter. Direct readings of capacity are obtained in this apparatus. There is also provision to measure tan δ, where δ is the loss angle and Q which is reciprocal of tan δ. Another provision is included to insert a headphone. The readings of the capacity of a condenser are taken from the graduated dial corresponding to the null-deflection of the indicating meter or from the minimum intensity of sound produced in the head-phone. Both these devices may be employed simultaneously quite independent of each other to determine the capacity of a condenser so as to ensure more correct readings.

5. EXPERIMENTAL

(a) In the first part of the present investigation, attempts were made to measure charges in the electrically treated dielectric material by means of an electrometer against time.

The hypothesis behind this measurement was that the molecules having dipole moments would align in the direction of the applied d.c. polarising field —field being applied in the molten condition of the dielectric material and continued so till the dielectric was solidified. So the surface near the positive electrode would be negative and that near the negative electrode positive. This dielectric system would then act as an electrostatic cell having two distinct positive and negative poles at the two faces but possessing no current supplying capacity, unlike the storage cell which can supply current. When such a cell is connected across a sensitive electrometer, there should be some deflection of the fibre of the electrometer, thereby proving the development of voltage due to charge formation at the surfaces. But when the experiment was performed, no deflection of the fibre was obtained even at the most sensitive condition of the electrometer.

In the next phase, this cell system being connected to the electrometer, the upper electrode was raised suddenly by holding the rod attached to the electrode by means of a polystyrene insulator (shown in the diagram figure 1a). This time the electrometer fibre was deflected and the deflection was also obtained when the electrode was suddenly brought near the surface of the dielectric but not physically touching it. This kind of operations of the electrode gave deflections of the fibre even when the two faces of the dielectric were earthed before each operation. The explanation of these observations will be given in the next section.

The experiment was not continued any more, as no convincing and consistant results were obtained with the electrometer which was supposed to be not sensitive enough for these measurements.

(b) Finding no promising results in the charge-measurement experiment, the direction of experiment on polarised dielectric material was turned to a different course. This time attempt was made to measure the change of dielectric constant ϵ and tan δ with time so as to obtain information of the amount of polarisation produced in the dielectric.

In connection with the measurements of dielectric constant ϵ and tan δ, the following experiments were performed with the help of the universal capacity bridge as described in the previous section :

(1) To measure the change with time the dielectric constant of a given wax material which was melted and subsequently allowed to solidify in a given electric field (figure 2*a*).

(2) To measure the variation of tan δ with time of the same specimen (figure 3).

(3) To study the effect of the strength of the initial polarising field on the subsequent change in the dielectric constant of the material with time (figures 2*a*, 4*a*).

(4) To study the effect of the temperature of the molten dielectric at the time of applying the polarising field, on the subsequent change with time of the dielectric constant of the material (figure 4).

(5) To measure the changes with time of the dielectric constants, both in the direction of the applied field and perpendicular to the direction of the applied field (figures 5*a*, 5*b*).

(6) To study the effect of melting the dielectric without any impressed field on the subsequent change of dielectric constant with time (figure 2*b*).

Experiment No. 6 served the purpose of a control.

6. RESULTS AND DISCUSSION

(a) The observations that were made in the measurement of charges were not consistent and conclusive, and so the results obtained have not been reported

in the present paper. A remarkable observation was however made viz., the fibre of the electrometer deflected when the upper electrode was suddenly raised from or brought near the surface. This finding can be explained only if the dielectric with the two electodes system is assumed to act as an electrophorous. The dielectric became polarised while an external electric field was applied in the molten condition of the dielectric. Subsequently, it was cooled in air without the applied voltage being withdrawn. No discharge could develop at that state. On the two opposite surfaces of the dielectric slab positive and negative free charges accumulate due to the applied field. This can be neutralised by a leak discharge through the body of the dielectric slab. In our case the leak discharge was extremely small and not detectable with the instrument used and the charge remained frozen-in.

Dielectric absorption observed in all solid dielectrics, is caused by delayed orientation of dipoles, molecular rearrangements, displacements of strain of covalent bond and ionic displacement in polarisation. On account of absorption,

TABLE I

Expt. No.	Value of air capacitor	Polarising field EKV/cm.	Temperature of the dielectric when the field was applied	Freq. of the measuring voltage	Results of experiment as obtained against time
1	2	3	4	5	6
1	33.5 $\mu\mu$f	11 6 Kv/cm	180°C	1000 c.p.s.	Fig. 2*a*
2	33 5 $\mu\mu$f	11.6 Kv/cm	180°C	1000 cp..s.	Fig. 3
3	33.5 $\mu\mu$f	11.6 Kv/cm	180°C	1000 c.p.s.	Fig. 2*a*
	28.5 $\mu\mu$f	5.06 Kv/cm	180°C	1000 c.p.s.	Fig. 4*a*
4	28.5 $\mu\mu$f	5.06 Kv/cm	180°C	1000 c.p.s.	Fig. 4*a*
	28.5 $\mu\mu$f	5.06 Kv/cm	90°C	1000 c.p.s.	Fig. 4*b*
5	2.1 $\mu\mu$f		180°C		Fig. 5b
	Perp. to Fiel				
	10.2 $\mu\mu$f	2 Kv/cm		1000 c.p.s.	
	Par^{l}. to Field		180°C		Fig. 5a
6	33.5 $\mu\mu$f	No field	180°C	10000 c.p.s.	Fig. 2B

[Table I shows the conditions under which the experiments were carried out Column (6) refers to the figures where the respective values of ε and tan δ are plotted against time. Column (3) shows the value of applied polarising field and column (4) the temperature when field was applied. Last row shows the experimental characteristic of the control specimen].

a capacitor containing solid dielectric can neither be charged nor discharged instantaneously. Dielectric absorption in combination with an adequate heat treatment produces the electret effect.

Further work in this line, with a much more sensitive electometer, is in progress.

(b) Experimental results of the dielectric constant ϵ and tan δ measurements of a typical sample of commercially available carnauba wax, are shown in the figures (2) to (5), and table I shows The different conditions of experiments in a summarised way.

In the present investigation, no attempt was made at securing high precision. Here the main object was to get information of the change of polarisation due to the action of electric field, in a very qualitative way. This in turn was obtained from the measurements of the dielectric constant. To that extent, the present investigation is a successful one. Not only dielectric constant ϵ but also tan δ, was measured in the same experiment. Knowing ϵ, tan δ and the period T of the a.c. measuring voltage, the conductivity was calculated by utilising the formula (9).

The results of the experiments performed are shown in the figures (2), (3), (4) and (5). The figure 2(C) shows the calculated a.c. conductivity of the polarised material against time.

I. (A). Figure 2, graph 2A shows the variation of dielectric constant ϵ against time. From the study of the graph 2A, it is evident that there is a gradual rise of the dielectric constant for the first 13 days. Then after the 18th day there is a sharp rise in the measure of ϵ. The value of the dielectric constant remains at that higher level—with many ups and downs—for about 68 days and after which there is a sharp fall . On close observation of the curve, it is found that the fluctuations in the measurements of the dielectric constant before the date of sharp rise have got some correspondence with the same after the date of fall. Moreover, in the measurements of the dielectric constant at the higher level state, it was noticed subjectively that the head-phone gave indications of tremendous noise and it was very difficult, sometimes it was practically impossible, to get the minimum sound-position at the highest sensitive condition of the measuring instrument. This excess noise may be attributed to be the cause of molecular re-arrangements due to internal induced field. Greater the number of dipoles aligned in the direction of the field, greater is the polarisation. Here it may be supposed that on the application of the field in the molten condition of the material some dipoles were aligned in parallel and some in antiparallel and the rest in all other directions according to the following statistical law, $n = n_0 e^{-\mu F/KT \cos\theta}$. where T is the temperature of the substance.

(B) *Interpretation of the mechanisms involved in the entire process of making electrets*

The wax material is kept for a few hours in molten condition in a strong electric field and then allowed to solidify with the field on, after which the external electric field is withdrawn.

We may picture the solidified wax material as follows:

(I) At the two ends are two strongly polarized electrets A_1 and A_2 in figure 6(a)

In between these two electrets are the wax dipole molecules, which try to orient themselves parallel to the direction of the field due to the two electrets A_1 and A_2. Such orientation are opposed by the viscous forces in the material of the wax. Gradually there will be increasing alignment of the wax molecules along the directions of the field due to A_1 A_2. The measure of this orientation will be the change in the value of dielectric co-efficient.

The variation of the predicted change of ϵ with T as illustrated in figure 6(b) corresponds roughly with the observed dependence of ϵ with T as given in figure 2(*o*).

(i) In first stage the portion AB of figure 6(b) represents an almost linear increase of dielectric coefficient with the applied finite A.C. field. This corresponds to the portion of the curve in 2(A) between 0 and 15 days.

(ii) in the second stage BC of figure 6(b) when the dielectric co-efficient increases very rapidly with the applied A.C. field corresponds to the portion of curve 2A between 15 and say, 22 days.

(iii) we can consider that corresponding to the portion CD of figure 6(b) is the portion between 22 and 90 days in the curve 2A.

(iv) there is an abrupt change in the dielectric coefficient curve 2A between 90 and 110 days. Probably more than one interpretation of this observed effect is possible. The following one appears to be reasonable.

During the stages (i) to (iii) the field due to the electret pair can be assumed to remain on the whole constant. Even during this period there is gradual loss of charges forming the electrets pair A_1 and A_2 due to

(a) loss of charge to the surrounding air and (b) due to conduction through the main body of the slightly leaking dielectric. When the charges on A_1 and A_2 become negligible, we arrive at a stage when there is a dielectric polarisation in a viscous dielectric body not maintained by any external electric field. The tendency towards random orientation of the dipole molecules in a zero external field which corresponds to an increase of entropy becomes effective and the wax body returns to its initial state.

(C) *Quantum-mechanical picture.*

In the language of quantum mechanics, it may be said that the molecules had moved to the state b from the state a. The state b represents a state for higher dielectric constant than that for states a. State of interchange of molecules were caused partially by the applied electrical field and subsequently the stage b was attained by the time dependent induction of field due to dipoles. The state b of the system of molecules is the unstable state. So the system returns to the stable state a after a length of time. The life of the state b depends upon the applied electric field. This is evident from the graphs 2A and 5A, as obtained in the present investigations. The entropy of the molecular system in the state b decreased as the system passed from the state a, where the entropy of the system was larger, to the state b. As the transport was forced, the systems reverted to the stable state a when the influence due to the applied field died down. This suggests the breakdown of the alignments of the domains.

2. Further it was found that the abnormally high value of the dielectric constant of the polarised material, came down to the normal value when the material was remelted. Melting of the material destroyed the aligned distribution of the dipoles and so there was no evidence of the increase in the value of the dielectric constant with time.

3. Tan δ which determines the loss, was measured with the capacity bridge. The plot of tan δ against time is shown in figure (3). From the graph, it is clear that the value of tan δ was very small at the start. But in five days, the values increased very rapidly. Subsequently it remained at the higher-value level having some fluctuations. From a comparative study of the curves for (i) dielectric constant ϵ against time (figure 2, curve A) and (ii) tan δ against time (figure 3), it is found that the value of dielectric constant dropped down to a lower level after about 90 days and thereafter gradually attained the values of ϵ nearing those of unpolarised material but the values of tan δ did not drop down to lower level. The cause for the attainment of lower values of c may be attributed to the breakdown of the alignment of the domains. That for the higher values of tan δ even when the values of ϵ came down to lower values, may be interpreted in the following way. Values of tan δ depend on the product of the dielectric constant and the resistance which is a hypothetical series or shunt resistance associated with the actual condenser to account for the loss in the dielectric. Since the mean values of tan δ as obtained in the present investigation are found constant, it may be inferred here that this constancy i.e. the product $\epsilon \times R$, can be maintained even when the value of ϵ dropped down to lower level, if there is a corresponding rise in the values of R. An increase in the value of κ is possible, if the alignments of the domains break down. In the present investigation, the results indicate that this state of affair might have occurred. These two observations on dielectric

constant and tan δ suggest that the alignments of the domains broke down after about 90 days and the material lost its electret property.

4. The a.c. conductivity of the material was calculated with the help of the equation (9). Calculation of κ required the measured values of ϵ and tan δ of the material and also T, the period of the measuring voltage. The plot κ against time is shown in the graph figure 2(C). Greater the development of surface charges, greater will be the a.c. conductivity. In the present investigation, the cause of the variation of a.c. conductivity of the material against time, may be attributed to the alignments of more and more dipoles in the direction of applied field, resulting thereby in greater amount of polarisation and hence surface charges which caused the increased value of a.c. conductivity.

5. The temperature of the molten material, at which the field is to be applied plays an important role in making electrets. Results of typical experiments performed, are shown in the graphs 4A and 4B. Here the applied voltage remained the same, but in one case the temperature was 180°C and in other 90°C. For this particular sample of the material, a compromising temperature of 180°C was found suitable for better results, without destroying the property of the material. Above 220°C, the material got charred. Considering these points, all the experiements were performed at 180°C.

6. In an experiment, the change of dielectric constants both in the direction of the applied field as well as at right angles to the field were measured. Results obtained are shown in graphs 5(a), 5(b) A and B. Figure 5(a) shows the change of dielectric constant along the direction of the field. Graph A of figure 5(b) shows the change of dielectric constant against time, when the system acted as a control and graph B of the same figure shows the variation at right angles to the applied field. Here it is apparent from the graphs A and B that the dielectric constant decreased with time, with the exception for a short period of 3 to 4 days, when the value of the dielectric constant was larger than the control. In all the experiments, where the dielectric constants were measured along the direction of the field, the values were always higher than those of the control from the very start of the experiment. This remarkable observation of the present investigation may be interpreted in the following way.

The domain structure may be supposed to have three axes of symmetry. Of the axes (X, Y, Z) say, the X axis was aligned in the direction of the field and the other two Y and Z at right angles to X, were oriented in any other direction. Under the joint action of the field induced by the dipoles and the measuring voltage one of the axes Y or Z was oriented in the direction at right angles to the field. So the dielectric constant increased. The curves are drawn in a magnified scale so as to show the small changes in the values of dielectric constant clearly.

7. The effects of the applied field on the making of electrets are shown in figures 2 and 4A. Larger the magnitude of the applied field, more enhanced

is the effect produced. Moreover, the life of the state *b* depends on the applied field. Results of the experiments as depicted in figures 2 and 4A support this view. Exact relationship between the applied field and the life of the state *b* of the electrically treated material cannot be decided at this early stage of experiments. For this, experiments in details are being undertaken.

The present investigations being preliminary, no attempt to theorise or go into the details of the experimental studies was made. Here the main object was to make an electret and then to employ it to generate ultrasonic energy. The preliminary observations on the first part are reported here. Works with greater details are in progress.

ACKNOWLEDGMENT

The author wishes to express his grateful appreciation to Dr. D. M Bose, Director, Bose Institute, Calcutta, for his keen interest.

REFERENCES

Adams. E. P., 1927 *J. Franklin Inst.* **204**, 469.
Eguchi, M., 1919, *Proc. Phys. Math. Soc. Japan*, **1**, 326.
1920, **2**, 45, 169, 192.
,, 1925, *Phil. Mag.*, **49**, 178.
Ewing, M., 1930, *Phys. Rev.*, **36**, 378.
Gemant, A., 1935, *Phil Mag.* **20**, 929.
Gutmann, F., 1948, *Rev. Mod. Phys.* **20**, 475.
Groos, B., 1949, *J. Chem. Phys.*, **17**, 866.
Kay, H. F., 1955, Report of Prog. Phys. Vol. XVIII.
Nakata, K., 1927, *Proc. Phys. Math. Soc. Japan.* **9**, 179.
Thiessen, P. A., 1936, *Physik Zeits.*, **37**, 511.
Chatterjee, S. D. and Bhadra, T. C., 1953, *Phys. Rev.*, **98**, 1728.
Other references will be available from the bibliographies given in these papers
Physical Chemistry by Glasstone, S.
Physical Chemistry by Partington, J. R.

Letters to the Editor

The Board of Editors will not hold itself responsible for opinions expressed in the letters, published in this section. The notes containing reports of new work communicated for this section should not contain many figures and should not exceed 500 words in length. The contributions must reach the Assistant Editor not later than the 15th of the second month preceding that of the issue in which the Letter is to appear. No proof will be sent to the authors.

3

DIURNAL VARIATION OF DEVIATIVE ABSORPTION IN THE F_2 REGION OF THE IONOSPHERE

S. K. SHARMA

RADIO COMMUNICATION LABORATORY, ENGINEERING COLLEGE,

BANARAS HINDU UNIVERSITY, BANARAS-5

In recent years many papers have appeared dealing with the non-deviative absorption occurring in the lower D, E and F_1 regions. Not much attention, however, appears to have been paid to the deviative absorption occurring in the F_2 region. An attempt has, therefore, been made in the present work to study the diurnal variation of deviative absorption occurring in the F_2 region by measuring total absorption of frequencies close to the critical frequency of the F_2 layer.

The total absorption of the waves has been calculated by modified method of Piggot (1953) from the amplitude measurement of first and second reflected echoes averaged over five minutes. The exploring frequencies were selected near the critical frequencies of F_2 layer, so that they might suffer heavy deviative absorption in the F_2 region. Curves I, II and III in the given figure show the diurnal variation of observed total absorption for three suitably spaced frequencies for a typical day. Curve IV shows the diurnal variation of maximum electron density in the F_2 layer calculated from critical frequencies. From the curves I, II and III it can be seen that there are two maxima of total absorption having a dip between them at local noon. The curves further indicate earlier decrease of total absorption at higher frequency than that at lower frequency.

The total absorption of such higher frequencies is made up of two components, namely, the non-deviative absorption in D, E and F_1 regions and deviative absorption in the F_2 region. It has been established theoretically by Appleton (1953) and later showed experimentally by many investigators that the non-deviative absorption acquires its maximum value after local noon due to slug-

gishness of these layers. The cause of two maxima, therefore, seems to be associated with the deviative absorption. It may be mentioned that the two maxima as shown by curves I, II and III are due to lowering of total absorption at local

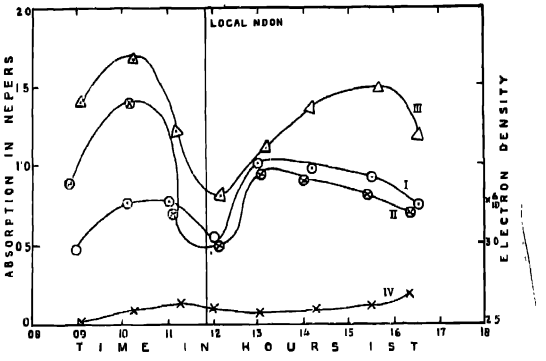

Fig. 1. (A) Diurnal variation of total absorption on 7–1–57.
(1) Curve I for 11.5 Mc/s.
(2) Cruve II for 12.5 Mc/s.
(3) Curve III for 12.5 Mc/s.
(B) Curve IV maximum electron density variation during the day.

noon. It therefore seems that deviative absorption is decreasing with the advance of the day which is further evident from the observation that the fall of total absorption at lower frequency starts a little later than that at higher frequency undergoing more deviative absorption. The lowering of deviative absorption with the advance of the day can not be explained in terms of electron limitation in the F_2 layer as the electron density is found practically constant throughout the hours of observations as can be seen from curve IV. It is therefore concluded that the lowering of deviative absorption in the F_2 region with the advance of the day is due to thermal expansion of the layer.

The author is highly indebted to Dr. S. S. Banerjee for constant guidance during the progress of the work.

REFERENCES

Piggot, W. R., *Proc. I. E. E.*, 1953, Vol. 100 61.
Appleton, E. V., *J. Atmos. Terr.* 1953, *Phys.*, 3 283.

INDEXED POWDER DIFFRACTION DATA ON DIHYDROXY-FUMARIC ACID, ANHYDROUS, $C_4H_4O_6$

M. P. GUPTA AND G. P. DUBE

DEPARTMENT OF PHYSICS, RANCHI COLLEGE, RANCHI

(*Received for publication, February 7, 1958*)

Chemical evidence that dihydroxyfumaric acid, $C_4H_4O_6$, has the trans-configuration has been given by Hartree (1953) while conclusive evidence regarding this acid having the trans-configuration in the solid state has also been given by Gupta (1953) using single crystals of dihydroxyfumaric acid, dihydrate, $C_4H_4O_6 \cdot 2H_2O$ and X-ray methods. Attempts to crystallize the anhydrous acid (i.e. without the molecules of water of crystallization) from absolute alcohol and other organic solvents by surrounding the solution with a packing of solid carbon dioxide have proved unsuccessful. The powder diffraction data of the anhydrous acid, however, are of such simplicity (figure 1) that it has been possible

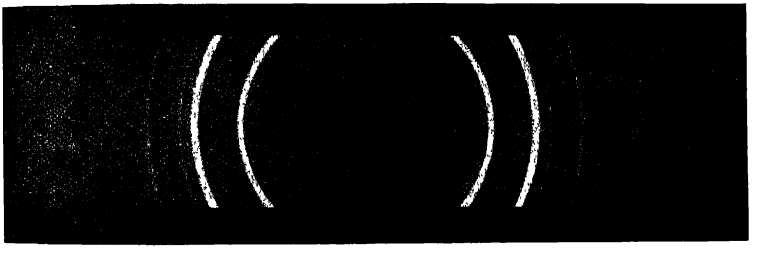

Fig. 1.

to index the data unambiguously after only a few trial combinations. This indexing leads to an orthorhombic cell with

$$a = 12.93\text{Å}, \quad b = 9.47\text{Å}, \quad c = 8.82\text{Å}.$$

The volume of the cell so chosen is 1081.2A^3. With the measured density of the powder material (1.80 gms/cc) this gives 8 formula units ($C_4H_4O_6$) of the anhydrous acid in the cell. Whether the cell is primitive or non-primitive, the available powder data are insufficient to give any correct indication. However, the very marked simplicity of the powder data and the absence of a large number of lines of simple indices indicate that both structurally as well as from the

space group symmetry the crystal would tend to show a hypercentric distribution (Lipson and Woolfson, 1952).

The powder diffraction data are given in Table I. Corrections for film shrinkage have been applied. The diffraction angles were checked independently by obtaining a diffraction curve on the Norelco Geiger counter diffractometer. There was good agreement regarding the diffraction angles but agreement with the film-method regarding intensity was only qualitative which may be due to preferred orientation in the sample prepared for the diffractometer.

TABLE 1

X-ray diffraction powder data

I/I_1	d (A) Observed	d (A) Calculated	hkl	I/I_1	d (A) Observed	d (A) Calculated	hkl
3	6.47	6.47	200	5	2.15	2.16	{014}
						2.15	{241}
1	4.73	4.73	020			2.15	{033}
3	4.41	4 41	002	1	2.04	2.04	{214}
						2 04	{233}
50	4.16	4.17	{102}				
			{021}	1	.98	1.98	{124}
						1.98	{423}
2	3.41	3 40	212				
				7	1.93	1.94	602
100	3.08	3.07	{410}				
		4.07	{130}	1	1.82	1.82	{250}
		3.06	{302}			1.82	{404}
15	2.84	2.84	230	1	1.76	1.75	442
1	2.69	2.70	231	1	1.69	1.69	721
1	2.58	2.57	213	1	1.59	1.59	640
20	2.45	2.45	123	10	1.54	1.54	604
1	2.31	2.33	{140}				
		2.33	{223}				

The experimental work was done during part of Exchange Visit Program P-72 at the Polytechnic Institute of Brooklyin, N. Y., and one of us (Gupta) is greatly indebted to Prof. I. Fankuchen for providing all the laboratory facilities.

REFERENCES

Gupta, M. P. 1953. *Jour. Amer. Chem. Soc.*, **75**, 6312.
Hartree, E. F. 1953, *Jour. Amec. Chem. Soc.*, **75**, 6244.
Lipson, H. and Woolfson, M. M. 1952, *Acta. Crys.*, **5**, 680.

5

AFTERGLOW IN p-CHLOROTOLUENE AT −180°C

D. C. BISWAS

OPTICS DEPARTMEMT, INDIAN ASSOCIATION FOR THE CULTIVATION OF SCIENCE, JADAVPUR

(*Received for publication, April 29, 1958*)

The luminescence spectra exhibited by *p*-chlorotoluene in the solid state at different low temperatures and also those exhibited by the substance dispersed in different rigid media were studied by Sirkar and Biswas (1956) and by Biswas (1956). It is, however, not known whether this luminescence consists only of fluorescence or any afterglow of comparatively longer duration is mixed up with fluorescence. As such an information would be extremely helpful in finding out the origin of the luminescence the method of Lewis and Kasha (1944) has been used to investigate the spectrum of the afterglow which is superposed on that due to fluorescence in the luminescence exhibited by crystals of *p*-chlorotoluene at −180°C.

The liquid sealed in a glass tube was dipped in liquid oxygen contained in a Dewar vessel of pyrex glass and the whole arrangement was next placed within a hollow metallic cylinder. This cylinder was provided with a rectangular aperture in its wall and it was rotated by a D.C. motor with 1450 r.p.m. at a uniform speed. The sample was illuminated from one side by the light from a mercury arc in Pyrex glass tube. The exciting radiation after passing through a light filter transmitting mainly the 3650 Å group of Hg lines was focussed on the sample by means of a cylindrical condenser. The light emitted by the sample in the transverse direction was focussed on the slit of the spectrograph. As the metallic cylinder was rotated the sample was alternately illuminated through the aperture and was focussed through the same aperture on the slit of the spectrograph. In this way, the light emitted by *p*-chlorotoluene approximately during the period from 0.5×10^{-2} sec. up to 10^{-2} sec. after the cessation of excitation was recorded by the spectrograph. A spectrogram of the afterglow emitted by *p*-chlorotoluene during the period mentioned above and photographed with an exposure of 5 hours is reproduced in figure 1.

A preliminary comparison of this spectrogram with that due to the total luminescence indicated that the intensity of the afterglow mentioned above constitutes a small fraction of the total luminescence. In order to make a more precise estimation of the relative intensities of the total luminescence and the afterglow mentioned above, the sample was illuminated constantly under identical conditions and the spectrum of the light emitted in the transverse direction was photographed with an exposure of about half an hour. The aperture in the

cylinder covers about one-tenth of the total area of the cylindrical surface and hence the exposure times of 5 hours and half an hour in the two cases mentioned above are effectively equal. Comparison of the two spectrograms reproduced in figures 1 and 2 shows that the luminescence emitted by *p*-chlorotoluene during

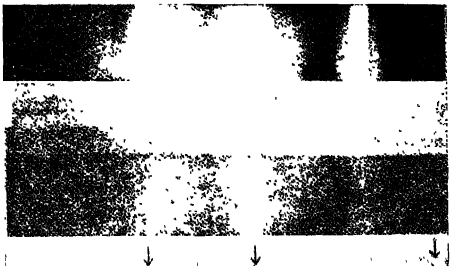

Fig. 1.

the period from 0.5×10^{-2} sec. to 10^{-2} sec. after the cessation of excitation is less than one fifteenth of the total luminescence emitted by the substance. The main contribution to the intensity of total emission is then due in all probability to luminescence having average life time shorter than 0.5×10^{-2} sec. More detailed investigation of this problem is proposed to be undertaken in this laboratory in future.

The author is grateful to Professor S. C. Sirkar, D.Sc., F.N.I. for his kind interest and guidance during the progress of this work.

REFERENCES

Biswas, D. C. 1956, *Ind J. Phys.*, **30**, 143.
Lewis, G. N. and Kasha, M, 1944, *Jour Am. Chem. Soc.*, 2100.
Sirkar,. S. C., and Biswas., D. C, 1956, *Jour. Chem. Phys.*, **24**, 470.

STUDIES ON A RHOMBIC ANTENNA WITH CYLINDRICAL HELICES AS THE ARMS

ASHOKE KUMAR SEN

INSTITUTE OF RADIO PHYSICS AND ELECTRONICS, UNIVERSITY OF CALCUTTA

(*Received for publication, April* 2, 1958)

ABSTRACT. The input impedance and the directivity of a rhombic antenna with arms in the form of cylindrical helices of constant pitch angle have been studied.

On the basis of certain plausible assumptions, theoretical expressions have been derived to obtain the input impedance and the directivity of the antenna. The results have been compared with experimentally observed values.

1. INTRODUCTION

The rhombic antenna is widely used in military and commercial services for point-to-point communication. It is a wide band antenna and possesses substantial degree of directivity. These two properties, as is well-known, result from the aperiodic nature of the system. The rhombic antenna, however, suffers from a number of limitations mentioned below:

(i) The horizontal and vertical radiation patterns being perceptibly dependent on one another, it is impossible to obtain high angle radiation except at very low gain and for very broad horizontal pattern;

(ii) Wastage of input energy at the terminating resistor, thereby greatly reducing the efficiency of the system;

(iii) Large plot of land is necessary for its erection.

The first difficulty is reduced to a considerable extent by using arrays of rhombic antennas in cascade, which, in addition, suppress smaller unwanted lobes of radiation and improve the radiation efficiency. The second difficulty is effectively minimised if the input impedance of the antenna is lowered by using multiple wires (space-tapered) instead of single conductors constituting the arms and also by feeding the energy at the terminal end back to the system in a manner that progressive waves flow round the network (Neimann, 1939).

In an attempt to reduce the third difficulty, the present author has investigated the possibility using cylindrical helices as the arms of the rhombic antenna. In a helix, the "axial" velocity of the electric wave is less than that along a linear conductor so that a rhombic antenna with helices as the arms should in effect correspond to a much longer rhombic antenna with linear arms. The antenna studied consists in each arm a helix designed for a midfrequency of

600 mc/s. The pitch angle and the length of each turn are 12° and 20 cm. respectively so that the helix operates predominantly in the "normal" mode over the entire frequency band.

The impedance characteristics and the radiation pattern of this antenna have been studied both theoretically and experimentally. The results of these investigations are reported in this paper.

2. EXPERIMENTAL ARRANGEMENTS AND MEASUREMENTS

The rhombic antenna has been designed to operate in the frequency range of 300 mc/s to 900 mc/s with the mid-frequency of 600 mc/s. Each arm of the antenna consists of a cylindrical helix of 10 turns made of hard-drawn copper-wire (1/8″ in diameter). The pitch angle of the helix is about 12° and the length of the wire in each turn is 20 cm. The total length of wire in each helix is 200 cm; that is, 4 wavelengths at the mid-frequency. The axial length of the helix is 40 cm. The inclination between the arms is made according to the standard design chart for the ordinary rhombic antenna (Smith, 1948), its value being about 145°. The included angle is adjusted to 35° so that the first maximum lobe may be directed along the major axis of the rhombus and its elevation is of the order of 17.5°. The elevation 17.5° is chosen because of convenience in the measurement of radiation patterns. The antenna is mounted horizontally over a copper-wire net at a height of about 3.75 wavelengths (corresponding to 600 mc/s) which satisfies the condition of maximum field intensity at the elevation angle of 17.5°. The copper net of close mesh provides the perfect "ground".

(i) *Measurement of impedance* :

The layout of the rhombic antenna with its measuring devices is shown in figure 1. The input impedance is measured by means of a twin-wire standing-

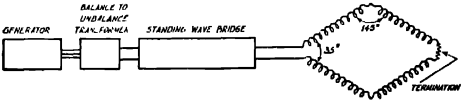

Fig. 1.—Block diagram of the experimental arrangement for the measurement of input impedance of the antenna.

wave bridge designed and constructed for the experiment. A balance-to-unbalance transformer is incorporated at the input end of the bridge since the generator output is taken through a co-axial cable.

Several wavelengths of line are placed between the bridge and the antenna, thereby eliminating the need for locating symmetrically both the operator and the measuring equipment. The line length, however, is so chosen that the

attenuation introduced by it may be neglected (Tomiyasu, 1949). The measurements have been made at frequencies from 300 mc/s to 900 mc/s. The impedance-frequency and standing-wave ratio characteristics are shown in figures 2-3.

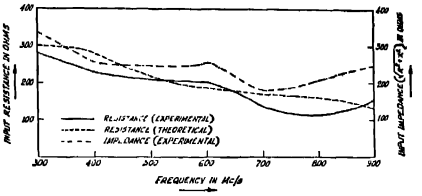

Fig 2.—Illustrating the variation of the calculated (dotted line) and the observed (solid line) values of the input resistance with frequency. Observed (chain line) values of input impedance $\sqrt{R^2+X^2}$ is also shown. Frequency range · 300 Mc/s to 900 Mc/s..

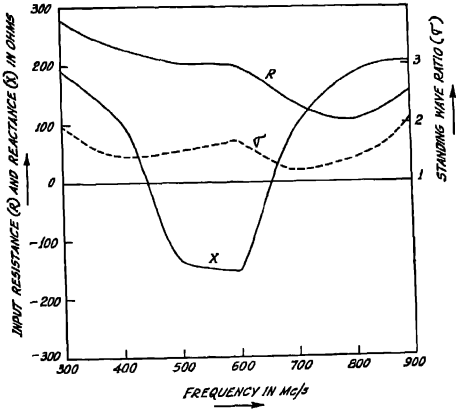

Fig. 3.—Observed values of the resistive (R) and the reactive (X) parts of the input impedance and also the SWR characteristics. Frequency range: 300 Mc/s to 900 Mc/s.

(ii) *Measurement of radiation pattern* :

The antenna together with the balance-to-unbalance transformer and the tapered feeder for impedance matching are erected horizontally above the ground. The height of the antenna from the copper net of close mesh which acts as ground, is adjusted so that the major radiation lobe satisfies the condition of maximum field intensity for an ordinary rhombic antenna. The receiving antenna is a dipole placed at a distance of about 10 wavelengths (corresponding to 600 mc/s) from the antenna under study. The height of the dipole is adjusted so that it receives

maximum "illumination" from the major radiation lobe, which makes an angle of 17.5° approximately with the plane of the rhombic antenna.

Imperfect termination of the antenna over the frequency-band generates back radiation due to the standing waves on the conductor arms, but its magnitude has been found to be small. Consequently, the measurement of the radiation pattern has been made only in the forward direction and the test antenna is swept through an angle of 180°. Both horizontally and vertically polarised components of the field have been measured only in the horizontal plane. The vertical-plane patterns, however, could not be measured because of experimental difficulties.

The crystal detector being a square-law device, accurate measurement of small side-lobe amplitudes is difficult. Hence, only the major lobes at different frequencies have been measured. The tendency of the major lobe to split up at the higher end of the frequency band has been shown in one particular case (figure 7f).

The plots of radiation patterns for different frequencies are shown in the figures 7–9.

3. THEORETICAL CONSIDERATIONS

(i) *Calculation of impedance* :

An approximate formula for the average characteristic impedance of the antenna has been derived by the standard method based on Schelkunoff's treatment of the biconical antenna (Schelkunoff, 1943). For the biconical antenna, Schelkunoff assumes that only the TEM transmission mode is present, so that both E and H lines are entirely transverse, that is, they have no radial component. This satisfies the boundary conditions since E is normal to the surface of the cones and the H lines are circles lying in planes normal to the polar axis. The voltage between points 1 and 2 on the cones at a distance r (figure 4) from the terminals is given by

$$V(r) = \int_{\theta_{h_e}}^{\pi-\theta_{hc}} E_\theta \, . \, r d\theta \qquad \ldots \quad (1)$$

where θ_{hc} is the half-angle of the cone.

The total current $I_{(r)}$ at the same point is obtained by Ampere's law,

$$I_{(r)} = \int_0^{2\pi} H\phi r \sin\theta d\phi = 2\pi r \sin\theta H\phi \qquad \ldots \quad (2)$$

If the biconical antenna is considered infinitely long, the ratio of $V_{(r)}$ and $I_{(r)}$ given by Eqns. (1) and (2) would give the characteristic impedance of the antenna

In the case of a rhombic antenna with cylindrical helices as the arms, the situation is evidently more complicated. For the sake of simplification, however, certain plausible assumptions may be made. These are discussed below:

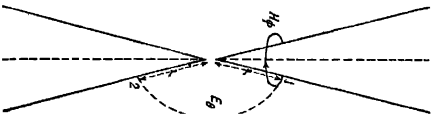

Fig. 4.—E_θ and H_φ lines of outgoing TEM wave on a biconical antenna.

(a) The average characteristic impedance of a rhombic antenna is approximately equal to the input impedance of infinitely long diverging wires of the same included angle (Schelkunoff, 1952).

(b) When two conical conductors of equal cone angles are kept inclined to each other symmetrically with repsect to a centre axis and are fed at the apex, the system radiates. Schelkunoff and others have shown that the interaction between the two diverging conductors may be neglected except in the vicinity of the input ends when the gap at the input end is large compared to the average radius of the conductors. On similar grounds we have also neglected any possible effect due to interaction between the arms of the antenna under study. Hence, the electromagnetic field may be considered uniform in the intervening region between the arms.

(c) It is known that strictly transverse electromagnetic waves cannot exist on non-conical wires (Schelkunoff, 1952). In the case of a helix, the field contains a voltage component due to the circumferential magnetic flux. But its magnitude being in our case relatively small, it may be neglected. The electromagnetic waves in the intervening region between the two arms may thus be assumed to be entirely transverse, as done by Schelkunoff in his treatment of the biconical antenna. The electric lines of force between the two arms, hence, will run principally along the great circles passing through the axes of the helix arms and the voltage will be the line integral of this electric field along the great circle.

(d) Since the antenna is terminated by its characteristic impedance and the conductors are assumed to be loss-less, the current distribution along the arms may be assumed uniform. Standing waves are, however, likely to exist on the conductors due to irregularities introduced at the side corners of the rhombic antenna and also due to the variation of characteristic impedance from point to point along the two diverging conductors. But these effects are usually negligible (Schelkunoff, 1952) and so, the current in the arm is primarily progressive. Consequently the principal wavefronts are spherical in nature. The effect is, therefore, like that of a current flowing 'axially' along the helices, the velocity of which is a function of the helix parameters. Pocklington (1897) has shown that for a

helix of dimensions comparable to the wavelength, the axial velocity is given by

$$v = c \sin \alpha \qquad \dots \quad (3)$$

where v is the phase velocity of the axial current; c, the velocity of light (3×10^{10} cm/sec.); and α, the pitch angle of the helix.

Since the field in the intervening region between the two arms is assumed entirely transverse, both E and H components can be expressed in terms of scalar potential functions. The potential function for the progressive travelling waves may be written as

$$T = A[K_0(\beta r_1) - K_0(\beta r_2)] \qquad \dots \quad (4)$$

where A is a constant; β, the axial phase constant $\left(=\frac{\omega}{v}\right)$; ω, the frequency in radians/sec., r_1 and r_2, the distances from the axes of the helix-arms of a point P in space on the meridian plane (figure 5), and K_0 is the modified Bessel function which is the solution of the modified Bessel equation of order zero, with the independent variable βr. It is known that the modified Bessel equation has two independent solutions involving I_0 and K_0. I_0, which is finite for all values of r and is only appropriate for source-free regions, is disregarded. The K_0-function however, vanishes at infinity and is retained, since it represents an outward travelling wave.

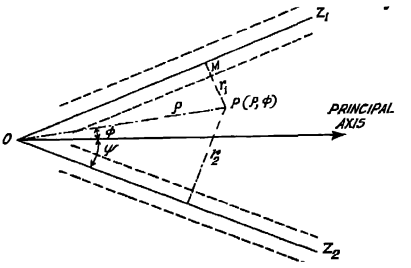

Fig. 5.—Illustrating the calculation of distance of a point 'P' in space from the two inclined arms of the antenna. The dotted lines indicate the outlines of the cylindrical helices and the solid lines OZ_1 and OZ_2, the axes thereof.

In figure 5, 2ψ is the included angle between the arms and (ρ, ϕ) are the coordinates of the reference point P on the meridian plane. Expressing r_1 and r_2 in terms of ρ, ψ and ϕ, the potential function takes the form

$$T = A[K_0\{\beta\rho \sin(\psi - \phi)\} - K_0\{\beta\rho \sin(\psi + \phi)\}] \qquad \dots \quad (5)$$

The azimuthal component of the magnetic field at P is given by the relation,

$$H_\phi = -\frac{1}{\rho}\cdot\frac{\partial T}{\partial \phi}$$
$$= -A\beta[K_1\{\beta\rho\sin(\psi-\phi)\}\cos(\psi-\phi) + K_1\{\beta\rho\sin(\psi+\phi)\}\cos(\psi+\phi)] \quad (6)$$

If the point is on the outer surface of the helix $(\psi-\phi)$ reduces to $\sin^{-1} a/\rho$ and $(\psi+\phi)$ to $(2\psi - \sin^{-1} a/\rho)$, where a is the radius of the outer surface of the helix. Substituting these values in Eqn.(6), the azimuthal component of the magnetic field H_{ϕ_s} just outside the surface of the helix arm is given by

$$H_{\phi_s} = -A\beta[K_1(\beta a)+K_1\{\beta\rho(\sin 2\psi - \frac{a}{\rho}\cos 2\psi)\}(\cos 2\psi - \frac{a}{\rho}\sin 2\psi)] \quad \ldots (7)$$

Now, for an infinitely long helix of radius a, we have, from Ampere's law,

$$I = \oint H_{\phi_s}\, ds = 2\pi a \,.\, H_{\phi_s} \quad \ldots (8)$$

On substitution, the current flowing axially through the helix arms is given by

$$I = -2\pi a \,.\, A\beta[K_1(\beta a) + K_1\{\beta\rho(\sin 2\psi - \frac{a}{\rho}\cos 2\psi)\}\times (\cos 2\psi - \frac{a}{\rho}\sin 2\psi)] \quad (9)$$

Now, the E_θ-field is given by the familiar relation,

$$E_\theta = Z_0 \,.\, H_\phi \quad (10)$$

where Z_0 is the characteristic wave imdedance.

Substituting the value of H_ϕ from Eqn. (6), we get,

$$E_\theta = -Z_0 \,.\, A\beta[K_1\{\beta\rho\sin(\psi-\phi)\}\cos(\psi-\phi)+K_1\{\beta\rho\sin(\psi+\phi)\}\cos(\psi+\phi)] \quad \ldots (11)$$

Hence, the transverse voltage tangential to the meridian plane is, from Eqn.(1),

$$V = \int_{-\psi}^{\psi-\sin^{-1}\frac{a}{\rho}} E_\theta \,.\, \rho d\theta = -Z_0 \,.\, 2A[K_0(\beta a)-K_0(\beta\rho\sin 2\psi)] \quad \ldots (12)$$

The upper limit of integration has been chosen to disregard the region inside the helix cylinder since it contributes little to the external field. From Eqns. (9) and (12), the characteristic impedance of the antenna is given as

$$Z_T = \frac{V}{I} = \frac{Z_0}{\pi a\beta}\cdot\frac{K_0(\beta a)-K_0(\beta\rho\sin 2\psi)}{K_1(\beta a)+K_1\left\{\beta\rho\left(\sin 2\psi - \frac{a}{\rho}\cos 2\psi\right)\right\}\left(\cos 2\psi - \frac{a}{\rho}\sin 2\psi\right)} \quad (13)$$

It is known that the characteristic wave impedance Z_0 is the same as the intrinsic impedance of free space ($= 120\pi$ ohms) for all transverse electromagnetic waves. Now, the phase velocity of the current wave along the two inclined arms of the antenna is reduced in the ratio β_0/β where $\beta_0 = \omega/c$ and the characteristic impedance of the system is inversely proportional to the phase velocity. It thus follows that the impedance will be increased in the ratio β/β_0. Accordingly Eqn. (13) reduces to

$$Z_T = \frac{120}{a\beta_0} \cdot \frac{K_0(\beta a) - K_0(\beta\rho \sin 2\psi)}{K_1(\beta a) + K_1\left\{\beta\rho\left(\sin 2\psi - \frac{a}{\rho}\cos 2\psi\right)\right\}\left(\cos 2\psi - \frac{a}{\rho}\sin 2\psi\right)} \quad \ldots (14)$$

The impedance of a rhombic antenna is found to vary perceptibly only upto a distance of $\lambda/2$ from the input ends (Schelkunoff, 1952); beyond this distance the variation is very small. The average characteristic impedance of the antenna will thus be given by

$$Z_{av} = \frac{1}{l}\left[\frac{120}{a\beta_0} \cdot \int_0^{\lambda/2} \frac{K_0(\beta a) - K_0(\beta\rho \sin 2\psi)}{K_1(\beta a) + K_1\left\{\beta\rho\left(\sin 2\psi - \frac{a}{\rho}\cos 2\psi\right)\right\}\left(\cos 2\psi - \frac{a}{\rho}\sin 2\psi\right)} d\rho\right.$$

$$+\left(l - \frac{\lambda}{2}\right) \cdot \frac{120}{a\beta_0} \cdot \frac{K_0(\beta a) - K_0\left(\beta\frac{\lambda}{2}\sin 2\psi\right)}{K_1(\beta a) + K_1\left\{\beta\frac{\lambda}{2}\left(\sin 2\psi - \frac{a}{\lambda/2} \cdot \cos 2\psi\right)\right\}\left(\cos 2\psi - \frac{a}{\lambda/2}\sin 2\psi\right)} \quad \ldots (15$$

where l is the axial length of each arm.

The expression for the average characteristic impedance is somewhat involved; however, for practical computation a number of approximations may be made, since the effects of some of the terms in the expression are small compared to others. For example, the quantities $\frac{a}{\rho}\cos 2\psi$ and $\frac{a}{\rho}\sin 2\psi$ have little effect on the variation of Z_{av} with ρ. Hence the denominator of the integrand reduces to $[K_1(\beta a) + K_1(\beta\rho \sin 2\psi)\cos 2\psi]$. The above expression is not integrable by any of the known methods. The integration is therefore performed numerically by the standard trapezoidal rule.

It is interesting to note that the expression on the right-hand side of Eqn. (15) is found to attain a constant value as ρ is increased beyond about 15 cm. This is in conformity with our assumption that the impedance is constant except near the input end. As the average characteristic impedance is approximately

equal to the input impedance [assumption (a)], the value of the expression on the right-hand side of Eqn. (15) should also represent the input impedance of the antenna at any frequency.

(ii) *Calculation of radiation pattern* :

In deriving expressions for the directivity of an ordinary rhombic antenna, Foster (1937) assumed that the current flows uniformly without attenuation from the input to the termination. This assumption neglects the effect of radiation and the mutual coupling between the arms. The derivation is thus not rigorous; however, it has been found that the shape of the directivity pattern is not particularly critical with regard to current distribution along the arms of the antenna (Christiansen, 1946).

The analysis of Foster, applicable to the case of a rhombic antenna with linear arms, should also hold good in the case of the antenna under study, except for the fact that the axial phase velocity in the helix arms is different from that in free space. Taking this departure into account, it may be readily seen that the relative directivities of the rhomic antenna under study for horizontal and vertical polarisations are approximately given by (Piggott, 1948; Harper, 1941).

$$D_h = A \cos \xi \left(\frac{\sin (\pi l k_1/\lambda_a)}{\pi l k_1/\lambda_a}\right)\left(\frac{\sin (\pi l k_2/\lambda_a)}{\pi l k_2/\lambda_a}\right) \cos \theta - \sin \xi \cos \Delta)$$
$$\times \sqrt{(1-\rho_h)^2 + 4\rho_h \cos^2 \left(\frac{\alpha_h}{2} - \frac{2\pi H}{\lambda} \sin \Delta\right.} \qquad (16)$$

and

$$D_v = A \cos \xi \left(\frac{\sin (\pi l k_1/\lambda_a)}{\pi l k_1/\lambda_a}\right)\left(\frac{\sin (\pi l k_2/\lambda_a)}{\pi l k_2/\lambda_a}\right) \sin \theta \,.\, \cos \Delta$$
$$\times \sqrt{(1-\rho_v)^2 + 4\rho_v \cos^2 \left(\frac{\alpha v}{2} - \frac{2\pi H}{\lambda} \sin \Delta\right)} \qquad (17)$$

where (figure 6),

l is the axial length of each arm ;

ρ_h, ρ_v —reflection coefficients of the ground, the suffixes h and v referring to the horizontal and vertejoı components;

α_h, α_v —phase changes due to the reflection;

Δ—elevation angle of the main radiation lobe with reference to the plane of the antenna;

2ξ —obtuse angle subtended by the adjacent helix-arms;

θ—aximuth angle of the axis of the major lobe referred to the major axis of the antenna;

H—height above the ground;

λ—free-space wavelength at the given frequency;

λ_a—effective 'axial' wavelength corresponding to frequency 'f' given by $\lambda_a = \frac{v}{f}$ where $v = \sin\alpha$;

$$k_1 = \frac{c}{v} - \cos\Delta \,.\, \sin(\xi + \theta)$$

$$k_2 = \frac{c}{v} - \cos\Delta \,.\, \sin(\xi - \theta)$$

k_1 and k_2 refer to the pick-up in the two pairs of the rhombic arms.

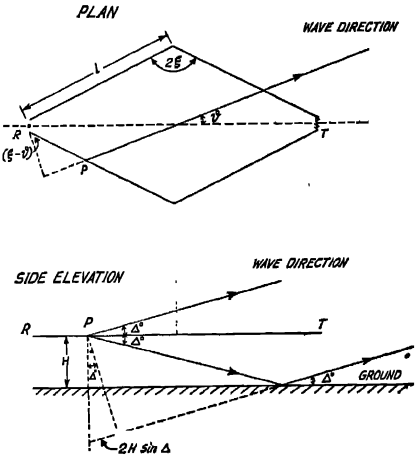

Fig. 6.—Illustrating the plan and the side elevation of the antenna when erected horizontally above the "ground".

For a perfectly conducting ground $\rho_h = 1$ and $\alpha_h = \pi$. The ground reflection factor in Eqn.(16) in case of the horizontally polarised component thus reduces to

$$R_h = 2 \sin\left(\frac{2\pi H}{\lambda} \sin\Delta\right) \qquad \ldots \quad (18)$$

For the vertically polarised component, however, both ρ_v and α_v are dependent on Δ and so, the reflection function, in Eqn.(18) hereafter represented by R_v, cannot be so replaced by a simple expression as in the case of R_h. Nevertheless, for approximate calculations, we may take $R_v \doteq 1$ for $\Delta \doteq 17.5°$ (Hamer, 1953).

It is seen from Eqns. (16) and (17) that the polar diagrams of the rhombic aerial are controlled by the product of three factors, viz., the integral functions $\frac{\sin(\pi l k_1/\lambda_a)}{\pi l k_1/\lambda_a}$, $\frac{\sin(\pi l k_2/\lambda_a)}{\pi l k_2/\lambda_a}$; the ground-reflection functions R_h, R_v; and the

projection functions $(\cos\theta - \sin\xi \cos\Delta)\cos\xi$, $(\sin\theta \,.\, \cos\Delta)\cos\xi$. It is apparent that if any of these factors is zero, the directivity must also be zero. This determines the positions of minima in the radiation pattern.

The ground-reflection functions (R_h, R_v) are dependent on Δ and H/λ and so, are fixed by the design of the antenna. For a particular frequency, the positions of maxima and minima in the polar diagram are dependent on the values of the projection functions as well as the integral functions. The shape of the polar diagram, however, is predominantly controlled by the integral function, or in other words, by the values of l/λ_a and k_1, k_2.

It is necessary that all the three functions should be large if a large directivity is required. In the case of the antenna under study, the values of the ground-reflection function and the projection function remain the same as in the case of a rhombic antenna with linear arms, but k_1 and k_2 assume very large values. These increments in the values of k_1, k_2 are due to the reduction in the phase velocity v. The magnitudes of the integral function thus are reduced, thereby causing a reduction in the value of the directivity of the antenna under study.

The directivity patterns, particularly for the horizontal polarisation in the azimuthal plane, show reasonable agreement with the theoretical values. The vertically polarised components of the field are present, though in smaller amplitudes, almost in the same direction as the horizontal components. This shows that the radiation field is somewhat elliptically polarised. The directivity patterns of the vertical components do not agree well with the theoretical values. This is

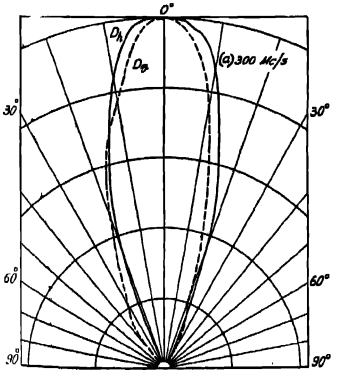

Fig. 7 (a).

D_h and D_v patterns of the antenna at 300 Mc/s.

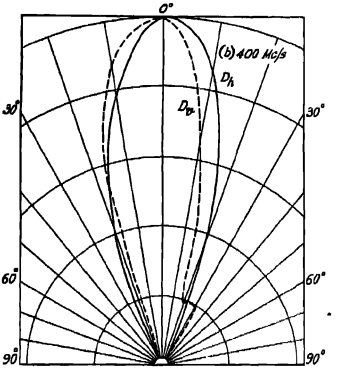

Fig. 7 (b).

D_h and D_v patterns of the antenna at 400 Mc/s.

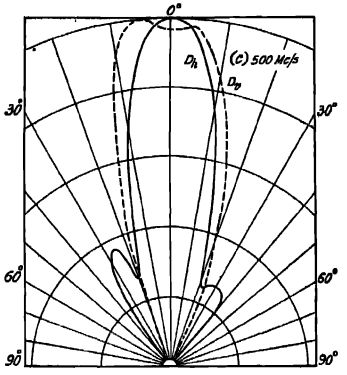

Fig. 7 (c).

D_h and D_v patterns of the antenna at 500 Mc/s.

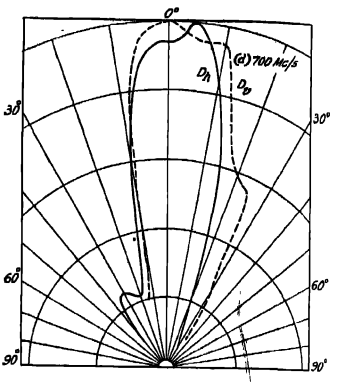

Fig. 7 (d).

D_h and D_v patterns of the antenna at 700 Mc/s.

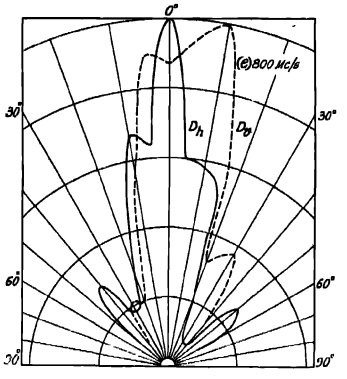

Fig. 7 (e).

D_h and D_v patterns of the antenna at 800 Mc/s.

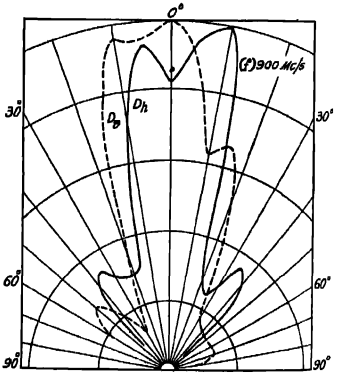

Fig. 7 (f).

D_h and D_v patterns of the antenna at 900 Mc/s.

as one would expect, for the derivation of the expressions for the directivity has been based on the assumption that the current in each helix arm can be replaced by an axial current which is not strictly true.

The patterns (figures 7-9) have been plotted after normalising the values. In figure 8, the experimental and theoretical polar diagrams of the antenna under study are compared for 600 mc/s excitation. Figure 9 has been shown to compare the theoretical polar plots (D_h) for the antenna with cylindrical helices as the arms and that with linear arms also at 600 mc/s excitation.

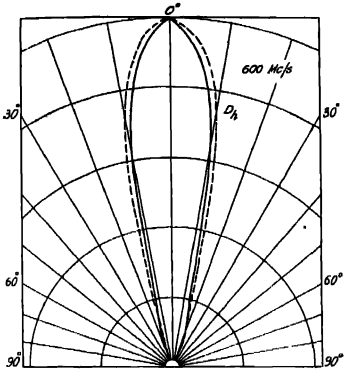

Fig. 8.

Calculated (dotted lien) and observed (solid line) D_h patterns at 600 Mc/s.

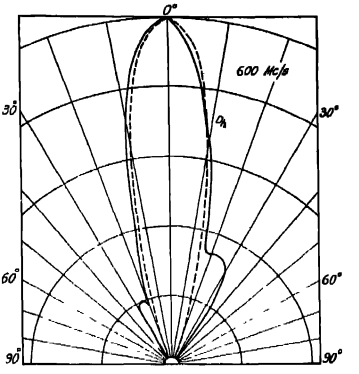

Fig. 9.

Calculated D_h patterns of the rhombic antenna with linear arms (dotted line) and of that with cylindrical helices as the arms (solid lines). Frequency, 600 Mc/s.

4. CONCLUDING REMARKS

It is evident from the observed impedance and the radiation characteristics of the antenna with helix arms that the wide-band properties and the directivity characteristics of a rhombic antenna with linear arms are more or less maintained in the case under study. There is, however, a decrease in gain. The reason may possibly be ascribed to the lesser "effective area" of the antenna under study in contrast to a corresponding antenna with linear arms.

It is found that at a particular frequency, the average characteristic impedance varies inversely as the radius of the helix cylinders. The impedance, again, varies from point to point near the input end and becomes constant after a distance. If the helices are suitably tapered towards the input ends the variation of impedance in the region may be reduced thereby enabling better match with the feeders.

ACKNOWLEDGMENTS

The author is grateful to Professor S. K. Mitra, F.R.S., for his kind interest in the work and to Professor J. N. Bhar for constant encouragement and enlightening discussions during the preparation of the paper. It is a pleasure to record his appreciation of the help and suggestions obtained from Professor J. S. Chatterjee and Mr. N. B. Chakravorty in course of the work. Thanks are also due to Mr. A. K. Choudhury for assistance in connection with the measuring equipments.

REFERENCES

Christiansen, W. N., 1947, *A.W.A. Technical Journal*, **7**, No. 4, 372.
Hamer, E. G., 1953, *Electronic Engg.*, **25**, 427.
Harper, E., 1941, Rhombic Antenna Design, D. Van Nostrand, New York,
Foster, D., 1937, *Proc. I.R.E.*, **25**, 1327.
Kraus, J. D., 1954, Antennas, McGraw-Hill Book Company, Inc., New York.
Neimann, M. S., 1939, *Izvestiya Electropram, Slab. Joka*, No. 1, **19**.
Piggott, W. R., A method of determining the Polar Diagrans of Long Wire and Horizontal Rhombic Aerials", 1948, D.S.I.R (U.K.), Radio Research Special Report, No. 16.
Pocklington, H. C., 1897, *Proc. Cambl Phil. Soc.*, **9**, 324.
Schelkunoff, I. S., 1943, Electromagnetic Waves, D. Van Nostrand, New York, 441.
Schelkunoff, I. S. and Friis, H. T., 1952, Antennas: Theory and Practice, John Wiley and Sons, New York, 427, 107.
Smith, W., Antenna Manual, Editors and Engineers Ltd., California, U.S.A., 213.
Tomiyasu, K., 1949, *J.A.P.*, **20**.

RADIAL PULSATIONS OF AN INFINITE CYLINDER IN THE PRESENCE OF MAGNETIC FIELD

J. N. TANDON

INDIAN NATIONAL COMMITTEE FOR THE I.G.Y., N.P.L., NEW DELHI-12

AND

S. P. TALWAR

DEPARTMENT OF PHYSICS, DELHI UNIVERSITY, DELHI

(*Received for publication, October* 28, 1957)

ABSTRACT. The general equation governing the radial pulsations of an infinite cylinder having volume currents has been derived and the integral formulae for the frequency of pulsations are deduced for two models of current density, viz., (i) circular currents and (ii) line currents. It is found that the cylinder remains dynamically stable for the two models of current systems.

The pulsations of an infinitely long cylindrical mass are of great significance for the cosmic bodies, e.g., spiral arm, solar ion streams etc. Chandrasekhar and Fermi (1953) have investigated the radial pulsations of such cylindrical masses in the presence of axial magnetic field. In the present note we investigate a similar problem in the presence of volume currents following the method adopted in our earlier paper (Talwar and Tandon, 1956) for the radial pulsations of spherical mass. Here, two special cases, (i) circular currents and (ii) axial line currents are discussed.

The equation of continuity and motion for the cylindrical fluid subjected to electromagnetic field can be written in the form

$$\frac{r}{r_0} \cdot \frac{\rho}{\rho} \cdot \frac{dr}{dr_0} = 1 \qquad \ldots \quad (1)$$

and

$$\rho \frac{\partial^2 r}{\partial t^2} = -\frac{\partial p}{\partial r} - \frac{2Gm(r)}{r} \rho + (\boldsymbol{j} \times \boldsymbol{H})_{radial} \qquad \ldots \quad (2)$$

Here all the physical quantities have their usual meaning and the electromagnetic field vectors $\boldsymbol{H}$ and $\boldsymbol{j}$ satisfy the usual Maxwellian relations. viz.,

$$\text{curl } \boldsymbol{H} = 4\pi \boldsymbol{j} \qquad \ldots \quad (3)$$

and

$$\text{div}\, \boldsymbol{H} = 0 \tag{4}$$

Distinguishing the values of various parameters for the equilibrium configuration by a subscript zero, we write

$$r = r_0 + \delta r, \qquad p = p_0 + \delta p, \qquad \rho = \rho_0 + \delta\rho \qquad \ldots \tag{5}$$

$$\boldsymbol{H} = \boldsymbol{H}_0 + \delta \boldsymbol{H} \quad \text{and} \quad \boldsymbol{j} = \boldsymbol{j}_0 + \delta \boldsymbol{j}$$

The variations in these parameters are assumed to be small so that the powers higher than the first can be neglected.

The equation (1) then gives

$$-\frac{\delta\rho}{\rho_0} = \frac{1}{r_0}\frac{\partial}{\partial r_0}(r_0 \delta r) \qquad \ldots \tag{6}$$

Taking the various terms in equation (2) in turn, we get

$$\rho \frac{\partial^2 r}{\partial t^2} = \rho_0 \frac{\partial^2 \delta r}{\partial t^2} \qquad \ldots \tag{7}$$

$$2Gm(r)\rho = \frac{2Gm(r_0)}{r} \rho_0 \left(1 - \frac{\partial \delta r}{\partial r_0}\right) \qquad \ldots \tag{8}$$

and

$$\frac{\partial p}{\partial r} = \frac{\partial p}{\partial r_0}\frac{\partial r_0}{\partial r}$$

$$= \frac{\partial p_0}{\partial r_0}\left(1 - \frac{\partial \delta r}{\partial r_0}\right) + \frac{\partial \delta p}{\partial r_0} \qquad \ldots \tag{9}$$

But for the equilibrium configuration equation (2) gives

$$\frac{\partial p_0}{\partial r_0} = -\frac{2Gm(r_0)}{r_0}\rho_0 + (\boldsymbol{j}_0 \times \boldsymbol{H}_0)_{radial} \qquad \ldots \tag{10}$$

and hence

$$\frac{\partial p}{\partial r} = \left[-\frac{2Gm(r_0)}{r_0}\rho_0 + (\boldsymbol{j}_0 \times \boldsymbol{H}_0)_{radial}\right] \qquad \ldots \tag{11}$$

$$\times \left(1 - \frac{\partial \delta r}{\partial r_0}\right) + \frac{\partial \delta \rho}{\partial r_0}$$

Now,

$$\frac{\partial \delta p}{\partial r_0} = \frac{\partial}{\partial r_0}\left[\frac{\Gamma p_0}{\rho_0}\delta p\right], \text{ Since } \frac{\delta p}{p_0} = \Gamma\frac{\delta \rho}{\rho_0}, \text{ (adiabatic pulsations)}$$

$$= -\Gamma\left[-\frac{2Gm(r_0)}{r_0}\rho_0 + (\boldsymbol{j}_0 \times \boldsymbol{H}_0)_{radial}\right]$$

$$\times \frac{1}{r_0}\frac{\partial}{\partial r_0}(r_0\delta r) \qquad \ldots (12)$$

$$-\Gamma p_0 \frac{\partial}{\partial r_0}\left\{\frac{1}{r_0}\frac{\partial}{\partial r_0}(r_0\delta r)\right\},$$

and hence equation (11) becomes

$$\frac{\partial p}{\partial r} = \left(1 - \frac{\partial \delta r}{\partial r_0}\right)\left\{-\frac{2Gm(r_0)}{r_0}\rho_0 + (\boldsymbol{j}_0 \times \boldsymbol{H}_0)_{radial}\right\}$$

$$-\Gamma\left\{-\frac{2Gm(r_0)}{r_0}\rho_0 + (\boldsymbol{j}_0 \times \boldsymbol{H}_0)_{radial}\right\} \qquad (13)$$

$$\times \frac{1}{r_0}\frac{\partial}{\partial r_0}(r_0\delta r) - \Gamma p_0 \frac{\partial}{\partial r_0}\left\{\frac{1}{r_0}\frac{\partial}{\partial r_0}(r_0\,\delta r)\right\}$$

Substituting equations (7), (8) and (13) in equation (2), we obtain, after some simplications.

$$\frac{\partial^2 \xi}{\partial r_0^2} + \left[\frac{2}{r_0} - \frac{2Gm(r_0)}{r_0}\frac{\rho_0}{p_0} + \frac{\Gamma+1}{\Gamma p_0}(\boldsymbol{j}_0 \times \boldsymbol{H}_0)_{radial}\right]\frac{\partial \xi}{\partial r_0}$$

$$+\left[\frac{4(1-\Gamma)}{\Gamma p_0}\frac{Gm(r_0)}{r_0^2}\rho_0 + \frac{1+2\Gamma}{\Gamma p_0}\frac{(\boldsymbol{j}_0 \times \boldsymbol{H}_0)_{radial}}{r_0}\right. \qquad \ldots (14)$$

$$\left. + \frac{\sigma^2 \rho_0}{\Gamma p_0}\right]\xi + \frac{[(\delta \boldsymbol{j} \times \boldsymbol{H}_0) + (\boldsymbol{j}_0 \times \delta \boldsymbol{H})]_{radial}}{\Gamma p_0 r_0}$$

$$= 0$$

where we have put

$$\delta r = \xi = \xi_0 e^{i\sigma t} \qquad \ldots (15)$$

The change in the magnetic field, δH, following the notion is given, (in a medium of infinite electrical conductivity), by

$$\delta \boldsymbol{H} = \text{curl}\ (\delta \boldsymbol{r} \times \boldsymbol{H}) + (\delta \boldsymbol{r} \cdot \text{grad})\,\boldsymbol{H} \qquad \ldots (16)$$

In any particular configuration where $\boldsymbol{j}_0$ and $\boldsymbol{H}_0$ are known, the change δj in current density, following the motion, can be evaluated by using equation (16) in conjunction with equation (3). Substituting the values of $\delta \boldsymbol{H}$ and $\delta \boldsymbol{j}$ thus obtained, in equation (14), we get the required equation for the radial pulsations of a cylindrical fluid, valid for all sorts of current system. We shall now deduce expressions for the frequency of pulsations in two special cases of current density.

Case (i) : Circular currents;

Let us consider that the circular currents are of the form

$$\boldsymbol{j} = \left(0, \frac{-kr}{4\pi}, 0 \right) \qquad \ldots \quad (17)$$

so that

$$\boldsymbol{H} = \left\{ 0, 0, \frac{K}{2}(r^2 - R^2) \right\} \qquad \ldots \quad (18)$$

and thus the only non-vanishing component for the change in the magnetic field following motion will be given by,

$$\delta H_z = - \left[2\xi + r_0 \frac{\partial \xi}{\partial r_0} \right] \left[\frac{K}{2}(r^2 - R^2) \right] \qquad \ldots \quad (19)$$

here K is a constant and R is the radius of the cylinder. Further, if ξ is assumed to be constant in space then

$$\delta \boldsymbol{H} = -2\xi \boldsymbol{H}_0 \qquad \ldots \quad (20)$$

and the change δj in current density (following motion) is given by

$$\delta \boldsymbol{j} = -3\xi \boldsymbol{j}_0 \qquad \ldots \quad (21)$$

Thus the pulsation equation (14) yields

$$\sigma^2 r_0 = 4(\Gamma - 1) \, . \, G\pi\rho_0 r_0 + \frac{2(2-\Gamma)}{} \times (\boldsymbol{j}_0 \times \boldsymbol{H}_0)_{radial} \qquad \ldots \quad (22)$$

Multiplying equation (22) by r_0 and integrating over the entire mass, we obtain (omitting the subscript zero)

$$\sigma^2 \, . \int^{m} r^2 dm = 2(\Gamma - 1) G M^2 + 2(2 - \Gamma) \int r \, . \, (j \times H) d\tau \qquad \ldots \quad (23)$$

where $d\tau$ is the volume element. Now

$$\int_V r \cdot (j \times H) d\tau = \frac{k^2 R^6}{48}$$

$$= 2 \int_V \frac{H^2}{8\pi} \, d\tau = 2\mathfrak{M} \text{ (say)} \qquad \ldots \quad (24)$$

Thus we have

$$\sigma^2 \int^M r^2 \, dm = 2(\Gamma - 1) GM^2 + 4(2 - \Gamma)\mathfrak{M} \qquad \ldots \quad (25)$$

It can readily be shown for the equilibrium configuration

$$\int_V r \cdot (j \times H) d\tau = GM^2 - 2(\Gamma - 1) U \qquad \ldots \quad (26)$$

where U is the internal energy of the system. Substituting equation (26) in equation (23) we obtain the expression for frequency of pulsation in terms of the internal energy, viz.,

$$\sigma^2 \int^M r^2 dm = -4(2 - \Gamma)(\Gamma - 1) U + 2GM^2 \qquad \ldots \quad (27)$$

or

$$\sigma^2 \int^M r^2 dm = 4(\Gamma - 1)^2 U + 2 \int_V \boldsymbol{r} \cdot (\boldsymbol{j} \times \boldsymbol{H}) d\tau \qquad \ldots \quad (28)$$

An expression similar to that of equation (28) was obtained earlier by Chandrasekhar and Fermi (1953)..

Case (ii). Line currents.

Let us consider the case in which the current density j is constant in the cylinder and is of the form

$$\boldsymbol{j} = \left((0, 0, \frac{K}{2\pi} \right) \qquad \ldots \quad (29)$$

where K is constant. The magnetic field will then be given by

$$\boldsymbol{H} = (0, Kr, 0) \qquad \ldots \quad (30)$$

For such a configuration

$$\delta \boldsymbol{H} = -\xi \boldsymbol{H}$$

and

$$\delta j = -2\xi j \qquad \dots \quad (31)$$

where ξ is a constant in space. Substituting these values in equation (14) we find

$$\sigma^2 \int^{M} r^2 dm = 2(\Gamma-1)GM^2 - 2(\Gamma-1)\int_V \boldsymbol{r}\,.\,(\boldsymbol{j}\times\boldsymbol{H})\,d\tau \qquad \dots \quad (32)$$

Using equation (26), we get

$$\sigma^2 \int^{M} r^2 dm = 4(\Gamma-1)^2 U \qquad \dots \quad (33)$$

as an expression for the frequency of pulsations in the presence of line currents in terms of internal energy, U. It can readily be shown that $\boldsymbol{r}.\,(\boldsymbol{j}\times\boldsymbol{H})$ is a negative quantity and hence the cylinder will be dynamically stable.

Equations (25) and (32) clearly show that the cylinder is stable for radial pulsations in the presence of circular as well as line currents. The lateral instability of the incompressible infinitely long cylindrical fluid mass has recently been discussed by Auluck and Kothari (1957). They have also shown that the magnetic field in general has a stabilizing effect.

REFERENCES

Auluck, F. C. and Kothari, D. S., 1957, *Z. Astrophys.* **42**, 101.
Chandrasekhar, S. and Fermi, *E.*, 1953, *Ap. J.*, **118**, 116.
Talwar, S. P. and Tandon, J. N., 1956, *Ind. J. Phys.*, **30**, 561.

ULTRAVIOLET ABSORPTION SPECTRA OF SOLUTIONS OF PYRIDINE IN DIFFERENT SOLVENTS AND AT DIFFERENT TEMPERATURES

S. B. ROY

OPTICS DEPARTMENT, INDIAN ASSOCIATION FOR THE CULTIVATION OF SCIENCE, JADAVPUR, CALCUTTA

(*Received for publication, March* 24, 1958)

ABSTRACT. The ultraviolet absorption spectra of solutions of pyridine in cyclohexane, 3-methyl pentane, carbon tetrachloride and isobutyl alcohol have been studied and the results have been compared with those for the vapour reported by previous workers. The two systems of bands due respectively to $n \rightarrow \pi^*$ and $\pi \rightarrow \pi^*$ transitions are observed in the spectra due to solutions in cyclohexane, 3-methyl pentane and carbon tetrachloride, but the first system is totally absent in the spectrum of the solution in isobutyl alcohol. The interval between the successive bands in the first system is 542 cm^{-1}, which agrees closely with that observed in the case of the vapour. It has further been observed that the 0, 0 band in the first system shifts by about 430 cm^{-1} when pyridine is dissolved in the first three solvents. It is pointed out that these results confirm the explanation put forward by previous workers for the absence of the first system of bands in the case of the solution in alcohol. The $n \rightarrow \pi^*$ transition does not occur in this case because a bond is formed between the pyridine molecule and the alcohol molecule through the non-bonding electron of the nitrogen atom, but no such bond formation takes place in the solutions in the other solvents.

INTRODUCTION

From theoretical considerations Kasha (1950) suggested the probabilities of two types of electronic transitions in the pyridine molecule, one due to the excitation of one nitrogen non-bonding electron to π molecular orbital being designated as $n \rightarrow \pi^*$ transition and the other a singlet-singlet $\pi \rightarrow \pi^*$ transition. On scrutinising the absorption spectrum of pyridine vapour reported by Sponer and Stücklen (1946), the existence of two systems of bands due to the transitions mentioned above was confirmed by Rush and Sponer (1952). The 0, 0 band due to $n \rightarrow \pi^*$ transition (called the 1st system) is at 34769 cm^{-1} and that due to $\pi \rightarrow \pi^*$ transition (called the 2nd system) at 38350 cm^{-1}.

The absorption spectra of solutions of pyridine were studied by Herington (1950) who measured the molecular dissociation constant but did not observe the 1st system of bands. Stephenson (1954) also studied the absorption spectrum of solutions of pyridine in iso-octane and alcohol. From a comparison of the two absorption curves he concluded that the 1st system of bands was present in

the case of the iso-octane solution and it was absent in the spectrum due to the solution in alcohol.

Recently, Banerjee (1956) studied the ultraviolet absorption spectrum of pyridine in the liquid state and in the solid state at $-180°C$ and found the first system of bands to be absent in both cases. He concluded that in the liquid and solid states, the pyridine molecule is attached to the neighbouring molecule through a new bond formed between non-bonding electron of the nitrogen atom and the hydrogen atom of the neighbouring molecule and therefore, the $n \rightarrow \pi^*$ transition does not occur.

The object of the present investigation was to study more exhaustively the influence of different environments and of temperature on both the systems of absorption bands of pyridine and to find out whether such bond formation is actually responsible for the disappearance of the first system of bands.

EXPERIMENTAL

The experimental arrangement was similar to that described in an earlier paper (Roy, 1956). Chemically pure pyridine from E. Merck was first fractionated and the proper fraction was redistilled under reduced pressure before use. The solvents used were cyclohexane, isobutyl alcohol, 3-methyl pentane and carbon tetrachloride. The solvents were found to have no absorption band in the region under consideration. The thicknesses of the two cells used were 5 mm and 3 cm. respectively and the strength of the solutions varied from .01% to .06% by weight. The spectra were photographed on Ilford HP3 films with a Hilger medium quartz spectrograph Iron arc spectrum was taken on each film as a comparison. Microphotometric records were taken with a Kipp and Zonen type self-recording microphotometer. The absorption spectra were calibrated with the help of the microphotometric records of iron lines using the method described in an earlier paper (Roy, 1956).

RESULTS

The microphotometric records of the absorption spectra of solutions of pyridine of different strengths in cyclohexane are given in figure 1 and those due to solutions in 3-methyl pentane, isobutyl alcohol and carbon tetrachloride are reproduced in figures 2 and 3. The frequencies of the absorption bands and probable assignemnts are given in Tables I, II and III. The data for the substance in the gaseous state reported by Rush and Sponer (1952) are also included in Table I for comparison.

DISCUSSION

It can be seen from figures 1(b) and 1(c) that the spectrum due to .06% solution in cyclohexane, with a cell thickness of 5 mm is identical with that

due to a thickness of 3 cm of .01% solution and there are three bands in the region, 35200 cm^{-1}—36284 cm^{-1}. The spectrum due to .01% solution of thickness

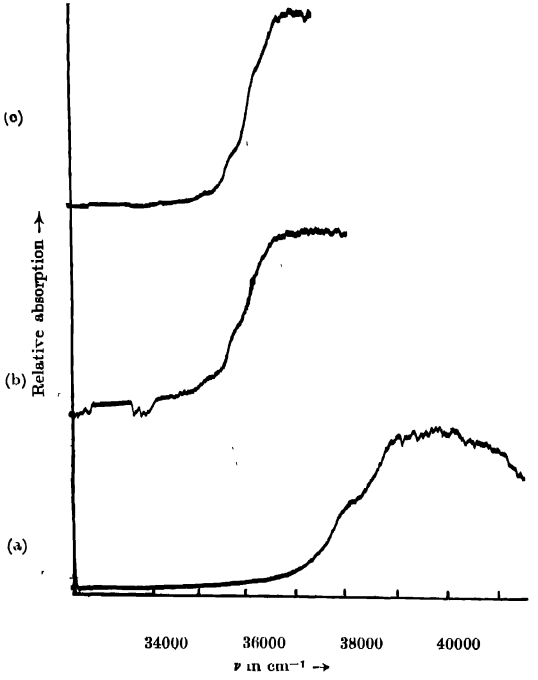

Fig. 1. Microphotomatric records of ultraviolet absorption spectra of solutions of pyridine in cyclohexane.

(a) .01 % solution in cyclohexane with 5 mm cell at 30°C
(b) .06 % " " " " " " " "
(c) .01 % " " " " 3 cm " " "

5 mm, however, does not show these bands but a second system of bands with the first band at 37924 cm^{-1} is observed. A thicker cell produces complete absorption in this region. Evidently, the solution yields two systems of absorption bands, the weaker one being due to $n \rightarrow \pi^*$ transition and the stronger one due to the $\pi \rightarrow \pi^*$ transition. The solution in 3-methyl pentane, also, shows these two systems as can be seen in figure 2. When the solution is frozen it becomes rigid glass and two extra bands appear on the shorter wavelength side in the

first system. The positions of the first three bands, however, remain unchanged when the solution is frozen and cooled to −180°C. This shows that

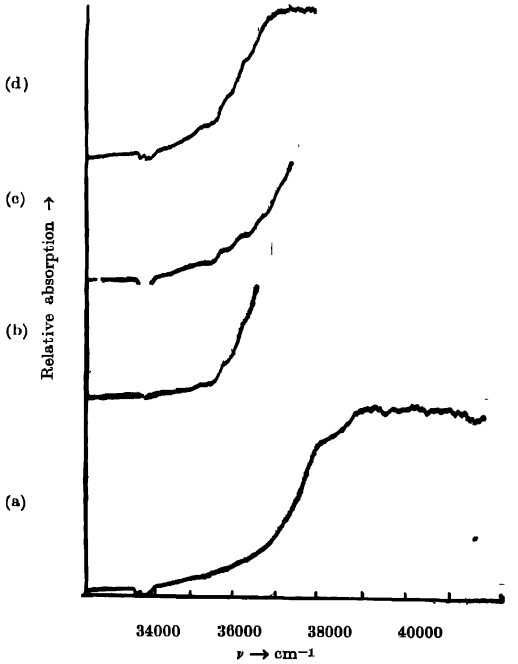

Fig. 2. Mycrophotometric records of ultraviolet absorption spectra of solutions of pyridine in 3-methyl pentane.

(a) .01% solution in 3-methyl pentane with 5mm cell at 30°C.
(b) .06% " " " " " 5 mm " " 30°C.
(c) .06% " " " " " 5 mm " " −180°C.
(d) .01% " " " " " 3 cm " " 30°C.

first band is to be assigned to 0→0 transition in the system and not to $V \rightarrow 0$ transition. Figure 3 shows that in the spectra due to solution in isobutyl alcohol, the first system of bands is totally absent, there being full transmission in the region of these bands. These results thus corroborate the view put forward by Stephenson(1954) that the disappearance of the bands in the spectrum due to the solution in alcohol is due to the formation of a bond through the non-bonding electron of the nitrogen atom and OH group of the alcohol molecule. It is further proved by these results that such bond formation does not take place in the solutions in cyclohexane and 3-methyl pentane.

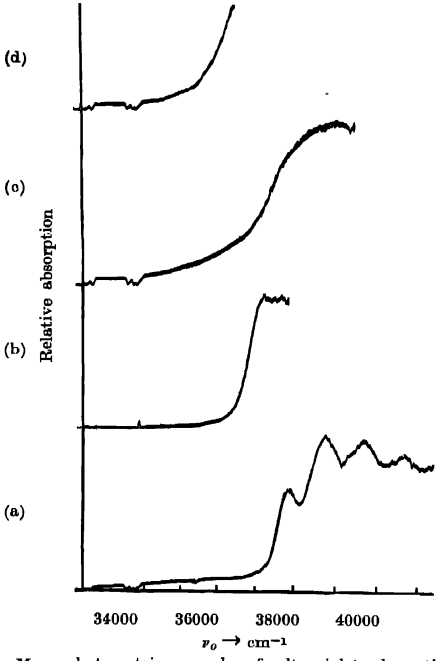

Fig. 3. Mycrophotometric records of ultraviolet absorption spectra of solutions of pyridine in different solvents.

(a) .01% solution in isobutyl alcohol with 5 mm cell at − 180°C.
(b) .06% ,, ,, ,, 5 mm cell at − 180°C.
(c) .01% ,, carbon tetrachloride with 5 mm cell at 30°C.
(d) .06% ,, ,, ,, 5 mm cell at 30°C.

The 0, 0 band in the first system due to pyridine vapour is at 34769 cm^{-1} (Rush and Sponer, 1952), but in the solutions either in cyclohexane or in 3-methyl pentane the band of the first system is at 35200 cm^{-1}. Hence this band is shifted towards shorter wavelength by about 431 cm^{-1} by the influence of the solvents. These bands are also much wider than the corresponding bands due to vapour. This broadening is evidently due to the fluctuation of the intermolecular forces in the solution. The interval between successive bands is 542 cm^{-1} which agrees closely with those observed in the case of the vapour (Rush and Sponer, 1952).

The spectrum due to the solution in carbon tetrachloride (figure 3) does not show discrete bands in the first system, but the absorption curves rise as steeply as in the case of solution in 3-methyl pentane. Probably, the bands are

TABLE I

Absorption spectra of pyridine

Vapour (prominent bands) Rush & Sponer, 1952		.01% sol. in cyclohexane .5cm cell (liq.)		.01% sol. in cyclohexane 3cm cell (liq.)		.06% sol. in cyclohexane .5cm cell (liq.)	
ν in cm^{-1}	Assignment	ν in cm^{-1}	Assignment	ν in cm^{-1}	Assignment	ν in cm^{-1}	Assignment
1st system		*1st system*		*1st system*		*1st system*	
34769	0, 0	No discrete band observed		35200	0, 0	35200	0, 0
35311	0+542			35742	0+542	35742	0+542
35633	0+864			36284	0+542×2	36284	0+542×2
35855	0+542×2						
36397	0+542×3						
2nd system		*2nd system*		*2nd system*		*2nd system*	
38350	0, 0	38070	0, 0	Total absorption		Total absorption	
		39020	0+950				
		39971	0+950×2				
		40821	0+950×3				

TABLE II

Absorption spectra of pyridine

.01% sol. in 3-methyl pentane .5cm cell (liq.)		.01% sol. in 3-methyl pentane 3cm cell (liq.)		.06% sol. in 3-methyl pentane .5cm cell (liq.)		.06% sol. in 3-methyl pentane (solid −180°C) .5cm cell	
ν in cm^{-1}	Assignment	ν in cm^{-1}	Assignment	ν in cm^{-1}	Assignment	ν in cm^{-1}	Assignment
1st system		*1st system*		*1st system*		*1st system*	
No discrete band observed		35200	0, 0	35200	0, 0	35200	0, 0
		35742	0+542	35742	0+542	35742	0+542
		36286	0+542×2	36286	0+542×2	36286	0+542×2
					—	36828	0+542×3
						37370	0+542×4
2nd system		*2nd system*		*2nd system*		*2nd system*	
38947	0+950	Total absorption		Total absorption		Total absorption	
39897	0+950×2						
40847	0+950×3						

TABLE III

Absorption spectra of pyridine

.01% sol. in isobutyl alcohol .5 cm cell		.06% sol. in isobutyl alcohol (solid −180°C) .5 cm cell		.01% sol. in carbon tetrachloride .5 cm cell		.06% sol. in carbon tetrachloride .5 cm cell	
ν in cm^{-1}	Assignment	ν in cm^{-1}	Assignment	ν in cm^{-1}	Assignment	ν in cm^{-1}	Assignment
1st system Absent		*1st system* Absent		*1st system* Unresolved		*1st system* Unresolved	
2nd system		*2nd system*		*2nd system*		*2nd system*	
37924	0, 0			37924	0, 0		
38874	0+950	Total absorption		38874	0+950	Total absorption	
39828	0+950×2						
40776	0+950×3						

much broader in this case and they are not resolved from each other. The nature of the curve shows, however, that in this case also, the first system shifts as much towards shorter wavelengths as in the solution in 3-methyl pentane.

In the absorption spectrum of pyridine in the liquid state and in the solid state at −180°C, the first system is totally absent (Banerjee, 1956). This shows that the non-bonding electron of the nitrogen atom forms a bond with the hydrogen atom of the pyridine ring. Hence the nature of the hydrogen atom in the ring is different from that of the hydrogen atom in cyclohexane or 3-methyl pentane.

ACKNOWLEDGMENT

The author wishes to record his grateful thanks to Professor S. C. Sirkar, D.Sc., F.N.I., for his kind interest and guidance in the work.

REFERENCES

Banerjee, S. B., 1956, *Ind. J. Phys.*, **30**, 480.
Herington, E. F. G., *Discussions of the Faraday Society*, **9**, 26.
Kasha, M., 1950, *Discussions of the Faraday Society*, **9**, 14.
Roy, S. B., 1956, *Ind. J. Phys.*, **30**, 267.
Rush, J. H. and Sponer, H., 1952, *J. Chem. Phys.*, **20**, 1847.
Sponer, H. and Stücklen, H., 1946, *J. Chem. Phys*, **14**, 101.
Stephenson, H. P., 1954, *J. Chem. Phys.*, **22**, 1077.

ON CORE-TO-PARTICLE INTERACTION FROM CLASSICAL POINT OF VIEW

S. MUKHERJEE AND A. GUPTA

INSTITUTE OF NUCLEAR PHYSICS, CALCUTTA

(*Received for publication August* 8, 1957)

ABSTRACT. The treatment of the extra-core particle in the semi-rigid model of nucleus, in a core plus one particle system, in a sense justifies the form of the interaction hamiltonian used, in such cases, by A. Bohr in his collective model of nucleus.

INTRODUCTION

In the collective model of nucleus (A. Bohr, 1952) one takes the interaction between a particle and the core, in a core plus one particle system, to be confined only on the surface, the interaction being represented by

$$_1H_{int} = -k\delta(r-R)\sum_{\mu=-\lambda}^{\lambda} \alpha_{\lambda\mu}\, Y^{\lambda}{}_{\mu}\,(\theta, \phi) \qquad \ldots \quad (1)$$

and as such the extra-core particle experiences no force when it goes within the nucleus. In this short note we have tried to find the order of magnitude of the force experienced by the extra-core particle when it goes within the liquid core, and to derive it we have followed a semi-rigid model for the whole system i.e. the rigid body motion of the extra-core particle and irrotational motion of the core. Classically the problem reduces to one of a small rigid sphere within a large volume of pulsating liquid of almost sperical shape and to seek an irrotational motion of the liquid consistent with the boundary conditions. We have found that the force experienced by the small sphere is derivable from a potential function and has exactly the form of an anisotropic harmonic-oscillator. We have also calculated the angular momentum and the magnetic moment of the system with the presence of the sphere within the nuclear fluid, and obtained a few correction terms in both cases over and above what A. Bohr (1952) has obtained for the same.

1. DERIVATION OF THE INTERACTION

Let the equation of the surface defining the boundary of the nucleus be given by

$$F \equiv R - R_0 \left\{1 + \frac{\alpha_{00}}{\sqrt{4\pi}} + \sum_{\mu=-2}^{2} \alpha_{2\mu}\, Y_{\mu}{}^{2}\,(\theta, \phi)\right\} = 0 \qquad \ldots \quad (2)$$

The condition at the boundary of the surface is

$$\frac{dF}{dt} = 0$$

or

$$\frac{\partial F}{\partial t} + u\frac{\partial F}{\partial r} + \frac{v}{r}\frac{\partial F}{\partial \theta} + \frac{w}{r\sin\theta}\frac{\partial F}{\partial \phi} = 0 \qquad \ldots \quad (3)$$

where u, v, w are the components of velocity in polar co-ordinates and the left hand side of (3) is evaluated at the surface given by (2).

Let us assume that the velocity potential at any point is given by

$$\phi = \sum_{\mu=-2}^{2} \beta_{2\mu}\, r^2 Y^2{}_\mu\,(\theta, \phi) \qquad \ldots \quad (4)$$

Then substituting for u, v, w in (3) by those calculated from (4), it is easily seen that the first order solution of the resulting equation is

$$\beta_{2\mu} = -\tfrac{1}{2}\dot{\alpha}_{2\mu}$$

or

$$\phi = -\tfrac{1}{2}\sum_{\mu=-2}^{2} \dot{\alpha}_{2\mu}\, r^2\, Y^2{}_\mu(\theta, \phi) \qquad \ldots \quad (5)$$

Now if a small sphere of radius δ is introduced within the fluid then the velocity potential given by (5) will be changed.

To facilitate the calculation of drag on this small sphere we change the origin to the centre of the sphere, without changing the direction of axes. Let (a, b, c) or (r_p, θ_p, ϕ_p) be the co-ordinates of the sphere referred to old system, and let (r', θ', ϕ') be the co-ordinate of any point in the new system which was (r, θ, ϕ) in the old system. Then equation (5) reduces to

$$\phi = -\tfrac{1}{2}\, r'^2 \sum_{\mu=-2}^{2} \dot{\alpha}_{2\mu}\, Y^2{}_\mu(\theta', \phi') - \tfrac{1}{2}\, r^2{}_p \sum_{\mu=-2}^{2} \dot{\alpha}_{2\mu}\, Y^2{}_\mu(\theta_p, \phi_p)$$

$$- r' \sum^{1} A_{\mu'}\, Y^1{}_{\mu'}(\theta', \phi') \qquad (6)$$

where

$$A_{\mu'} = r_p \sum_{m=-1} C^{\mu'}{}_m \dot{\alpha}_2 m + \mu'\, Y^1{}_m\,(\theta_p, \phi_p) \qquad (7)$$

and $C_m{}^{\mu'}$ is given by

$$\sqrt{\frac{3}{10\pi}}\, C^{\mu'}{}_m \equiv \begin{array}{c|ccc} m \backslash \mu' & -1 & 0 & 1 \\ \hline -1 & 1 & \frac{1}{\sqrt{2}} & \frac{1}{\sqrt{6}} \\ 0 & \frac{1}{\sqrt{2}} & \sqrt{\frac{2}{3}} & \frac{1}{\sqrt{2}} \\ 1 & \frac{1}{\sqrt{6}} & \frac{1}{\sqrt{2}} & -1 \end{array} \qquad (8)$$

The additional condition to be satisfied by the new velocity potential Φ is

$$-\frac{\partial \Phi}{\partial r'}\bigg|_{r'=\delta} = \text{velocity of the sphere in that direction}$$

$$= -\frac{\dot{a}-i\dot{b}}{2}\sqrt{\frac{8\pi}{3}}\, Y^1{}_1(\theta', \phi') + \dot{c}\sqrt{\frac{4\pi}{3}}\, Y^1{}_0(\theta', \phi') + \frac{\dot{a}+i\dot{b}}{2}\sqrt{\frac{8\pi}{3}}\, Y^1{}_{-1}(\theta', \phi') \quad \ldots (9)$$

So we take Φ in the form

$$\phi = -\left(r' + \frac{D}{r'^2}\right)\sum_{\mu'=-1}^{1} A_{\mu'}\, Y^1{}_{\mu'}(\theta', \phi') - \tfrac{1}{2}\left(r'^2 + \frac{E}{r'^3}\right)\sum_{\mu=-2}^{2} \dot{\alpha}_{2\mu}\, Y^2{}_{\mu}(\theta', \phi')$$

$$+ \frac{\delta^3}{r'^2}\sum^{1} B_{\mu'}\, Y^1{}_{\mu'}(\theta', \phi') \quad \ldots (10)$$

By (9) and (10) one easily obtains D, E and $B_{\mu'}$.

To calculate the thrust experienced by the sphere we use Bernoulli's equation

$$\frac{p}{\rho} = \frac{\partial \Phi}{\partial t} - \frac{1}{2} q^2 \quad \ldots (11)$$

where ρ is the density of the fluid, q, p are the velocity and the pressure at any point. In our case δ^3 is of the order $\frac{1}{A}$, where A is the mass number of the nucleus. So retaining terms of the order $\frac{1}{A}$ and neglecting all higher order

terms, it is easily seen that the force experienced by the small sphere due to the pressure and velocity distribution given by (11) and (10) respectively, is derivable from a potential function and the dominant terms are given by

$$V = -\frac{3M\rho}{2\rho+4\sigma} r_p^2 \sum_{\mu=-2}^{2} \dot{\alpha}_{2\mu} Y^2_\mu (\theta_p, \phi_p) \qquad \ldots \quad (12)$$

where M, σ are the mass and the density of the small sphere and the potential is measured from the surface of the nucleus. It is easily seen that the hamiltonian of the core will not change (up to the order of approximation we are concerned with) from that of A. Bohr (1952) who calculated the same with a velocity potential which is the same as our unperturbed Φ given by (5). Therefore up to $\frac{1}{A}$ order accuracy we may say that the potential energy of the particle at (r, θ, ϕ) within the nucleus, referred to its value at the surface, due to the surface oscillation is given by

$$H_{\text{int}} = -K_1 . \frac{1}{2} M r^2 \omega^2 \sum_{\mu=-2}^{2} \alpha_{2\mu} Y^2_\mu (\theta, \phi) \qquad \ldots \quad (13)$$

where $K_1 = \frac{3\rho}{\rho+2\sigma}$ and $\omega = \omega_2$ of A. Bohr (1952). This is to be compared with the interaction hamiltonian (1) of A. Bohr. The matrix element of K in (1) has been estimated (A. Bohr (1953)) to be of the order of 40 Mev, whereas the corresponding term in case of our interaction comes out to be of the order of 2 Mev (taking $\sigma \simeq \rho$; M = mass of a proton). So it turns out that the classical value of the interaction strength is too small compared to what is required emperically. The empirical way of defining the core-to-particle interaction only at the surface (if it serves some purpose) is then perhaps justified, so far as the present model is concerned.

2. ANGULAR MOMENTUM

We calculate the angular momentum using the formula (A. Bohr (1952)).

$$\boldsymbol{m} = \int \rho(\boldsymbol{r} \times \boldsymbol{v}) d\tau \qquad \ldots \quad (14)$$

with

$$\boldsymbol{v} = -\text{grad } \Phi \qquad \ldots \quad (15)$$

We write this as

$$\boldsymbol{m} = i B \sum_{\mu', \mu=-2}^{2} \dot{\alpha}_{2\mu'} \alpha^*_{2\mu} \boldsymbol{M}_{\mu', \mu} + \text{correction terms} \qquad \ldots \quad (16)$$

where the first term in (16) is the same as that obtained by A. Bohr (1952) and the other leading terms are of the form

$$i\rho D\sum_{\mu'=-1}^{1}\sum_{s=-1}^{1}\sum_{\mu=-2}^{2}\sum_{t=1}^{3}\sum_{L=t-1}^{t+1} C_s^{\mu'}\,\alpha_{2s+\mu'}\,\alpha^*_{2\mu}$$

$$\times\left\{\sum_{m=-t}^{t}\frac{3(2t+1)}{\sqrt{5(2L+1)}}\begin{pmatrix}t&1&2\\0&0&0\end{pmatrix}\begin{pmatrix}t&1&L\\0&0&0\end{pmatrix}\begin{pmatrix}t&1&2\\m&\mu'&m+\mu'\end{pmatrix}\begin{pmatrix}t&1&L\\m&s&s+m\end{pmatrix}r_p^2 f_k(r_p,\delta)\right.$$

$$Y^L_{s+m}(\theta_p,\phi_p)\boldsymbol{M}_{m+\mu',\mu}$$

$$-\sum_{m=-2}^{2}\sqrt{\frac{45}{2L+1}}\begin{pmatrix}2&1&t\\0&0&0\end{pmatrix}\begin{pmatrix}t&1&L\\0&0&0\end{pmatrix}\begin{pmatrix}2&1&t\\m&\mu'&m+\mu'\end{pmatrix}\begin{pmatrix}t&1&L\\m+\mu'&s&m+\mu'+s\end{pmatrix}r_p^2 f_k(r_p,\delta)$$

$$\left.Y^L_{m+\mu'+s}(\theta_p,\phi_p)\boldsymbol{M}_{m,\mu}\right\}$$

where $\begin{pmatrix}j_1&j_2&j\\m_1&m_2&m\end{pmatrix}$ is the Clebsch-Gordan coefficient $\langle j_1\,j_2\,m_1\,m_2\mid j_1 j_2 jm\rangle$ of Condon and Shortley (1953), $f_k(r_p,\delta)$ is some function of r_p and δ, and $D=\frac{1}{2}\delta^3$.

Magnetic moment is given by, (in the notation of *E*.Feenberg 1955)

$$\langle \nu\, j\, k;\ II \mid m_z \mid \nu j\, k\,;\, I\, I\rangle$$

where j, k, I are the total angular momentum of the extra-core particle, core and the nucleus respectively, ν is the phonon number. For the nuclei with $j=I$, and in case of one phonon excitation the contribution from the correction term becomes

$$F\begin{pmatrix}I&2&I\\I-1&1&I-1\end{pmatrix}^2\sum_{t=1}^{3}\sum_{L=t-1}^{t+1}\begin{pmatrix}I&L&I\\I-1&0&I-1\end{pmatrix}\begin{pmatrix}l&L&l\\0&0&0\end{pmatrix}\begin{pmatrix}t&1&2\\0&0&0\end{pmatrix}\begin{pmatrix}t&1&L\\0&0&0\end{pmatrix}^2\begin{pmatrix}t&1&2\\0&1&1\end{pmatrix}$$

$$\times U(\tfrac{1}{2}l\,I\,L;\quad I\,l)(2t+1)\quad f_k(r_p,\delta)$$

where l is the orbital angular momentum of the extra-core nucleon, F is a constant of the order $\frac{1}{A}$, U is the U-coefficient of Jahn (1952), and in this expression we have replaced the matrix element of r_p by its average value. It is seen from this expression that for $j=I=1/2$ the correction term does not contribute anything to the magnetic moment, and for all other I there is a non-zero contribution. But as the factor F is of the order $\frac{1}{A}$, it turns out that the contribution affects

only the second place in decimals, and as such the results of A. Bohr (1952, 1953) remain practically unchanged. It can also be verified that the results of quadrupole moments of A. Bohr also remain practically unaltered, if our form of interaction is superimposed on the kind of surface interaction used by him. So it may be concluded by saying that the semi-rigid model of nucleus does not affect the results of A. Bohr, so far as the points which we have investigated here are concerned.

N.B. It should be noted that the semi-rigid model of nucleus that we have used here is a bit idealisation of the same proposed by Moszkowski (1956).

ACKNOWLEDGMENTS

The authors have great pleasures in expressing their deep gratitude to Professor A. K. Saha. They would also like to thank Dr. M. K. Banerjee, Mr. M. K. Pal, Mr. P. N. Mukherjee for their helpful criticisms.

REFERENCES

Bohr, A., 1952, *Dan. Mat. Fys. Medd.* **26**, 14.
Bohr, A., 1953, *Dan. Mat. Fys. Medd.* **27**, 16.
Condon and Shortley., 1953, Cambridge.
Feenberg, E., 1955, Shell Theory of Nucleus, Princeton Univ. Press.
Jahn, H. A., 1951, *Proc. Roy. Soc.*, A. **205**, 192.
Moszkowski, Steven. A., 1956, *Phys. Rev.* **103**, 1328.

SCATTERING OF ELECTRON FROM FIVE DIMENSIONAL WAVE EQUATION

A. K. MITRA

DEPARTMENT OF THEORETICAL PHYSICS

INDIAN ASSOCIATION FOR THE CULTIVATION OF SCIENCE, CALCUTTA

(*Received for publicationApril* 22, 1958)

ABSTRACT. The solution of the radial part of the five dimensional wave equation for the case of scattering of an electron in a Coulomb field has been considered and it is found that half integral quantum numbers appear in the solution which lends support to the idea that the influence of the fifth coordinate is somewhat analogus to the existence of the spin

INTRODUCTION

Banerjee (1958) has shown that if one assumes that the electron obeys a five dimensional wave equation, then the given values of the angular momentum for such an electron are half integral; the appearance of half integers strongly suggests that the five dimensional wave equation incorporates the spin of the electron in a way not quite apparent on theoretical grounds.

In the present paper, the author intends to indicate that the solution of the radial part of the five dimensional wave equation for the case of scattering of electron in a Coulomb field contains half integral quantum numbers which again lends support to the idea that the influence of the fifth coordinate is the same as the existence of the spin.

THEORY

We consider the case of stream of electrons moving past a Coulomb field given by $-\frac{Ze}{r}$ where Ze is the charge of the source of the field and r is the distance of the electron from the source-point.

We consider the relativistic wave equation in five dimensional space- time similar to the Klein-Gordon equation, i.e.

$$\frac{\partial^2\psi}{\partial x^2}+\frac{\partial^2\psi}{\partial y^2}+\frac{\partial^2\psi}{\partial z^2}+\frac{\partial^2\psi}{\partial s^2}+\left(\frac{E^2-m^2c^4}{\hbar^2c^2}-\frac{2EZe^2}{\hbar^2c^2r}+\frac{Z^2e^4}{c^2\hbar^2r^2}\right)\psi=0 \quad \ldots (1)$$

If we change over to polar coordinates

$$x = r \sin\theta \cos\phi \sin\chi$$
$$y = r \sin\theta \sin\phi \sin\chi$$
$$z = r \cos\theta \sin\chi$$
$$s = r \cos\chi$$

then equation (1) reduces to

$$\frac{\partial^2\psi}{\partial r^2} + \frac{3}{r}\frac{\partial\psi}{\partial r} + \frac{1}{r^2}\cdot\frac{1}{\sin^2\chi\sin\theta}\frac{\partial}{\partial\theta}\left(\sin\theta\frac{\partial\psi}{\partial\theta}\right)$$

$$+\frac{1}{r^2}\cdot\frac{1}{\sin^2\chi\sin^2\theta}\frac{\partial^2\psi}{\partial\phi^2} + \frac{1}{r^2}\cdot\frac{1}{\sin^2\chi}\frac{\partial}{\partial\chi}\left(\sin^2\chi\frac{\partial\psi}{\partial\chi}\right)$$

$$+\left(\frac{E^2-m^2c^4}{\hbar^2c^2} - \frac{2EZe^2}{\hbar^2c^2r} + \frac{Z^2e^4}{\hbar^2c^2r^2}\right)\psi = 0 \qquad \ldots \quad (2)$$

The solution ψ of (2) can be written in the form $\psi = \psi_r \cdot \psi_\theta \cdot \psi_\varphi \cdot \psi_\chi$ where ψ_r is the solution of

$$\frac{\partial^2\psi_r}{\partial r^2} + \frac{3}{r}\frac{\partial\psi_r}{\partial r} + \left[\frac{E^2-m^2c^4}{\hbar^2c^2} - \frac{2EZe^2}{\hbar^2c^2r} + \frac{Z^2e^4}{\hbar^2c^2r^2} - \frac{l(l+2)}{r^2}\right]\psi_r = 0 \qquad \ldots \quad (3)$$

where l is a positive integer.

If we put $\rho = kr$, $\quad \dfrac{E^2-m^2c^4}{\hbar^2c^2} = k^2$, $\dfrac{EZe^2}{k\hbar^2c^2} = \alpha$

and $\dfrac{Z^2e^4}{c^2\hbar^2} = \beta$, then equation (3) reduces to

$$\frac{\partial^2\psi_r}{\partial\rho^2} + \frac{3}{\rho}\frac{\partial\psi_r}{\partial\rho} + \left[1 - \frac{2\alpha}{\rho} + \frac{\beta - l(l+2)}{\rho^2}\right]\psi_r = 0 \qquad \ldots \quad (4)$$

If we put $\psi_r = \rho^l e^{i\rho} F$, equation (4) reduces to

$$\frac{d^2F}{d\rho^2} + \frac{2}{\rho}\left\{l + \frac{3}{2} + i\rho\right\}\frac{dF}{d\rho} + \frac{2}{\rho}\left\{\left(l + \frac{3}{2}\right)i - \alpha + \frac{\beta}{2\rho}\right\}F = 0$$

i.e.

$$\rho\frac{d^2F}{d\rho^2} + \frac{2}{\rho}\left\{l + \frac{3}{2} + i\rho\right\}\frac{dF}{d\rho} + 2\left\{\left(l + \frac{3}{2}\right)i - \alpha + \frac{\beta}{2\rho}\right\}F = 0 \qquad \ldots \quad (5)$$

Putting $\rho = \frac{1}{2} iz$ in (5) we get

$$z \frac{d^2F}{dz^2} + (2l+3-z) \frac{dF}{dz} - \left(i\alpha+l+ \frac{3}{2} - \frac{\beta}{z} \right) F = 0 \qquad \dots (6)$$

Neglecting the term $\frac{\beta}{z}$, as β is very small, we get from (6)

$$z \frac{d^2F}{dz^2} + (2l+3-z) \frac{dF}{dz} - \left(i\alpha+l+ \frac{3}{2} \right) F = 0 \qquad \dots (7)$$

Two independent solutions of (7) are as follows

$$W_{1,2}(i\alpha+l+3/2,\ 2l+3,\ z) \qquad \dots (8)$$

In the case of Klein-Gordon equation, the equation for the radial wave function

$$\frac{\partial^2\psi_r}{\partial r^2} + \frac{2}{r} \frac{\partial\psi_r}{\partial r} + \left[\frac{E^2-m^2c^4}{\hbar^2c^2} - \frac{2EZe^2}{\hbar^2c^2r} + \frac{Z^2e^4}{\hbar^2c^2r^2} - \frac{l(l+1)}{r^2} \right] \psi_r = 0 \qquad \dots (9)$$

Proceeding exactly in the same manner as in the case of five dimensional continuum we get in this case two independent solutions

$$W_{1,2}\ (i\alpha+l+1,\ 2l+2,\ z) \qquad \dots (10)$$

Comparing (8) and (10) we notice that equation (10) goes over to equation (8) if $l \to l+\frac{1}{2}$. The addition of half to l in equation (8) suggests that the spin of the electron has entered into the formalism in suitable way.

In the case of scattering in a Coulomb field the radial part of the Schrodinger's equation is of the form

$$\frac{\partial^2\psi_r}{\partial r^2} + \frac{2}{r} \frac{\partial\psi_r}{\partial r} + \left[\frac{2m}{\hbar^2} \left(E - \frac{Ze^2}{r} \right) - \frac{l(l+1)}{r^2} \right] \psi_r = 0 \qquad \dots (11)$$

l being a positive integer.

The two independent solutions are

$$W_{1,2}\ (i\alpha+l+1,\ 2l+2,\ z)$$

where
$$k^2 = \frac{2mE}{\hbar^2},\ \alpha = \frac{Ze^2}{\hbar v},\ \rho = kr \qquad \dots (12)$$

and
$$z = -2i\rho$$

If we add an extra space dimension to the Schrodinger's equation the radial part becomes

$$\frac{\partial^2\psi_r}{\partial r^2} + \frac{3}{r} \frac{\partial\psi_r}{\partial r} + \left[\frac{2m}{\hbar^2} \left(E - \frac{Ze^2}{r} \right) - \frac{l(l+2)}{r^2} \right] \psi_r = 0 \qquad \dots (13)$$

Proceeding as before we get two independent solutions

$$W_{1,\,2}\,(i\alpha+l+\tfrac{3}{2},\ 2l+3,\ z) \qquad \ldots \quad (14)$$

Here we notice the same difference between equations (12) and (14) as in case of (8) and (10).

ACKNOWLEDGMENT

In conclusion the author expresses his sincere thanks to Prof. D. Basu for his kind guidance in this work.

REFERENCES

Banerjee, C. C., 1958, *Ind. J. Phys.*, **32**, 179.
Mott and Massey, The Theory of Atomic Collisions (Second Edition) P. 52.

Letters to the Editor

The Board of Editors will not hold itself responsible for opinions expressed in the letters, published in this section. The notes containing reports of new work communicated for this section should not contain many figures and should not exceed 500 words in length. The contributions must reach the Assistant Editor not later than the 15th of the second month preceding that of the issue in which the Letter is to appear. No proof will be sent to the authors.

6. RELATIONSHIP BETWEEN ADIABATIC COMPRESSIBILITY AND CONCENTRATION OF SOLUTIONS OF ELECTROLYTES

SATISH CHANDRA SRIVASTAVA

DEPARTMENT OF PHYSICAL CHEMISTRY,

INDIAN ASSOCIATION FOR THE CULTIVATION OF SCIENCE,

JADAVPUR, CALCUTTA-32

(*Received for publication January* 14, 1958)

It was pointed out by Mohanty and Deo (1955) that the ultrasonic velocity in magnesium and zinc sulphate solutions as well as the adiabatic compressibility vary linearly with concentration. Recently, Panda and Mohanty (1957) have concluded that the adiabatic compressibilities of cobalt and cadmium sulphate solutions vary linearly with concentration This may be represented by the following equations:

$$V = k'C + X \qquad .. \quad (1)$$

$$\beta = k'C + Y \qquad .. \quad (2)$$

where V is the ultrasonic velocity, β is the adiabatic compressibility, C is the concentration of the solution, k and k' are proportionality constants and X and Y are constants.

It is known that

$$\beta = \frac{1}{V^2\rho} \qquad ... \quad (3)$$

where ρ is the density of the solution.

From (1) and (3) we may write

$$\beta = \frac{1}{(K.C+X)^2\rho} \qquad ... \quad (4)$$

It seems clear that equation (2) and (4) can not hold good at the same time. Naturally, the statement that adiabatic compressibility for four electrolytes studied is linear with concentration seems to be incorrect. However, on plotting the graph it appears that there is very slight curvature and the plots are not exactly straight lines.

Bachem (1936), Brathel (1954), Krishnamurthi (1950) and many others have suggested different relations but at the same time there has been considerable amount of controversy.

Prakash and Srivastava (1958) themselves suggested one equation relating the velocity of ultrasonic waves in solutions of electrolytes with the ionic strength of the solution From the same relation the following equation may be derived :

$$\left(\frac{\rho}{\beta}\right)^{1/4} = \frac{P}{(2I)^{1/2}} + \frac{BZi^2(2\mu)}{D^2T(I)^{1/2}}$$

where $B = \dfrac{N^2.e^4}{1000.2\sqrt{2}.R.}$, N is avagadro number, e is electronic charge, R is gas constant.

Zi is valency of ions, D is dielectric constant of the solution,

T is temperature, I is ultrasonic intensity,

P is the pressure experienced by the solution internally if the salts are not ionised.

It is observed that the above equation holds good for the four bivalent sulphates studied by Mohanty and Deo (loc. cit) and Panda and Mohanty (loc cit). Also it is seen that the plot for all the four straight lines $\left[\left(\frac{\rho}{\beta}\right)^{1/4} \text{ against } \mu\right]$ has almost the same slope as is expected from the equation itself. The equation is also valid for potassium nitrate and strontium nitrate as is seen from the data of Krishnamurthi (loc. cit), but for sodium nitrate it shows a minimum.

REFERENCES

Bachem, 1936, *Z. Physik*, **101**, 541.
Brathel, R., 1954, *J. Acoust. Soc. Am.*, **26**, 227.
Krishnamurthi, B. H., 1950, *J. Sci. Ind. Res.* **9** , 215.
1951., *ibid.* **10B**, 49.
Prakash and Srivastava S. C., 1958, *Ind. J. Phys.*, **32**, 62.
Mohanty, B. S. and Deo, B. B., 1955, *Ind. J. Phys.*, **29**, 578.
Panda, S. and Mohanty, B. S., 1957, *Ind. J. Phys.*, **31**, 560.

7. FIVE DIMENSIONAL WAVE-EQUATION FOR HYDROGEN ATOM

V. B. KELKAR AND K. M. GATHA

INSTITUTE OF SCIENCE, MAYO ROAD, BOMBAY 1.

(*Received for publication April* 18, 1958)

Introducing a new co-ordinate s on par with the usual x, y and z co-ordinates, Banerjee (1957) has set up the five dimensional wave equation given by

$$[c^2(p_x^2+p_y^2+p_z^2)+p_s^2)+m_0^2c^4]\psi = [W-V(r)]^2\psi \qquad \ldots \quad (1)$$

Taking $V = (-Ze^2/r)$ as the hydrogen atom potential, he has solved this equation in four dimensional polar co-ordinates to obtain the solution

$$\psi(r, \theta, \phi, \chi) = DR_{n_r,l}{}^{(r)}P_l^m(\cos\theta)e^{im\varphi}\sin^l\chi \qquad \ldots \quad (2)$$

The eigenvalues of W, corresponding to the above eigen-functions, have been shown to be those given by Sommerfeld's (1916) formula.

The above wave-equation possesses the usual disadvantages associated with second order temporal differentiation contained therein. Further, the degeneracy is given by $(2l+1)$ which is unlike that of the Dirac levels. However, the equation for χ given as

$$\left[\frac{\partial}{\partial\chi}(\sin^2\chi\frac{\partial}{\partial\chi}+\left\{K\sin^2\chi-l(l+1)\right\}\right]U(\chi) = 0 \qquad \ldots \quad (3)$$

can be shown to possess polynomial solutions of the form

$$U(\chi) = \sum_{\mu=0}^{l'} a_\mu \sin^{l+2\mu}\chi$$

which leads to the degeneracy $\{(l+2l'+1)(l+2l'+2)/2\}$ which is again unlike that obtained for Dirac levels.

Banerjee has given the radial equation as

$$\left[\frac{d^2}{dr^2}+\frac{3}{r}\frac{d}{dr}+\left(A+\frac{2B}{r}+\frac{C}{r^2}\right)\right]R(r) = 0 \qquad \ldots \quad (4)$$

where $\quad A = \dfrac{w^2-m_0^2c^4}{\hbar^2c^2}$; $B = \dfrac{WZe^2}{\hbar^2c^2}$ and $c = [a^2Z^2-l(l+2)]$

The only difference introduced by using the above polynomial solutions for χ would be to replace l by $(l+2l')$. Substituting $R(r) = e^{-\rho/2}v(\rho)$ with $\rho = (2r/r_0)$ where $r_0 = \dfrac{1}{\sqrt{-A}}$, one obtains

$$v''+v'\left(\frac{3}{\rho}-1\right)+\left[\left(\frac{B}{\sqrt{-A}}-\frac{3}{2}\right)\frac{1}{\rho}+\frac{c}{\rho^2}\right]v=0 \qquad \ldots \quad (5)$$

It may be noted that this equation differs from that given by Banerjee in the appearance of 3/2 in place of unity. As a result, one obtains the eigenvalue expression

$$W = m_0c^2\left[1+\frac{\alpha^2z^2}{\{(n_r+\frac{1}{2})+\sqrt{(l+2l'+1)^2-\alpha^2z^2}\}^2}\right]^{-\frac{1}{2}} \qquad \ldots \quad (6)$$

which differs from the Sommerfeld's formula in the replacement of n_r by $(n_r+\frac{1}{2})$.

It is, therefore, concluded that the new degree of freedom, obtained by introducing the fifth dimension, does not produce the same effects as the electron spin.

REFERENCES

Banerjee, C. C., 1957, *Ind. J. Phys.* **31**, 242.
Sommerfeld, A., 1916, *Ann. der Physik*, **51**, 1.

ON THE INFRA-RED SPECTRA OF SOLUTIONS OF *O*-CHLOROPHENOL AND PHENOL

S. C. SIRKAR, A. R. DEB AND S. B. BANERJEE

OPTICS DEPARTMENT, INDIAN ASSOCIATION FOR THE CULTIVATION OF SCIENCE, CALCUTTA-32

(*Received for publication, June 7, 1958*).

ABSTRACT. The infra-red absorption spectra of solutions of *o*-chlorophenol and phenol in carbon tetrachloride and cyclohexane and also of the pure liquids have been recorded with a Perkin-Elmer Model 21 spectrophotometer in the region from 2800 cm^{-1} to 3700 cm^{-1}. The strong absorption maximum at 3533 cm^{-1} and the low inflexion at 3595 cm^{-1} due to 5% solution of *o*-chlorophenol are found to shift to 3540 cm^{-1} and 3605 cm^{-1} respectively when the solvent is changed from carbon tetrachloride to cyclohexane. As the concentration is increased to 30% a new broader and weaker maximum appears on the lower frequency side of the main peak. In the case of pure liquid two new broad peaks appear with greater height, but the maximum at 3500 cm^{-1} persists and an inflexion at 3600 cm^{-1} is also observed.

In the case of 5% solution of phenol in carbon tetrachloride a sharp peak is observed at 3605 cm^{-1} with a broad and higher maximum at 3380 cm^{-1} and the height of the latter diminishes as the concentration is reduced.

These results have been compared with those reported by previous workers. It has been concluded that the maximum at 3540 cm^{-1} given by the solution of *o*-chlorophenol in [illegible] due to valence oscillation in the O-H group in the *trans* configuration and that

ERRATA

On the Making of Electret and Measurement of the Changes of Dielectric Constant of a Polarised Electret Forming Material with Time, by T. C. Bhadra, Bose Institute, Calcutta. (Ind. Jour. Phys., **32**, 281, June, 1958),

Following corrections are to be made :

Page	*Line*	*For*	*Read*
282	9	electro-strition	electro-striction
,,	13	baror	bar or
286	9	dipoles of the	dipoles or the
287	In Eqns. (8) & (9)	All R	κ
292	7	The	the
294	38	value of κ is	value of R is

ON THE INFRA-RED SPECTRA OF SOLUTIONS OF *O*-CHLOROPHENOL AND PHENOL

S. C. SIRKAR, A. R. DEB AND S. B. BANERJEE

OPTICS DEPARTMENT, INDIAN ASSOCIATION FOR THE CULTIVATION OF SCIENCE, CALCUTTA-32

(*Received for publication, June 7, 1958*).

ABSTRACT. The infra-red absorption spectra of solutions of *o*-chlorophenol and phenol in carbon tetrachloride and cyclohexane and also of the pure liquids have been recorded with a Perkin-Elmer Model 21 spectrophotometer in the region from 2800 cm^{-1} to 3700 cm^{-1}. The strong absorption maximum at 3533 cm^{-1} and the low inflexion at 3595 cm^{-1} due to 5% solution of *o*-chlorophenol are found to shift to 3540 cm^{-1} and 3605 cm^{-1} respectively when the solvent is changed from carbon tetrachloride to cyclohexane. As the concentration is increased to 30% a new broader and weaker maximum appears on the lower frequency side of the main peak. In the case of pure liquid two new broad peaks appear with greater height, but the maximum at 3500 cm^{-1} persists and an inflexion at 3600 cm^{-1} is also observed.

In the case of 5% solution of phenol in carbon tetrachloride a sharp peak is observed at 3605 cm^{-1} with a broad and higher maximum at 3380 cm^{-1} and the height of the latter diminishes as the concentration is reduced.

These results have been compared with those reported by previous workers. It has been concluded that the maximum at 3540 cm^{-1} given by the solution of *o*-chlorophenol in cyclohexane is due to valence oscillation in the O-H group in the *trans* configuration and that the assignment of this frequency to the *cis* configuration made by previous workers is not correct mainly for the reasons that the frequency is found to depend on the environment, that the O-H frequency of phenol should be higher than that of free O-H group in *o*-chlorophenol molecule, and that the interval between this maximum and the low peak at about 3600 cm^{-1} remains constant when either the liquid is dissolved in different solvents or the temperature of the solution is changed.

INTRODUCTION

It was first suggested by Pauling (1936) that the two peaks at 6910 cm^{-1} and 7050 cm^{-1} observed in the infra-red spectrum of solution of *o*-chlorophenol in carbon tetrachloride (Wulf and Liddel, 1935) are due to the first harmonic of the valence oscillations of the O-H group in the *cis* and *trans* configurations respectively with respect to the chlorine atom. Later, Davies (1938) investigated the infra-red spectrum in the 2.8μ region of the solution of *o*-chlorophenol in CCl_4 at 18°C and 73°C and observed that at 18°C there was a strong peak at 2.825μ (3540 cm^{-1}) and a very weak peak at 2.775μ (3600 cm^{-1}) and that the intensity of the latter peak increased when the solution was heated to 73°C. He pointed out that these results confirmed the hypothesis of Pauling mentioned above. He

further calculated from the intensity-ratio the energy-difference between the two states and found it to be 1420 cal/mole. Recently, Mukherjee (1958) studied the Raman spectra of solutions of *o*-chlorophenol of different concentrations in different solvents and observed that the intensity of the line 3533 cm^{-1} due to OH valence oscillation in the pure liquid increases when the substance is dissolved in carbon tetrachloride and it increases further with the diminution in the concentration of the solutions. Similar results were observed in the case of solutions in cyclohexane, but the line is situated at 3550 cm^{-1} in this case. He has concluded from these results that as this line is attributed to the OH valence oscillation of the O-H group in the *trans* position, the number of such molecules increases with diminution of concentration of the solution in carbon tetrachloride. He further suggested that the line 3550 cm^{-1} observed in the solution in cyclohexane might represent the frequency of free O-H valence oscillations and that in the solution in carbon tetrachloride the frequency is lowered to 3533 cm^{-1} by the influence of the chlorine atoms in carbon tetrachloride molecules

The frequency 3540 cm^{-1} reported by Davies (1938) in the infra-red spectrum is slightly higher than the Raman frequency 3533 cm^{-1} observed by Mukherjee (1958) in the Raman spectrum of the solution in carbon tetrachloride. Also the influence of different solvents on the infra-red spectrum was not investigated by previous workers. It was further noticed that the energy-difference of the two configurations deduced by Davies for the solution in carbon tetrachloride was much smaller than that for the vapour (Zumwalt and Badger, 1940). It was, therefore, thought worthwhile to find out this influence in solutions of different strengths in different solvents and to correlate the results of such investigations with those on the Raman spectra of the solutions of *o*-chlorophenol published by previous workers. With this object in view studies have been made of the infra-red spectra of solutions of different strengths of *o*-chlorophenol in carbon tetrachloride and cyclohexane and similar investigations on the spectra of phenol have also been carried out for comparison. The influence of temperature on the infra-red spectra of the solutions of *o*-chlorophenol has also been studied.

EXPERIMENTAL

The infra-red spectra were recorded with a Perkin-Elmer Model 21 infra-red spectrophotometer provided with a rock salt prism and wave number scale in the counter. The slit was adjusted by putting the resolution dial at about 916. Atmospheric absorption had to be correctly compensated by adjusting the balance in order to get reliable results. The gain in the amplifier required for satisfactory operation was found to be 6.0. For calibration in the region 3000 cm^{-1}—3800 cm^{-1} the C-H band of benzene at 3046 cm^{-1} was recorded with the double beam arrangement and this band was put at 3046 cm^{-1} in the counter. It was found, however, that when operated as a single beam instrument to record

the atmospheric water band at 3740 cm^{-1} the position of the band indicated by the counter was only about 3732 cm^{-1}. So, no attempt was made to make the counter read correctly beyond 3600 cm^{-1}. The instrument was placed in an air-conditioned room, the temperature of which was maintained at about 27°C.

Chemically pure *o*-chlorophenol purchased from B.D.H. was redistilled under reduced pressure. Phenol of the same quality was purified by repeated crystallisation. Carbontetrachloride and cyclohexane used as solvents were also of chemically pure quality and these two liquids were also distilled in vacuum before being used as solvents.

In the case of *o*-chlorophenol the strengths of the solutions used were 30% and 5% for the solution in carbon tetrachloride and 30%, 5% and 3% for the solution in cyclohexane. The spectrum due to pure *o*-chlorophenol was also recorded for comparison. Similar studies were made with solutions of phenol of strengths 5% and 1% in carbon tetrachloride and 4% and 1% in cyclohexane. The thickness of the cell was 0.1 mm in the case of dilute solutions and .025 mm in the case of the pure liquids and their concentrated solutions

In order to find out whether the position of the absorption maximum due to the solution of *o*-chlorophenol in carbon tetrachloride depends on temperature, the curve due to a 5% solution at 70°C was recorded and compared with the curve recorded for the solution at 27°C. This was a repetition of the investigation made by Davies (1938), but special care was taken to resolve the structure and to find out whether any small shift of the maxima took place with the change of temperature of the solution. A cylindrical electrical heater was used to heat up the cell up to 70°C, the temperature being observed with an ordinary mercury thermometer. Similar investigation was carried out in the case of a 3% solution of *o*-chlorophenol in cyclohexane. Compensation cell was used in the reference beam in the case of all the solutions.

RESULTS AND DISCUSSION

The absorption curves due to *o*-chlorophenol and its solutions of certain concentrations in carbon tetrachloride and cyclohexane at 27°C are reproduced in figure 1. A comparison of the curves II and III due respectively to 30% and 5% solutions of *o*-chlorophenol in carbontetrachloride shows that in the latter case there is a sharp peak at about 3533 cm^{-1} having a very weak maximum at 3595 cm^{-1}. The latter peak is resolved only when full compensation of the atmospheric bands is achieved; otherwise only an inflexion is recorded in this place. In the case of the 30% solutions the maximum is broadened towards lower frequencies and extends up to 3300 cm^{-1}, a new broad peak being present at 3450 cm^{-1}. In the case of the pure liquid the maximum is still broader towards lower frequencies and the absorption in the 3300 cm^{-1} region is very much larger than that in the curve due to the 30% solution. So, it appears

that as the concentration increases, the molecules of *o*-chlorophenol in the solution have greater chance of coming together and the new absorption in the region 3300 cm^{-1} —3450 cm^{-1} is probably produced by some sort of association of molecules. In the case of the pure liquid the maximum absorption is at 3500 cm^{-1} and even at 3300 cm^{-1} the absorption is only slightly less than the maximum, but at frequencies lower than 3300 cm^{-1} the absorption falls off sharply. The nature of the broad absorption peak observed in this case suggests that the peak is produced by superposition of three main broad peaks at 3320 cm^{-1}, 3450 cm^{-1} and 3520 cm^{-1} respectively. There is also an inflexion at 3620 cm^{-1}.

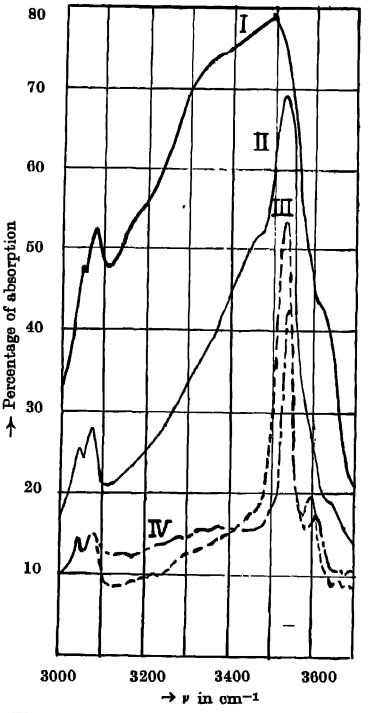

Fig. 1. Infra-red absorption spectra
Curve I. Pure *o*-chlorophenol
" II. 30% solution of *o*-chlorophenol in CCl_4
" III. 5% " " " " "
" IV. 3% " " " " cyclohexane.

In the region of first harmonic of this frequency due to pure *o*-chlorophenol in the liquid state Errera and Mollet (1935) observed a peak at 6620 cm^{-1}, there being very small absorption in the region of 7020 cm^{-1}. For a comparison of the results published by them with those observed in the present investigation it is to be found out whether the frequency of the first harmonic is exactly double of the fundamental or it is slightly different. The frequency of the strong fundamental in the solution in carbon tetrachloride is 3533 cm^{-1} at 27°C and not 3540 cm^{-1} as reported by Davies (1938). This discrepancy is due probably to slight error in the calibration of the spectra reported by him. Actual measurement on the peak reproduced by him shows that the frequency may be 3533 cm^{-1}. The frequency of the corresponding harmonic in the dilute solution in carbon tetrachloride reported by Wulf and Liddel (1935) is 6910 cm^{-1}, because the other peak observed by them at 7050 cm^{-1} is only one tenth as intense as the peak at 6910 cm^{-1}. Hence it appears that the frequency of the first harmonic is slightly less than double the fundamental frequency. If such a rule were applied to the frequencies observed in the case of the pure liquid the peak observed by Errera and Mollet (1935) at 6620 cm^{-1} would correspond to a fundamental frequency at about 3385 cm^{-1}, but the maximum observed in the present investigation is at 3500 cm^{-1}. So, there seems to be some discrepancy between the data for the region of the first harmonic and those for the fundamental observed in the present investigation. These latter data show that the funamental O-H frequency is probably altered in the pure liquid due to association of the molecules. Pauling (1945) suggested that the liquid may consist of dimers, and in that case two different O-H frequencies would be expected, one due to the O-H group in which the hydrogen atom is attached to the oxygen atom of the neighbouring molecule and the other due to the O-H group of which the hydrogen is attached to the chlorine atom in the *cis* position in the same molecule. Probably, these two frequencies are respectively 3320 cm^{-1} and 3450 cm^{-1}. Some of the molecules may be associated in a different way in the liquid and the absorption in the 3500 cm^{-1} region may be due to the OH group in these molecules.

The discrepancy between the results reported by Errera and Mollet (1935) and those observed in the present investigation mentioned above can, however, be explained by assuming that a combination frequency due to the C-H and O-H valence oscillations superposed on each other produces a peak at about 6600 cm^{-1} in the absorption curve due to the first harmonic of the broad peak represented by curve I in figure 1. Mukherjee (1958) also suggested that a combination frequency might produce the maximum at 6620 cm^{-1} in the case of the pure liquid.

It can be seen from curve IV in figure 1 that the absorption peak due to 3% solution of *o*-chlorophenol in cyclohexane is at 3540 cm^{-1} and there is a weak broad maximum at 3605 cm^{-1}. A 5% solution also gives similar results and a

30% solution gives new broad maxima as in the case of the 30% solution in carbon tetrachloride. It is thus evident that the position of this weak peak changes from 3595 cm^{-1} to 3605 cm^{-1} when the main peak shifts from 3533 cm^{-1} to 3540 cm^{-1} with the change of the solvent from carbon tetrachloride to cyclohexane. The interval between the main peak and the weak one is thus maintained constant and is about 62 cm^{-1}. The shift of the main peak with the change of the solvent shows that probably the OH group giving this frequency is free and is in the *trans* position, otherwise it would not be affected so much by the molecules of the solvent.

There is another stronger reason to justify this assumption. The frequencies of the second harmonic of the O-H oscillation diminishes by about 100 cm^{-1} when the chlorine atom of the *o*-chlorophenol molecule is replaced by a bromine atom. So, it is expected that when a chlorine atom substitutes a hydrogen atom in the O-H group of the phenol molecule, the O-H frequency should be lowered by more than 30 cm^{-1} in the fundamental mode. As the O-H frequency of the phenol molecule is 3605 cm^{-1}, we can expect a frequency of about 3550 cm^{-1} in the case of free O-H oscillation in *o*-chlorophenol molecule. Actually, we observe a frequency 3540 cm^{-1} in the case of the solution in cyclohexane. The influence of carbon tetrachloride molecules probably lowers the value still further to 3533 cm^{-1} in the solution in carbon tetrachloride. Hence, the assignment of the peak at 3595 cm^{-1} due to the solution in carbon tetrachloride to free O-H oscillation is probably not correct. The curves due to 5% solution of *o*-chlorophenol in carbon tetrachloride at 27°C and 70°C are reproduced in figure 2. It can be seen that at 27°C the main peak is at about 3533 cm^{-1} and the low peak is at about 3595 cm^{-1}, but they shift to 3540 cm^{-1} and 3603 cm^{-1} respectively when the solution is heated to 70°C. These results confirm the view that the influence of carbon tetrachloride molecules lowers the O-H frequency in the solution. At the higher temperature this influence diminishes owing to larger distances between the molecules. The results further show that the weak maximum also shifts by the same amount as the strong one with the change of temperature, and the interval of about 62 cm^{-1} is maintained constant. This indicates that probably the weak peak is due to a combination frequency, one of the frequencies being 3533 cm^{-1} and the other about 62 cm^{-1}. The latter may be that of torsional oscillation of the OH group. So, this maximum is in all probability not due only to the valence oscillation of the free O-H group.

Davies (1938) did not observe any resolved peak at 3595 cm^{-1} in the spectrum due to the solution of carbon tetrachloride at 18°C, but he observed such a maximum when the solution was heated to 73°C. In the present investigation, however, even at 27°C a resolved low peak is observed at 3595 cm^{-1}. As can be seen from figure 2, the height of the maximum does not increase appreciably at 70°C. Hence the value of the ratio of the number of molecules of the *cis* form to that of

trans form calculated by Davies has very little significance. It might be mentioned here that the low maximum is resolved from the main maximum only when

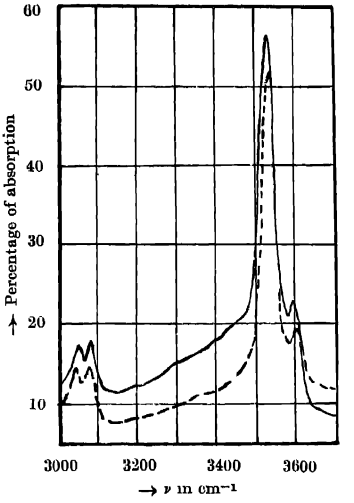

Fig. 2. Infra-red absorption curves.
—— 5% solution of *o*-chlorophenol in CCl_4 at 27°C.
.... „ „ „ „ at 70°C.
(The dotted curve is displaced downwards for clarity).

there is perfect compensation of the bands in the region 3740 cm^{-1} due to water vapour. If there be slight unbalance, the peak disappears and an inflexion is observed in its place. It has also been verified that the solvent used does not give even any weak peak in the whole region between 3000 cm^{-1} and 3800 cm^{-1}. In the case of the solution in cyclohexane no change in the spectrum is observed with the change of temperature.

It is thus observed that the relative intensities of the maxima at 3533 cm^{-1} and 3595 cm^{-1} and the interval between them remain almost constant when the liquid is dissolved in different solvents and the temperature of the solutions is changed. Also in the absorption curve due to the pure liquid the inflexion at 3610 cm^{-1} is distinctly visible. All these results lead to the conclusion that the low peak in the 3600 cm^{-1} region is not due to valence oscillation in the free O-H group but it is due to a combination frequency. The main peak at 3533 cm^{-1} due to the solution in carbon tetrachloride is thus to be assigned to valence oscillation in the free O-H group in the *trans* position. The curve due to the pure liquid shows that this frequency is reduced to about 3500 cm^{-1} and this may

indicate that although the O-H group is in the *trans* position in some of the molecules it is not free but probably it is linked to the chlorine atom of a neighbouring molecule. The frequency is further reduced when the dimer is formed through the O-H linkage as suggested by Pauling (1945).

Comparison with phenol

The curves I and II in figure 3 show that the solution of phenol in carbon tetrachloride gives one broad maximum with its centre at 3380 cm^{-1} and another sharp maximum at 3605 cm^{-1}, besides the sharp peak at 3046 cm^{-1} due to C-H oscillation. The ratio of the heights of the first two peaks diminishes as the concentration is diminished from 5% to 1%. Each of curves III and IV in figure 3 due respectively to 4% and 1% solutions of phenol in cyclohexane, on the other hand, shows a broad maximum at about 3340 cm^{-1} and sharp peak at 3600 cm^{-1}, but the latter peak is lower than that due to solution in carbon tetrachloride. It appears from these results that in phenol the frequency of free O-H valence oscillation is probably 3605 cm^{-1}, but the number of such molecules is small even in

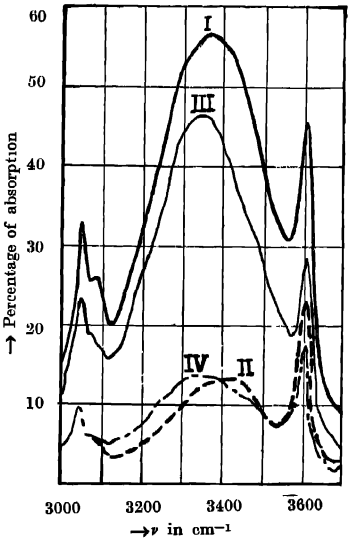

Fig. 3. Infra-red absorption curves of phenol.
Curve I and II. 5% and 1% solutions in CCl_4
Curve III and IV. 4% and 1% solutions in cyclohexane.

4% solution in carbon tetrachloride and in the solution in cyclohexane the number is still smaller. The broad peak at 3340 cm^{-1} may be due to dimers formed by strong association of the molecules. It appears that by the influence of chlorine

atoms in the carbon tetrachloride the dimers are split up into single molecules, but they persist in the solution in cyclohexane. The formation of such dimers or larger associated groups may be responsible for the high viscosity of pure phenol. If the formation of dimers in *o*-chlorophenol in the liquid state through a linkage between the hydrogen atom of the O-H group and the oxygen atom of a neighbouring molecule reduces the O-H oscillation frequency to 3320 cm^{-1} the formation of similar linkage is to be postulated in the case of phenol also, because in this case also the mean O-H frequency of the broad peak is 3320 cm^{-1}. It is interesting that there is no indication of absorption in the region 3450 cm^{-1} in the spectrum due to solution of phenol in carbon tetrachloride while a 30% solution of *o*-chlorophenol in carbon tetrachloride shows a peak at 3450 cm^{-1}. This maximum is therefore to be attributed to the frequency of oscillation in O-H group in the *cis* position with respect to the chlorine atom in the *o*-chlorophenol molecule and no such configuration of the phenol molecule is possible. These results clearly show that the fundamental O-H oscillation in single molecule of phenol has the frequency 3606 cm^{-1}. As pointed out above, the corresponding frequency in the *o*-chlorophenol molecule should be a little less than 3606 cm^{-1} and therefore the frequency 3540 cm^{-1} observed in the spectrum of solution of *o*-chlorophenol in cyclohexane is to be assigned to the free O-H group in the *trans* position.

Comparison of the infra-red and the Raman spectra

It has already been pointed out that the Raman spectrum of *o*-chlorophenol in the liquid state shows only a broad band at 3533 cm^{-1}. The width of the band estimated from the spectra reproduced by Mukherjee (1958) is about 25 cm^{-1}. On the other hand, the corresponding maximum in the infra-red spectrum reproduced in figure 1 has a width more than 300 cm^{-1} and extends from about 3250 cm^{-1} up to about 3600 cm^{-1}. So, the infra-red absorption in the region from 3250 cm^{-1} up to 3500 cm^{-1} is not represented in the Raman spectrum. It could be inferred from these facts that probably the absorption in this region is produced by the O-H oscillation in the dimer proposed by Pauling (1945) and that in the model of the dimer proposed by him the O-H stretching oscillation produces a very small change in the polarisability of the dimer. It can be easily seen from the model that when the stretching oscillations in the two OH groups are in phase the oscillation in the H-O-H group in the dimer is asymmetric. Probably, the oscillation in the two O-H groups in phase is more probable than those in opposite phases. The weak band at 3533 cm^{-1} in the Raman spectrum of the pure liquid is evidently due to the small number of associated molecules of other type and monomers present in the liquid. The increase in the number of single molecules in solutions, as indicated by the maxima in the infra-red spectra reproduced in figure 1, is responsible for the increase in the intensity of the Raman line at 3533 cm^{-1}. The shift of the Raman line due to the solution in cyclo-

hexane observed by Mukherjee (1958) is also confirmed by the curve due to the infra-red spectrum reproduced in figure 1. Thus the results on the investigation on the Raman spectra agree satisfactorily with those on the infra-red spectra.

REFERENCES

Davies, M. M., 1938, *Trans. Faraday Soc.*, **34**, 1427.
Errera, J. and Mollet, P., 1935, *Jour. de Physique*, **6**, 281.
Mukherjee, Deb Kumar, 1958, *Ind. J. Phys.*, **32**, 192.
Pauling, L., 1936, *J. A. C. S.*, **58**, 94.
Pauling, L., 1945, Nature of the Chemical Bond, p. 324.
Wulf, O. R. and Liddel, U., 1935, *J. A. C. S.*, **57**, 1464.
Zumwalt, L. R. and Badger, R. M., 1940, *J. A. C. S.*, **62**, 305.

POLARISATION OF A DIRAC PARTICLE AND PROTON-NEUTRON SCATTERING

S. P. MISRA

MATHEMATICS DEPARTMENT, RAVENSHAW COLLEGE, CUTTACK-3

(*Received for publication March, 13, 1958*).

ABSTRACT. The purpose of this paper has been to consider the polarisation problem for nucleon-nucleon scattering in the pseudoscalar meson theory. Attempts have always been made to explain polarisation in case of scattering by expanding in terms of centre of mass angular momentum and considering the scattering problem with the help of phase shifts in the different angular momentum and spin states. This procedure often contains the error of keeping only a few phase shifts without any theoretical justification We have avoided this source of error by taking the usual S-matrix in the second and fourth orders. Using this direct method, it has been observed that polarisation in case of such a scattering, when initially the partciles are unpolarised, is zero, which is in contradiction to the experimental results

INTRODUCTION

It is well known that the nuclear forces are best explained, at least in a qualitative manner, with the help of psudoscalar meson theory. We wish to consider polarisation in case of nucleon-nucleon scattering in this theory.

Since the experimental discovery of polarisation in case of scattering, many attempts have been made to explain them with the help of different models or from field theory with approximate calculations (Bhatia, 1950 ; Verde, 1955 ; Lepore, 1950). The approach of these attempts are similar to that of Mott (1932) and makes use of the centre of mass angular momentum expansion of the incoming and outgoing waves, and the subsequent calculations of different angular momentum states phase shifts only a few of which can be retained. Thus, besides the usual inaccuracy of the perturbation approach for the meson theories, the inaccuracy of retaining only a few angular momentum states without any theoretical justification in the individual cases, is further added.

To avoid at least the second error, we have considered the scattering problem from the general scattering matrix in the second and fourth orders for the particular case of neutron-proton scattering. We assume the incident particles to be unpolarised and calculate the cross-section for an arbitrary direction of polarisation of the outgoing proton beam. The dependance of this cross-section on the state of polarisation of the proton will give us the amount of polarisation of this

beam as a result of scattering, and by angular momentum conservation, we shall automatically obtain the polarisation of the neutron beam.

It is, however, found that the scattering cross-section does not depend on the state of polarisation of the outgoing proton, thus going against the experimental result that polarisation should be obtained in case of such a scattering.

It is to be noticed, however, that the scatterers in the case of experiments are not free particles, but are bound. This might be the source of error in taking as we have done, the wave functions to be all those of free particles.

RELATIVISTIC POLARISATION STATES OF A SINGLE DIRAC PARTICLE

The four spinor wave function of the Dirac particle of energy-momentum p will be taken in the positive energy states as

$$\psi(p) = k \begin{pmatrix} \psi_{Ip} \\ \psi_{IIp} \end{pmatrix}$$

where the small component $\psi_{IIp} = \dfrac{\vec{\sigma} \cdot \vec{p}}{E_p + M} \psi_{Ip}$ and $\psi_{Ip} = \begin{pmatrix} \cos \dfrac{\alpha}{2} \\ \sin \dfrac{\alpha}{2} \exp(i\beta) \end{pmatrix}$

The invariant normalisation $\bar{\psi}(p)\psi(p) = 1$ gives us $k = \sqrt{\dfrac{E_p + M}{2M}}$. We adopt the notation of Heitler (1954) as regards the γ-matrices the energy-momenta and the summation conventions. We define the anti-symmetric polarisation operator as

$$\sigma_{\mu\nu} = 1/2i(\gamma_\mu\gamma_\nu - \gamma_\nu\gamma_\mu)$$

such that the Pauli spin matrices $\vec{\sigma}$ are given as $\vec{\sigma} = (\sigma_{23}, \sigma_{31}, \sigma_{12})$. The relativistically covariant polarisation tensor is defined as

$$P_{\mu\nu} = \bar{\psi}(p)\sigma_{\mu\nu}\,\psi(p)$$

for the particle represented by the 4-spinor $\psi(p)$. Hence

$$\vec{P} = \bar{\psi}(p)\,\vec{\sigma}\,\psi(p)$$

$$= \frac{E_p}{M}\,\vec{P}_{NR} - \frac{(\vec{p} \cdot \vec{P}_{NR})}{M(E_p + M)}\,\vec{p} \qquad \ldots (1)$$

where

$$\vec{P}_{NR} = \psi^*_{Ip}\,\vec{\sigma}\,\psi_{Ip} = (\sin\alpha\cos\beta,\ \sin\alpha\sin\beta,\ \cos\alpha)$$

is the non-relativistic polarisation vector.

Again,
$$\vec{\sigma}_{k4} = (\sigma_{14}, \sigma_{24}, \sigma_{34}) = \begin{pmatrix} 0 & \vec{\sigma} \\ \vec{\sigma} & 0 \end{pmatrix}$$

gives us

$$\vec{P}_{k4} = \frac{i}{M}\,\vec{p}\times\vec{P}_{NR}$$

or,
$$\vec{P}_{k0} = \frac{\vec{p}}{M}\times\vec{P}_{NR} \qquad \ldots \quad (2)$$

It is easily seen that

$$\tfrac{1}{2}\,P_{\mu\nu}P^{\mu\nu} = \vec{P}\,.\,\vec{P} - \vec{P}_{k0}\,.\,\vec{P}_{k0} = 1$$

by eqns. (1) and (2) and further simplification, as we should expect of the polarisation.

From the above-mentioned equations it is also clear that the strictly space part (1) of the polarisation depends on the momentum of the particle unless we quantise polarisation parallel to the direction of the momentum itself, in which case $\vec{P} = \vec{P}_{NR}$. In such a case, the strictly relativistic part (2) also vanishes altogether.

In the general case, however, both the parts of the anti-symmetric tensor $P_{\mu\nu}$ stay, and have to be taken into account while considering coupling of this polarisation with any other tensor for an invariant description of such problems. It is also to be seen, that, if we consider, say, only positive energy states, then such states as $\exp(ipx)\begin{bmatrix}1\\0\\0\\0\end{bmatrix}$ are impossible.

If we replace α by $\pi-\alpha$ and β by $\beta+\pi$, such that

$$\psi_{Ip} \text{ changes to } \begin{pmatrix} \sin\frac{\alpha}{2} \\ -\cos\frac{\alpha}{2}\exp(i\beta) \end{pmatrix}$$

then the new $\psi(p)$ thus obtained is orthogonal to the original one, and has just the opposite polarisation even in the relativistic limit.

SECOND AND FOURTH ORDER PERTURBATION CALCULATIONS

In the specific problem of proton-neutron scattering, we take p_1, p_2 and p_3 and p_4 as the four-momenta of the incident proton and neutron and the outgoing proton and neutron respectively. The interaction hamiltonian density is taken as

$$H_i(x) = ig\bar{\psi}(x)\gamma_5\, \tau_k\psi(x)\phi_k(x) \qquad \ldots \quad (3)$$

The meson and nucleon propagation functions are respectively as

$$K_M\,(x_1-x_2) = -\frac{i}{(2\pi)^4}\int \frac{\exp\{(ik(x_1-x_2)\}}{k^2+\mu^2}\,dk$$

and

$$K_N(x_1-x_2) = \frac{i}{(2\pi)^4}\int \frac{(i\gamma k-M)}{k^2+M^2}\;\exp\{ik(x_1-x_2)\}dk.$$

In the above, μ and M are respectively the meson and nucleon masses. Throughout, natural units $c = \hbar = 1$ have been chosen.

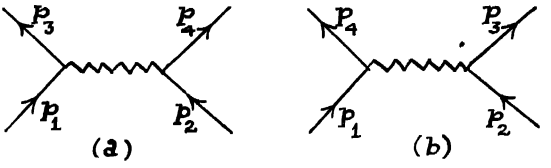

Fig. 1(a) & (b)

With summation over isotopic spin indices, the second order matrix elements become

$$S_2 = S_2^{(1)}+S_2^{(2)}, \qquad \ldots \quad (4)$$

$$S_2^{(1)} = ig^2(2\pi)^4\bar{\psi}(p_3)\gamma_5\,\psi(p_1)\bar{\psi}(p_4)\gamma_5\psi(p_2)[q^2+\mu^2]^{-1}$$

$$S_2^{(2)} = 2ig^2(2\pi)^4\psi(p_3)\gamma_5\,\psi(p_2)\bar{\psi}(p_4)\,\gamma_5\psi(p_1)[(q-p)^2+\mu^2]^{-1}$$

In the above result, $\psi(p_1)$ and $\bar{\psi}(p_3)$ are proton states and $\psi(p_2)$ and $\bar{\psi}(p_4)$ are neutron states, and $p = p_1-p_2$ and $q = p_1-p_3$.

For calculating the fourth order matrix element, we consider moderately high energies so that only the graphs figure 2 (a & b) and the graphs with p_1 and p_2 interchanged contribute the maximum.

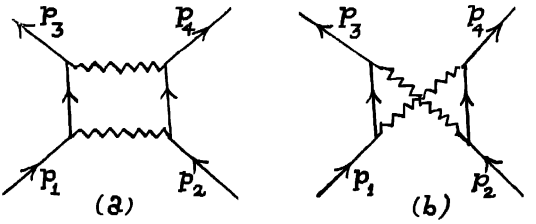

Fig. 2(a) & (b)

Then we easily obtain the respective scattering matrix elements as

$$S_4^{(a)} = g^4 \frac{1}{\underline{|4}} \cdot 4 \int d^4k \bar{\psi}(p_3)\gamma_5\tau_k\{i\gamma(p_1-k)-M\}\gamma_5\tau_l\psi(p_1)$$

$$\times\bar{\psi}(p_4)\gamma_5\tau_k\{i\gamma(p_2+k)-M\}\gamma_5\tau_l\psi(p_2)\times[k^2-2kp_1]^{-1}[k^2+2kp_2]^{-1}$$

$$[k^2+\mu^2)^{-1}[(q-k)^2+\mu^2]^{-1}$$

$$=5/6g^4\bar{\psi}(p_3)\gamma_\mu\psi(p_1)\bar{\psi}(p_4)\gamma_\nu\psi(p_2)I_{\mu\nu} \qquad \ldots \quad (5)$$

where

$$I_{\mu\nu} = \int d^4k\, k_\mu k_\nu[k^2+\mu^2]^{-1}[k^2-2kp_1]^{-1}[k^2+2kp_2]^{-1}\times[(q-k)^2+\mu^2]^{-1} \qquad \ldots(5a)$$

Similarly

$$S_4^{(b)} = -1/6g^4\bar{\psi}(p_3)\gamma_\mu\psi(p_1)\bar{\psi}(p_4)\gamma_\nu\psi(p_2)\, J_{\mu\nu} \qquad \ldots \quad (6)$$

where

$$J_{\mu\nu} = \int d^4k k_\mu\, k_\nu[k^2+\mu^2]^{-1}[k^2-2kp_1]^{-1}[k^2-2kp_4[(k-q)^2+\mu^2]^{-1} \qquad \ldots \quad (6a)$$

There will be two other matrix elements with the exchange of p_1 and p_2 (or p_3 and p_4) given as

$$S_4^{(a')} = -2/3\, g^4\bar{\psi}(p_3)\gamma_\mu\psi(p_2)\;\bar{\psi}(p_4)\;\gamma_\nu\psi(p_1)\, I_{\mu\nu}' \qquad \ldots \quad (7)$$

where

$$I_{\mu\nu}' = I_{\mu\nu}(p_1 \Longleftrightarrow p_2) \qquad \ldots \quad (7a)$$

and

$$S_4^{(b')} = -\frac{2}{3}g^4\bar{\psi}(p_3)\gamma_\mu\,\psi(p_2)\bar{\psi}(p_4)\,\gamma_\nu\,\psi(p_1)J'_{\mu\nu} \qquad \ldots \quad (8)$$

where

$$J'_{\mu\nu} = J_{\mu\nu}(p_1 \Longleftrightarrow p_2) \qquad \ldots \quad (8a)$$

The numerical coefficients are seen to be different in the latter two cases from a consideration of the specific isotopic spin states of the neutrons and the protons and taking summation over such states for the intermediate nucleons.

Hence finally we obtain the scattering matrix up to fourth order as

$$\begin{aligned} S &= S_2 + S_4 \\ &= i[g^2 Q \bar{\psi}(p_3)\gamma_5\, \psi(p_1)\, \bar{\psi}(p_4)\, \gamma_5\, \psi(p_2) + g^2 Q' \bar{\psi}(p_3)\, \gamma_5\, \psi(p_2)\, \bar{\psi}(p_4)\gamma_5\, \psi(p_1) \\ &\quad + g^4 Q_{\mu\nu}\, \bar{\psi}(p_3)\gamma_\mu\, \psi(p_1)\, \bar{\psi}(p_4)\, \gamma_\nu\, \psi(p_2) + g^4 Q'_{\mu\nu}\, \bar{\psi}(p_3)\gamma_\mu\, \psi(p_2)\, \bar{\psi}(p_4)\gamma_\nu\, \psi(p_1)] \end{aligned} \qquad \ldots (9)$$

where

$$Q = (2\pi)^4[q^2 + \mu^2]^{-1}, \qquad Q' = 2(2\pi)^4[(q-p)^2 + \mu^2]^{-1}$$

$$iQ_{\mu\nu} = \frac{5}{6} I_{\mu\nu} - \frac{1}{6} J_{\mu\nu} \qquad \ldots (9a)$$

and

$$iQ'_{\mu\nu} = -\frac{2}{3} I'_{\mu\nu} - \frac{2}{3} J'_{\mu\nu}$$

For the evaluation of the respective $I_{\mu\nu}$ and $J_{\mu\nu}$ integrals, we make use of the representation.

$$1/(a\ b\ c\ d) = 6 \int_0^1 dx \int_0^1 dy \int_0^1 dz\, x(1-x)[ay + b(1-y))x + (cz + d(1-z)(1-x)]^{-4}$$

and employ the wellknown techniques of Feynman to evaluate the resulting integrals.

Thus we shall have

$$I_{\mu\nu} = i\pi^2 \int_0^1 dx \int_0^1 dy \int_0^1 dz[D_1^{-2}\ P_{1\mu}(x, y, z) P_{1\nu}\ (x, y, z) + \tfrac{1}{2}\, \delta_{\mu\nu}\, D_1^{-1}] \qquad \ldots (10)$$

where

$$P_{1\mu}\,(x, y, z) = p_{1\mu}\, x(1-y) - p_{2\mu}\, xy + q_\mu\,(1-x)z, \qquad \ldots (10a)$$

$$\Delta = -(1-x)(\mu^2 + q^2 z)$$

and

$$\begin{aligned} D_1 &= -(P_1(x, y, z)^2 - \Delta \\ &= M^2 x^2 (1-2y)^2 + \mu^2(1-x) + q^2 z(1-x) \\ &\quad - p^2 x^2 y(1-y) - 2(pq)\, x\,(1-x) yz \end{aligned} \qquad \ldots (10b)$$

The integrals $J_{\mu\nu}$, $I'_{\mu\nu}$ and $J_{\mu\nu}'$ can also be written down in a similar way and will have the same form as above. Hence by (9a), (10a) and (10), we have

$$\begin{aligned} Q_{\mu\nu} &= A\, \delta_{\mu\nu} + S_{\mu\nu} \\ Q'_{\mu\nu} &= A'\, \delta_{\mu\nu} + S'_{\mu\nu} \end{aligned} \qquad \ldots (11)$$

where A and A' are real invariant functions of momenta and $S_{\mu\nu}$ and $S'_{\mu\nu}$ are the components of the sum of symmetric tensor products of the momentum-energy four vectors. Hence in (11), we have

$$S_{\mu\nu} = S_{\nu\mu}$$

and also S_{kl}, S'_{kl} $(k, l = 1, 2, 3)$ and S_{44}, S'_{44} are all real and all the remaining components of S and S' are pure imaginary.

Hence we have

$$\begin{aligned} Q^*_{kl} &= Q_{kl}, \qquad k, l = 1, 2, 3, \\ Q^*_{4k} &= -Q_{4k}, \end{aligned} \qquad \ldots \quad (12)$$

and the Q's as well are also symmetric.

We shall now adopt the properties (12) of $Q_{\mu\nu}$ and $Q'_{\mu\nu}$ and employ the expression (9).

In (9), we shall explicitly take $\psi(p_3)$ to be in the positive energy state with a definite polarisation given as

$$\psi(p_3) = \frac{1}{\sqrt{2M\,(E_{p_2}+M)}} \begin{bmatrix} E_{p_3}+M \\ \vec{\sigma} \cdot \vec{p}_3 \end{bmatrix} \psi_{Ip_3}, \qquad \ldots \quad (13)$$

$$\psi_{Ip_3} = \begin{bmatrix} \cos\frac{\alpha}{2} \\ \sin\frac{\alpha}{2} \exp(i\beta) \end{bmatrix}.$$

$\frac{1}{4} \sum_{p_1, p_2, p_3} |S|^2$ with the notation that $\sum_p$ indicates summation over the spin states of particles of momentum p, will give us the scattering cross-section when the outgoing proton has a definite state of polarisation given by (13) and the incident beams are unpolarised. In the calculation of $\sum_{p_1, p_2, p_4} |S|^2$, we shall have to employ the positive energy state projection operators $\Lambda_+(p_1)$, $\Lambda_+(p_2)$ and $\Lambda_+(p_4)$,

$$\text{where } \Lambda_+(p) = \frac{-i\gamma p + M}{2E_p}\beta$$

$$= \frac{1}{2E_p} \begin{bmatrix} E^+_p & \vec{\sigma} \cdot \vec{p} \\ \vec{\sigma} \cdot \vec{p} & E^-_p \end{bmatrix} \qquad \ldots \quad (14)$$

with the abbreviation $E^+_p = E_p + M$ and $E^-_p = E_p - M$.

$\sum_{p_1, p_2, p_4} |S|^2$ will give rise to sixteen terms in all, many of which will vanish. The different types of terms that will occur have been considered in the appendix.

When expressed in terms of the Pauli spin matrices, all of them will be of the form

$$\bar{\psi}(p_3)\begin{bmatrix} A_1+\vec{\sigma}\,.\,\vec{B}_1 & A_2+\vec{\sigma}\,.\,\vec{B}_2 \\ A_3+\vec{\sigma}\,.\,\vec{B}_3 & A_4+\vec{\sigma}\,.\,\vec{B}_4 \end{bmatrix}\psi(p_3) \qquad \ldots \quad (15)$$

which, by (13), will simplify to

$$\frac{1}{2ME^{+}_{p_3}}\ \psi^{*}I_{p_3}\{(E_{p_3})^2A_1-|\vec{p}_3|^2A_4+E^{+}_{p_3}(\vec{B}_2-\vec{B}_3).\ \vec{p}_3$$

$$+\vec{\sigma}\,.\,[E^{+}_{p_3})^2\vec{B}_1+|\vec{p}_3|^2\vec{B}_4-2(\vec{p}_3\,.\,\vec{B}_4)\ \vec{p}_3$$

$$+E^{+}_{p_3}(A_2-A_3)\vec{p}_3+iE^{+}_{p_3}(\vec{B}_2+\vec{B}_3)\times\vec{p}_3]\}\psi I_{p_3} \qquad \ldots \quad (15a)$$

In order that the scattering cross-section may depend on the state of polarisation of $\psi(p_3)$, the sum of the terms arising from the square bracket in (15a) from all the individual terms should not vanish. Since the final sum of all the terms must be real, in terms like (15a) we must consider only the real parts of A_1, A_4, $\vec{B}_2$ and $\vec{B}_3$ for the scattering cross-section that does not depends on the spin states of $\psi(p_3)$ and to obtain the spin dependance of the cross-section, we must consider the real parts of A_2, A_3, $\vec{B}_1$ and $\vec{B}_4$ and the pure imaginary parts of $\vec{B}_2$ and $\vec{B}_3$. It will however be seen in the appendix that in any matrix

$$O=\begin{bmatrix} A_1+\vec{B}_1\,.\,\vec{\sigma} & A_2+\vec{B}_2\,.\,\vec{\sigma} \\ A_3+\vec{B}_3\,.\,\vec{\sigma} & A_4+\vec{B}_4\,.\,\vec{\sigma} \end{bmatrix}$$

considered in (15), A_2 and A_3, $\vec{B}_1$ and $\vec{B}_4$ are pure imaginary and $\vec{B}_2$ and $\vec{B}_3$ are real. This shows that there is no preferred orientation of the spin of the proton as a result of scattering.

APPENDIX

The type of terms that will occur in $\sum_{p_1,p_2,p_4}|S|^2$ are the following : (neglecting real coefficients which are unimportant for our purpose)

(1) $\bar{\psi}(p_3)\gamma_5\wedge_{+}(p_1)\gamma_5\beta\psi(p_3)\ Sp[\beta\gamma_5\wedge_{+}(p_2)\gamma_5\beta\wedge_{+}(p_4)]$

(2) $\bar{\psi}(p_3)\gamma_5\wedge_{+}(p_1)\gamma_5\beta\wedge_{+}(p_4)\beta\gamma_5\wedge_{+}(p_2)\gamma_5\beta\psi(p_3)$

(3) $\bar{\psi}(p_3)\gamma_\mu\wedge_{+}(p_1)\beta\gamma_\lambda\psi(p_3)Q_{\mu\nu}Q_{\lambda k}\ Sp\,[\beta\gamma_\nu\wedge_{+}(p_2)\beta\gamma_k\wedge_{+}(p_4)]$

(4) $\bar{\psi}(p_3)\gamma_5 \Lambda_+(p_1)\beta\gamma_\mu\psi(p_3)Q_{\mu\nu}Sp[\beta\gamma_5 \Lambda_+(p_2)\beta\gamma_\nu \Lambda_+(p_4)]$

(5) $\bar{\psi}(p_3)\gamma_5 \Lambda_+(p_1)\beta\gamma_\nu \Lambda_+(p_4)\beta\gamma_5 \Lambda_+(p_2)\beta\gamma_\mu\psi(p_3)Q_{\mu\nu}$

(6) $\bar{\psi}(p_3)\gamma_\mu \Lambda_+(p_1)\beta\gamma_k \Lambda_+(p_4)\beta\gamma_\nu \Lambda_+(p_2)\beta\gamma_\lambda\psi(p_3)Q_{\mu\nu}Q'_{\lambda k}$

There will be two terms, each of the type (1), (2), (3) and (6) and four terms each of the type (4) and (5).

In the above expressions, while simplifying, we can very easily get rid of the γ_5's when they occur in pairs by transposing and putting $(\gamma_5)^2 = 1$, which introduces a change of sign at every step when a γ_5 crosses a γ_μ. It can be easily seen that the terms like (4) which do not contain γ_5 in suitable pair will vanish since the spur becomes identically zero.

To consider the matrix elements between $\bar{\psi}(p_3)$ and $\psi(p_3)$ in the different type of terms, we shall first prove the following result : When

$$\begin{bmatrix} a_1+i\vec{\sigma}\,.\,\vec{b}_1 & ia_2+\vec{\sigma}\,.\,\vec{b}_2 \\ ia_3+\vec{\sigma}\,.\,\vec{b}_3 & a_4+\vec{\sigma}\,.\,\vec{b}_4 \end{bmatrix} \begin{bmatrix} a_1'+i\vec{\sigma}\,.\,\vec{b}_1' & ia_2'+\vec{\sigma}\,.\,\vec{b}_2' \\ ia_3'+\vec{\sigma}\,.\,\vec{b}_3' & a_4'+i\vec{\sigma}\,.\,\vec{b}_4' \end{bmatrix}$$

$$= \begin{bmatrix} A_1'+i\vec{\sigma}\,.\,\vec{B}_1' & iA_2'+i\vec{\sigma}\,.\,\vec{B}_2' \\ iA_3'+\vec{\sigma}\,.\,\vec{B}_3' & A_4'+i\vec{\sigma}\,.\,\vec{B}_4' \end{bmatrix} \qquad \ldots \text{(A1)}$$

and if a_k, $\vec{b}_k$, a_k', $\vec{b}_k'$ $(k = 1, 2, 3, 4)$ are all real, then also A_k', $\vec{B}_k'$ $(k = 1, 2, 3, 4)$ are all real; *i.e.* the product of any two (and hence any number) of matrices of the above form (A1) remains unaltered in form with the real and imaginary parts remaining in tact. This result may be verified by direct multiplication.

It can very easily be checked that (1) does not contain any polarisation term. In the second, we find that once we get rid of the γ_5's the remaining matrices will be of the form (A1) and hence their products will also have the same form, and thus by (15*a*) will not give rise to any polarisation dependent scattering cross-section when we add to it the complex conjugate expression.

For considering the terms of type (3), we first consider the case that $Q_{\mu\nu}$ is expressed as direct product of two energy-momentum vectors. In this case, clearly the operator within $\bar{\psi}(p_3)$ and $\psi(p_3)$ is of the form (A1) as is easily seen by multiplying by $-i^2$ and noticing that $i\gamma_p$ for all values of p is of the form (A1). The spur in this term is easily seen to be real, and hence this term does not contribute anything to a polarisation dependant cross-section. In an exactly similar manner we can also see that when $Q_{\mu\nu}$ or $Q_{\mu\nu}'$ are (or as a corollary, sums of) momenta, none of the other types of terms can contribute anything to any dependance on polarisation.

Even when one (both) of $Q_{\mu\nu}$ and $Q_{\lambda k}'$ is replaced by $\delta_{\mu\nu}$ or (and) $\delta_{\lambda k}$ with other real coefficients, it can be seen in these terms that they will be sum of terms with all their matrices of the form (A1). This can be proved, for example, by separating a $\gamma_\mu \ldots \gamma_\mu$ summation into two parts, as $\gamma_k \ldots \gamma_k$ (with $k = 1, 2, 3$) and $\gamma_4 \ldots \gamma_4$. It will be seen that we shall either require two i's to make the matrices of the form (A1) and with real coefficients, or they will be automatically of that form.

As stated in the main text, this leads to the conclusion that the scattering cross-section will be independent of the polarisation state of $\psi(p_3)$.

ACKNOWLEDGMENT

The author wishes to express his sincere thanks to Prof. D. Basu, Ph. D. of the Indian Association for the Cultivation of Science for many fruitful discussions.

REFERENCES

Bhatia, A. B., 1950, *Proc. Phys. Soc.* (*Lond.*) *A*63, 502.
Heitler, W., 1954, The Quantum Theory of Radiation.
Lepore, J. V., 1950, *Phys. Rev.* **79**, 137.
Mott, N. F., 1932, *Proc. Roy. Soc.*, *A*135, 429.
Verde, M., 1955, *Nuvovo Cim.*, **12**, 452.

DIPOLE MOMENTS OF SOME SUBSTITUTED BENZENES AND PYRIDINES. PART II META DISUBSTITUTED BENZENES

C. R. K. MURTY

PHYSICS DEPARTMENT, ANDHRA UNIVERSITY, WALTAIR

(*Received for publication, April* 11, 1958)

ABSTRACT. The dipole moments of *m*-fluorochloro, *m*-fluorobromo and *m*-fluoroiodo benzenes were determined in dilute solution in-benzene. For meta compounds the values agree with those calculated by simple vectorial addition of the group moments, indicating the absence of induced effects.

INTRODUCTION

A survey of the literature on dipole moments shows that not many fluoro compounds have been investigated either in the gaseous state or in the solution state probably because of the difficulty in their preparation. The author could obtain a supply of these compounds through the generosity of Dr. Finger of the Illinois State Geological Survey, to whom he is particularly grateful. For these meta compounds no dipole moment data have been published previously. The author has determined the dipole moment values, making observations in dilute solution in benzene. The values for the ortho compounds have been published by Bergmann *et al.* (1930). Hurdis and Smyth (1942) have determined the dipole moments of para fluorobromo and fluoroiodo benzenes in the vapour phase. The present results would complete the observations on this group of molecules.

EXPERIMENTAL

The experimental arrangement used for measurement of dielectric constants and refractive index of solutions and the method of calculation of dipole moments from the experimental quantities and from the group moments, have been described previously by the author (Murty, 1957). The group moments and polarisabilities used for calculating the dipole moments using Smallwood and Herzfeld's method, are given below:

Group	Moment	Polarisability $\alpha \times 10^{24}$c.c.
F	1.45D	0.57
Cl	1.55	2.51
Br	1.50	3.63
I	1.25	5.46

RESULTS AND DISCUSSION

The experimental results are shown in Tables I, II, and III and consolidated in Table IV together with the calculated values. In Table V are given the observed and calculated values for all these fluoro compounds.

Table V shows that for the meta compounds the simple vectorial moment is in fair agreement with the observed values, whereas for the ortho compounds the agreement is not good—this fact shows that the ortho effects are appreciable for the halogen substituents, although a definite variation with size and polarisability of the substituent group is not noticeable. When the moments are calculated by the Smallwood and Herzfeld method, a much closer agreement is observed for the ortho compounds also. This may further indicate that the ortho effects could be accounted for mostly by mutual inductive effects, the effect due to steric repulsion being negligible.

TABLE I

m-Fluorochloro benzene

W	ε_{12}	$\Delta\varepsilon$	$\Delta\varepsilon/W$	n^2_{12}	n^2_{12}	Δn^2	$\Delta n^2/W$
0.01581	2.2960	0.0320	2.023	1.49348	2.23049	0.00017	0.011
0.02189	2.3074	0.0434	1.983	1.49347	2.23044	0.00021	0.010
0.04384	2.3477	0.0837	1.908	1.49347	2 23044	0.00021	0.005
0.06061	2.3776	0.1136	1.875	1.49343	2.23032	0.00033	0.005
0.07630	2.4047	0.1407	1.844	1.49340	2.23024	0.00041	0.005

$P_d = 50.0$ c.c. $\mu = 1.52$ D.

TABLE II

m-Fluorobromo benzene

W	ε_{12}	$\Delta\varepsilon$	$\Delta\varepsilon/W$	n_{12}	n^2_{12}	Δn^2	$\Delta n^2/W$
0.01311	2.2818	0.0178	1.361	1.49421	2.23269	0.00204	0.156
0.02116	2.2925	0.0285	1.347	1.49471	2.23417	0.00352	0.116
0.03365	2.3103	0.0463	1.377	1.49479	2.23439	0.00374	0.111
0.04832	2.3313	0.0673	1.393	1.49498	2.23497	0.00432	0.089
0.06184	2.3493	0.0853	1.380	1.49493	2.23482	0.00417	0.067
0.08718	2.3843	0.1203	1.380	1.49527	2.23583	0.00518	0.059

$P_d = 39.4$ c.c. 1.40 D.

TABLE III

m-Fluoroiodo benzene

W	ε_{12}	$\Delta\varepsilon$	$\Delta\varepsilon/W$	n_{12}	n^2_{12}	Δn^2	$\Delta n^2/W$
0.03779	2.3058	0.0418	1.105	1.49591	2.23775	0.00711	0.188
0.04930	2.3184	0.0544	1.104	1.49655	2.23965	0.00900	0.183
0.06034	2.3300	0.0660	1.094	1.49697	2.24093	0.01028	0.170
0 07698	2.3473	0.0833	1 082	1.49770	2.24311	0.01246	0.162
0 10420	2.3782	0.1142	1.096	1.49879	2.24637	0.01572	0.151
0.12880	2.4027	0.1387	1.076	1.49985	2.24955	0.01890	0.147

P_d = 38.3 c.c. μ = 1.38 D.

TABLE IV

Molecule	Calculated Vector	Calculated S and H	Observed
m-Fluorochloro benzene	1.50	1.45	1.52 D
m-Fluorobromo benzene	1.48	1 42	1.40
m-Fluoroiodo benzene	1.36	1 31	1.38

TABLE V

Molecule	Calculated Vector	Calculated S and H	Observed
o-Fluorochlorobenzene	2.60	2.43	2.38 D
m- ,,	1.50	1.45	1.52
p- ,,	0.10	0.08	0.95*
o-Fluorobromobenzene	2.56	2 36	2.27
m- ,,	1.48	1.42	1.40
p- ,,	0.05	0.05	0.50
o-Fluoroiodobenzene	2.34	2.10	2.00
m- ,,	1.36	1.31	1.38
p- ,,	0.20	0.26	0.90

* Value determined by the author for the pure liquid.

For para compounds there are large differences between the calculated and observed values. The values calculated by taking inductive effects are not very different from those calculated by simple vectorial method. The calculated values show that the moments of these para compounds should be roughly zero.

The large values observed may represent the contributions by atomic polarisations or resonance effect; the possible presence of small amounts of ortho compounds as impurities cannot also be ruled out.

ACKNOWLEDGMENTS

The author is very much indebted to Prof. K. R. Rao for his kind and constant guidance. He is grateful to Dr. Finger of the Illinois State Geological Survey for supplying the fluoro compounds.

REFERENCES

Bergmann, E., Engel, L., and Sandor, S., 1930, *Z. Physik, Chem.*, **10B**, 307.
Hurdis, E. C., and Smyth, C. P., 1942, *J. A. C. S.*, **64**, 2212.
Murty, C. R. K., 1957, *Ind. J. Phys.* **31**, 256.

AN ELECTRON DIFFRACTION CAMERA OF SIMPLIFIED DESIGN

S. N. CHATTERJEE

BIOPHYSICS DIVISION, INSTITUTE OF NUCLEAR PHYSICS, CALCUTTA-9.

(*Received for publication, April* 9, 1958)

Plate IX A & B

ABSTRACT. A simple electron diffraction camera has been designed where the majority of the specimen motions required for all types of diffraction work has been transmitted into vacuum through a Wilson seal using a rubber gasket only. Diffraction photographs can be taken from four specimens without disturbing the vacuum and with an accuracy better than 1%. The camera is adapted to the electron microscope after its projector lens which can be adjusted to have a shadow micrograph of the specimen under examination.

INTRODUCTION

For electron diffraction work, various rotational and translational motions have to be imparted to the specimen while inside the vacuum The transmission of these motions is generally effected with the help of sylphon bellows and ground joints (Finch and Quarrel, 1933, Germer, 1935; Thiessen and Schoon, 1937, Pinsker, 1953). The conical ground joints require frequent greasing for the maintenance of proper vacuum with the possibility of the contamination of the specimen (Hillier and Baker, 1946). As electron diffraction work requires extreme purity of the specimen, it is preferable to avoid the greased ground joints. Moreover, for transmission of all possible types of motion, the specimen holding mechanism may often be very complicated. In the present work, a specimen chamber is designed in a very simple way avoiding the ground joints

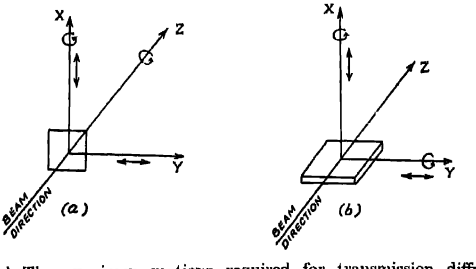

Fig. 1. a) The specimen motions required for transmission diffraction.
b) The specimen motions required for reflection diffraction.

and sylphon bellows. Here the necessary motions have been imparted through a particular type of Wilson seal (Cailson, 1941) using only rubber gaskets.

DESCRIPTION

The different specimen motions required are illustrated in the figures 1(a) and (b). Figure 1(a) refers to the transmission electron diffraction. With the electron beam travelling in the positive direction of the Z-axis, the specimen region giving diffraction patterns of clearest and sharpest definition is to be selected first. This requires a provision for the motion of the specimen along X- and Y- axes. To determine the orientation of the crystals the specimen must be rotated about two axes: the X- axis in order to obtain a different inclination of the crystal planes towards the electron beam and the Z-axis in order to change the orientation in azimuth (important for the study of monocrystalline films). Figure 1(b) refers to the reflection electron diffraction. In this case the correct position is obtained by turning it about the Y- axis and by displacing it either side in the direction of the X-axis. A motion along the Y- axis will leave scope for exploring the specimen. Finally in the case of the single crystal one must be able to rotate the specimen about the X-axis.

In the present work, the realisation of the majority of these motions was made by the use of a Wilson seal of the type shown in figure 2. From figure 2 it

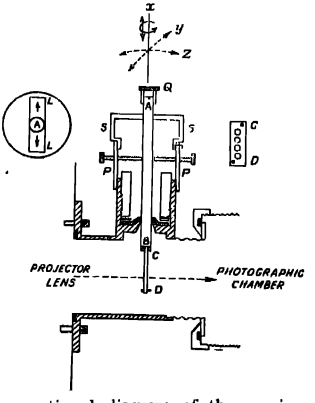

Fig. 2. The sectional diagram of the specimen chamber.

will be evident that the specimen has got both rotational and translation motion along X-axis. Translation is also possible along Y- and Z- axes but they are not linear. It can be easily seen that this will not affect in any way the main objectives since the motions required are very small. The only specimen movements

that are not permissible are (a) rotational motion along Y- axis and (b) rotationl motion along Z-axis.

Figure 2 shows the design of the specimen chamber using the above type of Wilson seal. The specimens for transmission work are held inside the grooves in a rectangular brass plate CD, drawn out from one end of the brass rod AB. The specimens are held on the collodion covered steel wire mesh normally used for the electron microscopy. To keep the specimens fixed in position during observation, copper rings are placed over these wire meshes and kept tight by means of another thin brass plate screwed into the former one. Four specimens can be examined one after another and within a very short time without disturbing the experimental conditions. To impart motions to the specimen, four screws at right angles to each other and all in the same horizontal plane pass through a brass cylinder, PP. The rotatory motion is imparted by means of the brass knob Q. Another brass cylinder SS, tightly fitted to PP and fixed in position by a screw, bears a rectangular slot LL on the top of width exactly equal to the diameter of the brass rod AB. The rectangular slot can be fixed normal to the electron optical axis of the camera and thus the motion of the specimen rod is restricted perpendicular to the beam. This prevents any variation of the diffraction during the examination of one specimen or in the course of changing from one length specimen to the next.

The specimen chamber is adapted to the horizontal electron microscope (Das Gupta *et al.*, 1948) built in this laboratory after its projector stage (Hillier *et al*, 1942; Cowley, 1953). There is no magnetic element between the diffraction specimen and the sensitive screen and hence there is no chance of any distortion of the diffraction diagram. Further, a large diffraction angle and hence greater number of diffraction rings are obtained for this position of the specimen.

Figure 3 shows the electron optical ray diagram for diffraction. The condenser lens, C forms an image of the cross over X from the electron gun. The

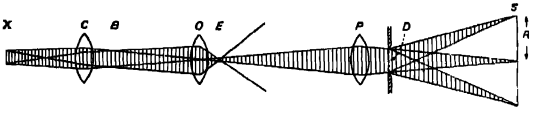

Fig. 3. Electron optical ray diagram for the diffraction work.

position of this image can be varied by varying the condenser current. The smallest cross section B of the beam from the condenser lens is focussed by the objective, O in front of the projector lens P at E. This is again focussed by the projector lens on the final screen in order to obtain sharp diffraction rings. The specimen is placed in the position D. The intensity of the diffraction diagram can be controlled by adjusting the objective and the condenser currents. The projector lens current can also be adjusted to obtain an electron optical shadow

micrograph of the specimen under observation. This allows an examination of the nature and the distribution of the diffraction specimen at a magnification of about 30X and ensures proper selection of the specimen area for diffraction work.

RESULTS

Plate IX A shows the diffraction photographs of the four gold films of the same thickness placed at the four positions of the holder. The ring diameters of the individual photographs were measured and are given in Table 1. The maximum deviations in the measured diameters of the corresponding rings as percentage of the mean diameter are given in the last column of the table. An accuracy better than 1% is achieved with this system.

TABLE I

Measurements on the diffraction patterns from the four gold films

hkl	Measured diameters (cm) from Plate IXA				Maximum deviation
	(a)	(b)	(c)	(d)	
111	1.462	1.465	1.467	1.460	0.5%
200	1.699	1.698	1.692	1.686	0.9%
220	2.389	2.380	2.389	2.382	0.4%
113	2.797	2.792	2.780	2.780	0.6%

The calibration of the camera was made from the diffraction pattern of a thallium chloride specimen (Plate IXB). $L\lambda$ was found to be 1.8464×10^{-8} cm^2. The normal diffraction pattern, the oblique texture pattern and shadow micrograph (125×) of a CdI_2 specimen are shown in Plate IXB b, c and d respectively.

ACKNOWLEDGMENTS

The author wishes to express his indebtedness to Prof. N. N. Das Gupta and Sri M. L. De for many helpful discussions. He is also indebted to Sri G. N. Sarkar for help in designing the diffraction adapter and to the Ministry of Education, Govt. of India, for the award of a Research Assistantship.

REFERENCES

Cowley, J. M., 1953, *J. Sc. Instr.*, **30**, 33.
Das Gupta, N. N. *et al.*, 1948, *Ind. Jour. Phys.*, **22**, 497.
Finch, G. I. and Quarrel, A. G., 1933, *Proc. Phys. Soc.*, *A*141, 399.
Germer, L. H., 1935, *Rev. Sci. Instr.*, **5**, 138.
Hillier, J., Baker, R. F. and Zworykin, V. K., 1942, *J. Appl. Phys.*, **13**, 571.
Thiessen, P. A. and Schoon, Th., 1937, *Z. Phys. Chem.*, *B*36, 195.
Wilson, R. R., 1941, *Rev. Sci. Inst.* **12**, 91.

Indian Journal of Physics, Vol XXXII, No. 8

(a)

(b)

(c)

(d)

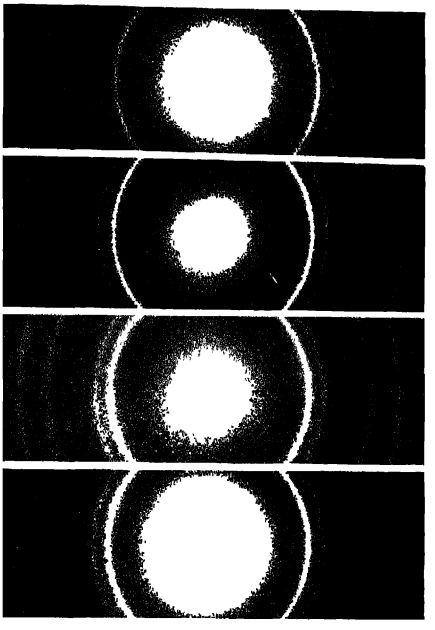

Electron diffraction photographs taken successively from four gold films of the same thickness from the four positions of the holder.

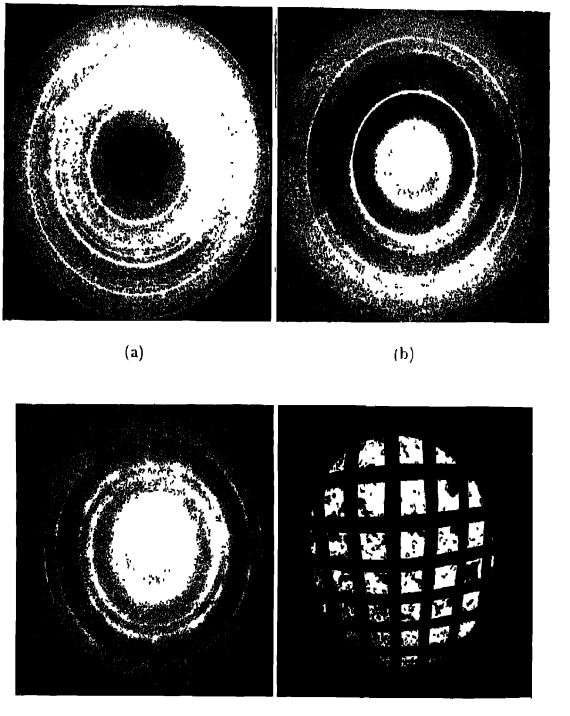

(a) (b)

(c) (d)

Electron diffraction photographs.

(a) Electron diffraction pattern of thallium chloride
(b) Normal diffraction pattern of CdI_2
(c) Oblique texture pattern of CdI_2
(d) Electron shadow micrograph of CdI_2 (125 ×).

RANGE-ENERGY RELATION FOR PROTONS IN VARIOUS SUBSTANCES

YATENDRA PAL VARSHNI

DEPARTMENT OF PHYSICS, ALLAHABAD UNIVERSITY, ALLAHABAD

(*Received for publication, March 6, 1958, after revision, June 9, 1958*)

ABSTRACT. A simple relation between the range (R) and energy (E) of heavy charged particles has been proposed : $R = a\,(E+c)^n$, where, a, c and n are constants. The relation has been shown to be quite successful for proton ranges in a number of substances, up to 100 Mev.

INTRODUCTION

All charged particles in their passage through matter lose energy by a number of processes. For not too high energies, the chief causes are the excitation and ionization of atoms and molecules of the medium. The practical problem of estimating the energy of a nuclear particle from its observed range in a known medium is of great importance and many experimental and theoretical studies have been made with the object of establishing standard range-energy relations. The subject has been reviewed in recent years by Taylor (1952), Bethe and Ashkin (1953), Allison and Warshaw (1953) and Uehling (1954).

It is convenient to distinguish the charged particles in two types : electrons and positrons on one hand and all charged particles heavier than electrons on the other In the present paper we would confine ourselves to heavier particles. In the following E is the energy of the particle in Mev, v is its velocity and R is its range. The different units of range are indicated at appropriate places.

Semi-theoretical or empirical relations are frequently employed for representing the relation between the energy and the range of a particle.

The best known of these relations is due to Geiger (1910) :

$$R = kv^3 = aE^{3/2} \qquad \ldots \quad (1)$$

Originally Geiger had suggested this for alpha particles having ranges between 3 and 7 cm.

For low energy alpha particles having ranges less than 4 mm., Blackett and Lees (1932) found the following equation to be satisfactory :

$$R = Cv^{1\cdot 43} \qquad \ldots \quad (2)$$

On the other hand, Briggs (1933) showed that for alpha particles having ranges greater than 5 cm., Geiger's relation should be modified to

$$R = kv^{3\cdot 26} \qquad \ldots \quad (3)$$

Rutherford, Wynn-Williams, Lewis and Bowden (1933) noticed deviations from the Geiger relation and gave a correction curve for the same.

Meyer (1935) put forward the following relation for alpha particles :

$$R = -r + Av + Bv^2 + Cv^3 \quad \ldots \quad (4)$$

where r, A, B and C are constants.

It becomes apparent that power relations have only limited applicability. Livingston and Bethe (1937) have given a graph showing the variation of the exponent n in Geiger law with E (figure 35, p. 278 of their paper).

Rogers and Rogers (1938) have proposed a number of relations for different energy intervals. For example, for protons in air, with R in cm. :

for $R \leqslant 6$

$$\log_{10}E = -.3845 + [.595 \pm .45e^{-4R} + \cdot 0025 \sin^2(2\pi R/9) \cos(\pi R/3)] \log_{10}2R \quad \ldots \quad (5a)$$

$6 \leqslant R \leqslant 30$

$$E = 1.819 + .16758(R-6) - .003(R-6)^2 + .00004(R-6)^3 \quad \ldots \quad (5b)$$

$30 \leqslant R \leqslant 90$

$$E = 4.661 + .08715(R-30) - .000454(R-30)^2 + .00000217(R-30)^3 \quad \ldots \quad (5c)$$

Wilson and Brobeck (Wilson 1947) found for protons in air :

$$R \text{ (in metres)} = (E/9.3)^{1.8} \quad \ldots \quad (6)$$

Rogozinski (1951) advocates :

$$R = a^{-1.8}E^{1.8} \quad \ldots \quad (7)$$

If R is in gm/cm^2, $a = 27.5$ for Al and $a = 29\ 0$ for air.

Cook, Jones and Jorgensen (1953) have employed a modification of Geiger relation for low energy protons (50—250 kev) :

$$R = C(E+E_1)^{3/2} \quad \ldots \quad (8)$$

where E_1 and C are constants.

Recently Kaila (1955) has deduced from semi-theoretical considerations an equation for the ranges of alphas in air. But the values of the constants are fitted empirically :

$$E = .4359R^{1/3} + 5.676R^{1/3} \log R + 1.477R^{-2/3} + .9712R^{-2/3} \log R \quad \ldots \quad (9)$$

The equation is useful below 2.5 Mev.

Another recent equation is due to Gobeli (1956). For ranges of alpha particles in three semiconductors, he finds that his results can be represented by

$$R = aE^n + b \quad \ldots \quad (10)$$

where a, b and n are constants. A similar equation has been used by Livesey (1956).

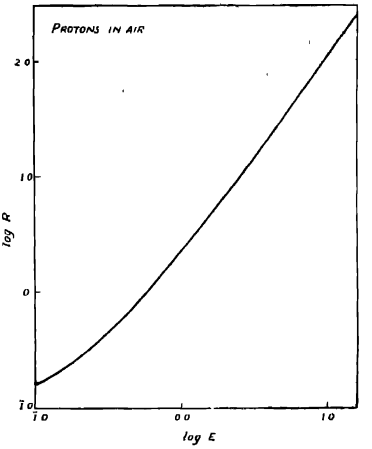

Fig. 1

NEW RELATION

From the above it will be evident that simple power relations hold only for small energy intervals. The point has been illustrated in figure 1, in which log R has been plotted against log E for protons in air for $E = 0.1$ to 15 Mev. For the applicability of the power relation, the curve should have been a straight line. Some of the relations proposed by earlier workers are rather complicated.

The present paper suggests a simple range-energy relation for heavy particles. The relation is

$$R = a(E+c)^n \qquad \ldots \quad (11a)$$

where a, c and n are constants.

The relation may be put as

$$\log_{10}R = n \log_{10}(E+c)+B \qquad \ldots \quad (11b)$$

Presently we would show its applicability to protons for wide energy intervals.

Range-energy data for protons in a number of substances are available from experimental determinations and /or theoretical calculations. Individual substances have been treated below separately.

AIR

Experimental determination of range-energy relation for protons in air have been made by a number of workers. These have been reviewed by Clarke and Bartholomew (1949), Bethe (1950), Jesse and Sadauskis (1950) and Bethe and Ashkin (1953). Theoretical calculations have been carried out by Smith

(1947) by numerical integration of the relativistic expression for dE/dx. The data for the region .05 Mev to 100 Mev can be represented by

$$\log R(\text{cm}) = 1.795 \log (E+0.13)+0.2598$$

Calculated values have been compared with experimental and theoretical values in Table I.

TABLE I

Air

E (Mev)	R (cm) Calc.	R (cm) Expt. & Theor.*	% error
0.05	0.0838	0.085	— 1 41
0.1	0.1301	0.15	—13.3
0.2	0.2486	0.285	—12.8
0.4	0.582	0.61	— 4 6
0.6	1.034	1.04	— 0.58
0.8	1 597	1.6	— 0 19
1.0	2.265	2.27	— 0.22
1.5	4.372	4.4	— 0.64
2 0	7.068	7.1	— 0.45
4.0	23.2	23	+ 0 87
6.0	47.14	46.7	+ 0 94
8.0	78.23	77.3	+ 1 20
10.0	116.1	114.8	+ 1 13
15.0	238.6	238.5	+ 0 04
19.0	363.4	362 3	+ 0.30
30	821.5	819.4	+ 0.26
40	1374	1374	0
50	2049	2053	— 0.19
60	2840	2849	— 0.32
70	3743	3756	— 0.34
80	4754	4769	— 0.31
90	5872	—	—
100	7095	7095	0

* Sources of data :

.05 — 1.5 Mev—Read from the curve given by Bethe (1950).

1.5 — 15 Mev—Read from curve given by Bethe and Ashkin (1953).

15 — 100 Mev—Theoretical calculations of Smith (1947).

BERYLLIUM

Aron (1951) has theoretically calculated the ranges, but as the value of the effective ionization potential used by him was found to be rather low, Bichsel, Mozley and Aron (1957) have recalculated ranges for energies between 1 to 21 Mev. From these the values of the constants in eq. (11b) were determined:

$$\log R\,(\text{mg/cm}^2) = 1.816 \log (E+0.18)+0.3443$$

Table II shows the results.

TABLE II

Beryllium

E (Mev)	R (mg/cm²) Calc.	R (mg/cm²) Theor.*	% error
1	2.99	3.0	—0.33
2	9.10	9.1	0
3	18.06	18.0	+0.33
4	29.67	29.6	+0.24
5	43.8	43.6	+0.46
6	60.37	60.1	+0.45
7	79.25	78.9	+0.44
8	100.4	100.0	+0.4
9	123.8	123.3	+0.4
10	149.4	148.8	+0.4
11	177.1	176.5	+0 34
12	206.8	206.3	+0.24
13	238.7	238.2	+0.21
14	272.7	272.1	+0.22
15	308.6	308.1	+0.16
16	346 5	346.1	+0.11
17	386.4	386.1	+0.08
18	428.3	428.1	+0.05
19	472.0	472.0	0
20	517.6	517.6	0
21	565.1	565.9	—0.14

* Theoretical values from Bichsel *et al.* (1957).

ALUMINUM

Aluminum is one of the most useful substances for range measurements at both low and high energy because it can be obtained both in thin foils and in bulk, with high purity and satisfactory uniformity. It is an element, hence preferable to mica whose chemical composition varies and it has at the same time sufficiently low atomic weight to permit the application of theory at relatively low energy.

Experimental results have been summarised by Bethe and Ashkin (1953). Smith (1947) has tabulated theoretical results for $E > 1$ Mev.

The data can be expressed by

$$\log R(\text{mg/cm}^2) = 1.777 \log (E+0.15)+0.4384$$

The calculated values by this relation together with Smith's values are recorded in Table III.

TABLE V

Silver

E (Mev)	R (mg/cm²) Calc.	R (mg/cm²) Theor.*
4	62.61	62.60
6	114.7	112.63
8	179.8	175.97
10	257.2	251.89
14	447.2	439.35
20	813.2	803.56
26	1272	1261.0
30	1624	1615.0
34	2014	2006.7
38	2439	2435.0
42	2901	2898.9
46	3396	3397.4
50	3923	3929.6
60	5389	5402.8
70	7050	7071.1
80	8902	8924.8
90	10940	10955
100	13150	13155

* Theoretical values from Aron (1951).

GOLD

For low energy region Wilcox (1948) gives a range-energy curve obtained by integrating the dE/dx curve. Theoretical values have been provided by Bichsel, Mozley and Aron (1957). Their data can be expressed by

$$\log R\ (\mathrm{mg/cm^2}) = 1.74 \log (E+1.15)+0.7329$$

Table VI shows the agreement between the two sets of values.

TABLE VI

Gold

E (Mev)	R (mg/cm^2) Calc.	R (mg/cm^2) Theor.*
2	39.8	39.7
3	64.3	64.3
4	93.62	93.6
5	127.5	127.3
6	165.7	165.5
7	208.1	207.8
8	254.5	254.2
9	304.8	304.5
10	359.1	358.6
11	417.0	416.4
12	478.4	477.8
13	543 4	542.9
14	612.0	611.5
15	684.2	683.5
16	759.7	759.0
17	838.3	837.8
18	920.0	920.0
19	1005.7	1005.5
20	1093.7	1094.2
21	1185.6	1186.2

* Theoretical values from Bichsel *et al* (1957).

GLYCEROL TRISTEARATE $C_{57}H_{110}O_6$

In many neutron experiments hydrogen is used in the form of an organic compound. Glycerol tristearate is one of the important ones. Hirschfelder and Magee (1948) have calculated ranges by a semi-theoretical method. The equation is

$$\log R\ (\mathrm{mg/cm^2}) = 1.81 \log (E+0.12)+0.2247$$

Table VII shows some of the theoretical values of Hirschfelder and Magee together with the calculated values from the above formula.

TABLE VII

Glycerol tristearate

E (Mev)	R (mg/cm²) Calc.	R (mg/cm²) Theor.*
0.02	0.0478	0.046
0.05	0.0679	0.068
0.1	0.1083	0.106
0.2	0.2132	0.205
0.4	0.5137	0.500
0.6	0.9256	0.911
0.8	1.442	1.430
1.0	2.060	2.050
1.2	2.773	2.767
1.4	3.579	3.576
1.6	4.477	4.476
1.8	5.464	5.464
2.0	6.536	6.539
2.2	7.697	7.698
2.4	8.937	8.941
2.6	10.26	10.267
2.8	11.67	11.673
3.0	13.16	13.160

* Theoretical values from Hirschfelder and Magee (1948).

PARAFFIN $(CH_2)_n$

Hirschfelder and Magee (1948) have tabulated theoretical results for paraffin also. The equation is

$$\log R\ (\mathrm{mg/cm^2}) = 1.834 \log (E+0.12) + 0.1905$$

Results are given in Table VIII.

TABLE VIII

Paraffin

E (Mev)	R (mg/cm²) Calc.	R (mg/cm²) Theor.*
0.05	0.06013	0.06096
0.1	0.0965	0.09613
0.2	0.1918	0.18908
0.4	0.4673	0.46833
0.6	0.8487	0.86101
0.8	1.331	1.35759
1.0	1.909	1.95202
1.5	3.756	3.83930
2.0	6.150	6.2683
3.0	12.50	12.652
4.0	20.81	20.960
5.0	31.00	31.118
6.0	43.00	43.070
7.0	56.75	56.771
8.0	72.23	72.182
9.0	89.34	89.275
10	108.1	108.022
11	128.5	128.40
12	150.5	150.40
13	174.1	173.99
14	199.2	199.17
15	225.9	225.91

* Theoretical values from Hirschfelder and Magee (1948).

NUCLEAR EMULSION

Due to the great importance of nuclear emulsion technique, extensive experimental and theoretical investigations have been carried out for establishing accurately the range-energy relation for the nuclear emulsions.

Simple power relations have been employed by some workers (Lattes, Occhialini and Powell, 1948 ; Bradner *et al*, 1950 ; Lees *et al*, 1953) for representing their data.

Recently Daniel, George and Peters (1955) have examined some of the experimental and theoretical data and given a 'best value' table of range and energy for Ilford C2 emulsion (density 3.94 gm/cm³). We have utilized their data for finding the values of the constants in the formula

$$\log R = 1.749 \log (E+0.25) - 2.0301$$

where R is in mm.

The calculated values by the above expression have been compared with the values given by Daniel *et al.* in Table IX.

TABLE IX

Ilford C2 nuclear emulsion

E (Mev)	R (mm) Calc.	R (mm) Expt. & Theor.*	% error
1	0.01379	0.0138	−0.07
1.5	0.02482	0.0255	−2.67
2	0.03854	0.0399	−3.4
3	0.07332	0.0746	−1.71
4	0.1172	0.1185	−1.1
5	0.1696	0.1725	−1.68
6	0.2301	0.2350	−1.96
7	0.2983	0.3030	−1.55
8	0.3740	0.3780	−1.06
10	0.5465	0.5540	−1.35
15	1.095	1.100	−0.45
20	1.799	1.815	−0.88
30	3.627	3.615	+0.33
40	5.977	5.960	+0 28
50	8.812	8.750	+0.71
60	12.11	11.85	+2.19
80	20.0	19.80	+1.01
100	29.50	29.70	−0.67

* Data from Daniel, George and Peters (1955).

DISCUSSION

The values of the constants in equation (11) for the various substances have been summarised in Table X.

TABLE X

Values of the constants (E in Mev)

Substance	Unit of R	n	c	B	a
Air	cm	1.795	0.13	0.2598	1.819
Beryllium	mg/cm²	1.816	0.18	0.3443	2.210
Aluminum	mg/cm²	1.777	0.15	0.4384	2.745
Copper	mg/cm²	1.778	0.5	0.5076	3.218
Silver	,,	1.768	0.9	0.5763	3.770
Gold	,,	1.74	1.15	0.7329	5.406
Glycerol tristearate	,,	1.81	0.12	0.2247	1.678
Paraffin	,,	1.834	0.12	0.1905	1.551
Nuclear emulsion	mm	1.749	0.25	−2.0301	0.009330

Though there is no regular variation in the values of the constants, yet a rough observation may be made that n has a tendency to decrease and C tends to increase as we go to substances of higher effective atomic numbers. Value of a is dependent on the unit of R. In those cases where R has been expressed in mg/cm^2 it may be noticed that a increases with increase in effective atomic number.

It will be observed from Tables I to IX that the agreement between the calculated values from eq. (11b) and the theoretical and/or experimental values is quite satisfactory up to 100 Mev. Errors are usually of the order of 1%. It may be added that the accuracy of theoretical and experimental figures is usually of the order of 2%. Further, the constants were not determined by the method of least squares; if they are determined by the method of least squares the results can be expected to be even better.

Below 0.1 Mev protons begin to capture electrons. The theory of the electron capture has not yet been fully worked out, though approximate studies have been made. In a number of cases (glycerol tristearate, paraffin etc.) theoretically calculated values are available for $E < 0.1$ Mev; but as these values do not include the effect of electron capture, they may be in error.

ACKNOWLEDGMENTS

The author is thankful to Prof. K. Banerjee for his kind interest in the work, and to the referee of the paper for helpful comments.

REFERENCES

Allison, S. K. and Warshaw, S. D., 1953, *Rev. Mod. Phys.*, **25**, 779.

Aron, W. A., 1951, Univ. of California Radiation Lab., Rept. UCRL-1325.

Aron, W. A., Hoffman, B. G. and Williams, F. C., 1949, Report AECU-663 and UCRL-121.

Bethe, H. A., 1950, *Rev. Mod. Phys.*, **22**, 213.

Bethe, H. and Ashkin, J., 1953, Experimental Nuclear Physics, (edited by E. Segre), Vol. 1, 166 (John Wiley and Sons Inc., New York).

Bichsel, H., Mozley, R. F. and Aron, W. A., 1957, *Phys. Rev.*, **105**, 1788.

Blackett, P. M. S. and Lees, D. S., 1932, *Proc. Roy. Soc.*, **A134**, 658.

Bradner, H., Smith, F. M., Barkas, W. H. and Bishop, A. S., 1950, *Phys. Rev.*, **77**, 462.

Briggs, G. H., 1933, *Proc. Roy. Soc.*, **A139**, 638.

Clarke, R. L. and Bartholomew, G. A., 1949, *Phys. Rev.*, **76**, 146.

Cook, C. J., Jones, E. and Jorgensen, T., 1953, *Phys. Rev.*, **91**, 1417.

Daniel, R. R., George, E. C. and Peters, B., 1955, *Proc. Indian Acad. Sci.*, **41**, 45.

Geiger, H., 1910, *Proc. Roy. Soc.*, **A83**, 492, 505.

Gobeli, G. W., 1956, *Phys. Rev.*, **103**, 275.

Hirschfelder, J. O. and Magee, J. L., 1948, *Phys. Rev.*, **73**, 207 and Erratum, 1950, *Phys. Rev.*, **79**, 1005.

Jesse, W. P. and Sadauskis, J., 1950, *Phys. Rev.*, **78**, 1.

Kaila, K. L., 1955, *Ind. J. Phys.*, **29**, 479.

Lattes, C. H. G., Occhialini, G. P. S. and Powell, C., 1948, *Proc. Phys. Soc.*, **61**, 173.
Lees, C. F., Morrison, G. C. and Rosser, W. G. V., 1953, *Proc. Phys. Soc.*, *A* **66**, 13.
Livesey, D. L., 1956, *Canad. J. Phys.*, **34**, 203.
Livingston, M. S. and Bethe, H. A., 1937, *Rev. Mod. Phys.*, **9**, 261.
Meyer, S., 1935, *Akad. Wiss. Wien. Ber.*, **144**, 317.
Rogers Jr., F. T. and Rogers, M. M., 1938, *Phys. Rev.*, **53**, 713.
Rogozinski, A., 1951, *J. Phys. Radium*, **12**, 955.
Rutherford, E., Wynn-Williams, C. E., Lewis W. B. and Bowden, B. V., 1933, *Proc. Roy. Soc.*, *A* **139**, 617.
Smith, J H., 1947, *Phys. Rev.*, **71**, 32.
Taylor, A. E., 1952, *Repts. Prog. Phys.*, **15**, 49.
Uehling, E. A., 1954, *Ann. Rev. Nuclear Sci.*, **4**, 315.
Wilcox, H. A., 1948, *Phys. Rev.*, **74**, 1748.
Wilson, R. R., 1947, *Phys. Rev.*, **71**, 385.

DIELECTRIC RELAXATION—EFFECT OF TEMPERATURE

K. V. GOPALA KRISHNA

MICROWAVE LABORATORY, ANDHRA UNIVERSITY, WALTAIR.

(*Received for publication, February* 25, 1958)

ABSTRACT. Dielectric relaxation times were determined over a wide range of temperatures for benzophenone, ethyl benzoate, α-nitro-naphthalene and ethyl adipate dissolved in heptane and ethyl adipate in decalin. The results have been discussed in the light of Eyring's theory on dipole rotation.

INTRODUCTION

Recent approaches to the problem of dielectric relaxation have involved the supposition that the dipole actually rotates between two positions of equilibrium separated by a potential energy barrier. If the height of the potential energy barrier is H_τ, then Frohlich (1949) has shown that the dielectric relaxation time τ, considered as a measure of the transition probability, is given by a relation of the form

$$\tau = \frac{C}{\omega_a} e^{H_\tau/KT} \qquad \ldots \quad (1)$$

where C is temperature-dependent to some extent, π/ω_a the average time required by an excited molecule to turn from one equilibrium direction to the other.

Eyring (1941), postulating an analogy between the processes of dipole rotation and of unimolecular chemical reactions, identifies H_τ with ΔF, the thermodynamic standard free energy associated with these processes. His theory leads to a value h/KT for the factor C/ω_a, h being the Planck's constant, and equation (1) can be written as

$$\tau = \frac{A}{T} e^{H_\tau/KT} \qquad \ldots \quad (2)$$

where $A/T = C/\omega_a$.

As in the dielectric relaxation, the conception of viscous flow as involving the surmounting by each molecule of a potential energy barrier of height H_η say, each time it moves, leads to a relation of the form

$$\eta = B\, e^{H_\eta/KT} \qquad \ldots \quad (3)$$

Eyring (1941) identified B with the factor hN/V, where h is the Planck's constant, N the Avogadro's number and V the molar volume.

This approach by Eyring to the understanding of relaxation as a rate process was investigated by Whiffen and Thompson (1946) by carrying out measurements on dilute solutions of chloroform, camphor, etc., in heptane. They observed a linear relationship between the logarithm of the relaxation time and the reciprocal of the absolute temperature. They pointed out, however, that a slight curvature to the graph, expected on the basis of Eyring's theory, could not be detected due to insufficient accuracy in their experimental results. Their observations indicated further an approximate equality of H_τ and H_η. They evaluated also the entropy change (ΔS) and heat content change (ΔH) for the process of activation and noticed that the entropy changes of activation were all small and negative. They said that the physical significance of such negative values should be left for later consideration but however indicated that this data might be informative about the packing of the molecules when compared with the corresponding values for other systems. Similar conclusions were drawn by Smyth *et al.* (1948) in their study on alkyl bromides. Recent investigation by Saxton (1952) on the effect of temperature on dielectric relaxation in the case of pure polar liquids, indicated a linear relationship between log $T\tau$ and $1/T$ in the case of methyl and ethyl alcohols but a curvature in the case of water. But in all the three liquids he found the plot of log $T\tau$ versus log η to be a perfect straight line with slope unity, thus showing that H_τ is identical with H_η. Further his observations on the two factors A and B indicated that, though they remained fairly constant over a wide range of temperatures in the case of alcohols, the values of the latter were found to be in reasonable agreement and those of the former to be significantly greater than the values predicted by Eyring. In the case of water he did not observe any constancy in the values of A and B, and this peculiar behaviour was attributed to the change of its co-ordinated structure with change in temperature.

A study of these observations on the effect of temperature on dielectric relaxation, so far recorded, seems to indicate that Eyring's theory on dipole rotation still remained open to discussion and requires a bulk of experimental data before any attempt is made to draw definite conclusions on this subject. Hence the present work has been undertaken with a view to studying Eyring's approach in understanding dielectric relaxation. Observations are recorded on benzophenone, ethyl benzoate, α-nitronaphthalene and ethyl adipate dissolved in heptane and ethyl benzoate in decalin. H_τ is found approximately equal to H_η in all the cases studied. The values for the factors A and B calculated from experimental observations are found to be constant in each liquid, and they are of the same order of magnitude though not in agreement, with those predicted by Eyring (1941).

EXPERIMENTAL

All the measurements on the effect of temperature were made at a wavelength of 3.28 cms.

The value of the dielectric relaxation time is evaluated at various temperatures by assuming Debye's equation for the complex dielectric constant as a function of frequency for a dilute solution of a polar compound in a non-polar solvent which can be written as

$$\frac{\epsilon^* - 1}{\varepsilon^* + 2} - \frac{\epsilon_\infty - 1}{\epsilon_\infty + 2} + \frac{4\pi n\mu^2}{9KT} \cdot \frac{1}{1 + i\omega\tau}$$

where n is the number of dipole molecules per c.c., ε^* is the complex dielectric constant of the solution.

Splitting the above expression into its real and imaginary parts, we obtain for the coefficient of imaginary part

$$\frac{3\epsilon''}{(\epsilon' + 2)^2 + \epsilon''^2} = \frac{4\pi\eta\mu^2}{9KT} \cdot \frac{\omega\tau}{1 + \omega^2\tau^2} \quad \ldots \quad (4)$$

where ε' and ε'' are dielectric constant and loss of the solution.

This equation can be written as

$$\frac{T\varepsilon''}{\{(\epsilon' + 2)^2 + \epsilon''^2\}d_{12}} = \frac{4\pi N\mu^2 W}{27KTM} \cdot \frac{\omega\tau}{1 + \omega^2\tau^2} \quad \ldots \quad (5)$$

since $n = Nd_{12}W/M$, where W is the weight fraction of the solute and M its molecular weight and N the Avogadro's number.

It can be seen that $T\epsilon''/\{(\epsilon'+2)^2+\varepsilon''^2\}d_{12}$ is maximum, when $\omega\tau = 1$, which gives the value of τ at that temperature. At any other temperature the ratio of the value of $T\varepsilon''/\{(\epsilon'+2)^2+\epsilon''^2\}d_{12}$ to its maximum value will be $2\omega\tau/(1+\omega^2\tau^2)$ in which τ is the relaxation time at that temperature. The choice between the two possible values of τ for one value of this ratio is determined by whether the temperature is above or below that corresponding to the maximum value.

It may be mentioned here that Whiffen and Thompson (1946) adopted this proeedure in their temperature measurements, but they have taken the following equation as the basis.

$$\tan\delta = \frac{(\varepsilon+2)^2}{\epsilon} \frac{4\pi\mu CN}{27KT} \cdot \frac{\omega\tau}{1+\omega^2\tau^2}$$

where ϵ is the dielectric constant of the solvent. This can be deduced from equation (4) if ϵ', the dielectric constant of the solution is assumed to be equal to that of the solvent and ϵ''^2 is neglected in comparison with $(\epsilon'+2)^2$. Further,

in their measurements, the dielectric constants of the solvent at different temperatures were estimated from that at 20°C by assuming that the molecular polarisability $\frac{\epsilon-1}{\epsilon+2} \cdot \frac{M}{\rho}$ is independent of temperature.

In the present work, no such approximations were made, and equation (4) was taken as the basis for the calculation. The values of ϵ' and ϵ'' of the solution at different temperatures were computed from the standing wave measurements by the method indicated by the author (1956).

The experimental set-up consists of Philips 55391 klysron oscillator with a frequency range 8500-9600 Mc/s fed by a stabilised power supply. In series with it are a matching unit a variable attenuator, a standing wave indicator and a silvered dielectric cell. The probe position in the standing wave indicator can be read to 0.002 cm. The dielectric cell and the standing wave indicator are vertically mounted to facilitate introduction of several temperature baths at the dielectric end without disturbing the main set-up. The design of the dielectric cell is such as to maintain constant thickness of the dielectric irrespective of the temperature for which it is exposed. A piece of waveguide, connected between the standing wave indicator and the dielectric cell, reduced to a great extent the transfer of heat to the crystal. In addition to this, forced air was blown at the extension guide which was found necessary to obtain reproducible results. The required temperatures were obtained by hot water, ice and precooled alcohol.

The densities of the solution at different temperatures were measured by a Westphal balance, which are accurate to one unit in the third decimal place.

RESULTS AND DISCUSSION

The experimentally obtained values of ϵ', ϵ'', and density together with the values, τ, log $T\tau$, and $1/T$ obtained on calculation for ethyl adipate, α-nitronaphthalene, ethyl benzoate and benzophenone dissolved in heptane and ethyl benzoate in decalin are given in Table I.

The values of the dipole moments are calculated from the maximum of $T\epsilon''/\{(\epsilon'+2)^2+\epsilon''^2\}d_{12}$, since at that point its value will simply be $2\pi N\mu^2 W/27KM$. The dipole moments calculated thus are compared with those taken from R.F. measurements (Tables of dipole moments, Wesson, 1948) in the following Table II

A reasonable agreement is found in all the cases and this can be taken as a satisfactory justification for using the Debye equations in calculating the values of τ.

The values of viscosity at various temperatures for the two solvents heptane and decalin are presented in Table III. The values of heptane are taken from

TABLE I

Temp °C	ε'	ε''	Density	τ	$10+\log T\tau$	$1/T$
1. *Ethyl adipate in heptane* (Weight fraction of the solute = 0.0454)						
−50	2.70	0.0711	0.794	27.5	1.788	4.48
−40	2.70	0.0724	0.784	21.8	1.706	4.29
−30	2.70	0.0704	0.775	17.4	1.626	4.12
−20	2.70	0.0656	0.766	14.4	1.561	3.95
−10	2.69	0.0593	0.757	12.0	1.500	3.80
0	2.69	0.0536	0.748	10.6	1.461	3.66
10	2.68	0.0498	0.739	8.5	1.381	3.53
20	2.66	0.0384	0.730	7.2	1.326	3.41
30	2.64	0.0330	0.721	6.4	1.286	3.30
40	2.63	0.0285	0.712	5.7	1.248	3.20
60	2.60	0.0201	0.694	4.2	1.148	3 00
70	2.56	0.0177	0.686	3.9	1.125	2.92
2. *α-nitronaphthalene in heptane* (Weight fraction of the solute = 0.0215)						
−20	2.78	0.1100	0.767	33.3	1.925	3 95
−10	2.75	0.1120	0.757	28.3	1.872	3.80
0	2.72	0 1127	0.748	23.6	1.810	3.66
10	2.69	0.1096	0.739	20 8	1.770	3.53
20	2.68	0.1056	0.730	17.4	1.707	3.41
30	2.67	0.0976	0.721	14.9	1.661	3.30
40	2.66	0.0927	0.711	13.7	1.632	3 20
50	2.58	0 0811	0.703	11.5	1.568	3.10
60	2.50	0 0722	0.694	10.5	1 542	3.00
70	2 46	0.0638	0.684	9 3	1.505	2.92
80	2.43	0.0560	0.675	8.2	1.462	2.83
3. *Ethyl benzoate in heptane* (Weight fraction of the solute = 0.0520)						
−40	2.69	0.0732	0.786	32.5	1.880	4.29
−30	2.69	0.0757	0.777	27.3	1.821	4.12
−10	2.68	0.0745	0.759	19.6	1 712	3.80
0	2.67	0.0712	0.750	17.4	1.677	3.66
10	2.67	0.0648	0.741	12 9	1.562	3.53
25	2.65	0.0563	0.728	10.9	1.510	3.36
40	2.62	0.0481	0.714	9.3	1.463	3.20
50	2.61	0.0423	0.705	8.1	1.420	3.10
60	2.59	0.0369	0.696	7.2	1.378	3.00
70	2.49	0.0315	0.688	6.5	1.347	2.92

TABLE I (*contd.*)

Temp °C	ε'	ε''	Density	τ	$10+\log T\tau$	$1/T$
4. *Benzophenone in heptane* (Weight fraction of the solute = 0.0407)						
0	2.65	0.0948	0.743	27.3	1.872	3.66
10	2.64	0.0952	0.734	23.5	1.823	3.53
20	2.63	0.0937	0.724	20.1	1.770	3.41
25	2.62	0.0912	0.719	19.0	1.753	3.36
30	2.61	0.0891	0 714	17.4	1.722	3.30
35	2.60	0.0864	0.710	16.7	1.711	3.25
40	2.56	0.0829	0.706	16.3	1.680	3.20
45	2.54	0.0800	0.702	14.9	1.675	3.15
50	2.52	0.0765	0.697	13.9	1.650	3.10
60	2.46	0.0692	0.688	12.4	1.615	3.00
70	2.45	0.0631	0.679	11.0	1.576	2.92
80	2.43	0.0568	0.671	9.8	1.538	2.83
Ethyl benzoate in decalin (Weight fraction of the solute = 0.0829)						
−20	2 23	0.0491	0.928	86.4	2.340	3.95
−10	2.21	0.0535	0.918	66.7	2.244	3.80
0	2.21	0.0663	0.908	54.3	2.171	3.66
10	2.20	0.0694	0.898	48.0	2.133	3.53
22 5	2.19	0 0790	0.885	36.5	2.033	3.39
29	2.17	0.0868	0 879	28 8	1.939	3.31
40	2.17	0.0915	0.868	21.1	1.819	3.20
49	2 15	0.0890	0 859	17 4	1.747	3.11
58	2.13	0.0818	0.850	13.1	1.637	3.02
70	2.12	0.0734	0.838	11.3	1.588	2.92
80	2.11	0.0661	0.828	10.0	1.546	2.83

TABLE II

Substance	Present investigation	R. F. measurements
Ethyl adipate	2.10	2.40
α-nitronaphthalene	3.92	3.88
Ethyl benzoate in heptane	1.84	1.82
in decalin	1.88	
Benzophenone	2.81	2.5 to 3.0

"Physico-Chemical constants" (Timmermans). The viscosity of decalin was determined using Ostwald type of viscometer, the accuracy of which may be within 2 per cent.

TABLE III

n-heptane		Decalin	
Temp. °C	Viscosity $\times 10^5$	Temp °C	Viscosity $\times 10^5$
6.6	480	0	3400
13.5	442	10	2590
21.7	403	14	2370
30.3	369	20	2170
38.3	340	27	1730
47.3	311	35	1430
55.0	289	45	1200
62 0	271	55	940
70.1	253	65	740
77.1	237		
85.5	222		

It is observed that the plots of log $T\tau$ versus $1/T$ yield a straight line, which means that H_τ is constant. The plots of log η and $1/T$ fall on a good straight line, indicating H_η to be constant. The values of H_τ and H_η, calculated from the slopes of the respective graphs log $T\tau$ versus $1/T$ and log η versus $1/T$ for the substances investigated at present, are given in Table IV.

TABLE IV

	ergs		
	$H_\eta \times 10^{13}$	$H_\tau \times 10^{13}$	
Ethyl adipate	1.35	1.36	Heptane
α-nitronaphthalene	1.32	1.36	Heptane
Ethyl benzoate	1.31	1.36	Heptane
Benzophenone	1.28	1 36	Heptane
Ethyl benzoate	2.45	2 81	Decalin

It can be seen that in all cases H_τ is approximately equal to H_η, and the difference is almost within the possible experimental error. It would thus appear that the heights of the potential energy barriers to be surmounted in the two processes of viscous flow and dipole rotation are almost equal.

The factors A and B

The values of the factors A and B, according to Eyring, as mentioned earlier, must be h/K and hN/V respectively. On this basis we might therefore expect A to be a constant for all the liquids, and B also for any liquid except for the small variation of the molar volume V, with temperature. This aspect of Eyring's theory was also studied in the present investigation.

The value of A is calculated at each temperature for the investigated molecules from equation (2) using the value of H_τ obtained from the slopes of the plots log $T\tau$ versus $1/T$. The results are given in Table V. It is observed that the values of A are fairly constant for each liquid, and they are in the same order of magnitude, but not in agreement, with the value h/K, which is 4.8×10^{-11}. It may be mentioned here that these observations are in accordance with those of Saxton (1952) in his studies on methyl and ethyl alcohols. His experimental results indicated that the values of A (average value 4.1×10^{-10} and 1.7×10^{-10} in methyl and ethyl alcohols respectively), though observed to be constant over the temperature range—10°C, to 50°C are significantly greater than h/K (4.8×10^{-11}.

The values of B (shown in Table VI) are also calculated from equation (3) using the values of H_η obtained from the slopes of the plots log η and $1/T$. In the case of the solvent decalin, the value of B (2.13×10^{-5}) is in reasonable agreement with the hN/V value calculated at 20°C which is 2.53×10^{-5}. But in the case of the solvent heptane, the experimentally determined value for B (1.45×10^{-4}) is greater than hN/V value calculated at 20°C which is 2.72×10^{-5}. Reference may again be made to the work of Saxton (1952), in the two alcohols, the values of which are presented below.

TABLE V

Values for factor A

Temp °C	Ethyl adipate	Ethyl benzoate	α-nitronaphthalene	Benzophenone	Ethyl benzoate in decalin
		in heptane A × 10″			
−50	7.60	—	—	—	—
−40	7.59	14.2	—	—	—
−30	7.50	13.5	—	—	—
−20	7.57	—	19.5	—	1.98
−10	7.64	14.1	19.9	—	2.08
0	7.99	14.9	19.7	25.4	2.24
10	7.55	12.9	20.3	25.4	2.59
20	7.48	13.5 (25°C)	19.7	25.2	2.67 (22.5°C)
30	7.62	14.5	19.7	25.0	2.45 (29°C)
40	7.75	14.1	20.4	25.1	2.29
50	—	14.0	19.4	25.6	2.27
60	7.43	13.9	19.9	25.7	2.04 (58°C)
70	7.67	14.1	19.9	25.5	2.20
80	—	—	19.5	25.2	2.32

TABLE VI

Values for factor B

Decalin		Heptane	
Temp. °C	$B \times 10^6$	Temp. °C	$B \times 10^4$
0	2.00	6.6	1.44
10	1.98	13.5	1.45
14	2.00	21.7	1.45
20	2.13	30.3	1.46
27	1.98	38.3	1.46
35	1.96	47.3	1.46
45	2.20	55.0	1.46
55	1.93	62.0	1.46
65	1.83	70.1	1.46
		77.1	1.45
		85.5	1.44

	Experimental observations	hN/V
Methyl alcohol	8.7×10^{-5}	10^{-4}
Ethyl alcohol	4.5×10^{-5}	6.9×10^{-5}

The values show a somewhat reasonable agreement in the two cases, and not as so in decalin.

Further, it may be seen for all the five solutions examined that the values of B are very much greater than A; thus, although H_τ is equal to H_η approximately molecular jumps over the potential energy barrier in viscous flow are accomplished more readily than those associated with dipole rotation.

Lastly, it may be mentioned that the suggestion put forth by Eyring for the possible separation of H_τ into internal energy change (ΔH) and entropy change (ΔS) has not been discussed in the present investigation, since this procedure will sometimes lead to false deductions concerning their magnitudes, especially when $h\,\omega_a/2\pi > KT$, as pointed out by Pelzer (1946) and when the entropy varies rapidly with temperature (Saxton 1946).

ACKNOWLEDGMENT

The author is highly indebted to Prof. K. R. Rao for his kind and valuable guidance during the progress of the work.

REFERENCES

Eyring, H., Glasstone, S., Laidler, K. J., 1941, The theory of rate process, pp. 477, New York, McGraw-Hill Book Co. Inc.

Fröhlich, H., 1949, Theory of Dielectrics, Clarendon Press, Oxford.
Gopala Krishna, K. V., 1956, *Trans. Farad. Soc.*, **52**, 1110.
Pelzer. H., 1946, *Trans. Farad. Soc.*, **42A**, 164.
Saxton, J. A., 1946 b, Meteorological factors in radio wave propagation, p. 306. London. The Physical Society.
Saxton, J. A., 1952, *Proc. Roy. Soc.*, **213A**, 473.
Smyth, C. P., Hennelly, E. J., Heston, W. M., 1948, *J. Amer. Chem. Soc.*, **70**, 4102.
Whiffen, D. H., Thompson, H. W., 1946, *Trans. Farad. Soc.*, **42A**, 114.

Letters to the Editor

The Board of Editors will not hold itself responsible for opinions expressed in the letters, published in this section. The notes containing reports of new work communicated for this section should not contain many figures and should not exceed 500 words in length. The contributions must reach the Assistant Editor not later than the 15th of the second month preceding that of the issue in which the Letter is to appear. No proof will be sent to the authors.

8. SOFT X-RAY EMISSION SPECTROSCOPY OF GRAPHITE AND THE SUGGESTION OF A SUITABLE BRILLOUIN ZONE FOR IT.

AJIT KUMAR DUTTA

DEPARTMENT OF MAGNETISM, INDIAN ASSOCIATION FOR THE CULTIVATION OF SCIENCE, CALCUTTA-32

Three different Brillouin zones for graphite have, from time to time, been proposed by different workers (Ganguli and Krishnan, 1941; Wallace, 1947; Dutta, 1957) the details of which are given in the table below.

No. of electrons that can be contained in the Brillouin zone	Boundary planes	Structure factor for the boundary planes	Value of K, the reciprocal lattice vector for the boundary planes in 10^8 cm^{-1}	Fermi energy calculated according to the simple Sommerfeld formula in electron volts
1	$\{\bar{1}10, 0$	1	1.47	8.4
	$000, 2\}$	4	0 92	
3	$\{\bar{2}\bar{1}1, 0$	4	2.55	17 6
	$000, 2\}$	4	0.92	
4	$\{220, 0$	1	2.95	22
	$000, 2\}$	4	0.92	

It is well known that soft X-ray emission spectrum can furnish direct evidences regarding the band structure of solids and an attempt is made here to utilise the available data to decide the proper Brillouin zone in graphite. The variation on $N(E)$, the density of state with E, the energy within a Brillouin zone has been obtained in the case of graphite from its soft X-ray spectroscopy by Skinner (1940) and is repersented in the adjoining graph. The nature of variation of $N(E)$ with E is obviously that of a semimetal (Wilson, 1954)—the first peak

from the left hand side indicating the touching of a set of Brillouin zone boundaries which, in view of the kink following, has evidently been overlapped ; the second peak indicating the maximum energy up to which the levels are filled under the normal state of the lattice as well as the contiguity of another set of bounding planes of Brillouin zone. The $N(E)$ value then falls rather sharply, the absorption edge lying near about the lowest point of this curve. The total band width is therefore about 24 ± 3 ev. From the above, the essential requirements of the proper Brillouin zone of graphite are : (i) it should be bounded by two independent sets of planes, one such set being overlapped; (ii) band width between

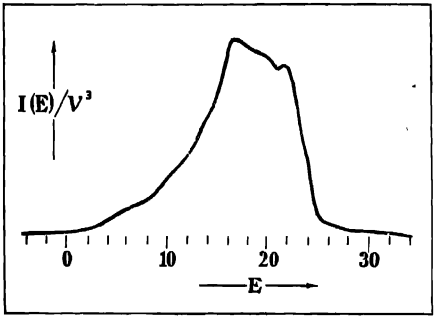

Fig. 1.—Intensity distribution of the soft X-ray emission spectra of graphite.
$I(E)$ = intensity in numbers of quanta per second of radiation in the emitted band in the unit range of quantum energy.
ν = absolute energy of transition
E = energy in electron volts ($\pm$ 3).

one set of planes should be much greater than that between the other set; (iii) the total band width should be about 24 ± 3 ev. On a reference to the table above it is evident that the one electron zone satisfies the requirements (i) and (ii), the three electron zone satisfies only (ii) and the four electron zone satisfies all the three conditions. Therefore, the four electron zone may now be considered to be the most suitable one for graphite. This acceptance of the four electron zone for graphite is further supported by the following essential considerations :

(1) It can be shown from a consideration of the nature of variation of $N(E)$ with E, the peculiar crystal structure of graphite and the electronic specific heat of graphite that 16 ev representing the position of the first peak from the left hand side correspond to a K-value equal to that for the $(2\bar{2}0, 0)$ planes. The band width between the kink and the absorption edge can also be shown to correspond to a K-value equal to that for the (000, 2) planes.

(2) The existence of π- and σ- electron interaction in the C-C bond formation in graphite which is also a necessary requirement of the acceptance of the 4-electron Brillouin zone has been proved amongst others by Coulson (1951 and 1952), Altman (1952) and others (March, 1952), Pariser (1953), Niira (1952), Davies, Hirschfelder and others (1955).

The details of these discussions have been dealt with in a separate paper and is in course of publication elsewhere.

ACKNOWLEDGMENT

The author wishes to express his best thanks to Prof. A. Bose for his kind interest in the work.

REFERENCES

Altman, S. L., 1952, *Proc. Roy. Soc.*, *A* **210**, 327, 343.
Coulson, C. A., Higgs, P. W. and March, N. H., 1951, *Nature* (London) **168**, 1039.
——— and Taylor, R., 1952, *Proc. Phys. Soc.*, *A* **65**, 815.
Davies, P. L. Dissertation for the doctorate degree, King's College, University, London (Quoted in Hirschfelder's paper).
Dutta, A. K., 1957, 'Magnetism', Indian Association for the Cultivation of Science, Calcutta–32, 147.
Ganguli, N. and Krishnan, K. S., 1941, *Proc. Roy. Soc.*, *A* **177**, 168.
Hirschfelder, J. O. and others, 1955, *J. Chem. Phys.*, **23**, 1778.
March, N. F., 1952, *Act Cryst.*, **5**, 157.
Niira, K., 1952, *J. Chem. Phys.*, **20**, 1498.
Pariser, R., 1953, *J. Chem. Phys.*, **21**, 568.
——— and Parr, R G., 1953, *J. Chem. Phys.*, **21**, 767.
Skinner, H. W. B., 1940, *Phil. Trans. Roy. Soc.*, *A* **279**, 95.
Wallace, P., 1947, *Phys. Rev.*, **71**, 622.
Wilson, A. H., 1954, Theory of Metals (Cambridge).

BOOK REVIEW

GEOMETRICAL AND PHYSICAL OPTICS—R. S. Longhurst. Pp. i-xvi+534. Longmans, Green and Co., London. 1957. Price 60 shillings net.

This is a text book intended primarily for students reading for the honours degree in physics, but some of the topics have been dealt with so elaborately as to make them useful to postgraduate students. Examples of such topics are : Multiple beam interferometry, Huygens' principle and the scalar theory of diffraction, Fraunhofer diffraction patterns, Monochromatic aberrations, the Electromagnetic theory of light, Reflection and refraction of waves, Propagation of light in crystals and the Velocity of light, discussed in Chapters IX, X, XI, XV, XIX, XXI, XXII and XXIV respectively. In fact, it was formerly difficult for the students to prepare for the complete course with the help of a single text book chosen from those published previously without consulting other books on interferometry and electromagnetic theory of light, but in the book under review this deficiency has been removed to a large extent.

The special feature of this book is the abundant use of neat and beautiful diagrams. Further, the author seems to have spent a little thought over making each of these diagrams instructive and self-explanatory. The large number of interference and diffraction patterns reproduced in Plates I-III (p. 16) seem to have been taken from new photographs. The images in optical instruments reproduced in Plate IV are highly instructive and have bearing on advanced theories of formation of images in different instruments under different conditions.

The author has scrupulously avoided any discussion on atomic spectra probably on the ground that such topics would be out of place in a text book on geometrical and physical optics So, students desirous of procuring some elementary knowledge in spectroscopy will have to consult some other suitable books, but as a text book on geometrical and physical optics this book will be immensely useful to students preparing for the B.Sc. (Hons.) and M.Sc. degrees of any Indian University. The get-up is excellent and the price is consistent with the volume and the quality of the printed matter.

S. C. S.

THE EMISSION SPECTRUM OF CHLORINE (Cl_2^+)

P. B. V. HARANATH AND P. TIRUVENGANNA RAO

PHYSICS DEPARTMENT, ANDHRA UNIVERSITY, WALTAIR

(*Received for publication, July* 18, 1958)

Plate X

ABSTRACT. The emission spectrum of chlorine as excited in a high frequency discharge from a 100 watt oscillator, is photographed in the visible region on Fuess and Hilger glass Littrow spectrographs. Photographs of the spectra reveal many more new bands, especially on the longer wavelength side. New vibrational analysis for these bands has been proposed. Most of the bands have been arranged into three systems designated as Systems I, II, III, having the vibrational frequencies of the upper and lower states approximately in the ratio of 1 : 2. The following vibrational constants are derived.

	ν_e	ω_e'	$x_e'\omega_e'$	ω_e''	$x_e''\omega_e$
System—I	20448.0	350.0	2.0	656 0	4.6
System—II	20736.0	375.0	2.6	656.0	4.7
System—III	20569.0	347.5	2.0	655.0	5.5

The occurrence of a fourth system consisting of the remaining unclassified bands is also suggested. From the equality of the vibrational constants of the lower states of Systems—I and II, it is concluded that they have a common lower level. The vibrational analysis of these emission bands is well supported by the observed chlorine isotope effect.

INTRODUCTION

In addition to its atomic line spectrum, chlorine has long since been known to emit a larger number of red degraded bands extending from λ6400 to λ3400. Ota and Uchida (1928) were the first to arrange them tentatively into three systems on the basis of their measurements of these emission bands. Later, Elliot and Cameron (to be referred to as EC) (1937) considered that some of the progressions in the vibrational schemes of Ota and Uchida are not genuine for want of sufficient accuracy in their measurement of band heads. These latter authors reinvestigated the spectrum under improved experimental conditions of excitation and were able to get more accurate measurements of band heads. They proposed the analysis of the bands as belonging to two sub-systems I and II having a common lower state, probably the ground state of the molecule. They suggested that the transition involved is, in all probability, a $^2\Pi$—$^2\Pi$, from a rotational analysis of some of the bands belonging to both the systems. They

further claim that although their vibrational schemes are rather meagre, their vibrational assignments are well supported by the observed chlorine isotope effect and also from the rotational analysis of some of the bands. Because of the large number of unclassified bands in the spectrum, they, however, did not rule out the possibility of a quartet system arising from the transition $^4\Delta - ^4\Delta$.

However, there are certain inconsistencies in EC's analysis of these emission bands, some of which have been pointed out by Howell (1953).

(a) The intensity distribution of the bands in each of the systems is inconsistent with the values of ω'_e and ω''_e as derived from the analysis. Further, large number of gaps in the vibrational arrays suggest a fundamental weakness in their schemes. Also a large number of bands remain unclassified.

(b) The value of the energy of dissociation of the ground state common to both the systems, derived from the Birge Sponer extrapolation method, is obtained as 4.4 ev. as against 2 23 ev. indirectly obtained from the values of the ionisation potentials I of Cl and Cl_2 and the dissociation energy D of Cl_2. Because the ionisation potentials of Cl and Cl_2 and the dissociation energy of Cl_2 are now well established and known to be extremely reliable, Howell considers that the above discrepancy should rather be attributed to the incorrectness of the analysis of the bands proposed by EC.

(c) The derived values of B_e and ω_e' from EC's analysis are not consistent with each other. For different band systems of a molecule, the ratio B_e/ω_e should be approximately constant. For the neutral halogen molecules the ratio B_e^2/ω_e is found to be constant. From the derived values of B_e and ω_e of the upper and lower states, it can be seen that the constancy of the ratio B_e^2/ω_e fails badly.

On the basis of electron configurations and predicted term types for Cl_2^+, (Mulliken, 1934), the ground state electron configuration of Cl^+_2 is now accepted as

$$(\sigma+\sigma, \sigma_g)^2 (\pi+\pi, \pi_u)^4 (\pi-\pi, \pi_g)^3 \ldots\ldots {}^2\Pi_{3/2g}, {}^2\Pi_{1/2g} \qquad \ldots \quad (1)$$

The first two excited electron configurations are respectively

$$\sigma_g^2\, \pi_u^3\, \pi_g^4 \ldots\ldots\ldots {}^2\Pi_{3/2u}, {}^2\Pi_{1/2u} \qquad \ldots \quad (2)$$

and

$$\sigma_g \pi_u^4\, \pi_g^4 \ldots\ldots {}^2\Sigma_g^+ \qquad \ldots \quad (3)$$

As can be seen from the configurations (2) and (3) an electron goes from a bonding orbital to an antibonding orbital. This means that the vibrational frequency of these excited states should be considerably reduced relative to that of the ground state. The derived ω_e' and ω_e'' values from EC's analysis are in disagreement with the above theoretical prediction. Further, according to the

vibrational analysis proposed by the authors (1955) for similar bands in the case of bromine, the vibrational frequency of the upper state of both the systems are considerably lowered relative to the vibrational frequency of the ground state viz., ($\omega_e'' = 376$ common to both the systems, $\omega_e' = 190$ and 152 for systems I and II).

In view of the above discrepancies in the EC's analysis of the emission bands of Cl_2^+, and also the results of our investigation on similar emission bands in the case of bromine molecule, it is thought desirable to reinvestigate the visible emission band spectrum of chlorine. The experimental results and the details of the vibrational analysis are described in the following pages. A preliminary report of the details of the analysis has already appeared in *Current Science* (1956).

EXPERIMENTAL

In the present work the spectrum of Cl_2^+ is excited, as in the case of bromine, in an electrodeless discharge from a high frequency high power oscillator of 16 Mcs. frequency and about 150 watt output power. The discharge tube made of pyrex glass of length 30 cm. and diameter 18 cm. has two side tubes along its length which contain small quantities of cupric chloride. One end of the tube is cemented with a glass or quartz window by means of shellac, while the other end is drawn into an adopter for connecting to a system of high vacuum pumps through a liquid air trap. Chlorine is generated by electrical heating of cupric chloride contained in the side tubes of the discharge tube. An Edwards Speedivac oil diffusion pump of single stage backed by a Cenco Hyvac pump provides a system to maintain chlorine at low pressures in the discharge tube. The pressure is also regulated by adjusting the current in the circuit of the heating coil. The current is so adjusted that a bluish emission free from any traces of usual impurities is observed in the discharge column.

Hilger three prism glass Littrow and Fuess spectrographs are used to photograph the spectra on Ilford Special Rapid Panchromatic plates. About four to five hours on the Littrow instrument, and one and a half to two hours on the latter instrument are found necessary to give rise to intense spectra. The spectra recorded on the Littrow spectrograph reveal, owing to the high dispersion, an open rotational structure of the bands. For the vibrational analysis of the bands, measurements of band heads are taken on plates recorded on Fuess instrument having a smaller dispersion. Measurements of band heads are taken on a good number of plates and it is found that they agree within one cm^{-1}.

RESULTS

Table I records the band head data and their quantum assignment in the different systems. The isotopes of the neighbouring bands are marked by the letter (i) in the assignment columns.

TABLE I

Authors Wave-length	Wave-number	E C Wave-number	Int.	Assignment System I v', v''	System II v', v''	System III v', v''
6434.3	15537		1			
6410.1	15596		1			
6402 8	15614		1			
6366.3	15703		1			
6344.0	15759		1			
6335.2	15780		1			
6323.6	15809		2	3, 9		
6281.2	15916		2			
6267.0	15952		2			
6254.9	15983		2			
6244.7	16009		2			
6230.6	16045		2			
6219.4	16074		2			
6210.2	16098		3			
6201.9	16120		3			
6192.8	16143		3	4, 9		
6171.8	16198		2	i		
6149.2	16258		3			
6094.4	16404		3			
6070.0	16470		3	5, 9		
6051.8	16519		1	i		
6036.0	16563		2			
6026.6	16588		4			
6019.9	16607		4			3, 8
6013.6	16624		4	2, 7		
6003.6	16654		4			
5995.6	16674		4	i		
5981.1	16715		4	4, 8		
5964.4	16761		4	i		
5945.0	16816		4			
5934.4	16863		4			
5905.2	16929		3			
5894.5	16960		3	3, 7		
5865 0	17046		5	5, 8		
5850.8	17087		3	i		
5821.9	17172		4			3, 7
5805.5	17220		3	2, 6		i
5792.8	17258		3	i		
5779.8	17297		4	4, 7		
5767.1	17335		3	i		
5750.2	17386		2			
5738.0	17423		2			
5720.8	17475		4	—		
5706.0	17521		4			
5693.7	17558		5	3, 6		
5682.2	17594		4	i		
5676.7	17611		2			
5670.5	17630		4	5, 7		
5654.2	17681		4			
5645.3	17709		3			

TABLE I (contd.)

Authors Wave-length	Wave-number	E C Wave-number	Int	Assignment System I v', v''	System II v', v''	System III v', v''
5632 5	17749		2			3, 6
5616.6	17799		2			
5607.2	17829		2			
5603.8	17840		3		6, 8	
5587.0	17894		3	4, 6		
5582.6	17908		4			
5577 4	17924		1	i		
5545.4	18028		2			
5538.4	18051		3			
5519.1	18114		4			
5503 9	18164		4			6, 7
5494.2	18196		2			1
5479 4	18245		4			
5469.6	18278		3	7, 7		
5460 9	18307		2	1		
5442.7	18368		2			
5432 9	18401	18401 4	4			5, 6
5423.7	18432	18431 9	4			1
5396 9	18524	18522 0	6			
		18541.8				
5389 6	18549	18546 9	5	6, 6		
5382.6	18573		3	1		
5375.5	18598	18598.2	3	8, 7		
5368.0	18624		2			
5349.2	18689		2			
5337.4	18730		2			
5330 8	18754		3			
5324 6	18775	18777 3	3			
5318.5	18797		3			
5314.3	18812		2			
5310.1	18827		4	5, 5	9, 8	
5305 0	18845		3	i		
5302 3	18854	18858.6	3		1	
5297.4	18872	18873.4	5	7, 6		
5291 4	18893		2	i		
5264.5	18990		6			5, 5
5259.0	19010		4		6, 6	i
5255 3	19023	19024.3	2			
5244.6	19062	19061.2	2			
5238.4	19084		2		8, 7	
5230.6	19113		4			
5223.7	19138	19137.9	4			
5219 4	19154	19152.8	4	6, 5	10, 8	
5212.0	19181	19182.6	3			
5209.1	19192	19192.6	3	8, 6		
5202 4	19217		3			
5189 3	19265		3			4, 4
5184.2	19284		3			1
5175.6	19316	19311.8	4			6, 5
5171.0	19333		4			1

TABLE I (contd.)

Authors Wave-length	Wave-number	E C Wave-number	Int.	Assignment System I v', v''	System II v', v''	System III v', v''
5167.9	19345	19349.4	3		7, 6	
5163.3	19362	19358 1	3		i	
5158 5	19380	19380.0	3			
5153.7	19398	19396.5	3			
5150.0	19412		4		9, 7	
5145.7	19428		2		i	
5136.4	19463	19463 1	3			
5132.5	19478	19479.7	4	7, 5		
5126.0	19503	19500 4	3			
5121.1	19522	19518 3	3			
5102 4	19593		2			5. 4
5099 3	19606		1			1
5094.9	19622	19624.0	2			
5080 8	19676	19676 1	7		8, 6	
5077 1	19691	19691 8	4		1	
5071 3	19713		3			
5065 4	19736		4		10, 7	
5059.8	19758	19758.8	5			
5049 6	19798	19800 3	2	8, 5		
		19816 0				
5023 4	19901	19903 2	4			
5020.1	19914	19913 3	6			
5010 5	19952		2			6, 4
5005.4	19973	19972.0	2			
5002 8	19983	19983.6	4			
4997.8	20003		1		9,6	
4977 9	20083	20083.0	4			
4969.5	20117	20118.4	2	9, 5		
4940 7	20234	20228.2	4			7, 4
4924.6	20301	20300.1	5			
4918.1	20327	20323 8	2		10, 6	
4903.9	20386	20383 5	3			
4897 2	20414	20416.0	4	8,4		
4882.6	20475		2			
4870 5	20526	20524 1	6			6, 3
4852 5	20602	20595 6	5		9, 5	
4837.3	20667	20668 2	5			
4826.3	20714	20711.3	5	7, 3		
4822.5	20730		2	9, 4		
4818.3	20748		2			
4799.4	20830	20828 6	5			
4795.0	20849	20852.3	8			7,3
4786.7	20885	20885.5	4			
4777 2	20927	20927.2	5		10, 5	
4704.2	20984		4			
4751.0	21041	21041.7	8	10, 4		
4732.4	21125	21121.6	7			
4726.2	21153		7			6, 2

TABLE I (contd.)

Authors Wave-length	Authors Wave-number	E C Wave-number	Int.	Assignment System I v', v''	Assignment System II v', v''	Assignment System III v', v''
4723.9	21163	21161 1	4			
4715.2	21202	21201.5	7			
4711.0	21221	21222.0	5			
4705.4	21246		3		11, 5	
4684.7	21340	21339 7	6	1		
4682.5	21349	21349.8	8	11, 4		
4677.1	21375		3			
4655.1	21476	21476.3	8			7, 2
4646.6	21515	21513 5	2			
4637.2	21559	21559.1	3		12, 5	
4616.3	21656	21659.0	6	1		
4613.6	21669	21668.7	6	10, 3		
4592.1	21770		2			1
4589 1	21785	21,783.0	4			8, 2
4579.4	21831	21831.5	5			
4571 3	21869	21872 2	1			
4552.6	21959	21959 0	7	1		
4549 1	21976	21976 4	8	11,3		
4521 1	22112	22111.5	4			
4509.7	22168	22168 5	6			
4506 2	22185	22186 2	6			
4491.3	22259	22260.3	4	1		
4487.0	22280	22277 3	5	12, 3 i		
4482.8	22301	22301.0	2	10,2		
4465 1	22390		3			10, 2
4462 8	22401	22402 7	2			
4459.2	22419		2			
4447.9	22476		3			
4442 4	22504	22504 5	5			
4437.6	22528	22529 3	3			
4433.7	22548		3			
4426 7	22584	22585 7	4	1		
4421 5	22610	22609 3	5	11, 2		
4410 4	22667	22671.5	4			i
4405 4	22694	22696.3	5			11, 2
4399.5	22724		2			
4385.6	22795	22793 0	3			
4381 2	22818	22819 7	3			
4371 3	22870		3			
4368 2	22886	22886.0	2	1		
4363.0	22914	22912.7	3	12, 2		
4358.9	22935		2			
4353.9	22961	22961.2	5			i
4348.5	22990	22990.0	3			12, 2
4341.3	23028		1			
4334 3	23065		2		1	
4330.6	23085		3		13, 3	
4322.2	23130	23130.3	3	1		
4316 2	23162	23163.4	5	15, 3		
4309.0	23200	23200 9	3			
		23264.9				

TABLE 1 (contd.)

Authors Wave-length	Wave-number	E C Wave-number	Int.	Assignmentœ System I v', v''	System II v', v''	System III v', v''
4291.5	23295	23295.5	3			i
4285.6	23327	23327.4	4			11, 1
4278.2	23368		3			
4273 0	23396		3			
4264.1	23445	23444.7	2			
4259.5	23470	23474.0	2	i		
4252.9	23507	23509 9	4	14, 2		
4238.6	23586	23586 6	3			i
4231.7	23624	23624.2	4			12, 1
4207.4	23761	23762.0	2			
4201.6	23794	23797.2	6	1		
4194.4	23835	23833.3	6	13, 1		
4185 4	23886	23887 8	4			i
4178 7	23925	23925.2	5			13, 1
4177 6	23930		3		i	
4171 7	23964	23964.4	4		16, 3	
4148 2	24100	24102 3	5	i		
4140.5	24145	24147.3	6	14, 1		
4127 6	24220	24215.2	4			1
4119.8	24266	24265 9	6		1	12, 0
4112.7	24308	24308 7	5		15, 2	
4107.5	24339		2			
4091.3	24435	24425 4	3	i		
4083 3	24485	24484 8	4	13, 0		
4078.3	24513		2			i
4071 6	24553	24551.7	4		1	
4070.1	24562		3			13, 0
4064 4	24597	24596.9	5		16, 2	
4041.7	24735	24735.1	4	1		
4033.0	24788	24788.3	5	14, 0		
4024.2	24843		2			
4015.1	24899	24896 0	3		i	
4007.2	24948	24948 1	3		15, 1	
3979 7	25120	25122.6	3			
3969.8	25183	25180.3	4		1	
3961.5	25236	25236.2	5		16, 1	
3940.5	25370	25365.4	4		i	
3932.0	25425	25426.3	5		19, 2	
3926 3	25462		4		1	
3917.7	25518	25526.5	5		17, 1	
3890.0	25700	25699.8	4			
3881.3	25757	25757.3	5			
3871.7	25821	25819.9	4		i	
3862.6	25882	25882.4	5		16, 0	
3829.7	26104		4		i	
3820.7	26166		5		17, 0	

TABLE II

Vibrational scheme for System I

v' \ v''	0	1	2	3	4	5	6	7	8	9
2							17220* 596 338	16624* 336		
3							17558* 598 336	16960* 337		15809* 334
4							17894* 597	17297* 582 333	16715* 572 331	16143* 327
5						18827* 327		17630* 584	17046* 576	16470*
6						19154 605 324	18549 323			
7				20714	X	19478 606 320	18872 593 320	18279* 319		
8					20414 616 316	19798 606 319	19192 594	18598		
9					20730* 613 311	20117				
10			22301 632 309	21669 628 307	21041 308					
11			22610 634 304	21976 627 304	21349					
12			22914 634	22280						
13	24485 650 303	23835 310								
14	24788 643	24145 638	23507							

Note. Bands marked with "*" are newly obtained in the present work.
The place marked (X) is superposed by atomic line.

TABLE III

Vibrational scheme for System II

v'' / v'	0	1	2	3	4	5	6	7	8
6							19010* 335		17840*
7							19345 331		
8							19676 592 327	19084* 328	
9						20602 599 325	20003* 591 324	19412* 585 324	18827* 327
10						20927 600 319	20327 591	19736* 582	19154
11						21246* 313			
12					22168 609	21559			
13				23085*					
14					X				
15		24948 640 288	24308 289						
16	25882 646 284	25236 639 282	24597 633	23964					
17	26166* 648	25518							
18									
19			25425						

Note. The place marked (X) is superposed by atomic line.
Bands marked with "*" are newly obtained in the present work.

TABLE IV

Vibrational scheme for System III

v' \ v''	0	1	2	3	4	5	6	7	8
3							17749* 577	17172* 565	16607*
4					19265* 328		X		
5					19593* 603 321	18990* 589 326	18401		
6			21153* 627 323	20526 612 323	19914 598 320	19316	X	18164*	
7			21476 627 309	20849 615	20234				
8			21785						
9			X						
10		X	22390* 304						
11		23327 633 297	22694 296						
12	24266 642 296	23624 634 301	22990						
13	24562* 637	23925							

Note. Bands marked with "*" are newly obtained in the present work.
The places marked (X) are superposed by atomic lines.

Photographs of the spectra of Cl^+_2 recorded on Fuess instrument are reproduced in Plate X. The spectrum extends from λ 6500 to λ 3400. All the bands are clearly red degraded. However, owing to the fall in intensity of the bands below λ 3800, they are not shown in the plate. The plate reveals a large number of additional bands, especially in the longer wavelength region of the spectrum which are not reported by EC. The bands which are bracketted in the plate are the isotope components belonging to the various systems.

VIBRATIONAL ANALYSIS

In the present investigations on the emission spectrum of chlorine, many more new bands especially in the region above λ 5200, and some additional bands in the central region of the spectrum have been obtained. This can be seen in Table I in which the measurements by authors are given in column one, while in column two those reported by EC are given for comparison. In view of this additional data obtained by the authors, it is considered worthwhile to attempt to analyse the bands in the light of the above predictions that were discussed for Cl^+_2. After a number of attempts, the following analysis seems to be a plausible one for the visible emission bands of Cl^+_2.

A prominent feature of the band spectrum is the presence of double headed bands especially on the short wave length side and in the central region. EC have indentified most of these double headed bands as due to the isotopic molecules $(Cl^{35}\ Cl^{35})^+$, $(Cl^{35}\ Cl^{37})^+$, from intensity considerations and also from a detailed study of the rotational analysis of some of the bands. The identification of these double heads as due to isotopes by EC is considered reliable.

With the ratio of the vibrational frequencies ω'_e and ω''_e being roughly 1/2, most of the bands could be arranged into three different systems designated here as Systems I, II, and III respectively. The location of the system origins and the assignments of the vibrational quantum numbers are made on the basis of the observed isotope separations in each case.

System I

System I consists of prominent double headed bands reported by EC. A few additional bands marked with * in its vibrational scheme, displayed in Table II are also found to belong to the same system. About 70 bands including isotopes are assigned to this system.

System II

The vibrational analysis of this system is presented in Table III. About half of the bands assigned in this scheme are those that are newly recorded in the present emission plates. About 50 bands including isotopic heads are assigned to this system.

Indian Journal of Physics, Vol. XXXII, No. 9.

PLATE X

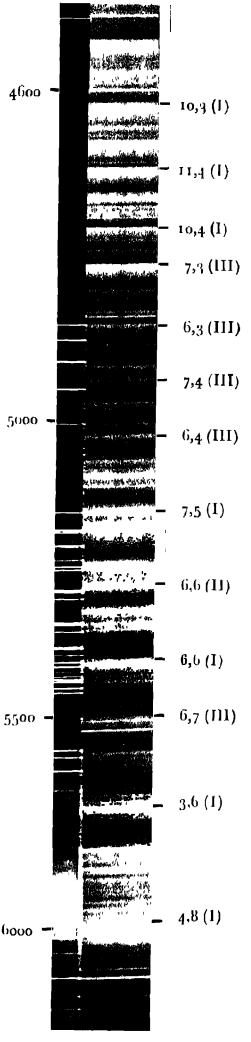

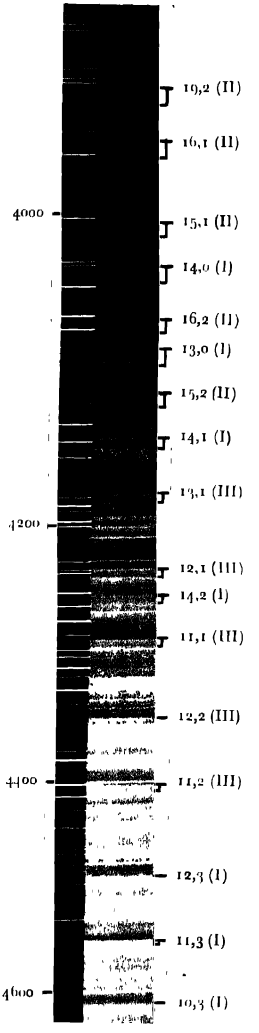

Emission spectrum of chlorine (Cl_2^+)

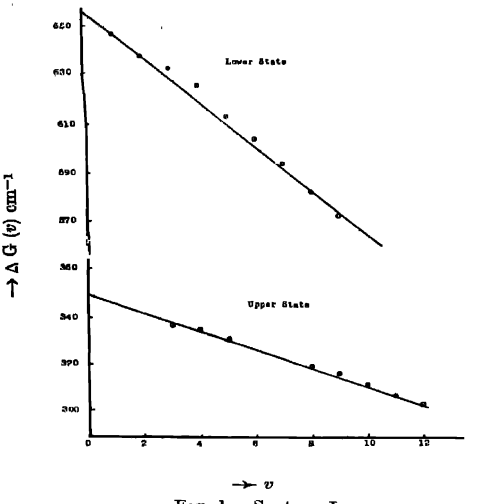

Fig. 1. System I

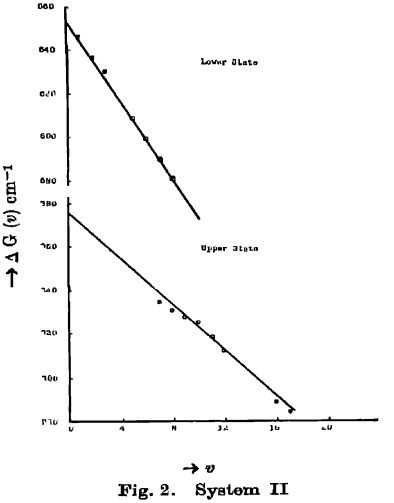

Fig. 2. System II

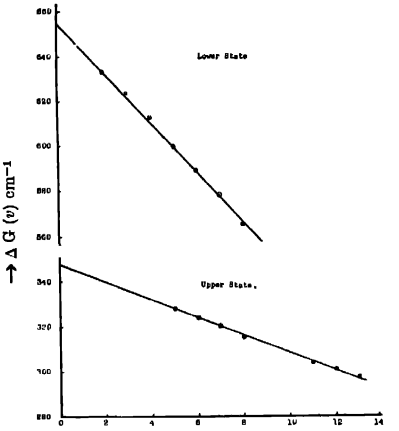

Fig. 3. System III

System III

The analysis of this system as shown in Table IV contains half of the bands that are newly recorded. About 50 bands including the isotopic components are found to belong to this system.

If linear curves are drawn by plotting the usual $\Delta G(v)-v$ values, the following vibrational constants for the above three systems, have been derived. The $\Delta G(v)-v$ curves are shown in figures 1, 2 and 3 for the three systems respectively.

Vibrational constants

	ν_e	ω_e'	$x_e\,\omega_e$	ω_e	$x_e\,\omega_e$
System I	20448.0	350.0	2.0	656.0	4 6
System II	20736.0	375.0	2.6	656.0	4.7
System III	20569.0	347.5	2.0	655.0	5.5

In addition to the bands assigned to the above three systems, there are some bands lying above λ 4400 and extending upto λ 6500 which could not be fitted into any one of these vibrational schemes. A recurring wave number interval of about 640 cm^{-1} among these bands suggests the possibility of yet another system in this region. No analysis could be presented for this system as its development is inadequate.

TABLE V

Isotope effect of chlorine

$(Cl^{35}Cl^{35})^+$ v'	v''	$(Cl^{35}Cl^{37})^+$ Calculated Separation	Observed Separation
		SYSTEM I	
14,	0	53.2	53
13,	0	49.9	50
14,	1	44.6	45
13,	1	41.8	41
14,	2	36.2	37
12,	2	29 5	28
11,	2	26 1	26
10,	2	22.6	21
12,	3	21.3	21
11,	3	17.9	17
10,	3	14.4	13
11,	4	9 9	9
5,	5	20.4	18
7,	6	20.0	21
6,	6	23.9	24
4,	6	32.0	30
3,	6	36.2	36
2,	6	40.5	38
7,	7	27 2	29
4,	7	39.2	38
2,	7	47.7	50
5,	8	42.0	41
4,	8	46.1	46
5,	9	48.7	49
4,	9	52.8	55
		SYSTEM II	
17,	0	63.3	62
16,	0	60.6	61

$(Cl^{35}Cl^{35})^+$		$(Cl^{35}Cl^{37})^+$ Calculated Separation	Observed Separation
17,	1	54.7	56
16,	1	52.0	53
15,	1	49 1	49
19,	2	53.4	55
16,	2	43.6	44
15,	2	40.7	42
16,	3	35 4	34
8,	6	14 5	15
7,	6	18.4	17
9,	7	17 8	16
9,	8	24.7	27
		SYSTEM III	
13,	0	49.5	49
12,	0	46 2	46
13,	1	40.9	39
12,	1	37.6	38
11,	1	34.2	32
12,	2	29.3	29
11,	2	25.9	27
10,	2	22 4	*
8,	2	15 0	15
7,	2	11.2	*
5,	4	12.6	13
5,	5	20.1	20
6,	5	16.1	17
5,	6	27.3	27
6,	7	30.1	32
3,	7	44.0	*48
3,	8	49.2	47

Note: The places marked (*) are superposed by atomic lines.

REMARKS

The following points which arise from the vibrational analysis of the emission spectrum of Cl_2^+ are in accordance with the theoretical predictions for Cl_2^+.

The intensity distribution in each of the above analysed systems is of an open Franck-Condon parabola type, that could be normally expected when the two frequencies ω_e' and ω_e'' are approximately in the ratio of 1 : 2.

From the equality of the vibrational constants of the lower states of systems I and II, it may be concluded that the two systems, as in the case of bromine, may have a common lower state, which is most probably the normal state of the molecule Cl_2^+. Using Birge Sponer extrapolation method, the dissociation energy of the ground state is obtained as 2.8 e.v. This value, although an approximate one, comes nearer the indirectly determined value 2.23 ev. for the ground state of Cl_2^+.

As shown in Table V the observed isotope separations agree closely with those calculated from the formula for a large number of bands in all the three systems.

$$\nu^1-\nu = (\rho-1)[\omega_e'(v'+1/2)-\omega_e''(v''+1/2)]$$
$$-(\rho^2-1)[x_e'\omega_e'(v'+1/2)^2-x_e''\omega_e''(v''+1/2)^2]$$

ν^1 is the wavenumber of the band head due to the less abundant molecule $(Cl^{35}\,Cl^{37})^+$, the more abundant molecule being $(Cl^{35}\,Cl^{35})^+$. For bands for which $\nu > \nu_e$ the interval $\nu^1-\nu$ is negative and for those for which $\nu < \nu_e$ the interval is positive. For the sake of convenience, the positive and negative signs are omitted in Table V. Because of the presence of four overlapping systems in the same region, a few of the isotope components of the bands belonging to one system coincide in position with those of the main bands belonging to one of the other systems.

If the emission bands of bromine reported earlier by the author are regarded as due to Br_2^+, a value of $\omega_e''(Br_2^+)/\omega_e''(Br_2)$ is obtained as 1.16. This is found to be equal to the ratio $\omega_e''(Cl_2^+)/\omega_e''(Cl_2)$ for each of the systems.

For the halogens the ratio B^2/ω_e is found to be approximately a constant for a pair of electronic states belonging to a system. Using the values of rotational constants B' and B'' obtained by EC it is found that the values of B^2/ω_e to be approximately constant for each of the above systems.

The rotational constants B_v' and B_v'' derived by EC from the combination relations are utilised by the authors to check the quantum assignments of band heads in the three systems. It is found that in each of these present systems, bands belonging to the same vibrational level (upper or lower) have the same values of B_v' or B_v'' respectively. This feature is shown in Table VI.

TABLE VI

Rotational constants

Band head	Assignment	B_v'	B_v''	Previous assignment
		SYSTEM—I		
21669*	10, 3	0.1753	0 2658	4, 2 (I)
21042*	10, 4	0.1770	0.2655	4, 3 (I)
21976	11, 3	0.1735	0.2650	5, 2 (II)
21350	11, 4	0.1733	0.2635	5, 3 (II)
		SYSTEM—II		
24948	15, 1	0.1645	0.2688	8, 0 (I)
25236*	16, 1	0.1668	0.2688	9, 0(II)
24308	16, 2	0.1640	0.2669	8,1 (I)
24597	16, 2	0.1660	0.2668	9, 1 (I)
25882*	16, 0	0.1615	0.2693	10, 0 (I)
26166*	17, 0	0.1598	0.2663	11, 0 (II)
		SYSTEM—III		
23327	11, 1	0.1693	0.2668	6, 1 (I)
23624	12, 1	0.1695	0.2665	7, 1 (II)
23924	13, 1	0.1658	0.2669	Unclassified
21476*	7, 2	0.1758	0 2640	Unclassified
22693	11, 2	0.1695	0.2655	6, 2 (I)
22990	12, 2	0.1698	0.2650	7, 2 (II)

The rotational constants for the bands marked with (*) are not accurate as was reported by EC.

ACKNOWLEDGMENT

The authors are grateful to Prof. K. R. Rao for his kind interest in the work.

REFERENCES

Elliot, A. and Cameron, W. H. B.,1937, *Proc. Roy. Soc. A.*, **158**, 681.
" 1938, " **164**, 531.
Haranath, P. B. V. and Tiruvenganna Rao, P., 1955, *Ind. Jour. Phy.*, **29**, 205
" " 1956, *Curr. Sci.*, **25**, 47.
Howell, H. G., 1953, *Proc. Phy. Soc., A.*, **66**, 759.
Mulliken, R. S., 1934, *Phys. Rev.*, **46**, 549.
Uchida, Y. and Ota, Y., 1928, *Jap. Jr. Phys.*, **5**, 53.

DETERMINATION OF THE BETA RAY ENERGY SPECTRUM FROM THE ABSORPTION CURVES OF BETA RAYS

N. K. SAHA AND K. L. KAILA

DEPARTMENT OF PHYSICS, UNIVERSITY OF DELHI, DELHI-8

(*Received for publication, July* 14, 1958)

ABSTRACT. An attempt is made to calculate the energy-distribution of the β-ray spectrum of RaE starting from the observed absorption curve of these β-rays. The absorption law of homogeneous β-rays, required as the basis of this calculation, is obtained here by a rigorous curve fitting of the existing data. Further, Katz and Penfold's (K.P.) remarkable range-energy relation for β-rays is utilised, which seems to avoid most of the limitations of the earlier relations Somewhat improved results compared to previous workers' are obtained in the present work, but still some divergence with the results of magnetic spectrograph remains. Possible causes of the divergence are discussed.

1. INTRODUCTION

Side by side with the elaborate standard methods of β-ray spectrometry, (e.g., the methods of magnetic focussing, scintillation and proportional counters etc.), the method of measuring the total intensity of transmitted beta -rays through various thicknesses of aluminium absorbers (the absorption method) may be considered as a simpler alternative. This method has been widely used in early days for quick and fairly accurate determination of the end-points of β-ray spectra In spite of its inherent defects, the simplicity of the absorption method and the much weaker beta-ray source that it needs compared to the standard methods, make it worthwhile to investigate whether the absorption method can be usefully extended to the determination of the energy spectrum of the continuous beta-rays. The problem, as we shall see presently, resolves essentially to the analysis of the mechanism of absorption of homogeneous beta-rays in a material and the effect of simultaneous absorption of a large number of such homogeneous groups present in the whole spectrum. Attempts have been made by Dass Gupta and Chaudhury (1948), Evans (1950), and Schopper (1951) to solve this problem with varying degrees of success. A review of these works, however, makes it clear that the problem is not yet satisfactorily solved. The energy spectrum determined by this method does not agree well with the results of the magnetic spectrometer. The purpose of the present work is to make a fresh attempt in the line with a closer analysis of the absorption curves of the homogeneous beta-rays on which, theoretically, the success of the whole

calculation should rest. The results derived are applied to the actual calculation of the RaE-β-ray energy spectrum which is compared with the observed spectrum. Some improvement is obtained over the previous position. Results are discussed in detail in the light of the mechanism of the absorption of β-rays.

2. REVIEW OF EARLIER WORKS

Let $\phi(x,R)$ denote the function representing the absorption of the homogeneous group of β-rays of the extra-polated range R(gm/cm^2) at an absorber thickness x(gm/cm^2) and $N(R)$ the number of the homogeneous β-rays of this group. Then the intensity of β-rays transmitted through the absorber thickness x and having a range lying between R and $R+dR$ is given by

$$dI = N(R)\,\phi(x,R)\,dR \qquad \ldots \quad (1)$$

Consider now a certain composite β-ray energy spectrum whose upper limit of range is x_0 gm/cm^2, i.e., at which absorber thickness the intensity of the β-rays falls off to zero. The total intensity of the β-rays of all different ranges which will be transmitted through the absorber thickness x is then given by

$$I(x) = \int_{R=x}^{R=x_0} N(R)\,\phi(x,R)\,dR \qquad \ldots \quad (2)$$

Thus knowing the function $\phi(x,R)$ and the absorption curve for the β-ray spectrum giving $I(x)$ as a function of x, the original intensity $N(x)$ of the homogenous β-rays of all ranges present at a given absorber thickness x can be determined by suitable solution of (2). The range distribution $N(x)$ would easily give us the energy distribution $N(E)$, provided the range energy relation is known.

Rutherford and others (1930) made extensive studies of the absorption of homogenous β-rays in aluminium and expressed the absorption function ϕ by the empirical relation.

$$\phi(x/R) = 1+a\left(\frac{x}{R}\right) + b\left(\frac{x}{R}\right)^2 + c\left(\frac{x}{R}\right)^3 + \ldots \qquad \ldots \quad (3)$$

the constants, a, b, c, etc., are completely arbitrary and are to be adjusted to fit in the experimental curve. A careful study of the absorption of monochromatic β-rays of different energies was afterwards done by Marshall and Ward (1937) for the two β-emitters RaE and UX. It becomes clear from the curves they obtain that near the full absorption thickness R_{max}, some amount of straggling effect takes place making the actual range rather uncertain. However, the extrapolated range measured agrees quite well with the results of previous works done by Schonland (1925), Varder (1915), Madgwick (1927), and Eddy (1929). Because of the certainty of the extrapolated range, it is generally to be preferred to the maximum range in all range considerations. In what follows, R stands

for the extrapolated range. For Ra E the various absorption curves for the constituent homogeneous groups of β-rays obtained by Marshall and Wards, when replotted as a function of x/R, fit well into a single common curve a, figure 1.

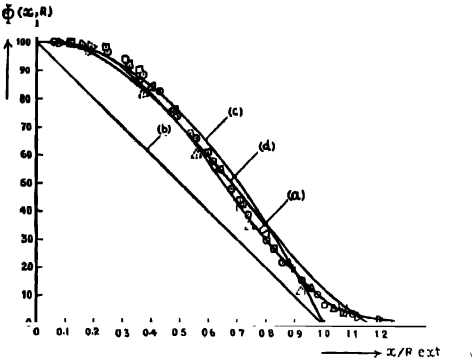

Fig. 1.—The transmission function ϕ (x/R) for beta-rays against x/R : (a) Replotted from Marshall and Wards' experimental absorption curves, (b) $\phi = 1-x/R$, (c) $\phi = 1-(x/R)^2$ and (d) $\phi = 1-1.25\ (x/R)^2 + 0.38\ (x/R)^4$.

Dass Gupta and Choudhury (1948) were the first to attempt a calculation of the energy distribution of Ra E β-rays from the absorption data by using in the first approximation, a linear relation,

$$\phi(x/R) = 1 - \frac{x}{R} \qquad \ldots \quad (4)$$

Introducing this in eqn. (2) and solving under the limiting conditions $\phi = 1$ at $x = 0$ and $\phi = 0$ at $x = R$, one obtains the range distribution

$$N(x) = x\, I''(x) \qquad \ldots \quad (5)$$

where I'' denotes the second derivative of I with respect to the absorber thickness x.

A plot of the above linear relation for ϕ (curve b, Fig. 1) against x/R shows, however, a wide divergence from the experimental curve for $\phi(x/R)$ cited above (curve a, Fig. 1). The evaluation of the second derivative $I''(x)$ from the experimental curve for $I(x)$ also involves considerable uncertainty. The energy distribution of the β-rays calculated by these authors is, therefore, not expected to yield good results.

H. D. Evans (1949) suggested an improvement in the evaluation of the derivatives $I'(x)$ and $I''(x)$ by introducing a logarithmic function $L(x) = \log_e I(x)$, so that (5) takes the form

$$N(x) = xI(x)[L''(x) + \{L'(x)\}^2] \qquad \ldots \quad (6)$$

Since $L''(x)$, as found from the experimental data, is generally small (about 10% to 20%) compared to $\{L'(x)\}^2$, the main contribution in (6) comes from $L'(x)$ which can be determined much more accurately than $L''(x)$. Although the derivative of $I(x)$ was thus quite accurately evaluated by Evans, the energy distribution of β-rays derived by him did not show any substantial agreement with the β-ray spectrometric results. Only improvement found by Evans seems to be that the distribution curve showed a maximum which was not present in Dass Gupta's result.

Hughes *et al.* (1949) have obtained very similar results with ^{64}Cu, ^{187}Au, ^{185}W and radium E and compared the energy distributions derived from absorption curves with magnetic spectrograph observations. They found that the end point energy agreed in the two methods for all cases, but the maxima of the calculated curves occurred at about 100 kev higher energy than the observed values.

H. Schopper (1951) suggested a parabolic relation for $\phi(x/R)$ as

$$\phi(x/R) = 1 - \left(\frac{x}{R}\right)^2 \qquad \ldots \quad (7)$$

This relation (curve *c*, Fig. 1) agrees much better with the experimental curve *a*, as compared to the linear relation (4), except for the values of x/R approaching 1.

Using the relation (7) and solving the differential equation obtained, he arrived at the expression

$$2N(x) = xI''(x) - I'(x) \qquad \ldots \quad (8)$$

Also by putting $L(x) = \log_e I(x)$ according to Evans, the above equation (8) becomes

$$2N(x) = I(x)\{x[L'^2(x) + L''(x)] - L'(x)\} \qquad \ldots \quad (9)$$

In a previous work Schopper showed that the intensity $I(x)$ of the transmitted β-rays at x can be represented empirically by the relation

$$I(x) = \text{const}\ \{(x_0 - x)^2 + 0.22(x_0 - x)\}^{n/2} \qquad \ldots \quad (10)$$

where x_0 is the maximum range obtained from the absorption curve and n is an exponent obtainable from a plot of the observed values of $\log I(x)$ against $\log\{(x_0 - x)^2 + 0.22(x_0 - x)\}$. By introducing (10) in eqn. (9) one obtains

$$N(x).\ \text{const} = n\{(x_0 - x)^2 + 0.22(x_0 - x)\}^{n/2-1}(x_0 + 0.11)$$
$$+ n(n-2)\{(x_0 - x)^2 + 0.22(x_0 - x)\}^{n/2-2}(x_0 - x + 0.11)^2 x \qquad \ldots \quad (11)$$

He further points out that the equation (11) would not be valid in the low energy region, since the analytical expression (10) used here suppresses the finer details

of the absorption curve at small absorber thicknesses. In the low energy region, therefore, the relation (9) is directly utilised for the calculation.

3. COMPARISON WITH EXPERIMENT

The β-ray energy spectrum of RaE has been accurately measured by the magnetic spectrometer by several authors (Neary, 1940; Flammerrfeld, 1939). The most satisfactory determination is due to Neary, the results of which are shown by the curve *a*, figure 2. The relation (11) derived by Schopper has been

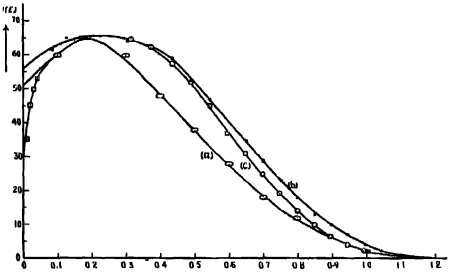

Fig. 2.—The energy distribution curve for Ra E β-rays : (*a*) The spectrometric measurements of Neary, (*b*) recalculated from H. Schopper's formula (8) and (9) using (12*a*), (*c*) calculated from relations (25) and (26).

used by him to calculate the energy distribution of β-rays from RaE, ^{32}P, $UX_1 + UX_2$ and $^{90}Sr + ^{90}Y$. For RaE, in the region of high energies, Flammersfeld's range-energy relation

$$E(x) = 1.92\sqrt{(x_0-x)^2+0.22(x_0-x)} \qquad \ldots \quad (12)$$

for β-rays has been used to obtain the necessary $\frac{dx}{dE}$ values. It is, however, clear that the last relation cannot be true at low energies, since according to this, $\frac{dx}{dE}$ tends to zero at x approaching zero, whereas experiment shows that $N(E) = N(x)\frac{dx}{dE}$ has a finite value at very low energies. In the low energy region Schopper, therefore, uses the relation (9) directly together with the values of $\frac{dx}{dE}$ obtained by himself earlier* and calculates the energy distribution. The latter values of $\frac{dx}{dE}$ near about the maximum of the distribution curve appear

* We are indebted to Dr. H. Schopper for his very friendly private communication this ubject.

to be somewhat higher than those obtained from Flammersfeld's relation. The RaE β-ray-spectrum calculated by Schopper by the above procedure shows considerable agreement with the experimental curve of Neary. It may be pointed out, however, that the $\frac{dx}{dE}$ values used by Schopper cannot be taken as quite certain unless they are confirmed by an independent relation which is known to be strictly valid throughout the entire energy range of the β-rays. Such a consistent range-energy relation for β-rays has recently been given by Katz and Penfold (1952) for aluminium absorbers. This is

$$R = 412\, E^n \text{ (mg/cm}^2\text{)}, \quad \text{where } n = 1.265 - 0.0954 \log_e E \quad \ldots \quad (12a)$$

and fits well with the most reliable published values of practical ranges of mono-energetic electrons and the maximum ranges of nuclear β-rays in energy region $0.01 \leqslant E \leqslant 2.5$ Mev. It would, therefore, be logical to recalculate the distribution curve by employing Schopper's formulae and using the dx/dE values derived from Katz and Penfold's relation (12a). The result of such a recalculation is shown in curve *b* of figure 2. Clearly enough, this curve does not show a good agreement with the experimental results (curve *a*) in the medium and the high energy regions. The apparent good agreement of Schopper's original results with experiments thus appears to be somewhat exaggerated.

In the present work we propose to review the relation representing the absorption of the homogeneous β-rays more critically with a view to achieving better agreement with Marshall and Ward's absorption curves than hither to obtained by previous authors. It appears that the addition of a fourth power term to the parabolic relation (7) gives some improvement in the fit. The plot of the relation

$$\phi(x/R) = 1 - 1.25(x/R)^2 + 0.38(x/R)^4 \quad \ldots \quad (13)$$

is shown in figure 1, curve *d*, where we also reproduce for comparison the curve *c* representing the parabolic relation, curve *b* representing the linear relation and the curve *a* the experimental results of Marshall and Ward. It is clearly seen that the curve *d* follows the experimental curve more closely than the others, although there is some departure in the high energy region. Taking equation (13) as the basic relation for $\phi(x/R)$, we carry out the calculations following the equation (2) and solve the differential equation resulting from that. The corresponding relation giving the energy distribution of β-rays is obtained by utilising the range energy relation of Katz and Penfold. Unfortunately a complete analytical solution cannot be achieved due to mathematical difficulties, but a method of successive approximations has been used as a first approach. The results obtained are shown in curve *c*, of figure 2 which suggest a slight improvement over previous results. It, however, appears that considerable divergence

from experimentally observed β-ray-spectrum still exists. The significance of this departure will be discussed later.

4. THE MODIFIED INTEGRAL DIFFERENTIAL EQUATION AND ITS SOLUTION

As already mentioned in section 3, the empirical relation (13) or

$$\phi(x/R) = 1+a(x/R)^2+b(x/R)^4 \qquad \ldots \quad (13a)$$

with $a = -1.25$ and $b = +0.38$ is used as the basis of our calculation.

Proceeding as in equation (2), we have

$$I(x) = \int_x^{R_0} \phi(x/R)N(R)dR \qquad \ldots \quad (14)$$

$$I'(x) = -(1+a+b)N(x)+\frac{1}{x}\int_x^{R_0}\left[\frac{2ax^2}{R^2}+\frac{4bx^4}{R^4}\right]N(R)dR \qquad \ldots \quad (15)$$

$$I''(x) = -(1+a+b)N'(x)-\frac{1}{x}[2a+4b]N(x)$$

$$+\frac{1}{x^2}\int_x^{R_0}\left(2a\frac{x^2}{R^2}+12b\frac{x^4}{R^4}\right)N(R)dR \qquad \ldots \quad (16)$$

If we write

$$\left.\begin{aligned} f(x) &= \int_x^{R_0}\left(\frac{x}{R}\right)^2 N(R)dR \\ \psi(x) &= \int_x^{R_0}\left(\frac{x}{R}\right)^4 N(R)dR \\ K(x) &= a\,f(x)+b\psi(x) \end{aligned}\right\} \qquad \ldots \quad (i)$$

we obtain

$$I(x) = \int_x^{R_0} N(R)dR + a\,f(x) + b\psi(x) \qquad \ldots \quad (17)$$

$$I'(x) = -(1+a+b)N(x)+\frac{2a}{x}f(x)+\frac{4b}{x}\psi(x) \qquad \ldots \quad (18)$$

$$I''(x) = -(1+a+b)N'(x) - \frac{1}{x}(2a+4b)N(x)$$

$$+ \frac{2a}{x^2} f(x) + \frac{12b}{x^2} \psi(x) \qquad \ldots \quad (19)$$

Also from the last equation of (i) we get

$$\psi(x) = \frac{K(x) - a f(x)}{b} \qquad \ldots \quad (20)$$

Substituting this in (18), we obtain

$$f(x) = -\left[I'(x) + (1 + a + b)N(x) - 4\frac{K(x)}{x} \right] \frac{x}{2a} \qquad \ldots \quad (21)$$

Substituting (21) in (20), results

$$\psi(x) = -\frac{K(x)}{b} + \frac{x}{2b}\left[I'(x)+(1+a+b)N(x) \right] \qquad \ldots \quad (22)$$

Also from (19) using (21) and (22) follows :

$$I''(x) = -(1+a+b)N'(x)+\frac{1}{x}(5+3a+b)N(x)-\frac{8K(x)}{x^2}+\frac{5}{x}I'(x)$$

or $$I''(x)-\frac{5}{x}I'(x)+\frac{8K(x)}{x^2} = -(1+a+b)N'(x)+\frac{1}{x}(5+3a+b)N(x)$$

Substituting for $K(x)$ from (17),

$$I''(x)-\frac{5}{x}I'(x)+\frac{8}{x^2}I(x)-\frac{8}{x^2}\int_x^{R_0} N(R)dR$$

$$= -(1 + a + b)N'(x) + \frac{1}{x}(5 + 3a + b)N(x)$$

$$= AN'(x)+\frac{B}{x}N(x) \qquad \ldots \quad (23)$$

where $A = -(1+a+b)$ and $B = (5+3a+b)$.

If we put $a = -1$ and $b = 0$, equation (23) should reduce to Schopper's equation. In this case equation (23) will become as

$$I''(x)-\frac{5}{x}I'(x)+\frac{8}{x^2}I(x)-\frac{8}{x^2}\int_x^{R_0} N(R)dR = \frac{2}{x}N(x) \qquad \ldots \quad (23a)$$

and equation (14) will give,

$$I(x) = \int^{R_0} N(R)dR - \int^{R_0} (x/R)^2 N(R)dR,$$

so that

$$\int_x^{R_0} N(R)dR = I(x) + \int_x^{R_0} \left(\frac{x}{R}\right)^2 N(R)dR \qquad (23b)$$

Substituting this in equation (23a), we obtain

$$I''(x) - \frac{5}{x} I'(x) - \frac{8}{x^2}\int_x^{R_0} \left(\frac{x}{R}\right)^2 N(R)dR = \frac{2}{x} N(x) \qquad \ldots \quad (24)$$

Also from equation (15) we have in this particular case,

$$I'(x) = -\frac{2}{x}\int_x^{R_0} \left(\frac{x}{R}\right)^2 N(R)dR \qquad \ldots \quad (24a)$$

Substituting this value in (24) we get,

$$2N(x) = xI''(x) - I'(x) \ (Eq.8)$$

which is exactly the same solution (8) obtained by Schopper, here appearing as a particular case of the solution (23).

Now our object will be to solve the equation (23). As is evident from the form of the equation, it will not be possible to get a simple solution in a very rigorous manner. Our attempt here will be to assume the solution (8) to be true to a first approximation and then by substituting in (23) to get a solution to the next higher approximation.

Thus we use for I(x) the expression from (23b) and for I′(x) from (24a) and rewrite the general relation (23).

Equation (23) then becomes

$$xI''(x) - I'(x) = Ax\, N'(x) + B\, N(x)$$

Again using (8),

$$2N'(x) = I''(x)+xI'''(x)-I''(x) = xI'''(x)$$

Substituting this above we get

$$xI''(x)-I'(x) = A\frac{x^2}{2}I'''(x) + B\,N(x)$$

or

$$BN(x) = -A\frac{x^2}{2}I'''(x) + xI''(x) - I'(x)$$

But $A = -(1+a+b) = -0.13$, $B = (5+3a+b) = 1.63$, because $a = -1.25$ and $b = 0.38$. Thus, we get finally

$$1.63N(x) = 0.065x^2I'''(x)+xI''(x)-I'(x) \qquad \ldots \quad (25)$$

and putting $L = \log_e I(x)$,

$$1.63N(x) = I(x)[0.065x^2\{L'^3+3L'L''+L'''\} + x\{L'^2+L''\}-L'] \qquad \ldots \quad (26)$$

Evidently, this final solution (25) differs from Schopper's solution by an extra term $0.065x^2I'''(x)$.

For calculating the energy distribution curve we have used for the medium and high energy regions relation (25), obtaining, I', I'' and I''' from Schopper's annalytical equation (10). As pointed out by Schopper, at low energies the finer variations of the absorption curve are suppressed if relation (10) is used. Therefore, for the low energy region, we have used equation (26) in which L', L'' and L''' are obtained from the plot of experimental values of L versus x given by Evans. Finally for obtaining $N(E)$ as a function of E, we have made use of Katz and Penfold's range energy relation, (12a). The results obtained are shown by the plot c in figure 2.

5. DISCUSSION

The energy spectrum of β-rays calculated according to the above procedure is shown in figure 2, curve c. The spectrometric measurements due to Neary are plotted in curve a, and the energy distribution recalculated from Schopper's formula by using Katz and Penfold's range-energy relation is also shown by the curve b for comparison. The five experimental points at $E \leqslant 0.05$ Mev energy are due to Pniewski and Danysz (1953). As already emphasized in section 3, the recalculated curve b shows considerable divergence from the experimental distribution, particularly at the high energy side beyond the maximum. In fact the recalculated maximum comes out to be very flat (inherent defect of

the procedure) and falls near about the position of the experimental maximum. The curve c obtained from our calculation shows a good agreement with the experimental curve towards the high energy region of the distribution curve, but the agreement in the intermediate region shows only a slight improvement. It is unlikely that the mathematical approximation involved in our calculation or the inaccuracies of the graphical estimates of L', L'' and L''' can account for the observed disagreement. It also seems clear that the introduction of still higher order terms in the expression (13) for $\phi(x/R)$ will not improve matters, since the fourth power term, added by us already, makes the agreement of $\phi(x/R)$ with its experimental values quite good. The reason for the disagreement seems to be more deep seated. Probably the analytical expression (10) for $I(x)$ in terms of the absorber thickness needs modification. It would be possible to modify it if the detailed mechanism of absorption of β-rays in absorber thickness could be exactly formulated theoretically. This possibility is not yet in sight. The other alternative is to look for uncertainty, if any, in the spectrometric determination of the β-ray energy distribution curve for RaE in the region of intermediate energies. The general accuracy of Neary's data is certainly better than 2%. It may, however, be pointed out that the results calculated from a set of theoretical formulae, as done by us, ultimately depend on the accuracy of the absorption measurements of the continuous β-rays. This accuracy is probably not very high (variable between 6.3% and 1% in Evan's measurements). For a strict comparison the conditions for the spectrometric and the absorption measurements should be identical. Probably not enough attention has yet been paid to this point.

When the main problem of theoretically calculating a single continuous β-ray energy distribution curve from the absorption data has been satisfactorily solved, one may probably attempt a possible extension of the theory in other directions. For example, one would like to ask : is it possible to apply the theory to the cases, where more than one continuous β-spectra with different end points are superimposed on each other, or when line spectra are superposed on a continuous β-spectrum ? Beta emitters of these complicated types are, of course, quite numerous. But it is too early to consider these questions now before the simplest problem outlined above has been completely solved.

ACKNOWLEDGMENTS

The authors wish to express their sincere thanks to Prof. D. S. Kothari for giving them facilities to carry out this work. They are also indebted to Prof. N. N. Dass Gupta for many stimulating discussions in the course of this work. Their thanks are also due to Dr. A. N. Mitra of the Muslim University, Aligarh for giving them mathematical help and to Dr. J. Varma (now in the Tata Institute of Fundamental Research, Bombay) for his interest in the early stage of the work.

REFERENCES

Dass Gupta, N. N. and Chaudhury, A. K., 1948, *Ind. Jour. Phys.* **22**, **27**.
Eddy, C. E., 1929, *Proc. Camb. Phil. Soc.*, **25**, 50.
Evans, H. D., 1950, *Proc. Phys. Soc. Lond.*, *A* **63**, 575.
Flammerfeld, A., 1939, *Zeit. Physik*, **112**, 727.
Hughes, D J., Eggler, C. and Huddleston, C. M., 1949, *Phy. Rev.*, **75**, 515.
Katz, L. and Penfold, A. S., 1952, *Rev. Mod. Phy.* **24**, 30.
Madgwick, E., 1927, *Proc. Camb. Phil Soc.*, **23**, 970.
Marshall, J. S., and Ward, A. G., 1937, *Canadian J. Res.*, *A* **15**, 39.
Neary, G. J., 1940, *Proc. Roy. Soc.*, *A* **175**, 71.
Pniewski, J. and Danysz, M., 1953, *Nature* (London), **171**, 694.
Rutherford, E., Chadwick, J. and Ellis, C. D., 1930, Radiations from radioactive substances, Cambridge University Press.
Schonland, B. F. J., 1925, *Proc. Roy. Soc. Lond*, *A* **108**, 187.
Schopper, H, 1951, *Zeit. f. Physik*, **129**, 416.
Varder, R. W., 1915, *Phil. Mag.* **29**, 725.

ON THE ABSORPTION COEFFICIENTS AND ENERGY SPECTRA OF GAMMA-RAYS FROM RA (B+C) UNDER THICK LAYERS OF Pb ABSORBER

P. K. SEN CHAUDHURY

DEPARTMENT OF PHYSICS, PRESIDENCY COLLEGE, CALCUTTA

(*Received for publication, June* 26, 1958)

ABSTRACT The absorption coefficients and energy spectra of gamma-rays from 500 mc of Ra in equilibrium were measured under thick layers of Pb from 18.5 to 27.5 cm with a sodium iodide (thallium activated) crystal in combination with a linear amplifier and differential energy discriminator. The absorption coefficient measured with absorber of very small lateral dimensions and for the gamma-rays of highest energy, *e.g.*, 2 494$\pm$0.073 Mev emitted by radium is about 8% less than the theoretical value. But when a strong and wide beam is used by placing the Ra source immediately below the absorber then the measured absorption coefficients show anomalous variations as previously reported by the author. The energy spectra measured under 18.5 cm and 20.5 cm of Pb absorber show three peaks at about 2.494$\pm$0.073, 2.220$\pm$0.065 and at 1.776$\pm$0.052 Mev and the energy spectra under 23.5 cm shows in addition to these three peaks indications of another peak at 1.469$\pm$0.043 Mev.

INTRODUCTION

A few years past the author (Senchaudhury, 1948, 51, 54) reported some anomalous variations in the experimental values of absorption coefficients of gamma-rays from radon in equilibrium under thick layers of Pb absorber and it was suspected that these might be due to some penetrating radiation of secondary origin. But the author's experiments were repeated by Dixon and Whyte (1952) in Canada and by Clay and co-workers (1952) in Amsterdam with conflicting results. Dixon and Whyte carefully did the experiment apparently under the same conditions as the author and obtained a constant absorption coefficient under 13 to 26 cm of Pb, whereas Clay with an ionisation chamber obtained the absorption coefficients monotonously decreasing to values far below the theoretical minimum values. Now a careful study of the paper by Dixon and Whyte showed that one of the main differences between their and author's previous experimental arrangements was that they used a highly canalised beam with a canal of depth 30 cm, whereas in author's experiments a radon capsule of length about 3 cm was placed in a cavity of only about 4 cm depth. This means a great difference, firstly although they have used a radium source of one curie strength, the intensity of the radiation on the absorber had been reduced by a factor of $1/30^2 = 1/900$, and the effective strength of the radiation

was about 1 mc only. They used 5 cm thick Pb shielding on the sides of the detector, whereas the author used only 1 cm thick Pb shield. In all the previous experiments the absorption coefficients for the integral beam only have been measured that is the average absorption coefficient of the highly heterogeneous beam of gamma-rays emitted by Ra and therefore the comparison of the experimental values with those of the theoretically calculated values are meaningless except that the absorption coefficients should not be less than the theoretical minimum values of about 0.47 cm^{-1} in Pb. There has also been some controversy about the energy spectra of gamma-rays from Ra (B + C) and Whyte (1952) only indirectly inferred the energy spectra from transmission curves under thick layers of Pb.

In view of all these the author was waiting for a suitable opportunity to repeat the former experiments and also to visualise directly the energy spectra under thick layer of Pb. absorber. By the courtesy of Prof. Lauterjung of the Institut für Physik Im Max-Planck-Institut fur Medicinische Forschung at Heidelberg it has been possible for the author to repeat the experiments more carefully during a study leave in West Germany. Several sets of measurements were made under different experimental arrangements with the two-fold objects, firstly, to investigate the anomalous variations in absorption coefficients under certain experimental conditions and the nature of secondary radiations producing such localised variation and secondly, to see how far the experimental values can be brought in agreement with the theoretically calculated values by elemmating all secondary radiation and measuring with nearly monochromatic radiation only.

EXPERIMENTAL ARRANGEMENTS

In these investigations a sodium-iodide (thallium activated) Harsha crystal of diameter and depth 5 cm with a linear amplifier and differential discriminator has been used as the detector and as a spectrometer. The linear amplifier used is model 218 and the differential discriminator is a single channel 510 pulse-height analyser of the Atomic Instrument Co, with resolving time 0.8μ sec. and 10μsec. respectively. The recorder was a 1000 scaler of Tracer Lab of resolving time 1μsec. The photomultiplier used was R.C.A. 6342 and the high voltage supplied to its cathode was from a model 312 super stable power supply. The differential discriminator was calibrated by the peak of Cs^{137} gamma-rays and the constancy of the linear scale was tested almost every time before and after each experiment. The strength of the Ra source was 500 mc. Mainly three sets of experimental arrangements have been used in these investigations e.g.

1. (a) Detector unshielded and the beam not canalised,
   (b) Same as (a) but with sides shielded detector,
2. Canalised beam and sides shielded detector,

3. Same as 2, but the lateral dimensions of the absorber used are very small.

The different experimental arrangements are shown in the figure 1. The experimental arrangements 1(a) are similar to the previous arrangements of

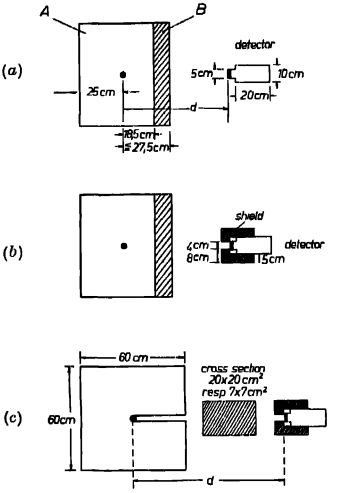

Fig. 1.—Experimental arrangements.

(*a*) Beam not canalised. Detector unshielded.

(*b*) As in (a) but detector shielded.

(*c*) Beam canalised, detector shielded and with two different lateral dimensions of the absorber.

the author except 30 cm Pb, shielding all but the front side of the Ra source to prevent any radiation escaping to he room other than through the front absorber. Under these conditions it was found that the counting rate by the detector reduced to that of the background when about 33 cm Pb absorber was used in the front. The detector sides were not shielded by Pb as preliminary experiments showed that such heavy shield appreciably reduce the absorption coefficients by scattering back to the detector some of the radiation scattered by the absorber. Further, any remaining scattered radiation by wall reflection etc., which are of very low energy, were cut off by the energy discriminator except for the total integral beam. The a rangements (b) are similar to (a) except 5 cm thick Pb shielded the sides of the detector. The experimental arrangements (c) with a canalised beam of canal depth 30 cm are exactly similar to that of Dixon and Whyte. Absorbers of two lateral dimensions, e.g., 20 cm × 20 cm and 7 cm × 7 cm were used.

EXPERIMENTAL RESULTS

The counting rates, subtracting the background with different thickness of Pb absorber and with different energy cut-offs under the experimental arrangements (a), are shown in logarithmic scale in the figure 2. The curves are represented by the number 1, and the size of the points represents the statistical error when it is not shown otherwise. The measured absorption coefficients for three different distances of the detector from the Ra source, e.g., 75 cm, 64 cm and 49 cm and for the integral beam of energy greater than 1.029 Mev. are shown in the figure 3 together with the mean curve under different thicknesses of Pb absorber. The absorption coefficients were measured from 18.5 cm to 27.5 cm Pb absorber at the interval of 1 cm only. It may be observed that

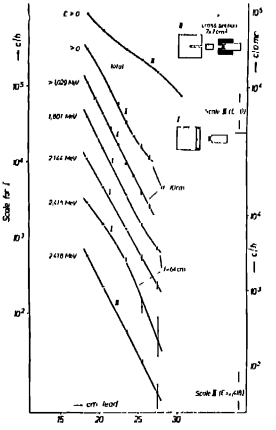

Fig. 2.—Counting rates from source radiations for different energy cut-off.
Curves I · Beam not canalised, detector unshielded (Expt. la)
Curves II : Beam canalised, detector shielded, absorber cross-sections 7×7 cm^2 arrangements according to Fig. 1(c).

in all the three curves the absorption coefficient steadily decreases to a minimum under about 21.5 to 22.5 cm Pb followed by a steady rise to a maximum under 23.5 cm Pb and a sharp fall again to a value much below the theoretically expected and the minimum value under 24 5 cm. In each curve a new rise again under 25.5 cm is indicated. The theoretically expected value is represented by the dotted line and it is nearer to the peak value under 23.5 cm Pb.. The measured absorption coefficients for the integral beam of all energy also shows exactly similar variations. The conditions of these measurements are nearly similar to those of the previous measurements by the author. In the previous

results there was a steady decrease of the measured absorption coefficients after 20 cm of Pb absorber to a minimum between 23 and 25 cm with a rise again after 25 cm. But in the previous measurements Pb absorber at the interval of 2 cm or more were used and probably therefore the additional increase under

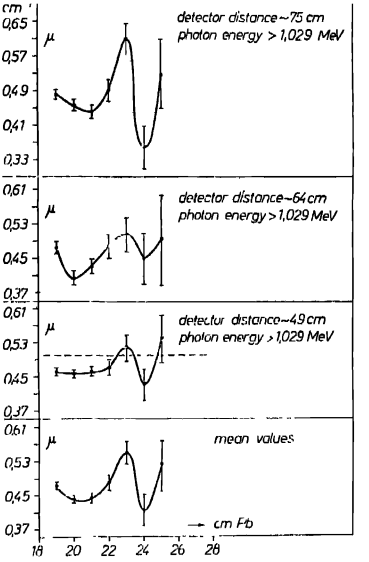

Fig. 3 —Absorption coefficients for the integral beam with $E > 1,029$ Mev under different absorber thickness measured at three different distances between the source and the detector. Beam not canalised, detector unshielded. Arrangements Ia Lower curve : Mean of three curves for different distances.

23.5 cm indicated by the present experiment, was not detected. But the measurements with the arrangements (b) shielding the sides of the detector by 5 cm thick Pb show that for the integral beam and for the integral beam of energy greater than 1 029 Mev, the absorption coefficients steadily decrease to a value below the theoretical minimum value after 23.5 cm of Pb absorber.

The experimental arrangements (c) are exactly similar to those of Dixon and Whyte (1952) and the measured absorption coefficients for the integral beam of all energy and for energy greater than 1.029 Mev. measured with Pb absorber of dimension 20 cm by 20 cm are also similar to those obtained by these workers. There are no anomalous variations and the measured absorption coefficients are nearly constant and equal to theoretically expected values. But

the measured absorption coefficients for higher energy cut-offs and nearly monochromatic radiations are always smaller than the theoretical values. In the final measurements with the arrangements (c) the absorbers of lateral dimension 7 cm × 7 cm were used and the absorption coefficients were measured for the integral beam of all energy and for the photons of energy 2.494±0.073 Mev, which the energy spectra measurements showed to be the highest energy component of gamma-rays from Ra (B+C) The log intensity curves are shown in the figure 2 with the curves marked III. The measured absorption coefficients for the integral beam are much smaller than the theoretical minimum values similar to those obtained by Clay (1952) and reduce to as low as 0.17 cm^{-1} under 23.5/cm Pb absorber. But it was observed that the counting rate by the detector could not be reduced to that of the background even after 40 cm of Pb absorber. It is therefore obvious that such low values of absorption coefficients are due to a considerable fraction of the scattered radiation from the absorber which is scattered back to the detector by the large Pb. shield surrounding its sides. For the Compton scattering is maximum in the forward direction and as the lateral dimension of the Pb absorber is very small, these scattered radiations are not further reabsorbed as the successive thickness of Pb absorber is increased. When the measurements were made for gamma-rays of highest energy 2.494±0.073 Mev. only cutting-off all scattered radiations of lower energy by the discriminator with narrow channel width, the measured absorption coefficient was about 0.455 cm^{-1} which is only about 8% less than the theoretical value.

ENERGY SPECTRA

For the experimental arrangements (a) the energy spectra of gamma-rays from Ra (B+C) were measured under 18.5 cm and 23.5 cm Pb absorber together with that of the background under 23.5 cm The measured spectra are represented in the figure 4, one volt pulse height is equivalent to 0.0342±.001 Mev. The energy spectra are shown for gamma-rays of energy greater than about one Mev. only for the energy spectra under 1 Mev show no peak but a continuous energy distribution. The energy spectra under 18.5 cm curve *A* show peaks at 1.77±0.065, 2.22±0.09 and 2.39±0.07 Mev The energy spectra under 23.5 cm curve (c) shows in addition to three peaks a new peak at 1.469±0.043 Mev. But slightly displaced towards higher energy there is also a peak in the background curve *B* at 1.537±0.045 Mev. The limit of error to each peak energy is the constant error of calibration and do not affect the relative position of the peaks. The constancy of the linear scale of the amplifier was tested by the constancy of position of Cs^{137} peak almost after every experiment.

For the experimental arrangements (c) the energy spectra were measured under 20.5 cm and 23.5 cm Pb absorber with the background spectra under 23.5 cm. The energy spectra under 20.5 cm shows three peaks at 2.49±0.073

Mev. 2.289±0.067 Mev. and at 1.7761±0.052 Mev. The energy spectra under 23.5 cm shows four peaks at 2 46±0.07 Mev, 2.280±0.06 Mev, 1.800±0.05 Mev and at 1.47±0.043 Mev. The peak at 2.49±0.07 Mev is very clear under this experimental arrangements though it was scarcely visible under the arrange-

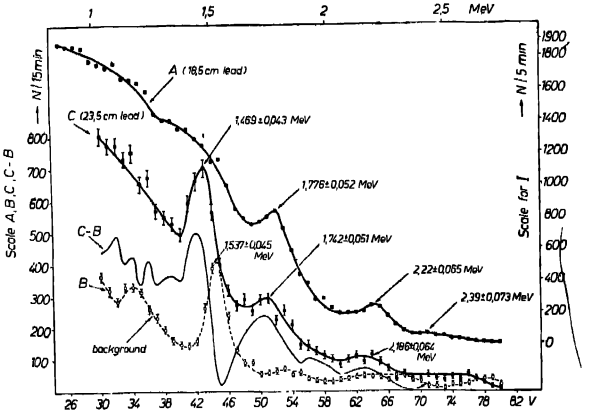

Fig. 4.—Energy spectra of the total radiation (source and background) under 18.5 and 23.5 cm Pb absorber (curve A and C).

Background without source radiation (curve B), curve (C-B) Photon spectra of the Ra source under 23.5 cm Pb absorber. Arrangements I(a).

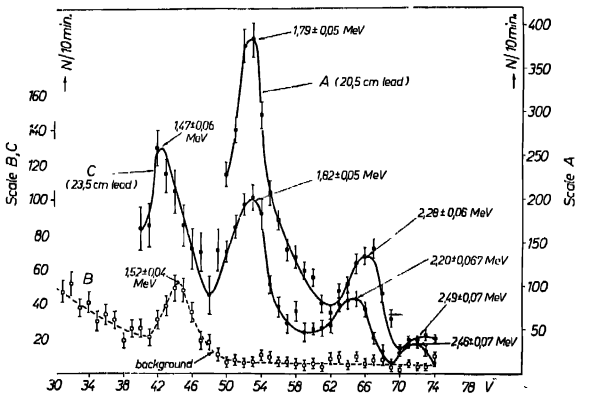

Fig. 5.—Energy spectra of the total radiation (source and background) under 20.05 cm (curve A) and under 23.5 cm Pb (curve C) together with the background (Curve B) Conditions : Beam canalised, detector shielded and absorber cross-sections 20 × 20 cm

ment (a). This peak was first reported by Lathyshev and co-workers (1947). Again the peak at 1.47 ± 0.043 Mev exactly coincides with that under the experimental arrangement (a) and there is also the background peak as in previous experiment at 1.537 ± 0.045 Mev. As the energy difference between these two peaks is very small it is natural to think that the peak with Ra source is simply the background peak shifted to lower energy due to increase in intensity with Ra source. To investigate this point the energy spectra of Cs^{137} gamma-rays were measured for different total intensities by changing the distance of the Cs^{137} source from the crystal detector and it was found that there was slight shift of the peak towards higher energy with the increase of the total intensity when the linear scale was calibrated at lower intensity. This is also expected from the slight decrease in sensitivity of the photo-cell cathode at higher intensity. The measured energy spectra of Ra gamma-rays under different thickness of Pb absorber also show that as the intensity is increased by decreasing the absorber thickness, there is slight shift towards higher energy of all the peaks except the new peak at 1.469 Mev which is at energy lower than its neighbour background peak. Also with the experimental arrangements (c) the total intensity was cut down by a factor of about 1/7 in comparison with that under (a) still the position of these two peaks remained exactly same Therefore, it is very unlikely that the peak with radium is the same peak ' he background.

DISCUSSIONS

Finally to summarise the results these investigations have shown that for the experimental arrangements with a wide and very strong incident beam on the absorber by placing 500 mc Ra immediately below it, the variations of absorption coefficients between 20.05 and 25.5 cm are anomalous as reported by the author previously. But the anomaly disappears when a highly canalised beam similar to that of Dixon and Whyte is used. Also when the absorption coefficients are measured for the gamma-rays of highest energy only cutting off all the secondary radiations of lower energy by the energy discriminator and using absorber of very small lateral dimension to prevent the production of appreciable secondaries by multiple scattering etc., the measured value is constant and only about 8% less than the theoretical value. It is, therefore, clear that the anomalies appearing under the experimental arrangements described above must be due to secondary radiations produced either by multiple scattering or these are produced locally in the anomalous region by some unknown process. But it is difficult to understand how multiple scattering which is a continuous process can produce such sharp localised increase and decrease in the absorption. Therefore the appearance of a new peak of energy 1.469 ± 0.043 Mev under 23.5 cm Pb may be significant It could, however, be still better decided if the energy spectra were measured in a laboratory where the neighbouring background peak due to radio-active contamination or cosmic-rays

was absent. A careful search was also made with a BF_3 counter if any appreciable number of neutrons were emitted by the 500 mc Ra source due to interaction with light elements in glass container etc., but no extra count over the natural background was detected.

ACKNOWLEDGMENTS

These investigations were done at the Institüt für Physik Im Max-Planck Institüt Für Medicinishe Forshung, Heidelberg, and the author expresses his grateful thanks to Prof. Dr. Lauterjung who very kindly provided the author with all the experimental facilities. The author is also very grateful to Prof. Dr. A. Ehmert and to Dr. G Pfotzer of the Max-Planck-Institut fur Physik Der Stratorphare Weissenau for much help. Finally the author is thankful to the Government of West Bengal, for the grant of a study leave.

REFERENCES

Clay, J. and Coworkers, 1952, *Physica*, **18**, 582.
Dixon, W. R. and Whyte, J. N., 1952, *Canad J. Phys.*, **30**, 438.
Lathyshev, G. D., 1947, *Rev. Mod. Phys.*, **19**, 132.
Senchaudhury, P. K, 1948, *Ind. J. Phys.*, **22**, 341.
Do 1951, *Phys. Rev.*, **81**, 274.
Do 1954, *Z. Naturforschung*, **9a**, 175.
Whyte, J. N., 1952, *Canad J. Phys*, **30**, 442.

ON THE VARIATION OF COMPRESSIBILITY OF WATER AND ELECTROLYTIC SOLUTIONS WITH TEMPERATURE

PRAFULLA KUMAR MAHAPATRA AND BAMAN CHARAN RAY

DEPARTMENT OF PHYSICS, RAVENSHAW COLLEGE, UTKAL UNIVERSITY, CUTTACK 3

(*Received for publication, May 22, 1956, received after revision, February 7, 1958*)

ABSTRACT. Ultrasonic velocities and compressibilities in water and some electrolytes have been measured. The results have been discussed in the light of the knowledge about their structures.

INTRODUCTION

Variation of ultrasonic velocity in water with temperature upto near about the boiling point of water has been measured by Neuman (1947) and Willard (1947). They have employed the methods of interference and diffraction respectively for the determination of the velocity at the higher temperatures. The measurement of ultrasonic velocity at high temperatures tends to be inaccurate as the diffraction patterns become increasingly diffuse with temperatures near the boiling point. The velocities measured by these workers do not agree, particularly at higher temperatures and we have therefore attempted to measure the variation of velocity with temperature for water and also for solutions of NaCl and $MgSO_4$. The tabulated values of the densities from the International Critical Tables, Vol. III at different temperatures have been used to give us the respective compressibilities at different temperatures.

EXPERIMENTAL RESULTS

The velocities of ultrasonic waves in solutions were determined from the measurement of Debye Sears diffraction patterns, obtained by running a 50 watt ultrasonic generator at 3 m/c through the liquids. The liquids were heated to different temperatures upto about 90°C, by passing steam through a glass tube immersed in the trough containing the experimental liquids. The velocities at different temperatures and in different solutions were obtained by comparison with the fringe width dw for water at a lower range of temperature, where the velocity V_w is accurately known from measurements of other workers. The unknown velocity is determined from the relation $V_x\, dx = V_w\, dw$, where V_x and dx represent the velocity to be determined and the corresponding fringe seperation respectively. The ultrasonic frequency and the photographic set-up were kept

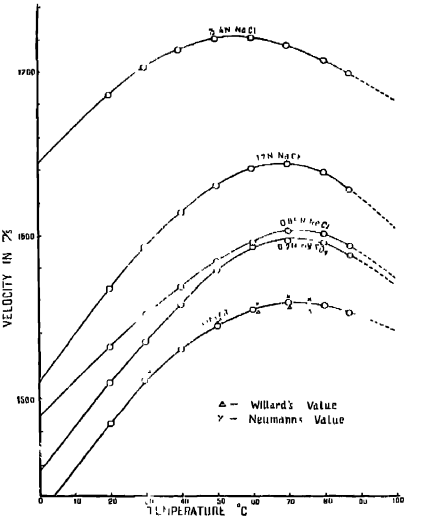
VELOCITY IN M/S
1700
1600
1500
Willard's Value
Neumann's Value
TEMPERATURE °C

Fig 1.

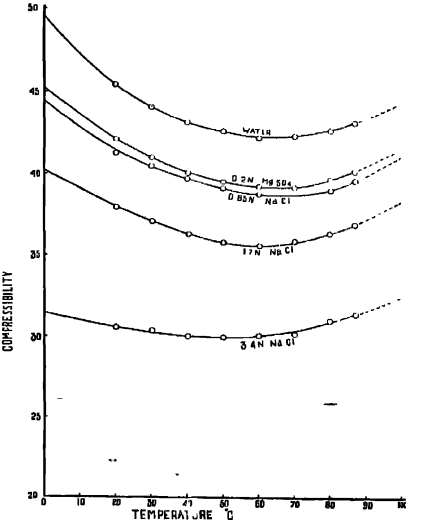
COMPRESSIBILITY
50
45
40
35
30
25
20
WATER
0.2N Na SO4
0.85N Na Cl
1.7N Na Cl
3.4N Na Cl
TEMPERATURE °C

Fig 2.

constant throughout the experiment. The velocities so determined for the experimental liquids have been plotted in figure 1 against the temperatures with extrapolations below room temperature and above 90°C. The electrolytes and their molar strengths and also the experimental points of Neuman and Willard for water have been indicated on the figures. The probable error in the measurement of velocity is of the order of ± 1 m/s. The calculated values of compressibilities obtained from these velocity values and the known density values have been shown in figure 2.

DISCUSSIONS

It will be observed from the compressibility graphs in figure 2 that the compressibilities for water as also for the electrolytic solutions at first decreases and then rises with temperature. To account for these, qualitatively, we take up the composition of water as proposed by Bernal and Fowler (1933). We may consider that at about 0°C. water consists of the tridymite structures mostly, which break up partially into the cubical structures by the rise of temperature or by the influence of the ionic pull.

According to the accepted ideas, the cubical water structure, so formed, tends to be more closely packed due to larger mutual attraction upon one another. This naturally tends to decrease the compressibility by rise of temperature. Further, according to the theory of Bernal and Fowler the structure of water near about 100°C is of the homogeneous cubical type. The decrease of compressibility with the increasing strength of any electrolyte at this temperature, as will be observed from the graphs, cannot therefore be due to the breaking up of more complex structure It must be purely an effect of ionic pull on the polarised water structures which increases proportionately with electrolytic strength. This effect is, however, expected to be weaker for larger mutual separations caused by any rise of temperature and thus causing an increased compressibility with temperature.

Besides, as in the case of all non-associated pure liquids, there should occur an increase of compressibility on account of larger mutual seperations, if there is any, as the temperature rises. The variation of compressibility for electrolytes with the rise of temperature is thus caused by the following effects, namely, the general increase of compressibility with larger spacings as for any homogeneous non-associated liquids; the increase of compressibility due to diminished strength of ionic pull at larger seperation, by the effect of temperature rise, and the increased ionic attraction, and a further decrease of compressibility due to the effect of the broken up cubical structure. It does not appear to be feasible at this stage to sort out the magnitude of the different effects. The comparative value of the decrease of compressibility for different concentrations of NaCl

and $MgSO_4$ indicates that the decrease of compressibility compared with water is proportional to the concentration and the bivalent salts give rise to an effect which appears to be nearly double the ionic charge or the square of the charge. Further experiments on this line are expected to give fruitful results.

ACKNOWLEDGMENTS

Our thanks are due to Prof. A. K. Dutta for his kind help and guidance throughout the course of the work.

REFERENCES

Bernal, J. D. and Fowler, R. H., 1933, *Jour. Chem. Phys.* **1**, 515.
Neuman, E. A., 1947, *Proc. Phys. Soc. Lond.*, **59**, 585.
Willard, G. W, 1947, *Journ. Acoust. Soc. Amer.*, **19**, 235.

CALORIMETER FOR THE MEASUREMENT OF SPECIFIC HEAT OF LAC

SURENDRA NATH SRIVASTAVA

DEPARTMENT OF PHYSICS, ALLAHABAD UNIVERSITY, ALLAHABAD

(*Received for publication, October* 16, 1957)

ABSTRACT. For the measurement of the specific heat of lac and other bad conducting materials, a rectangular type of copper calorimeter is designed, which eliminates the sources of errors of the calorimeter used by Bhattacharya (1940). Specific heat of Kusum lac has been measured from room temperature to 110°C, at intervals of 5°C. The variation of its specific heat with temperature is discussed.

INTRODUCTION

Measurement of the specific heat of lac was undertaken to examine the behaviour of the variation of specific heat of lac at higher temperatures. The specific heat was measured from room temperature to 110°C, with a newly designed rectangular type of calorimeter. It is not desirable to extend this range beyond 110°C since the lac polymerises quickly after this temperature. Even in this short range several interesting features were revealed and it is hoped that a complete study may be useful for judging the quality and age of lac sample.

EXPERIMENTAL

The measurement of the specific heat of lac was made by Sen (1938-39) and Bhattacharya (1940) from 10°C to 40°C. The apparatus used by them consists of two hollow cylinders of same the length l and radii R and $2R$. Heating wire is wound round the inner cylinder and the thermometer is placed on the common axis for recording the temperature. The whole calorimeter is filled with lac. In such an arrangement following defects were felt.

1. The volume of lac contained inside the inner cylinder is $\pi R^2 l$. and that contained in the interspace of the cylinders is $\pi(2R)^2 l - \pi R^2 l = 3\pi R^2 l$. That is, on one side of the heater the material is three times that on the other side of it, and therefore the average temperature of lac in the two compartments cannot be expected to remain the same.

2. The thermometer is placed on the axis of the cylinders ; hence it will not record the average temperature of lac of the inner cylinder.

3. Lac is a bad conductor of heat, and no attempt seems to have been made towards the attainment of uniform temperature in the mass of the substance.

Considering these defects the calorimeter finally adopted, (figure 1) consists of a hollow rectangular copper vessel, with the closed bottom. A flat heater divides the vessel in two rectangular chambers along its length. Thus there are

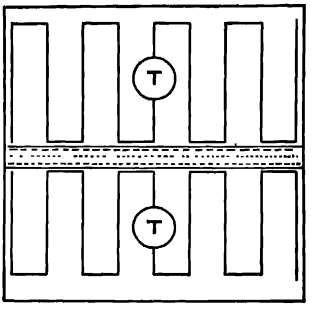

Fig. 1. Cross-sectional view of the calorimeter.

equal volumes of substance on the two sides of the heater in the two chambers, and the error due to the first objection is eliminated. Two thermometers, enclosed in copper covers, are placed such that their bulbs occupy the central positions in the two chambers. This rules out the second objection. Finally, two copper sheets are introduced in the zig-zag way in the two chambers to ensure the uniformity of temperature.

The dimensions of the actual calorimeter used were $1'' \times 1'' \times 4''$. Heating coil of approximately 30 ohms was wound flat on a thin insulator, and was finally covered by two thin insulating papers. Over these papers two copper sheets were placed, and the whole assembly was kept in the exact central position of the calorimeter, dividing it in two equal rectangular chambers. Four inches wide copper sheet was bent in the form of a rectangular wave with wave-length of $1/5''$ and amplitude of $3/16''$. It was placed in the calorimeter as shown in figure 1, in cross-section. Thus no part of the substance is farther than $1/20''$ from the highly conducting surface of copper sheet. Thus only in two minutes after the passage of current the temperature became constant.

The calorimeter was placed in a glass bottle, and the bottle was kept in a glycerine bath. The temperature of the bath could be increased by a heater and maintained constant by a thermo regulator and stirrer, and could be read by a thermometer. Current at nearly 16 volts was passed through the heater

of the calorimeter for about a minute and the rise in temperature was noted. Radiation correction was also applied. Water equivalent of empty calorimeter was determined in the routine way. Calorimeter was then filled with lac, and the specific heat computed after passing current and noting the rise in temperature, which was recorded by a thermometer which could read to 0 1°C. The rise is adjusted nearly 5°C for each determination, after which the temperature of the bath is kept constant for 15 minutes, and the thermometer is also seen to record the constant temperature for at least 10 minutes, before every fresh determination.

RESULTS

Specific heats of Kusum shellac of fresh and heat-hardened samples were measured and are tabulated in the Table I. Lac is polymerised after a few years of storage, and is rather useless for many purposes There are a number of prescribed tests to judge the quality of lac. However, the measurement of specific heat of a sample can enable us to estimate its age from the difference between its specific heat and that of the fresh sample at that temperature.

TABLE 1.

Temperature in °C	Specific heat of Lac Fresh	Heat hardened	Temperature in °C	Fresh	Specific heat of Lac Heat hardened
20–25	.33		65–70	.66	.53
25–30	.34	.30	70–75	.71	.53
30–35	.39	.32	75–80	.65	.53
35–40	.40	.34	80–85	58	
40–45	.45	.37	85–90	.57	
45–50	.54	.45	90–95	.57	
50–55	.57	.47	95–100	.57	
55–60	.64	.47	100–105	.57	
60–65	.62	.53	105–110	.56	

It may be noted that the specific heat varies very slowly in the range 20°C to 40°C, rising gradually from 0.33 to 0.40, while after this temperature it rises very rapidly, attaining a maximum value of 0.71 at 75°C. After 75°C it falls abruptly to a value of 0.58 at 85°C, and remains more or less constant upto 110°C, which is the maximum of the range. Bhattacharya (1940) has attributed the rapid rise to a continuousrate of fusion. Such a variation of specific heat for lac is due to its being a complicated mixture of various complex

organic substances of which little is known. However, lac has been separated in three portions hard and soft resins, and the lac wax, by physical means. These three fractions themselves contain innumerable complex organic substances. Thus from the variation of the specific heat it appears that as the temperature is raised, more and more constituents of lac begin melting resulting in an abnormal rise in the specific heat of lac. The maximum value of specific heat at 75°C and the abrupt fall in its value after this temperature indicate that maximum fraction of lac melts at 75°C, and the constancy in specific heat after this indicates that no more of the lac melts till the maximum range of measurement. Hence 75°C is taken to be the melting point of lac.

ACKNOWLEDGMENTS

The author is thankful to Dr. S. V. Puntambekar, Director, Indian Lac Research Institute, for his guidance, and to Dr. Yatendra P. Varshni, for his useful suggestions throughout the progress of the work.

REFERENCES

Bhattacharya, G. N., 1940, *Ind. J. Phys.*, **14**, 415.
Sen, 1938-39, I. L. R. I. Ann. Repts.

Letters to the Editor

The Board of Editors will not hold itself responsible for opinions expressed in the letters, published in this section. The notes containing reports of new work communicated for this section should not contain many figures and should not exceed 500 words in length. The contributions must reach the Assistant Editor not later than the 15th of the second month preceding that of the issue in which the Letter is to appear. No proof will be sent to the authors.

9

ON THE MAGNETIC SUSCEPTIBILITY AND ANISOTROPY OF V^{3+} UNDER A CRYSTALLINE ELECTRIC FIELD HAVING PREDOMINANTLY CUBIC SYMMETRY WITH A SMALL TRIGONAL COMPONENT

A. S. CHAKRABORTY

DEPARTMENT OF MAGNETISM, INDIAN ASSOCIATION FOR THE CULTIVATION OF SCIENCE
CALCUTTA-32

(*Received for publication, June* 26, 1958)

The equation for magnetic susceptibility of vanadium ammonium alum in a crystalline electric field of predominantly cubic symmetry with a small trigonal distortion has been deduced by Siegert, (1937) assuming a breakdown of the Russel-Saunders (ll) coupling and neglecting the effect of admixtures from the higher orbital levels Γ_5, Γ_2 and ^3P configuration. It is found that though this expression fits well with the experimental mean values of susceptibility of vanadium ammonium alum in liquid hydrogen and helium temperature range, there is appreciable deviation in liquid air to room temperature range It is very probable that in these V^{3+} salts the binding is only partially covalent in nature (Owen, 1955) and though the spin-orbit coupling has broken down, the R–S (ll) coupling is not (Van Vleck, 1939). Further the admixtures from upper levels may not be quite neglgible as has been shown by Abragam and Pryce (1951).

We have, therefore, deduced the expression for mean gm. ionic susceptibility using Abragam and Pryces' Hamiltonian and the wave functions. The expression for susceptibility is

$$K = \frac{8NB^2}{3k} \frac{\frac{1}{T}\left[A+B\,\mathrm{Exp}\left(-\frac{402}{T}\right)+C\,\mathrm{Exp}\left(-\frac{602.6}{T}\right)\right]+E\left\{\mathrm{Exp}\left(\frac{D}{kT}\right)-1\right\}}{2+\mathrm{Exp}\left(\frac{6.9}{T}\right)+2\,\mathrm{Exp}\left(-\frac{402}{T}\right)+2\,\mathrm{Exp}\left(-\frac{602.6}{T}\right)} + K_c \quad \ldots (1)$$

where, $K_0 = 200.5 \times 10^{-6}$, $A = 0.9313$, $B = 0.8438$, $C = 2.078$, $E = 0.2377$ and $D/K = 6.9$, obtained with the trial value of Δ (the trigonal field orbital splitting) $= -400$ cm^{-1}, the effective Lande factors $\alpha = 1.25$ and $\alpha' = 0.60$ and λ (the spin-orbit coupling constant) $= 104$ cm^{-1}, as a result of which we obtain

$$g_{\parallel} = 1.93$$

$$g_{\perp} = 1.82$$

and $$D = 4.8 \text{ cm}^{-1}$$

N = number of magnetic ions per gram molecule

β = Bohr magneton

k = Boltzmann factor

Since in these alums there are four trigonally distorted clusters arranged in cubic symmetry in the unit cell (Pa 3), the crystal does not show any anisotropy and the experimental mean susceptibility of the crystal, which is the same as that of the ion, is all that we can compare with the theory.

In recent years Dutta-Roy (unpublished) has very carefully measured the value of K for vanadium ammonium and potassium alums in the range 300°K to 100°K using sensitive techniques developed in this laboratory (Dutta-Roy, 1956). These are in general agreement with the results of van den Handel and Siegert in the same range but with some small deviations the nature of which will be discussed in a separate paper by Dutta-Roy.

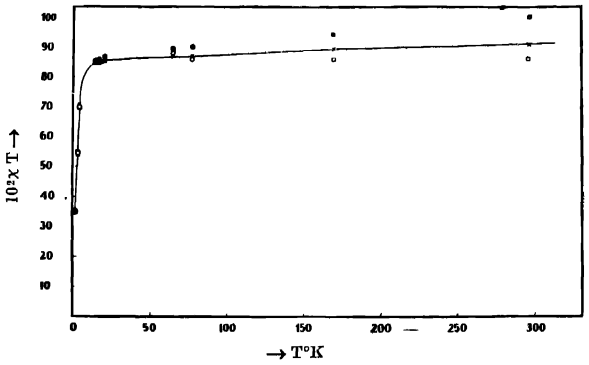

Fig. 1. Variation of moment ($10^2\chi$ T) with temperature for vanadium ammonium alum.

O Shows our theoritical values
X ,, the experimental ,,
● ,, Siegert's theoretical values.

A curve for 10^2KT against T is plotted in figure 1 and compared with the experimental values. It will be seen that the agreement is on the whole very satisfactory in the low temperature region (liq. He and H_2) and is also quite good in the liquid air range.

It is found that the "crystalline spectroscopic splitting factors" $g_{\|} = 1.93$ and $g_{\perp} = 1.82$ so that the anisotropy of the $[V(H_2O)_6]^{3+}$-complex may be small. The anisotropy will, however, also depend to appreciable extent on the large spin separation $D = 4.80$ cm^{-1}. The Van Vleck high frequency term in equation (1) $= 0.42 \times 10^{-6}$ for the above quoted values of α, α', Δ and λ, in good agreement with Van Vleck's estimated 0.3×10^{-6}

The value of the parameter α' appears to be too low perhaps due to the inclusion of the covalency factor in these parameters. Perhaps a somewhat better reasonable fit might be obtained by adjusting the parameters further, but this may not be very fruitful in the absence of experimental justification for the chosen values of α, α', Δ, $g_{\|}$, $g_{\perp}$ and D from measurements on absorption spectra and paramagnetic resonance which is not yet available. Thus these coefficients are to some extent arbitrary, though generally reasonable from the theoretical and experimental investigations on other salts of the iron group of elements. The fact that these parameters may also change with temperature (Bose *et al.*, 1957 and 1958 ; Dutta-Roy, 1956) makes the situation further complicated. These facts will be discussed soon in details in a further paper.

ACKNOWLEDGMENTS

The author's most sincere thanks are due to Prof A Bose, D.Sc., F.N I. for suggesting the problem and for his constant advice and encouragement during the progress of this work and to S. K. Dutta-Roy for making his excellent data on V^{+3} alums available. My sincere thanks are also due to Dr. D. K. Roy of the Institute of Nuclear Physics, Calcutta, for his many valuable suggestions and stimulating discussions in developing the paper and Miss G. Bhowmik for her help in calculations.

REFERENCES

Abragam, A. and Pryce, M. H. L, 1957, *Proc. Roy. Soc.*, *A*205, 135,
Abragam, A. and Pryce, M. H. L., 1951, *Proc. Roy. Soc.*, *A*, **206**, 164.
Bose, A., Mitra, S. C. and Dutta, S. K., 1957, *Proc. Roy. Soc. A*, **239**, 165.
Bose, A., Mitra, S. C., and Dutta, S. K., 1958, *Proc. Roy. Soc. A*, (incourse of publication
Dutta Roy, S. K., 1956, *Ind. Jour. Phys.*, **30**, 169.
Handel, van den and Siegert, 1937, *Physica*, **4**, 871.
Owen, J., 1953, *Proc. Roy. Soc.*, *A*228, 183.
Siegert, A., 1937, *Physica*, **4**, 138.
Van Vleck, J. H., 1939, *Jour. Chem. Phys.*, **7**, 61.

BOOK REVIEW

INTRODUCTION TO PHYSICAL CHEMISTRY. VOL. 1.

by Prof. S. N. Mukherjee, D. Sc.

Published by : Art Union Printing Press, Price 11/-

This is a useful book for the undergraduate students of the Indian Universities. The present book covers the syllabus of the 1st year Honours course in the three-year Honours course. The topics in this volume are mainly represented by the properties of gases, liquids and solids and thermodynamics.

Utilizing his rich experience as a teacher, the author has developed the topics in a clear and logical manner, elaborating the fundamental principles in a lucid style. He has taken meticulous care in presenting the basic concepts of physical chemistry and their applications to various physico-chemical phenomena. The book would be suitable as a text book not only to the degree students but also to a great measure to the post graduate students of Indian Universities.

Some typograpical and other mistakes have crept into this book and it is hoped that the author would take cognizance of such matters in the second edition of this book.

S. R. P

INFRA-RED ABSORPTION SPECTRA OF SOLUTIONS OF ETHYLENE DICHLORIDE IN CERTAIN SOLVENTS*

MONOMOHAN MAZUMDER

OPTICS DEPARTMENT, INDIAN ASSOCIATION FOR THE CULTIVATION OF SCIENCE, JADAVPUR, CALCUTTA-32

(*Received for publication July* 18, 1958)

ABSTRACT. The infra-red absorption spectra of pure ethylene dichloride and of its solutions in carbon tetrachloride, methyl cyclohexane and heptane of different concentrations recorded with a Perkin-Elmer Model 21 spectrophotometer have been compared with each other. The integrated intensities of the absorption peaks 1297 cm^{-1} and 1236 cm^{-1} have been measured in each case and it is observed that in the case of 20% solutions in heptane and methyl cyclohexane the ratio A_{1297}/A_{1236} is less than that for the pure liquid and that the ratio diminishes by about 50% when the strength of the solution is diminished to 3%. In the case of solutions in CCl_4 the changes in the ratio mentioned above are much smaller.

The spectra due to 5% solution of $C_2H_4Cl_2$ in heptane were recorded with the solution at 27°C and 70°C and it was observed that the ratio is slightly smaller at higher temperature than at the room temperature.

It is pointed out that such changes in the ratio A_{1297}/A_{1236} are in complete disagreement with those expected from the energy-difference of the two types of molecules in the solution calculated by previous workers. It is concluded that the results can be explained on the assumption that formation of virtual H–Cl linkages in the liquids is responsible for the origin of the gauche molecules.

INTRODUCTION

The existence of rotational isomers in the liquid state of some substituted ethane compounds was first demonstrated by Mizushima and Morino (1938). From the values of dielectric constant of gaseous ethylene dichloride Watanabe *et al.* (1942) found the difference of energy between the trans and gauche configurations of the molecule to be 1.22 KCal/mole, and taking into account the respective partition functions and also the two alternative configurations of the gauche molecule, they calculated the ratio of the number of gauche and trans molecules and found it to be 0.34 : 1 in the vapour state at the boiling point of the liquid. By comparing the intensities of the Raman lines 666 cm^{-1} and 768 cm^{-1} both in the case of vapour state and also for the liquid state they concluded that the value of the ratio of gauche and trans molecules in the liquid state is 1.3 : 1. Watanabe *et al.* (1943) tried to explain this change in the ratio of population of the two types of molecules with change of state by assuming

* Communicated by Prof. S. C. Sirkar.

that in the liquid state the gauche molecule acquires an excess of electrostatic energy which is equal to $-\left(\frac{\epsilon-1}{2\epsilon+1}\right)\frac{\mu^2}{a^3}$, where ϵ is the dielectric constant of the liquid, μ the permanent electric moment of the gauche molecule and a is its radius assuming the molecule to be a sphere. They showed that the influence of this electrostatic energy would diminish the energy-difference of the two types of molecules to a very small value in the liquid state. Actually, from the temperature-dependence of the ratio of intensities of the lines mentioned above they concluded that the electrostatic energy of the gauche molecules in the liquid state explains the observed change in energy-difference.

From the results of measurements of the infra-red absorption bands 1235 cm^{-1} and 1291 cm^{-1} of ethylene dichloride in the vapour state at different temperatures Bernstein (1949) concluded that the ratio (N_g/N_t) of the gauche (C_2) and trans (C_{2h}) molecules increases at higher temperatures indicating an energy-difference of about 1140 cal/mole between the two configurations. The value of N_g/N_t at 424.4°K was found by him to be 0.574, while from the ratio of the intensities of the Raman lines 666 cm^{-1} and 768 cm^{-1} in the vapour state at 443°K Watanabe *et al* (1943) found the value of N_g/N_t to be 0.47. The present author (1953) also measured the ratio of the intensities of the two Raman lines due to ethylene dichloride at 135°C and found it to be 1 · 4.5. When these results were compared with those published by Watanabe *et al* (1943), the change in the ratio of intensity of the two lines mentioned above with change of temperature of the vapour indicated very small energy-difference of the two types of molecules. Thus these results are at variance with each other.

Rank, Kagarise and Axford (1949) found the value of energy-difference of the two types of molecules in the liquid state to be almost zero. This would lead to a value of N_g/N_t equal to 1.90 according to Watanabe *et al* (1942). Actually, however, with the value of the energy-difference deduced from the dielectric measurements and from the ratio of intensities of the Raman lines 666 cm^{-1} and 768 cm^{-1} of ethylene dichloride in the vapour and liquid states, they got the value 1.3 · 1 for N_g/N_t in the liquid state. So the value of N_g/N_t found out by Watanabe *et al* is not in agreement with the value of energy-difference in the liquid state reported by Rank *et al.*

It was suggested earlier by Bishui (1948) that the gauche type of molecule of ethylene dichloride in the liquid state might be produced by association of the neighbouring molecules. Kuratani (1952), however, studied the infra-red absorption bands of ethylene dichloride in solution in a few solvents and measured the intensity-ratio of the absorption bands 1284 cm^{-1} and 1230 cm^{-1} and found that the ratio did not change with the change of concentration of the solution. From these results he concluded that the band 1284 cm^{-1} was not produced by associated molecules as suggested by Bishui (1948). Later, Banerjee (1954)

measured the intensities of the Raman lines 654 cm^{-1} and 755 cm^{-1} of ethylene dichloride dissolved in more suitable solvents such as heptane and cyclohexane with different concentrations ranging from 35% to 65% and found that the ratio of intensities of the two lines diminishes with the diminution of concentration of the solutions. From these results he concluded that when suitable solvents are used some of the associated groups which produce the gauche type of molecule break up into single molecules and the number of gauche molecules is thus reduced at higher dilutions.

Kuratani (1952) measured the ratio of intensities of the infra-red absorption bands 1284 cm^{-1} and 1230 cm^{-1} of the solutions of ethylene dichloride in benzene, CCl_4, CS_2 and acetonitrile of different concentrations. If, however, the ratio of the intensities of the same infra-red absorption bands were measured for the solutions in some other suitable solvents the results might show more conclusively whether the ratio of the intensity of the bands due to the two types of molecules changes with concentration or not. For this reason, the investigation of the ratio of intensities of the infra-red absorption bands of solutions of ethylene dichloride of different concentrations in heptane, methyl cyclohexane and CCl_4 was undertaken and the results have been discussed in the present paper. The solvents heptane and methyl cyclohexane were chosen to find out whether at concentrations lower than those used by Banerjee (1954) any remarkable changes occur in the ratio N_g/N_t.

EXPERIMENTAL

Chemically pure ethylene dichloride obtained from E. Merck was dehydrated and fractionated and the fraction boiling at 83.7°C was collected and redistilled under reduced pressure. The liquids heptane, methyl cyclohexane and carbon tetrachloride were also of chemically pure quality and were distilled several times in vacuum before being used as solvents.

The strengths of the solutions in heptane and methyl cyclohexane were 3%, 10% and 20% and in CCl_4 3% and 15%.

The infra-red spectra were recorded with a Perkin-Elmer Model 21 spectrophotometer with a sodium chloride prism. The resolution dial was placed at about 916. The absorption bands due to solvents were compensated by using suitable compensation cells in the reference beam. The thickness of the cell was 0.1 mm in the case of dilute solutions and 0.025 mm in the case of concentrated solutions. The spectra due to pure liquids were recorded by using very thin films formed between two plane parallel sodium chloride plates.

In order to find out whether the ratio of the intensities of the bands 1236 cm^{-1} and 1297 cm^{-1} of ethylene dichloride solutions changes with change of temperature of the solution the spectrum due to 5% solution in heptane at 70°C was recorded and compared with that recorded for the solution at 27°C.

RESULTS AND DISCUSSION

The values of A_{1297}/A_{1236} of pure ethylene dichloride and its solutions in carbon tetrachloride and methyl cyclohexane at 27°C and in heptane at 27°C and 70°C are given in Table 1. The absorption curves due to the pure liquid, 15% and 3% solutions in CCl_4, and 20%, 10% and 3% solutions in methyl cyclohexane and heptane are reproduced in figures 1, 2, 3 and 4 respectively. Figure 5 shows the absorption curves due to 5% solution of ethylene dichloride in heptane at 27°C and 70°C.

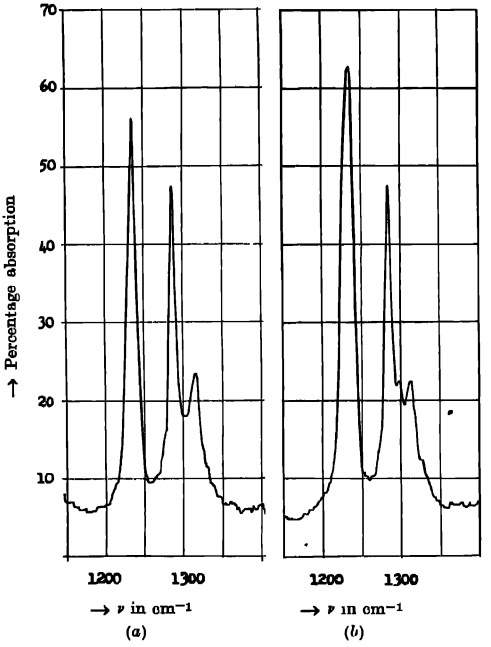

Fig. 1. Infra-red absorption curves of pure ethylene dichloride.
(*a*) Thin film of the liquid. (*b*) Thin film under slight pressure.

In the case of pure liquid it was found that the band 1297 cm^{-1} split up into three components in some cases and into two components in other cases, the three components appearing only when the cell was extremely thin and the liquid film was under slight pressure and two components in the case of thicker films or solutions. When the ratio of the integrated intensities of all the components of the band 1297 cm^{-1} to that of the band at 1236 cm^{-1} was calculated, it was found to be identical in both the cases. Apparently, however, the com-

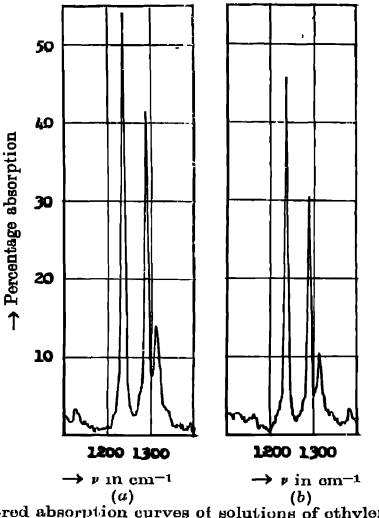

Fig. 2. Infra-red absorption curves of solutions of ethylene dichloride in carbon tetrachloride.
(*a*) 15% solution in 0.025 mm cell. (*b*) 3% solution in 0.1 mm cell.

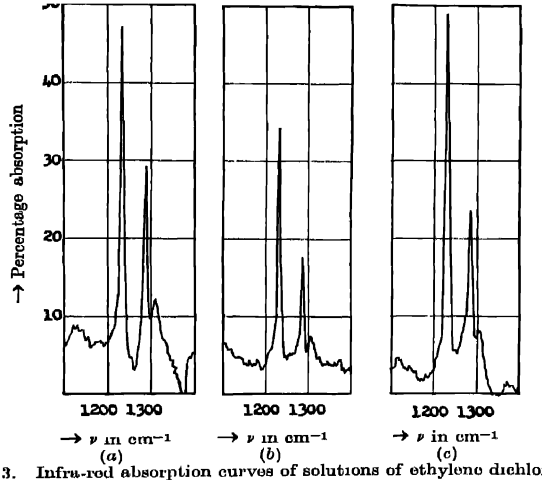

Fig. 3. Infra-red absorption curves of solutions of ethylene dichloride in methyl cyclohexane.
(*a*) 20% solution in 0 025 mm coll.
(*b*) 10% ,, ,, ,, ,,
(*c*) 3% ,, ,, 0.1 mm ,,

ponent at 1286 cm^{-1} was found to be relatively stronger when the band 1297 cm^{-1} was split up into two components. The bands observed in both the cases are reproduced in figures 1(a) and 1(b). In calculating the relative intensities of the two bands the integrated intensity of both the components of the band 1297 cm^{-1} was taken into consideration.

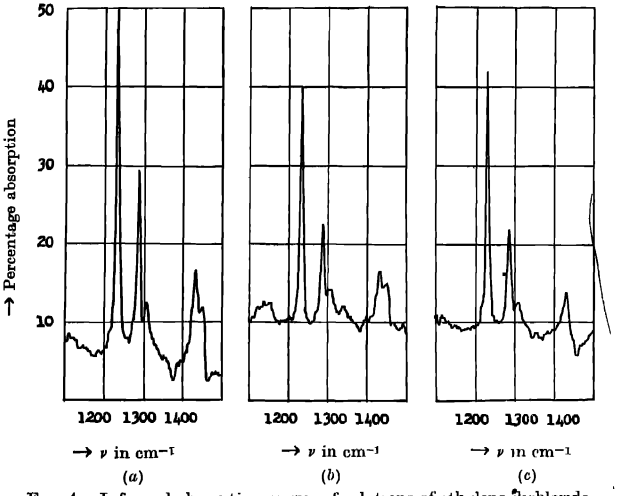

Fig. 4. Infra-red absorption curves of solutions of ethylene dichloride in heptane.

(a) 20% solution in 0 025 mm cell.
(b) 10% ,, ,, 9 025 mm ,,
(c) 3% ,, ,, 0.1 mm ,,

It can be seen from Table I that the ratio A_{1297}/A_{1236} changes very slightly when ethylene dichloride is dissolved in CCl_4 to make a 15% solution and that the ratio diminishes again very slightly when the solution is diluted to 3%. The ratio, however, changes more markedly when the liquid is dissolved either in heptane or in methyl cyclohexane even to make a 20% solution and when the solutions are diluted the ratio diminishes still further. For example, the ratio changes from 0.833 to 0.526 when pure liquid is dissolved in heptane to make a 20% solution, and the ratio is reduced to 0.357 when the strength of the solution is changed to 3%. In the cases of solutions in methyl cyclohexane also similar results are observed.

In order to understand the significance of these results it would be interesting to compare them with those expected from the values of energy-difference calculated by Wada (1954) taking into consideration the influence of different

TABLE I

Ratio of integrated absorption at the bands 1297 cm^{-1} and 1236 cm^{-1}

Solvent	Strength of solution	Temperature	A_{1297}/A_{1236}
Pure $C_2H_4Cl_2$	100%	27°C	0.833
CCl_4	3%	,,	0.645
	15%	,,	0.733
Heptane	3%	,,	0.357
	10%	,,	0.400
	20%	,,	0.526
	5%	,,	0.36
	5%	70°C	0.32
Methyl cyclohexane	3%	27°C	0 384
	10%	,,	0.476
	20%	,,	0 58

solvents on the energy-difference. He has shown that if 1270 cal/mole be taken as the energy-difference between the two types of molecules in gaseous state the value should be reduced to zero in the pure liquid. Actually also, from the measurement of temperature-dependence of the relative intensities of the Raman lines 654 cm^{-1} and 755 cm^{-1} of ethylene dichloride it has been concluded by Rank *et al* (1949) that the energy-difference in the liquid state is zero. There is, however, some difficulty about such a conclusion because the ratio N_g/N_t would be 1.9 · 1 when $\Delta E = 0$, but actually it is 1.3 : 1 as reported by Watanabe *et al* (1942). So, there is some discrepancy between the values of N_g/N_t calculated by Watanabe *et al* and that expected in the case of absence of any energy-difference (ΔE) between the two types of molecules.

In the case of solutions, the general nature of the change in ΔE due to the influence of solvent molecules calculated by Wada (1954) was shown to be in agreement with that observed experimentally by different workers. In the case of solution in CCl_4, however, the value of ΔE expected from his theory was about 790 cal/mole, but Kuratani (1952) observed the value to be 510 cal/mole. Again, the latter worker also reported that the ratio A_{1297}/A_{1236} did not change with the change of concentration of the solution, but in the present investigation it has been found that the ratio changes from 0.733 to 0.645 when the strength of the solution is changed from 15% to 3%. When there are large number of hydrogen atoms in the molecule of the solvent, such as heptane and methyl cyclohexane, the ratio mentioned above changes more rapidly with the

increase in dilution. It can be seen from Table I that the value of the ratio A_{1297}/A_{1236} for the 3% solution in heptane is even smaller than that observed in the case of ethylene dichloride vapour (Bernstein, 1949). These facts indicate that the ratio of population of the two types of molecules is not determined solely by the energy-difference, but there is some other cause which is responsible for the origin of the gauche molecules.

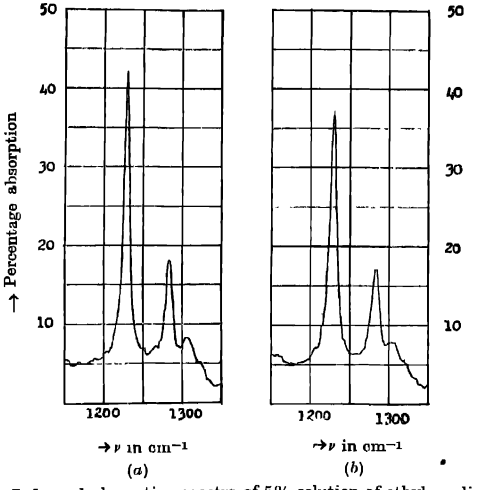

Fig. 5. Infra-red absorption spectra of 5% solution of ethylene dichloride in heptane at (*a*) 27°C and (*b*) 70°C.

In order to test the correctness of such a conclusion the temperature-dependence of the value of the ratio A_{1297}/A_{1236} in the case of 5% solution of ethylene dichloride in heptane was determined at two different temperatures of the liquid and the absorption curves reproduced in figure 5 show that the band 1236 cm^{-1} becomes a little broader at 70°C than that at 27°C. If the integrated intensities are taken into consideration the ratio mentioned above has the value 0.36 at 27°C but it diminishes to 0.32 when the temperature of the solution is raised to about 70°C. On the other hand, if the value of ΔE were 900 cal/mole as calculated by Wada (1954), the value of A_{1297}/A_{1236} would increase and become 0.378 with the rise of temperature of the solution from 27°C to 70°C. Thus it is quite evident that the energy-difference alone does not determine the relative population of the two types of molecules in the solution.

All the results mentioned above can be explained quite satisfactorily on the hypothesis that some virtual linkage between the Cl atoms of $C_2H_4Cl_2$ molecules of the H atoms of the solvent molecules is responsible for the origin of most

of the gauche molecules present in the solution. In pure liquid also there is possibility of formation of groups of such associated molecules and this may explain the discrepancy between the observed and calculated values of the relative populations of the two types of molecules in the liquid mentioned earlier. When CCl_4 is used as a solvent there is very little tendency of the Cl atoms of the solvent molecules to break up the Cl–H linkage formed in the associated groups of $C_2H_4Cl_2$ molecules. This explains why the value of A_{1297}/A_{1236} does not change very much when ethylene dichloride is dissolved in carbon tetrachloride and also explains the large discrepancy between the value of ΔE calculated by Wada (1954) on his theory and that observed by Kuratani (1952) for this particular solution. In the case of solutions in heptane and methyl cyclohexane on the other hand, the influence of H atoms on the Cl atoms of the $C_2H_4Cl_2$ molecules is so great that the value of the ratio N_g/N_t is even less than that for the vapour. This fact furnishes an additional evidence for the fact that association between neighbouring molecules is responsible for the preponderance of the gauche molecules in the pure liquid. The results of some recent investigations in the Raman spectra of ethylene dichloride, ethylene dibromide and ethyle chlorhydrin carried out in this laboratory have furnished further evidence in support of the conclusion mentioned above These results will be discussed in a separate paper.

ACKNOWLEDGMENTS

The author is indebted to Professor S. C. Sirkar, D.Sc., F.N.I. for kindly suggesting the problem and for his helpful guidance throughout the progress of the work.

REFERENCES

Banerjee, S. B., 1954, *Ind. J. Phys.*, **28**, 205.
Bernstein, H. J., 1949, *J. Chem. Phys.*, **17**, 258.
Bishui, B. M., 1948, *Ind. J. Phys.*, **22**, 253.
Kuratani, K., 1952, *Rept. Inst. Sci. and Technol. Univ. Tokyo*, **6**, 221.
Mazumder, M., 1953, *Ind. J. Phys.*, **27**, 406.
Mizushima, S. and Morino, Y., 1938, *Proc. Ind. Acad. Sc.*, **A8**, 316.
Rank, D. H., Kagarise, R. E. and Axford, D. W., 1949, *J. Chem. Phys.*, **17**, 1354.
Wada, A., 1954, *J. Chem. Phys.*, **22**, 198.
Watanabe, I., Mizushima, S. and Morino, Y., 1942, *Sc. Pap. I. P. C. R.* (Tokyo), **39**, 401.
Watanabe, I., Mizushima, S. and Masiko, Y., 1943, *Sc. Pap. I. P. C. R.* (Tokyo), **40**, 425.

CRYSTAL STRUCTURE OF FROZEN CYCLOHEXANE AT −180°C*

G. S. R. KRISHNA MURTI

OPTICS DEPARTMENT, INDIAN ASSOCIATION FOR THE CULTIVATION OF SCIENCE, CALCUTTA-32

(*Received for publication, July* 22, 1958)

Plate XI

ABSTRACT. The Debye-Scherrer patterns of frozen cyclohexane at −5°C and at −180°C have been photographed and analysed. It has been found that the crystal at −5°C is cubic with the edge of the unit cell $a=8$ 80 A.U. At −180°C the crystal has been found to be monoclinic with the unit cell dimensions as $a=8.82$ A.U., $b=9$ 84 A.U., $c=15.90$ A.U. and $\beta=109°$. The density of cyclohexane at −180°C has been measured and the number of asymmetric molecules in the unit cell has been found to be 8. The space group C_h^3 has been assigned to the crystal.

INTRODUCTION

The crystal structure of cyclohexane was first studied by Hassel and Kringstad (1930) who found the crystal to belong to the cubic system with unit cell dimensions $a = 8.43$ A.U. They studied the Debye-Scherrer pattern of the substance at −80°C, by freezing the liquid with solid CO_2-acetone mixture. The crystal structure of the substance was re-examined by Hassel and Sommerfeldt (1938) at −8°C and −40°C and they also found the crystal to be cubic with $a = 8.76$ A.U. at both the temperatures. They further tried to determine the space group and concluded that the space group might be T_d^1. Lonsdale and Smith (1939) studied the crystal structure of the substance at −180°C and reported that the powder pattern obtained by them did not correspond to any one of cubic, tetragonal or hexagonal lattices. They further pointed out that the crystal might have a low temperature modification of low symmetry or at that particular temperature two crystalline forms might have been present simultaneously. They used the results of the investigation by Hassel and Kringstad (1930) to find out the space group of the crystal at −80°C and concluded that the space group might be either T_h^2 or O_h^4.

The structure of the crystal of cyclohexane at −180°C was therefore not known. An attempt has been made to study the Debye-Scherrer pattern of the crystal at −180°C and to compare it with that due to the crystal at −5°C in

* Communicated by Prof. S. C. Sirkar.

order to find the space group to which the crystal at –180°C belongs. As shown below it has been found that the crystal at –180°C belongs to monoclinic system and the space group has also been determined.

TABLE I

Spacings of cyclohexane

Cubic form			Monoclinic form at –180°C		
Indices	Observed at –5°C	From the data of Hassel and Sommerfeldt (1938) at –40°C observed	Indices	Observed	Calculated from the proposed structure
111	5 08 (s)	5 06 (vs)	111	5 39 (ms)	5 39
			020	4 92 (vs)	4.92
			113	4.54 (w)	4.54
200	4.40 (m)	4.37 (vs)	200	4.17 (m)	4 17
210		3 93 (vw)	104	3.92 (vs)	3 94
211		3.62 (w)	004	3.76 (m)	3.76
			122, 211	3 46 (w)	3.46
220		3 14 (vw)	202, 222	3 22 (w)	3.22
			124, 104	3.09 (vw)	3.08
300, 221		2.93 (ms)	$30\bar{2}$	2 94 (vw)	2.94
310		2.82 (vw)	300	2 77 (m)	2.78
311	2 65 (vw)	2 65 (vw)	$10\bar{6}$	2 66 (m)	2 655
222		2.54 (w)	006	2 515 (w)	2.51
321		2.30 (vw)	040	2.45 (m)	2.46
400		2.23 (w)	404	2 15 (w)	2 15
411, 330		2.09 (w)	044	2 06 (m)	2.06
421		1.93 (vw)	051, $40\bar{6}$	1.94 (w)	1.94
			308	1 87 (w)	1.87
			340	1.84 (vw)	1 84
			060	1.64 (m)	1.64
			128	1 62 (vw)	1.62
			520	1.57 (vw)	1.58
			$30\bar{10}$, $43\bar{9}$	1.55 (vw)	1.55
			048	1.495 (w)	1.495
			453, 228	1.47 (vw)	1.464, 1.468

EXPERIMENTAL

Pure cyclohexane, distilled under low pressure, was used in obtaining the Debye-Schorrer patterns of the crystal. The photographs at −180°C were taken by the method described earlier (Krishna Murti and Sen, 1956) with the camera of special design (Biswas, 1958). The Dewar vessel was modified so as to allow only the liquid oxygen vapour to pass on the specimen in order to record the pattern at a temperature just below 0°C and the temperature obtained in this way was −5°C as shown by a thermometer.

A Seifert X-ray tube running at 32 KV, 26 ma. was used to photograph the patterns. The X-ray tube was provided with a copper target and a nickel filter was used to cut off the Kβ radiation. An exposure of about 3.5 hours was sufficient to record the patterns with moderate densities. The radius of the camera was measured by photographing a Debye-Scherrer pattern due to aluminium powder and was found to be 4.5 cms.

RESULTS AND DISCUSSION

The photographs of the Debye-Scherrer patterns obtained at different temperatures are reproduced in Plate XI. The spacings calculated from the Debye-Scherrer patterns of cyclohexane at different temperatures are given in Table I. The intensities of different rings in the patterns estimated visually are given along with the spacings as very strong (vs), strong (s), medium (m), weak (w) and very weak (vw).

It is found that the spacings obtained for the crystal at −5°C correspond to those of a cubic crystal with the edge $a = 8.80$ A.U. This is in confirmity with the results reported by earlier authors.

It can be easily seen from the patterns reproduced in Plate XI that the crystal structure of the substance at −180°C is quite different from that at −5°C. Attempts were made to analyse the pattern by the methods of Hesse (1948) and Lipson (1949) and it was found that the pattern does not correspond to cubic, tetragonal, hexagonal or orthorhombic system. Since it appears to belong to a lower symmetry it was assumed that it might belong to monoclinic symmetry, as it is the next in order of symmetry. A trial and error method was used and as the crystal belongs to a cubic system at −5°C, it was assumed that a distortion is produced in the crystalline lattice.

The spacings 4.92 A.U., 4.17 A.U. and 3.76 A.U. have been assigned to the indices (020), (200) and (004) and the spacing 5.39 then agrees with that of the plane $(1\bar{1}1)$, if $\beta = 109°$. The unit cell dimensions of the crystal calculated with the above data are $a = 8.82$ A.U., $b = 9.84$ A.U., $c = 15.90$ A.U. and $\beta = 109°$. By trial the indices of all the planes giving the lines in the pattern have been found. It can be seen from Table I that it has been possible to

Indian Journal of Physics, Vol. XXXII, No. 10.

(a)

(b)

Debye-Scherrer patterns of solid cyclohexane

(a) Crystals at $-5°C$

(b) ,, ,, $-180°C$

assign indices to all the spacings and that the observed and calculated spacings agree closely with each other.

The density of frozen cyclohexane at −180°C was measured by the method used earlier in this laboratory (Biswas and Sirkar, 1957) and was found to be 0.8561. The number of molecules in the unit cell was calculated using this value of density and it was found to be 8. It can be seen from Table I that all the (hkl) spacings with (k+1) odd are absent. So the space group C_s^3 is ascribed to the crystal.

Hence it can be concluded that the crystal is cubic at −5°C but it has a low-temperature modification of lower symmetry at −180°C, the lattice at −180°C being monoclinic and the space group C_s^3.

ACKNOWLEDGMENT

The author is indebted to Professor S. C. Sirkar, D.Sc., F.N.I., for his kind interest and guidance during the progress of the work.

REFERENCES

Biswas, S. G., 1958, *Ind. J. Phys.*, **32**, 13.
Biswas, S. G. and Sirkar, S. C., 1957, *Ind. J. Phys.*, **31**, 141.
Hassel, O. and Kringstad, H., 1930, *Tidsskr. Kjemi. og. Bergv.*, **10**, 128.
Hassel, O. and Sommerfeldt, A. M., 1938, *Zeit. f. Phys. Chem.*, **B40**, 391.
Hesse, R., 1948, *Acta, Cryst.*, **1**, 200.
Krishna Murti, G. S. R. and Sen, S. N., 1956, *Ind. J. Phys.*, **30**, 242.
Lipson, H., 1949, *Acta. Cryst.*, **2**, 109.
Lonsdale, K. and Smith, H., 1939, *Phil Mag.*, **28**, 614.

A COMPACT INSTRUMENT FOR THE MEASUREMENT OF SURFACE TENSION OF LIQUIDS

P. D. PATHAK AND R. M. PATEL

M. G. SCIENCE INSTITUTE, AHMEDABAD

(*Received for publication, January* 8, 1958)

ABSTRACT. An instrument for the measurement of surface tension of liquids by a null method is described. The method of balancing the downward force of surface tension on the edge of a thin glass plate by the upward hydrostatic pressure of the liquid is used. The instrument is quite compact, handy and sensitive and can be used for rapid measurement on a number of samples.

INTRODUCTION

Except perhaps du Nouy's tensiometer, compact instruments for the measurement of surface tension are not available. Invariably it is required to assemble a number of loose pieces and it is difficult to obtain accurate results unless extreme care is taken in their manipulation.

Meier (1949) has described a method on which the present instrument is based. He balanced the downward pull due to surface tension on a vertical wire immersed in water by the upthrust of water. Vankataraman (1955) has investigated the scope of the method in detail and found that it is capable of giving results with an accuracy of less than 0.1%. It was thought desirable, therefore, to devise a compact instrument, which should have an advantage of sensitivity, accuracy and rapidity.

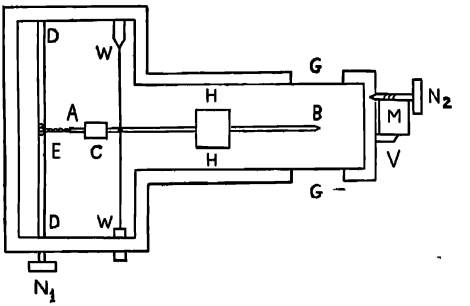

Fig. 1

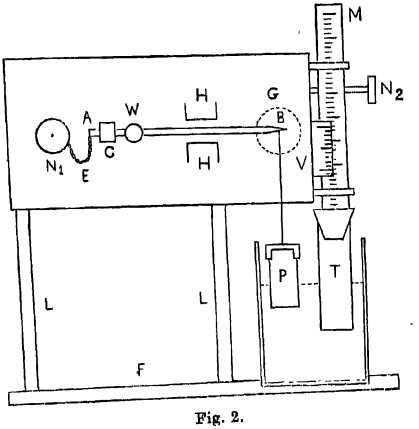

Fig. 2.

DESCRIPTION OF THE INSTRUMENT

The instrument is described in figures 1 and 2. *WW* is the torsion wire. *AB* is the torsion arm fixed at the centre of the wire. The glass plate *P* is suspended from the end *B*. *C* is the compensating weight.

Since the instrument is generally kept closed to avoid disturbances due to draught, etc., it was inconvenient to adjust the weight *C* every time to restore the horizontality of the torsion arm A light metal chain *E* was wound on the rod *DD* and its other end was attached to the end *A* of the torsion arm. By turning the knob N_1, the chain could be wound or unwound, thus decreasing or increasing a slight weight on the end *A*. The supports *HH* are fixed in the box to allow the torsion arm to deflect in a restricted range. A rod *M* with a centimetre scale marked on it and a vernier *V* are attached at the end of the instrument. The vernier is fixed while the rod *M* can be moved up and down by the rack and pinion motion with the help of the knob N_2. A glass tube *T* with a flat bottom is attached to the rod *M* through a rubber cork as shown in figure 2. The whole assembly rests on the pillars *LL* fixed to the base *F*.

OPERATION OF THE INSTRUMENT

The glass plate *P* is suspended from the end *B* and the weight *C* adjusted to keep the arm nearly horizontal. (Once adjusted, this position of the weight is not to be disturbed so long as the glass plate is the same.) The knob N_1 is then rotated until the arm is exactly horizontal. The glass plates *GG* are put to illuminate the end *B*. Although we used a microscope to see the image of *B*, the observation could be taken without it. For this a small horizontal line is marked at the centre of each glass plate. The end *B* is observed from the side

and the knob N_1 is turned until the lines and the end B are one behind the other. The liquid is then poured in the beaker until its level is just near the lower edge of B. The glass tube is lowered by turning the knob N_2 so that the liquid level just touches the lower edge of P. This reading (H_1) on the scale M is noted. When the liquid level touches the plate, the latter is drawn downward by the force of surface tension. This force is balanced by the upthrust of the liquid by raising the level of the liquid sufficiently. This is done by lowering the glass tube T until the end B is restored to its original position. The reading (H_2) on the scale is again noted and the difference H_2–H_1 is found.

When the torsion arm is restored to its horizontal position, the forces of surface tension and upthrust are equal.

$$\therefore \quad \gamma \cdot 2\,(l+t) = \rho g h \cdot lt \qquad \ldots \quad (1)$$

where γ is the surface tension of the liquid, l the length of the edge of the glass plate in contact with water, t the thickness of the plate, ρ the density of the liquid and h the height through which the liquid level is raised.

The height h is connected with H $(= H_2 - H_1)$ by the relation

$$h\,[\,\pi\,(R^2 - r^2) - l \cdot t\,] = \pi\, r^2 H \qquad \ldots \quad (2)$$

where R = radius of the beaker and r = radius of the glass tube T.

$$\therefore \quad h = \frac{\pi\, r^2 H}{\pi\,(R^2 - r^2) - l \cdot t} \qquad \ldots \quad (3)$$

Substituting this value of h in eq. (1) we get

$$\gamma \cdot 2\,(l+t) = \frac{\rho\, g l t \cdot \pi\, r^2 H}{\pi\,(R^2 - r^2) - lt}$$

or

$$\gamma = \frac{\rho\, g\, l\, t \cdot \pi\, r^2 H}{2\,(l+t)\,[\,\pi\,(R^2 - r^2) - lt\,]} \qquad \ldots \quad (4)$$

The above equation can be written as

$$\gamma/\rho = C \cdot H \quad \text{for a given instrument} \qquad \ldots \quad (5)$$

where

$$C = \frac{\pi\, r^2 \cdot g\, l\, t}{2(l+t)\,[\,\pi\,(R^2 - r^2) - lt\,]}$$

Thus by drawing a graph of γ/ρ against H for different known liquids the constant C of the instrument can be determined. Such a graph drawn from observation on some known liquids like benzene, carbon disulphide, chloroform is shown in figure 3.

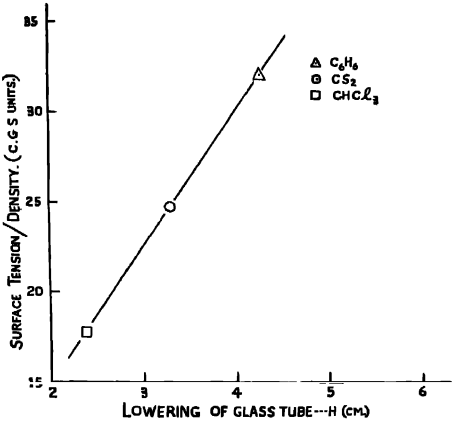

Fig. 3.

Typical observations on benzene are given below :

Temperature of the liquid = 26°C
Radius of the tube $T = r$ = 1.22 cms.
Radius of the beaker = R = 3.28 cms.
Mean $H_2 - H_1 = H$ = 4.280 cms.
Length of the plate = l = 1.550 cms.
Thickness of the plate = t = 0.101 cm.
Density of benzene = ρ = 0.875 gm./c.c.
g = 980 cm./Sec^2
Surface tension = γ = 28.08 ($\pm$ 0.088) dynes/cm. from equation (4).

The accuracy of our method (0.32%) may be compared with that obtained by Sugden (1921) with the capillary tube method where it is stated that the possible errors in the method may amount to 0.3%.

REFERENCES

Meier, F. A., 1949, *School Science Review*, **30**, 112.
Sugden, Samual, 1921, *Jour. Chem. Soc.*, **119**, 1483.
Venkataraman, S., 1955, *Ind. J. Phys.*, **29**, 522.

150 KV COCKCROFT-WALTON TYPE PARTICLE ACCELERATOR

C. S. KHURANA* AND H. S. HANS

PHYSICS DEPARTMENT, MUSLIM UNIVERSITY, ALIGARH

ABSTRACT. Details of the 150KV Cockcroft-Walton type particle accelerator, which has been constructed in this laboratory, are given. Use of radio-frequency ion-source, and 250KV isolation transformer for supplying voltage to the various circuits in the ion-source head, are its main features. A steady current of protons of more than 100 micro-amperes at the target has been obtained.

INTRODUCTION

A low voltage Cockcroft-Walton (C-W) type particle accelerator can be utilized excellently for the production of neutrons from the exothermic reactions viz., D (d, n) He^3 and D (t, n)He^4. This gives a cheap and copious source of monoenergetic neutrons of about 2.8 Mev and 14 Mev energy respectively from the two reactions. To start work in neutron reactions, we have constructed a C-W type accelerator in our laboratory, details of which are given below.

Figure 1 shows the block diagram of the C-W accelerator which is self explanatory.

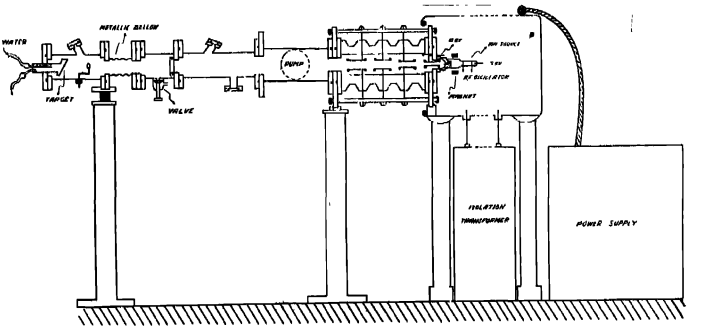

Fig. 1. Block diagram of the 150KV cockcroft-Walton type particle accelerator.

150KV POWER SUPPLY

For the generation of 150 KV, we have a Beta-electric company's power supply (Beta Electric Corp. New York, N.Y.) Model No. 2150-2R (2-5-1) which

* Junior Research Fellow, Ministry of Education, Government of India.

is based on a standard doubler circuit. Three transformers of 50KV each, in series, serve as the main high voltage transformers, and the two special X-ray tubes Eureka EV-3-75-T as the rectifier tubes. All the components of the high voltage power supply are placed inside a box 30″×30″×30″ filled with Burma Shell Diala-B oil. The high voltage can be varied from 0-150KV, with the help of a variac in the control panel, which is meant for operating the power supply from a distance.

Safety measures include the following ; (i) On over-voltage or over-load the high voltage is automatically removed, which can be put on again only if one starts from zero voltage. (2) Two inter-locks insure that no person can approach the high voltage side, without putting off the high voltage. (3) Spark-gaps inserted in the various points of the circuit, remove the momentary surges without damaging the main components. (4) When the high voltage is switched off, the high voltage point is automatically earthed.

ION SOURCE AND ASSOCIATED CIRCUITS

Our ion-source is essentially the same as that of Moak, Reese and Good (1951), the only difference being that the pyrex envelope of our ion-source is of a little bigger diameter than that of theirs. The ion-source base is connected through a palladium tube to a cylinder containing the gas to be used in the ion-source i e. dydrogen or deuterium. By controlling the temperature of the palladium tube, the flow of the gas to the ion-source is regulated,. A variable 24 volts A.C. transformer is used for this purpose. A 100MC oscillator of the same type as that of Moak, Reese and Good (1951) excites the discharge in the ion-source. A variable 1000 volts positive power supply provides the voltage to the oscillator. A variable positive voltage of 0-5000 volts is applied to the probe on the top of the ion-source to direct the positive ions towards the cathode. A coil of 2½″ internal diameter consisting of 1400 turns of no. 22 enamelled copper wire serves as the magnet. It serves the purpose of increasing the path length of electrons in the ion-source and hence intensifies the discharge. The current of this is supplied by a 50 volts 3 amperes power supply, using selenium rectifiers.

All the ion-source accessaries are placed inside an aluminium box 5′×3′×3′ with rounded exteriors. The output from the 150KV power supply is connected to the box through a special insulated cable. Since the whole box is at high voltage, it is essential to insulate the A.C. voltage supplied to the various circuits in the box. We have achieved this by a 2KW isolation transformer of 220 volts primary and 220 volts secondary with 250KV insulation between the primary and secondary. The isolation transformer placed in a container having nearly 80 gallons of Diala B oil is put just below the aluminium box. It was considered more advantageous to use this isolation transformer than the usual method of an A.C. generator in the box, driven by a motor below through an insulated

belt etc. In our case, we are saved of the jerks to the box and the accelerating column.

ACCELERATING COLUMN

The accelerating column consists of alternate conducting and insulating sections. The insulating sections are porcelain cylinders each of 2½″ length, 6″ internal diameter and of 2″ thickness. The two ends of the cylinders are ground flat. The remaining surface is glazed to ensure absence of porousness. The conducting sections are steel plates with holes in the centre, placed between these insulating cylinders. The joints are made vacuum-tight by a special cement i.e. Epibond (obtainable from Furnace Plastics, Los Angeles, California, U.S.A.)

The final accelerating column consists of 4 sections with an over-all length of 11 inches. The two extreme faces of the column were further joined to two circular steel plates of 18″ diameter, with a hole of 5½″ diameter. Three perspex rods were fixed between these plates at the periphery to increase the mechanical strength of the accelerating column.

The metal plates carry cylindrical electrodes at their centre. These electrodes, which can be fitted from out-side, shape the electric field along the tube axis, so as to accelerate and focus the charged particles, At the same time they are designed to shield the tube walls from the stray ions.

150KV is distributed over a chain of resistors of 1200 Meg ohms. The tapping after every 300 Meg. ohms is connected to the cylindrical electrodes inside the accelerating column.

The positive ion beam from the ion-source is extracted by placing an electrode just below the ion-source hole to which a negative voltage with respect to the cathode of the ion-source is applied. The negative voltage can be varied from 0 to 15KV. This electrode also serves as the main focussing electrode.

INSULATION

The box with ion-source accessaries weighing about 500 lbs is supported by four perspex pillars which also serve the purpose of insulating the box from the ground. As these pillars were not commercially available, four perspex sheets (obtainable from ICI) were joined together by perspex screws and were turned on a lathe to get circular pillars of 4″ diameter. Though the pillars are of 4 feet height, the nearest distance of the box from the electrical ground is one foot.

VACUUM SYSTEM

The vacuum in the whole system is maintained by an MCF-700 oil diffusion pump of capacity 650 lit/sec. with a backing Duo-Seal mechanical pump of capacity 380 lit/min. A freon gas cold trap just above the diffusion pump is used to cool

the oil vapours. Pressure of the order of 10^{-6} mm of mercury is maintained in the whole system. Even when satisfactory vacuum-tightness has been obtained, a high pumping speed has to be maintained, as the ions admitted for acceleration are always accompanied by neutral gas which would build up a pressure. An NRC type 501 thermocouple gauge and a 507 ionization gauge are included in the system just above the cold trap to measure the pressure.

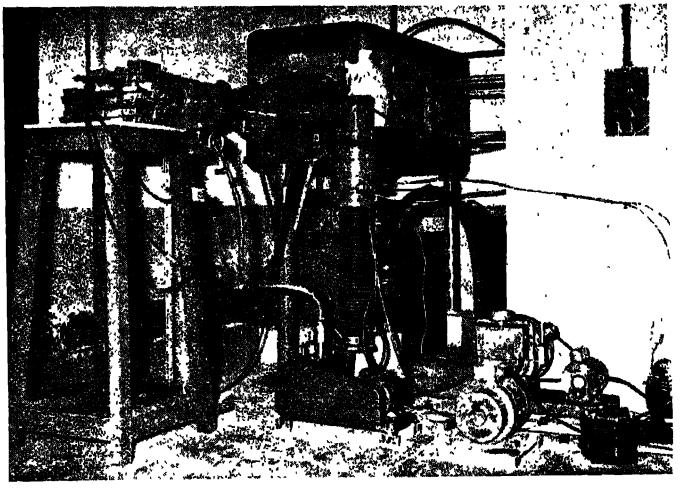

Fig. 2. A photograph of the 150KV Cockcroft-Walton type particle accelerator.

The various parts in the vacuum system after the accelerating column are (i) A 'T'-shaped copper tubing which connects the diffusion pump to the main vacuum system side. (2) A metallic system containing a vacuum-tight valve which by manual operation from out-side can separate the system on the acceleration column side from the target side. This portion also contains a second valve to let in air or pump the target side when necessary. (3) A metallic bellow to adjust target to bring the beam in the centre. (4) The target end which includes a quartz piece and a side window in front of the quartz to see the flourescence pattern of the beam when it falls on the quartz. The actual target is put on the end of this piece.

Whenever A.C. mains supply fails or at night when no body is attending the accelerator, a convertor run on the D.C. battery set, available in the laboratory, is used to keep the mechanical pump running. Also included in the diffusion pump heater-circuit is an automatic swith, so that if the water supply to the diffusion pump fails, the heater voltage should go off.

CONTROL ROOM

The voltage of the various power supplies inside the box containing ion-source accessaries are varied from the control room with the help of perspex rods. These rods are fixed to the variacs in the input of the power supplies on one side, and to the control knobs in the control room on the other side. By rotating these rods from the control room, the variacs can be adjusted to give the desired voltages in the power supplies. The control room also contains (1) : Control panel for 150KV power supply. (2) Ionization guage circuit to measure vacuum in the system. (3) Beam current integrator etc. (4) A telescope to read the various meters in the box, through a hole in the wall of the control room. (5) Detecting equipment.

OPERATION

The accelerator has been in operation for the last many months, using a proton beam. Beam current of protons of more than 100 micro-amperes has been obtained on the target, about 5 feet away from the ion-source. Beam can be kept steady continuously for many hours. No insulation breakdown troubles have been encountered.

ACKNOWLEDGMENTS

The authors are deeply indebted to Prof. P. S. Gill for his kind interest and continuous encouragement in the setting up of the accelerator. We also wish to acknowledge the active co-operation of the workshop personnel.

REFERENCE

Moak, C. D., Reese, H. Jr., and Good, W. M., 1951, Nucleonics, 9, 3, 18.

EVIDENCE FOR FORMATION OF MOLECULAR GROUPS IN LIQUIDS AT LOW TEMPERATURES*

G. S. KASTHA

OPTICS DEPARTMENT, INDIAN ASSOCIATION FOR THE CULTIVATION OF SCIENCE, CALCUTTA-32

(*Received for publication, July* 24, 1958)

ABSTRACT. The intensity-distribution in the wing accompanying the Rayleigh line scattered by pyridine, *a*-picoline, *o*-cresol, *o*-chlorophenol and *p*-xylene at temperatures near about the freezing points of the liquids has been studied by the method of photographic spectrophotometry and it has been compared with that observed at higher temperatures in each case. It has been found that in all the cases the intensity of the wing in the region from the centre of the Rayleigh line upto a distance of about 25 cm^{-1} decreases with the lowering of temperature and at the lower temperature there appear in the wing at distances beyond 45 cm^{-1} from the Rayleigh line additional intensities from new sources. The intensity of the wing beyond 45 cm^{-1} due to the liquid at low temperatures has been compared with the intensity of the low-frequency Raman lines observed in the region 45–137 cm^{-1} in the spectra due to the frozen liquids. It has been concluded that the additional intensity mentioned above may arise from vibration in groups of loosely attached molecules formed in the liquid near its freezing point and that the size of these groups and also the strength of the intermolecular bond in the groups increase with solidification of the liquid.

INTRODUCTION

The intensity-distribution in the wing accompaying the Rayleigh radiation scattered by various substances in gaseous and liquid states has been studied by many workers and different workers have put forward different hypotheses to explain the origin of the wing. Bhagavantam (1933) pointed out that most of the liquids cannot be treated as aggregates of freely rotating molecules and as such the theory developed in the case of gases does not apply to the liquids. From theoretical considerations he suggested that the intensity in the wing due to the liquids might arise from superposition of contributions from the partly gas-like and partly solid-like character of the liquid state. Gross and Vuks (1935), on the other hand, attributed the origin of the wing to vibrations of lattices in quasi-crystalline liquids analogous to those in the solid state. Later, Bhagavantam (1935) postulated that the hindered rotation of molecules pivoted in the lattice-like structure of the liquid was responsible for the occurrence of the wing. Rousset (1935), however, pointed out that for the amplitudes of hindered oscillations proposed

* Communicated by Prof. S. C. Sirkar.

by Bhagavantam (1935), the intensity of the wing for large frequency-shifts would be quite negligible and postulated the influence of formation of cybotactic groups in the liquid state on the rotational energy levels of the freely rotating molecules. He also considered the broadening of the exciting Rayleigh line due to the fluctuation of the intermolecular field caused by the impact of neighbouring molecules on the scattering centres as pointed out by Cabannes and Rocard (1929). Sirkar (1936) and Sirkar and Mookerjee (1936) made thorough investigations of the intensity-distributions in the wings due to some aliphatic and aromatic organic compounds in the liquid state and in sloutions and pointed out that the results obtained by them were not in complete agreement with the hypotheses put forward by the previous workers mentioned above. Sirkar and Mookerjee (1936) concluded that the intensity in a portion of the wing near the Rayleigh line might be produced by both rotational Raman scattering and broadening of Rayleigh line due to fluctuation of intermolecular field as pointed out by Cabannes and Rocard (1929), and the other portions of the wing might be due to vibrations of associated groups of molecules present in the liquid state. They also showed that the intensity in the wing depends on the anisotropy and nature of grouping of the molecules in the liquid state and that the major portion of the wing is in no way connected with the new Raman lines which are observed in the low-frequency region in the case of the solid state. Similar conclusions were also arrived at by Pniewski (1938a, b) from results of investigations on the wing due to carbon disulphide, chloroform and carbon tetrachloride. Gross and Raskin (1945) suggested that vibrations of molecules in the liquid analogous to those of the molecules in the lattice might give rise to the wing. Raskin (1948), however, concluded more recently from the results of investigations on the low-frequency Raman lines and the wing accompaying Rayleigh line due to phenol and diphenyl methane that the phenomenon of the wing cannot be treated as evidence of persistence of quasi-crystalline remnants in the liquid state.

The different hypotheses mentioned above do not seem to agree with each other completely and it appears that no single hypothesis is sufficient to explain the orign of the whole portion of the wing satisfactorily. So, it was intended to test the correctness of the various view points and to obtain some information which might lead to an unequivocal conclusion regarding the origin of the different portions of the wing. For this purpose the dependence of distribution of intensity in the wing due to a few typical aromatic liquids on temperature has been investigated quantitatively and the results have been discussed in the light of the various hypotheses mentioned above.

EXPERIMENTAL

In order to study the distribution of intensity in the wing due to any liquid at different temperatures ranging from −70°C to 150°C, three different arrangements were made. The experimental arrangement used in photographing the

spectra of the light scattered by the liquids at temperatures below 0°C was the same as that used for studying the wing due to liquid oxygen (Kastha, 1954). A mixture of liquid oxygen and ethyl alcohol at a definite proportion was used to obtain a bath at a particular low temperature which was measured with a pentane thermometer, For temperature above 0°C but below 20°C, the Dewar vessel and the liquid container were replaced by a double jacketed Wood's tube through which cold water maintained at proper temperatures was circulated with a pump. The temperature of the outgoing water was measured and kept constant within 1°C. For temperatures above 100°C the liquid in its container was placed in a cylindrical heater provided with two long slits parallel to the axis.

The liquids investigated were pyridine, α-picoline, *o*-cresol, *o*-chlorophenol and para-xylene. These were supplied by E. Merck, Fischer Scientific Co. and B. D. H. Each of the liquids was fractionated and the proper fraction was repeatedly distilled under reduced pressure to make it dust-free.

The spectrograph used in the present investigation has a dispersion of about 11 A.U./mm in the region 4047 A.U. and on the Stokes side the line is absolutely free from coma. This line was therefore chosen to study the distribution of intensity in the wing due to the liquid at different temperatureres.

The same slit width was used throughout the investigation. Ilford Zenith plates were used to photograph all the spectra and since a quantitative measurement of intensity was aimed at the exposures were so adjusted as to give a clear background and Raman lines of suitable densities in the spectrograms.

The microphotometric records of the various spectrograms were taken with a Kipp and Zonen self-recording microphotometer of the Moll type using a 8 : 1 magnification ratio.

The details of the method followed in converting the blackening due to the wing and the Raman lines into intensity readings and for obtaining the relative intensity-distribution in the wing taking into account the widening of the Rayleigh line, were the same as described in an earlier paper (Kastha, 1954). The intensities $I_{\Delta\nu}$ at distances $\Delta\nu$ from the centre of the Rayleigh line 4047 A.U. due to any of the liquids at a given temperature were compared with the intensity of a suitable Raman line (I_R). The lines 654 cm^{-1} in the case of pyridine and the line 810 cm^{-1} in the case of α-picoline were used as the reference Raman lines. The Raman lines 680, 750 and 647 cm^{-1} served as reference lines in the case of *o*-chlorophenol, *o*-cresol and *p*-xylene respectively. The values of $I_{\Delta\nu}/I_R$ were plotted against the distances $\Delta\nu$ from the centre of the Rayleigh line to obtain the true intensity-distribution in the wing for the liquid at the particular temperature. Such data obtained for the liquid at different temperatures furnished information regarding the dependence of the intensity of any portion of the wing on temperature.

RESULTS

The curves showing the distribution of intensity in the wing accompaying the Hg line 4047 A.U. scattered by the liquids at different temperatures are reproduced in figures 1-5. The changes in the intensity-distribution which take place with change of temperature of the different liquids studied in the present investigation are stated below.

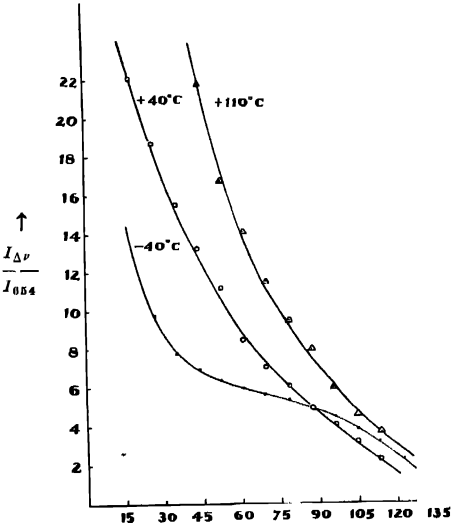

Fig. 1. Pyridine

(a) *Pyridine* : It can be seen from figure 1 that the intensity in the wing due to pyridine at 40°C is large at distances less than 25 cm^{-1} and beyond this distance it gradually decreases with increasing distances from the centre of the Rayleigh line. When the temperature of the liquid is raised to 110°C the intensity of the portion of the wing lying within 40 cm^{-1} from the Rayleigh line increases remarkably while that of the portion beyond 40 cm^{-1} increases only slightly. When the liquid is cooled to -40°C the intensity-distribution in the wing changes completely and the intensity at each point in the wing upto 90 cm^{-1} is reduced considerably. It is also found that at -40°C throughout the region between 45-90 cm^{-1} the intensity at different points is almost the same, but beyond 90 cm^{-1} the intensity at any point in the wing is larger than that observed in the case of the liquid at 40°C. The wing however extends upto 140 cm^{-1} at both the temperatures.

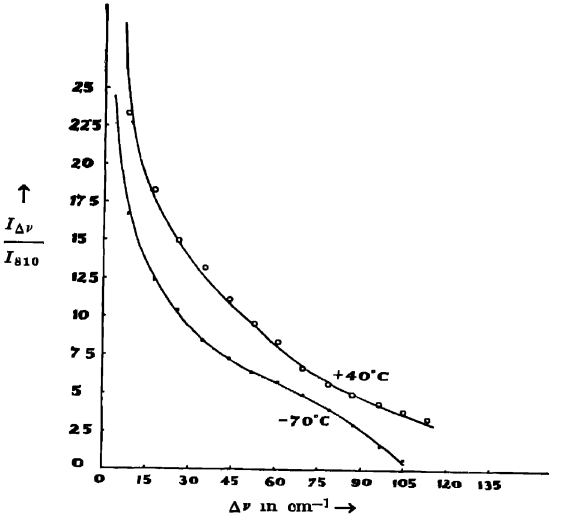

Fig. 2. α-Picoline

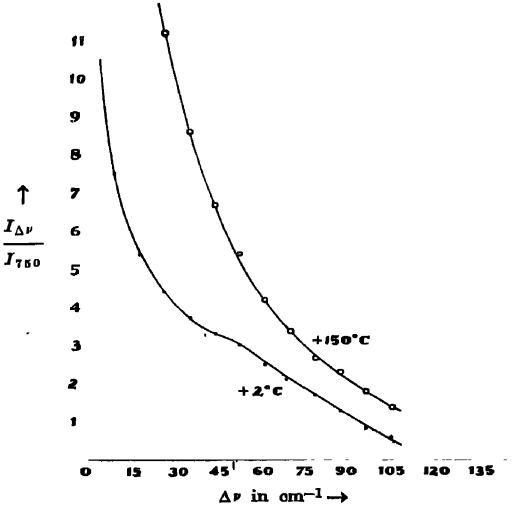

Fig. 3. o-Cresol

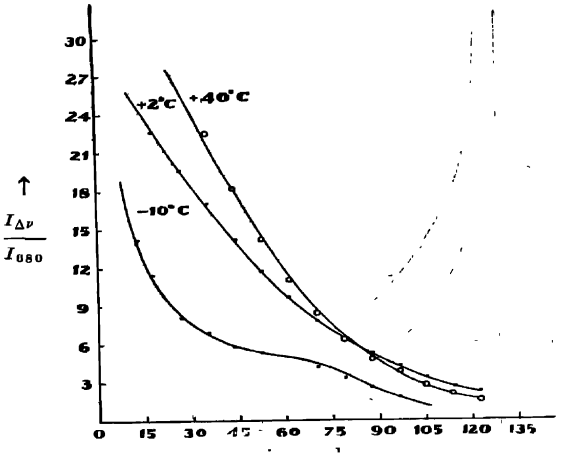

Fig. 4. *o*-Chlorophenol

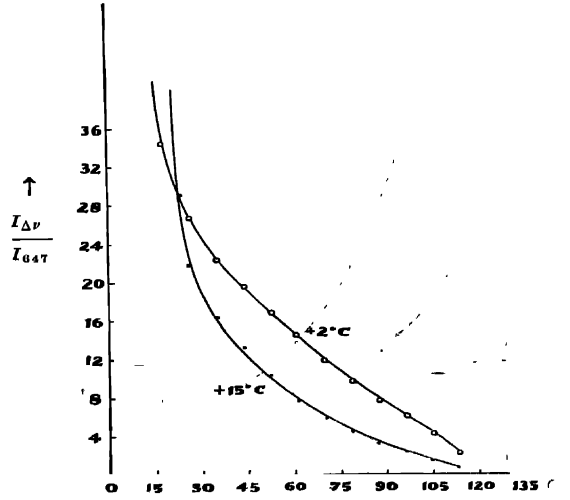

Fig. 5. *p*-Xylene

(b) *α-picoline* : It is seen from figure 2 that the intensity-distribution in the wing due to this liquid at 40°C is similar to that observed in the case of pyridine at the same temperature. When the liquid is cooled to −70°C the intensity in the region very near to the Rayleigh line is greatly reduced and an inflexion in the intensity-$\Delta\nu$ curve appears at about 45 cm^{-1}, beyond which the intensity slowly decreases to zero at about 105 cm^{-1}.

(c) *o-Cresol* : In this case when the liquid is super cooled to 2°C (figure 3) the intensity of the wing close to the Rayleigh line is greatly reduced and an inflexion in the intensity-distribution curve appears at 45 cm^{-1}. The intensity of the wing beyond 45 cm^{-1} falls off rapidly and becomes negligible at about 110 cm^{-1}.

(d) *o-Chlorophenol* : In this case the intensity-distribution in the wing due to the liquid at 40°C and 2°C shown in figure 4 is similar to that observed in the case of pyridine at 40°C. The intensity-distribution curve for *o*-chlorophenol at −10°C is similar to that in the wing due to pyridine at −40°C, but in the former case the intensity extends upto 120 cm^{-1}.

(e) *p-Xylene* : It can be seen from figure 5 that the intensity-distribution curves due to *p*-xylene at 2°C and 15°C respectively intersect each other at about 25 cm^{-1} and that the intensity beyond 25 cm^{-1} from the Rayleigh line increases while that in the portion nearer to the Rayleigh line diminishes considerably when the liquid is cooled to 2°C.

DISCUSSION

The results described above indicate that in all cases the intensity in the region adjacent to the Rayleigh line is very large and it increases rapidly with the rise of temperature of the liquids and diminishes considerably when the temperatures of the liquids are lowered. The intensity at large distances from the Rayleigh line, however, increases in the case of *p*-xylene and pyridine and diminishes in other cases when the liquids are cooled to low temperatures. The above-mentioned changes in the intensity of the portion of the wing near to the Rayleigh line, with change of temperature of the liquids, suggest that a part of the intensity in this portion of the wing may be due to rotational Raman scattering. Another part may arise out of contributions from Rayleigh radiation broadened in the process of scattering of light by molecules in motion due to collision as suggested by Cabannes and Rocard (1929). According to the theory of rotational Raman scattering the intensity of the wing would be zero at the centre of the Rayleigh line and a maximum of intensity in the wing would be expected at distances varying from 8 cm^{-1} to 18 cm^{-1} from the centre of the Rayleigh line due to the different liquids studied. On this would be superposed the intensity of the edges of the broadened Rayleigh radiation mentioned above. The relative contributions to the intensity of the wing

from these two causes cannot be determined from the results obtained, because the intensity-distribution in the wing at distances less than 15 cm^{-1} from the Rayleigh line could not be determined on account of insufficient dispersion of the spectrograph used and the blackening produced in the neighbourhood of Rayleigh line due to scattering in the photographic emulsions. Since the forces hindering rotations and other type of movements of the molecules increase with lowering of temperature of the liquid, the intensity of the portion of the wing close to the Rayleigh line is expected to decrease when the liquids are cooled to low temperatures. However, the increase in the intensity of the wing beyond 25 cm^{-1} and 90 cm^{-1} in the case of *p*-xylene at 2°C and pyridine at –40°C respectively indicates clearly, that the intensities in these regions of the wing are not wholly due to rotational scattering or to broadening of Rayleigh line arising out of molecular collisions. Moreover, since it is known that almost all the molecules of *o*-chlorophenol in the liquid state exist as dimers at room temperature (Pauling, 1945, Sirkar *et al.*, 1958) and the motion of these dimers is hindered to a greater extent when the temperature of the liquid is lowered, the intensity in the wing at distances beyond 50 cm^{-1} from the Rayleigh line which diminishes only slightly with lowering of temperature to –10°C, cannot be due either to rotation or to collisions of the molecules. Thus it seems plausible to assume that a major part of the intensity of the wing at distances beyond 50 cm^{-1} from the Rayleigh line observed in the present case originates from vibrations of groups of molecules which are formed in the liquids at low temperatures and since some of these groups of molecules would be expected to break up with increase of temperatures the contribution due to vibrations of such groups to the intensity of the part of the wing mentioned above, would diminish at higher temperatures. Also, as there is some contribution to the intensity in this part of the wing from rotational scattering these groups are small enough to permit rotation of other free single molecules. It must be pointed out, however, that these groups are different from the cybotactic groups postulated by Rousset (1935). Since the latter groups give rise to X-ray diffraction haloes, the size of the groups must be large and as such groups are continuously formed and broken within the volume of the liquid the binding forces between adjacent molecules in those groups are small and the intensity of the wing at large distances from the Rayleigh line cannot be attributed to any intermolecular vibration in such groups. Moreover, the appreciable intensities beyond 50 cm^{-1} observed in the wing due to these liquids at low temperatures indicate that the groups are formed by molecules attached to each other through weak linkages. These forces are stronger than the Van der Waals' forces but much weaker than the forces due to regular bonding. The continuous nature of the scattering due to vibrations in such groups in the liquid may be due to the fact that the frequencies of vibrations of these groups of molecules overlap each other on account of fluctuations in the strength of binding due to impact of neighbouring molecules. Formation of such groups of

molecules in the liquid state was also inferred by Sirkar and Mookerjee (1936) from results of investigation of the wing due to a few organic liquids in the pure state and in solutions and by Pniewski (1938a, b) who measured the intensity in the wings due to CS_2, $CHCl_3$ and CCl_4.

In this connection it would be interesting to compare the intensity-distribution in the wing due to the liquids at low temperatures with the intensities and positions of the low-frequency Raman lines which are observed in the spectra when the liquids are solidified. For this purpose, the positions of the low-frequency lines and their intensities estimated visually with respect to the intensity of a Raman line chosen in each case for obtaining the intensity-distribution in the wing due to the liquid are given in Table I. The figures in parentheses indicate these intensities.

TABLE I

Substance	Reference Raman line (R) $\Delta\nu$ in cm^{-1}	Low-frequency Raman lines $\Delta\nu$ in cm^{-1}			
Pyridine (−180°C) (Kastha, 1956)	654	58 (1)	82 (1)	97 (1)	137 (½)
α-Picoline (−180°C) (Kastha, 1957)	810	45 (½)	70 (½)	94 (1)	
o-Chlorophenol (−30°C) (Biswas, 1954a)	680	51 (½)	63 (¾)	94 (1b)	
o-Cresol (−30°C) (Biswas, 1955)	750	45 (½)	90 (1b)		
p-Xylene (−30°C) (Biswas, 1954b)	647	55 (½)	91 (4b)		

It can be seen from Table I and figures 1–5 that the low-frequency lines appear in each case in regions which correspond to those in the wing due to the liquid state at low temperature in which there is continuous Raman scattering which has been attributed to vibrations in groups of molecules. Also, the low-frequency lines are not observed in other regions in which the wing has no appreciable intensity. These facts suggest that the same groups of molecules which are responsible for the intensity observed in the wing beyond 45 cm^{-1} due to liquids at low temperatures are also responsible for the origin of the low-frequency lines which appear in the spectra when the liquids are frozen. It can be seen from figures 1–5 and Table I that the intensity of the low-frequency lines taken together is much less than the aggregate intensity of the wing beyond 45 cm^{-1} in all cases. Since the variation in the strength of binding among the molecules in the groups due to impact from neighbouring molecules ceases as the liquids are frozen, the frequencies of vibrations due to these groups are expected to become discrete in the solid state. The dimunition in the intensity of these lines may be explained

in the following way. When the liquid is frozen the groups of molecules mentioned above may link up with other neighbouring groups to form larger aggregates in the solid state. In some modes of vibrations of the groups in the liquid state involving angular motions, the change in the polarisibility produced in some of the smaller groups of molecules diminishes enormously in the solid state because of restriction of such modes in the larger groups. Also the scattering arising from rotation of some individual molecules still present in the liquid state ceases completely with solidification of the liquids. These two reasons taken together may account for the feebleness of the low-frequency lines compared to the intensity of the part of the wing beyond 45 cm^{-1} due to the liquids at low temperatures.

These results thus indicate the formation of groups of molecules in the liquid state and increase in the size of these groups with solidification of the liquids. The large frequency-shifts of the low-frequency Raman lines also indicate that the binding forces between the molecules in these groups are much larger than Van der Waals' existing in the liquids at ordinary temperatures. If the melting point of the crystal be slightly below the room temperature, groups of molecules may be present in the liquid even at the room temperature, as in the case of diphenyl ether (Sirkar, 1936).

ACKNOWLEDGMENTS

The author's grateful thanks are due to Professor S. C. Sirkar, D.Sc., F.N.I., for his kind interest during the progress of the work.

REFERENCES

Bhagavantam, S., 1933, *Ind. J. Phys.*, **8**, 97.
„ 1935, *Proc. Ind. Acad. Sc.*, **2**, 63.
Biswas, D. C., 1954a, *Ind. J. Phys.*, **28**, 85.
„ 1954b, *Ind. J. Phys.*, **28**, 303.
„ 1955, *Ind. J. Phys.*, **29**, 257.
Cabannes, J. and Rocard, Y., 1929, *Jour. de Phys.*, **10**, 52
Gross, E. and Vuks, M., 1935, *Nature*, **135**, 100, 431, 998.
Gross, E. F. and Raskin, Sh., 1945, *Bull. Acad Sci. U.R.S.S. Sér. Phys.*, **9**, 184.
Kastha, G. S., 1954, *Ind. J. Phys.*, **28**, 329.
„ 1956, *Ind. J. Phys.*, **30**, 519
„ 1957, *Ind. J. Phys.*, **31**, 395.
Pauling, L., 1945, Nature of the Chemical Bond, p. 324.
Pniewski, J., 1938a, *Bull intern. Acad. Polon Sci., Classe. Sci. math. nat., Serie A*. 136.
„ 1938b, *Act. Phys. Polon.*, **7**, 186.
Rousset, A., 1935, *Thesis*, Paris.
Sirkar, S. C., 1936, *Ind. J. Phys.*, **10**, 75 ; 108.
Sirkar, S. C., Deb, A. R. and Banerjee, S. B., 1958, *Ind. J. Phys.*, **32**, 345.
Sirkar, S. C. and Mookerjee, B. K., 1936, *Ind. J, Phys.*, **10**, 375.

ON THE ELECTRON PRODUCTION RATE IN THE F_2 REGION OF THE IONOSPHERE

S. DATTA

INSTITUTE OF RADIO PHYSICS AND ELECTRONICS

92, UPPER CIRCULAR ROAD, CALCUTTA-9

ABSTRACT. A column of unit cross section of the F_2 region extending from the "bottom" to the height of its maximum electron density is divided into four columns of equal length. Mean production rate in each of the columns is calculated. For this purpose, diurnal variation of the total number of electrons in each of the columns and the height variation of the attachment coefficient suggested by Ratcliffe *et al* (1956) are utilised.

This method of computation leads to a regular consistent diurnal variation of the electron production rate with a single peak at about half an hour before noon time and eliminates the anomalous results that are sometimes obtained when other methods of computation are employed.

INTRODUCTION

The electron production rate $q(h)$ in the F_2 region of the ionosphere at any height h may be calculated from the equation :

$$q(h) = \frac{dN(h)}{dt} + K(h) \cdot N^k(h) \tag{1}$$

where $N(h)$ is the electron density and $K(h)$ is the loss coefficient at the height h, the value of k depending upon the electron loss process is 1 or 2.

One may also consider the mean production rate $\bar{q}$. This computation (Datta, 1957) is based on the diurnal variation of the total number of electrons n in a column of unit cross section from the "bottom" to the height of maximum electron density. The equation utilised is

$$\frac{dn}{dt} = \bar{q} \cdot ym - \bar{\alpha} \left(\frac{n}{y_m} \right)^2 \cdot y_m \tag{2}$$

where $\bar{\alpha}$ is the mean recombination coefficient and y_m is the layer semithickness. For parabolic distribution of electron density $\bar{\alpha} = 1.2\ \alpha_m$ and under equilibrium conditions $\bar{q} = \frac{8}{15} q_m$ where α_m and q_m are the recombination coefficient and electron production rate at the height of maximum electron density.

To determine $q(h)$ from Eq. (1) one assumes either a fixed value of the loss coefficient or its symmetrical diurnal variation. When calculations are made

with the latter assumption the $q(h)$ values so determined show necessarily diurnal symmetry having anomalous midday dip and sometimes zero, even negative values. This happens, in particular, at the maximum electron density height due to the well-known midday "bite out" in the diurnal variation of maximum electron density in the F_2 region. Both the calculations, namely, that assuming symmetrical diurnal variation and that with a fixed value of the loss coefficient are affected by the bodily movement of the layer as a whole and by dilution and contraction of the layer due to thermal changes and electronic drift.

When computations are made from the diurnal variation of n utilising Eq. (2) the anomalous negative and zero values of the electron production rate obtained at the height of maximum electron density height, disappear. The anomaly of middy dip in the diurnal variation of the production rate, however, persists though less markedly. The method also minimises the effects of dilution and of contraction of the layer due to thermal changes and electronic drift on the production rate computation. However, it does not give any information about production rate variations at different parts of the F_2 region.

In the method of analysis, as presented in this paper, a column of unit cross section extending from the "bottom" to the height of maximum electron density is divided into four columns of equal length and mean electron production rate in each of the columns is computed from the diurnal variation of the total number of electrons in each of the columns. Effects of layer movement as a whole, and layer contractions and dilution due to thermal changes and electronic drift are then minimised, since the computations are from the total number of electrons in unit column in some definite fraction of the layer thickness, irrespective of the total layer thickness and the layer height. The data actually used for computation for the F_2 region were those of Slough : mean hourly values of $N(h)$ at a series of heights for the month of January, 1950, on international quiet days computed by Schmerling and Thomas (1956). For the height variation of the attachment coefficient that suggested by Ratcliffe *et al.* from night time observations over Slough, Watheroo and Huancayo, was utilised. "Tables of F_2-layer Electron Density on International Quiet Days" were obtained from Radio Group, Cavendish Laboratory, Cambridge, England.

It is proposed to make a similar analysis in a subsequent paper for the F_2 region over Haringhata when the work, already in progress in this laboratory for the determination of the distribution of electrons in "mean quiet F_2-layer" and a model for the height variation of the loss coefficient over Haringhata, is completed.

THE METHOD

A column of unit cross section extending from the "bottom" of the F_2 region to the height of maximum electron density is divided into a number of columns

of equal length. Let n_r be the total number of electrons in the rth unit column —the first column being the lowest one. Then

$$n_r = \int_{(r-1)\frac{T}{x}}^{r \cdot \frac{T}{x}} N(h) \cdot dh \qquad \ldots \quad (3)$$

where T is the thickness of the layer from the "bottom" ($h_0 F_2$) to the height of maximum electron density ($h_m F_2$) when height is measured from the bottom of the layer and x is the number of equal unit columns. It is to be noted that the total number of electrons n in the unit column extending from the "bottom" to the maximum electron density height is given by

$$n = \int_{h_0 F_2}^{h_m F_2} N(h) \cdot dh = \sum_{1}^{x} n_r \qquad \ldots \quad (4)$$

In case of a parabolic region, it can be shown that

$$n_r = \frac{1}{x} \left[1 - \frac{1}{3x^2} \{1+3(x-r)^2+3(x-r)\} \right] \cdot T N_m \qquad \ldots \quad (5)$$

where T is the semi-thickness of the parabolic region and N_m is the maximum electron density.

The diurnal variation of n_r is governed by the equation

$$\frac{dn_r}{dt} = Q_r - L_r \qquad \ldots \quad (6)$$

where Q_r is the total production rate and L_r is the total loss rate in the column considered and they are given by

$$Q_r = \int_{(r-1)\frac{T}{x}}^{r \cdot \frac{T}{x}} q(h)\, dh \qquad \ldots \quad (7)$$

and

$$L_r = \int_{(r-1)\frac{T}{x}}^{r \cdot \frac{T}{x}} K(h) \,.\, N^k(h) dh \qquad \ldots \quad (8)$$

$k = 1$ when the electron decay process is attachment type.

and $k = 2$ when the electron decay process is recombination type.

If q_r be the mean electron production rate in the rth column, then

$$q_r = \frac{x}{T} \cdot Q_r \qquad \ldots \quad (9)$$

Thus from the diurnal variation of n_r and the values of L_r, Q_r [from (6)] and hence the mean rate of production q_r [from (9)] can be computed.

Values of n_r and L_r may be calculated by numerical integration utilising Eqs. (3) and (8). These computations obviously require knowledge of the height variation of the loss coefficient $K(h)$, height distribution of electron density $N(h)$ and the electron decay process.

RESULTS

Recent work of Ratcliffe *et al.* indicates that the electron decay process in the F-region above 240 Km is of the attachment type. From night time observations (Ratcliffe 1956) over Slough, Huancayo and Watheroo they conclude that the attachment coefficient $K(h)$ at a height h between 250 Km and 350 Km is given by

$$K(h) = 10^{-4} \cdot \exp\left(\frac{300-h(K_m)}{50}\right) \text{sec.}^{-1} \qquad \ldots \quad (10)$$

For our purpose, Eq. (10) is extrapolated to a height of 200 Km as shown in figure 1.

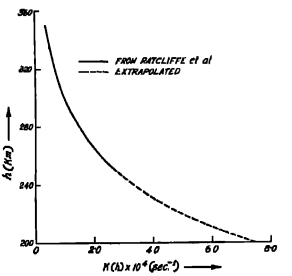

Fig. 1. Variation of the attachment coefficient with height.

A column of unit cross section from the bottom to the height of maximum electron density in the F_2 region is divided into four columns of equal length. From the "Tables of F_2-layer electron density on international quiet days", height distribution of electron density for every hour was drawn and total number of electrons in each of the four columns was calculated by Simpson's rule for numerical integration. The diurnal variation of the total number of electrons in a column of unit cross section from the bottom to the height of maximum

electron density is shown in figure 2. figure 3 shows the diurnal variation of the numbers n_1, n_2, n_3 and n_4 of electrons in the 1st, 2nd, 3rd and 4th columns respectively when taken in order from the bottom.

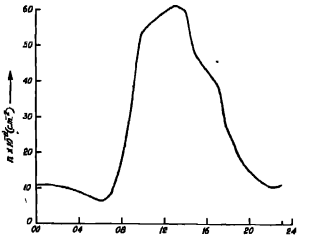

Fig. 2. Diurnal variation of the total number of electrons in a column of unit cross section extending from the bottom to the height of maximum electron density.

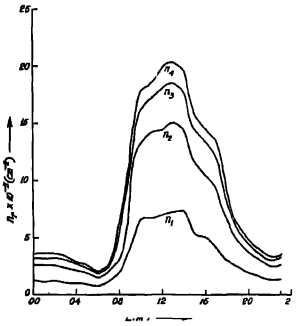

Fig. 3. Diurnal variation of the number of electrons n_1, n_2, n_3 and n_4 in the 1st, 2nd, 3rd and 4th columns respectively when taken in order from the bottom.

Hourly values of the loss rate in each column were also calculated by numerical integration utilising Eqn. (8) by Simpson's rule. $K(h)$ values given by (10) were used for the purpose.

To obtain half hourly values of $\frac{dn_r}{dt}$ for each of the columns, a linear change between the hourly values of n_r was assumed. For each column, mean of the two hourly values of L_r was taken as the half hourly value between the two hours. Thus half hourly values of mean production rate in each column were calculated from Eqs. (6) and (9). The diurnal variations of mean production rates q_1, q_2, q_3 and q_4 in the 1st, 2nd, 3rd and 4th column respectively are shown in figure 4.

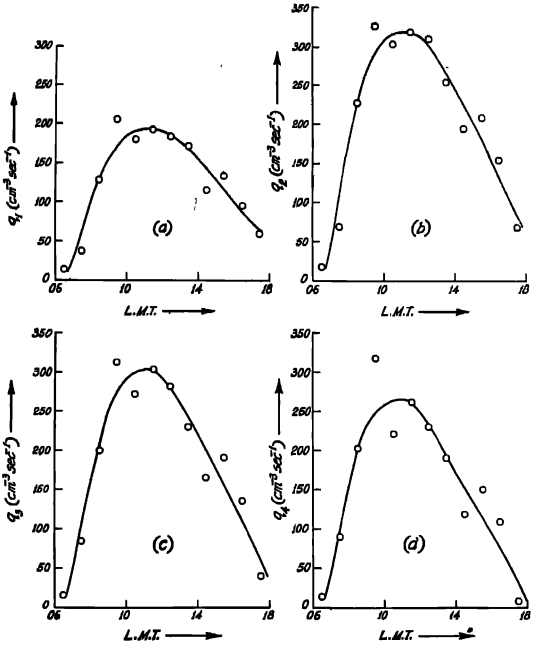

Fig. 4. Diurnal variation of mean production rate q_1, q_2, q_3 and q_4 in the 1st, 2nd, 3rd and 4th columns respectively when taken in order from the bottom.

The production rate Q of the electrons in a column of unit cross section from the bottom to the height of maximum electron density height is given by

$$Q = \frac{T}{4}(q_1+q_2+q_3+q_4) \qquad \ldots \quad (11)$$

Figure 5 shows that diurnal variation of the prouction rate Q. Figure 6 shows the diurnal variation of the mean electron production rate Q/T in the F_2-region. For comparison the value of Q from the hypothesis of Bradbury (1938) for the formation of the F_2-layer, may be calculated as follows.

If a gas of constant scale height H is ionized by a monochromatic radiation, then the value of $q(h)$, when the solar zenithal angle is χ, is given by the expression due to Chapman (1931a)

$$q(h) = q_0 \exp(1-Z-e^{-z}\sec\chi) \qquad (12)$$

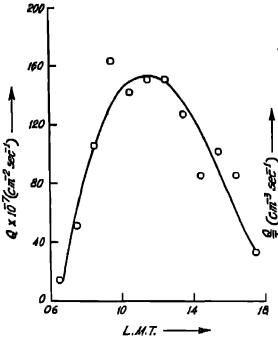

Fig. 5. Diurnal variation of electron production rate Q in a column of unit cross section extending from the bottom to the height of maximum electron density.

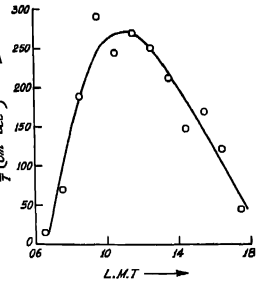

Fig. 6. Diurnal variation of the mean electron production rate Q/T in the F_2-region.

Half hourly values of electron production rate Q in a column of unit cross section entending from bottom of the F_2 region to the maximum electron density height

TABLE I

Hour L. M. T.	$Q \times 10^{-7}$ per cm² per sc
0630	13
0730	51
0830	106
0930	163
1030	141
1130	151
1230	151
1330	127
1430	86
1530	102
1630	86
1730	33

where $Z = \dfrac{h-h_0}{H}$ and h_0 is the height of maximum production rate q_0 when $\chi = 0$.

According to Bradbury, F_1 and F_2 layers are both produced by the same ionization process with the height of peak production rate near the level of F_1 layer peak and the F_2 layer peak is formed due to the rapid decrease of the electron loss rate above F_1 layer. According to this hypothesis the value of Q in the F_2 region when the solar zenithal angle is χ, is given by

$$Q = \int_{h_0F_2}^{h_mF_2} q(h)dh = q_0 H\cos\chi \{\exp(1-e^{-z_2}\sec\chi) - \exp(1-e^{-z_1}\sec\chi)\} \quad \ldots \quad (13)$$

where $$Z_2 = \frac{h_mF_2 - h_0}{H}$$

and $$Z_1 = \frac{h_0F_2 - h_0}{H}$$

According to Ratcliffe *et al*

$$q_0 = 280\,(1+1.4\times10^{-2}\bar{R})\ \mathrm{cm}^{-3}\cdot\mathrm{sec}^{-1} \quad \ldots \quad (14)$$

where $\bar{R}$ = monthly average relative Zürich sunspot number.

$h_0 = 180$ Km and $H = 45$ Km.

For the month of January 1950 ($\bar{R} = 100$) at Slough, the value of Q at noon from the expression (13) is found to be 105×10^7 cm^{-2} sec.$^{-1}$ while the value of Q at noon shown in Table I is 151×10^7 cm.$^{-2}$ sec.$^{-1}$

CONCLUSION

Diurnal variations of mean electron production rate in different parts of the F_2 region, when computed by taking account of the height variation of attachment coefficient suggested by Ratcliffe *et al.* show quite consistent results. The mean production rates have all maximum near about 1130 hr. Unlike other methods of electron production rate computation, this method does not lead to anomalous value or midday dip in the diurnal variation.

ACKNOWLEDGMENTS

This work forms part of the programme of Radio Research Committee of the Council of Scientific and Industrial Research, Government of India, and the author wishes to express his thanks to the Council for financial assistance.

The author is indebted to Professor S. K. Mitra, F.R.S., for clarifying discussions. He is grateful to Prof. J. N. Bhar, D.Sc., F.N.I., for his interest and encouragement throughout the progress of the work.

Thanks are also due to Dr. A. K. Saha for many suggestions

REFERENCES

Ratcliffe, J. A., Schmerling, E. R. Setty, C. S. G. K. and Thomas, J. O., 1956, *Phil Trans. A*, 248, 621.

Datta, S., 1957, *Ind. Jour. Phys.*, 31, 43.

Schmerling, E. R. and Thomas, J. O , 1956, *Phil Trans. A*, 248, 609.

Schmerling, E. R. and Thomas, J. O., 1955, Tables of F2-layer Electron density on International Quiet days, Cavendish Laboratory, Cambridge, England.

Bradbury, N. E., 1938, *Terr. Magn. Atmos. Elect.* **43**, 55.

Chapman, S., 1931a, *Proc. Phys. Soc.*, **43**, 26.

DIPOLE MOMENTS OF SOME SUBSTITUTED BENZENES AND PYRIDINES. PART III. CHLORO-AND BROMO ETHYL BENZENES

C. R. K. MURTY

PHYSICS DEPARTMENT, ANDHRA UNIVERSITY, WALTAIR

(*Received for publication, May* 27, 1958)

ABSTRACT. The dipole moments of six ethyl substituted benzenes were determined in dilute solution in benzene. The effects of methyl and ethyl groups on other substituents in the benzene ring have been discussed in the light of the observed moments.

INTRODUCTION

A large number of methyl substituted benzenes have been investigated both in vapour and solution phases and their dipole moments determined. Using the dipole moment data, the structure of the methyl benzenes has been extensively discussed in regard to their effect on other substitutions and their inductive and resonance effects on the benzene ring itself (Smyth and Lewis, 1940). Similar investigations have not so far been carried out with ethyl substitution. Only two of these, namely, ethyl benzene and pentachloro ethyl benzene have been studied (Baker and Groves, 1939 and Smyth and Lewis, 1940). In the present investigation the dipole moments of six ethyl substituted benzenes have been determined in dilute solution in benzene, in order to understand the effect of replacing the methyl group with ethyl group in the benzene compounds.

EXPERIMENTAL

The experimental arrangement and the method of calculation are the same as described previously (Murty, 1957). All the ethyl benzenes were supplied by L. Lights and Co., England and were of analytical reagent standard of purity. The solvent benzene was also of A.R. grade of purity. The group moments and polarisabilities used in the calculation are given below.

Group	Moment	Polarisability $\alpha \times 10^{24}$ cc
Cl	1.55	2.51
Br	1.50	3.63
C_2H_5	0.58	4.21

RESULTS AND DISCUSSION

TABLE I

o-Chloro ethylbenzene

W	ε_{12}	$\Delta\varepsilon$	$\Delta\varepsilon/W$	n_{12}	n^2_{12}	Δn^2	$\Delta n^2/W$
0.00962	2.2833	0.0193	2.007	1 49425	2.23277	0 00212	0.220
0 01397	2.2907	0 0267	1 908	1 49437	2.23315	0 00250	0 179
0 01954	2.2995	0.0355	1.817	1.49437	2 23315	0 00250	0 128
0 03522	2.3241	0.0601	1.707	1.49468	2.23406	0 00341	0.097
0 04420	2.3374	0.0734	1.661	1 49483	2.23451	0 00386	0.087
0.05164	2.3482	0.0842	1.631	1.49489	2.23470	0.00405	0 078

$(\Delta\varepsilon/W)_W$ $(\Delta n^2/W)_{W\to 0}$

$P_d = 49.6$ c.c. $\mu = 1.57$ D.

TABLE II

m-Chloro ethylbenzene

W	ε_{12}	$\Delta\varepsilon$	$\Delta\varepsilon/W$	n_{12}	n_{12}^2	Δn^2	$\Delta n^2/W$
0.00730	2 2826	0 0186	2 544	1 49384	2.23155	0.00090	0.123
0.02024	2.3159	0.0519	2.563	1.49408	2.23227	0.00162	0.080
0.03132	2.3435	0.0795	2.537	1.49423	2.23273	0.00208	0.066
0 04107	2.3661	0.1021	2.485	1.49459	2.23380	0.00315	0.077
0.05824	2.4063	0.1423	2.444	1.49479	2 23439	0.00374	0 064
0 07949	2 4556	0 1916	2.411	1.49505	2.23519	0 00454	0 057
0.09879	2.4988	0.2348	2.378	1.49545	2.23636	0 00571	0.058

$(\Delta\varepsilon/W)_{W\to 0}=2\ 558$ $(\Delta n^2/W)_{W\to 0}=0\ 085$

$P_d=65\ 8$ c.c. $\mu=1.81$ D.

TABLE III

p-Chloro ethylbenzene

W	ε_{12}	$\Delta\varepsilon$	$\Delta\varepsilon/W$	n_{12}	n^2_{12}	Δn^2	$\Delta n^2/W$
0.03126	2.3581	0.0941	2.926	1.49429	2.23292	0.00227	0 071
0.04401	2.3840	0.1200	0.728	1.49434	2.23306	0 00241	0.055
0.05876	2.4187	9.1547	2.632	1.49444	2 23332	0.00267	0.045
0.07459	2.4516	0.1876	2.516	1.49468	2.23398	0 00333	0.044
0.09454	2.4943	0.2303	2.437	1.49508	2.23528	0 00463	0 043

$(\Delta\varepsilon/W)_{W\to 0}=3.10$ $(\Delta n^2/W)_{W\to 0}=0\ 080$

$P_d=80.4$ c.c. $\mu=2.00$ D

TABLE IV

o-Bromo ethylbenzene

W	ε_{12}	$\Delta\varepsilon$	$\Delta\varepsilon/W$	n_{12}	n^2_{12}	Δn^2	$\Delta n^2/W$
0 02250	2.3184	0.0544	2.419	1.49419	2.23261	0.00196	0.087
0.03968	2.3604	0.0964	2 429	1.49451	2.23368	0 00303	0.076
0.05608	2.3977	0.1337	2.384	1.49523	2.23571	0.00506	0.090
0.07352	2.4360	0.1720	2.339	1.49553	2.23667	0.00602	0.082
0 09053	2.4725	0.2085	2.303	1.49605	2.23815	0.00750	0.083
0.10760	2.5075	0.2435	2.261	1 49682	2 24047	0.00982	0.091

$P_d = 85\ 5$ c.c. $\mu = 2.06$ D.

TABLE V

m-Bromo ethylbenzene

W	ε_{12}	$\Delta\varepsilon$	$\Delta\varepsilon/W$	n_{12}	n^2_{12}	Δn^2	$\Delta n^2/W$
0.01260	2.2945	0.0305	2.423	1.49383	2.23158	0 0093	0.074
0 02231	2.3179	0 0539	2 415	1 49417	2.23250	0 00185	0.083
0 02925	2.3333	0.0693	2.370	1.49450	2 23353	0.00288	0.098
0.04887	2.3793	0.1153	2 360	1.49499	2.23500	0.00435	0.089
0.06322	2.4104	0.1464	2.316	1.49555	2 23666	0.00601	0.095
0 08221	2.4512	0 1872	2 277	1 49591	2.23776	0.00711	0.087
0 10140	2 4908	0.2268	2.236	1 49663	2.23990	0 00925	0.091

$(\Delta\varepsilon/W)_{W\to 0} = 2.454$ $(\Delta n^2 W)_{W\to 0} = 0.081$

$P_d = 83.1$ c.c. $\mu = 2.03$ D.

TABLE VI

p-Bromo ethylbenzene

W	ε_{12}	$\Delta\varepsilon$	$\Delta\varepsilon/W$	n_{12}	n^2_{12}	Δn^2	$\Delta n^2/W$
0.02113	2.3190	0.0550	2.602	1.49458	2 23376	0.00311	0.147
0.03375	2.3642	0.0822	2.435	1.49499	2.23511	0.00446	0.132
0.04981	2.3802	0 1162	2.333	1.49571	2.23715	0.00650	0 131
0.06814	2.4194	0.1554	2.281	1 49637	2.23912	0.00847	0 124
0.09239	2.4706	0.2066	2.238	1.49707	2.24122	0.01057	0.114
0.12450	2.5421	0.2781	2.236	1.49783	2.24350	0.01285	0.103

$(\Delta\varepsilon/W)^{W\to 0} = 2.640$ $(\Delta n^2 W)_{W\to 0} = 0.151$

$P_d = 87.2$ c.c. $\mu = 2.08$ D.

TABLE VII

Molecule	Calculated Vector	Calculated S & H	Observed
o-Chloro ethyl benzene	1.36	1.79	1.57
m-Chloro ethyl benzene	1.91	2 01	1.81
p-Chloro ethyl benzene	2.13	2 23	2 00
o-Bromo ethyl benzene	1.31	2.01	2.06
m-Bromo ethyl benzene	1.86	1.99	2.03
p-Bromo ethyl benzene	2.08	2.18	2.08

Table VII shows that there is considerable amount of disagreement between the calculated and observed values Even when inductive effects are considered the disagreement exists; in fact, the values calculated by simple vectorial method are better, in particular as we go to meta and para-chloro ethyl benzenes. It indicates that the induced effects are slight. The disagreement between the calculated and the observed values may be attributed to the assumed group moment of 0.58 for C_2H_5 which may be rather high. Unfortunately, there is no solution value available for ethyl benzene. A comparison with the corresponding chlorotoluene values reveals that the calculated values are 0.22 to 0.28 higher for the chloroethyl benzenes. The slight induced effects present in chloroethyl benzenes may be due to the higher polarisability of the ethyl group.

In the absence of induced and resonance effects, the chloro and bromo ethyl benzenes should have almost the same dipole moment as the corresponding substituted toluenes. It is also reasonable to expect slightly higher values for ethyl compounds owing to the slightly larger dipole moment and polarisability of the ethyl group. Examination of Table VIII (which gives the comparative data) indicates that the experimentally observed values for ethyl benzenes support the expectations.

TABLE VIII

	Ortho		Meta		Para	
	Cal.	Obs.	Cal.	Obs.	Cal.	Obs.
Chlorotoluene*	1.41	1.43	1.79	1.77	1.95	1.94
Chloro ethyl benzene	1.79	1.57	2.01	1.81	2.23	2.00
Bromotoluene*	1.38	1.44	1.76	1.75	1.92	1.93
Bromo ethyl benzene	2.01	2.06	1.99	2.03	2.18	2.08

* Moore and Hobbs (1948)

The agreement between the observed and calculated values of chloro and bromo toluenes, the fact that chloromesitylene has the same moment 1.55 as chlorobenzene while bromomesitylene and bromodurene have moments 1.52 and 1.55 respectively as compared to 1.50 for bromobenzene and that chloro ethyl benzenes have approximately same values as the corresponding toluenes show that effects of the methyl and ethyl groups upon the structures contributing to the moments of chloro and bromo benzenes as well as the inductive effect between the halogen and the adjacent methyl or ethyl groups are too small to be detected in the moments (Smyth and Lewis, 1940).

In the case of bromoethyl benzenes there is little variation in observed moment values from ortho- to para- position which is unexpected since for the corresponding bromotoluenes there is a definite increase of moment from ortho- to para-substitution. It is also interesting to note that while the calculated values by vector method show the increase from ortho-to para-substitution, the Smallwood and Herzfeld method does not give values with any definite indication of increase from ortho- to para- positions. The experimental observations were taken on two different samples obtained at differnt times but the same values of dipole moments for the three bromo ethyl benzenes were obtained. It is felt that further determinations on dipole moments should be carried out on other polysubstituted benzenes containing the ethyl group before attempting an explanation of the observed moments.

ACKNOWLEDGMENT

The author is deeply indebted to Prof. K. R. Rao for his kind and constant guidance.

REFERENCES

Baker, J. W., and Groves, L. G., 1939,, *Jour. Chem. Soc.*, 1144.
Moore, E. M., and Hobbs, M. E., 1949, *Jour. Am. Chem. Soc.*, **71**, 411.
Murty, C. R. K., 1957, *Ind. J. Phys.*, **31**, 256.
Smyth, C. P., and Lewis, G. L., 1940, *Jour. Am. Chem. Soc.*, **62**, 721.

STRUCTURE OF THE SPECTRUM OF SINGLY IONISED BROMINE

Y. BHUPALA RAO*

PHYSICS DEPARTMENT, ANDHRA UNIVERSITY, WALTAIR

(*Received for publication April* 10, 1957)

Plates XII & XIII

ABSTRACT. The earlier analysis is revised in several respects and very much extended. 76 levels belonging to the $4p^4$, $4p^5$, 5s, 4d, 5p, 6s, 5d and 4f configurations are newly idontified involving the classification of nearly 400 additional lines in the region 10000 A in the photographic infra-red, to 350 A in the vacuum ultraviolet. This brings the total of classified lines to about 540. Almost all the intense lines are classified except about a dozen and some faint lines. The second ionisation potential is established to be 21.80 volts.

INTRODUCTION

Besides the very early work summarised in Kayser's Handbuch der Spectroscopie, Vol. 8, the previous important work on the description and analysis of the spectrum of singly ionised bromine consists essentially of the investigations of Bloch and Bloch (1927), Bloch, Bloch and Lacroute (1934), Lacroute (1935), Tolansky and Trivedi (1940), Ramanadham and Rao (1944), and Ranade (1951). Bloch and Bloch (1927) have first given a fairly extensive and accurate wavelengths of the lines of bromine between 6750 and 2250A using a source of electrodeless discharge and later, along with Lacroute (1934), reported the identification of 45 levels of Br II based on the ^4S and ^2D states of the Br III ion, involving the classification of about 170 lines, and have also given from Zeeman effect studies, the values of the g-factor for some of the levels Lacroute (1935) has measured the spectrum in the region 2280–649 A as recorded on a 1-metre vacuum grating spectrograph using a source of electrodeless discharge similar to the one employed by Bloch and Bloch (1927) and confirmed some of the levels by a study of the Zeeman effects. The Zeeman patterns of several other lines also were recorded.

Ramanadham and Rao (1944) have revised and extended the earlier analysis. They have made changes in the designations and values of the 4d $^3D^0$ and $^1D^0$ levels to bring them into conformity with their positions in isoelectronic and analogous spectra and assigned the $^5D^0$ term identified earlier to the 5d instead of the 4d configuration as the latter is expected to be deeper than the 4d $^3D^0$

* Present address : ONG Commission, Dehra Dun.

term and of the same order of magnitude as the $5s$ terms. They have rejected the levels given in the earlier investigation as $5s'\ ^1D_2^0$ and $5d'\ ^3D_2^0$ as unreal since combinations with them occur elsewhere and omitted the levels given by the previous workers as $4d\ ^3D_{2,1}^0$ since their reality could not be well established though some combinations with the 5p terms and with $4p^4\ ^3P_2$ were present. They have further identified the $4p^4\ ^3P_{0,1}$, $5p'\ ^3F_4$ levels, $5d\ ^3D^0$ term and several $5d'$ levels. The $6s'$ levels are also given by them but as tentative.

Tolansky and Trivedi (1940) reported measurements of the hyperfine structure for four lines of Br II. Ranade (1951) has analysed the hyperfine structure of some lines and confirmed the analysis of the combinations involving the deeper terms given by Bloch, Bloch and Lacroute (1934).

Moore (1952) has compiled all the energy levels in the book "Atomic Energy Levels, Vol. II" in the ascending order of magnitude with the ground level $4p^4\ ^3P_2$ as zero and has calculated the g-values for some of them with the help of the Zeeman patterns obtained by Lacroute. She has also suggested that the levels 96439.4 and 98807.3 given by Bloch, Bloch and Lacroute as $4d\ ^3D_{2,1}^0$ and omitted by Ramanadham and Rao might be $4p^5\ ^3P_{2,1}^0$ levels.

Still several and some very strong lines in the spectrum remain unclassified and as remarked by Moore in the book referred to above the analysis is far from complete and well worth further observation. Some of the levels identified in previous work need confirmation and on close scrutiny other levels appear to be either unreal or not correct in designation. In the present work an extensive study of the spectrum over the entire range from the photographic infra red to the vacuum ultraviolet (10000 to 350A) is made with the purpose of obtaining a complete analysis of the spectrum. As a result, several new levels belonging to the $4p^4$, $4p^5$, $4d$, $5s$, $5p$, $5d$, $6s$ and $4f$ configurations are identified leading to the classification of nearly 400 additional lines bringing the total of classified lines to about 540. Almost all the intense lines are now interpreted except for about a dozen and some faint lines.

A preliminary note giving the newly identified levels is already published (Bhupala Rao, 1956).

EXPERIMENTAL

The source of radiation chiefly used in this investigation is a H-shaped pyrex glass discharge tube with a capillary of 1 to 2 mm. in diameter and about 2 cm. in length excited by a transformer giving 20000 V in the secondary. In the uncondensed discharge tube, the arc lines of bromine and a few lines involving combinations between deep levels of Br II appear. When the pressure is low the capillary is light red in colour and this is the condition best suited for obtaining the arc lines. As the gas pressure is increased the colour of the discharge in the capillary changes to greyish blue and some of the prominent first spark

lines also appear. Kiess and de Bruin (1929) have reported a similar observation. Most of the arc lines occur in the infra-red while the resonance group $4s^2 4p^5\ ^2P^0.4s^2-4p^4\ (^3P)5s\ ^4P,\ ^2P$ is in the region 1650 to 1300 A. In the condensed discharge with a condenser of capacity approximately 1.8×10^{-3} mfd kept in parallel with the transformer, the colour of the discharge in the capillary is bluish white and all the lines due to the singly and doubly ionised atoms are recorded with good intensity while the arc lines are generally diminished in intensity though some of them in the infra-red appear fairly strong. As one goes to lower wavelengths, lines due to still higher stages of ionisation also appear with comparable intensity. When an inductance of 0.5 m.h. is introduced into the circuit in series with the discharge tube, the intensity of Br II lines remains unchanged or even increases in several cases. But the lines of Br III are either partially or completely suppressed except in the vacuum ultraviolet region where they also appear fairly intense.

The discharge is also excited by 10000 V rectified by a kenotron 8013A and condensed by capacities of (a) 0.5 m.fd. and (b) 0.2 m.fd. In this condition, particularly with 0.5 m.fd and narrow capillary, a strong background is generally present and all the important lines of the various stages of ionisation appear. When an inductance of 0.5 m.h. is introduced in series with the discharge tube, the intensity of the background is reduced

The spectrum is obtained also in a high frequency discharge tube using a 100-watt H.F. oscillator operating at a frequency of about 11 M.c/s. In the visible region several lines of Br I, a few lines of Br II and a good number of bands of bromine molecule appear. But in the near ultraviolet only a fairly strong continuum is recorded. Again below 2000 A the bands of bromine molecule appear.

The spectrum is phographed in the infra-red on Kodak I.Q. and I.N. plates with Fuess and Hilger Glass Littrow spectrographs. In the vacuum ultraviolet region 1-metre Normal Incidence Vacuum Grating spectrograph set up by the author in this laboratory is used, (15000 lines per inch); the grating was kindly supplied by Prof. Siegbahn. The spectrum is recorded on Ilford Q_2 plates and extends upto 350 A with 6 hours exposure in condensed discharge condition.

In addition to the data obtained from the above methods a large number of photographs were also kindly made available to the author by Prof. K. R. Rao. These are pictures taken at Upsala with a Grazing Incidence Spectrograph long ago and well preserved, extending from 1085 to 480 A. The dispersion about 3.2 A/m.m. near 950 A. The source consisted of a vacuum spark between electrodes tipped with Rb Br and Cs Br ; full details regarding the pictures are given by Rao and Badami (1931) in the paper on Se IV.

The important multiplets involving the newly identified levels are given in Tables II to VI. The intensities for the lines specified there are the intensities in condensed discharge with inductance. Newly classified lines not contained in the multiplet tables are given separately in Table VIII with their intensities in condensed discharge with inductance, wavelengths and wavenumbers. All the values above 2000 A are from Littrow measurements.

ANALYSIS

The predicted terms of Br II are given in Table I. The observed terms are all underlined and those identified in previous investigations are marked with an asterisk also. All the newly observed energy levels are given in the preli-

TABLE I

Terms of Br II

Configuration	Terms								
$4s^2\ 4p^4$			$^3P^*$	^1D		^1S			
$4s\ 4p^5$			$^3P^0$		$^1P^0$				
Basic terms of Br III	^4S			^2D				^2P	
$4s^2\ 4p^3$									
$4s^2\ 4p^3\ 5s$	$^5S^0{}^*$			$^3D^0{}^*$				$^3P^0{}^*$	
	$^3S^0{}^*$			$^1D^0{}^*$				$^1P^0$	
$4s^2\ 4p^3\ 5p$	$^5P^*$	$^3F^*$	$^3D^*$	$^3P^*$			^3D	^3P	^3S
	$^3P^*$	$^1F^*$	$^1D^*$	$^1P^*$			^1D	^1P	^1S
$4s^2\ 4p^3\ 4d$	$^5D^0$	$^3G^0$	$^3F^0$	$^3D^0$	$^3P^0$	$^3S^0$	$^3F^0$	$^3D^0$	$^3P^0$
	$^3D^0{}^*$	$^1G^0$	$^1F^0$	$^1D^0$	$^1P^0$	$^1S^0$	$^1F^0$	$^1D^0$	$^1P^0$
$4s^2\ 4p^3\ 6s$	$^5S^0{}^*$			$^3D^0$				$^3P^0$	
	$^3S^0{}^*$			$^1D^0$				$^1P^0$	
$4s^2\ 4p^3\ 5d$	$^5D^0{}^*$	$^3G^0$	$^3F^0{}^*$	$^3D^0$	$^3P^0$	$^3S^0$	$^3F^0$	$^3D^0$	$^3P^0$
	$^3D^0{}^*$	$^1G^0$	$^1F^0$	$^1D^0$	$^1P^0$	$^1S^0$	$^1F^0$	$^1D^0$	$^1P^0$
$4s^2\ 4p^3\ 4f$	^5F	^3H	^3G	^3F	^3D	^3P	^3G	^3F	^3D
	^3F	^1H	^1G	^1F	^1D	^1P	^1G	^1F	^1D

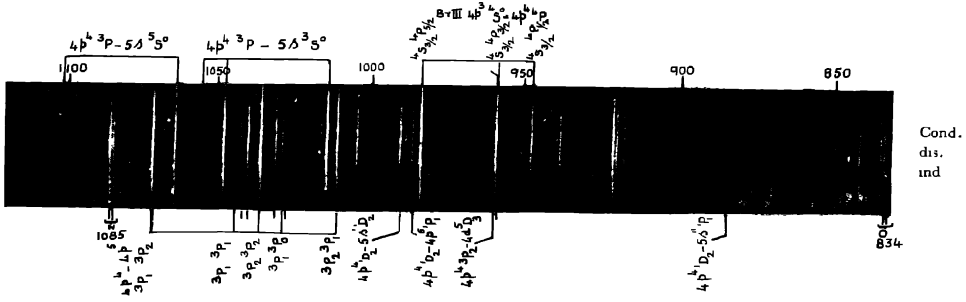

a $4p^4\,{}^3P - 4p^3\,{}^3P^0$, $4p^4\,{}^3P - 5s^5\,S^0$ and $4p^4\,{}^3P - 5s^3\,S^0$ multiplets

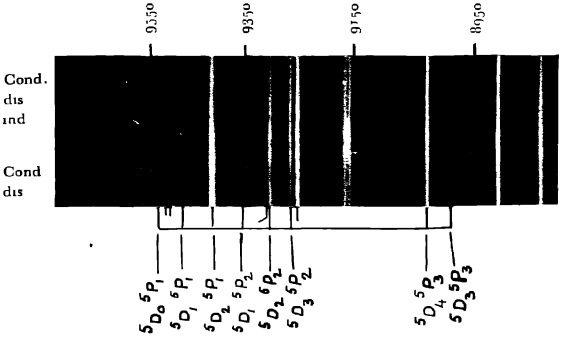

$4\,d^5\,D^0 - 5\,p^5\,P$ multiplet

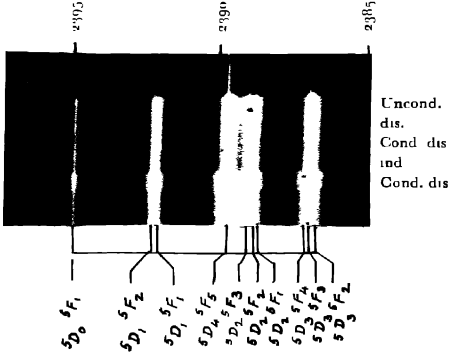

$4\,d^5\,D^0 - 4\,f^5\,F$ muluplet

BHUPALA RAO

$4p^5\,{}^3P - 5p\,{}^3P$, $5s\,{}^3D - 4f\,{}^3F$, $4d\,{}^3D - 4f\,{}^3F$ multiplets

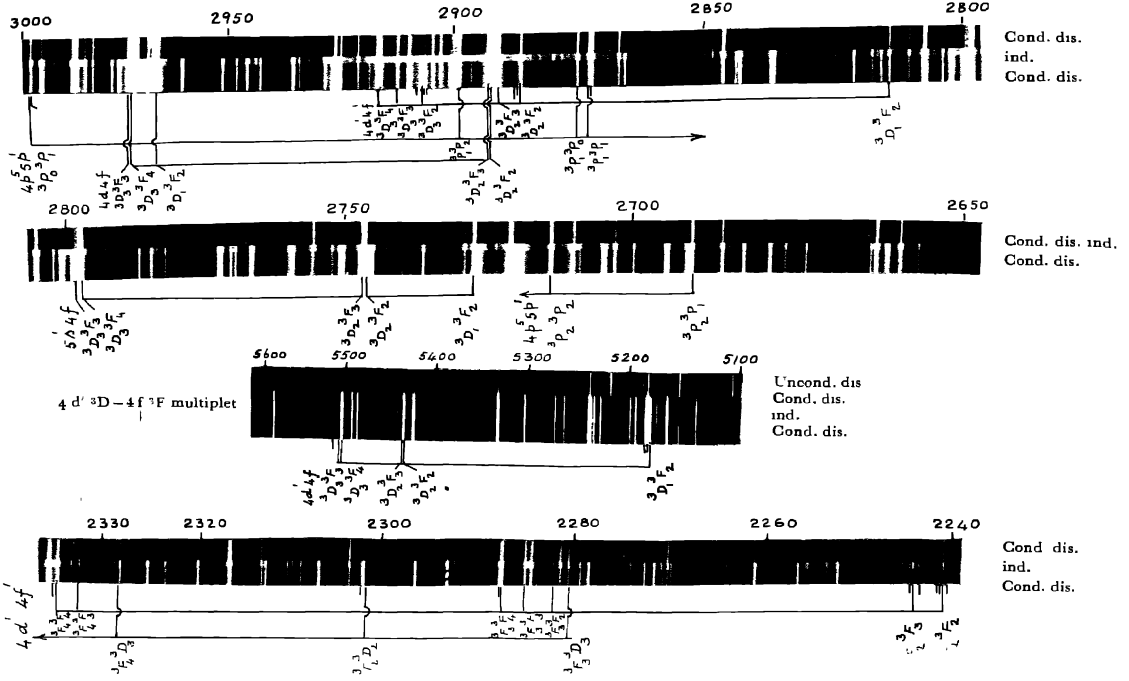

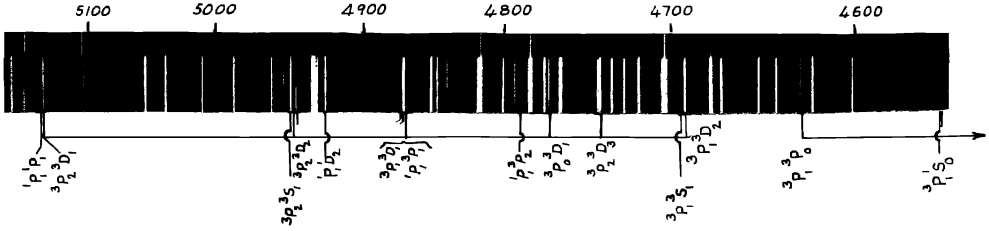

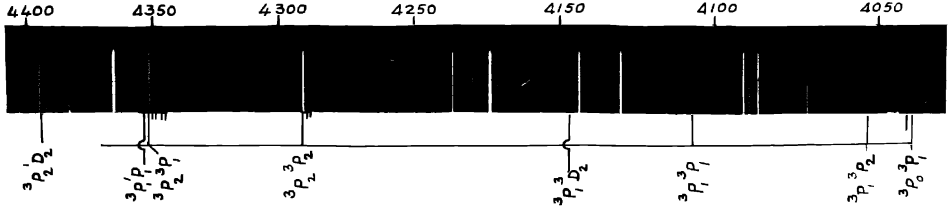

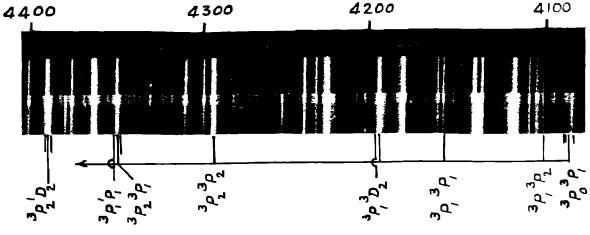

5 s" – 5 p" multiplets.

minary note (Bhupala Rao, 1956). Several of them are contained in the multiplet tables also. The rest are given in Table VII. The values of some of the levels of 4d $^5D^0$, 4f ^5F and ^3F terms differ slightly from those given in the preliminary note since these had to be readjusted in the final calculation. The levels 161526.4 and 161896.2 appearing as 4f'$^1D_4$ and 4f'$^1G_2$ in the preliminary note are actually 4f' $^1G_4$ and 4f' $^1D_2$ respectively.

The lines 98476, 95336 and 93921 cm^{-1} (1015.5, 1048.9 and 1064.7 A respectively) in the vacuum ultraviolet region are very prominent and longer than the other lines [Plate XII A (1)] which suggest that they form the resonance lines. Their intensity and characteristics confirm the identification of the 4p^4 ^3P levels. The lines, 98804, 96430 and 93295 cm^{-1} (1012.1, 1037.0 and 1071.9 A respectively) also shown in Plate XII A(1) are equally strong and have the same characteristics as the resonance lines lending strong support to the suggestion that the levels 96439.4 and 98807.3 may be 4p^5 $^3P^0_{2,1}$ levels. Hence it is accepted as the correct designation of the two levels and only the 4p^5 $^3P^0_0$ level remains to be identified. These two levels give combinations with several 4p^4, 5p, and 5p' levels. The multiplet 4p^5 $^3P^0$ 5p' ^3P is particularly well developed giving intense lines (Plate XII B). A comparison of the values and intervals of the $4p^5$ $^3p^0$ levels with those in Kr III (Humphreys, 1935 and Boyce, 1935) leads to a value of about 1400 cm^{-1} for the 4p^5 $^3P_0^0$—$^3P_1$ interval, by which the 4p^5 $^3P_0^0$—5p' $^3P_1$ line should be in the region of ν 33400 cm^{-1}. From an examination of the plate for a line in that region with the same characteristics as the other lines of the multiplet, the line 33358.9 cm^{-1} is identified to be the 4p^5 $^3P_0^0$—5p' $^3P_1$ combination. It is confirmed by the combinations of the resulting level 100242.2 with seven other even levels.

The 4p^5 $^1P_1^0$ level is expected to give strong lines with 5p' $^1D_2$ and 5p' $^1P_1$ levels. Ramanadham and Rao have suggested the 5d' $^1P_1^0$ level entirely by the pair of lines 17481.6 and 23364.4 cm^{-1}. But this pair is found to be more completely suitable for the 4p^5 $^1P_1^0$ level of magnitude 113342.8 cm^{-1} which is consistent with the expected value from a study of the analogous spectra. Its combinations with twelve other even levels confirm the identifications. The combinations of the 4p^5 levels with the even levels are given in Tables II to IV.

Of the remaining unclassified lines, the group of close lines at 41800 cm^{-1} (2390 A) stands most prominent appearing prominently even under the weakest excitation including the uncondensed discharge. An attempt was made at first to see if they could be accounted for as combinations involving 5p and 5p' terms, but this attempt proved unsuccessful. A close examination of the lines shows they are all very diffuse and have strong satellites very close to them. A study of the position of the 4d $^5D^0$ term in the isoelectronic sequence Se I, (Ruedy and Gibbs, 1934) Br II, Kr III leads to a value of about 104000 cm^{-1} in Br II.

TABLE II

Odd levels \ Even levels		$4p^4$ $^3P_0$ 3840	$^3P_1$ 3139	$^3P_2$ 0	$5p$ $^5P_1$ 114682 8	$^5P_2$ 114818 1	$^5P_3$ 115176.2	$^3P_0$ 117834.3	$^3P_1$ 117561.5	$^3P_2$ 117767.6
$4p^5$ $^3P_0$	100242.2		97098 (1)							
$^3P_1$	98807.3		95658 (2)	98804 (6)		16011 3 (1)		19027.4 (1)	18754.5 (8)	18960.4 (6)
$^3P_2$	96439.4		93295 (6)	96430 (6)	18243 3 (2)		18736.9 (2)		21122.2 (1)	21327.8 (00)
$4d$ $^5D_0$	104206.1		101055 (0)		10477 (1)					
$^5D_1$	104151.7		101002 (0)		10531 (3)	10666 (0)				
$^5D_2$	104086.1				10597 (6)	10732 (2)				13680 (2)
$^5D_3$	104044.6			104042 (0)		10774 (4)	11132 (2)			13722 (1)
$^5D_4$	104097.9						11078 (7)			
$4d'$ $^3F_2$	117744.6									
$^3F_3$	118509.1			118498 (1)						
$^3F_4$	119432.1									
$^3D_1$	126788.2	122945 (1)	123651 (0)	III? 126794 (00)						
$^3D_2$	127687.7		124544 (3)	127688 (0)						
$^3D_3$	127940.6			127939 (2)						10171 (1)
$^1D_2$	128890.5		125751 (00)	128881 (1)			(I) 13713 (00)			

Assuming the 4f orbit to be hydrogen like, the value of 4f ^5F term is most likely to be of the order of 146000 cm^{-1} and the 4d $^5D^0$—4f ^5F multiplet should then be expected in the neighbourhood of 42000 cm^{-1}. From these considerations the group at 41800 cm^{-1} is classified as the 4d $^5D^0$ 4f ^5F multiplet. This classification is confirmed by the presence of the entire multiplet 4d $^5D^0$—5p ^5P in the region 10500-11000 cm^{-1} and supported by several intercombinations. These two multiples are shown in Plates XII A(i) and (ii). Further confirmation is obtained by the identification of the 4f ^3F term within 200 cm^{-1} from the 4f ^5F term giving very strong combinations with 5s′ $^3D^0$, $^1D^0$ and 4d $^3D^0$ and 4d′ $^3D^0$ terms. [Plates XI A(ii), (iii) and XIIB]. These multiplets are given in Tables II and V.

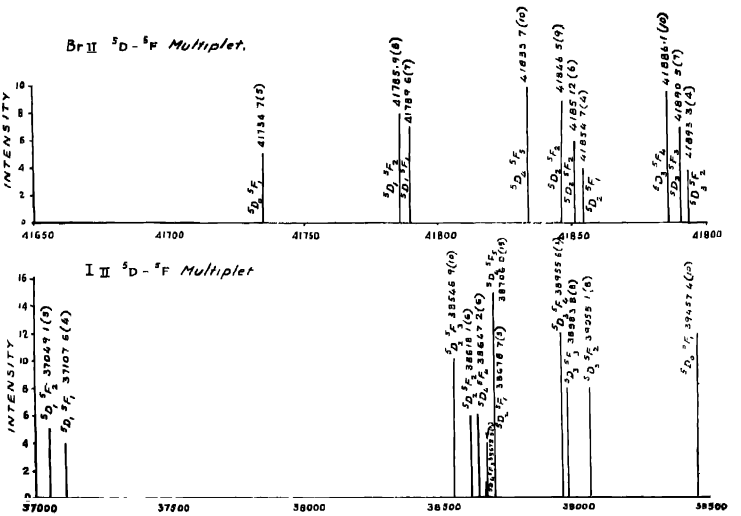

Fig. 1

In the spectrum of singly ionised iodine, Murakawa (1938) has classified a similar group as 5d $^5D^0$—5f ^5F multiplet. A plot of this multiplet in Br II and III presented in figure 1 brings out the similarity between the two. Here it may be observed that this ^5F term of absolute value 28600 cm^{-1} in III may more probably belong to the 4f electron consistent with its hydrogen like nature. On this basis the absolute value of the 5f term will be of the order of 17600 cm^{-1}. In Cl II also Murakawa (1935) has identified a term as 4f ^3F but Kiess and de Bruin (1939) have rejected the suggestion on the ground that the term does not exhibit the combination characteristics of ^3F terms though its magnitude is of

the correct order, its combinations are sharp without shading or satellites. But in view of the identification of the corresponding multiplet in Br II and III it is likely that there may be scope for further consideration of the assignment given by Murakawa.

Ramanadham and Rao have based the identification of the $5s''\ ^3P^0$, $^1P^0$ terms purely on combinations with the ground term in the vacuum ultraviolet region. The $5s''\ ^3P^0$ levels are of the right order of magnitude and are confirmed by the new combinations identified in this investigation. But the $5s''\ ^1P_1^0$ level given by them is based on only a single combination 105377 cm^{-1} with the level 11409 (absolute value 162710 in their paper); this level 11409 is found to be unreal, the line 105377 cm^{-1} defining this level having been distinctly classified as Br III $4p^3\ 4S_{3/2}-4p^4\ ^4P_{1/2}$ combination (Bhupala Rao, 1956a). Further, the value 116786 (absolute value 57333.0 in their paper) for the $5s''\ ^1P_1^0$ level is too deep and not consistent with the progression of values in spectra isoelectronic with BrII.

The 5p″ levels are estimated to be of the order of 144000 cm^{-1}. With the help of the $5s''\ ^3P^0$ intervals which are already identified, the $5p''\ ^3D$ levels could be established easily by searching for the appropriate interval and are confirmed by the presence of the $5s'\ ^3D^0-5p''\ ^3D$ and $4d\ ^3D^0-5p''\ ^3D^0$ multiplets. But the identification of the $5p''\ ^3P$ term has proved to be more difficult because of the intensity anomalies in the $5s''\ ^3P^0-5p''\ ^3P$ multiplet, the great irregularity in the variation of the intervals between its levels and the few combinations it gives with the $5s'\ ^3D^0$, $4d\ ^3D^0$ and $4p^5\ ^3P^0$ term. It may be noted, however, that a similar intensity anomaly in the $5s''\ ^3P^0-5p''\ ^3P$ multiplet and irregularity in the intervals of the $5p''\ ^3P$ term are present in Kr III also. Some of the lines included in this multiplet were classified by Ramanadham and Rao as combinations between 5p′ and 5d′ terms. But the present assignment seems to be more consistent and appropriate. The two levels 144517.7 and 145370.0 are designated as $5p''\ ^1P_1$ and $5p''\ ^1D_2$ respectively due to their combining properties. With the help of the interval between these, the $5s''\ ^1P_1^0$ level is found to be 125058.7 which is supported by several intercombinations. The scheme of all these combinations is given in Table IV. The $5s''-5p''$ multiplets are shown in Plate XIII.

The $4p^4\ ^1D_2$ level was suggested by Ramanadham and Rao on the basis of two lines 101532 (10) and 98284 (0) cm^{-1} given as the combination $4p^4\ ^1D_2-5s'\ ^2D^0$ and the intercombination $4p^4\ ^1D_2-5s'\ ^3D_2^0$ respectively. But the line 101532 defining the $4p^4\ ^1D_2$ level is distinctly classified as Br III $4p^3\ ^4S_{3/2}^0-4p^4\ ^4P_{5/2}$ combination (Bhupala Rao, 1956a). A search among the vacuum ultraviolet lines for the interval $5s'\ ^1D^0-5s''\ ^1P_1^0$ has led to the identification of the $4p^4\ ^1D_2$ level at 12098 and it is confirmed by its combinations with seventeen other odd levels. All these combinations are given in Table IV.

TABLE V

Odd levels \ Even levels		4f							
		$^5F_1$ 145941.1	$^5F_2$ 145937.3	$^5F_3$ 145932.9	$^5F_4$ 145929.9	$^5F_5$ 145931.6	$^3F_2$ 146087.5	$^3F_3$ 146081.6	$^3F_4$ 146095.1
$4p^5$	$^3P_0^*$	100242.2	45698.3 (2)						
	$^3P_1$	98807.3		47130.6 (0)					
	$^3P_2$	96439.4							
	$^1P_1$	113342.8					32745.0 (2)		
$4d$	$^5D_0$	104206.1	41734.7 (5)						
	$^5D_1$	104151.7	41789.6 (7)	41785.9 (8)					
	$^5D_2$	104086.1	41854.7 (4)	41851.2 (6)	41846 5 (9)				
	$^5D_3$	104044 6		41893.3 (4)	41890 5 (7)	41886 1 (10)			42051.0 (00)
	$^5D_4$	104097.9				41833.7 (10)			
	$^3D_1$	112395 9					33691.8 (8H)		
	$^3D_2$	111530 5					34557 4 (2)	34551 3(8H)	
	$^3D_3$	112460.5						33621.2 (5)	33634 6 (10H)
$5s'$	$^3D_1$	109428.2					36659.0 (5H)		
	$^3D_2$	109682.5					36404.7(1H)	36399.0(7H)	
	$^3D_3$	110378 2						35703.0(1h)	35716 4(5h)
	$^1D_2$	112939.5					33147.3 (2)	33141 6 (6h)	
$4d'$	$^3D_1$	126788.2					19299.6 (6)		
				III?					
	$^3D_2$	127687.7		18246.6 (0)			18399.9 (2)	18393.9 (6)	
	$^3D_3$	127940 6						18141.4 (3h)	18154.7 (10)

A search among the vacuum ultraviolet lines for the intervals of the ground term $4p^4\ ^3P$, 701 and 3139, has led to the identification of the $4d'\ ^3D^0$, $^1D^0$ terms (Table II). The presence of the $4d'\ ^3D^0-4f\ ^3F$ multiplet with good intensity (Table V) and the multiplet $4d'\ ^3D^0-5p''\ ^3P$ (Table IV) point to their correct identification. But combinations of the $4d'\ ^3D^0$ levels with $5p''\ ^3D$ levels are only a few as can be seen in Table IV Starting with $4d'\ ^3D^0$, $^1D^0$ terms it has been possible to arrive at the $4f'$ (^3F, ^3D, ^1H, ^1G, ^1F, ^1D) and $4d'$ ($^3F^0$, $^1G^0$, $^1F^0$) terms and the $4f'\ ^3G_3$ level. The $4d'-4f'$ combinations are all diffuse in varying degrees. The $4f'\ ^3F$, ^3D terms are inverted and their overall intervals are very small (–103.7 cm^{-1} –51.7 cm^{-1} respectively even though the interval between the ^2D levels of the parent configuration is 1195 cm^{-1}. The $4d'$—$4f'$ combinations are given in Table VI and some of the multiplets are shown in Plate XII B.

The $4d''$ levels could not be located since even with the most favourable estimate their combinations with the $5p'$ and $5p''$ levels are expected to occur beyond the photographic infra-red region; consequently it is not possible to identify the $4f''$ levels also.

Several of the $5d'$ and $6s'$ levels given by Ramanadham and Rao had to be altered. The changes are discussed below.

1. The $5d'\ ^3G_5^0$ level was fixed only by a single line 24529.2 cm^{-1}. This is classified otherwise as $5p'\ ^3P_2$—$5d'\ ^3D_3^0$. Another line at 25010.2 cm^{-1} is taken as $5p'\ ^3F_4$—$5d'\ ^3G_5^0$ consistent with the intensities of the combinations $^3F_2$—$^3G_3^0$ and $^3F_3$—$^3G_4^0$. The new level is 156756.6.

2. The levels $5d'\ ^3F^0_{2,3}$ do not appear to be quite correctly identified. The combination $5p'\ ^3F_3$—$5d'\ ^3F_3^0$ expected to be strong is absent and the combination $5p'\ ^3F_2$—$5d'\ ^3F_2^0$ is also absent on the author's plates, probably not resolved from the stronger line 24983.4 cm^{-1} very close to it. The alternative levels suggested now are 157226.9 and 158327.4 for $5d'\ ^3F_3^0$, $^3F_2^0$ respectively, which give strong $^3F_3$—$^3F_3^0$ and $^3F_2$—$^3F_2^0$ lines but the combinations with $5p'\ ^3D$ levels are not of the expected intensity. Further, with the alternative choice the $5d'\ ^3F^0$ term is inverted with a total interval of –1643.0 cm^{-1}. This is doubtful when the other $5d'\ ^3G^0$, $^3D^0$ terms do not show this inversion or partial inversion. Therefore the levels designated by Ramanadham and Rao are retained and the two new levels 157226.9 and 158327.4 are given under the designations $5d'\ a^0_3$ and $5d'\ b^0_2$ respectively.

3. The magnitude of the $5d'\ ^3D^0$ term identified by Ramanadham and Rao seemed to be too deep and inconsistent with the general progression of values $5d'\ ^3(G^0, F^0, D^0, P^0, S^0)$ although the component levels are regarded as real. Hence the suggested $5d'\ ^3D^0$ term is adopted as the $6s'\ ^3D^0$ term, the identification of the latter being considered unsatisfactory. An entirely new set of levels is suggested as $5d'\ ^3D^0$ term, the component levels being 157369.7, 157632.8 and 157808.3. The level 151458.3 given by Ramanadham and Rao as $6s'\ ^3D_1^0$ is,

however, retained as a separate level b^0 since it gives three cobminations with $5p/^5P$ term though its combinations with all other levels are accounted for otherwise.

4. The 5d′ $^3P^0$ term also had to be altered, the 5d′ $^3P^0_1$ level having been regarded as 5d′ $^3D^0_2$ on account of the existence of another combination between this and 5p′ $^3F_3$. The level 5d′ $^3P^0_0$ was based on two lines 30581.9 and 25655.4 cm^{-1}. Of these, 30581.89 cm^{-1} is classified otherwise which makes the identification of the level uncertain. The two components of the 5d′ $^3P^0$ term newly identified are 159778.4 and 159910.8. The third component 5d′ $^3P^0_0$ level could not be located.

The designation and reality of the level 158234 are not certain; its combination with 5p′ $^3D_3$ (ν 27579.4) is accounted for otherwise (table 8). Hence the level is left out.

5. The identification of the 5d′ $^3S_1^0$ level was based on two lines one of which is not found on the author's plates. The other line 24448.5 cm^{-1} is now classified otherwise as $5s^{0''}$ $^3P^0_0$—5p″ $^3P_1$. The new level is 156512.2. It gives three combinations with 5p″ levels. Two of them are classified otherwise also but their intensity for the other combinations seems to be too large. Hence their double classification is considered justified.

6. Of the singlets, the level 5d′ $^1G_4^0$ was fixed by two lines, the important one among which (23295.9 cm^{-1}) is now classified otherwise as 5s″ $^3P^0_2$—5p″ $^3P_2$. The level 160887.7 identified as 5d′ $^1F^0_3$ has to be altered as 5d′ $^1D^0_2$ since it has given a combination with 5p′ $^1P_1$. The 5d′ $^1D^0_2$ has been assigned as 6s′ $^1D^0_2$, the magnitude of the level being consistent with the newly identified 6s′ $^3D^0$ levels. The two lines defining the 5d′ $^1P^0_1$ level are otherwise classified as combinations of the $4p^5$ $^1P^0_1$ level with 5p′ $^1D_2$, $^1P_1$. Hence the new identifications are made.

The 5d′ $^1G^0_4$ level is virtually based only one combination 5p′ $^1F_3$—5d′ $^1G^0_4$ (25273.7(5) cm^{-1}) the intercombination 5p′ $^3F_3$—5d′ $^1G_4^0$ (25655.4(00) cm^{-1}) being very weak. An alternative level is 158820.7 which gives the lines 27130.4 (3) and 27512.1 (4) cm^{-1}) with 5p′ $^1F_3$ and 5p′ $^3F_3$ respectively. But since the intensity of 27512.1 cm^{-1} is not only greater than that of the other line but much more than what can be reasonably expected for such an inter-combination, this level is not adopted as 5d′ $^1G_4^0$ and also not included in the table given in the preliminary note. All the 5p′—6s′, 5d′ combinations are given in Table III.

An attempt to identify the 6s″ and 5d″ terms with the help of ther intervals of the 5p″ levels has led to the identification of only the 6s″ $^3P^0_1$ level definitely and the 6s″ $^1P^0_1$, 5d″ $^1D^0_2$, $^1P^0_1$ levels with a certain amount of confidence. Other levels could not be suggested at all, the multiplets with these levels are too weak. But a number of levels are found with the anticipated order of magnitude.

Hence these are given as tentative levels in the preliminary note (1956) under the designations 6s″ a^0 and 5d″ (a^0, b^0, c^0 d^0) suggesting their possible J values.

The level 138127.0 given by Ramanadham and Rao as 6s′ a is retained as a^0 even though its reality is not yet confirmed.

IONISATION POTENTIAL

The absolute term values are calculated from the $^5S^0$ and $^3S^0$ terms of the 'ns' series using the Rydberg formula. The values are found to be 5s $^5S^0_2$=81771.3 and 5s $^3S_1{}^0$=77552.7 with effective quantum numbers 2.317 and 2.379 respectively. When their separations from the ground level 93927.5 and 98476.4 are added they give 175698 and 176029 cm^{-1} respectively for the distance separating the ground levels of Br II and Br III. Their mean comes to 175869 cm^{-1}, the same value arrived at by Moore (1952).

From the ns' $^3D_3{}^0$ levels converging to 4p^3 $^2D^0_{5/2}$ of Br II the absolute value of 5s′ $^3D^0_3$ is obtained to be 81908.6 giving the value 192286.8 for the limit 4p^3 $^2D^0_{5/2}$ of Br III reckoned from the ground level 4p^4 $^3P_2$ of Br II. The difference between the two limits is 16418 cm^{-1} which is in very good agreement with the interval 4p^3 $^4S^0_{3/2}$—4p^3 $^2D^0_{5/2}$ in Br III equal to 16300 cm^{-1} (Bhupala Rao, 1956a).

Though Moore has arrived at the value 175870 cm^{-1} (I.P. 21.80 V) for the limit, she has retained the value 174119 cm^{-1} (I.P. 21.6 V) given by Bloch, Bloch

TABLE VII

Configuration	Designation	J	Level	Interval
4s^2 4p^4	4p^4 ^1S	0	27876	
4s^2 4p^3 (^4S) 6s	6s $^5S^0$	2	135794.3*	
4s^2 4p^3 (^4S) 6s	6s $^3S^0$	1	137608.0*	
	a^0	1	138127.0*	
4s^2 4p^3 (^4S) 5d	5d $^5D^0$	0	140223.5*	
				−0.8
		1	140222.7*	
				284.3
		2	140507.0*	
				−212.5
		3	140294.5*	
				−2.4
		4	140292.1*	
	b^0	2	151458.3*	
4s^2 4p^3 (^2P) 6s	6s″ a^0	2	166487.2	
4s^2 4p^3 (^2P) 6s	6s″ $^1P^0$	1	167439.0	

TABLE VII (*contd.*)

Configuration	Designation	J	Level	Interval
$4s^2\ 4p^3\ (^2P)\ 5d$	$5d''\ a^0$	2 or 3	169127.6	
$4s^2\ 4p^3\ (^2P)\ 5d$	$5d''\ b^0$	2 or 3	169368.1	
$4s^2\ 4p^3\ (^2P)\ 5d$	$5d''\ c^0$	2	169676.2	
$4s^2\ 4p^3\ (^2P)\ 5d$	$5d''\ d^0$	2 or 3	169768.9	
$4s^2\ 4p^3\ (^2P)\ 5d$	$5d''\ {}^1D^0$	2	170703 1	
$4s^2\ 4p^3\ (^2P)\ 5d$	$5d''\ {}^1P^0$	1	170827.4	
Br III ($^4S^0_{1\frac{1}{2}}$)	LIMIT		175870	

* Identified in previous investigations

TABLE VIII

Intensity	λ(air)	ν(vac)	Classification	Remarks
1	8725.3	11458	$4d'\ {}^3F_3{}^0-5p'\ {}^3D_2$	
0	8417.5	11877	$4d'\ {}^3F_4{}^0-5p'\ {}^3F_3$	
1	8231.0	12146	$4d'\ {}^3F_3{}^0-5p'\ {}^3D_3$	
1	7552.2	13238	$4d'\ {}^3F_4{}^0-5p'\ {}^3F_4$	Br I
0	6768.8	14770	$4d'\ {}^3F_3{}^0-5p'\ {}^3P_2$	
2	6168.49	16207.0	$5p''\ {}^3D_3-5d'\ {}^3P_2{}^0$	
00	5643.37	17715.0	$5s'\ {}^1D_2{}^0-5p'\ {}^3D_3$	
00	5611.42	17815.9	$5p''\ {}^3D_1-5d'\ {}^3P_2{}^0$	
4	5199 35	19227.8	$4d\ {}^3D_3{}^0-5p'\ {}^3F_3$	
2	5055.87	19773.5	$5p\ {}^3P_0-6s\ {}^3S_1{}^0$	
1	4941.24	20232.2	$5s'\ {}^3D_3{}^0-5p'\ {}^3F_2$	
2	4861.11	20565.7	$5p''\ {}^3P_2-6s''\ a_2{}^0$	
3	4777.04	20927.6	$5s'\ {}^3D_2{}^0-5p'\ {}^3F_2$	
00vbb	4578.07	21837.2	$5p''\ {}^3P_1-6s''\ {}^1P_1{}^0$	
0	4465.18	22389.3	$5p\ {}^3P_0-5d\ {}^5D_1{}^0$	
1	4388.20	22782.0	$5p''\ {}^3D_3-6s''\ a_2{}^0$	
0	4361.54	22921.3	$5p''\ {}^1P_1-6s''\ {}^1P_1{}^0$	
2H	4308.00	23206.1	$5p''\ {}^3P_2-5d''\ a_2{}^0$ or 3	
1	4261.22	23460.9	$5s''\ {}^3P_2{}^0-4f\ {}^3F_2$	

TABLE VIII (*contd.*)

Intensity	λ(air)	ν(vac)	Classification	Remarks
2	4208.51	23754.7	$5p''\ ^1D_2-5d''$ a_2^0 or 3	
			$5p''\ ^3P_2-5d''$ c_2^0	
00	4192.40	23846.0	$5p''\ ^3P_2-5d''$ d^0_2 or 3	
0	4129.33	24210.2	$4d\ ^3D_1^0-5p'\ ^1D_2$	
2	4118.56	24273.0	$4d'\ ^3F_4^0-5p''\ ^3D_3$	
1	4115.71	24290 3*	$5p''\ ^3P_0-6s''\ ^1P_1^0$	
1	4106.39	24345.5	$4d'\ ^3F_3^0-5p''\ ^3D_2$	
0	4105.50	24350.7	$4d'\ ^3F_2^0-5p''\ ^3D_1$	
1	4097.90	24395.9	$5p''\ ^1D_2-5d''\ d_2^0$ or 3	
0	4034.11	24781.6	$5p''\ ^3P_2-5d''\ ^1D_2^0$	
00	3963.18	25225.2	$5p''\ ^3P_1-5d''\ ^1P_1^0$	Br III line?
3	3946.86	25329.5	$5p''\ ^1D_2-5d''\ ^1D_2^0$	
0b	3944.55	25344.3	$5p''\ ^3D_3-6s''\ ^1P_1^0$	
00	3932.27	25423.4	$5p''\ ^3D_3-5d''\ a_2^0$ or 3	
0	3927.42	25454.8	$5p''\ ^1D_2-5d''\ ^1P_1^0$	
0	3895.52	25663.3	$5p''\ ^3D_3-5d''\ b_2^0$ or 3	
0	3850.94	25960.4	$4d'\ ^3F_2^0-5p''\ ^3D_1$	
0b	3849.28	25971.6	$5p''\ ^3D_3-5d''\ c_2^0$	
0	3835.82	26062.7	$5p''\ ^3D_3-5d''\ d_2^0$ or 3	
1	3817.85	26185.4	$5p''\ ^1P_1-5d''\ ^1D_2^0$	
2	3811.37	26229.9	$5s'\ ^3D_3^0-5p'\ ^1D_2$	
0b	3799.80	26309.7	$5p''\ ^1P_1-5d''\ ^1P_1^0$	
0	3778.43	26458.5	$5d\ ^5D_1^0-5p'\ ^3F_2$	
2h	3770.41	26514.8	$5p''\ ^3D_2-5d''\ b_2^0$ or 3	
1	3762.82	26568.3	$4d\ ^5D_2^0-5p'\ ^3D_3$	
1	3756.84	26610.6	$4d\ ^5D^0_3-5p'\ ^3D_3$	coincidence with a Br III line
1	3749.43	26663.2	$4d'\ ^3F_4^0-4f\ ^3F_4$	Br III line
00	3733.99	26773.4	$4d'\ ^3F_2^0-5p''\ ^1P_1$	
0	3727.29	26821.5	$5p''\ ^3D_2-5d''\ c_2^0$	Br III line?
3h	3725.46	26834.7	$5p''\ ^3S_1-5d''\ c_2^0$	?

TABLE VIII (*contd.*)

Intensity	λ(air)	ν(vac)	Classification			Remarks
00	3721.25	26865.1	$4d'$	$^3F_3^0-5p''$	$^1D_2$	
3	3714.45	26914.3*	$5p''$	$^3D_2-5d''$	d^0_2 or 3	
00	3712.93	26925.3	$5s'$	$^3D_2^0-5p'$	$^1D_2$	
2	3678.24	27179 2	$5s'$	$^3D_1^0-5p'$	$^1D_2$	
2	3624 87	27579 4	$4d'$	$^3F_3^0-4f$	$^3F_2$	
			$5p''$	$^3D_1-5d''$	c_2^0	
1	3623.88	27586.9	$4d'$	$^3F_3^0-4f$	$^3F_1$	
3	3622.06	27600.8	$4d$	$^5D_2^0-5p'$	$^1F_3$	
0	3615.92	27647.6	$4d$	$^5D_4^0$ $5p'$	$^3F_4$	
1	3608.98	27700.8	$4d$	$^5D_3^0-5p'$	$^3F_4$	
1	3527.98	28336.8	$4d'$	$^3F_2^0-4f$	$^3F_3$	Br III line
0h	3527.06	28344.2	$4d'$	$^3F^0_2-4f$	$^3F_2$	
00	3480.59	28722.6	$5p'$	$^1D_2-6s''$	$^3P_1^0$	
1	3432 33	29126.4	$4d$	$^5D_1^0-5p'$	$^3P_2$	
0	3419.82	29233.0	$4d$	$^5D_3^0-5p'$	$^3P_2$	
0	3400.93	29395.3	$4d$	$^5D_0^0-5p'$	$^3P_1$	
1	3397.88	29421.7	$4d$	$^5D_1^0-5p'$	$^3P_0$	Br III line
1	3387.18	29514.6	$4d$	$^5D_2^0-5p'$	$^3P_1$	
1	3310.28	30200.3	$5s$	$^3S_1^0-5p'$	$^3D_1$	
1	3174.66	31490.4	$5s$	$^3S_1^0-5p'$	$^3D_2$	
1h	3150.94	31727.4	$5p'$	$^3P_1-6s''$	$^3P_1^0$	
1	2958.07	33796.0	$5p$	$^3P_1-6s'$	$^3D_1^0$	
?	2945.55	33939.6	$5p$	$^3P_1-6s'$	$^3D_2^0$	coincidence with a Br III line?
0	2888.29	34612.4	$5p$	$^3P_2-6s'$	$^3D_3^0$	
00h	2834.41	35270.4	$5p$	$^3P_1-6s'$	$^1D_2^0$	
1H	2725.32	36682.1	$5s$	$^5S_2^0-5p'$	$^3F_2$	
00	2715.16	26819.4	$5p$	$^5P_1-6s'$	$^3D_2^0$	
2H	2578.66	38768.2	$4d$	$^5D_2^0-5p''$	$^3D_2$	
2	2393.32	41770.2	$4d$	$^5D_1^0-5p''$	$^3P_2$	
00	2372.05	42144.7	$5p$	$^3P_2-5d'$	$^4P_2^0$	

TABLE VIII (*contd.*)

Intensity	λ(air)	ν(vac)	Classification	Remarks
0	2344.92	42632.3	$5p\ ^5P_3$–$5d'\ ^3D_3^0$	Br III line
3	1410.2	70911	$4p^4\ ^1S_0$–$4p^5\ ^3P_1^0$	?
1	1226.3	81545	$4p^4\ ^1S_0$–$5s'\ ^3D_1^0$	
1	1170.2	85453	$4p^4\ ^1S_0$–$4p^4\ ^1P_1^0$	Br III line?
1	1029.0	97183	$4p^4\ ^1S_0$–$5s''\ ^1P_1^0$	
0	947.1	105591	$4p^4\ ^3P_0$–$5s'\ ^3D_1^0$	
0	889.9	112375	$4p^4\ ^3P_2$–$4d\ ^3D_1^0$	?
1	786.4	127160	$4p^4\ ^1D_2$–$5d\ ^3D_3^0$	
00	743.8	134454	$4p^4\ ^3P_1$–$6s\ ^3S_1^0$	
0	710.6	140726	$4p^4\ ^1D_2$–$6s'\ ^1D_2^0$	

* Also classified otherwise in previous investigations.

† double classification.

and Lacroute (1934) feeling that the new value is probably too high. Lacroute (1935, page 70) stated that the absolute values were obtained from the $ns\ ^5S_2^0$ series and remarked that the calculation made from two terms could not be considered as very accurate. From the results of the calculations by Moore and in the present investigation it appears that Lacroute's estimate is in error On a perusal of the table of binding energies of electrons of singly-ionised atoms (Moore and Russell, 1952) the value derived for Br II on the basis of 174119 cm^{-1} for the limit seems to be too small and not consistent with the general progression of values in the first spark spectra of neighbouring elements. With 175870 cm^{-1}

TABLE IX

Spectrum	4p	4d	5s	5p	5d
Se II	$4p^3\ ^4S_{3/2}^0$ 21.5		$5s\ ^4P_{1/2}$ 9.70	$5p\ ^4P_{1/2}^0$ 7.50	$5d\ ^4F_{3/2}$ 4 36
Bloch	21.6	—	9.94	7.37	4.32
Br II	$4p^4\ ^3P_2$	$4d\ ^5D_3^0$	$5s\ ^5S_2^0$	$5p\ ^5P_1$	$5d\ ^3D_3^0$
Author	21.80	8.90	10.16	7.58	4.54
Kr II	$4p^5\ ^2P_{3/2}^0$ 24.56	$4d\ ^4D_{7/2}$ 9.66	$5s\ ^4P_{5/2}$ 10.58	$5p\ ^4P^0_{5/2}$ 7.96	$5d\ ^4P_{1/2}$ 4.63

for the limit they appear to be of the right order of magnitude and are given in Table IX along with the old ones based on Bloch's value for the limit and those for Se II and Kr II.

A comparison of the effective quantum numbers $n^*=4\ R/T$ corresponding to the deepest terms of the 5s electron in the first spark spectra of bromine and its neighbouring elements is made in Table X as in the case of As 1. (Meggers, Shenstone and Moore, 1950).

TABLE X

Spectrum	Term	T (Absolute value)	$4R/T$	$n^*=(4R/T)^{1/2}$
Ga II	$5s\ ^3S_1$	62515	7 022	2.650
Ge II	$5s\ ^2S_{1/2}$	66116	6.639	2.577
As II	$5s\ ^3P_0^0$	84271	5.209	2.282
Se II	$5s\ ^4P_{3/2}$	78287.0	5.607	2.368
Br II	$5s\ ^5S_2^0$	81905.1	5.359	2 315
Kr II	$5s\ ^4P_{5/2}$	85352.0	5 143	2 268
Rb II	$5s\ ^3P_2^0$	88504.7	4.960	2 227
Sr II	$5s\ ^2S_{1/2}$	88964.0	4.934	2.221

By interpolation the value of n^* for 5s in Br II is obtained as 2.315. The corresponding term $T=4R/(n^*)^2$ has a numerical value $(4\times109737.1)/(2.315)^2=81905.1$ and gives the limit as 175832.6 cm^{-1} agreeing very well with the value derived from the "ns" series. This value 2.315 of n^* for 5s $^5S^0_2$ derived in this way is in good agreement also with the value 2.317 derived from the "ns" series. In view of the above considerations it appears that the value 175870 cm^{-1} for the limit may not be high and may be adopted as the limit corresponding to a second ionisation potential of 21.80 volts. This is therefore given as the limit.

Comparison with other spectra

A perusal of the final analysis shows that the term intervals are in general smaller than the separations between different terms and there is not much mixing up of levels of different terms. But the interval ratios within the terms are not in accord with the theoretical values derived from L-S coupling. The spectrum has very great resemblance to Kr III in several respects.

A comparison of the relative positions of $(n+1)s\ ^5S^0$, $nd\ ^5D^0$ and $np^5\ ^3P^0$ terms in the analogous spectra will be of interest here. The values are taken from Moore's "Atomic Energy Levels" Vols. I and II (1949 and 1952) and are collected in Table XI. The values of the limit and 4d $^5D^0_4$ for Br II are from the present

analysis. A striking feature of the structure of these spectra is the increasing stability with atomic number of the np^5 and nd configurations. In both the isoelectronic sequences the $(n+1)\ ^5S^0$ term lies deepest in the first members, SI and SeI, followed by $nd\ ^5D^0$ and $np^5\ ^3P^0$. In the case of the second members, Cl II and Br II, they are all of the same order and a crossing of the levels takes place.

TABLE XI

Spectrum	Limit	n	$(n+1)s\ ^5S_2^0$	$nd\ ^5D_4^0$	$np^5\ ^3P_2^0$
S I	83559.3	3	52623.9	67878.0	72025.5
Cl II	192000	3	107878 5	110295.8	93366.6
A III	32996.58	3	174375.0	144907 0	113800.7
Se I	78658.2	4	48182.2	63370 1	—
Br II	175870	4	93927.5	104097.9	96439.4
Kr III	298020	4	145720.0	138650.3	115932

When we go to the third members, A III and Kr III, the order of the terms is $np^5\ ^3p^0$, $nd\ ^5D^0$ and $(n+1)s\ ^5S^0$. The $np^5\ ^3p^0$ terms are all inverted. The intervals of the $nd\ ^5D^0$ terms are all small and they are inverted except in A III and Kr III.

ACKNOWLEDGMENTS

The author is very much indebted to Prof. K. R. Rao for his very kind and valuable guidance throughout the progress of this work. The author wishes to take this opportunity to express his grateful thanks to Prof. Manne Siegbahn for his very kind interest and help in securing the 1-metre grating for the vacuum grating spectrograph and to Prof. S T. Krishnaswamy Chetty for very kindly making a mount for the grating. The author is thankful to Dr. C. Ramasastry for the kind help in securing the infra-red plates and to all his friends for their kind help. The author is thankful to the Government of India for the award of a research scholarship.

REFERENCES

Bhupala Rao, Y. 1956, *Ind. J. Phys.*, **30**, 95.
Bhupala Rao, Y. 1956a, *Ind, J. Phys.* **30**, 371.
Bloch L. and Bloch, E. 1927, *Ann. de. Phys.*, **7**, 205.
Bloch, L. Bloch E. and Lacroute, P. 1934, *Compt. Rend.*, **199**, 41.
Boyce, J. C. 1935, *Phys. Rev.*, **47**, 718.
Humphreys, C. J. 1935, *Ibid*, **47**, 712.

Kiess C. C. and Bruin, T. L. de 1929, *Bur. Std. Jour. of Research*, **4**, 667.

Kiess C. C. and Bruin, T. L. de 1939, *Bur. Std. Jour. of Research* **23**, 443.

Lacroute, P. 1935, *Ann. de Phys.*, **3**, 3.

Meggers, W. F. A. G. Shenstone and C. E. Moore, 1950, *Bur. Std. Jour. of Research*, **45**, 346.

Moore, C. E. 1949, Atomic Energy Levels, Vol. I.

Moore, C. E. 1952, Atomic Energy Levels, Vol. II.

Moore, C. E. and Russell, H. N. 1952, *Bur. Std. Jour. of Research*, **48**, 61.

Murakawa, K. 1935, *zeits. f. Phys.*, **96**, 117.

Murakawa, K. 1938, *zeits. f. Phys.* **109**, 162.

Ramanadham R. and Rao, K. R. 1944, *Ind. J. Phys.*, **18**, 317.

Ranade, J. D. 1951, *Phil. Mag.*, **42**, 284.

Rao K. R. and Badami, J S. 1931, *Proc. Roy. Soc. Lond. A.*, **131**, 154.

Ruedy J. E. and Gibbs, R. C. 1934, *Phys. Rev.*, **46**, 880.

Tolansky S. and Trivedi, S. A. 1940, *Proc. Roy. Soc. Lond. A.*, **175**, 366.

DIPOLE MOMENTS OF SOME SUBSTITUTED BENZENES AND PYRIDINES

C. R. K. MURTY

PHYSICS DEPARTMENT, ANDHRA UNIVERSITY, WALTAIR

(*Received for publication September* 16, 1958)

ABSTRACT. The dipole moments of seven substituted pyridines have been determined in dilute solution in benzene. The moment values are also calculated using group moments and vectorial method. The differences in moments between the calculated and observed values have been discussed.

INTRODUCTION

Since the publication of the electron diffraction results on pyridine by Schomaker and Pauling (1939), considerable interest was shown on the investigation of the dipole moments of these compounds. The electron diffraction studies have revealed that pyridine has a structure similar to that of benzene. The determination of the dipole moments of γ-substituted pyridines by Leiss and Curran (1945) has confirmed the similarity between the benzene and pyridine rings. To determine whether or not the carbon nitrogen linkage can be adequately represented by a single constant in heterocyclic ring systems, Schneider (1948) has determined the dipole moments of diazines and drawn the following conclusions : (1) the carbon nitrogen electric moment apparently has a constant value in the heterocyclic compounds investigated, (2) a heterocyclic ring of the pyridine type can be represented by a plane hexagon and (3) in the compounds investigated, all bonds between nitrogen and carbon seem to be electrically equivalent so far as dipolar characteristics are concerned.

The present investigation on substituted pyridines has been undertaken primarily to obtain dipole moment data on as many pyridine compounds as possible in order to understand their structure.

The experimental arrangement used for measurement of dielectric constant and refractive index of solutions and the method of calculation of dipole moments from the experimental observations had been described previously by the author (1957). All the substituted pyridines were supplied by L. Lights and Co., England and were reported to be of a high standard of purity. The solvent benzene was also of A.R. grade of purity.

CALCULATION OF μ FROM GROUP MOMENTS

For the calculation of dipole moment in the case of 2-and 3-acetyl pyridines, group moments of 2.22 and 2.89 have been assumed for N– and acetyl

groups respectively. It has also been assumed that the acetyl group moment makes an angle of 55° with the C-C bond to the ring (Smyth, 1955). This value of the angle has been obtained from the dipole moment of *p*-diacetyl benzene.

In the case of amino methyl pyridines, the group moments 0.40 and 1.53 have been assumed for CH_3 and NH_2. It is also assumed that the moment of NH_2 acts along the C–C bond to the ring following the example of other substituted pyridines investigated by Curran (1945). If it is assumed that NH_2 group moment makes an angle of 38° with the C–C bond following the example of substituted anilines, the calculated values are very much different from the observed values.

RESULTS AND DISCUSSION

Dipole moments of seven substituted pyridines have been determined and the results are given in Tables I to VII. The observed and calculated values of dipole moments are given in Table VIII.

TABLE I

2-Acetyl pyridine

W	ε_{12}	$\Delta\varepsilon$	$\Delta\varepsilon/W$	n_{12}	n^2_{12}	Δn^2	$\Delta n^2/W$
0 01204	2.3639	0.0999	8 290	1.49416	2 23252	0.00187	0.155
0 02223	2.4398	0 1758	7 911	1 49432	2 23289	0 00224	0.101
0 03479	2 5335	0.2695	7.745	1.49454	2.23364	0.00299	0.086
0 04851	2 6360	0 3720	7.670	1.49454	2 23364	0.00299	0.062
0.06299	2.7448	0 4808	7.632	1.49459	2 23381	0.00316	0.050
0.07645	2.8489	0 5849	7.650	1.49474	2.23425	0.00360	0.047

$(\Delta\varepsilon/W)_{W\to 0}=8.08$, $(\Delta n^2/W)_{W\to 0}=0\ 124$. $P_d=163.4$ c.c. $\mu=2.85$D

TABLE II

3-Acetyl pyridine

W	ε_{12}	$\Delta\varepsilon$	$\Delta\varepsilon/W$	n_{12}	n^2_{12}	Δn^2	$\Delta n^2/W$
0.02276	2.4109	0.1469	6.455	1.49522	2.23569	0 00504	0.221
0.03499	2.4829	0.2189	6.253	1.49577	2.23733	0.00668	0.191
0.04908	2.5722	0.3082	6.280	1.49598	2.23795	0.00730	0.149
0.06272	2.6550	0.3910	6.234	1.49633	2 23901	0.00836	0.133
0.07352	2.7247	0.4607	6.266	1.49668	2.24007	0.00942	0.128

$(\Delta\varepsilon/W)_{W\to 0}=6.48$, $(An^2/W)_{W\to 0}=0.262$. $P_d=128.6$ c.c. $\mu=2.53$D

TABLE III

2-Amino-3-methyl pyridine

W	ε_{12}	$\Delta\varepsilon$	$\Delta\varepsilon/W$	n_{12}	n^2_{12}	Δn^2	$\Delta n^2/W$
0.00263	2.2776	0.0136	5.190	1.49383	2.23154	0.00089	0.383
0.00448	2.2880	0.0240	5.348	1.49399	2.23202	0.00137	0.306
0.00856	2.3125	0.0485	5.665	1.49421	2.23267	0.00202	0.236
0.01417	2.3477	0.0837	5.912	1.49467	2.23404	0.00339	0.239
0.01820	2.3726	0.1086	5.971	1.49473	2.23423	0.00358	0.197

$(\Delta\varepsilon/W)_{W\to 0}=5.08$, $(\Delta n^2/W)_{W\to 0}=0.342$. $P_d=94.9$ c.c. $\mu=2.17$ D

TABLE IV

2-Amino-4-methyl pyridine

W	ε_{12}	$\Delta\varepsilon$	$\Delta\varepsilon/W$	n_{12}	n^2_{12}	Δn^2	$\Delta n^2/W$
0.00207	2.2843	0.0203	9.766	1.49386	2.23163	0.00098	0.473
0.00436	2.2987	0.0347	7.943	1.49414	2.23246	0.00181	0.415
0.00721	2.3179	0.0539	7.482	1.49419	2.23261	0.00196	0.272
0.01021	2.3353	0.0713	6.984	1.49444	2.23335	0.00270	0.264
0.01267	2.3438	0.0798	6.306	1.49464	2.23396	0.00331	0.261

$(\Delta\varepsilon/W)_{W\to 0}=8.67$, $(\Delta n^2/W)_{W\to 0}=0.550$. $P_d=141.0$ c.c. $\mu=2.65$D

TABLE V

2-Amino-5-methyl pyridine

W	ε_{12}	$\Delta\varepsilon$	$\Delta\varepsilon/W$	n_{12}	n^2_{12}	Δn^2	$\Delta n^2/W$
0.00202	2.2782	0.0142	7.021	1.49411	2.23237	0.00172	0.851
0.00294	2.2819	0.0179	6.103	1.49427	2.23284	0.00219	0.747
0.00678	2.3026	0.0386	5.689	1.49462	2.23390	0.00325	0.479
0.00993	2.3181	0.0541	5.450	1.49462	2.23390	0.00325	0.327
0.01371	2.3353	0.0713	5.198	1.49464	2.23396	0.00331	0.241

$(\Delta\varepsilon/W)_{W\to 0}=6.32$, $(\Delta n^2/W)_{W\to 0}=0.880$. $P_d=111.4$ c.c. $\mu=2.35$ D

TABLE VI

2-Amino-6-methyl pyridine

W	ε_{12}	$\Delta\varepsilon$	$\Delta\varepsilon/W$	n_{12}	n^2_{12}	Δn^2	$\Delta n^2/W$
0.01405	2 3157	0.0517	3.678	1.49561	2.23686	0.00621	0.442
0.01899	2.3348	0.0708	3.729	1.49633	2.23900	0.00835	0.440
0.02816	2.3699	0 1059	3.761	1 49692	2 24078	0 01013	0.360
0.03601	2 4023	0 1383	3.840	1.49756	2.24269	0.01204	0.334
0.04561	2.4400	0 1760	3.859	1.49783	2.24350	0.01285	0.282

$(\Delta\varepsilon/W)_{W\to 0}=3.605$, $(\Delta n^2/W)_{W\to 0}=0\ 510$. $P_d = 63\ 2$ c.c. $\mu = 1.77$ D

TABLE VII

2-Amino-4-6-dimethyl pyridine

W	ε_{12}	$\Delta\varepsilon$	$\Delta\varepsilon/W$	n_{12}	n^2_{12}	Δn^2	$\Delta n^2/W$
0 01112	2 3138	0 0498	4.483	1 49528	2.23586	0.00521	0 469
0.01738	2.3389	0.0749	4 308	1 49587	2 23763	0 00698	0 402
0 02518	2 3664	0 1024	4.069	1 49629	2 23890	0 00825	0.328
0.03487	2.3999	0 1359	3.896	1.49668	2.24007	0.00942	0.270
0.04056	2 4133	0.1493	3.696	1.49747	2 24242	0.01177	0 290

$(\Delta\varepsilon/W)_{W\to 0}=4.72$, $(\Delta n^2/W)_{W\to 0}=0.520$ $P=97\ 7$ c.c. $\mu=2.20$D

TABLE VIII

Substance	μ observed	μ calculated
2-Acetyl pyridine	2 85	2 81 D
3-Acetyl pyridine	2.53	0.71
2-Amino-3-methyl pyridine	2 17	2.35
2-Amino-4-methyl pyridine	2.65	2.28
2-Amino-5-methyl pyridine	2.35	1.92
2-Amino-6-methyl pyridine	1.77	1.59
2-Amino-4 : 6-dimethyl pyridine	2 20	1.92

In the case of acetyl pyridines, the agreement between calculated and observed values is satisfactory when the acetyl group is in the α-position. For β-acetyl

pyridine the calculated value is very low compared to the observed value of 2.53. This difference is so much that it cannot be accounted for by experimental errors. The discrepancy may be understood when the γ-acetyl pyridine is also investigated.

The group moments of CH_3 and NH_2 have the same sign but opposite to that of pyridine moment. As the group NH_2 is fixed in the α-position in all the compounds investigated, the moment to be expected for 2-amino-3-methyl pyridine is that of 2-amino pyridine plus the small contribution of CH_3. The observed value appears to be somewhat less than the expected value. When CH_3 is in the γ-position the moment observed is maximum indicating negligible effect of NH_2 on CH_3 and an approximate moment of $2.17+0.40 = 2.57$ may be expected for this compound. The observed value of 2.65 shows fair agreement with the expected value though considerably greater than the calculated value obtained by simple vectorial method. The value of 2.17 for 2-amino pyridine includes the inductive and resonance effects between pyridine and NH_2 group.

In the case of 2-amino-5-methyl pyridine the CH_3 group is in the meta-position relative to N– and away from NH_2 unlike in 2-amino-3-methyl pyridine. Assuming negligible effect of NH_2, a moment of 2.39 is to be expected which is close to 2.35 observed for this compound. 2-amino-6-methyl pyridine should have the minimum moment since both NH_2 and CH_3 are ortho-to N. The observed value of 1.77 is minimum for all these compounds and is slightly greater than the value of 1.65 observed for 2 : 6-dimethyl pyridine as is to be expected.

The moment value for 2-amino-4-6-dimethyl pyridine should be obtained by adding CH_3 group moment to that of 2-amino-6-methyl pyridine since CH_3 which is added is para-to N. The observed value of 2.20 is in reasonable agreement with 2.17 which is the expected value.

In conclusion, the author considers that a much larger amount of data on pyridine compounds with various substitutions in different positions have to be collected before the structure and resonance effects in these compounds can be completely discussed.

ACKNOWLEDGMENT

The author is very much indebted to Prof. K. R. Rao for his kind and constant guidance throughout the progress of the work.

REFERENCES

Curran, B. C., and Leiss, D. G., 1945, *J. Am. Chem. Soc.*, **67**, 79.
Murty, C. R. K., 1957, *Ind. J. Phys.*, **31**, 256.
Schneider, W. C., 1948, *J. Am. Chem. Soc.*, **70**, 627.
Schomaker, V., and Pauling, L., 1939, *J. Am. Chem. Soc.*, **61**, 1769.
Smyth, C. P., 1955, Dielectric Behavior and Structure, McGraw-Hill Book Co., pp. 343.

CORRECTION FOR STOKES' LAW

N. R. GOKHALE AND K. M. GATHA

PHYSICS DEPARTMENT, INSTITUTE OF SCIENCE, BOMBAY-1

Received for publication, May 22, 1958

ABSTRACT. Millikan's correction to Stokes' law for water droplets falling through air has been measured. Some necessary improvements over Millikan's method have been introduced. The present direct measurement yields the value $A = 0.701$ for the relevant correction constant

INTRODUCTION

To study the rate of evaporation of unattached water droplets, they have been allowed to evaporate at a controlled temperature and pressure within Millikan's oil-drop apparatus, containing air at some specified relative humidity With the help of Stokes' law, the droplet radii have been calculated by measuring the values of velocity under gravity at intervals in the usual manner. The range of the droplet radii in the present series of experiments varies from 5×10^{-5} cm to 2×10^{-4} cm. Since such droplet radii are not large compared to the mean free path in air at room temperature and atmospheric pressure, Millikan's correction to Stokes' law has been experimentally determined for water droplets falling through air.

MILLIKAN'S CORRECTION TO STOKES' LAW

In gases at ordinary pressures the slip due to molecular inhomogeneities makes Stokes' law slightly incorrect even for spheres with radii as large as 0.005 mm Millikan has suggested that the usual Stokes' law should be replaced by an equation of the general form,

$$X = 6\pi\eta R V_g(1+A'l/R)^{-1} \qquad \ldots \quad (1)$$

where l is the molecular mean free path in air and

$$A' = A+Be^{-CR/l} \qquad \ldots \quad (2)$$

where A and B are constants depending on the nature of the gas and the drop substance, while C is equal to 1.25 Millikan determined the values of A' by the oil-drop method, for a wide range of the ratio l/R, for different drop substances and media.

The correction $(1+A'l/R)^{-1}$ can also be written as $(1+b/pR)^{-1}$, where b is a constant and p is the pressure.

DETERMINATION OF A' FOR WATER DROPLETS FLLING THROUGH AIR

It may be noted that as the readings in the present series of experiments are taken at atmospheric pressure, the second term in equation (2) would become quite negligible and A' is equal to A

The higher rate of evaporation of water, as compared to that of oil, makes the application of Millikan's procedure to determine the value of A' for water rather difficult. In order to avoid any appreciable evaporation of the observed droplet, the following three precautions have been taken:

(i) The air inside the chamber was made saturated with water vapour by keeping four small water-boats inside this chamber

(ii) With the above arrangement the air inside the chamber is made saturated for plane water surface. However, small drops with radii of the order of 10^{-4} to 10^{-5} cm will evaporate as the vapour pressure on a convex surface is more than that on a plane surface Hence before

TABLE I

Observed relation between $(e_1^{2/3})$ and $(1/pR)$

Observat numbe	t_g (sec)	t_f (sec)	$v_g \times 10^3$ (cm/sec)	$v_f \times 10^3$ (cm/sec)	$e_n \times 10^{10}$ (e.s.u.)	n	$e_1 \times 10^{10}$ (e.s.u.)	$e_1^{2/3} \times 10^8$	$R \times 10^5$ (cm)	p (cm of Hg)	$1/pR$
1	2	3	4	5	6	7	8	9	10	11	12
1	40.0	3.2	2.025	25.31	17 91	3	5.970	70 89	4 142	76.40	316.0
2	25.3	4.5	3 202	18.00	17.46	3	5.820	69.69	5.208	76.30	251.7
3	8.5	14.7	9.530	5.511	21.36	4	5.340	66.20	8.984	76.40	145.6
4	14 0	8.8	5.786	9 204	16.60	3	5.533	67.39	7.001	76.35	187 1
5	30.7	6.2	2 638	13.06	11 73	2	5.865	70 06	4 729	76.45	276.7
6s	21.5	5 3	3.768	15.29	17.02	3	5 673	68 52	5.649	76 45	231.5
7	16.0	7.3	5.063	11.10	16.74	3	5.580	67.76	6 549	76.40	199.8
8	41.0	11.0	1.975	7.364	6.042	1	6.042	71.47	4.091	76.40	320.0
9	7.5	24.6	10.80	3.294	21.31	4	5.327	65.70	9.566	76.50	136.7
10	11.9	12.0	6.808	6.750	16.28	3	5.426	66.53	7.600	76.50	172.1
11	9.9	9.9	8.183	8.183	21.54	4	5 385	66.19	8.326	76 35	157.3
12	27.6	6.8	2.935	11.91	11.70	2	5.850	69.95	4.986	76.30	262.8

starting to take observations on a droplet, considerable spraying caused numerous droplets to enter the chamber and evaporate for some time. This procedure further reduced the rate of evaporation of the droplet under observation

(iii) The time for which the droplet was under observation was minimized so as to make its evaporation negligible for all practical purposes. The procedure of taking observations has therefore been altered from that followed by Millikan The velocity under gravity for the droplet was measured and almost immediately its velocity in the opposite direction, with the electric field on, was noted

Only two such observations were recorded for each droplet. The variation in the values of the electronic charge ascertained by preliminary observations, was from 5×10^{-10} e.s.u. to 6×10^{-10} e.s u. for the dorplet radii in the present series of experiments. Hence it was possible to guess correctly the value of n when the same was small. It is for this reason that the value is chosen equal to or less than 4.

A number of preliminary observations were taken to calculate approximately the value of e_1. But only those observations, with n between 1 and 4 were used

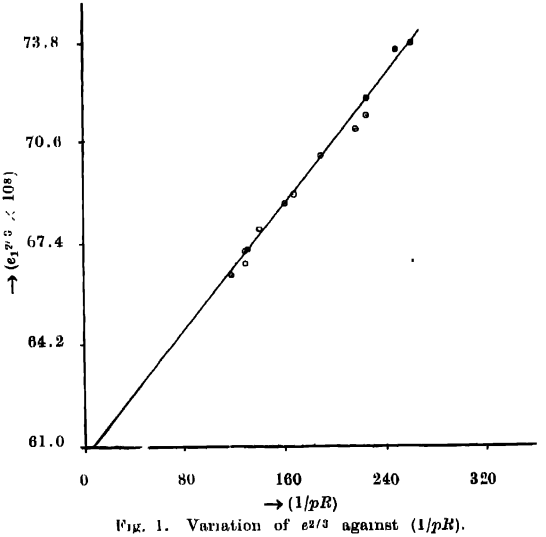

Fig. 1. Variation of $e^{2/3}$ against $(1/pR)$.

for further calculations. These observations are presented in Table I. In making these calculations, the density of the liquid $\sigma = 0.996$ gm cm^{-3}, the density

of the medium $\rho = 0.00129$ gm cm^{-3} and the viscosity of the medium $\eta = 183.2 \times 10^{-6}$ dynes per sq. cm. per unit vel. grad. have been used. Further, one division of the tele-microscope equals 0.081 cm. The second column of Table I gives the values of the time t_g taken by the droplet to traverse one division in the tele-microscope under the gravitational field alone. Whereas, the third column gives the values of the time t_f taken by the dorplet to travel one such division when the electric field is applied. After calculating V_g and V_f, e_n is calculated with $F = 2.183$ volts cm^{-1}. The values e_1 and $e_1^{2/3}$ are presented in the eighth and ninth columns respectively The tenth column gives the values of R and the last column gives the values of $(1/pR)$ varying between 136.7 and 320.

The graph showing the variation of $e_1^{2/3}$ against $(1/pR)$ is shown in figure 1. The points lie fairly well on a straight line that passes through the calculated value of $e^{2/3}$ when $(1/pR)$ is zero The constant b was calculated from the slope of this straight line giving $b = 0.000512$ Taking $l = 9.6 \times 10^{-6}$ cm and noting that $A = b/pl$, the value of A was calculated giving $A = 0.701$.

REFERENCES

Millikan, R A, 1912, Electron
Millikan, R A, 1920, *Phys. Rev.*, **15**, 545
Millikan, R. A, 1923, *Phys. Rev.*, **21**, 217
Millikan, R. A., 1923, *Phys Rev.*, **22**, 1.
Stoke, 1851, *Cambr. Trans.* 9 & *Mathematical and Physical Papers* **3**, 59.

ELECTRONIC SPECTRA OF *o*-CHLOROPHENOL IN DIFFERENT ENVIRONMENTS AND AT DIFFERENT TEMPERATURES*

S. B. ROY

OPTICS DEPARTMENT, INDIAN ASSOCIATION FOR THE CULTIVATION OF SCIENCE, JADAVPUR, CALCUTTA-32

(*Received for publication, September* 19, 1958)

ABSTRACT. Investigations have been carried out on the ultraviolet absorption spectra of pure *o*-chlorophenol and its solutions in CCl_4, cyclohexane, 3-methyl pentane and isobutyl alcohol at different temperatures. Both the pure liquid and .01% solution in CCl_4 show band systems with the 0,0 band at 35475 cm^{-1}, the bands in the former case being much broader. From a comparison of these spectra with those due to the vapour it has been concluded that some of the molecules in the pure liquid and most of the molecules in the solution are of trans configuration. Broadening of the bands in the spectrum due to pure liquid is ascribed to the presence of dimers in the liquid.

The spectra due to .01% solution in 3-methylpentane or cyclohexane are found to consist of a strong system of bands accompanied by a much weaker system displaced from the former towards higher energies by 346 cm^{-1} The stronger system has been assigned to trans molecules and the weaker one to molecules which form H-Cl bonds with neighbouring solvent molecules

The spectrum due to .01% solution in isobutyl alcohol shows a band system shifted towards longer wavelengths with respect to that in the case of the pure liquid by about 400 cm^{-1}. This unusually large shift towards red has been accounted for by assuming a strong interaction between solvent and solute molecules resulting in the formation of a compound similar to a trisubstituted benzene compound.

INTRODUCTION

It was first pointed out by Pauling (1936) that the two peaks at 6910 cm^{-1} and 7050 cm^{-1} observed by Wulf and Liddel (1935) in the infra red spectrum of solution of *o*-chlorophenol in CCl_4, might be due to the first harmonic of O-H valence oscillation in the cis and the trans configuration respectively. Later, Davies (1938) in repeating the same investigation in the region of 3450-3600 cm^{-1} at different temperature, supported the hypothesis of Pauling.

Errera and Mollet (1935) observed a broad absorption peak with a maximum at 6620 cm^{-1} in the infra red spectrum of the pure liquid. Pauling (1945) interpreted the result by suggesting that the further lowering of O-H frequency even below 6910 cm^{-1}, might be due to formation of dimers in which

* Communicated by Prof. S. C Sirkar,

the hydrogen atom of the O-H group in the trans molecule is linked with the oxygen atom of O-H group in the cis molecules in the liquid.

W. Lüttke and R. Mecke (1950) also investigated the infrared spectrum of *o*-chlorophenol in solution of CCl_4 in the region of 10000–10500 cm^{-1} and reported that the strong band at 10090 cm^{-1} and weak band at 10325 cm^{-1} are due to second harmonic of the O-H valence oscillation in the cis and the trans form respectively. These frequencies are not one and half times of those reported by Wulf and Liddel (1935).

Recently. Sirkar *et al* (1958) investigated the infrared spectrum of *o*-chlorophenol in the liquid state and its solution in CCl_4 and cyclohexane at various concentrations and temperatures in the region 3000–3700 cm^{-1}. They reported that the broad absorption bands due to *o*-chlorophenol in the pure liquid might be produced by the superposition of the three main broad bands at 3320, 3450 and 3500 cm^{-1} with a small inflexion at 3620 cm^{-1} They ascribed the first peak to dimers as proposed by Pauling and the second one at 3450 cm^{-1} to the cis molecules. From the spectrum due to 5% solution of *o*-chlorophenol in CCl_4, Sirkar *et al* concluded that the strong absorption peak at 3533 cm^{-1} is due to the O-H valence oscillation in trans molecules and suggested that 3595 cm^{-1} might be due to a combination frequency

From an investigation of the Raman spectra of solutions of *o*-chlorophenol in different solvents Mukherjee (1958) reported that the intensity of O-H line 3533 cm^{-1} increases with decrease of concentration of the solution. He concluded that the molecules of trans configuration become predominant in weak solution.

It is well known that the ultraviolet absorption spectra of substituted benzenes are affected appreciably by environment (Roy, 1956). It would, therefore, be interesting to study the influence of environment on the ultraviolet absorption spectrum of the ortho chlorophenol molecule. The object of the present investigation was to study such spectra of solutions of *o*-chlorophenol in different solvents in the liquid and solid states with a view to finding out whether the data furnished any information regarding the configuration of the molecule in the state of aggregation. The results discussed in the later sections show that different solvents have influences of different nature on the absorption spectra of the molecule.

EXPERIMENTAL

The experimental arrangement is similar to that described in an earlier paper (Roy, 1956). The solvents used were CCl_4, cyclohexane, 3-methyl pentane and isobutyl alcohol. The latter two solvents form rigid glass at −180°C. All the solvents were found to have no absorption in the region under consideration. *o*-Chlorophenol obtained from B.D.H. was of chemically pure quality. It was fractionated and the proper fraction was redistilled under reduced pressure.

The spectra were photographed on Ilford HP3 films with a Hilger medium quartz spectrograph. Iron arc spectrum was taken on each film as a comparison. Microphotometric records were taken with a Kipp and Zonen type microphotometer. The absorption spectra were calibrated with the help of microphotometric records of iron lines using the method described earlier (Roy, 1956).

RESULTS AND DISCUSSION

The microphotometric records of the absorption spectra of *o*-chlorophenol in the liquid and the solid state and its solution in CCl_4 are given in figure 1; those of

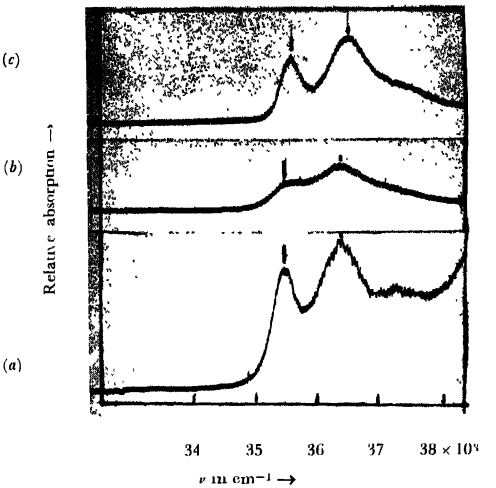

Fig. 1. Microphotometric records of absorption spectra of *o*-chlorophenol
(*a*) 01 % solution in CCl_4 with 5 mm cell at 30°C
(*b*) Pure liquid at 30°C
(*c*) Pure solid at −180°C

the solutions in cyclohexane, 3-methyl pentane and isobutyl alcohol are given in figures 2 and 3. The frequencies of the absorption bands and their probable assignments are given in Tables I, II and III. The data for the gaseous state (Ramasastri, 1951) are included in Table I for comparison

It can be seen from figure 1(a) that the spectrum due to .01% solution of *o*-chlorophenol in CCl_4 consists of three sharp bands with the 0, 0 band at 35475 cm^{-1} and excited state vibration frequency 917 cm^{-1}, whereas in the vapour state the 0, 0 band is at 35892 cm^{-1} and the corresponding excited state frequency is 953 cm^{-1}. So the solvent produces a shift of the band system

to lower energies of about 417 cm^{-1} and slight lowering of excited state frequency. The pure liquid shows much broader bands with their centres in the same positions as in the spectrum due to the solution in carbon tetrachloride. It is thus evident that the cause of this lowering of excited state energy of the molecule is the same in both the cases. Only chlorine atom is common in both the carbon tetrachloride molecule and *o*-chlorophenol molecule and probably the influence of the chlorine atom of a neighbouring molecule is responsible for this shift of the 0, 0 band. In that case it appears that the chlorine atom of the *o*-chlorophenol molecule in the liquid state is free to form some sort of linkage with the hydrogen atom of the benzene ring in the neighbouring molecule and in the solution in CCl_4, the chlorine atom of the solvent molecule may form such linkages with the hydrogen atom of benzene ring of the *o*-chlorophenol molecule.

In the solution each molecule of the solute is surrounded by large number of atoms of the solvent molecules and therefore there is higher probability of more than one C-H group being under the influence of surrounding chlorine atoms than in the pure liquid If such an influence in the solution on more than one C-H group would shift the 0, 0 band to 35475 cm^{-1}, only a fraction of the total number of the molecules may be under such an influence in the pure liquid and in the rest only one CH group may be under the influence of the chlorine atom of a neighbouring molecule. The shift of the 0, 0 band in the case of these latter molecules from its position in the spectrum due to vapour is expected to be smaller. The position of the broad 0, 0 band on the shorter wavelength side of 35475 cm^{-1} may be produced by these latter molecules and also by the dimers which may be present in the liquid (Paulung, 1945)

Thus it can be concluded from these results that in the pure liquid some of the molecules have the chlorine atom free from the influence of the O-H group and these molecules are of the trans configuration. Hence it can be seen from the above arguments that in the solution in carbon tetrachloride most of the molecules of the solute have the trans configuration. This conclusion is in agreement with those arrived at by Sirkar *et al.* (1958) from the results of the investigation on the infrared absorption spectra of solutions of *o*-chlorophenol.

The spectrum due to pure solid at −180°C (figure1 c), however, consists of three bands which are slightly sharper than that due to pure liquid and the 0, 0 band at 35600 cm^{-1}, is shifted towards shorter wavelength from the main peak at 35475 cm^{-1} in the spectrum due to pure liquid. This main peak is due to the molecules in which more than one CH group are under the influence of chlorine atom of the neighbouring molecules and the portion on the shorter wavelength side of the band at 35475 cm^{-1} has been assigned to those molecules in which only one CH group has been affected by the chlorine atom of the neighbouring molecule. So it appears that in the solid state the number of latter molecules increases and the number of those molecules in which more than one

CH group are affected, diminishes. If the position of the broad band due to the liquid further away from 35475 cm^{-1} towards shorter wavelength be assigned to dimers in which O–H–O is formed between two molecules, it appears that the number of such molecules in the solid state is much smaller because the absorption in this region in the solid state is very small.

Figure 2(a) shows that in the spectrum due to solution of orthochlorophenol in 3-methyl pentane in addition to three strong bands, as in the case of solution in CCl_4, three other weaker bands appear and the 0, 0 band at 35640 cm^{-1} is shifted

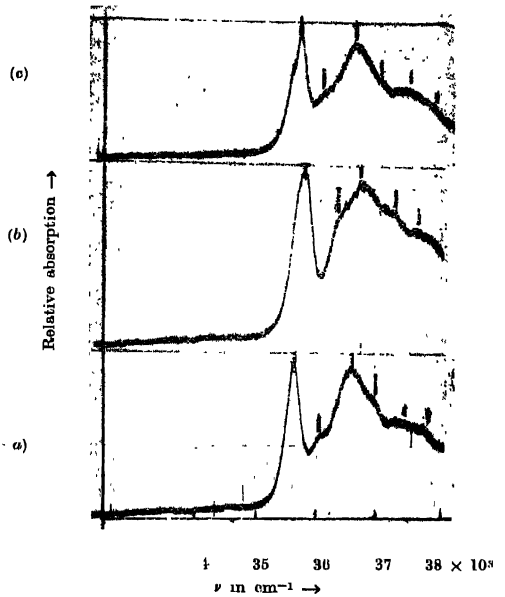

Fig. 2. Microphotometric records of the absorption spectra of o-chlorophenol.
(a) .01% solution in 3 methyl pentane with 5 mm cell at 30°C.
(b) .01% solution in 3 methyl pentane with 5 mm cell at −180°C.
(c) .01% solution in cyclohexane with 5 mm cell at 30°C.

towards higher energy by 165 cm^{-1} with respect to that due to the liquid. This shift can be explained by assuming that as the chlorine atom is surrounded by large number of hydrogen atoms in the solvent molecules, the O-H group is set free and the molecules assume trans configuration. If in some of these molecules the chlorine atom would form a virtual bond with the hydrogen atom of the solvent

molecule, the migration effect would be reduced and the band system would shift to higher energies. The weak band at 35986 $cm^{-1}$and the other two such bands on the shorter wavelength side may be due to these molecules. It is seen from figure 2(b) that when solution is frozen and cooled to −180°C, the intensity of the weaker band system increases and the bands are shifted towards higher energies. This is expected according to the hypothesis mentioned above, because at lower temperature, the distance between molecules diminishes and the probability of H–Cl bond formation increases and also the strength of the bond is expected to increase at closer distances.

TABLE I

Absorption spectra of *o*-chlorophenol

Vapour (Ramasastri, 1951) Prominent bands		Liquid at 28°C		Solid at −180°C		.01% sol. in CCl_4 (liquid at 28°C)	
ν in cm^{-1}	Assignment	ν in cm^{-1}	Assignment	ν in cm^{-1}	Assignment	ν in cm^{-1}	Assignment
35892 (vs)	ν_0	35475 (b)	ν_0	35600 (s)	ν_0	35475 (s)	ν_0
36387 (w)	ν_0+495	36392 (b)	ν_0+917	36512 (s)	ν_0+912	36392 ((s)	ν_0+917
36527 (m)	ν_0+635	37310 (b)	$\nu_0+2\times917$	37426 (w)	$\nu_0+2\times912$	37310 (w)	$\nu_0+2\times917$
36693 (m)	ν_0+801						
36845 (s)	ν_0+953						
36982 (m)	ν_0+1090						
37092 (w)	ν_0+1200						
37377 (vw)	ν_0+1485						

TABLE II

Absorption spectra of *o*-chlorophenol

.01% sol. in 3-methyl pentane (liq. at 28°C)		.01% sol. of 3-methyl pentane (solid at −180°C.)		.01% sol. in cyclohexane (liquid at 28°C)	
ν in cm^{-1}	Assignment	ν in cm^{-1}	Assignment	ν in cm^{-1}	
35640 (s)	ν_0	35767 (s)	ν_0	35729 (s)	ν_0
35986 (w)	ν_0'	36286 (m)	ν_0'	36079 (w)	ν_0'
36552 (s)	ν_0+912	36672 (s)	ν_0+905	36645 (s)	ν_0+916
36903 (w)	$\nu_0'+912$	37191 (m)	$\nu_0'+905$	36998 (w)	$\nu_0'+916$
37470 (m)	$\nu_0+2\times912$	37580 (w)	$\nu_0+905\times2$	37556 (w)	$\nu_0+916\times2$
				37917(vw)	$\nu_0'+916\times2$

TABLE III

Absorption spectra of *o*-chlorophenol

.01% sol. in isobutyl alcohol (liq. at 28°C)		.01% sol. in isobutyl alcohol (solid at −180°C)		20% sol. in isobutyl alcohol (liq. at 28°C)		20% sol. in isobutyl alcohol (solid at −180°C)	
ν in cm^{-1}	Assignment	ν in cm^{-1}	Assignment	ν in cm^{-1}	Assignment	ν in cm^{-1}	Assignment
35065 (m)	ν_0	35065 (m)	ν_0	35488 (b)	ν_0	35475	ν_0
35241 (s)	ν_0'	35241 (s)	ν_0'	36405 (b)	ν_0+917	36392	ν_0+917
35488 (m)	ν_0''	35488 (m)	ν_0''	37329 (b)	$\nu_0+917\times2$	37316	$\nu_0+917\times2$
35985 (s)	ν_0+920	35985 (s)	ν_0+920				
36168 (s)	$\nu_0'+917$	36168 (s)	$\nu_0'+917$				
36405 (m)	$\nu_0''+917$	36401 (m)	$\nu_0''+917$				
36902 (w)	$\nu_0+2\times917$	36902 (w)	$\nu_0+2\times917$				
37094 (w)	$\nu_0'+2\times917$	37094 (w)	$\nu_0'+2\times917$				
37329 (vw)	$\nu_0''+2\times917$	37329 (vw)	$\nu_0''+2\times917$				

Similar results are also observed in the case of solution of *o*-chlorophenol in cyclohexane at room temperature.

It can be seen from figure 3(d) Table III that the 0,0 band in the spectrum due to .01% solution of *o*-chlorophenol in isobutyl alcohol at room temperature is shifted towards longer wavelengths even with respect to the 0, 0 band due to the pure liquid by about 410 cm^{-1}. This large shift towards red suggests that some strong interaction takes place between *o*-chlorophenol and isobutyl alcohol molecules. Strong interaction between *o*-chlorophenol and alcohol molecules was also reported by Rene Freymann (1940) from the intensity of .99μ band in the infrared absorption spectrum of solution of *o*-chlorophenol in alcohols. It is evident from the amount of shift of the band system that the interaction between *o*-chlorophenol molecule and isobutyl alcohol molecules is different from that between *o*-chlorophenol in methyl pentane or cyclohexane. In this case formation of some new types of bonds between O–H group of alcohol and hydrogen atom of CH group of chlorophenol may take place, and thereby a trisubstituted benzene-like compound is produced. This explanation is supported by the fact that the calculated position of the 0, 0 band at 35130 cm^{-1} in the spectrum due to pure 1, 3, 5-trichlorobenzene in the liquid state is near to the band at 35065 cm^{-1} in the spectrum due to .01% solution of *o*-chlorophenol in the liquid state. The spectrum due to frozen .01% solution of *o*-chlorophenol in isobutyl alcohol

is similar to that due to same solution in liquid state, but bands become sharper at the lower temperature.

The spectrum due to 20% solution of *o*-chlorophenol in isobutyl alcohol is similar to that of the pure substance, only with slight shift towards longer

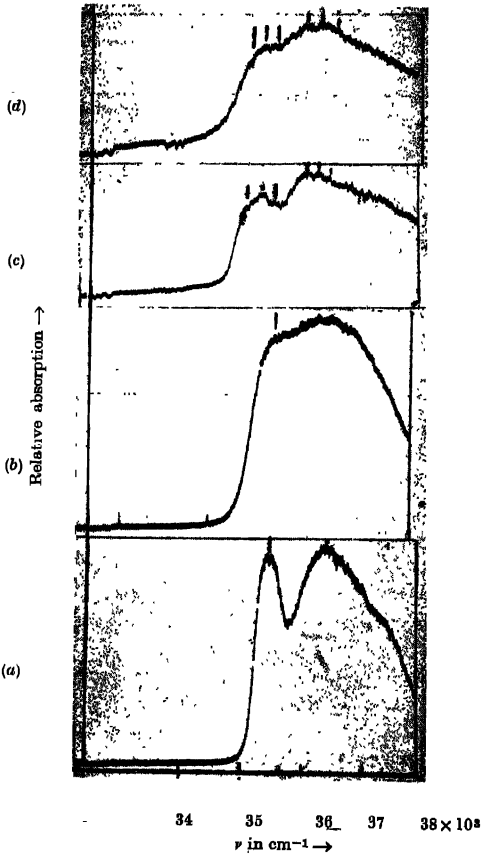

Fig. 3. Microphotometric records of the absorption spectra of *o*-chlorophenol.

(*a*) 20% solution in isobutyl alcohol at −180°C.
(*b*) " " " " " 30°C.
(*c*) .01% " " " " " −180°C.
(*d*) " " " " " " 30°C.

wavelength. So, as in the case of pure liquid most of the *o*-chlorophenol molecules in 20% solution remain in groups and give spectrum like that of the pure substance.

ACKNOWLEDGMENT

The author is indebted to Professor S. C. Sirkar, D.Sc. F. N.I., for his kind help and guidance during the progress of this work.

REFERENCES

Davies, M. M., 1938, *Trans. Farad. Soc.*, **34**, 1427.
Errera, J. and Mollet, P., 1935, *Jour de Physique*, **6**, 281.
Lüttke, W. and Mecke, R., 1950, *Zeit. Phys. Chem.*, **196**, 56.
Mukherjee, D. K., 1958, *Ind. J. Phys.*, **32**, 192.
Pauling, L., 1936, *J. A. C. S.*, **58**, 94.
" 1945, Nature of Chemical Bond, p. 324.
Ramasastri, C., 1951, *Proc. Nat. Ins. Sc.* (Ind.), **17**, 349.
Rene Freymann, 1940, *Comp. Rend.*, **211**, 386.
Roy, S. B., 1956, *Ind. J. Phys.*, **30**, 267.
Sirkar, S. C., Deb. A. R. and Banerjee, S. B., 1958, *Ind. J. Phys.*, **32**, 345.
Wulf, O. R. and Liddel, U., 1935, *J. A. C. S.*, **57**, 1464

Letters to the Editor

The Board of Editors will not hold itself responsible for opinions expressed in the letters, published in this section. The notes containing reports of new work communicated for this section should not contain many figures and should not exceed 500 words in length. The contributions must reach the Assistant Editor not later than the 15th of the second month preceding that of the issue in which the Letter is to appear. No proof will be sent to the authors.

10

CHARGE-TRANSFER TRANSITION IN Cl_2^+

V. VENKATESWARA RAO AND P. TIRUVENGANNA RAO

SPECTROSCOPIC LABORATORIES, ANDHRA UNIVERSITY, WALTAIR

(*Received for publication September* 8, 1958)

Recently the authors (Rao and Rao, 1958) have carried out detailed rotational analysis of some of the prominent bands of systems I and III analysed by Haranath and Rao (1956) in the visible emission spectrum of Cl_2^+. The rotational analysis shows that systems I and III arise respectively from $^2\Pi_{1/2}$—$^2\Pi_{1/2}$ and $^2\Pi_{3/2}$—$^2\Pi_{3/2}$ components of a $^2\Pi_{(a)}$—$^2\Pi_{(a)}$ transition. The two systems were interpreted on the basis of predicted electronic states from electron configurations by Mulliken (1934) in Cl_2^+, with lower $^2\Pi$ states arising from the ground state configuration $(\sigma_g 3p)^2 (\pi_u 3p)^4 (\pi_g 3p)^3$, $^2\Pi_{3/2g}$, $_{1/2g}$ and the upper states from the first excited electron configuration $(\sigma_g 3p)^2 (\pi_u 3p)^3 (\pi_g 3p)^4$, $^2\Pi_{3/2u}$, $_{1/2}{}^u$.

Most of the prominent bands in the visible emission spectrum of Cl_2^+ belong to these two systems. It is tempting to explain the rather high intensity of the bands of subsystems I and III on the basis of a charge-transfer spectrum. The transition of an electron in a diatomic molecule from a bonding to the corresponding antibonding orbital is always an allowed transition. The intensity of such a transition in a molecule was first shown by Mulliken (1939) to be high The 'f' value for such a transition has been shown to be of the same order as for the first members of a Ryderg series. Such transitions were called by Mulliken as charge-transfer spectra. Examples of these transitions are known in the spectra of H_2, H_2^+, O_2, O_2^+ and the halogen molecules. In O_2 the transition from the ground state .....$(\pi_u 2p)^4 (\pi_g 2p)^2$, $^3\Sigma_g^-$ to the excited state.....$(\pi_u 2p)^3 (\pi_g 2p)^3$, $^3\Sigma_u^-$ represents the Schuman-Runge bands in absorption. In this transition an electron goes from the bonding $(\pi_g 2p)$ orbital to the corresponding antibonding $(\pi_g 2p)$ orbital. As this is an example of charge-transfer spectrum,

a considerable intensity is expected, and indeed observed. Further, the vibrational frequency in the excited state is reduced to 819 cm^{-1} from a value of 1580 cm^{-1} in the ground state. The ultraviolet bands of O_2^+ observed in emission arising from the transition

$$\ldots\ldots (\pi_u 2p)^3 (\pi_g 2p)^2,\ ^2\Pi_u \rightarrow (\pi_u 2p)^4 (\pi_g 2p),\ ^2\Pi_g$$

are another example of this type. In the excited state, an electron goes from the bonding $(\pi_u 2p)$ orbital to the corresponding antibonding $(\pi_g 2p)$ orbital. Since there are 4 electrons in the $(\pi_u 2p)$ orbital which can carry out this transition, a considerable intensity is expected. The observed high intensity of the ultraviolet bands of O_2^+ is in agreement with this conclusion. Also the vibrational frequency in the excited state is reduced to 900 cm^{-1} from 1876 cm^{-1} in the ground state. By analogy with the above two cases we may consider the

$$\ldots\ldots (\pi_u 3p)^3 (\pi_g 3p)^4,\ ^2\Pi_u \rightarrow (\pi_u 3p)^4 (\pi_g 3p)^3,\ ^2\Pi_g$$

transition observed in emission in Cl_2^+ as an example of a charge-transfer spectrum. In this case also an electron goes from the bonding $(\pi_u 3p)$ orbital to the corresponding antibonding $(\pi_g 3p)$ orbital in the excited state. Again since there are 4 such electrons in the $(\pi\ 3p)$ orbital that can carry out this transition, a considerable intensity may be expected as in O_2^+. The observed high intensity of the bands of systems I and III support this conclusion. Further, similar to O_2 and O_2^+, the vibrational frequency in the excited state reduces to 348 cm^{-1} from in the ground state.

REFERENCES

Haranath, P. B. V. and Rao, P. T., 1956, *Curr. Sci.*, **25**, 47.
Haranath, P. B. V. and Rao, P. T., *Ind. Jour. Phys.* (in press).
Mulliken, R. S., 1934, *Phys. Rev.*, **46**, 549.
Mulliken, R. S., 1939, *J. Chem. Phys.*, **7**, 20.
Rao, V. V. and Rao, P. T., 1958. *Canad. Jour. of Phys.*, (in press).

A NEW WIDEBAND DISCRIMINATOR

N. B. CHAKRABORTI*

INSTITUTE OF RADIO PHYSICS AND ELECTRONICS, UNIVERSITY OF CALCUTTA

(*Received for publication, September* 30, 1958)

ABSTRACT. The present note describes a discriminator, employing transmission lines, designed to have linear response over a wide range of frequency deviation as is required in wideband FM work. It has been shown that linearity of response can be obtained without difficulty up to a fractional frequency deviation as high as 50 per cent.

INTRODUCTION

Conventional tuned circuit discriminators give linear response for frequency deviations which are at best small fractions of the central carrier frequency and are hence unsuitable for wideband FM work. In this paper a new type of discriminator has been described which can be arranged to give linear response over a range even wider than is necessary for wideband FM work in current use. Theoretically, the output of the discriminator is shown to be linear to within 5% up to a fractional frequency deviation as high as 70%. In a practical arrangement, however the range of linearity is reduced to about 50%, but even this range is considerably higher than what can be approached with ordinary tuned circuit discriminators. The discriminator employs physical or artificial transmission lines for the generation of sinusoidal frequency functions which are then combined to give the familiar '*S*' characteristic.

Circuit arrangements for different frequency regions are described.

PRINCIPLE OF THE CIRCUITS

Let us consider the circuit of figure 1(a). The voltage V_{BC} across BC, is the sum of the voltage drops V_{DC} and V_{BD}. Each of these voltages is developed across resistance R_0 which is the characteristic impedance of the transmission line of delay δ. Since the travelling current wave at B appears δ secs. after the application of the input at A, the voltage V_{BC} can be written as

$$V_{BC}(t) = R_0[I(t)+I(t-\delta)],$$

and operationally as

$$V_{BC}(p) = R_0(1+e^{-p\delta}) \, . \, I(p)$$

*Now at J. K. Institute of Applied Physics. Allahabad University.

Hence for a sinusoidal current $Ie^{j\omega t}$

$$V_{BC}(j\omega) = R_0[1+e^{-j\omega\delta}]I = 2R_0 I \cos\frac{\omega\delta}{2} \cdot e^{j\frac{\omega\delta}{2}},$$

or

$$|V_{BC}| = 2R_0 I \cos\frac{\omega\delta}{2} \qquad \ldots \quad (1)$$

The input impedance Z_{AC} equals $2R_0$; hence the input voltage is $2R_0 I$. The voltage across AB is the difference between the input voltage V_{AC} and the voltage V_{BC}. Hence

$$V_{AB}(j\omega) = (1-e^{-j\omega\delta})R_0 I = 2R_0 I \sin\frac{\omega\delta}{2} \cdot e^{j\frac{\omega\delta}{2}+j\pi/2}$$

or

$$|V_{AB}| = 2R_0 I \sin\frac{\omega\delta}{2} \qquad (2)$$

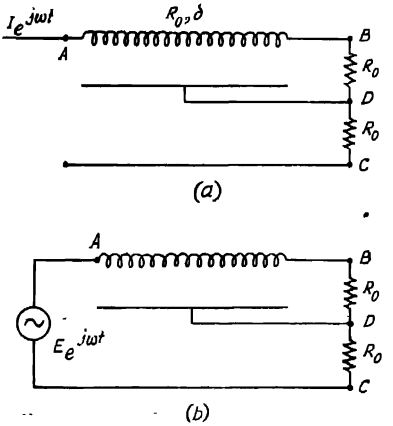

Fig. 1. Schematic diagram of a transmission line arrangement for producing sinusoidal voltage output.

If the circuit be voltage fed as in figure 1(b), the voltage drops are given by

$$|V_{BC}| = E \cos\frac{\omega\delta}{2} \qquad \ldots \quad (1.1)$$

$$|V_{AB}| = E \sin\frac{\omega\delta}{2} \qquad \ldots \quad (2.1)$$

Now the voltages V_{BC} and V_{AB} which are sinusoidal functions of frequency ω can be combined to give a discriminator characteristic. Thus, from elementary

trigonometry, the difference of two voltages of the form $A_1 \sin \frac{\omega\delta}{2}$ and $A_2 \cos \frac{\omega\delta}{2}$ can be written as :

$$A_1 \sin \frac{\omega\delta}{2} - A_2 \cos \frac{\omega\delta}{2} = A_0 \sin \left(\frac{\omega\delta}{2} - \phi \right) \qquad \ldots \quad (3)$$

$$= V_0, \text{ say,}$$

where $\quad A_0 = \sqrt{A_1^2 + A_2^2}$ and $\phi = \tan^{-1} \frac{A_2}{A_1}$;

It is seen that V_0 is zero at a frequency defined by

$$\omega_0 = \frac{\tan^{-1} \frac{A_2}{A_1}}{\delta/2}. \qquad (4)$$

For any other frequency

$$\omega = \omega_0 + \Delta\omega,$$

$$V_0 = A_0 \sin \left(\Delta\omega \, . \, \frac{\delta}{2} \right. \qquad \ldots \quad (5)$$

Now $\sin \theta/\theta$ is nearly equal to unity for small values of θ. In fact, up to $\theta = \pi/6$ radians, $\sin \theta/\theta$ does not depart from unity by more than 5%. Hence it follows that the difference voltage V_0 will be linearly related to $\Delta\omega$, for values of $\Delta\omega \, . \, \frac{\delta}{2}$ up to $\pi/6$ radians, the departure not exceeding 5%.

Now, for $\quad \Delta\omega \, . \, \frac{\delta}{2} = \pi/6, \; \frac{\Delta\omega}{\omega_0} = \frac{\pi/6}{\tan^{-1} \frac{A_2}{A_1}}$, from Eq. (4).

If $\; A_1 = A_2, \qquad \frac{\Delta\omega}{\omega_0} = \frac{2}{3} \, . = 66.6\%$

It is thus clear that by combining differentially the two voltages V_{AB} and V_{BC}, as given by eqns. (1) and (2) or by eqns. (1.1) and (1.2), a discriminator may be arranged. The output of such a discriminator, working with FM waves of carrier frequency ω_0 with a frequency deviation $\Delta\omega$, will obviously be linear (to within 5%) for fractional frequency deviations as large as 67%.

It should be noted that this limiting figure is obtained with the constraint that $A_1 = A_2$. If, however, this constraint is removed and the magnitudes of

A_1 and A_2 are suitably adjusted, the linearity can be extended even up to 100% frequency deviation.

It may be noted that the component functions $\cos\frac{\omega\delta}{2}$ and $\sin\frac{\omega\delta}{2}$ themselves provide discriminator characteristics around the centre frequencies $\omega = (2K+1)\frac{\pi}{\delta}$ and $\omega = \frac{2K\pi}{\delta}$ respectively while the combined characteristics $\sin\left(\frac{\omega\delta}{2} - \phi,\right)$ as seen above, is centered round $\omega = \frac{(\phi+K\pi)}{\delta/2}$ where K is any integer. Thus there will be harmonic response. It is therefore necessary to provide the required attenuation at all but the desired mode. The separation between successive "modes" in all the three cases is $2\pi/\delta$, but the ratio between the centre frequencies corresponding to the first two modes can be made higher in the combined characteristics than in the other two cases. What is more important is that the S/N ratio is better in the balanced form, and the maximum fractional frequency deviation is the largest.

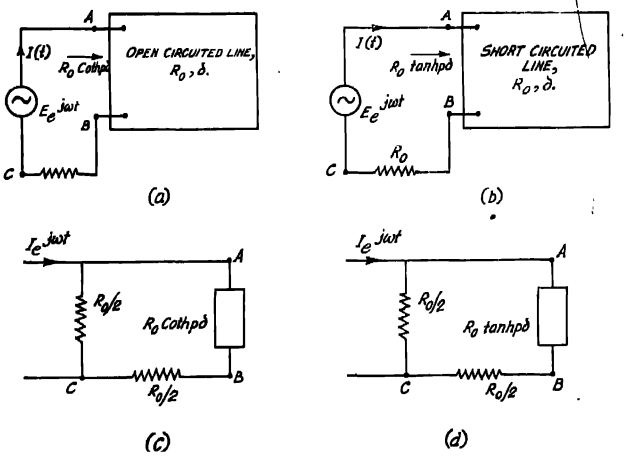

Fig. 2. Arrangements employing a single transmission line for generating sinusoidal magnitude functions.

Other circuit arrangements for realising sinusoidal magnitude function and hence discriminator characteristics are shown in figure 2. Thesea rrangements utilise reflections at the end of the transmission line and are discussed below.

Figure 2(*a*) :

$$I(t) = \frac{E(t)}{2R_0} - \frac{E(t-2\delta)}{2R_0}$$

and $$I(j\omega) = \frac{E}{R_0} \sin \omega\delta \,.\, e^{j(\omega\delta + \pi/2)}.$$

Hence the voltage $$V_{BC} = j\,E \sin \omega\delta \; e^{j(\omega\delta + \pi/2)}$$

and $$V_{AB} = E \cos \omega\delta \,.\, e^{j\omega\delta} \,,$$

$$V_0 = |V_{BC}| - |V_{AB}| = \sqrt{2}E \sin(\omega\delta - \pi/4) = \sqrt{2}E \sin \Delta\omega \,.\, \delta,$$

for $$\omega = \omega_0 + \Delta\omega, \text{ where } \omega_0 = \pi/4\delta.$$

Figure 2(*b*) :

$V_{AB} = jE \sin \omega\delta \,.\, e^{j\omega\delta}$ and $V_{BC} = E \cos \omega\delta \,.\, e^{j\omega\delta/2}$ and hence
$V_0 = |V_{AB}| - |V_{BC}| = \sqrt{2}\, E \sin(\omega\delta - \pi/4)$.

Both the systems 2(*a*) and 2(*b*) are fed from a constant voltage generator.

Figure 2(*c*) :

The current in the branch *CRA* is

$$I_B = \frac{R_0/2}{R_0 + R_0 \tanh p\delta} \,.\, I = \frac{I}{2} \cdot \frac{1}{1 + \tanh p\delta}$$

Here the voltage $$|V_{AB}| = \frac{I.R_0}{2} \sin \omega\delta$$

and $$|V_{BC}| = \frac{IR_0}{4} \cos \omega\delta,$$

Hence, $$V_0 = |V_{AB}| - |V_{BC}| = \frac{IR_0}{4} \,.\, \sqrt{5}.\, \sin(\omega\delta - \tan^{-1} 0.5)$$

For $$\omega = \omega_0 + \Delta\omega, \text{ where } \omega_0 = \tan^{-1} \frac{0.5}{\delta},$$

$$V_0 = \frac{IR_0}{4} \,.\, \sqrt{5} \sin(\Delta\omega \,.\, \delta).$$

Figure 2(*d*) :

$$|V_{AB}| = \frac{IR_0}{2} \cos \omega\delta,$$

$$|V_{BC}| = \frac{IR_0}{4} \sin \omega\delta,$$

and $$V_0 = |V_{BC}| - |V_{AB}| = \frac{IR_0}{4} \,.\, \sqrt{5} \sin(\delta\omega - \tan^{-1} 0\,2).$$

In figure 3, are shown arrangements where the sinusoidal functions are generated by means of two lines, one open and the other short circuited.

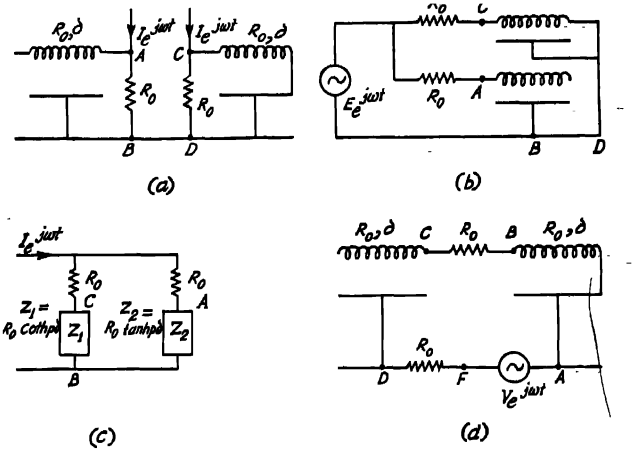

Fig. 3. Arrangements employing two transmission lines for generating sinusoidal magnitude functions.

Figure 3(a) :

$$|V_{AB}| = IR_0 \sin \omega\delta, \quad |V_{CD}| = IR_0 \cos \omega\delta,$$

and

$$V_0 = |V_{AB}| - |V_{CD}| = \sqrt{2}\, IR_0 \sin(\omega\delta - \pi/4).$$

Figure 3(b) :

$$|V_{AB}| = E \cos \omega\delta, \quad |V_{CD}| = E \sin \omega\delta,$$

$$V_0 = |V_{AB}| - |V_{CD}| = \sqrt{2}\, E \sin(\omega\delta - \pi/4).$$

In figure 3(b) the input impedance is R_0; the equivalent current fed form is as shown in figure 3(c).

Figure 3(c) :

$$|V_{AB}| - |V_{CB}| = \sqrt{2}\, R_0 I \sin(\omega\delta - \pi/4).$$

Figure 3(d) :

$$|V_{BA}| = \frac{V}{2}(1 - \cos 2\omega\delta), \quad |V_{CD}| = \frac{V}{2}(1 + \cos 2\omega\delta),$$

$$|V_{CA}| = V \sin \omega\delta, \quad |V_{FC}| = V \cos \omega\delta.$$

The arrangements described in the foregoing discussion are physically realisable at u.h.f. as well as in the r.f. and lower frequency ranges.

It is also to be noted that in the arrangements of figure 1 and figure 2, both voltage fed and current fed systems are equally practicable. Further, in the system of figure 2, one can employ lumped equivalents of the input impedance of open- or short-circuited transmission lines, some of which are shown in figure 4. Now

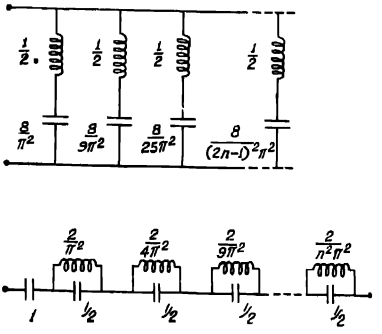

Fig. 4. Lumped equivalent of the input impedance of an open ended transmission line. The capacitances are in units of $\frac{\delta}{R_0}$ and the inductances are in units of δR_0.

for operation at higher frequencies, δ and hence R_0 have necessarily to be small, thus requiring the use of current fed forms. If high impedance cables are available, one may use the voltage fed forms.

Variation of the centre frequency : A variation of the centre frequency can be effected by adjusting the relative magnitudes of the two voltages (i.e., A_1 or A_2). It is observed from Eq.(4) that a variation of the amplitude factor in the cosine component by 50% results in a variation of the centre frequency by 25%. This, however, involves a change in the difference output.

EXPERIMENTAL ARRANGEMENT

An experimental arrangement as shown in figure 5 was made. The value of R chosen was one that gave a square pulse with step input to the system with least reflections. The characteristic impedance was 950 Ω and the total delay (one way) 0.28μ secs. The output impedance of the cathode follower was about 200Ω. The voltage across the resistance R was consequently reduced by the factor $\frac{15}{19}$ and the centre frequency shifted to a value greater than $\frac{1}{8\delta}$. The latter could, however, be moved back by adjusting the potentiometer shown in figure 5. The system was tested by applying C. W. signal from a standard signal

generator and observing the detected outputs $|V_{AB}|$ and $|V_{BG}|$. It is found from figure 6 that the detected difference output is substantially linear over the frequency range 200 kc/s to 600 kc/s, the centre frequency in this case being 400 kc/s.

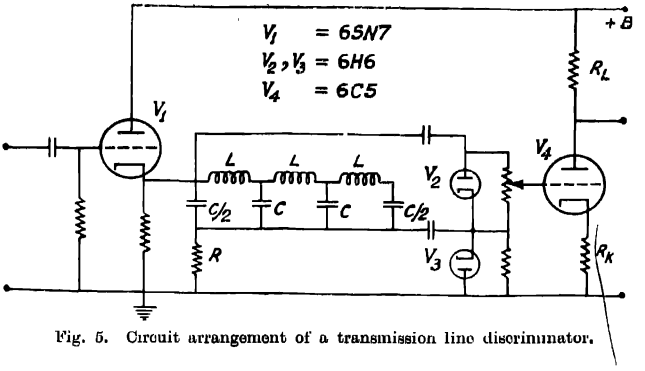

Fig. 5. Circuit arrangement of a transmission line discriminator.

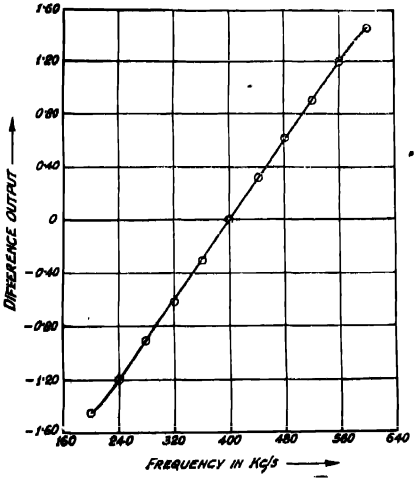

Fig. 6. Measured characteristics of the system of figure 5.

Another arrangement corresponding to the system in figure 3(c) was also made as shown in figure 7 and tested. The results obtained are presented in figure 8 which shows that almost perfect linearity extends up to ±3mc/s round the centre frequency of 6.4 mc/s.

It is thus seen that in both the discriminator arrangements the output is quite linear up to a frequency deviation of about 50% of the centre frequency.

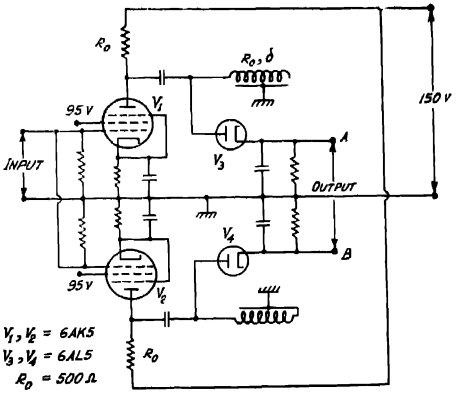

Fig. 7. Alternative circuit arrangement of a transmission line discriminator.

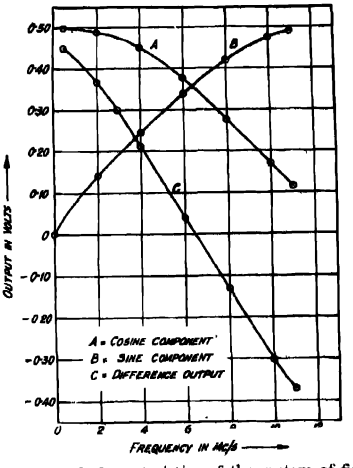

Fig. 8. Measured characteristics of the system of figure 7.

ACKNOWLEDGMENTS

This work formed part of a programme of research of the Electronic Circuitry Laboratory of the Institute of Radio Physics and Electronics, and was supported

by a Senior Research Training Scholarship under the Ministry of Education, Government of India, to which the author is grateful.

The author is deeply indebted to Professor J. N. Bhar for guidance and helpful suggestions and to Mr. A. K. Choudhury and Mr. B. R. Nag for valuable assistance. The author would also express his gratitude to his superiors in the J. K. Institute of Applied Physics, University of Allahabad, for the help accorded in the publication of the paper.

REFERENCE

Tibbs, C. E., Frequency Modulation Engineering.

CALCULATIONS OF THE DIPOLE MOMENTS OF TRI-SUBSTITUTED BENZENES.—1, 2, 3-, 1, 2, 4-AND 1, 3, 5-SUBSTITUTIONS

D. V. G. L. NARASIMHA RAO

PHYSICS DEPARTMENT, ANDHRA UNIVERSITY, WALTAIR

(*Received for publication October* 12, 1958)

ABSTRACT. The previous calculations of the author on the dipole moments of 1, 2, 4 tri-substituted benzenes are now extended to the other two—1, 2, 3 and 1, 3, 5 substitutions. The equations of Frank are used in computing the induced moments since the dielectric constant of the internuclear space is introduced directly in these equations to account for its effect on the induced moments. Previous calculations on 1, 2, 4 substitution are also revised. The equation are applied in the first instance to a few typical molecules for which observed moments are available in the literature. Agreement between the calculated and observed values is found to be satisfactory for a majority of cases investigated. The calculated values also compared well with those deduced empirically by a previous worker.

INTRODUCTION

A general method was given by the author (Narasimha Rao, 1955) for calculating the dipole- moments of 1, 2, 4 tri-substituted benzenes assuming the group moments as may be obtained from the observations on the corresponding mono-substituted compounds. The equations of Smallwood Herzfeld (1930) were used in computing the mutual induction of the three primary dipoles on one another and also the moments induced in the -CH and -C–C bonds of the hydrocarbon residue by the primary dipoles. The effect of the dielectric constant of the internuclear space was not considered in these equations. To allow for this effect the author has applied a correction by multiplying the total induced moment by the factor $\epsilon+2/3\epsilon$ where ϵ is the dielectric constant of the internuclear space assumed as 2.40 following Le Fevre and Le Fevre (1937). It was found that improved values could be obtained for the calculated moments when this correction was applied.

The calculations are now extended to the other two substitutions also, 1, 2, 3, and 1, 3, 5. The field equations of Frank (1935) are used in computing the induced moments since the dielectric constant of the internuclear space is directly involved in these equations so that no correction need be applied at the end. The previous calculations on 1, 2, 4 substitution are also revised and presented in the following pages.

CALCULATIONS

1, 2, 3 *substitution.* Figure 1 represents the case of a 1, 2, 3 substituted compound. The appropriate angles and distances are shown in the figure. ξ_1, ξ_2 and ξ_3 are the X-components, η_1, η_2, and η_3 are the Y-components of m_{01},

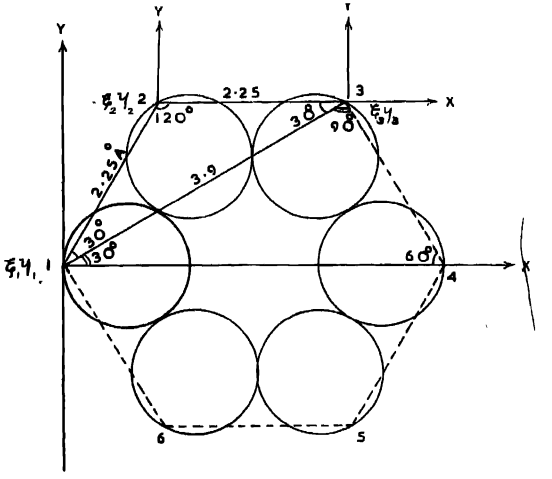

Fig. 1. 1 : 2 : 3 substitution.

m_{02} and m_{03} respectively (the actual group moment m_0 is given as $m_e = 1.843m_0$ where m_e is the moment of the mono-substituted compound). Applying the equations of Frank, the interaction of the three primary dipoles gives the follow-equations :

$$\begin{aligned}
&\xi'_1 + 0.1528a_1\xi'_2 - 0.7939a_1\eta'_2 - 0.7640a_2\xi'_3 - 0.7939a_2\eta'_3 = \xi_1\\
&\eta'_1 - 0.7939a_1\xi'_2 - 0.7640a_1\eta'_2 - 0.7939a_2\xi'_3 + 0.1528a_2\eta'_3 = \eta_1\\
&0.1528b_1\xi'_1 - 0.7939b_1\eta'_1 + \xi'_2 - 1.2224b_1\xi'_3 = \xi_2\\
&0.7939b_1\xi'_1 + 0.7640b_1\eta'_1 - \eta'_2 - 0.6112b_1\eta'_3 = -\eta_2\\
&0.7640c_2\xi'_1 + 0.7939c_2\eta'_1 + 1.2224c_1\xi'_2 - \xi'_3 = -\xi_3\\
&-0.7939c_2\xi'_1 + 0.1528c_2\eta'_1 + 0.6112c_1\eta'_2 + \eta'_3 = \eta_3 \qquad \ldots (1)
\end{aligned}$$

where

$$\begin{aligned}
&\alpha_1/r^3_1 = a_1, \quad \alpha_1/r^3_2 = a_2, \quad \alpha_1/r^3_3 = a_3\\
&\alpha_2/r^3_1 = b_1, \quad \alpha_2/r^3_2 = b_2, \quad \alpha_2/r^3_3 = b_3\\
&\alpha_3/r^3_1 = c_1, \quad \alpha_3/r^3_2 = c_2, \quad \alpha_3/r^3_3 = c_3. \qquad \ldots (2)
\end{aligned}$$

α_1, α_2, α_3 are the polarisabilities of the three substituent groups. In setting up these equations the fields of the induced moments are also considered since we have written $\xi' = \xi + \xi_i$ and $\eta' = \eta + \eta_i$. Thus as a result of dipolar induction

each ξ is modified to a certain ξ' and each η to a certain η'. In order to obtain the numerical values of ξ' and η', the six equations (I) are solved by the method of post-multiplication (Frazer, Duncan and Collar-1938) giving the values of the six variables.

The induced moments in the remaining —CH groups at 4, 5, 6 positions are calculated along similar lines. Values of the necessary angles and distances are given in Table I below.

TABLE I

Group		(4)	(5)	(6)
1	r	4.5	3.9	2.25 Å
	v	0°	−30°	−60°
2	r	3.9	4.5	3 9
	v	−30°	60°	−90°
3	r	2.25	3.9	4 5
	x	−60°	−90°	−120°

The final values are given as

$$\Sigma\xi_i = 0.008424\xi'_1 - 0.0543\eta'_1 + 0.0005861\xi'_2 - 0.01445\eta'_2 - 0.01663\xi'_3 - 0.03985\eta'_3$$
$$\Sigma\eta_i = -0.05433\xi'_1 + 0.03780\eta'_1 - 0.01445\xi'_2 + 0.01728\eta'_2 - 0.03985\xi'_3 + 0.06284\eta'_3 \quad \ldots (3)$$

In evaluating the induced moments in the –C–C bonds the various angles and distances are shown in Table II.

TABLE II

Group		(1)	(2)	(3)	(4)	(5)	(6)
1	r	1.3	2.6	3.438	3.438	2.6	1.3Å
	v	30°	30°	10°54′	−10°54′	−30°	−30°
2	r	1.3	2.6	3.438	3.438	2.6	1 3
	v	−30°	−30°	−49°6′	−70°54′	−90°	−90°
3	r	1 3	2.6	3.438	3.438	2 6	1.3
	v	−90°	−90°	−109°6′	−130°54′	−150°	−150°

The sum of the induced moments in –C–C bonds is given as

$$\Sigma\xi'_1 = 0.8265\xi'_1 + 0.07124\xi'_2 - 0.4359\eta'_2 + 0.07124\xi'_3 + 0.4359\eta'_3$$
$$\Sigma\eta'_i = -0.1806\eta'_1 - 0.4359\xi'_2 + 0.5746\eta'_2 + 0.4359\xi'_3 + 0.5746\eta'_3 \quad \ldots (4)$$

The total contribution due to induction in the unsubstituted —C—H groups and in the —C—C bonds is obtained as

$$\Sigma(\xi_i+\xi'_i) = 0.8349\xi'_1-0.05433\eta'_1+0.7183\xi'_2-0.4504\eta'_2+0.05461\xi'_3+0.3961\eta'_3$$
$$\Sigma(\eta_i+\eta'_i) = -0.05433\xi'_1-0.1427\eta'_1-0.4504\xi'_2+0.5919\eta'_2+0.3961\xi'_3+0.6374\eta'_3 \quad \ldots (5)$$

Finally the resultant moment of the molecule is given as

$$\mu = (M^2_x + M^2_y)^{\frac{1}{2}}$$

where $M_x = \Sigma(\xi_i + \xi'_i) + \xi'_1 + \xi'_2 + \xi'_3$

$$= 1.8349\xi'_1-0.05433\eta'_1+1.07183\xi'_2-0.4504\eta'_2+1.05461\xi'_3+0.3961\eta'_3$$

$$M_y = \Sigma(\eta_i+\eta'_i)+\eta'_1+\eta'_2+\eta'_3$$
$$= -0.05433\xi'_1+0.8573\eta'_1-0.4504\xi'_2+1.5919\eta'_2+0.3961\xi'_3+1.6374\eta'_3 \quad (6)$$

1 : 2 : 4 *Substitution.* Figure 2 gives a picture of this type of compound. A consideration of the interaction of the three primary dipoles gives the relations

$$\xi'_1+0.1528a_1\xi'_2-0.7939a_1\eta'_2-1.2224a_3\xi'_3=\xi_1$$

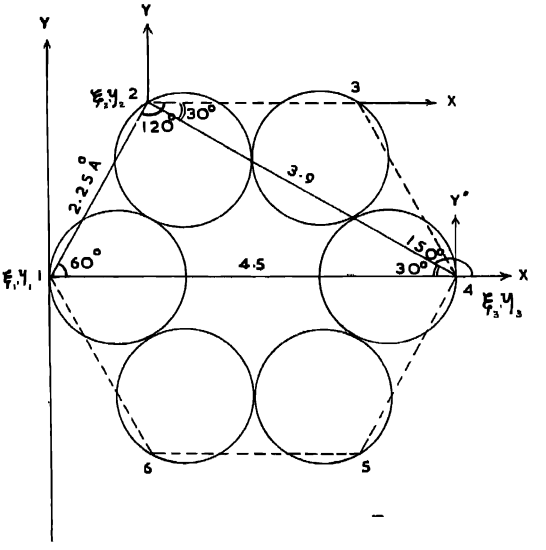

Fig. 2. 1 : 2 : 4 substitution

$$\eta'_1-0.7939a_1\xi'_2-0.7640a_1\eta'_2+0.6112a_3\eta'_3=\eta_1$$
$$0.1528b_1\xi'_1-0.7939b_1\eta'_1+\xi'_2-0.7640b_2\xi'_3+0.7939b_2\eta'_3=\xi_2$$
$$-0.7939b_1\xi'_1-0.7640b_1\eta'_1+\eta'_2+0.7939b_2\xi'_3+0.1528b_2\eta'_3=\eta_2$$

$$-1.2224c_3\xi'_1-0.7640c_2\xi'_2+0.7939c_2\eta'_2+\xi'_3=\xi_3$$
$$0.6112c_3\eta'_1+0.7939c_2\xi'_2+0.1528c_2\eta'_2+\eta'_3=\eta_3 \qquad \ldots \quad (7)$$

In this case the sum of the contributions of the induced moment in the unsubstituted —C—H and —C—C bonds (the necessary distances and angles are given in Tables I and II of the previous paper—Narasinha Rao 1955) is

$$\Sigma(\xi_i+\xi_i')=0.8343'\xi_1+0.04558\eta'_1+0.1337\xi'_2-0.4416\eta'_2+0.8149\xi'_3+0.008752\eta'_3$$
$$\Sigma(\eta_i+\eta'_i)=-0.04558\xi'_1-0.1400\eta'_1-0.4416\xi'_2+0.5584\eta'_2+0.008752\xi'_3-$$
$$0.09450\eta'_3 \qquad \ldots \quad (8)$$

The resultant moment is again

$$\mu=(M_x^2+M_y^2)^{\frac{1}{2}}$$

with $M_x=1.8343\xi'_1+0.04558\eta'_1+1.1337\xi'_2-0.4416\eta'_2+1.8149\xi'_3+0.008752\eta'_3$
$M_y=-0.04558\xi'_1+0.8600\eta'_1-0.4416\xi'_2+1.5584\eta'_2+0.008752\xi'_3+0.9055\eta'_3$
$\ldots \quad (9)$

1, 3, 5 *substitution.* The method of calculation may be understood from figure 3. The induced effects in the primary dipoles give the following equations.

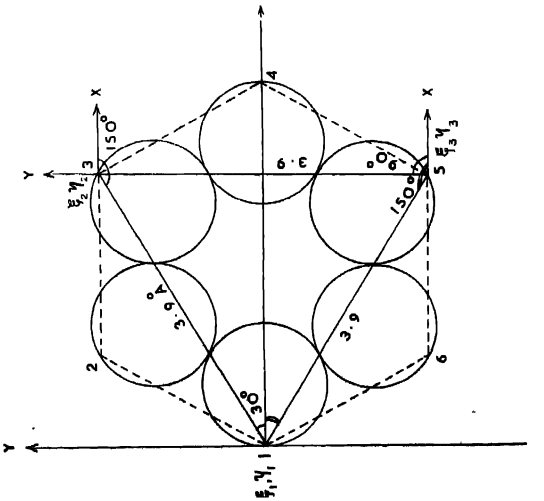

Fig. 3. 1 3 : 5 substitution

$$\xi'_1-0.7640a_2\xi'_2-0.7939a_2\eta'_2-0.7640a_2\xi'_3+0.7939a_2\eta'_3=\xi_1$$
$$\eta'_1-0.7939a_2\xi'_2+0.1528a_2\eta'_2+0.7939a_2\xi'_3+0.1528a_2\eta'_3=\eta_1$$

$$-0.7640b_2\xi'_1-0.7939b_2\eta'_1+\xi'_2+0.6112b_2\xi'_3=\xi_2$$
$$-0.7939b_2\xi'_1+0.1528b_2\eta'_1+\eta'_2-1.2224b_2\eta'_3=\eta_2$$
$$-0.7640c_2\xi'_1+0.7939c_2\eta'_1+0.6112c_2\xi'_2+\xi'_3=\xi_3$$
$$0.7939c_2\xi'_1+0.1528c_2\eta'_1-1.2224c_2\eta'_2+\eta'_3=\eta_3 \qquad \ldots \quad (10)$$

In computing the induced moments in the unsubstituted –C–H groups and –C–C bonds the angles and distances are given in Tables III and IV respectively.

TABLE III

Group		(2)	(4)	(6)
1	r	2.25	4.5	2.25Å
	x	60°	0°	−60°
2	r	2.25	2.25	4.5
		180°	−60°	−120°
3	r	4.5	2.25	2.25
	v	120°	60°	180°

TABLE IV

Group		(1)	(2)	(3)	(4)	(5)	(6)
1	r	1.3	2.6	3.438	3.438	2.6	1.3Å
	v	30°	30°	10°54′	−10°54′	−30°	−30°
2	r	1.3	2.6	3.438	3.438	2.6	1.3
	v	−90°	−90°	−109°6′	−130°54′	−150°	−150°
3	r	1.3	2.6	3.438	3.438	2.6	1.3
	v	150°	150°	130°54′	109°6′	90°	90°

For this substitution

$$\Sigma(\xi_i+\xi'_i) = 0.8179\xi'_1+0.1315\xi'_2+0.3961\eta'_2+0.1315\xi'_3-0.3961\eta'_3$$
$$\Sigma(\eta_i+\eta'_i) = -0.1361\eta'_1+0.3961\xi'_2+0.5887\eta'_2-0.3961\xi'_3+0.5887\eta'_3 \qquad \ldots \quad (11)$$

Finally the total moment of the molecule is given as

$$\mu = (M_x^2+M_y^2)^{\frac{1}{2}} \qquad \text{with}$$

$$M_x = 1.8179\xi'_1+1.1315\xi'_2+0.3961\eta'_2+1.1315\xi'_3-0.3961\eta'_3$$
$$M_y = 0.8634\eta'_1+0.3961\xi'_2+1.5887\eta'_2-0.3961\xi'_3+1.5887\eta'_3 \qquad \ldots \quad (12)$$

RESULTS AND DISCUSSION

The method described above is applied to specific cases in the first instance to a few typical molecules for which the observed values are obtained from the compilation of Wesson (1948) and listed in the following Table V. The deviations

$\Delta = \mu_{obs.} \sim \mu_{calcd.}$ and $\delta = \mu_{obs.} \sim \mu_{vector}$ are also given in the table for comparison. A particular point to be noted is the choice of the moment m_e of the mono-substituted benzene to be used in the calculation, since for the same molecule various values have been reported in the literature. Values of m_e considered to be the most probable by the author and hence used throughout are given in Table VI.

TABLE V

Compound	$\mu_{obs.}$	$\mu_{calcd.}$	μ_{vector}	Δ	δ
2, 3-Dichloronitrobenzene	3.86	4.34D	4.78	0 48	0.92
2, 4-Dichloronitrobenzene	2.66	3.01	3 45	0.35	0.79
2, 5-Dichloronitrobenzene	3 45	3.64	3 95	0 19	0.50
2, 6-Dichloronitrobenzene	4.18	4.76	5 50	0.58	1 32
3, 5-Dichloronitrobenzene	2 66	2.49	2.40	0.17	0.26
1, 3-5, Trichlorobenzene	0.28	0.00	0.00	0 28	0.28
1, 3-5, Triiodobenzene	0 24	0.00	0.00	0.24	0.24
3, 5-Dinitrotoluene	4 05	4.16	4.34	0 11	0 29

TABLE VI

Group	m_e
NO_2	−3.95
Cl	−1.55
I	−1.25
CH_3	+0.39
NH_2	+1.53

Conventionally the group moment is considered positive when the dipole moment vector of the group is directed towards the centre of the benzene ring and negative when it is directed away from the centre. The polarisability values α of the various groups are assumed from Smallwood and Herzfeld's results (1930). Judged from the magnitudes of Δ and δ in Table V it may be seen that for all the molecules studied the calculated moments are nearer the observed values when the induced moments are taken into account. For the two symmetric substitutions, 1, 3, 5 tri-chloro- and 1, 3, 5 tri-iodo benzenes, the induced moments get cancelled and the author's detailed calculation also gives a zero moment. The reported

values may be due perhaps to the neglect of atom polarisation as in the similar case sym- tri-nitrobenzene.

The first five molecules listed in the table are the subject of investigation by Thomson (1944)—a sixth isomer is also studied by him— to ascertain whether there is any steric inhibition of resonance of the nitro group due to vicinal Cl groups. The molecular solution volumes and molecular refractivities support the view that in 2, 6-dichloronitrobenzene where there are two Cl groups ortho to NO_2 group, resonance between the NO_2 group and benzene ring is to a large extent inhibited. It is suggested that even one Cl ortho to NO_2 will have a certain inhibitory effect on the resonance. Variations in the parachors are of the same magnitude and sign as variations in molecular solution volumes. It may hence be expected that the dipole moment of 2, 6-dichloronitrobenzene will be lower than the calculated value even after allowance for inductive effects. He points out that values found for dipole moments "are not inconsistent with this view". Calculated moments are obtained by Thomson using certain empirical rules regarding the interaction of Cl and NO_2 groups. (a) Each chlorine ortho to a nitro group will result in a diminution of moment of 0.59D. This correction includes at least two factors- the effect of induction and the effect of inhibition of resonance. (b) A chlorine meta to a nitro- group will result in an increase of moment by 0.15. In his calculations the assumed values of moments are $C_6H_5NO_2$—3.97, *o*-$C_6H_4Cl_2$—2.25, *m*-$C_6H_4Cl_2$—1.48, *p*-$C_6H_4Cl_2$. A comparison is made between the values calculated by the author and those of Thomson in Table VII below.

TABLE VII

Compound	(Thomson) $\mu_{calcd.}$	(author) $\mu_{calcd.}$	Δ
2, 3-Dichloronitrobenzene	3.97	4.34	0.37
2, 4-Dichloronitrobenzene	3.03	3.01	0.02
2, 5-Dichloronitrobenzene	3.38	3.64	0.26
2, 6-Dichloronitrobenzene	4.27	4.76	0.49
3, 5-Dichloronitrobenzene	2.49	2.49	0.00

The difference between the two types of calculation is shown under Δ′ in the table. Δ′ may be taken as an extent of the inhibition of resonance, since a correction for this effect is applied by Thomson inherent in rule (ā) whereas the author's values take account of induction only. There is no method at present to make an exact estimate of this effect by simple theory. As a logical consequence of the arguments of Thomson, we may expect that in 2 : 6 dichloronitrobenzene in which the proposed effect must be most pronounced, the nitro-group moment may have approximately the same value as the corresponding aliphatic compound-

nitromethane. If now the calculations are repeated using this value for m_e the observed moment may be explained. Such a procedure has been worked out assuming $m_e = 3.10$D and as per our predictions the calculated moment turns out as 3.94 D which is slightly less than the observed value 4.18 indicating that resonance of the NO_2 group is inhibited to a large extent, thus establishing the essential point of Thomson.

In 3, 5-dinitro-toluene no such complications are expected since there are no methyl or Cl groups ortho to the NO_2 group and as expected the agreement between calculated and observed values is within experimental error.

A critical account of the assumptions made in the procedure worked out for calculating the induced moments and their validity has been given in the previous paper by the author.

ACKNOWLEDGMENTS

The author is deeply indebted to Prof. K. R. Rao for his kind and constant guidance throughout the progress of work. He is also grateful to the Council of Scientific and Industrial Research for financial assistance.

REFERENCES

Frank, ., 1935, *Proc. Roy. Soc.* (*Lond*), A152, 171.
Frazer, , Duncan, . and Collar, , 1938, Elementary Matrices, Cambridge University Press, London, pp 126.
Le Fevre and Le Fevre, 1937, *J. Chem. Soc.* 196.
Narasimha Rao, ., 1955, *Ind. J. Phys.*. 29, 49
Smallwood. . and Herzfeld, ., 1930, *J. Am. Chem. Soc.*, 52, 1919.
Thomson, ., 1944, *J. Chem. Soc.*, 404.
Wesso ., 1948, Tables of Electric Dipole Moments. The Technology Press, M.I.T.

THE DIELECTRIC PROPERTIES OF ROSIN

A. K. SEN AND G. N. BHATTACHARYA

DEPARTMENT OF APPLIED PHYSICS, UNIVERSITY OF CALCUTTA,

(*Received for publication, October* 14, 1958)

ABSTRACT. The dielectric properties of w. w. rosin have been measured over a wide range of temperature and frequency, viz., from 20°C to 150°C and from 1 kc/s to 500 kc/s. Within the temperature range of investigation rosin behaves as a typical polar resin in the anomalous dispersion range. The range of dispersion is wide and this may be explained from the distributed relaxation times of its polar units. With the help of melt viscosity data of this resin the size of its rotating unit has been calculated following Debye's relations and the calculated radius comes out to be 4.6 Å.

INTRODUCTION

It has been recently observed (Sen and Bhattacharya, 1958) that ester gum, which is the glycerol ester of rosin, behaves as a typical polar resin. Its loss curve is a typical absorption curve but owing to its somewhat large molecule it has a distributed range of relaxation time due to which it has a wide range of dispersion as well as a diminished value of the dielectric loss. The application of Stokes' law for estimation of the radius of the rotating unit has revealed that probably a part of the molecule only rotates and the ester gum molecule as a whole does not take part in the orientation. Chemically speaking ester gum is mainly glyceryl tri-abietate i.e., glycerol ester of abietic acid, the chief constituent of rosin. It is of interest, therefore, to study the dielectric properties of rosin, the raw material for ester gum in order to account for its dielectric loss and to obtain an idea of the size of the rotating unit in this case.

There are two types of rosin available at present—one is "gum rosin" obtained from the resinous exudation of the pine tree and the other is "wood rosin" extracted from stumps of rosin-bearing wood. Nearly the entire production of Indian rosin is of the gum type. Though extensive work has been done in America on the various physical and chemical properties of rosin produced there, very little information is available about Indian rosin. Rau and Simonsen (1924) however have shown that the abietic acid isolated from rosin derived from Indian Pinus Longifolia is identical in all respects with the acid present in the rosin from American Pinus Palustris.

THEORETICAL

The relation between the dielectric constant ϵ' and loss factor ϵ'' of a substance which exhibits the phenomenon of absorption is expressed as

$$\epsilon'' = \epsilon' \tan \delta$$

where $\tan \delta$ is the power factor of the condenser filled with the given dielectric material and δ is its loss angle. The dielectric constant ϵ' and the power factor $\tan \delta$ of the condenser may be determined in the usual manner and the dielectric loss may be computed.

Now, the current in phase with the voltage in a condenser having dielectric loss is

$$I_r = I \tan \delta = \omega C V \tan \delta$$

$$= 2\pi f C V \frac{\epsilon''}{\epsilon'} .$$

But the value of C for a parallel plate condenser of area A and the dielectric thickness d is given by

$$C = \frac{A \times \epsilon'}{4\pi d \times 9 \times 10^{11}} \text{ farads.}$$

Therefore substituting this value of C, we have

$$I_r = \frac{f A V \epsilon''}{18 \times 10^{11} \times d}$$

Again, if K_t is the total conductance of this condenser, then

$$I_r = \frac{A V K_t}{d}$$

Therefore,

$$\epsilon'' = \frac{18 \times 10^{11} \times K_t}{f}$$

But $K_t = K_0 + K$, where K_0 and K are the d.c. and a.c. conductance respectively. Hence pure a.c. loss would be

$$\epsilon'' = \frac{18 \times 10^{11} (K_t - K_0)}{f}$$

EXPERIMENTAL

Apparatus :—The bridge, oscillator and amplifier null detector employed for capacity and power factor measurements in the present investigation were the same as reported previously (Sen and Bhattacharya, 1958) for ester gum. The cell used was also the same.

Material :—The sample of rosin used was of the "water white" commercial grade and was obtained from Napier Paint Works Ltd., Calcutta. The softening point of the sample determined by the mercury surface method was 67°C.

Method of procedure :—The procedure followed for the measurement of capacity and power factor as well as for filling up the experimental cell has already been described in some detail elsewhere (Sen and Bhattacharya, 1958).

D.c. conductivity was measured at different temperatures using the same cell. The values of d.c. conductance reported here were obtained after 2 minutes of electrification. For this measurement direct deflection method was used employing a precision universal shunt and a sensitive galvanometer. The viscosity of the sample was determined using Lee's modified viscometer (Lee, 1934) as reported previously (Sen and Bhattacharya, 1957).

DISCUSSION

The results of measurements of power factor tan δ, the dielectric constant ϵ' and the dielectric loss factor ϵ'' for various temperatures and frequencies are shown graphically in figures 1, 2 and 3. These curves, it may be seen, indicate

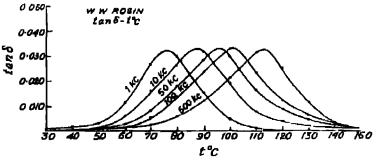

Fig. 1.

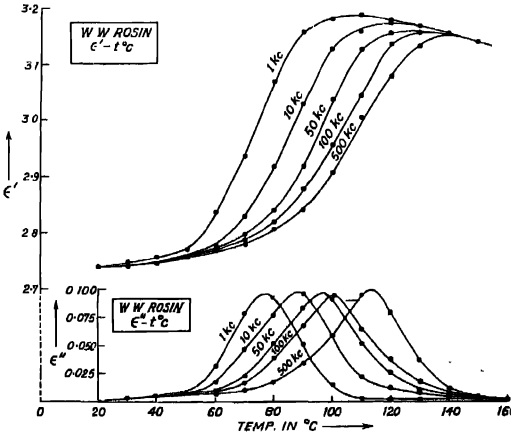

Fig. 2. and Fig. 3.

the characteristics of a typical polar resin in the anomalous dispersion range. Almost similar curves were obtained in our previous investigation on ester gum and the general interpretations given in our previous paper (Sen and Bhattacharya, 1958) as regards its behaviour at different temperatures and frequencies hold good in the present case also. A detailed discussion on the electrical behaviour of this resin is therefore omitted here.

The power factor as well as the dielectric loss curves of rosin begin to rise from about 40°C. The dielectric constant is also very small below this temperature. The maximum value of power factor remains practically the same for all frequencies and is about 0.033. The region of temperature within which the power factor peaks are distributed is about 37°C, the peak for 1 kc/s occurring at 76°C while that for 500 kc/s occurring at 113°C.

The values of dielectric constant and power factor reported here are in good agreement with those mentioned by Clare (1949) or by Kitchin and Muller (1928), although the samples used by these investigators are of different origin. It would be reasonable to think therefore that the basic constituent of rosin primarily responsible for its dielectric behaviour is the same in all samples irrespective of different methods of processing and different countries of origin.

As is well known most of the resins are characterised by a band of distributed relaxation time instead of a single one as demanded by Debye's orginal theory. Various workers have demonstrated the effect of such distributed relaxation times and have indicated the mechanism of such distribution of relaxation times in resins. Fuoss and Kirkwood's (1941) theory which accounted for the existence of such bands in high polymers can be used to calculate this factor of distribution in resins. Yager (1936) has also shown from theoretical considerations that the

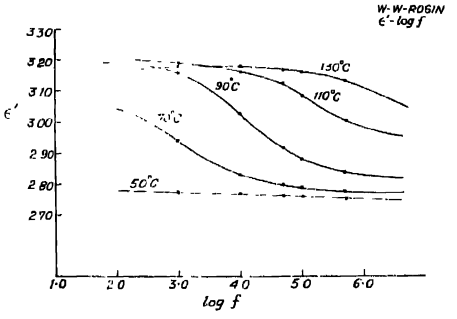

Fig. 4

effect of distributed relaxation times in a polar resin is to diminish the maximum loss factor ε_m'' and also to widen the dispersion band. These two phenomena

often serve as an indication of the existence of distributed relaxation times in the molecule. In this case the calculated value of ϵ_m'' at 90°C, for example, comes

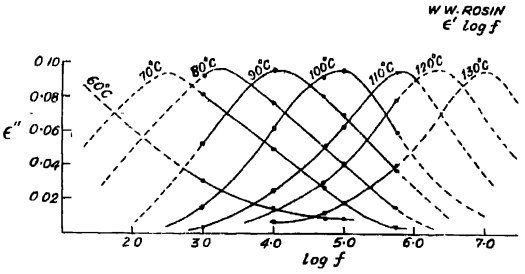

Fig. 5.

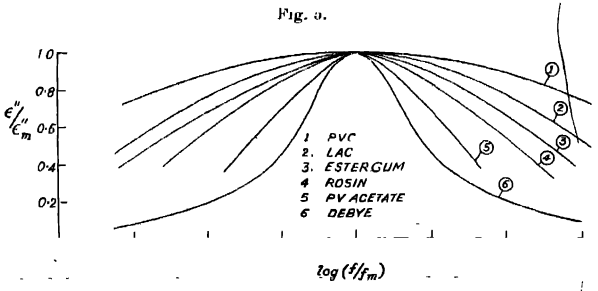

Fig. 6.

out to be 0.20 and the observed maximum loss factor (from figure. 5) is 0.096 i.e., about half of the theoretical value. The dispersion band also spreads over a wide range—for at least 5 or 6 decades of frequency.

From both these considerations, viz., the diminished value as well as a wide-spread dispersion range, a distributed range of relaxation time of the rosin molecule suggests itself. It can be seen also from a study of the bluntness or flatness of the $\frac{\epsilon''}{\epsilon_m''}$ vs. $\frac{f}{f_m}$ curve for this sample compared with the Debye graph in figure 6. A comparative study of the degree of such an effect in different substances may be made by plotting such curves in one graph where blunter curves will indicate greater effect of distributed relaxation times.

In the case of a liquid where Stokes' law is applicable the relaxation time τ is given by the relation, due to Debye, viz,

$$\tau = \frac{4\pi\eta a^3}{KT}$$

where η = coefficient of viscosity and a = radius of the rotator,

This simple relation of Debye has been found to hold good in cases of liquids having molecules of smaller size and simpler shape and proper values of melecular radii are obtained by putting the macroscopic value of viscosity for η in it.

But the propriety of substituting the macroscopic value of viscosity for the coefficient of internal friction in the above relation in cases of resins having larger and more complex molecular structure is often open to criticism.

In fact, some workers are of opinion that the internal friction experienced by the polar groups in their orientation is something quite different from the macroscopic viscosity and as such dimensions of the polar units obtained by using the macroscopic viscosity for η in this relation may not represent true values. But at the same time it must also be remembered that the the number of cases in which proper dimensions of the polar units have been obtained by using the macroscopic viscosity in this relation, is not quite a few. It is well known that strikingly good agreement between the observed and theoretical values were obtained in Mizushima's (1927) experiments. Since then many workers have obtained for various substances the correct values of radii of their rotating units. Race (1931), for example, calculated the dimension of polar particles in mineral oils in fair agreement with their correct values. Hartshorn and his co-workers (1940) from their study on a number of phenolic resins obtained the dimensions of the hydroxyl group, the most probable group of the resin molecule for orientation. One of us (Bhattacharya, 1944a. 1944b) also found similar results in the case of lac and some of its constituents.

Again we can write, $$\tau = \frac{\xi}{2KT} = \frac{C\eta}{T}$$

if it is assumed that the inner frictional torque is proportional to macroscopic viscosity.

Therefore $$\log T\tau = C' + \log \eta$$

But since $\log \eta = A + \frac{Q}{RT}$, which may be seen from the viscosity-temperature graph in figure 8 to hold good in this case,

$$\log T\tau = C'' + \frac{Q}{RT}$$

where Q = molar activation energy, and R = molar gas constant.

If the above assumption is true, a straight line graph is expected when $\log T\tau$ is plotted against $1/T$.

Here the relaxation time τ has been calculated from the relation

$$\tau = \frac{1}{\omega\epsilon''} \cdot \frac{\epsilon_\infty' + 2}{\epsilon_0' + 2} \{\epsilon_m'' \pm \sqrt{\epsilon_m''^2 - \epsilon''^2}\}$$

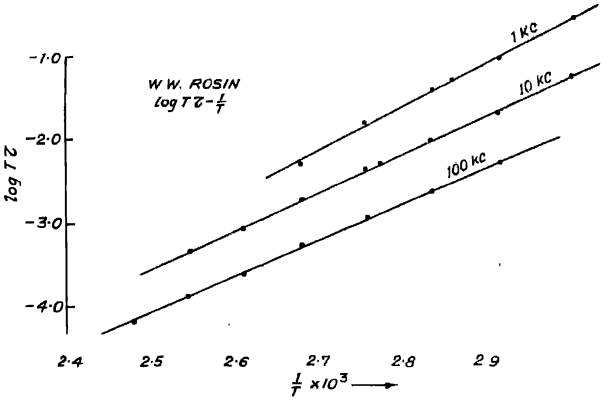

Fig. 7.

for frequencies of 1 kc/s, 10 kc/s, and 100 kc/s over the investigated range of temperature and the results of computation are tabulated in Table I.

The calculated values of log $T\tau$ for different frequencies are plotted against $\frac{1}{T}$ and the graphs are shown in figure 7. All these graphs are straight lines which justify our previous assumption.

The resistivity of an insulating material is due to lack of mobility of its charge carriers and so depends on its inner viscosity. Hence the resistivity and inner viscosity are related to temperature in a similar fashion. We find, however,

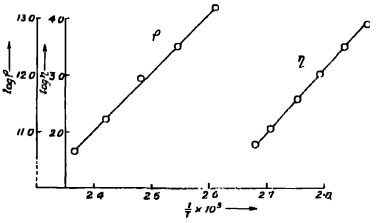

Fig. 8.

from the results of resistivity and viscosity determinations at different temperatures shown in Tables II and III respectively that the resistivity and macroscopic viscosity behave similarly with temperature. In figure 8 logarithms of both d.c. resistivity and viscosity are plotted against $\frac{1}{T}$ and it may be seen that both

the graphs are straight lines and they are almost parallel, signifying that they have almost same value of molar activation energy.

TABLE I

Frequency in kc/s	Temperature $t°C$	$T°K$	$\frac{1}{T} \times 10^3$	Relaxation time in sec	log $T\tau$
1	60°	333	3.003	9.13×10^{-4}	−0.517
	70°	343	2.915	2.70×10^{-4}	−1.003
	77°	350	2.857	1.48×10^{-4}	−1.286
	80°	353	2.833	1.21×10^{-4}	−1.369
	90°	363	2.755	4.44×10^{-4}	−1.703
	100°	373	2.681	1.20×10^{-5}	−2.349
10	60°	333	3.003	1.62×10^{-4}	−1.268
	70°	343	2.915	5.60×10^{-5}	−1.717
	80°	353	2.833	3.06×10^{-5}	−1.961
	88°	361	2.773	1.48×10^{-5}	−2.272
	90°	363	2.755	1.28×10^{-5}	−3.323
	100°	373	2.681	5.02×10^{-6}	−2.728
	110°	383	2.611	1.85×10^{-6}	−3.150
	120°	393	2.545	1.19×10^{-6}	−3.330
100	70°	343	2.915	1.51×10^{-5}	−2.286
	80°	353	2.833	6.71×10^{-6}	−2.626
	90°	363	2.755	3.47×10^{-6}	−2.900
	100°	373	2.681	1.48×10^{-6}	−3.258
	110°	383	2.611	5.70×10^{-7}	−3.661
	120°	393	2.545	3.12×10^{-7}	−3.911
	130°	403	2.481	1.39×10^{-7}	−4.251

TABLE II

D.C. conductivity and resistivity—temperature

Temperature $t°C$	$T°K$	$\frac{1}{T} \times 10^3$	D.C. Conductivity K_0 mho-cm^{-1}	D.C. Resistivity ρ ohm-cm.	log ρ
110°	383	2.611	6.5×10^{-14}	1.54×10^{13}	13.1871
120°	393	2.545	3.16×10^{-13}	3.16×10^{12}	12.5003
130°	403	2.481	1.14×10^{-12}	8.77×10^{11}	11.9341
140°	413	2.421	5.89×10^{-12}	1.70×10^{11}	11.2299
150°	423	2.364	2.24×10^{-11}	4.46×10^{10}	10.6498

TABLE III

Viscosity—Temperature

Temperature			Viscosity	
$t°C$	$T°K$	$\frac{1}{T} \times 10^3$	η in poise	$\log \eta$
75	348	2.874	7,870	3.896
80	353	2.833	3,020	3.480
85	358	2.793	1,060	3.025
90	363	2.755	372	2.573
95	368	2.717	112	2.050
100	373	2.681	60	1.778

Hence from all these evidences it would not be very much wrong to assume that the macroscopic viscosity is the inner friction for our purpose here.

In order to obtain the dimension of the rotating unit from the relation

$$\tau = \frac{4\pi\eta a^3}{KT}$$

we should know the value of the relaxation time τ This may be calculated from another relation due to Debye, viz.,

$$\omega\tau = \frac{\epsilon'_\infty + 2}{\epsilon'_0 + 2}$$

at the point where the maximum dielectric loss takes place for any frequency in the loss factor—temperature (ϵ''–temp) graph, ϵ'_∞ being the value of the dielectric constant at very high frequency and ϵ'_0 is the dielectric constant at very low frequency i.e., the static dielectric constant. These values of ϵ'_∞ and ϵ'_0 are estimated from ϵ'—$\log f$ graph corresponding to a temperature at which the dielectric loss is maximum for a particular frequency f and are used in the calculation of the relaxation time τ. Now knowing the viscosity corresponding to the temperature at which the loss maximum occurs and using it in the equation

$$\tau = \frac{4\pi\eta a^3}{KT}$$

the radius of the rotating unit can be obtained. Table IV shows the results of such calculations, from which it may be seen that the values, though computed from different data, are more or less in close agreement. The range of variation is narrow around the most probable value of 4.6Å.

TABLE IV

Calculated relaxation time and radius of the rotator

Loss maximum temperature °C	Relaxation time τ in sec	Frequency in kc/s	log η	Radius of the rotator 'a' in Å
77°	1.48×10^{-4}	1	3.80	4.55
88°	1.48×10^{-5}	10	2.78	4.60
96°	2.97×10^{-6}	50	2.10	4.55
100°	1.48×10^{-6}	100	1.78	4.65

The average dimension of the rotating unit so obtained reveals an interesting fact. The radius of the abietic acid molecule, the chief constituent of rosin, theoretically calculated from its established chemical structure is of the same order. This suggests that abietic acid molecule as a whole takes part in the orientation.

It may be mentioned here that from a similar study of the dielectric properties of a sample of wood rosin, Kitchin and Muller (1928) also obtained the dimension of the rotating unit as 4.8Å which is almost equal to the value obtained here.

REFERENCES

Bhattacharya, G. N., 1944a, *Ind. J. Phys.*, **18**, 1.

Bhattacharya, G. N., 1944b, *Ind. J. Phys.*, **18**, 97.

Claro, I. C., 1949, Elastomers and Plastomers (Elsevier Publishing Co., New York) **2**, 388.

Fuoss, R. M. and Kirkwood, J. G., 1941, *J. Chem. Phys.*, **9**, 329.

Hartshorn, L., Megson, N. J. L. and Rushton, E., 1940, *Proc. Phys. Soc.*,**52**, 790.

Kitchin, D. W. and Muller, H., 1928, *Phys. Rev.*, **32**, 979.

Lee, A. R., 1934, *J. Soc. Chem. Ind.*, **53**, 69*T*.

Mizushima, S., 1927, *Sci. Papers, Inst. Phys. Chem. Research (Tokyo)*, **5**, 201.

Race, H. H., 1931, *Phys. Rev.*, **37**, 430.

Rau, M. G. and Simonsen, J. L., 1924, Indian Forest Records, **11**, 207.

Sen, A. K. and Bhattacharya, G. N., 1957, *J. Assoc. App. Physicists*, **4**, 72

Sen, A. K. and Bhattacharya, G. N., 1958, *Ind. J. Phys.*, **32**, 49.

Yager, W. A., 1936, *Physics*, **7**, 434.

COLOUR CENTRES IN PENTAHYDRATE CRYSTAL OF SODIUMTHIOSULPHATE

KAPIL DEO PRASAD

DEPARTMENT OF PHYSICS, PATNA UNIVERSITY

(*Received for publication, May* 23, 1958)

ABSTRACT. It has been observed that pentahydrate crystals of sodium thiosulphate develop a yellow coloration after a few hours of irradiation by X-rays. Spectrophotometric analysis revealed that the coloured crystal has an absorption maxima at about 400 mμ. Even when kept in darkness, the crystal loses its coloration at a rate depending on the temperature. For example, at –5°C the colour persists for about 15 days without any appreciable bleaching and at 29°C it persists for 36 hours with a lot of bleaching.

The induced coloration disappears rapidly when the crystal is exposed to monochromatic radiation of a wave-length lying in the region of its absorption band. A new absorption band at about 1000 mμ is developed after bleaching of the crystal in complete darkness, whereas two new absorption bands, one at 1000 mμ and the other at about 580 mμ, the F′ band, appear after bleaching the coloured crystal by light of a wave-length lying in its X-ray induced abosrption band.

INTRODUCTION

The study of the physical properties of crystals, which have been coloured either by exposure to X-rays, or cathode rays or by stoichiometric excess of the alkali metals, occupies an interesting place in the solid state physics. It appears that the coloration of crystals of alkali halides by cathode ray bombardment and subsequently by X-ray irradiation, was first observed by Goldstein (1896). Pohl (1937, 1938) gave the name of F band to the absorption band in the visible region developed in these crystals and ascribed the absorption to the production of absorbing centres in the crystals, which they called F centres (from the German word Farbzentren or colour centres).

Molnar (Seitz, 1946) observed that the coloration produced tends to a saturation value depending on temperature, the nature of the crystal and the intensity of the X-ray beam and that besides the F band, a new absorption band (called the V band) on the ultra-violet side of the F band and another (called the M band) on its infra red side are also produced by X-ray irradiation.

The F band is also induced in alkali halide crystals when they are heated in an atmosphere of the alkali metal vapour and then cooled rapidly to room temperature (*i.e.*, quenched). If instead of quenching, the crystal is cooled slowly after heating, an additional absorption band is observed and this is probably due to the formation of colloidal aggregates of the excess alkali metal (Hirschlaff,

1938). This additional absorption band lies between 550—600 mμ in NaCl depending on the size of the colloidal aggregates, the wavelength of the peak of the absorption band increasing with the size of the colloidal aggregates. The crystal appears blue by transmitted light.

Besides the coloration of alkali halides, the coloration of a few other crystals like that of chrome-alum (Braun, Many and Simchen, 1954), BaF_2 and CaF_2 (Smakula, 1950), etc. by X-ray irradiation, has been observed and studied. It appears that no previous worker has studied the coloration effects in sodium thiosulphate crystals by X-ray irradiation and therefore the present investigation has undertaken to study this phenomenon.

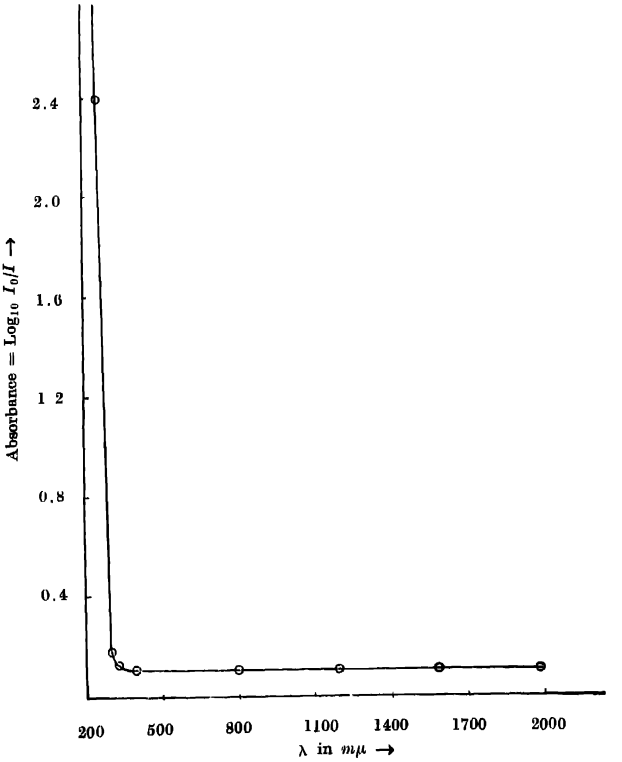

Fig. 1.

EXPERIMENTAL

Pentahydrate crystals of sodium thiosulphate were prepared in the laboratory from saturated solutions of Merck's sample of the salt in distilled water. The single transparent crystal was cut to the suitable size (2.0 cm × 1 cm × 0.5 cm) so as to fit in the cell holder of the Beckmann's Du model spectrophotometer. The transmittance of the unexposed and uncoloured crystal was first measured in the wavelength region 200 mμ to 2000 mμ Figure 1 shows the plot of the absorption of the crystal calculated from the measured transmittances.

The crystal was then irradiated for about 5 hours at room temperature (about 20°C) by unfiltered radiation of a copper target emerging through a beryllium window, the tube current being 8 mA at 50 KV The crystal developed a yellow coloration Its transmittances for different wavelengths were measured immediately after completion of irradiation and Curve 1 of figure 2 shows its

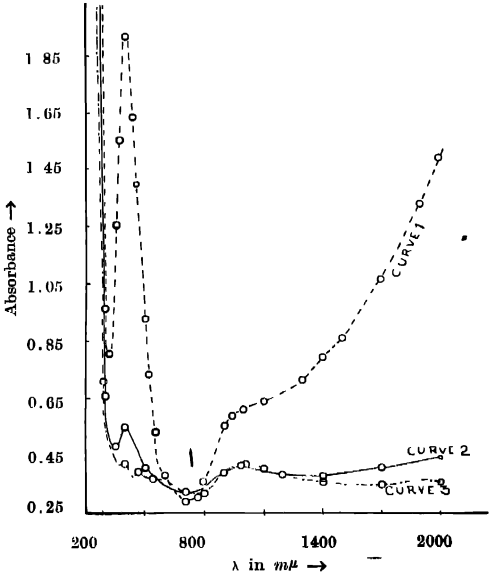

Fig. 2.

absorption calculated from the transmittance data. Curves 2 and 3 of figure 2 show its absorption in different wavelength regions observed after the crystal had been in dark at room temperature for five days and 54 days respectively.

It has also been found that the coloured crystal can be bleached by irradiation by a light of wavelength in the region of its absorption band. A second crystal was coloured by X-ray irradiation and its absorption curve (curve 1 of figure 3) was obtained immediately afterwards. The coloured crystal was then irradiated by light of the wavelength in the absorption band (*i.e.*, 405 mμ) for about 7 hours by placing it in the monochromated beam of 405 mμ in the DU model of Beckmann

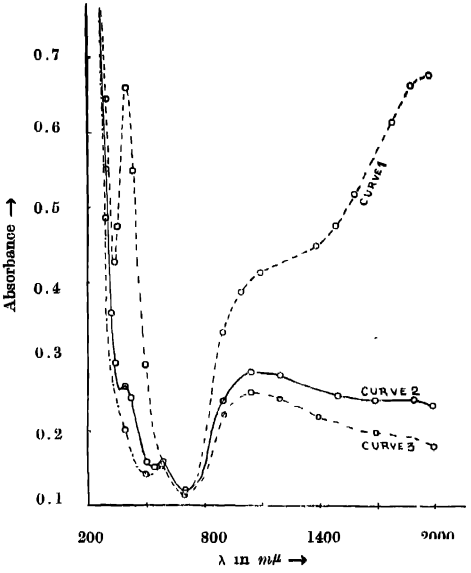

Fig. 3.

spectrophotometer. Table I is the observation for such irradiation. Curve 2 of figure 3 shows the extent of bleaching effected by exposure to light of wavelength in the region of its absorption band. The crystal was then left in dark at room temperature for 15 days more and Curve 3 of figure 3 shows its absorption after this period.

DISCUSSION OF RESULTS

It is clear from figure 1 that unexposed, colourless and transparent single crystals of sodium thiosulphate have negligible absorption in the region 300 mμ to 2000 mμ and perhaps beyond 2000 mμ also. After irradiation by X-ray the crystal is coloured and this coloration is due to an absorption band at about 400 mμ. From Curve 1 of figure 2 there is an indication of the presence of another band beyond 2000 mμ. Measurement could not be extended beyond 2000 mμ on

account of the non-availability of an infra red spectrophotometer. I shall call the absorption band at 400 mμ as the F band and that beyond 2000 mμ as the M band corresponding to the F and M bands developed in alkali halide crystals. The mechanism of the production of the colour centres responsible for these absorption bands are probably the same as that for alkali halide crystals, namely, the trapping of electrons and holes produced by energetic photo-electrons released by the impact of X-ray photons.

Curve 2 of figure 2 shows that the F and M centres are not stable but decay with time even in complete darkness probably due to thermal impacts. Those curves also show that while F and M bands are bleached almost completely, a new absorption band appears at about 1000 mμ. This is most likely due to the gradual drifting of the trapped electrons in the F and M centres to centres of greater stability.

Curve 3 of figure 2 shows that after 54 days the F and M bands are almost completely bleached while the band at 1000 mμ still persists together with the formation of a band at about 460 mμ which may be ascribed either to the formation of colloidal aggregates during the process of bleaching or to the drifting of the trapped electrons to centres of greater stability. After the above process of self-bleaching, the crystal still retains a faint bluish tinge.

Curve 1 of figure 3 is the absorption curve of another crystal of sodium thiosulphate coloured by X-ray irradiation. The crystal was then irradiated with light of wavelength 405 mμ, and the resulting decrease in its absorption is given in Table I. The increase in per cent transmittance with time has been plotted in figure 4. It is seen that in this case also the F and M bands are bleached just

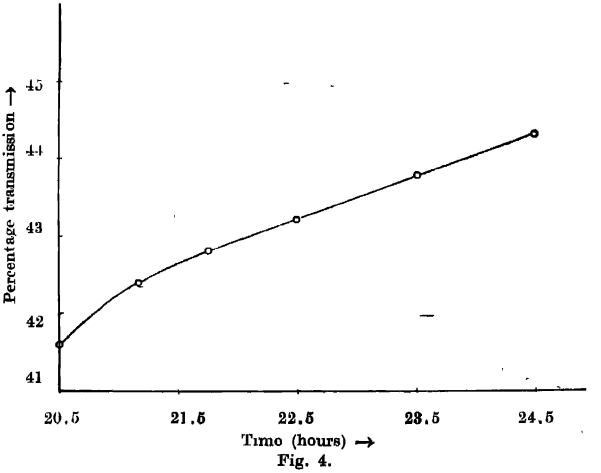

Fig. 4.

as when the coloured crystal is left in darkness for a long time; but in the present case the bleaching time is much smaller In this case also a new band at 1000 mμ and another at 580 mμ appear after bleaching. I shall call for the present the band at 580 mμ, the F′ band. This F′ band lasts for a much longer time when the crystal is left in darkness.

The number of F centres per c.c. formed in the crystal as a result of X-ray irradiation was calculated from the equation (Pohl, 1937)

$$N_0 = 1.31 \times 10^{17} \frac{n_0}{(n_0^2+2)^2} K_{max} H. \qquad \ldots \quad (1)$$

Where, N_0 is the number of colour centres per unit volume.

n_0 ,, ,, refractive index of the crystal = 1.5

K_{max} ,, ,, absorption constant for the band maxima in cm^{-1}

H ,, ,, half width of the band in ev

The values of the number of the colour centres per c.c. present in the crystal at various stages have been calculated and are given in tabular form in Table II.

The pentahydrate crystal of sodium thiosulphate, $Na_2S_2O_3+5H_2O$, has a complex structure while the alkali halide crystals have relatively much simpler structure. Further studies on other physical properties associated with the formation of colour centres by X-ray irradiation, are necessary before venturing to explain all the observations reported above.

TABLE I

Time (hours)	% Transmission	Absorbance
0	24.4	613
1	26.6	.575
Dark interval for 19½ hours		
20½	41.6	.381
21½	42.4	.373
21¾	42.8	.369
22½	43.2	.364
23½	43.8	.358
24½	44.3	.354
Dark interval for 22 hours		
46½	52.2	.282
48	52.7	.278
48½	52.9	.276

TABLE II

Fig.	Curve	K_{max}	H	N_0
	1	7.70	1.01	84.5×10^{15}
2	2	2.21	41	$9.85 \times$,,
	3	1.67	.12	$2.20 \times$,,
	1	3.05	.59	19.57×10^{15}
3	2	1.20	.16	$2.07 \times$,,
	3	.92	0	$0 \times$,,

ACKNOWLEDGMENTS

The author indebted to the Government of India for the award of a scholarship which has enabled him to carry out the work on this subject. He is thankful to his supervisor Prof. M. N. Varma for his keen interest in the work and for valuable suggestions. He is also indebted to the Head of the University Department of Physics, Patna University, for providing all necessary laboratory facilities for the work. His thanks are also due to the Director of the Indian Institute of Technology, Kharagpur, for permission to visit the Physics laboratory with a view to acquainting himself with works on similar lines in progress there and to Dr. J. Sharma of the Department of Physics of the same institute for certain valuable suggestions.

REFERENCES

Braun, E. A., Many, A. and Simchen, A. E., 1954, *Phys. Rev.*, 96, 1505.
Goldstein, E., 1896, *Zeits. f. Instrumentkunde*, 16, 211.
Hirschlaff, E., 1938, "Flourescence and Phosphorescence" Methuen's monographs on physical subject.
Pohl, R. W., 1938, *Physik Zeits* 39, 36.
Pohl, R. W., 1937, *Proc. Phys. Soc.*, 49, (extra part), 3.
Seitz, F., 1946, *Rev. Mod. Phys.*, 18, 384.
Smakula, A., 1950, *Phys. Rev.*, 77, 408.

ABSORPTION OF MICROWAVES IN SOLUTIONS OF ORTHO-CHLOROPHENOL*

TARAK JIBAN BHATTACHARYYA

OPTICS DEPARTMENT, INDIAN ASSOCIATION FOR THE CULTIVATION OF SCIENCE, CALCUTTA-32

(*Received for publication, October* 14, 1958)

ABSTRACT. The absorption of 3.18 cm microwaves in solutions of *o*-chlorophenol in CCl_4 has been studied using optical method. It has been found that the 15% solution exhibits maximum absorption at 0°C and the 7 5% solution shows the maximum at −13°C. The aggregate absorption is found to increase with lowering of concentration. These results have been discussed in the light of those observed in the investigations on the infra-red and Raman spectra of solutions of the compound in different solvents reported by previous workers. It has been concluded that in dilute solution in CCl_4, the OH group in most of the molecules possesses freedom of rotation

INTRODUCTION

The Raman spectra of solutions of *o*-chlorophenol in different solvents have been studied by Mukherjee (1958) and it has been observed that the intensity of the line 3533 cm^{-1} increases when the liquid is dissolved in the solvents and it increases further when the concentration is diminished from 30% to 15%. He pointed out that as this line is assigned to the OH valence oscillation in the molecule with the OH group in the *trans*-position, such molecules become predominant in very dilute solutions. He further pointed out that the assignment made by Pauling (1936) of the strong infrared absorption peak at 6910 cm^{-1} in CCl_4 observed by Wulf and Liddel (1935) is probably not correct. More recently, Sirkar, Deb and Banerjee (1958) from an investigation on infrared spectra of the solutions of *o*-chlorophenol concluded that in dilute solutions most of the molecules have the OH group in the *trans* configuration. They observed that the spectrum due to pure *o*-chlorophenol in the liquid state consists of three broad absorption maxima indicating the presence of large number of double-molecules as suggested by Pauling (1945) and also some molecules of *cis* and *trans* configurations. Similar conclusions were also arrived at by Roy (1958) who studied the electronic spectra of *o*-chlorophenol in different solvents at different temperatures.

The absorption of 3.18 cm microwaves in *o*-chlorophenol and *p*-chlorophenol was studied by Ghosh (1955*a*) who found that although *p*-chlorophenol shows absorption in the range 50°C—170°C with the maximum at 85°C, *o*-chlorophenol

* Communicated by Prof. S. C. Sirkar.

does not show any absorption throughout the temperature range from the freezing point up to the boiling point of the substance. He explained this by assuming that most of the molecules in the liquid state are of the *cis* form.

The results of the investigations on the Raman spectra and the infrared absorption spectra of solutions of *o*-chlorophenol mentioned above indicate, however, that the OH group has freedom of rotation in some of the molecules in the solutions. In that case such solutions should exhibit absorption of microwaves at proper concentrations and temperatures to produce proper values of coefficient of viscosity. The present investigation was undertaken to find out whether such absorption takes place in the 3-cm region.

EXPERIMENTAL

The experimental arrangements and the method of determining absorption maxima were similar to those used by Ghosh (1954*a*). A klystron oscillator of the type 793A was used as the source of microwaves of frequency 9415 Mc/sec.

Chemically pure samples of *o*-chlorophenol and carbon tetrachloride were dehydrated and fractionated. Proper fractions were collected and redistilled under reduced pressure. Solutions with 15% and 7.5% molar concentrations of *o*-chlorophenol in CCl_4 were used. In the case of 15% solution the absorption was studied in the temperature range from 40°C to about −20°C. The solution was diluted to 7.5% and its temperature was lowered up to −50°C in order to find out the temperature at which maximum absorption takes place in this case. The values of the static dielectric constant, refractive index and the coefficient of viscosity were required for the calculation of the radius of the rotor. These data of the solutions of *o*-chlorophenol in CCl_4 were not available in the standard literature. The dielectric constant was measured in the laboratory. A tuned circuit with a special type of cell connected parallel to a standard condenser was loosely coupled to the coil of a constant frequency oscillator. The cell used for this purpose consists of a gold plated brass cylinder placed coaxially inside another hollow gold plated cylinder and the inner cylinder is kept insulated from the outer one with the help of a polystyrene cap. The thickness of the annular space between the cylinders is 3 mm.

The values of coefficient of viscosity η of the solutions at the required temperatures were calculated from the formula $\eta = x_1\eta_1^{\frac{1}{3}} + x_2\eta_2^{\frac{1}{3}}$, where x's and η's are the mole-fractions and coefficients of viscosity of the pure components at the temperature concerned. The coefficients of viscosity of pure *o*-chlorophenol and pure carbon tetrachloride were obtained by extrapolating the data given in the International Critical Tables.

From the refractive indices of the pure substances, the refractive indices of the solutions were calculated by using the standard formula.

RESULTS AND DISCUSSION

The coefficient of absorption μ was calculated from the formula :

$$\mu x = \log_e(I_0/I)$$

where x is the thickness of absorption cell and I_0/I is the ratio of the currents in the detector without and with the cell in its position respectively. The values of log I_0/I plotted against temperature of the 7.5% and 15% solutions are shown in the two curves reproduced in figure 1.

The maximum absorption in 15% solution takes place at 0°C and that for 7.5 % occurs at −13°C for microwaves of frequency 9415 Mc/sec. The relaxation time τ was calculated from Debye's equation .

$$\omega\tau = \frac{\epsilon_0 + 2}{\epsilon_1 + 2}\sqrt{\frac{\epsilon_1}{\epsilon_0}}$$

where ϵ_1 is the static dielectric constant of the solution and ϵ_0, the dielectric constant of the solution at frequencies in the optical range which was taken to be the square of the refractive index n of the solution at 20°C for sodium D-line, as the values of refractive indices at lower temperatures were not available.

The value of the radius a of the rotor was calculated from Debye's equation

$$a^3 = \frac{\tau KT}{4\pi\eta}$$

where η is the coefficient of viscosity at the temperature T°K. The values of a and the constants used in the calculation of a are given in Table I.

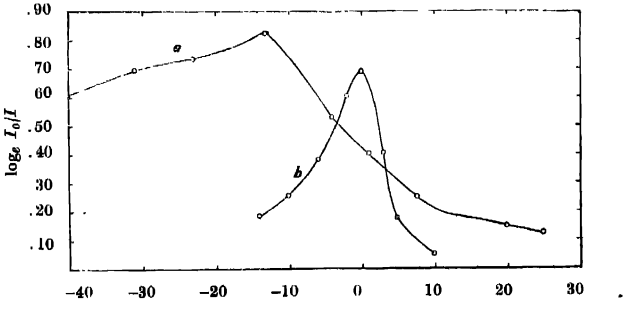

Fig. 8. Absorption of 3.18 cm microwaves in solution of o-chlorophenol in CCl_4.
Curve A – 7.5% solution (molar concentration).
Curve B – 15% „ („).

TABLE I

Molar Concentrations of *o*-chlorophenol in CCl_4 sol.	Temp. for maximum absorption in °K	Static dielectric constant of sol.	n	$\eta \times 100$	$\tau \times 10^{11}$ (in sec.)	$a \times 10^8$(cm)
15%	273°K	3.71	1.47	1 9	1.67	1.39
7.5%	260°K	2.60	1.47	2.7	1.63	1.43

It can be seen from figure 1 that the solution of *o*-chlorophenol exhibits absorption in 3-cm microwave region. The maximum absorption occurs at −13°C for the 7.5% solution and that for the 15% solution occurs at 0°C. The peak of the curve for 7.5% is higher and much broader than the peak of the other curve. The radius of the rotor calculated by using Debye's formula is found to be approximately 1.4 Å in both the cases. It is of the same order as that of the freely rotating OH groups observed by Ghosh (1954*b*; 1955*b*, *c*) in phenols and alcohols

Ghosh (1955*a*) did not observe any absorption of 3.18 cm waves in pure *o*-chlorophenol throughout the temperature range from the freezing point to the boiling point of the liquid. He concluded that most of the molecules have their OH group in *cis* position with respect to the chlorine atom of the same molecule in the pure liquid. The results of the present investigation, however, show that in solutions of *o*-chlorophenol in CCl_4 the OH group is free in some of the molecules and the radius of the rotor is found to be of the same order as that of the freely rotating OH group. It is, therefore, clear that hydrogen atoms of OH groups in the molecules of *o*-chlorophenol in solutions in CCl_4 are not chelated as observed by Ghosh (1955*b*) in pure liquid. The fact that the peak of the curve for 7.5% solution is higher and broader than that of the other curve indicates that the intensity of absorption is higher for 7.5% solution than for the 15% solution. Hence the number of molecules with free OH group is greater in 7.5% solution than that in 15% solution. Thus the observations in present work suggest that the OH group in most of the molecules of *o*-chlorophenol in dilute solution in CCl_4 possesses freedom of rotation about an axis coinciding probably with the diameter of benzene ring passing through the carbon atom to which the OH group is attached. This further shows that in the dilute solutions of *o*-chlorophenol in CCl_4, a predominantly large number of molecules of *o*-chlorophenol have their OH groups turned to the *trans*-position with respect to the chlorine atom by the influence of the solvent molecules.

Mukherjee (1958) concluded from the results of investigation on the Raman spectra of the solutions of *o*-chlorophenol in different solvents. that the OH group is free in most of the molecules in the solution. Sirkar, Deb and Banerjee

(1958) investigated the infra-red absorption spectra of the solutions of *o*-chlorophenol in carbon tetrachloride and cyclohexane of different strengths and also of the pure liquid. In the case of pure *o*-chlorophenol they concluded from the results that there are some dimers in the liquid as proposed by Pauling (1945) and the feeble absorption produced in the region 3500 cm^{-1}—3600 cm^{-1} might be due to OH oscillation in a small percentage of single molecules of *trans*-configuration. They further observed that with the change of concentration from 30% to 5% the number of such single molecules of *trans* configuration increases rapidly. The results of the present investigation corroborate the conclusions drawn by the above workers, because at the lower concentration the aggregate absorption is much larger than that in the 15% solution.

ACKNOWLEDGMENT

The author is indebted to Professor S. C. Sirkar, D.Sc., F.N.I., for suggesting the problem and for his guidance throughout the progress of the work.

REFERENCES

Ghosh, D. K., 1954*a*, *Ind. J. Phys.*, **28**, 191.
,, 1954*b*, *Ind. J. Phys.*, **28**, 485.
,, 1955*a*, *Ind. J. Phys.*, **29**, 450.
,, 1955*b*, *Ind. J. Phys.*, **29**, 161
,, 1955*c*, *Ind. J. Phys.*, **29**, 581.
Mukherjee, D. K., 1958, *Ind. J. Phys.*, **32**, 192.
Pauling, L., 1936, *J. Am. Chem. Soc.*, **58**, 94.
,, 1945, Nature of Chemical bond, p. 324.
Roy, S. B., 1958, *Ind. J. Phys.*, **32**, 525.
Sirkar, S. C., Deb, A. R. and Banerjee, S. B., 1958, *Ind. J. Phys.*, **32**, 345.
Wulf, O. R. and Liddel, U., 1935, *J. Am. Chem. Soc.*, **57**, 1464.

Letters to the Editor

The Board of Editors will not hold itself responsible for opinions expressed in the letters, published in this section. The notes containing reports of new work communicated for this section should not contain many figures and should not exceed 500 words in length. The contributions must reach the Assistant Editor not later than the 15th of the second month preceding that of the issue in which the Letter is to appear. No proof will be sent to the authors.

11

THERMOLUMINESCENCE AND PHOSPHORESCENCE SPECTRA OF SOME PURE AND IMPURITY ACTIVATED ALKALI HALIDES

B. C DUTTA* AND A. K. GHOSH+

KHAIRA LABORATORY OF PHYSICS, UNIVERSITY COLLEGE OF SCIE CALCUTTA.

(*Received for publication, September* 25, 1958)

In order to have a better insight into the mechanism of luminescence emission the thermoluminescence spectra of NaCl, NaF, NaI, KI, LiCl and also those of thallium activated NaCl, NaBr, KI were studied. The measurements were confined in the spectral range 330 mμ—650 mμ.

Glow peaks were observed both above and below room temperature. On examination of the results it will be evident that most of the glow peaks observed are below room temperature. This is possibly because of the fact that the irradiation by 10 KV cathode rays had been done mostly at liquid oxygen temperature and so the high temperature glow peaks are either weak or absent.

All alkali halides have visible thermoluminescence emission. There may be different spectral bands in the same glow peak. The thermal activation energy for visible and ultra-violet emissions may or may not be different, i.e., there may be visible and ultra-violet emissions in the same glow peak or only visible or only ultra-violet emission.

Coincidence of thermal bleaching of colour centres and thermoluminescence has been reported by many workers (Dutton *et al.*, 1953 : Sharma 1952, 1956 , Halperin *et al*, 1957) and it is assumed that the two processes are closely related to each other. Both may have the same origin or one may be the cause of the other. In most cases it is observed that the samples are coloured on irradiation This colour disappears or changes at specific temperatures indicating a change in the absorption band.

*Now at Birkbeck College, London.

†Now at University of Notre Dame, U.S.A.

On incorporation of impurities into the host crystal there is generally an increase in the liminescence intensity ; trapping and luminescence centres are perturbed or destroyed and new centres created.

The observed emissions for the pure sample are assumed to be due to release of trapped electrons (holes) and its recombination with holes (electrons). In some cases there may be tunnelling of trapped electrons to trapped holes. Excitons probably play an intermediate role in the luminescence emission process.

TABLE I

Thermoluminescence spectra

Phosphor	Glow peak temperature in °K	Luminescence band maxima in m μ	Remarks
NaCl	160	432,540	After 10KV cathode ray irradiation at 90°K.
	232	484	,,
	545	416,519	After 10KV cathode ray irradiation at 300°K
NaI	164	522	After 10KV cathode ray irradiation at 90°K
NaF	185	403	,,
	290	415	,,
KI	104	568	,,
	190	570	,,
	320	478	,,
LiCl	118	423,528	,,
	226	460	,,
	314	547	,,
NaCl : Tl (2.5%)	163	416, 510	,,
	227	418,515	,,
	489	470	,,
	493	510	,,
NaBr : Tl (2.5%)	109	510	,,
	184	550	,,
	279	448	,,
	423	560	,,
KI : Tl (2.5%)	224	450	,,

TABLE II

Phosphorescence spectra

Phosphor	Luminescence band maxima in m μ	Remarks
NaCl	435, 540	After 10KV cathode ray irradiation at 90°K
KI	570	,,

The authors wish to thank Prof. S. N. Bose for his constant interest in the work.

REFERENCES

Dutton, D. and Maurer, R. J., 1953, *Phys. Rev.*, **90**, 126.

Sharma, J., 1952, *Phys. Rev.*, **85**, 692 and **87**, 335; 1956, *Phys. Rev.*, **101**, 1295.

Halperin *et al.*, 1957 *Phys. Rev.*, **108**, 928, 932.

ON THE CALCULATION OF RELAXATION TIMES

C. R. K. MURTY

PHYSICS DEPARTMENT, ANDHRA UNIVERSITY, WALTAIR

(*Received for publication, September* 30, 1958)

Chau, Le Fevre and Tardif[1] have suggested an empirical equation to calculate the relaxation times of polar molecules in dilute solution in non-polar solvents. From the known physical properties of the solute and solvent they have calculated the relaxation times for a number of polar molecules in different solvents using the equation

$$\tau = \pi\eta_1(\exp \Delta_1)ABC/2(\epsilon_1+2)kT \qquad \ldots \quad (1)$$

where η_1, Δ_1 and ϵ_1 are the viscosity, depolarisation factor observed in Rayleigh scattering and the dielectric constant of the non-polar solvent, while ABC are the dimensions pertaining to the solute molecule. They have compared the calculated relaxation times with their observed values and found reasonable agreement.

Another empirical equation namely,

$$\tau = 6\pi\eta_1\alpha/(\epsilon_1+2)kT \qquad \ldots \quad (2)$$

is now suggested in which η_1 and ϵ_1 are the viscosity and dielectric constant of the solvent and α is the polarisability of the solute molecule. This equation avoids the necessity of knowing Δ_1 and ABC, the quantities which cannot be easily obtained. α can be easily computed from a knowledge of the refractivity of the solute molecule.

The relaxation times calculated using equations (1) and (2) are given in the following table together with the observed values as given in reference (1). The data necessary for the calculation have been taken from (Chau *etal*, 1957).

An examination of the table shows that equation (2) in its simpler from gives equally satisfactory values for relaxation times as equation (1). The equation (2) has been tested for a number of other solutes and is found to give reasonable values for τ. Full details will be published elsewhere.

TABLE I

Solute	Solvent	$\tau_{eq(1)}$	$\tau_{eq(2)}$	$\tau_{obs} \times 10^{12}$ SeC.
Nitrobenzene	CCl_4	13	14	13–20
	C_6H_6	13	9.0	11–15
Nitronaphthalene	CCl_4	19	21	25
	C_6H_6	18	14	20
Nitroanthracene	CCl_4	24	30	23
	C_6H_6	23	20	28
Pyridine	CCl_4	20	9.6	7.2
	C_6H_6	10	6.3	4.4
Quinoline	CCl_4	15	16	14
	C_6H_6	14	11	10
iso-Quinoline	CCl_4	16	17	21
	C_6H_6	14	11	15
Acridine	CCl_4	19	24	26
	C_6H_6	18	16	20
4–Nitrodiphenyl	CCl_4	20	23	21
	C_6H_6	20	15	30

REFERENCE

Chau, J. Y. H., Le Fevre, R. J. W., and Tardif, J., 1957, *J. Chem. Soc.*, 2293.

CONFIGURATIONAL INTERACTION IN MOLECULAR ORBITAL THEORY AS APPLIED TO INDENE

S. RAMAMURTY

MATHEMATICAL PHYSICS DEPARTMENT, ANDHRA UNIVERSITY, WALTAIR

(*Received for publication, November* 12, 1958)

From the work of Craig, Jacobs, Coulson and Altmann (1950a), it is clear that to get reliable estimates of the energy levels of the molecules it is necessary to take into account the considerations that molecular states arise from superposition of configurations, that the influence of σ electrons must not be ignored and that $3p$ orbitals play an important role in the structure of molecules. Pariser and Parr (1950b) have given a method of calculating the effect of interaction of configurations which, in a fairly simply way, enables us to take into account also the influence of σ electrons. Adopting this method, further calculations have been made on indene, following up the author's previous simple ASMO treatment of this molecule (Coulson and Jacob, 1951).

The molecular orbitals and their energies have been obtained by setting up and solving the secular equation, ignoring overlap and non-neighbour resonance integrals as a first approximation.

The configurations which have been selected for interaction are the ground configuration and all the singly excited configurations. The formulae expressing the interaction between the configurational wave functions have been obtained using McWeeny's results (Coulson and Craig, 1951). The required integrals over M. O.'s have been numerically obtained by a matrix procedure. The C.I. matrix has been diagonalized, yielding the energy values as also the coefficients of the configurational wave functions in the state wave functions. The results of the calculations together with the experimental data are given in the following table.

TABLE

Calculated and Experimental Spectral positions

Calculated (e.V)	Experimental (e.V) Vapour	Solution	Difference
3.7	4.3	4.3	-0.6
4.7	4.9	4.6	-0.2
6.3	5.5	5.6	0.8

There is agreement between the predicted and observed values to within one electron volt which may represent the order of accuracy in such calculations.

Full details of the calculation will be published shortly.

ACKNOWLEDGMENT

The author is deeply indebted to Prof K. R. Rao for his kind and invaluable guidance throughout the progress of the work.

REFERENCES

Altmann, S. L., 1952, *Proc. Roy Soc.*, *A* **210**, 327.
Altmann, S. L, 1952, *Proc. Roy Soc.*, *A* **210**, 343.
Craig, D. P., 1950*a*, *Proc. Roy. Soc.*, *A* **200**, 474.
Craig, D. P., 1950*b*, *Proc. Roy Soc.*, *A* **202**, 498
Coulson, C. A., Jacob, J, 1951, *Proc. Roy. Soc.*, *A* **206**, 287.
Coulson, C. A., Craig, D. P, and Jacobs, J., 1951, *Proc. Roy Soc.*, *A* **206**, 297.
Jacobs, J., 1955, *Proc. Phys. Soc.*, *A* **68**, 72.
McWeeny, R., 1955, *Proc. Roy. Soc. A* **232**, 114.
Pariser R, and Parr, R. G., 1953, *J. Chem. Phys.*, **21**, 446.
Pariser R, and Parr, R. G., 1953, *J. Chem. Phys.*, **21**, 767.
Pariser, R. 1956, *J. Chem. Phys.*, **24**, 250.
Ramamurty, S, 1953, *Ind. J. Phys*, **27**, 504.

PREDICTED ELECTRONIC SHIFTS IN FLUORINATED NAPHTHALENES

S. RAMAMURTY

MATHEMATICAL PHYSICS DEPARTMENT, ANDHRA UNIVERSITY, WALTAIR

(*Received for publication, November* 12, 1958)

Murrell and Longuet-Higgins (1955) developed a method of calculating inductive perturbations taking configurational interaction into account and obtained satisfactory results in the case of benzene. Using this method and the available experimental data corresponding to system I of the vapour absorption bands of α and β fluoronaphthalenes (Ramamurty and Rao, 1957), the values of the parameters A and δ have been found to be

$$A = -0.0252, \qquad \delta^2 = 0.1304$$

For the significance of A and δ reference may be made to the paper of Murrell and Longuet-Higgins (1955).

Using these values the shifts corresponding to the system in other fluorinated naphthalenes may be calculated. The values thus predicted for some of these are given below ·

TABLE I

	Molecule	Shift to the red in e.V.
1, 2	Fluoronaphthalene	0.0587
1, 3	,,	0.0556
1, 4	,,	0.0606
1, 2, 3	,,	0.0894
1, 2, 4	,,	0.0900
1, 2, 3, 4	,,	0.0987

Experimental work on the absorption of these and other fluorinated naphthalenes is desirable to enable a verification of the correctness of these predictions. This work is proposed to be taken up as soon as the substances become available. Full details of the calculations will be published shortly.

ACKNOWLEDGMENTS

The author is deeply indebted to Prof. K. R. Rao for his kind and invaluable guidance throughout the progress of the work.

REFERENCES

Hurrell, J. N., and Longuet-Higgins, H. C., 1955, *Proc. Phys. Soc.*, *A* 68, 329.

Ramamurty, S., Jagannadha Rao, M., and Ramakrishna Rao, V., 1957, *Ind. J. Phys.*, 31, 497.

The following special publications of the Indian Association for the Cultivation of Science, Jadavpur, Calcutta, are available at the prices shown against each of them :—

TITLE	AUTHOR	PRICE
Methods in Scientific Research	Sir E. J. Russell	0 6 0
The Origin of the Planets	Sir James H. Jeans	0 6 0
Separation of Isotopes	Prof. F. W. Aston	0 6 0
Garnets and their Role in Nature	Sir Lewis L. Fermor	2 8 0
(1) The Royal Botanic Gardens, Kew.	Sir Arthur Hill	1 8 0
(2) Studies in the Germination of Seeds.	"	
Interatomic Forces	Prof. J. E. Lennard-Jones	1 8 0
The Educational Aims and Practices of the California Institute of Technology	R. A. Millikan	0 6 0
Active Nitrogen— A New Theory.	Prof. S. K. Mitra	2 8 0
Theory of Valency and the Structure of Chemical Compounds.	Prof. P. Ray	3 0 0
Petroleum Resources of India	D. N. Wadia	2 8 0
The Role of the Electrical Double-layer in the Electro-Chemistry of Colloids.	J. N. Mukhrjee	1 12 0
The Earth's Magnetism and its Changes	Prof. S. Chapman	1 0 0
Distribution of Anthocyanins	Robert Robinson	1 4 0
Lapinone, A New Antimalarial	Louis F. Fieser	1 0 0
Catalysts in Polymerization Reactions	H. Mark	1 8 0 (2*s*.6*d*.—foriegn)
Constitutional Problems Concerning Vat Dyes	Dr. K. Venkataraman	1 0 0
Non-Aqueous Titration	Santi R. Palit, Mihir Nath Das and G. R. Somayajulu	3 0 (foreign $ 1.00 or 5s)

A discount of 25% is allowed to Booksellers and Agents.

RATES OF ADVERTISEMENTS

1. Ordinary Pages :
   - Full page .. .. Rs. 50/- per insertion
   - Half page .. .. Rs. 28/- per insertion
2. Pages facing 1st inside cover, 2nd inside cover, and first and last page of book matter :
   - Full page .. .. Rs. 55/- per insertion.
   - Half page .. .. Rs. 30/- per insertion.
3. Cover page .. .. by negotiation.

25% Commissions are allowed to *bona fide* publicity agents securing orders for advertisements.

CONTENTS

Indian Journal of Physics Vol. 32, No. 12 December 1958

PAGE

66. A New Wideband Discriminator —N. B. Chakraborti 537
67. Calculations of the Dipole Moments of Tri-Substituted Benzenes 1, 2, 3-, 1, 2, 4-and 1, 3, 5-Substitutions —D. V. G. L. Narasimha Rao ... 547
68. The Dielectric Properties of Rosin —A. K. Sen and G. N. Bhattacharya 556
69. Colour Centres in Pentahydrate Crystal of Sodiumthiosulphate —Kapil Deo Prasad 566
70. Absorption of Microwaves in Solutions of Ortho-Chlorophenol —Tarak Jiban Bhattacharyya 573

LETTERS TO THE EDITOR

11. Thermoluminescence and Phosphorescence Spectra of some Pure and Impurity Activated Alkali Halides —B. C. Dutta and A. K. Ghosh ... 578
12. On the Calculation of Relaxation Times —C. R. K. Murty 580
13. Configurational Interaction in Molecular Orbital Theory as Applied to Indene —S. Ramamurty 582
14. Predicted Electronic Shifts in Flourinated Napthalenes —S. Ramamurty 584

SCIENTIFIC 'PYE' INSTRUMENTS

for

Industrial and Academic Research

Such as

Electronic Instruments, Galvanometers, Electrometers, Magnetic Instruments like Fluxmeters, Measuring Microscopes and Cathetometers, Potentiometers, Resistance Bridges and Boxes, Stop Clocks, Tuning Forks, etc. etc.

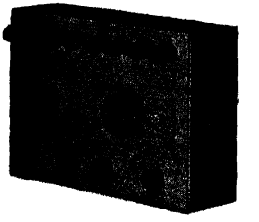

Potentiometer (Cat. 7554)

by

Messrs. W. G. PYE & CO. LTD. Granta Works, Cambridge, England.

SOLE AGENTS IN INDIA:

TOSHNIWAL BROTHERS PRIVATE LIMITED

198, Jamshedji Tata Road, BOMBAY-1.

BRANCHES:

14-B/4 N. E. A. NEW DELHI 5 — 'RIVAL' Kacherry Road, Ajmer. — ROUND TENA, Mount Road, Madras — 172, Dharamtalla Street CALCUTTA 13

PRINTED BY KALIPADA MUKHERJEE, EKA PRESS, 204/1, B. T. ROAD, CALCUTTA-35
PUBLISHED BY THE REGISTRAR, INDIAN ASSOCIATION FOR THE CULTIVATION OF SCIENCE
2 & 3, LADY WILLINGDON ROAD, CALCUTTA-32